Nitrogen-rich poly(pseudohalogenido) complexes of silicon, germanium, tin and lead

Zoe M. Smallwood

A thesis submitted in partial fulfilment of the requirements for the degree of
Doctor of Philosophy

The University of Sheffield
Faculty of Science
Department of Chemistry

February 2020

Abstract

Investigations into the coordinative behaviour of nitrogen-rich pseudohalogenido ligands towards *p*-block elements are generally less extensive than the analogous *d*-block complexes. In this study, several pseudohalides ($Y^- = N_3^-$, CN^-, CHN_4^-, $N(CN)_2^-$) were investigated as ligands in new poly(pseudohalogenido) complexes of group 14 elements, as E(IV) (E = Si−Pb) or E(II) (E = Ge, Pb).

The anionic complexes, $[E(Y)_6]^{2-}$ were stabilised as PPN salts ($[PPN] = \{Ph_3P\}_2N^+$). The preparation of $[PPN]_2[E(CN)_6]$ (E = Ge, Sn) required several synthetic strategies to account for the varying reactivity of the coordination centres and complete ligand exchange. Cycloaddition reactions involving $[PPN]_2[Sn(CN)_6]$ resulted only in ligand exchange. All attempts to isolate $[Pb(N_3)_3]^-$ were unsuccessful. The $[N(CN)_2]^-$ anion proved unsuitable owing to its weak coordination ability and varying denticity. $Ge(N_3)_2$ and $Pb(N_3)_4$ were stabilised for the first time by the inclusion of mono- or bidentate Lewis bases, as $Ge(N_3)_2(L)_2$ (L = py, pic, ^tBupy) and $Pb(N_3)_4(bipy)$. The limited stabilisation resulted in highly reactive adducts which frequently decomposed into more-stable oxidation states. Decoordination of volatile ancillary ligands in $Ge(N_3)_2(L)_2$ formed a germanium nitride under mild conditions, a process unknown for any group 14 poly(azido) complex. The pseudohalogen character of the N_5^- anion was evaluated for the first time, but the inability to prepare analytically pure N_5^- salts limited investigations to mass spectrometric studies. Crystallographic and electrochemical studies of arylpentazoles identified inter- and intramolecular interactions and examined the feasibility of N_5^- generation, respectively.

These studies give new and further insight into the coordination behaviour of common pseudohalides towards group 14 elements, including reactivity varying by ligand type, centre and oxidation state. This work further demonstrates the importance of the type and extent of stabilisation for nitrogen-rich complexes from both an energetic materials perspective and for decoordination of ancillary ligands to form novel compounds under mild conditions.

Acknowledgements

Firstly, I would like to thank my supervisor, Dr Peter Portius, for all of his help and guidance throughout this project, ranging from instruction in a wide number of practical techniques to extended discussion of results, answering my many questions and translating literature. This project would not have been possible without his support and I am grateful for the skills, knowledge, persistence and expertise I have gained over the last five years.

I would also like to acknowledge the huge support of Harry Adams and Dr Craig Robertson, who provided expert instruction and pratical support in X-ray crystallography, and assisted with the structure solutions of some of the compounds presented in this work. I am grateful for their support and their persistence, patience and expertise in helping to solve some of the more tricky structures. Dr Craig Robertson is also thanked alongside Dr Tom Roseveare for assisting with powder X-ray diffraction studies and the crystallographic studies of HOP-N_5. I would like to thank Dr Sandra van Meurs for recording low-temperature, solid-state, ^{119}Sn and ^{207}Pb NMR spectra. Simon Thorpe and Sharon Spey (mass spectrometry), Stephen Atkin (elemental analyses) and Rob Hanson (HPLC and TGA) are also acknowledged. Dr Grant Hill is thanked for conducting theoretical studies of the hexa(cyanido) complexes. Thanks also to Dr Marco Conte for allowing the use of his tube furnace, James Railton for his support during those studies, and Dr Nik Reeves-McLaren for Raman microscopy. I am indebted to Prof. František Hartl and James Taylor at The University of Reading for undertaking OTTLE studies on the arylpentazoles and arylazides, Dr Simon Parker at The University of Sheffield for help with cyclic voltammetry, and Dr Tony Haynes for loan of his low-temperature spectroscopic cell.

A number of individuals within the Portius group have assisted with some of the work undertaken in this project and I am grateful for the assistance of Lucas Pitzalis and Matthew Allen ($[N(CN)_2]^-$ compounds), George Szolin-Jones (Pb(IV) azido complexes) and Bradley Westwater (arylpentazoles and N_5^-). In addition, I would like to thank the members of the group both past and present, in particular Drs Rory Campbell, Ben Crozier and Ben Peerless for their practical support as well as helping to clear my plate at the Notty House. Thank you also to Babs and Andy, for your support, and Dr Amanda Newbold, for first inspiring me to study chemistry in the first place.

Last but not least, I am so grateful to all of my friends and colleagues who have made the last five years not only bearable but also enjoyable, especially the other Graduate Teaching Assistants and my friends who I have spent many a morning tea break or summer tournament match with. Equally important are those who may never have set foot in the lab- a big thank you to James as well as Alice, Luke, Hannah and my other friends for the endless support, love, kindness and laughter whilst reminding me that a world exists outside of a Schlenk tube. However, the biggest thanks are to my parents, who have been there throughout with words of encouragement, many cups of tea and slices of cake, even if you haven't always understood exactly what all the chemistry means. I couldn't have done it without you.

Contents

Chapter 1. Introduction

1.1 The Pseudohalogen Concept

The pseudohalogen concept was first proposed in 1925 by Birckenbach and defines a pseudohalogen, Y, as a compound which exhibits similar behaviour and reactivity to a halogen.[1] This essential characteristic allows the definition of a set of criteria which should be fulfilled by any pseudohalogen candidate (table 1), which include: [2,3]

Criterion	Description	Formula
A	Formation of radical anions	$Y^{\cdot}$
B	Existence of anionic species	Y^{-}
C	Formation of solid precipitates as silver, lead or mercury salts	e.g. AgY
D	Capable of acting as a ligand to form coordination complexes	MY_n
E	Existence of a protonated form	HY
F	Oxidation of anionic species to form dimeric molecules	$2Y^{-} \rightarrow Y_2$
G	Formation of mixed-pseudohalogen molecules	$Y-Y'$

Table 1. Criteria for identification of a species as a pseudohalogen.

The first species formally defined in Birckenbach's seminal report included the cyanide (CN^-), cyanate (OCN^-), thiocyanate (SCN^-) and azide (N_3^-) anions, which meet many of the behaviours listed above (table 2,3).[1] Later, other species such as the dicyanamide ($[N(CN)_2]^-$) and tricyanomethanide ($[C(CN)_3]^-$) anions were added to the classification. As demonstrated by even the first pseudohalogens, not all criteria are achieved by every compound. For example, although the azide anion is stable can be protonated to form HN_3, the dimeric form (hexazene, $\{N_3\}_2$) is unknown. Likewise, many coordination complexes of the dicyanamide anion, $[N(CN)_2]^-$ are known, but the protonated form ($HC(CN)_2$) has never been isolated from solution and has been described as extremely unstable.[4,5]. Whilst many pseudohalides form salts and coordination complexes, the respective protonated or dimeric forms are often unstable (i.e., $HN(CN)_2$, HN_3, $HSCN$) or even unknown ($\{N_3\}_2$, $\{OCN\}_2$) (table 3, figure 1).

Criterion		CN^-	N_3^-	Cl^-
Formation of radicals	A	$CN^{·\,a}$	$N_3^{·\,b}$	$Cl^{·\,c}$
Existence of anions	B	CN^-	N_3^-	Cl^-
Solid precipitates with $Ag^+/Pb^{2+}/Hg^{2+}$	C	$AgCN$	AgN_3	$AgCl$
Formation of coordination complexes	D	$[Fe(CN)_6]^{3-\,d}$	$[Fe(N_3)_6]^{2-\,e}$	$FeCl_3$
Protonated form	E	HCN	HN_3	HCl
Formation of dimeric molecules	F	$(CN)_2$	$-$	Cl_2
Mixed pseudohalogen compounds	G	$CN-N_3^{\,f}$		$Cl-Br^{\,g}$

Table 2. Examples of behaviour of pseudohalides (CN^- and N_3^-) versus a halide (Cl^-). [a-g] references [6–12] ; $-$ unknown.

	A	B	C	D	E	F	G
CN^-	●	●	●	●	●	●	●
N_3^-	●	●	●	●	●		●
CNO^-	●	●	●	●	●	*	●
SCN^-	●	●	●	●	●	●	●
$[N(CN)_2]^-$	●	●	●	●	○		
$[C(CN)_3]^-$	●	●	●	●	●	●	●

Table 3. Summary of fulfilment of pseudohalogen criteria for known pseudohalogen species. * speculated ; ○ not isolated.

$(N_3)_2$
Category F
unknown

$OCN(N_3)$
Category G
unknown

$HN(CN)_2$
Category E
unstable
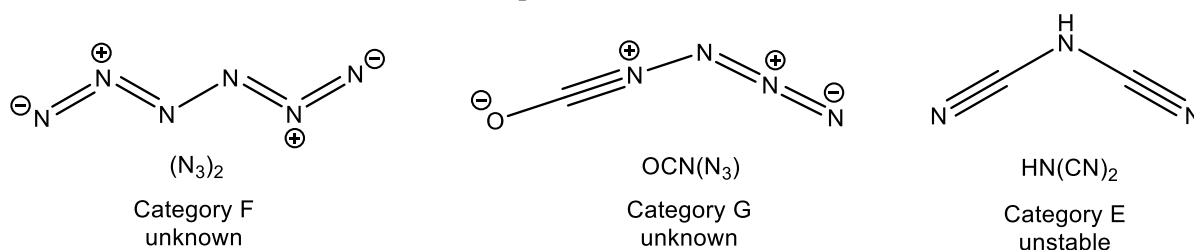
Figure 1. Examples of unknown pseudohalogen derivatives which represent the absence of particular categories of pseudohalogen behaviour.

Many small molecules have since been proposed as pseudohalogens, including selenocyanogen, $(SeCN)_2$, dithiocyanogen, $(SCN)_2$, and the tricyanomethanide ($[C(CN)_3]^-$) and azidothiocarbonate ($[CS_2N_3]^-$) anions.[13–15] Many standard pseudohalide reactivities are observed for these compounds, including the existence of neutral protonated forms, ionic salts, insoluble silver salts and complexation reactions (e.g., table 4). The formation of several isovalent or isoelectronic derivatives to known pseudohalides, such as the trinitromethanide ($[C(NO_2)_3]^-$), cyanotellurate ($[TeCN]^-$) and dicyanooxymethanide ($[OC(CN)_2]^-$) anions, is an important strategy for the preparation of novel pseudohalogen candidates.[16–22]

Criterion	$[C(CN)_3]^-$	$[C(NO_2)_3]^-$	CHN_4^-	Refs.
A	$(NC)_3C-C(CN)_3$[a]	$(NO_2)_3C-C(NO_2)_3$	$(CHN_4)_2$ [b]	23,24
B	$K[C(CN)_3]$	$K[C(NO_2)_3]$	$NaCHN_4$	16,25
C	$Ag[C(CN)_3]$	$Ag[C(NO_2)_3]$[c]	$AgCHN_4$	25,26
D	$[Cu\{C(CN)_3\}_3]^+$	$H_3B\{C(NO_2)_3\}$	$Fe(CHN_4)_2Cl_4$	27,28
E	$HC(CN)_3$	$HC(NO_2)_3$	CH_2N_4	16,25
F	$[C(CN)_3]^-$	$[C(NO_2)_3]^-$	$[CHN_4]^-$	16,25
G	$(CN)_3C-CN$	$(NO_2)_3C-CN$	CHN_4-CN	29,30

Table 4. Comparison of pseudohalide criteria of $[C(CN)_3]^-$, the isovalent derivative $[C(NO_2)_3]^-$ and $[CHN_4]^-$. [a] not prepared from $[C(CN)_3]^-$; [b] not prepared from $[CHN_4]^-$; [c] soluble in H_2O.

The identification of a set of defined characteristics for pseudohalogen character allows any chemical species to be evaluated as a pseudohalogen, provided sufficient information regarding the reactivity and chemical behaviour of the anion is known. The aromatic tetrazolate anion, CHN_4^-, is a common functional group in many new nitrogen-rich energetic materials owing to the consistently high levels of energetic performance and stability.[31,32] Tetrazole displays many of the characteristics of pseudohalogens including the formation of salts,[33] existence of a stable protonated form,[33] the formation of coordination complexes[34] and the existence of inter-pseudohalogen dimers (as cyanotetrazole, $NC-CHN_4$)[35]. Dimeric bis(tetrazole) is also known, but is not prepared by the direct oxidation of the tetrazolate anion.[36] Therefore, although the anion has never been *formally* defined as a pseudohalogen (a brief mention in literature aside)[37], the close analogy with many of the criteria met by 'conventional' pseudohalogens allows the compound to be considered as such (table 4).

The propensity to form pseudohalogenido coordination complexes allows control of the reactivity, structure and subsequent behaviour of the complexes through the tailoring of characteristics such as ligand identity, coordination number, coordination centre and counter-ions. Complexes containing pseudohalogenido ligands have been examined in many applications from molecular magnetism ($[Fe\{N(CN)_2\}_3]^{2-}$) to ionic liquids ($[^nBu(C_3N_2H)][C(CN)_3]$), supramolecular chemistry ($\{R_2CuN_3\}_2$) and dye-sensitised solar cells ($\{SeCN\}_2$).[22,38–40]

1.2 Conventional Energetic Materials and their problems

An energetic material can be defined as "a compound or mixture of substances which contains both the fuel and the oxidiser and reacts readily with the release of energy and gas".[41] Energy release occurs through the generation of heat, light and sound. Energetic materials have numerous, wide-ranging and significant applications, on multi-tonne scales in fields such as construction (demolition, mining) to defence (rocket propellants) and aesthetic displays (pyrotechnics). The role and application of an energetic material is greatly influenced by its sensitivity, performance and initiation properties. For example, primary explosives initiate decomposition upon the application of relatively mild stimuli (i.e., impact, friction and electrostatic discharge) and detonate rapidly, whilst those which require the decomposition of an additional energetic material for initiation are classified as secondary explosives.[42] Energetic character can be afforded by several strategies, including the presence of ring or cage strain and substituents which readily decompose to form stable products.[43]

High Energy Density Materials (HEDM's) are energetic materials that have a large amount of energy released per unit volume. The density of an energetic material is correlated with the detonation performance, which is usually evaluated by examination of the detonation velocity (D). An increased density is usually accompanied by a higher detonation velocity and (usually) a greater performance.[44,45] The precise boundary conditions for a HEDM are difficult to define, but conventional HEDM's often possess high detonation velocities. Not all energetic materials are used as explosives and detonation is not required for propellants. Likewise, the desired values for detonation velocity of explosives vary between primary (where D must only be sufficient to initiate a secondary explosive) and secondary classifications (where the desired value of D is limitless).[45] Despite these variations, the calculation of detonation velocities can be considered as a useful indicator of explosive power and performance.[46]

Many energetic materials currently in use (herein referred to as 'conventional') are predominantly carbon-based and form CO_2 as the primary decomposition product, provided there is sufficient oxygen available. However, often the rate of decomposition is too fast to facilitate complete combustion and additional products of incomplete combustion such as CO or solid carbon ('soot') are formed. This is demonstrated in the decomposition of trinitrotoluene, TNT (scheme 1). The formation of solid carbon presents both aesthetic and health issues, through the reduction of visibility in pyrotechnic formulations to breathing difficulties through inhalation by nearby individuals.[47]

$$CO_2 + 3CO + 3C_{(s)} + 1.5H_2 + H_2O$$
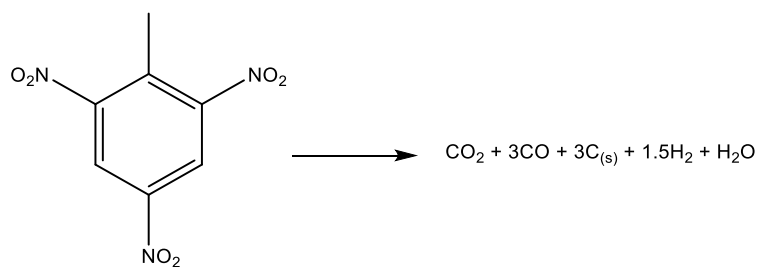
Scheme 1. Incomplete combustion of TNT into CO_2, CO and soot (C).

Not all visible residue from the decomposition of an energetic material is solid carbon. In pyrotechnics, the formation of solid metal oxides from colourant additives can significantly increase the amount of particulate matter released into the environment.[47] Although the reduction of visibility is an aesthetically undesirable consequence (figure 2), the effects of solid particulates on humans are more adverse. Studies have shown that increased concentrations of fine particulate matter (i.e., ≤ 10 μm) are associated with lower life expectancy, including an increased number of deaths from respiratory or cardiovascular issues.[48,49] The increase of particulate matter can be significant following a pyrotechnic release. In one instance, the concentration of sub-particulates (<2.5 μm) at one location adjacent to a firework display site were observed to increase by 370% across the 24 hours following the display.[50]

In pyrotechnical applications, reduced visibility can be negated by the addition of more colourants to shine through the smoke and solid matter. However, these colourants are often heavy metal salts, e.g. barium or strontium nitrates, and are highly toxic to both wildlife and humans.[47] Where pyrotechnics are released during snowfall, barium is a particularly prevalent contaminant, with levels increasing by up to 500 times those prior to release. The same study showed that snow contaminated by *solid* pyrotechnic residue was, alarmingly, observed to contain barium levels some 50,000 times greater than before the display occurred.[51] Another alternative to increasing the amount of colourant additives is the provision of an external source of oxygen, increasing the chance of complete combustion into CO_2 and minimising soot formation. This is achieved by the addition of external oxidisers such as perchlorate salts. However, the adverse effects of perchlorate compounds on kidney and thyroid function are well-documented in both humans and other animals, and the high water solubility of perchlorate anions leads to rapid contamination of groundwater and the surrounding environment.[52,53] In one study, the concentration of perchlorate anions in a lake situated next to a firework display increased by up to 1028 times in the period after the conclusion of the display.[54] The presence of a dipole moment in CO_2 and H_2O results in the absorption of infra-

red radiation (the 'greenhouse gas' effect) and introduces environmental issues even when combustion is complete. These environmental and health impacts result in a trade-off between the adverse effects of the additives and products of varying extents of combustion. The widespread and regular use of fireworks adds an additional pressure to reduce the amount and environmental toxicity of products released upon their use; for example, in 1999, over 30,000 tons of fireworks were released in Germany alone.[55] Therefore, the excess usage of toxic colourant or oxidiser components in formulations is undesirable.
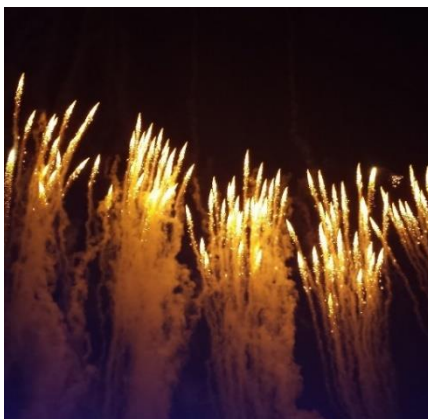
Figure 2. Photograph showing solid residue observed during a pyrotechnic display. The solid residue is hypothesised to contain a mixture of solid metal oxides and soot. *Photo credit: own photograph.*

Significant research efforts have targeted the reduction of both the amount and toxicity of additive components in energetic materials.[56] Evaluation of both current and novel energetic compounds allows the formulation of a list of targets and qualities for an optimum energetic material:

i. Decompose solely into either CO_2, H_2O or N_2, or a combination thereof, without the need for external oxidisers;

ii. Contain minimal or no toxic additives, such as heavy metal colourants or perchlorates,

iii. Demonstrate low sensitivity towards energetic stimuli, allowing safe handling, transport and manufacture;

iv. Possess long-term stability in ambient conditions with no change in performance, properties or sensitivity;

v. Can be prepared by facile, accessible procedures involving minimally-hazardous precursors and processes;

vi. Possess performance, reliability, stability and cost-effectiveness that is comparable or better than the materials used currently.
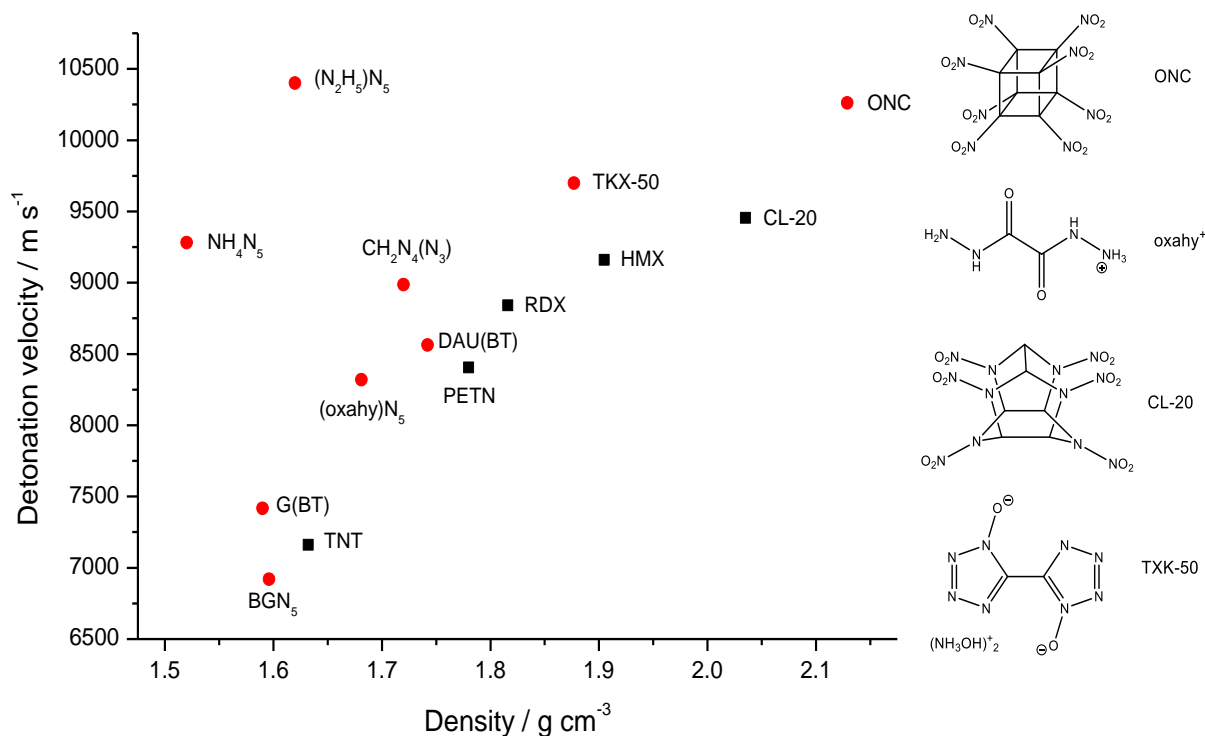
1.3 Nitrogen-rich energetic materials

Over the past two decades, research has focused on the use of nitrogen-rich compounds (i.e., those which contain $\geq$60% nitrogen by weight) in energetic materials. The key advantage of nitrogen-rich energetic materials versus the conventional carbon-based counterparts such as TNT or RDX is the relative strength of the N$\equiv$N triple bond ($\Delta H_f = 946\,kJ\,mol^{-1}$) and weakness of the N=N and N$-$N bonds versus those of the carbon-carbon bonds of the same order (table 5). Repulsion of lone pairs of electrons from both nitrogen atoms weakens the N$-$N single bond.[57] These two factors mean that decomposition of a compound through N$-$N bond cleavage to form N_2 (i.e., N$\equiv$N) is highly enthalpically favourable in comparison to the formation of CO_2 or H_2O.[58] The formation of gaseous N_2 provides an additional entropic driving force. The strong enthalpic and entropic driving force of N_2 formation results in an improved energetic performance through an increased detonation velocity, energy density or detonation pressure. Consequently, many nitrogen-rich energetic materials possess greater detonation velocities per density unit than conventional carbon-based examples such as TNT or RDX (figure 3).

	E$-$E	E=E	E$\equiv$E
N	160	418	946
C	346	598	813

Table 5. Bond dissociation enthalpies ($kJ\,mol^{-1}$) of E_2 bonds (E = C, N).[44,57,58]

The formation of N_2 confers further advantages beyond energetic performance. Nitrogen gas is colourless, odourless and non-toxic, allowing its safe release without any adverse environmental, health or aesthetic effects. The absence of a dipole moment means N_2 is IR inactive and cannot absorb infra-red radiation in the same manner as H_2O and CO_2. An increased nitrogen content (and the formation of N_2) reduces the amount of carbon in the compound, increasing the chance of complete combustion and concurrently reducing both the amount of smoke produced and the amount of external oxidiser required in the formulation. The improved visibility afforded by less smoke allows the reduction of the amount of colourant additives required to create the desired effect, in turn decreasing the amount of harmful particulate matter and toxic heavy metal salts released into the environment. The combination of high performance and low environmental impact has led to the investigation of many nitrogen-rich compounds as 'green' energetic materials, in applications from primary and secondary explosives to colourants in pyrotechnic formulations.[44,47,59–61] These benefits are summarised in table 6.

Figure 3. Relationship between density and calculated detonation velocity of some conventional (■) and nitrogen-rich (●) energetic materials. PETN = $C(CONO_2)_4$; G = guanidinium; BG = bisguanidinium; BT = bis(tetrazolate); RDX = $\{NC(NO_2)\}_3$; HMX = $\{NC(NO_2)\}_4$. Data taken from references [46,62–68].

Feature	Benefits
Decreased heavy metal content	Less harmful to environment and humans Less particulate matter released
Lower carbon content	Less smoke/soot and particulate matter released Less CO_2 and CO released Improved visibility of effects Less additives required for visible effects
High enthalpy of formation of N_2	Improved energetic performance Increased efficiency
Greater oxygen balance	Less smoke/soot and CO released Increased combustion efficiency Less external oxidiser required
Decreased oxidiser content	Less harmful to environment and humans
N_2 primary decomposition product	Colourless, odourless, non-toxic No dipole moment Release of less greenhouse gases (CO_2, H_2O)

Table 6. Summary of key benefits of nitrogen-rich energetic materials.

1.4 Polynitrogen species

Although nitrogen-rich compounds are common, polynitrogen species (those comprised of entirely nitrogen) increase in rarity as the number of nitrogen atoms increases and very few are isolable at ambient conditions. The absence of N_4 as an isolable compound is presumed to be due to the aforementioned $N\equiv N$ bond dissociation enthalpy favouring the dissociation of N_4 to two moles of gaseous N_2. Polynitrogen, N_∞, would be the ideal candidate for a nitrogen-rich energetic material but is observed only at extremely high pressures and temperatures (110 GPa and >2000 K) or under ambient conditions using highly specialised plasma-assisted syntheses. These extreme synthetic conditions render N_∞ unsuitable for applications of any type.[69,70] Despite calculations predicting its stability, octomeric nitrogen (N_8) remains unknown.[71] Although N_2 is stable and extremely abundant, the extremely high bond dissociation enthalpy of the $N\equiv N$ triple bond renders dinitrogen too stable for any energetic materials applications.

Owing to the rarity of isolable, suitable polynitrogen compounds, nitrogen-*rich* compounds which are accessible and isolable at ambient conditions are extremely desirable for the preparation of new nitrogen-rich energetic materials. The azide anion, N_3^-, has been known for over 100 years and is isolable in the form of inorganic salts, such as NaN_3, and the less-stable protonated form hydrazoic acid, HN_3. The latter species possesses one of the highest nitrogen contents of any isolable nitrogen-rich compound to date.[72] More recently, Christe and co-workers succeeded in preparing N_5^+ from diazofluoride cations and HN_3.[73] The N_5^+ cation possesses a bent, linear structure with almost equal $N-N$ bond lengths throughout and has been isolated in salts containing bulky, phlegmatising anions such as $[AsF_6]^-$.[73,74] Anion exchange with nitrogen-rich anions resulted in energetic salts; the nitrogen content of pentazenium tetra(azido)borate, $N_5[B(N_3)_4]$ (figure 3), ranks slightly below N_∞ and is one of the highest of a compound which is isolable at ambient conditions to date (table 7). The nitrogen-rich pentazenium salts are characterised by extremely high energetic character and sensitivities, with even single millimolar amounts exploding with sufficient force to damage apparatus.[74] The more stable pentazenium salts that do not contain nitrogen-rich anions are extremely powerful oxidisers and must be synthesised and handled under specialist conditions (i.e., HF solvent, inert conditions, low temperatures). Despite their extremely high nitrogen content and predicted energetic performance, the extreme sensitivity to energetic stimuli and moisture means that the use of N_5^+ salts in energetic materials applications is currently unfeasible.
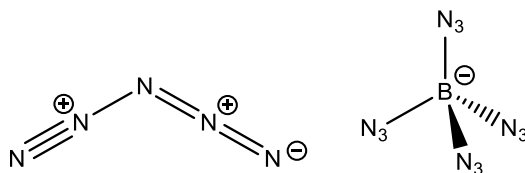
Figure 3. Structure of pentazenium tetra(azido)borate, $N_5[B(N_3)_4]$ (97% N).[74]

The pentazolate anion, N_5^-, was first detected experimentally in the mass spectrum of an arylpentazole ($R\text{-}C_6H_5\text{-}N_5$) compound in solution. Several years later, the first bulk synthesis of the pentazolate anion was reported, including studies demonstrating its remarkably high thermal stability.[75,76] The presence of hydrogen bonding and aromaticity of the N_5^- anion results in stabilities which far outrank those of the pentazenium salts of comparable nitrogen content, including towards energetic stimuli. For example, ammonium pentazolate, NH_4N_5, has a comparable nitrogen content to $N_5[B(N_3)_4]$ but has a thermal stability that is several orders of magnitude higher than the latter (table 7). Although the isolation of N_5^- occurred relatively recently, investigations into energetic pentazolate salts show promising detonation performances that suggest pentazolate salts may be suitable compounds in new energetic materials. For example, the detonation velocity of NH_4N_5 is calculated to be almost identical to RDX (hexogen, $\{NC(NO_2)\}_4$) with significantly improved friction and thermal sensitivities versus the latter, whilst bis(guanidinium)pentazolate, $GU(N_5)$, possess lower energetic sensitivities towards friction and impact than RDX, but alongside a reduced detonation velocity and thermal stability.[66] Although energetic pentazolate salts as promising candidates for the preparation of high-performing, insensitive secondary explosives, more research is required in order to optimise the stability, performance and synthetic cost (in both monetary and difficulty) of such compounds. The latter is a critical factor in the accessibility of such compounds owing to the current generation of the N_5^- anion from a single precursor using specialised, low-temperature synthetic methods.[66] The preparation of powerful, highly sensitive near total-nitrogen compounds demonstrate that a balance is required for nitrogen-rich energetic materials between performance, ease of synthesis and sensitivity to both environmental conditions and energetic stimuli.
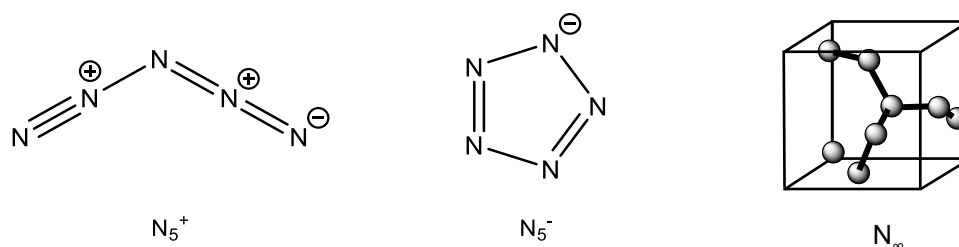
Figure 4. Novel polynitrogen compounds of N_5^+ (left), N_5^- (centre) and N_∞ (right). Structure of N_∞ based on that reported in reference [69].[69,73,76]

Compound	Nitrogen content by weight (%)	Refs.
z	65	[72]
CH_2N_4	80	[33]
$CHN_4(N_3)$	88	[77]
$N_5[P(N_3)_6]$	91	[74]
$C(N_3)_4$	93	[78]
NH_4N_5	95	[66]
$N_5[B(N_3)_4]$	97	[74]
HN_3	98	[79]
$N_5^+N_5^-$	100	— [a]
N_∞	100 [b]	[69]

Table 7. Summary of some polynitrogen compounds with the highest nitrogen contents by weight (to date) versus NaN_3. [a] currently unknown; [b] stable only at 110 GPa and >2000 K.

1.5 Nitrogen-rich pseudohalides

Several nitrogen-rich compounds that possess an optimal compromise between energetic sensitivity, nitrogen content and energetic performance are based upon pseudohalogens (figure 5). Owing to their decreased toxicity and increased performance versus conventional energetic materials, nitrogen-rich tetrazolato compounds have produced some of the most promising energetic candidates. The dihydroxylammonium salt of 5,5'-bistetrazole-1,1'oxide, TKX-50, has an energetic performance and stability which equals or outperforms many commercial and industrial secondary explosives with a significantly decreased synthetic cost.[65] Tri(1-ethyl-5-aminotetrazolyl)borate (abbreviated here as TEATB) has been investigated as a replacement for green barium colourants in pyrotechnical applications, whilst formulations containing alkali metal bistetrazolate salts have been identified as colourant formulations which produce less smoke than the corresponding alkali metal nitrates.[31,80,81] Potassium dinitraminobistetrazole, K_2DNABT, is a primary explosive which has been proposed as a potential lead-free, less toxic and higher-performing replacement for $Pb(N_3)_2$ with no increase in sensitivity to energetic

13

stimuli.[82] Hydrazinium nitroformate, $H_5N_2[C(NO_2)_3]$ has been investigated as a perchlorate-free oxidising agent.[83]
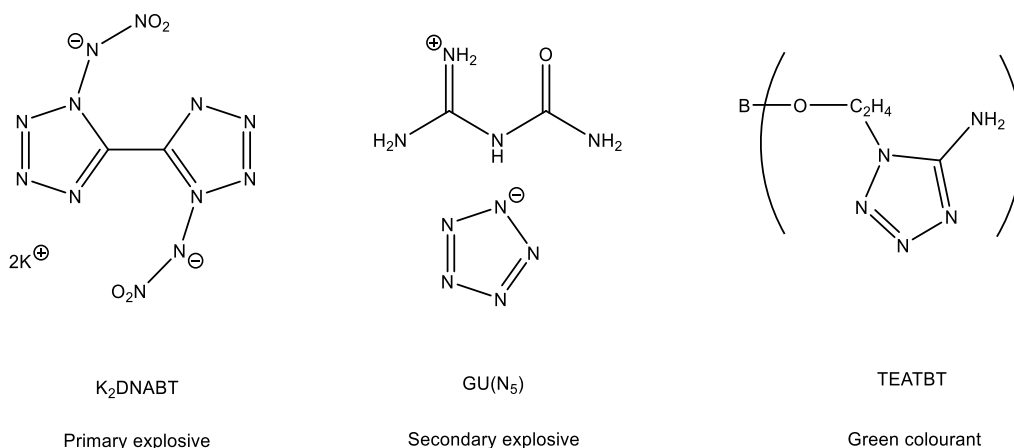
Figure 5. Structure and proposed application of some novel nitrogen-rich compounds.

1.6 Hypervalent and Hypercoordinate Coordination Centres

From an energetic materials perspective, an increased number of nitrogen-rich ligands in a complex will result in a higher nitrogen content, energy density and, ultimately, energetic performance. The presence of a hypercoordinate coordination centre can increase the coordination number and many coordination complexes containing *p*-block centres can be described as hypervalent or hypercoordinate. A coordination centre can be defined as hypervalent if the number of Lewis electron pairs involved in coordination exceeds the number of valence electrons on the central element, i.e., the Octet rule appears broken by the presence of more than four electron pairs on the central atom.[84,85] 'Hypervalent' complexes of *p*-block elements include SF_6 and PCl_5.[86,87] Although the concept was originally defined for elements in groups 15−18, hypervalent complexes containing centres of group 14 elements have since been reported.[84,88–90] The propensity of hypervalency increases with element mass and size.[91,92] Significant differences in the electronegativity between the ligands and coordination centres increases the chances of a complex being hypervalent and an increase in the ligand-centre bond lengths of the analogous neutral complex is also attributed as an indicator of hypervalency.[93] The origin of hypervalency has been the subject of considerable debate and it was not until recently that theoretical calculations eliminated mixing of *d-* and *p-* orbitals in hypercoordinate centres as a cause.[87,94] Instead, the partial ionisation of coordinative interactions of ligands or the formation of multiple-centre, multiple-electron bonds are hypothesised to occur, preserving the octet with a valency that merely *appears* exceeded (figure 6).[91]
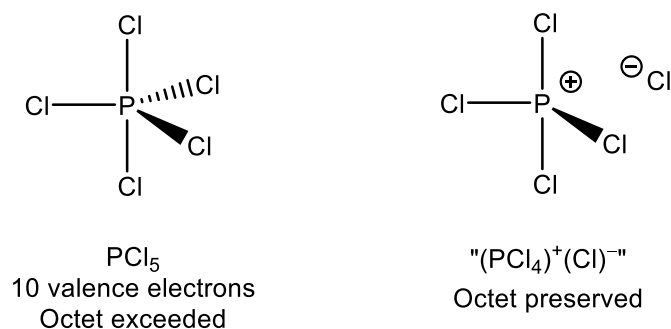
Figure 6. Bonding structure of hypervalent PCl_5.

An alternative concept to hypervalency is hypercoordination. If the coordination number of a main-group element exceeds four (i.e., the number afforded by adherence to the Octet rule), the element is defined as hypercoordinate. Hypercoordination can involve lone pair donation from coordinating ligands and therefore a hypercoordinate complex is not necessarily hypervalent.[93] The wider definition of hypercoordination means many 'non-hypervalent' complexes can be included in the classification, such as anionic complexes of group 13. The coordination chemistry of hypercoordinate complexes of group 14 has been reviewed extensively.[93] The effect of hypercoordination on the nitrogen content of a complex is demonstrated by the formation of poly(azido) complexes of group 14 elements as $[E(N_3)_n]^{4-n}$. An increase in the greatest value of the coordination number (n) down the group from carbon ($n = 4$) to silicon, germanium, tin and lead ($n = 6$) offsets the decreased nitrogen content afforded by heavier coordination centres in the charge-neutral tetraazides of the same elements (table 8).[78,95–97]

	Nitrogen Content (wt%)				
Complex	**C**	**Si**	**Ge**	**Sn**	**Pb**
$E(N_3)_4$	93	86	70	59	(45)
$[E(N_3)_6]^{2-}$	(95)	90	78	68	55

Table 8. Nitrogen contents of regular- ($E(N_3)_4$) and hyper- ($[E(N_3)_6]^{2-}$) coordinate homoleptic azido complexes of group 14 centres. Values listed in brackets denote an unknown compound.

1.7. Nitrogen-rich coordination compounds

Coordination compounds containing nitrogen-rich pseudohalogenido ligands are an alternative to polynitrogen salts. The varying energetic sensitivities of coordination complexes facilitates applications in different fields to that of secondary explosives occupied by other energetic salts. However, to date the number of energetic nitrogen-rich coordination complexes is comparatively lower than nitrogen-rich energetic salts, possibly due to the presence of toxic

15

metal centres in the former, e.g. Pb(N$_3$)$_2$, or a decreased performance of energetic coordination complexes versus salts.

The most notable example of nitrogen-rich pseudohalide ligands is the azido ligand. The azide anion has already been demonstrated as an ideal candidate for the synthesis of numerous nitrogen-rich coordination complexes, as complexes of both *d-* and *p*-block elements with varying coordination numbers and oxidation states.[97–99] The most widespread example is lead diazide, Pb(N$_3$)$_2$, a primary explosive which is used on industrial scales as an initiator for other energetic materials, including secondary explosives in detonator devices (figure 7).[59] However, lead exposure has significant impacts on the environment and human health, including long-term contamination of groundwater and significant health issues such as neurological effects, and therefore the development of lead-free replacements is a significant area of research in the field of energetic materials.[59,100,101] Unusually, a number of lighter *p*-block poly(azido) complexes are known in addition to Pb(N$_3$)$_2$, such as the hexa(azido) complexes of silicon, germanium and tin as [E(N$_3$)$_6$]$^{2-}$ or neutral base-stabilised tetra(azido) complexes of the same elements.[95,96,102] Poly(azido) complexes have been prepared with both phlegmatising (e.g. [PPN]$^+$) or, less-commonly, nitrogen-rich or energetic (e.g., G$^+$, N$_5^+$) counter-ions.[74,95]

Owing to the high nitrogen content (up to 81% by weight) and, until recently, its status as the most nitrogen-rich and isolable aromatic ring system, tetrazole rings offer an alternative nitrogen-rich ligand. Unlike the azido ligand, the presence of a CH unit allows easy derivatisation of tetrazoles to afford additional nitrogen or oxygen content such as nitro-, oxido- or azido-tetrazolate anions.[59,68] Substituent modification can serve a number of purposes, from increasing or decreasing the nitrogen content or energetic behaviour to facilitating the formation of extended nitrogen-rich frameworks or increasing the ligating ability of the coordinating atom. The ammonium salt of the tetrakis(nitrotetrazolato)cuprate(I) anion, (NH$_4$)[Cu{CH$_2$N$_4$(NO$_2$)}$_4$(H$_2$O)$_2$], is a rare example of a nitrogen-rich coordination complex with an energetic performance that exceeds known primary explosives such as lead azide and lead styphnate, with the additional advantage of a lead-free composition (figure 7).[59] This reactivity has already been investigated in the numerous examples of bistetrazolates and other derivatives, but investigations into *p*-block coordination complexes containing tetrazolato ligands are more recent. Anionic hexakis(tetrazolato) complexes of the same elements have also been prepared and represent only the second known nitrogen-rich complexes of group 14.[103,104]

Although research into pentazolato complexes is still in its infancy, a number of monomeric transition metal salts, three-dimensional structures (described as 'metal-inorganic frameworks') and coordination polymers have already been prepared.[75,105–108] Numerous examples of energetic metal-organic frameworks exist which contain energetic linker ligands such as functionalised furazans, triazoles and tetrazoles.[109–112] The formation of three-dimensional structures from pentazolato coordination complexes opens the possibility of inclusion of N_5^- to form nitrogen-rich energetic metal-organic frameworks, such as in $Cd_3(NH_4CHN_4)_4(N_3)_2$.[113] In contrast to the nitrogen-rich azido and tetrazolato ligands, homoleptic poly(pentazolato) complexes are unknown, as are heteroleptic pentazolato complexes containing any *p*-block centre. The many examples of energetic pseudohalogenido complexes suggest that the combination of hypercoordinate coordination complexes containing nitrogen-rich pseudohalide ligands is a promising strategy for the development and investigation of new nitrogen-rich energetic materials.
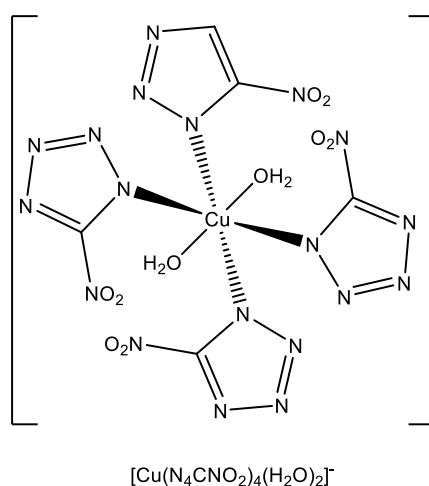
Figure 7. Structure of the tetrakis(nitrotetrazolato)cuprate(I) anion in $NH_4[Cu(N_4CNO_2)_4(H_2O)_2]$.

Chapter 2. Research Questions

This research aimed to investigate and evaluate the inclusion of several pseudohalogenido ligands in novel nitrogen-rich coordination compounds of group 14, either through direct coordination of a nitrogen-rich ligand or by indirect formation of novel tetrazolato- ligands *in situ*. A range of pseudohalide ligands, coordination centres and oxidation states were investigated in order to quantify the reactivity and stability of both known and novel group 14 pseudohalogenido complexes and to facilitate comparisons to analogous *d-* or *p*-block complexes already investigated. The following research questions are proposed:

1. Can novel pseudohalogen coordination complexes of group 14 ($Y = CN$, N_3, $N(CN)_2$) be prepared?
    i. How does the reactivity of these complexes differ with respect to the analogous *d*- and *p*-block complexes already known?
    ii. Can these pseudohalogenido ligands undergo further reactions to facilitate the *in situ* preparation of novel nitrogen-rich ligands?

2. Can nitrogen-rich complexes containing group 14 elements in their less-abundant oxidation states be prepared?
    i. Are charge-neutral Ge(II) and Pb(IV) polyazides, e.g. $Ge(N_3)_2(L)_2$ or $Pb(N_3)_4(L)$, isolable?
    ii. How does the reactivity, decomposition and chemical behaviour of these species compare to the analogous complexes in the more common oxidation states?
    iii. Are such complexes comparable in stability and energetic sensitivities to other *p*-block nitrogen-rich complexes and conventional energetic materials?

3. Can a reliable method for the electrochemically induced formation of N_5^- from arylpentazoles (ArN_5) be developed?
    i. How does this method compare with the preparative method already known?
    ii. Can N_5^- be formed using any alternative chemical methodologies or precursors?

4. Can the N_5^- anion be considered a pseudohalide?
    i. Can the N_5^- anion act as a ligand towards *p*-block coordination centres?
    ii. How does the ligating ability of N_5^- compare to the azide anion (N_3^-)?
    iii. Can novel salts containing N_5^- be prepared?

Chapter 3. Homoleptic cyanido complexes of group 14 elements

3.1 Introduction

The cyanide anion (CN^-) was one of the first pseudohalogens described by Birckenbach.[1,2] Since the discovery of "Prussian Blue", $K_3[Fe(CN)_6]$, over 150 years ago, homoleptic poly(cyanido) complexes containing d-block coordination centres have been studied extensively and are known for almost every transition metal coordination centre.[6,114,115] The ability of the cyanido ligand to bridge between two adjacent d-block centres also facilitates the formation of many dimeric poly(cyanido) complexes, which display behaviours including switchable magnetism, luminescence and hydrogen storage capability.[116–118] Transition metal complexes involving monomeric (i.e., M−CN) and bridging (i.e., M−CN−M) cyanido ligands have been reviewed in great detail and will not be discussed further here. In contrast to, and despite, the extensive knowledge of the reactivity of the cyanido ligand towards d-block coordination centres, investigations towards coordination centres of p-block elements (groups 13−15) are rarer and have only recently been investigated in detail.

3.1.1 p-block poly(cyanido) complexes of groups 13−15

The trend in reactivity for the formation of both charge-neutral and anionic tricyanides of group 13 (E = B−Tl) and 15 (E = P−Bi) decreases down each group, with the formation and reactivity of anionic poly(cyanido) complexes containing lighter coordination centres varying largely to the heavier congeners. Charge-neutral homoleptic poly(cyanido) complexes are known for both group 13 and 15 centres but the number and stability of anionic complexes is far greater for complexes containing group 13 elements than for those of group 15.

Boron tricyanide is prepared by the reaction of BCl_3 with AgCN. The complex has been investigated as a precursor to the formation of boron-carbon-nitride-type ceramics.[119,120] Tetra(cyanido)borate salts, $(cat)[B(CN)_4]^-$ (cat^+ = e.g. K, Bu_4N), are prepared from the reaction of BX_3 (X = Cl, Br, I), (cat)BX and KCN and have been investigated for use in ionic liquids.[121] Reduction by an alkali metal in liquid ammonia or ^nBuLi forms $[B(CN)_3]^{2-}$, which can be subsequently oxidised to form $[B_2(CN)_6]^{2-}$.[122–125] Aluminium tricyanide and lithium tetra(cyanido)aluminates are prepared by the reaction of HCN with AlH_3 or $Li[AlH_4]$, respectively.[126] A single report details the preparation of $[Al(CN)_6]^{3-}$ from $Al(OH)_2$ and HCN, but is not characterised and remains unknown, despite the prediction of its stability in a later

theoretical study.[127,128] $Ga(CN)_3$ is prepared by the reaction of $GaCl_3$ with the covalent cyanide transfer reagent TMS−CN. Inclusion of a cyanide salt in the reaction mixture, or treatment of $Ga(CN)_3$ and LiCN, forms $[Ga(CN)_4]^-$.[129] However, attempts to prepare aluminium and indium tricyanides through reaction of the corresponding trifluorides with TMS−CN were unsuccessful and necessitated the use of much harsher synthetic conditions, such as the reaction of gaseous HCN on AlH_3, cyanogen $\{CN)_2\}$ with InOI, or indium metal with $Hg(CN)_2$.[126,130,131] Thallium tricyanide, $Tl(CN)_3$, exists only with HCN in equilibrium with $[Tl(CN)_4]^-$ and neither complex has been isolated.[132,133] In contrast to the formation of the tetra(cyanido)borate and gallate anion, the reaction between TMS−CN, a cyanide salt and EF_3 affords the *penta*(cyanido) anions as $[E(CN)_5]^{2-}$ (E = In, Tl).[130] The monoanionic tetracyanido complexes, $[E(CN)_4]^-$ (E = In, Tl) are unknown (E = In) or exist only in equilibrium with the neutral tricyanide (E = Tl).[130,132,133] In(II) dicyanide, $In(CN)_2$, can be prepared from the reaction of HCN and indium metal. $In(CN)_2$ and $[B(CN)_3]^{2-}$ are the only examples of the rare class of low-valent homoleptic cyanido complexes of group 13.[134]

The charge-neutral tricyanides of group 15, $E(CN)_3$ (E = P−Bi) are prepared from the reaction of ECl_3 with either ionic (AgCN) or covalent (trimethylisocyanosilane, Me_3SiNC) cyanido transfer reagents.[135,136] It is unclear if the use of an *iso*cyanosilane instead forms the coordinatively isomeric tri(isocyanido) complexes, i.e., $E(NC)_3$. The anionic di(cyano) complex of nitrogen (dicyanamide, $[N(CN)_2]^-$) is itself defined as a pseudohalogen and can coordinate to both *d*- and *p*-block centres, although no homoleptic poly(dicyanamido) complexes of group 13 or 15 are known.[137,138] The reactivity of the dicyanamide ligand is discussed in chapter 7. Tricyanamide, $N(CN)_3$, remains unknown. The reaction of $P(CN)_3$ with NaCN does not form $[P(CN)_4]^-$ but instead undergoes disproportionation to form $[P(CN)_2]^-$ and a dimeric phosphorus cyanide.[139,140] The $[E(CN)_5]^{2-}$ anions (E = Sb, As) can be prepared from EF_3, Me_3SiCN and an ionic cyanide transfer reagent in a similar strategy to the syntheses of the $[E(CN)_4]^-$ anions of group 13 (E = B, Ga). The formation of $E(CN)_3$ as a reaction byproduct is unobserved for the group 13 complexes and demonstrates an alternative method for the preparation of the neutral group 15 tricyanides. With the exception of bismuth, hexa(cyanido)complexes of group 15 as $[E(CN)_6]^{3-}$ are unknown (E = P, As) or debated (E = Sb).[122,141,142] All attempts to form $[P(CN)_6]^{2-}$ from the reaction between $[PF_6]^{2-}$ and Me_3SiCN resulted in incomplete ligand exchange.[142]

3.1.2 Poly(cyanido) complexes containing group 14 centres (E = Ge−Sn)

The tricyanomethanide cation, $[C(CN)_3]^+$, is also a pseudohalide and is the only known cationic homoleptic group 14 complex to date. Tricyanomethanide salts are prepared from the reaction of a cyanide salt with dibromomalononitrile, $C(CN)_2Br_2$. Subsequent reaction of $Ag[C(CN)_3]$ and XCN (X = Cl, Br) affords $C(CN)_4$.[29] The protonated form, tricyanomethane ($HC(CN)_3$), is prepared from acidification of tricyanomethanide salts at low temperatures. Although initially reported to be stable only at low (−40 °C) temperatures, tricyanomethane was later isolated at ambient temperatures.[25,143,144] The chemistry and coordination behaviour of the tricyanomethanide group has been studied extensively elsewhere and will not be discussed further here.[40]

Reports of other charge-neutral group 14 tetracyanides are scarce. Despite several preparation attempts by the reaction of silicon tetrahalides with both ionic (AgCN) and covalent (HCN) cyanide transfer reagents, $Si(CN)_4$ is unknown.[145,146] The preparation of the $[Si(CN)_6]^{2-}$ anion as $(cat)_2[Si(CN)_6]$ (cat = e.g. $[PPN]^+$, Et_3NH^+, Li^+) represent the only isolation of anionic hexa(cyanido) complexes of group 14, one salt of which (1-butyl,3-methylimidazolium hexa(cyanido)silicate, $BMIm[Si(CN)_6]$) has been investigated as a candidate for ionic liquids.[147,148] $Ge(CN)_4$ is prepared from ligand exchange between $GeCl_4$ and AgCN.[135,149] As discussed for the group 15 tetracyanides, it is unclear if coordination isomerism is present in $Ge(CN)_4$ formed by the reaction of $GeCl_4$ and TMSNC.[135] $Sn(CN)_4$ is briefly reported without characterisation data and $Pb(CN)_4$ is unknown.[150,151] Both $[Ge(CN)_6]^{2-}$ and $[Pb(CN)_6]^{2-}$ are unknown; $[Sn(CN)_6]^{2-}$ is described as unisolable and has only been previously characterised by *in situ* ^{119}Sn NMR spectroscopy.[152]

E = Ge, Sn R = Ag$^+$
E = Ge, R = Me$_3$Si

E = Si, cat$^+$ = e.g. PPN$^+$, Et$_3$N$^+$, BMIm$^+$
E = Sn, cat$^+$ = ^{n}Bu$_4$N$^+$
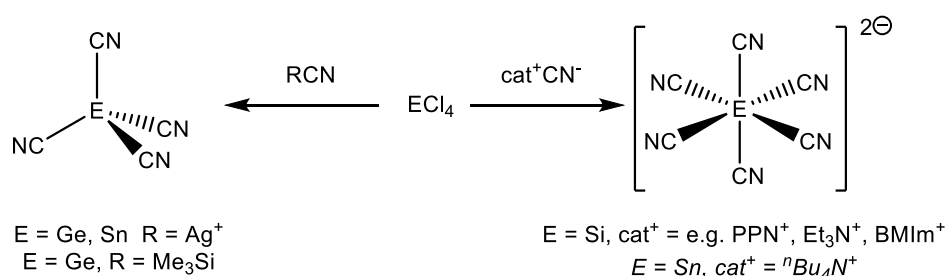
Scheme 2. Syntheses of known poly(cyanido) complexes of group 14. Annotations in i*talics* denote a complex that was not isolated.

A small number of sparsely-characterised, charge-neutral and homoleptic poly(cyanido) complexes are reported for low-valent group 14 elements. Whilst $Ge(CN)_2$ is prepared from the reaction of GeX_2 with an ionic (X = Cl) or covalent (X = F) cyanide transfer reagent as an extremely air sensitive oil, the heavier congeners are prepared by decomposition of high-valent precursors. $Sn(CN)_2$ is formed by the protonolytic reduction of bis(cyclopentadienyl)tin(IV) by HCN, whilst a single report details the preparation of $Pb(CN)_2$ from thermal decomposition of $R_2Pb(CN)_2$ (R = alkyl).[153–155] These complexes represent the only homoleptic poly(cyanido) complexes of group 14 which are not prepared by ligand exchange. No further studies of either compound are reported and consequently it is unclear if the preparation of $Sn(CN)_2$ from SnX_2 and a cyanide transfer reagent, in analogy to the formation of $Ge(CN)_2$, is feasible.
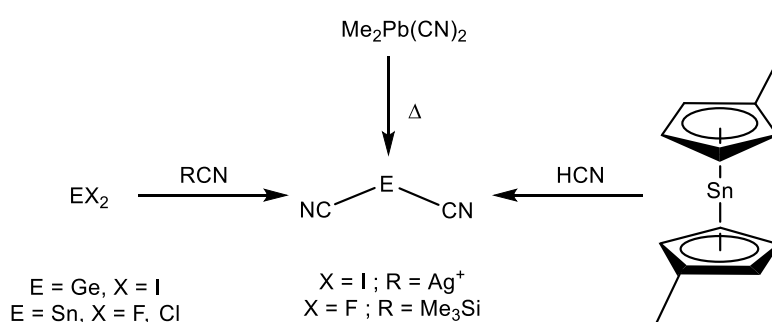
Scheme 3. Syntheses of known poly(cyanido) complexes of E(II) (E = Ge−Pb).

Homoleptic complexes of group 14 in either oxidation state are significantly fewer and less characterised compared to those of groups 13 and 15. Many reports are restricted to brief descriptions with sparse or even absent characterisation data. The recent investigations into poly(cyanido) complexes of groups 13 and 15 demonstrate varying trends in reactivity, stability and bonding. By comparison, the relatively few examples of the analogous group 14 complexes precludes the examination of similar trends in reactivity and behaviour for this group. The comparative infrequency of poly(cyanido) versus poly(azido) complexes of group 14 is in stark contrast to the large number of extensively-characterised examples of the latter. As such, few comparisons can be drawn regarding the reactivity of CN^- and N_3^- towards the same group 14 elements. The preparation of poly(cyanido) complexes of group 14 would allow the investigation of structure, behaviour and reactivities of these elements towards the cyanido ligand and facilitate comparisons with both other psuedohalogenido complexes and poly(cyanido) complexes of neighbouring groups. Although not nitrogen-rich, the preparation of these complexes could facilitate the *in-situ* formation of novel nitrogen-rich tetrazolato ligands through cycloaddition reactions.

Period	13	14	15
1	B(CN)$_3$ [B(CN)$_4$]$^-$ [B(CN)$_3$]$^{2-}$ [B$_2$(CN)$_6$]$^-$	[C(CN)$_3$]$^+$ C(CN)$_4$	[N(CN)$_2$]$^-$
2	Al(CN)$_3$ [Al(CN)$_4$]$^-$ [Al(CN)$_6$]$^{3-}$	[Si(CN)$_6$]$^{2-}$	P(CN)$_3$ [P(CN)$_2$]$^-$
3	Ga(CN)$_3$ [Ga(CN)$_4$]	Ge(CN)$_2$ Ge(CN)$_4$	Bi(CN)$_3$ [Bi(CN)$_5$]$^{2-}$ [Bi(CN)$_6$]$^{3-}$ [Bi$_2$(CN)$_{11}$]$^{5-}$
4	In(CN)$_3$ [In(CN)$_5$]$^{2-}$ In(CN)$_2$	Sn(CN)$_4$ [Sn(CN)$_6$]$^{2-}$ [b] Sn(CN)$_2$	As(CN)$_3$ [As(CN)$_5$]$^{2-}$
5	Tl(CN)$_3$ [a] [Tl(CN)$_4$]$^-$ [a]	Pb(CN)$_2$	Sb(CN)$_3$ [Sb(CN)$_5$]$^{2-}$
Refs.	121,123,156–158,124–126,130–134	29,147,150–154,159	1,136,139,160–163

Table 9. Reported homoleptic poly(cyanido) complexes of groups 13−15.
[a] present only in equilibrium with each other and HCN; [b] observed *in situ.*

3.2 Results and Discussion

3.2.1 Synthesis of [PPN]$_2$[Ge(CN)$_6$]

In analogy to the preparation of [Si(CN)$_6$]$^{2-}$, the reaction of GeCl$_4$ with excess [PPN]CN was speculated to form [PPN]$_2$[Ge(CN)$_6$] (scheme 4).[147]

$$GeCl_4 + ex.PPNCN \xrightarrow{MeCN} (PPN)_2[Ge(CN)_6] + PPNCl$$
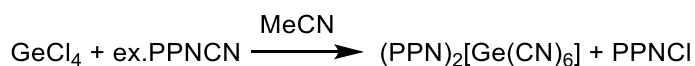
Scheme 4. Proposed synthesis of [PPN]$_2$[Ge(CN)$_6$].

Treatment of GeCl$_4$ with excess [PPN]CN formed a microcrystalline solid. The observation of two ν(CN) bands in the IR spectrum contrasted the single ν(CN) band expected for a perfectly octahedral complex with O$_h$ symmetry, such as [Ge(CN)$_6$]$^{2-}$. The presence of an additional ν(CN) band is indicative of either incomplete chloro/cyanido ligand exchange or a non-octahedral complex. The former hypothesis is consistent with the requirement for two treatments of excess [PPN]CN to prepare chlorine-free [PPN]$_2$[Si(CN)$_6$] and suggested that a mixed-ligand complex as [PPN]$_2$[Ge(CN)$_x$Cl$_y$] ($x + y = 6$) was formed. The observation of two signals associated with cyanido ligands in the ^{13}C NMR spectrum (figure 8) contrasted the

single signal observed for $[PPN]_2[Si(CN)_6]$ and gave further evidence for the formation of $[PPN]_2[Ge(CN)_xCl_y]$.
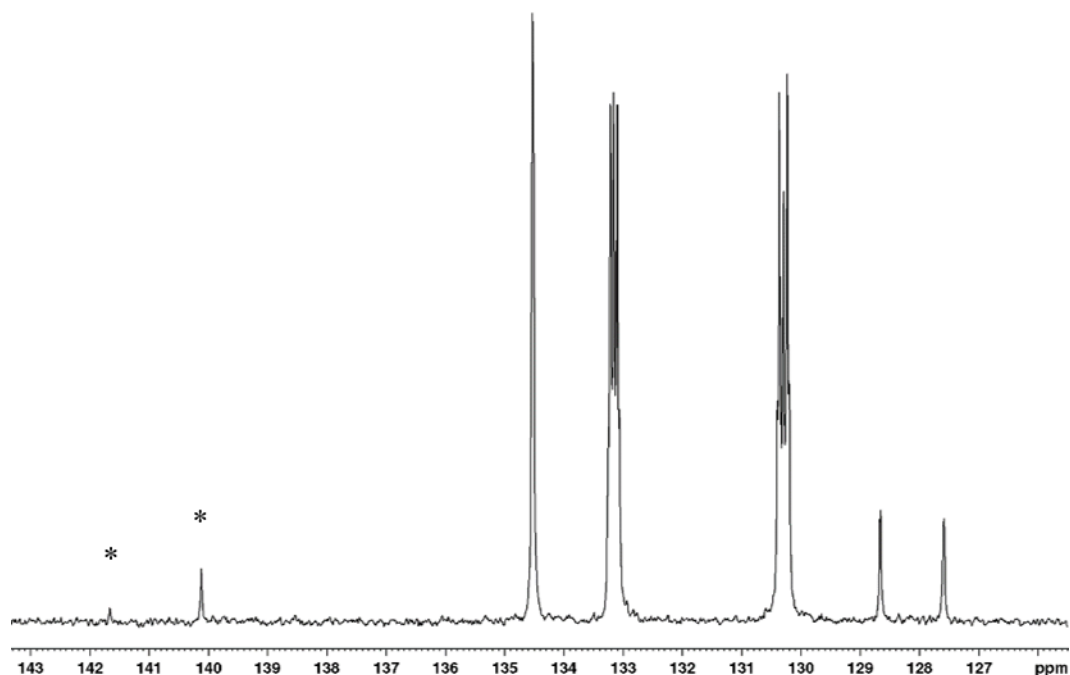
Figure 8. Expansion of the ^{13}C NMR spectrum of $[PPN]_2[Ge(CN)_xCl_y]$ in CD_3CN. The signals marked with asterisks (*) are attributed to cyanido ligands; all other signals are attributed to $[PPN]^+$.

Elemental analysis confirmed that ligand exchange was incomplete and identified the presence of a solid solution of chloro-cyano germanate salts which included $[PPN]_2[Ge(CN)_6]$, $[PPN]_2[Ge(CN)_5Cl]$, $[PPN]_2[Ge(CN)_4Cl_2]$ and PPNCl (table 10). Recrystallisation from hot MeCN afforded colourless block-shaped crystals. Crystallographic studies showed large amounts of disorder in the cyanido ligands when solved as $[PPN]_2[Ge(CN)_6]$, arising from the presence of unmodelled chlorine.

	C (%)	H (%)	N (%)	Cl (%)
$w = 1, x = 0.1, y = 0.2, z = 2.6$	73.44	4.94	5.60	3.03
Observed values	74.87	5.48	5.94	2.95
Difference (%)	-1.43	-0.54	-0.34	+0.08

Table 10. Microanalytical data for a solid solution of $[PPN]_2[Ge(CN)_6]$,$[PPN]_2[Ge(CN)_5Cl]$, $[PPN]_2[Ge(CN)_4Cl_2]$ and $[PPN]Cl$ (w, x, y and z, respectively) versus the observed values.[164]

Treatment of the crystallised mixed-ligand complex with additional, excess [PPN]CN failed to complete chlorido/cyanido ligand exchange. The solubility of all starting materials, intermediates and products in MeCN was hypothesised to form an equilibrium which impeded

the formation of chlorine-free $[Ge(CN)_6]^{2-}$ (scheme 5). An additional thermodynamic or entropic driving force, such as the formation of a removable insoluble or gaseous byproduct, is required to favour the selective formation of $[Ge(CN)_6]^{2-}$. The reaction between GeF_4 and the covalent cyanide transfer reagent TMS−CN may provide sufficient additional thermodynamic and entropic driving forces to complete ligand exchange through the formation of strong Si−F bonds ($\Delta H_{(Si-F)} = 582$ kJ mol^{-1}) in gaseous TMS−F and prepare $Ge(CN)_4$ (scheme 6). Subsequent reaction of $Ge(CN)_4$ with chlorine-free [PPN]CN could result in the formation of pure $[Ge(CN)_6]^{2-}$. However, owing to the need for specialist equipment to handle gaseous GeF_4, this strategy was unfeasible and was not attempted. $Ge(CN)_4$ was not formed from the reaction between $GeCl_4$ and TMSCN in MeCN, contrasting the report detailing the formation of $Ge(CN)_4$ from TMSNC and $GeCl_4$ in xylene.[135] This is speculated to be due to the decreased thermodynamic and entropic driving forces for the formation of TMS−Cl versus TMS−F (table 11), although the reason for the differing reactivity between TMSCN and TMSNC is unclear.[165]

	$\Delta H_{(Si-X)}$ / kJ mol^{-1}	b.p. / °C
TMS−F	582	15
TMS−Cl	391	58

Table 11. Comparison of bond enthalpies and boiling points of TMS−F and TMS−Cl.[58,165]

$$GeCl_4 + PPNCN \longrightarrow (PPN)_2[Ge(CN)_xCl_y] + PPNCN \rightleftharpoons (PPN)_2[Ge(CN)_6] + PPNCl$$
$$x + y = 6$$
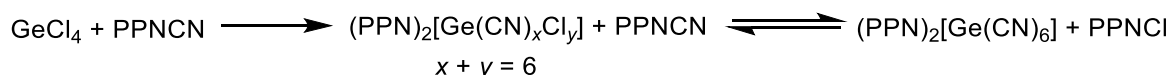
Scheme 5. Proposed equilibrium between $GeCl_4$, [PPN]CN and $[PPN]_2[Ge(CN)_6]$.

$$GeF_4 + 4Me_3SiCN \longrightarrow Ge(CN)_4 + 4Me_3SiF_{(g)} \xrightarrow{PPNCN} (PPN)_2[Ge(CN)_6]$$
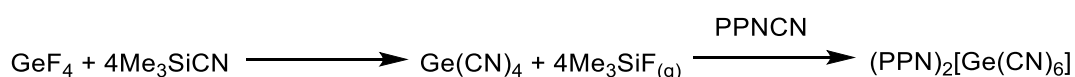
Scheme 6. Proposed synthesis of $[PPN]_2[Ge(CN)_6]$ from GeF_4.

The use of NaCN as an ionic cyanide transfer reagent was trialled to determine if the formation of an insoluble byproduct (NaCl) from the equilibrium between [PPN]CN, [PPN]Cl and $[PPN]_2[Ge(CN)_xCl_y]$ would form $[Ge(CN)_6]^{2-}$. Although insoluble in MeCN, the residual solubility of NaCN at elevated temperatures (65 °C) proved sufficient for a reaction to occur and allow IR spectroscopic monitoring (scheme 7). Elemental analysis of the obtained crystalline material confirmed that pure $[PPN]_2[Ge(CN)_6]$ was formed with a chlorine content below detectable levels (<0.3%), and demonstrated that the formation of an insoluble byproduct was required to achieve complete chloro/cyanido ligand exchange. The IR spectrum of $[PPN]_2[Ge(CN)_6]$ showed two distinctive ν(CN) bands in the solid state and only one in

solution (figure 9). The analytical purity of the complex precluded the possibility of the additional ν(CN) band arising from chlorine contamination, and is instead due to the imperfect octahedral geometry of the $[Ge(CN)_6]^{2-}$ anion. An additional band is also observed in the solid state IR spectrum of $[PPN]_2[Si(CN)_6]$.[147]

$$GeCl_4 \xrightarrow[\substack{MeCN \\ -PPNCl}]{ex.PPNCN} (PPN)_2[Ge(CN)_xCl_y] \xrightarrow[\substack{MeCN \\ -NaCl_{(s)}}]{ex.NaCN} (PPN)_2[Ge(CN)_6]$$
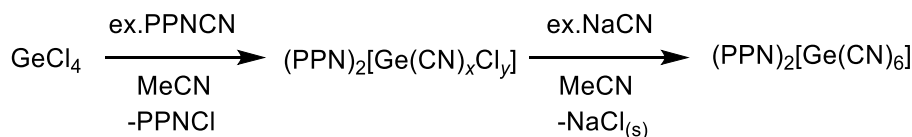
Scheme 7. Synthesis of $[PPN]_2[Ge(CN)_6]$ from $[PPN]_2[Ge(CN)_xCl_y]$ ($x + y = 6$).
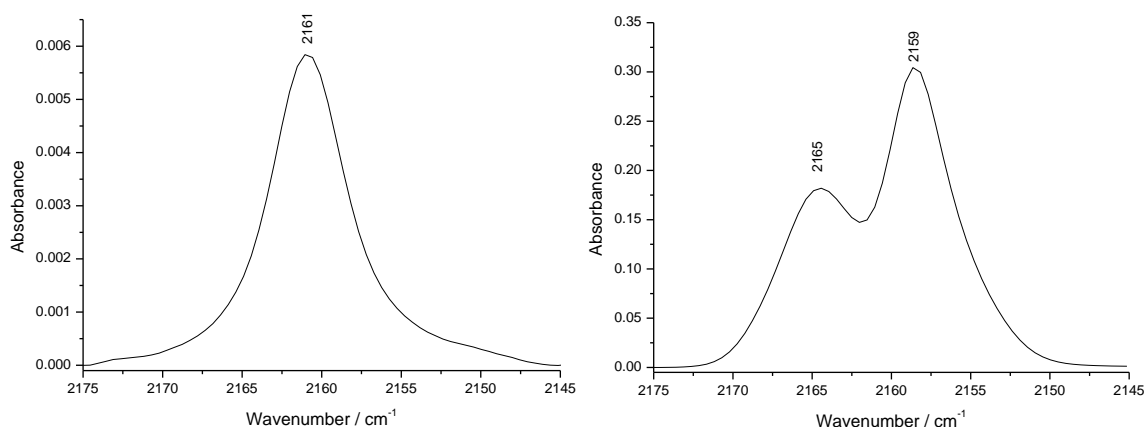
Figure 9. IR spectra of $[PPN]_2[Ge(CN)_6]$ between 2180-2145 cm^{-1} in MeCN solution (left) and as a nujol mull (right).

The ^{13}C NMR spectrum of $[PPN]_2[Ge(CN)_6]$ showed a single carbon resonance ($\delta = 140.0$ ppm) which is attributed to the $[Ge(CN)_6]^{2-}$ anion adopting perfect octahedral geometry in solution. This observation is consistent with the detection of a single ν(CN) band in solution-phase IR spectroscopic studies. When crystallised, the packing-induced distortion of the anion from perfect octahedral geometry should generate additional carbon resonances, in analogy to the additional ν(CN) bands observed in the IR spectrum of the solid compound. However, the resonances observed in solid-state ^{13}C NMR measurements proved indistinguishable from those arising from the PPN cation (figure 10) and no further information regarding the solid-state geometry of the anion could be gathered from this technique. Comparison of the ^{73}Ge chemical shift of $[Ge(CN)_6]^{2-}$ to $[Ge(SCN)_6]^{2-}$ ($\delta = -443.0$ ppm), $Ge(NCO)_4$ ($\delta = -88.9$ ppm) and $[Ge(N_3)_6]^{2-}$ ($\delta = -290.6$ ppm), could elucidate the position of the CN ligand in an approximate spectrochemical series of homoleptic pseudohalogenido complexes of Ge(IV).[96,166,167] However, the lack of sensitivity of the ^{73}Ge nucleus in the range of the spectrometer probe meant that no ^{73}Ge NMR spectra of the complex could be recorded.
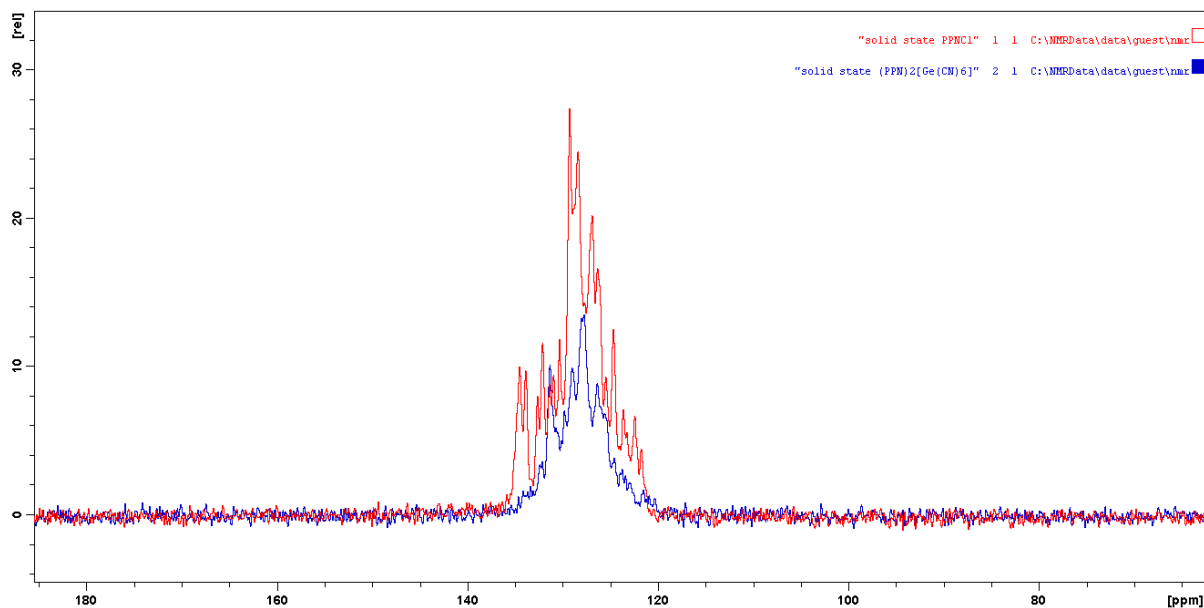
Figure 10. ^{13}C MAS NMR spectra of [PPN]Cl (red line, —) and $[PPN]_2[Ge(CN)_6]$ (blue line, —).

Recrystallisation from MeCN gave colourless block crystals of $[PPN]_2[Ge(CN)_6]$ in space group $P2_1/c$ (figure 11). Crystallographic analysis shows that the $[Ge(CN)_6]^{2-}$ anion in $[PPN]_2[Ge(CN)_6]$ possesses six crystallographically independent ligands in a distorted octahedral geometry and is the first example of an octahedral Ge−C$_6$ network, accompanying the observation of the first Si−C$_6$ framework in $[Si(CN)_6]^{2-}$. The amount of disorder in the crystal structure of the $[Ge(CN)_6]^{2-}$ anion is lower than in $[PPN]_2[Ge(CN)_xCl_y]$ owing to the absence of chlorine above detectable limits. The C−N bond in all six cyanido ligands are almost identical to the standard C≡N bond length ($d = 1.14$ Å).[168] All six Ge−C−N bond angles deviate from 180° in an imperfectly octahedral geometry which results in the contraction of one Ge−C bond in the crystal structure. The C(6)−N(6) ligand displays the largest deviation from the perfect linearity expected for a cyanido group ($\angle = 174.11°$).

The origin of the distorted octahedral geometry is attributed to the packing interactions of the anions in the crystal form and accounts for the observation of an additional ν(CN) band in the IR spectrum of the solid. Similar distortion is observed in the crystal structures of the $[Si(CN)_6]^{2-}$ salts, including those which contain smaller and less sterically-hindering cations to $[PPN]^+$, and appears to be an inherent feature of cyanido ligands in coordination complexes of this type.[147,148,169] Although several short contact interactions are observed between the terminal nitrogen atoms of the CN ligands and the $[PPN]^+$ cations, these differ to those observed in salts of $[Si(CN)_6]^{2-}$ and are believed to arise as a secondary consequence from the packing arrangements in the unit cell (figures 12, 13).
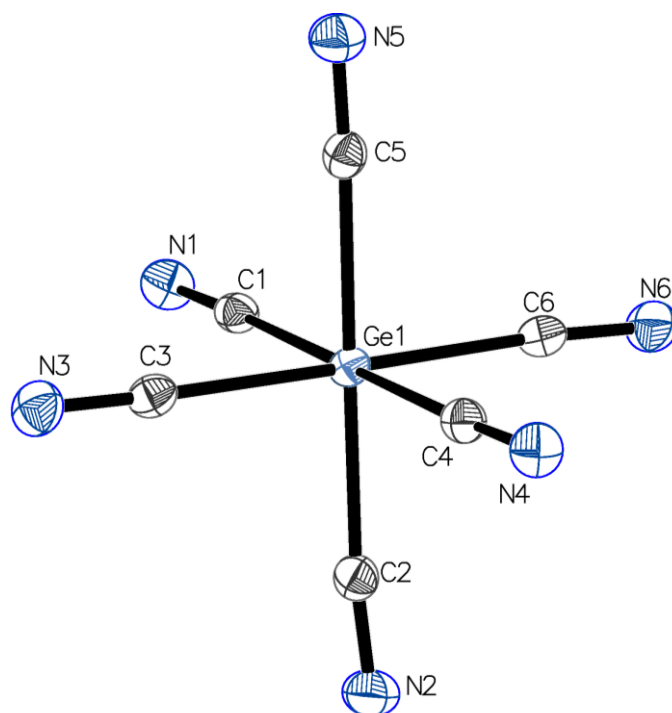
Figure 11. Structure of the $[Ge(CN)_6]^{2-}$ anion in $[PPN]_2[Ge(CN)_6]$. Selected bond lengths (Å) and angles (°): Ge(1)−C(1) 2.0589(13), Ge(1)−C(2) 2.0406(14), Ge(1)−C(3) 2.0564(14) , Ge(1)−C(4) 2.0484(13), Ge(1)−C(5) 2.0484(14), Ge(1)−C(6) 2.0441(14), C(1)−N(1) 1.1458(18), C(2)−N(2) 1.1444(18), C(3)−N(3) 1.1471(18), C(4)−N(4) 1.1461(18), C(5)−N(5) 1.1469(18), C(6)−N(6) 1.1454 (18); N(1)−C(1)−Ge(1) 176.62(12), N(2)−C(2)−Ge(1) 176.20(12), N(3)−C(3)−Ge(1) 177.23(12), N(4)−C(4)−Ge(1) 174.94(12), N(5)−C(5)−Ge(1) 174.89(12), N(6)−C(6)−Ge(1) 174.11(12).

$d_{min,max}(Ge-C)$ / Å	$d_{min, max}(C-N)$ / Å	$\angle_{min, max}(Ge-C-N)$ / °
2.0406(14), 2.0589(13)	1.1444(18), 1.1471(18)	174.11(12), 177.23(12)

Table 12. Ranges of bond lengths and angles observed for the $[Ge(CN)_6]^{2-}$ anion in the crystal structure of $[PPN]_2[Ge(CN)_6]$.
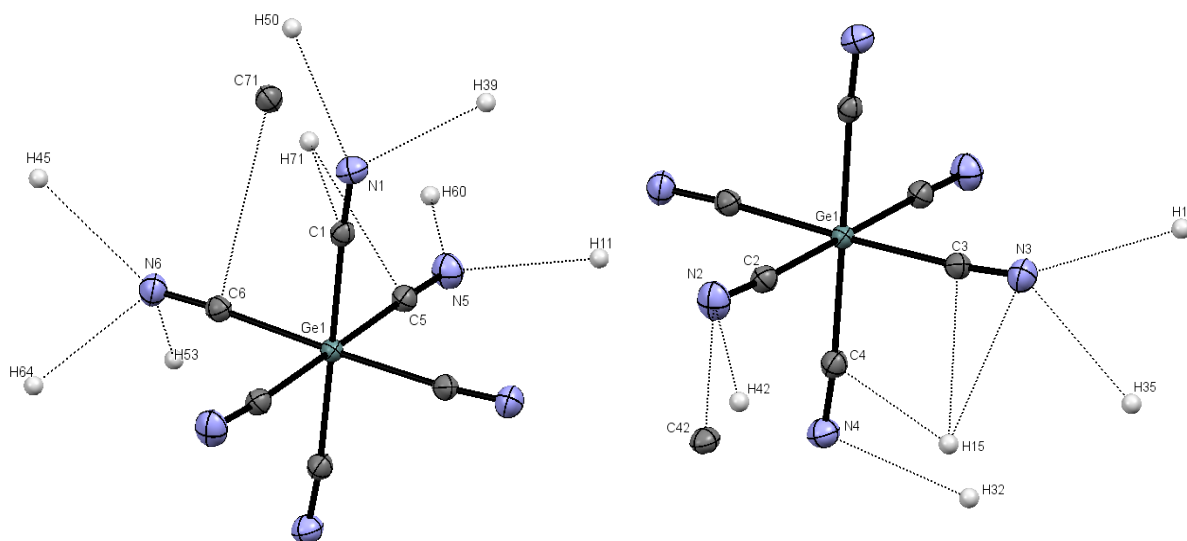
Figure 12. Selected short contact interactions between the CN ligands of $[Ge(CN)_6]^{2-}$ and $[PPN]^+$.

28
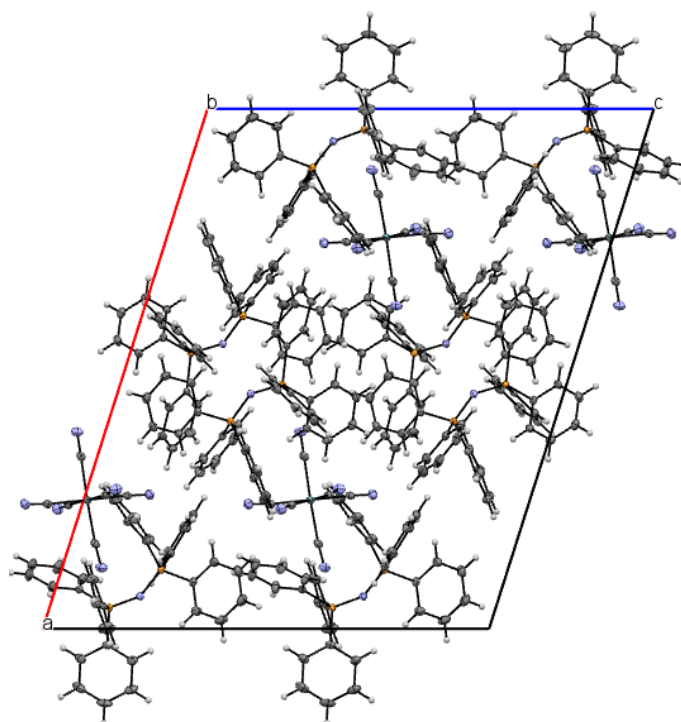
Figure 13. Packing of [PPN]$_2$[Ge(CN)$_6$] in the crystal lattice, viewed down the crystallographic *b* axis.

The preparation of [PPN]$_2$[Ge(CN)$_6$] from [PPN]$_2$[Ge(CN)$_x$Cl$_y$] was also attempted using AgCN. Crystallographic analysis of the colourless crystals isolated from the supernatant solution showed that [PPN][Ag(CN)$_2$]·MeCN had formed instead of [PPN]$_2$[Ge(CN)$_6$] (scheme 8, figures 14, 15). The fate of the germanium coordination centre is unknown but is speculated to form another anionic chloro-cyano germanate complex. The dicyanoargentate anion is known alongside several other bis(pseudohalogenido)argentate anions as [AgY$_2$]$^-$, Y = CN, N$_3$, NCO, SCN.[170–173]

$$(PPN)_2[Ge(CN)_xCl_y] + ex.AgCN \xrightarrow{\text{MeCN}} (PPN)[Ag(CN)_2]\cdot MeCN$$
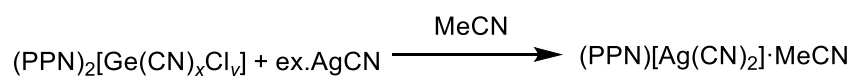
Scheme 8. Synthesis of [PPN][Ag(CN)$_2$]·MeCN from [PPN]$_2$[Ge(CN)$_x$Cl$_y$] and AgCN.
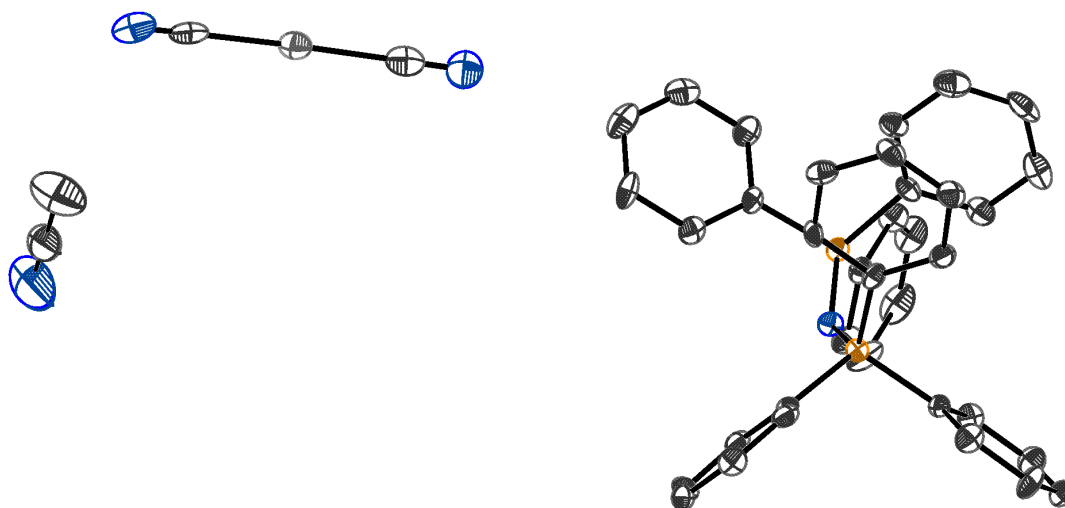
Figure 14. Asymmetric unit of the crystal structure of [PPN][Ag(CN)$_2$]·MeCN. Hydrogen atoms omitted for clarity. Grey = carbon, blue = nitrogen, light grey = silver, orange = phosphorous.
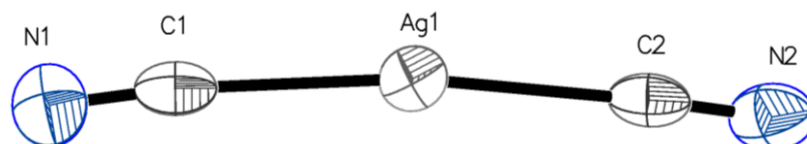
Figure 15. Crystal structure of the [Ag(CN)$_2$]$^-$ anion in [PPN][Ag(CN)$_2$]·MeCN. Grey = carbon, light grey = silver, blue = nitrogen. Selected bond lengths (Å) and angles (°) : Ag(1)−C(1) 2.064(8), Ag(1)−C(2) 2.064(8), C(1)−N(1) 1.101(8), C(2)−N(2) 1.082(8) ; C(1)−Ag(1)−C(2) 172.0(3), N(1)−C(1)−Ag(1) 174.1(6), N(2)−C(2)−Ag(1) 177.4(7).

[PPN][Ag(CN)$_2$]·MeCN crystallises from MeCN as colourless blocks with space group *P*2$_1$/c. The [Ag(CN)$_2$]$^-$ anion does not exhibit any hydrogen-bonding intermolecular interactions. Whilst all bond lengths are comparable with the previously-reported THF and CH$_2$Cl$_2$ solvates (table 13), the MeCN solvate prepared in this study is the least planar.[172,173] The IR spectrum of solid [PPN][Ag(CN)$_2$]·MeCN shows a sharp ν(CN) band associated with the [Ag(CN)$_2$]$^-$ anion at 2135 cm^{-1}. An additional sharp ν(CN) band at 2159 cm^{-1} is caused by the imperfect linearity of the [Ag(CN)$_2$]$^-$ anion, whilst bands at 2169 and 2148 cm^{-1} arise from solvated MeCN (figure 16). The spectral position of the main ν(CN) band is consistent with the other solvates.[172,173] The [Ag(CN)$_2$]$^-$ anion in the CH$_2$Cl$_2$ solvate is the most linear and consequently only one ν(CN) band is observed. As the anion becomes less linear, alongside the change in solvate, the symmetry of the anion decreases and the number of ν(CN) bands rises.

Description	Solvate		
	MeCN	**THF** [a]	**CH₂Cl₂**
Temperature / K	100	195	150
$d_{min,max}$(Ag−C) / Å	2.064(8)	2.029, 2.054	2.046(5), 2.059(6)
$d_{min,max}$(C−N) / Å	1.082(8), 1.101(8)	1.111, 1.165	1.133(6), 1.063(6)
$\angle$(C−Ag−C) / °	172.0(3)	176.46	179.10
Deviation from 180° bond angle / °	8.03	3.54	0.90
ν(CN) / cm^{-1}	2135, 2159	2131, 2138	2137
Refs.	This work	[172]	[173]

Table 13. Comparison of bond angles and ν(CN) bands asymmetric CN stretching frequencies for the three crystallographically-studied solvates of [PPN][Ag(CN)₂]. [a] no errors reported.
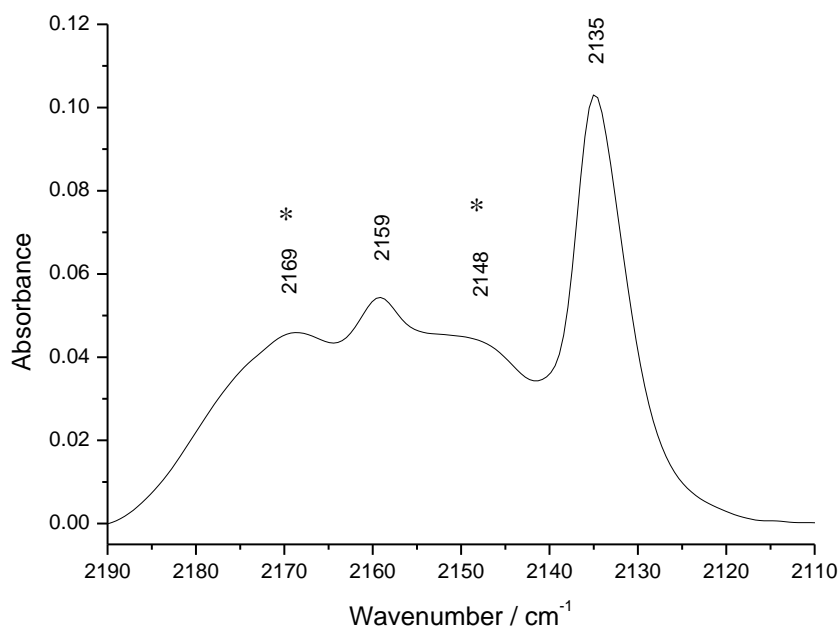
Figure 16. IR spectrum of [PPN][Ag(CN)₂]·MeCN between 2190−2110 cm^{-1}. Bands marked with asterisks (*) are attributed to solvated MeCN.

The formation of [Ag(CN)₂]$^{-}$ demonstrates the unsuitability of AgCN as an ionic cyanide transfer reagent for the preparation of group 14 cyanido complexes and was not investigated further. It is therefore hypothesised that the contrasting effectiveness of NaCN as an ionic cyanide transfer reagent may be due to the absence of competing complexation reactions between CN ligands and the non-coordinating sodium cation.

3.2.2 Synthesis of Sn(CN)₄(L)₂ (L = MeCN, py)

In analogy to the silicate and germanate analogues, the reaction between [PPN]CN and SnCl₄ was attempted to prepare the $[Sn(CN)_6]^{2-}$ anion as [PPN]₂[Sn(CN)₆] (scheme 9). As observed for the reaction with GeCl₄, treatment of SnCl₄ with one batch of excess [PPN]CN resulted in a microcrystalline solid and ligand exchange could not be completed despite further reaction with fresh, excess [PPN]CN. Microanalysis identified the composition of the crystalline solid as an approximately equal mixture of [PPN]₂[Sn(CN)₅Cl] and [PPN]₂[Sn(CN)₆] (table 14). Crystallographic analysis showed a disordered $[Sn(CN)_6]^{2-}$ anion, consistent with the structure of the anion in [PPN]₂[Ge(CN)ₓClᵧ].

$$SnCl_4 + ex.PPNCN \xrightarrow{\text{MeCN}} (PPN)_2[Sn(CN)_6] + PPNCl$$
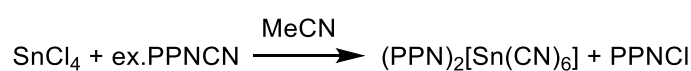
Scheme 9. Proposed synthesis of [PPN]₂[Sn(CN)₆].

	C (%)	H (%)	N (%)	Cl (%)
[PPN]₂[Sn(CN)₆] (A)	69.28	4.48	8.29	0
[PPN]₂[Sn(CN)₅Cl] (B)	67.91	4.44	7.20	2.61
1:1 A + B	68.59	4.46	7.75	1.31
Observed Values	68.52	4.52	7.53	1.00
Difference between observed values and B (%)	0.07	−0.06	0.22	0.31

Table 14. Microanalytical results for [PPN]₂[Sn(CN)ₓClᵧ].

Owing to the difficulty in completion of ligand exchange between SnCl₄ and [PPN]CN, charge-neutral adducts of tetracyanotin were investigated as alternative precursors for the formation of [PPN]₂[Sn(CN)₆] through their reaction with [PPN]CN (scheme 10). In contrast to the germanium analogue, SnF₄ is a stable solid and reacted readily at room temperature with TMSCN in MeCN to form an insoluble off-white solid in near-quantitative yield.

$$SnF_4 + 4Me_3SiCN \longrightarrow Sn(CN)_4 + 4Me_3SiF_{(g)} \xrightarrow{\text{PPNCN}} (PPN)_2[Sn(CN)_6]$$
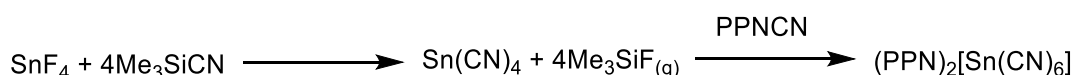
Scheme 10. Proposed synthesis of [PPN]₂[Sn(CN)₆] from SnF₄ and TMS−CN.

An extremely strong, sharp ν(CN) band was observed at 2182 cm⁻¹ in the IR spectrum which appears to possess a weak shoulder at 2179 cm⁻¹ (figure 17). Bands consistent with coordinated MeCN at 2290 and 2320 cm⁻¹ confirmed the formation of an adducted acetonitrile complex.

Replication of the reaction in pyridine instead of MeCN afforded a compound in similar yield which exhibited a single strong $\nu(CN)$ band (figure 17) at a slightly lower spectral position than the main $\nu(CN)$ band of the MeCN adduct ($\tilde{\nu} = 2165$ cm^{-1} vs 2182 cm^{-1}, respectively). The coordination of pyridine was evidenced by the observation of an additional band at 1610 cm^{-1}. Although the exact number of coordinated ancillary ligands in each complex was unable to be determined, the formation of bis-solvated adducts of other tetra(pseudohalogenido) complexes of Sn(IV), such as $Sn(N_3)_4(py)_2$, suggests that the reactions described here afforded binary solvent adducts of tin tetracyanide as $Sn(CN)_4(L)_2$ (L = MeCN, py, scheme 11).[102]

$$SnF_4 + 4Me_3SiCN \xrightarrow{\quad L \quad} Sn(CN)_4(L)_2 + 4Me_3SiF_{(g)}$$
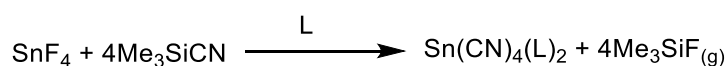
Scheme 11. Synthesis of $Sn(CN)_4(L)_2$ (L = MeCN, py).
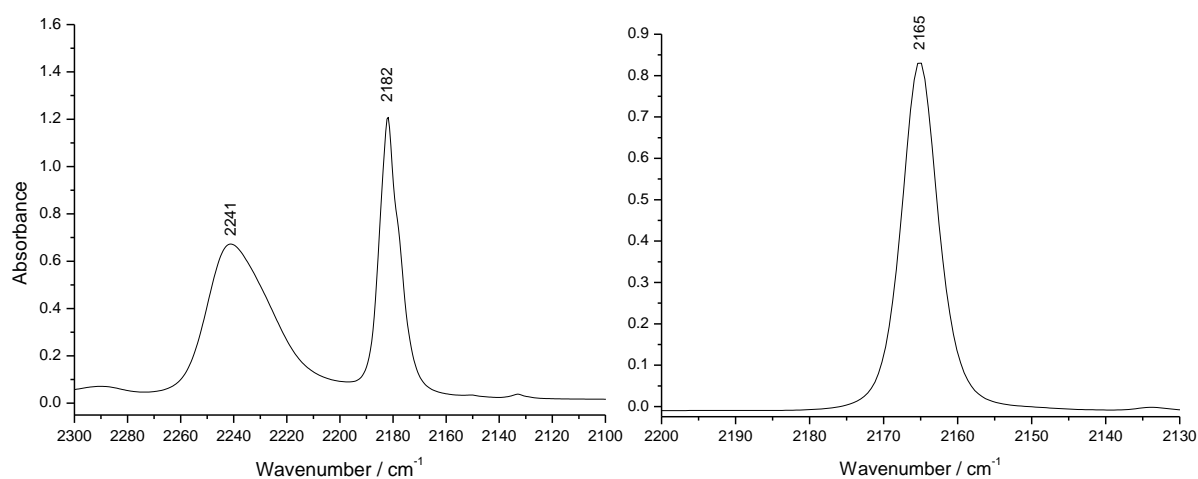
Figure 17. IR spectrum of $Sn(CN)_4(MeCN)_2$ between 2300-2100 cm^{-1} (left) and $Sn(CN)_4(py)_2$ between 2200-2130 cm^{-1} (right), nujol mull.

Both adducts are extremely air sensitive and immediately turned yellow when exposed to air, resulting in an intense odour of both HCN and ancillary ligand (MeCN or py). Despite attempts to minimise air exposure through sample preparation in a glovebox and immediate analysis, the extreme air sensitivity of both complexes prevented the determination of reliable microanalytical values. The obtained values were inconsistent with $Sn(CN)_4$, $Sn(CN)_4(L)$ or $Sn(CN)_4(L)_2$ and are instead assigned to hydrolysis products of unknown identity, which formed almost immediately upon air exposure.

The insolubility of both complexes in common, non-coordinating solvents limited spectroscopic analysis to NMR studies in coordinating solvents. The absence of any signals in the ^{19}F NMR spectrum of $Sn(CN)_4(py)_2$ in DMSO-d_6 confirmed that exchange of all four fluoride ligands was complete, supported by one ^{13}C NMR resonance at $\delta = 113.8$ ppm,

attributed to the single cyanido carbon environment of $Sn(CN)_4$. All other carbon resonances were consistent with uncoordinated pyridine and indirectly confirmed that an adducted complex was initially present prior to displacement of the pyridine ligands by DMSO-d_6 (figure 18). It is unclear if the ancillary ligand decoordination observed in the NMR spectra occurs spontaneously or only upon displacement by a more strongly coordinating ligand, as observed here. The ^{1}H NMR spectrum of the same compound shows signals attributed to uncoordinated pyridine and HCN, the latter arising from decomposition in air during analysis.[169,174] The decomposition of $Sn(CN)_4(py)_2$ during spectroscopic studies prevented the determination of the ratio of cyanido to pyridine ligands through integral ratio analysis.
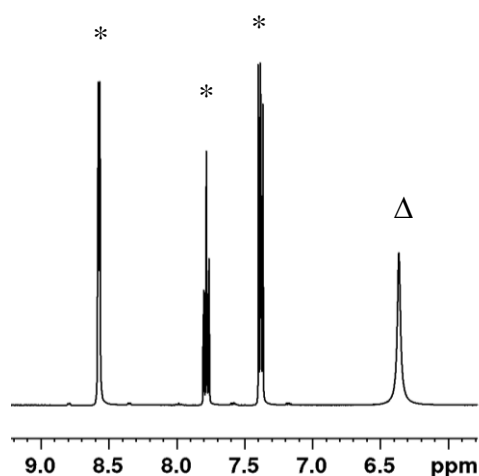
Figure 18. ^{1}H NMR spectrum of $Sn(CN)_4(py)_2$ in DMSO-d$_6$, showing the presence of uncoordinated pyridine (*) and water (Δ).

Attempts to crystallise $Sn(CN)_4(py)_2$ from hot pyridine resulted in a non-crystalline precipitate. No precipitation was observed upon crystallisation attempts from DMF, presumably due to the displacement of both pyridine ligands to form a highly-soluble DMF adduct as $Sn(CN)_4(DMF)_2$. The absence of accurate microanalytical and crystallographic data prevented the confirmation of the identity of both complexes. However, the observation of a single ν(CN) band in the IR spectrum, one CN environment in the ^{13}C NMR spectrum and the absence of any ^{19}F NMR signals support the hypothesis for the formation of $Sn(CN)_4(py)_2$ (table 15).

	Sn(CN)$_4$(MeCN)$_2$	Sn(CN)$_4$(py)$_2$
ν(CN) / cm^{-1}	2165	2182
ν(L) / cm^{-1}	2290, 2320	1610
δ(CN) / ppm	−	113.8

Table 15. Characterisation data for Sn(CN)$_4$(L)$_2$ (L = MeCN, py). The insolubility of Sn(CN)$_4$(MeCN)$_2$ in non-coordinating solvents precluded NMR spectroscopic studies.

Sn(CN)$_4$(MeCN)$_2$ was heated under high vacuum in an attempt to afford pure Sn(CN)$_4$ (scheme 12). Despite several hours of heating at 60°C, no change in the IR spectrum was observed and the bands attributed to coordinated MeCN remained. The extremely strong coordination of the ancillary ligands means that removal is only possible through displacement by a more strongly coordinating ligand such as DMF, as evidenced during crystallisation attempts and spectroscopic studies described above. As a result, Sn(CN)$_4$ remains uncharacterised.[150,151]

$$Sn(CN)_4(MeCN)_2 \xrightarrow[\;60°C\;]{\text{high vacuum}} \!\!\!\!\times\!\!\!\! \rightarrow Sn(CN)_4 + 2MeCN$$
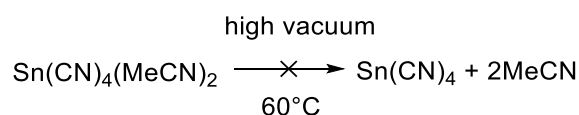
Scheme 12. Attempted preparation of Sn(CN)$_4$ from Sn(CN)$_4$(MeCN)$_2$.

3.2.3 Synthesis of [PPN]$_2$[Sn(CN)$_6$] from Sn(CN)$_4$(MeCN)

The reaction of Sn(CN)$_4$(MeCN)$_2$ with an excess of [PPN]CN formed a white solid which, in analogy to [PPN]$_2$[Ge(CN)$_6$], displayed two ν(CN) bands in the solid-state IR spectrum and one in solution (figure 19). Both precursors were chlorine-free and therefore incomplete chloro/cyanido ligand exchange was not possible. Elemental analysis confirmed the formation of analytically-pure [PPN]$_2$[Sn(CN)$_6$] and, indirectly, the formation of Sn(CN)$_4$(MeCN)$_2$ in the previous step.
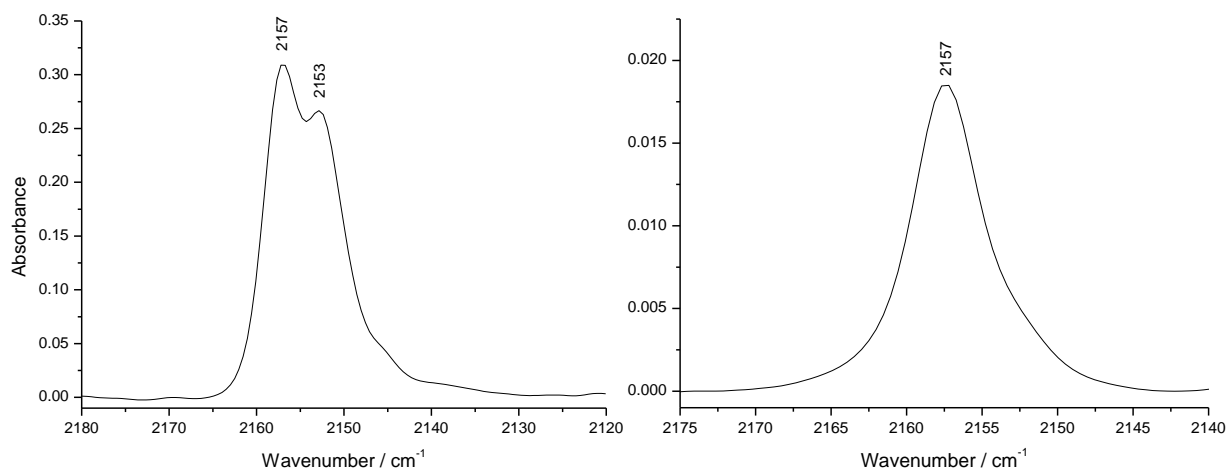
Figure 19. IR spectra of [PPN]$_2$[Sn(CN)$_6$] between 2180−2120 cm^{-1} (left, nujol) and 2175−2140 cm^{-1} (right, MeCN).

Surprisingly, two resonances were observed for the [Sn(CN)$_6$]$^{2-}$ anion in the solution-state ^{13}C NMR spectrum of [PPN]$_2$[Sn(CN)$_6$] (figure 20). As the spectrum was recorded in solution, the second signal (δ = 139.5 ppm) cannot arise from imperfect octahedral geometry and is instead attributed to a hydroxyl- or oxo-stannate anion formed by hydrolysis of [Sn(CN)$_6$]$^{2-}$ in air during analysis. Two resonances were also observed in the ^{119}Sn NMR spectrum of the compound in solution, the higher of which (δ = 879 ppm) is attributed to [Sn(CN)$_6$]$^{2-}$ and the identity of the lower (δ = 851 ppm) speculated as the stannate hydrolysis product. In contrast, the solid-state ^{119}Sn NMR spectrum showed only a single resonance, at a comparable spectral position (δ = 871 ppm) to those observed in solution. This finding supports the hypothesis that the second signal observed in solution is generated from rapid hydrolysis. A weak signal at δ = 362 ppm in the ^{15}N NMR spectrum is attributed to the bridging nitrogen atoms of the PPN cations and no cyanido ligand resonances were observed. The long proton relaxivity time (ca. 25 seconds) rendered confirmation of this assignment through ^{13}C/^{15}N cross-polarisation studies unfeasible.
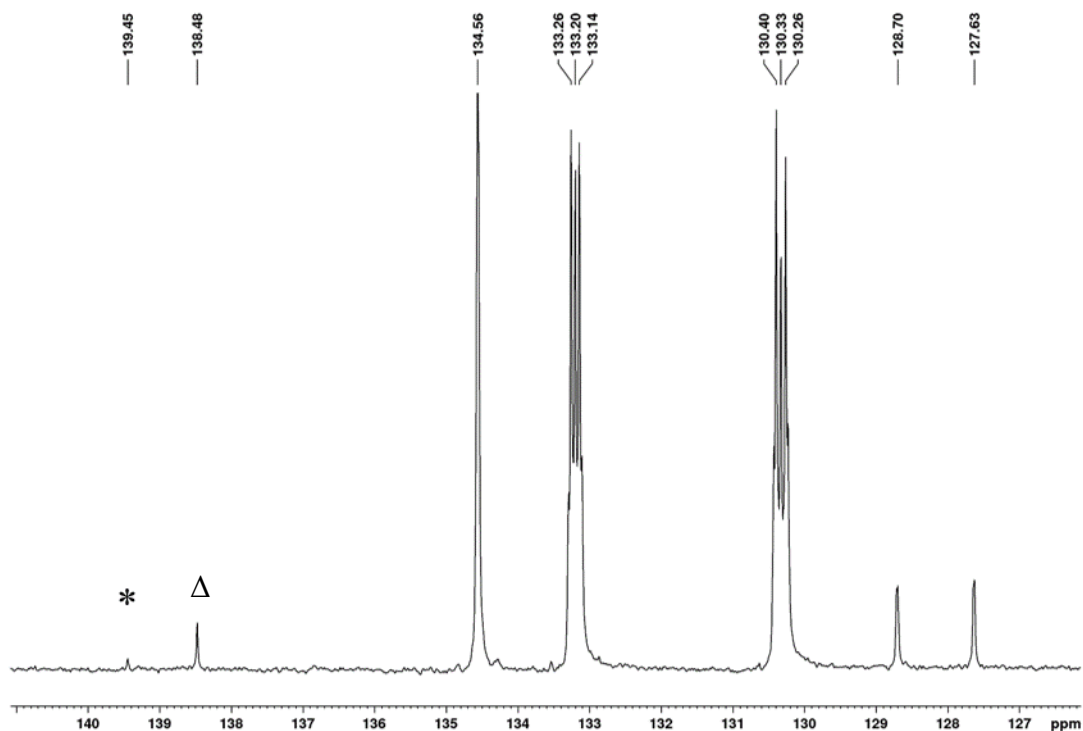
Figure 20. ^{13}C NMR spectrum of $[PPN]_2[Sn(CN)_6]$ in CD_3CN, showing the presence of $[Sn(CN)_6]^{2-}$ (Δ) and an unidentified decomposition product arising from air exposure (*). The other signals are attributed to $[PPN]^+$.

The only prior reported characterisation of the $[Sn(CN)_6]^{2-}$ anion is a single ^{119}Sn NMR chemical shift ($\delta = -961$ ppm), recorded following the *in situ* synthesis of $(NH_4)_2[Sn(CN)_6]$ from $SnCl_4$ and NH_4CN.[152] It is not clear why the complex was not isolable. The reported resonance deviates largely from the values in both solution and solid states observed in this study (table 16) and the absence of further reported characterisation of $[^nBu_4N]_2[Sn(CN)_6]$ precluded further comparisons with $[PPN]_2[Sn(CN)_6]$. The isolation of analytically pure $[PPN]_2[Sn(CN)_6]$, in combination with the marked similarity in both solid-state and solution ^{119}Sn NMR chemical shift values, appears to indicate that the previously reported chemical shift of $[Sn(CN)_6]^{2-}$ instead arises from another anionic cyanostannate complex of unknown identity.

	[PPN]₂[Sn(CN)₆]		**[ⁿBu₄N]₂[Sn(CN)₆]** [152]
δ(Sn) / ppm	−879.46, −850.17* [a]	−871.46 [b]	−916.2 [b]

Table 16. Comparison of ^{119}Sn NMR data for $(cat)_2[Sn(CN)_6]$ (cat = $[PPN]^+$ and $[^nBu_4N]^+$). [a] solution state; [b] solid state; * hydrolysis product.

[PPN]$_2$[Sn(CN)$_6$] crystallises from MeCN solution in space group *P*2$_1$/*n* as colourless blocks which appear pale yellow in the bulk (figure 21). A point of inversion at the coordination centre of the imperfectly-octahedral [Sn(CN)$_6$]$^{2-}$ anion results in three crystallographically independent CN ligands. This symmetry is analogous to the [Si(CN)$_6$]$^{2-}$ anion in [PPN]$_2$[Si(CN)$_6$] but not [PPN]$_2$[Ge(CN)$_6$], which contains six crystallographically independent CN ligands.[147,169] The distance of the Sn−C bonds is greater than for the lighter homologues (table 17). The non-linearity of the Sn−C−N bonds and imperfect octahedral geometry of the anion is consistent with both of the hexa(cyanido)silicate and -stannate anions and accounts for the presence of more than one ν(CN) band in the IR spectrum. No hydrogen-bonding interactions are present but, in analogy to the [Ge(CN)$_6$]$^{2-}$ anion, several short contacts are observed (figure 22) which may arise from similar packing-based distortion to the former. The [Sn(CN)$_6$]$^{2-}$ anion is only the second example of an octahedral Sn−C$_6$ coordination skeleton after the larger (and therefore more sterically hindered) substituted pyridyl complexes prepared by Schrader *et al.* in 2014 (figure 23).[175]
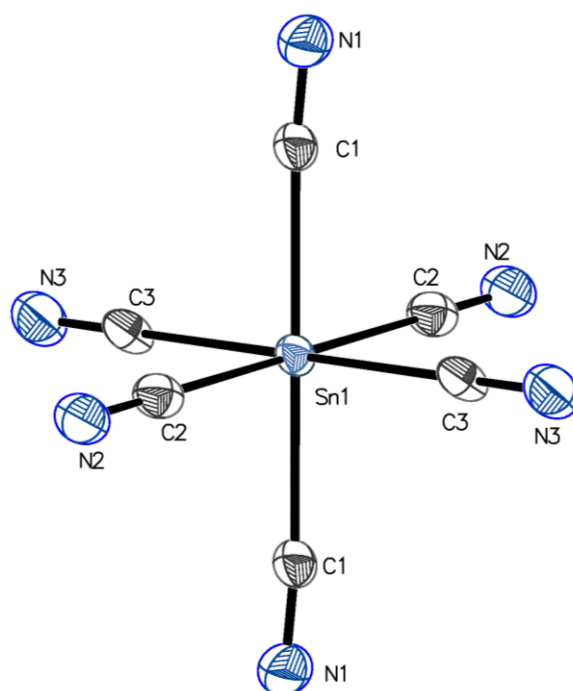
Figure 21. Thermal ellipsoid plot of the [Sn(CN)$_6$]$^{2-}$ anion in [PPN]$_2$[Sn(CN)$_6$]. Selected bond lengths (Å) and angles (°) : Sn(1)-C(1) 2.225(2), Sn(1)-C(2) 2.229(2), Sn(1)-C(3) 2.203(2), N(1)-C(1) 1.134(3), N(2)-C(2) 1.146(3), N(3)-C(3) 1.159(3); C(3)-Sn(1)-C(1) 91.65(8), C(3)-Sn(1)-C(1) 88.35(8), C(3)-Sn(1)-C(2) 88.43(8), C(3)-Sn(1)-C(2) 88.92(8), C(1)-Sn(1)-C(2) 91.08(8), C(3)-Sn(1)-C(2) 91.58(8), C(1)-Sn(1)-C(2) 88.92(8), N(1)-C(1)-Sn(1) 174.89(19), N(2)-C(2)-Sn(1) 175.73(19), N(3)-C(3)-Sn(1) 179.1(2).
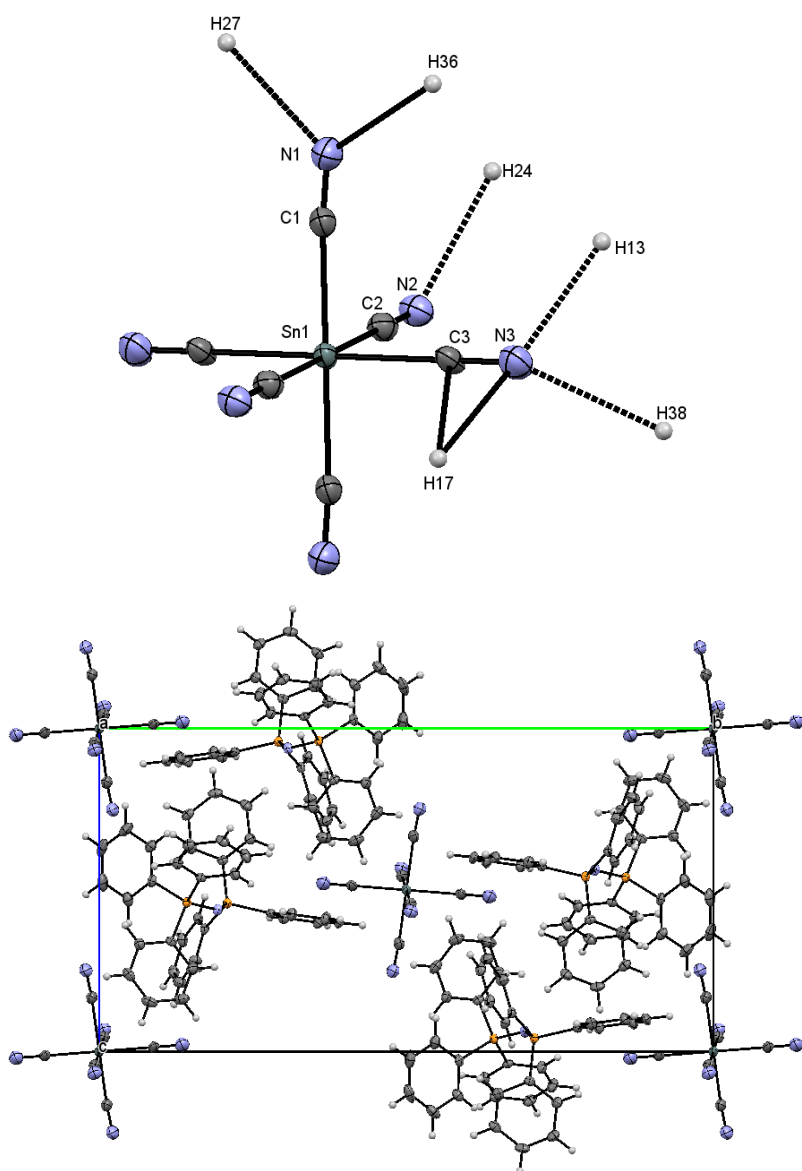
Figure 22. Top: short contact interactions for each of the crystallographically independent CN ligands in the $[Sn(CN)_6]^{2-}$ anion. Bottom: packing diagram of $[PPN]_2[Sn(CN)_6]$ in the crystal lattice, viewed down the crystallographic *a* axis.

Zahn *et al.*,
2014

This work
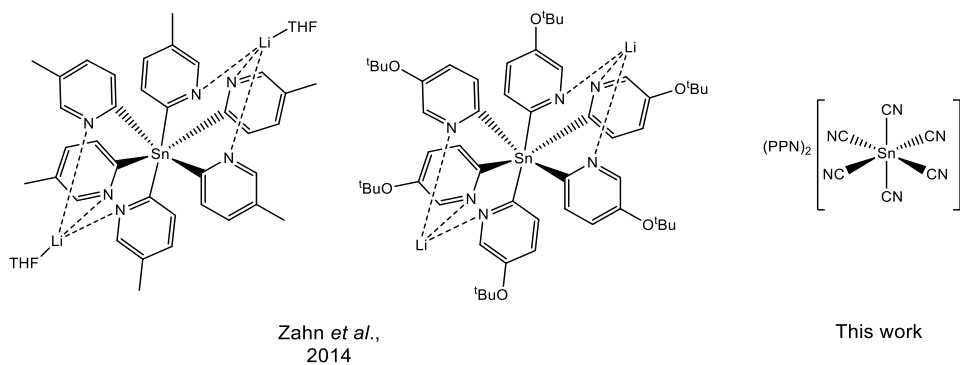
Figure 23. Structure of known $Sn-C_6$ coordination skeletons.[175]

$[E(CN)_6]^{2-}$	Space Group	n	$d_{min,max}(E-C)$ / Å	$d_{min,max}(C-N)$ / Å	$\angle(E-C-N)$ / °
E = Si	P_{bca}	3	1.9501(15),	1.115(2),	175.27(14),
			1.9588(15)	1.152(2)	178.01(13)
E = Ge	$P2_1/c$	6	2.0406(14),	1.1444(18),	174.11(12),
			2.0589(13)	1.1471(18)	177.23(12)
E = Sn	$P2_1/n$	3	2.203(2),	1.134(3),	174.89(19),
			2.229(2)	1.159(3)	179.1(2)

Table 17. Summary of crystallographic data of the $[E(CN)_6]^{2-}$ anions in $[PPN]_2[E(CN)_6]$ (E = Si, Ge, Sn). n represents the number of crystallographically independent ligands.[169]

3.2.4 Synthesis of Sn(CN)$_2$(L)$_2$ (L = MeCN, py)

Following the preparation poly(cyanido) complexes of Sn(IV) by reaction between SnF$_4$ and TMSCN, the same synthetic strategy was extended to Sn(II) centres. The reaction between SnF$_2$ and TMS−CN in MeCN or py afforded a solid which appeared similar to Sn(CN)$_4$(L)$_2$ (L = MeCN, py) and was hypothesised to be Sn(CN)$_2$(L)$_2$ (L = MeCN, py). Both adducts possess distinctive ν(CN) bands located ca. 25 cm^{-1} below the ν(CN) bands of the Sn(IV) analogues (figure 24, table 18). In further analogy to the latter, both adducts of Sn(CN)$_2$(L)$_2$ were extremely air-sensitive and poorly soluble in non-coordinating solvents, preventing crystallisation and full characterisation.
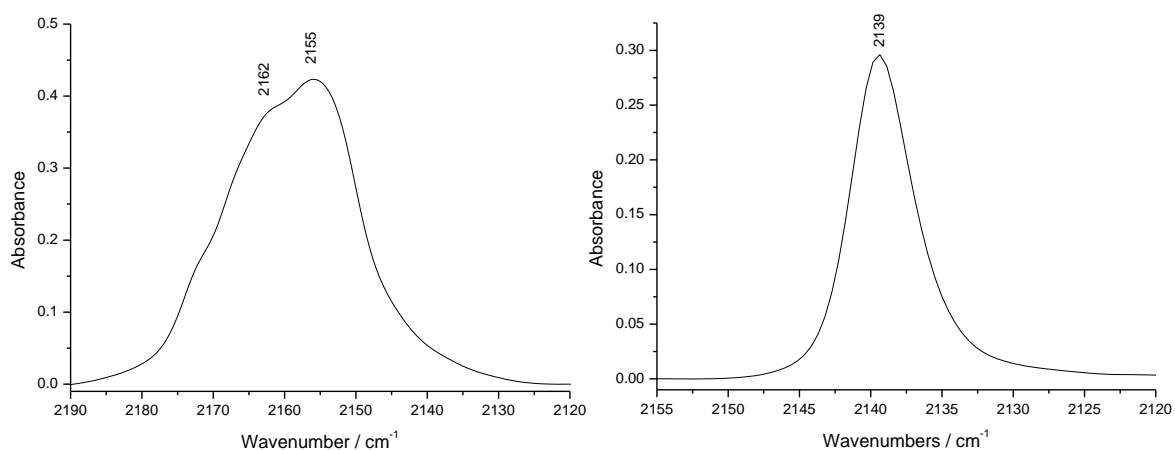
Figure 24. IR spectrum of Sn(CN)$_2$(MeCN)$_2$ between 2190−2120 cm^{-1} (left) and Sn(CN)$_2$(py)$_2$ between 2155−2120 cm^{-1} (right) as nujol mulls. ATR spectra were unable to be recorded owing to the air sensitivity of both complexes.

A sample of Sn(CN)$_2$(MeCN)$_2$ was placed under high vacuum in an attempt to form Sn(CN)$_2$ through the decoordination of both ancillary ligands. Mass loss was accompanied by the

formation of several new $\nu(CN)$ bands in the IR spectrum, the two most intense of which were almost identical to those previously reported for samples of $Sn(CN)_2$ prepared through protonolysis of $Sn(Cp^*)_2$ (Cp^* = methylcyclopentadiene) (table 18).[154] However, the preservation of the characteristic bands of coordinated MeCN ($\nu(CN)$ = 2252, 2296 cm^{-1}) denoted that ancillary ligand decoordination was incomplete and it is proposed that a mixture of bi, tri- and tetra-coordinate cyanotin products ($Sn(CN)_2(MeCN)_x$, x = 0, 1 or 2) were formed. The inherent instability of tricoordinate, neutral $Sn(CN)_2(MeCN)$ would likely result in rapid formation of $Sn(CN)_2$; it is therefore hypothesised that the product mixture is predominantly $Sn(CN)_2(MeCN)_2$ and $Sn(CN)_2$.

	$Sn(CN)_4(L)_2$ Sn(IV)	$Sn(CN)_2(L)_2$ Sn(II)
L = MeCN	2182	2155, 2162
L = py	2165	2139
L = none	–	2173, 2163 (*2179, 2168*)[154]

Table 18. Summary of $\nu(CN)$ bands observed in the IR spectra of neutral homoleptic cyanido complexes of Sn(IV) and Sn(II). Values in *italics* denote those reported previously.

In analogy to the synthesis of $[PPN][Sn(N_3)_3]$ from $Sn(N_3)_2(py)_2$, $Sn(CN)_2(py)_2$ was reacted with [PPN]CN to prepare $[PPN][Sn(CN)_3]$.[176] Despite treatment of a MeCN suspension of $Sn(CN)_2(py)_2$ with several portions of [PPN]CN at elevated temperatures (conditions which afforded $[PPN]_2[Sn(CN)_6]$ from $Sn(CN)_4(L)_2$), no reaction was observed (scheme 13, top).[176] The absence of $[Sn(CN)_3]^-$ and the ready loss of ancillary ligands from $Sn(CN)_2(L)_2$ contrast the behaviour exhibited by the high-valent Sn(IV) analogues and confirms that both CN^- and MeCN coordinate more weakly to Sn(II) centres than Sn(IV). The reported preparation of $[Sn(N_3)_3]^-$ from the rapid reaction between SnF_2, $[PPN]N_3$ and $TMSN_3$ further demonstrates the decreased coordination strength of the cyanido ligand in comparison to the azido ligand (scheme 13, top).[176]
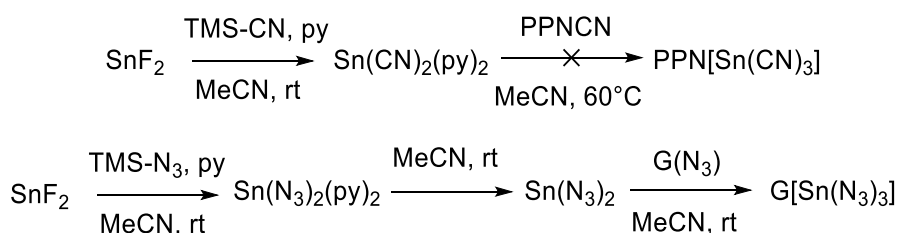
Scheme 13. Reactivity of cyanido (top) and azido (bottom) transfer reagents towards SnF_2.[176]

3.2.5 Attempted Synthesis of [PPN]$_2$[Pb(CN)$_6$]

The reported synthesis of the [Pb(N$_3$)$_6$]$^{2-}$ anion, as [Ph$_4$As]$_2$[Pb(N$_3$)$_6$], demonstrates the ability of hypercoordinate Pb(IV) coordination centres to stabilise pseudohalide ligands in the same manner as the lighter congeners of Si$-$Sn.[97,177,178] Despite this, the [Pb(CN)$_6$]$^{2-}$ anion is unknown and its preparation was therefore attempted, in order to quantify the reactivity of the CN ligand towards Pb(IV) centres and allow comparison with the azido ligand. In principle, the reaction of a covalent cyanide transfer reagent (e.g. TMSCN) with PbF$_4$ would afford Pb(CN)$_4$(L)$_2$ (L = e.g. MeCN, py). Subsequent reaction with [PPN]CN could form [PPN]$_2$[Pb(CN)$_6$], in analogy to the preparation of [PPN]$_2$[Sn(CN)$_6$] from SnF$_4$. However, the inability to obtain PbF$_4$ in sufficient purity precluded reliable characterisation of all solid products formed from the reaction between "PbF$_4$" and TMS$-$CN. This, combined with the instability of PbCl$_4$, necessitated the reaction between the more stable [PbCl$_6$]$^{2-}$ anion and ionic cyanide transfer reagents as the only feasible strategy towards [Pb(CN)$_6$]$^{2-}$ (scheme 14).
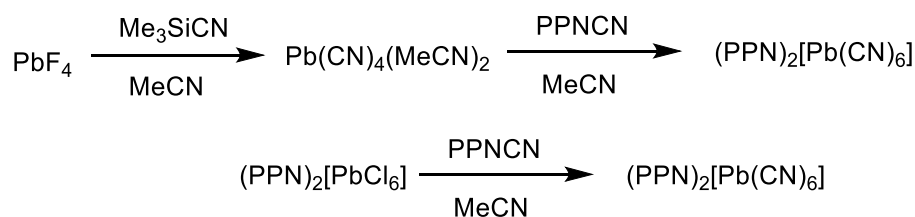
Scheme 14. Proposed synthetic routes towards [PPN]$_2$[Pb(CN)$_6$] using covalent (TMS$-$CN) and ionic ([PPN]CN) cyanide transfer reagents.

A solution of [PPN]$_2$[PbCl$_6$] in MeCN was treated with [PPN]CN under identical conditions to those which afforded the hexa(cyanido)germanate anion. Despite the use of multiple batches of excess [PPN]CN, IR spectroscopic monitoring showed no reaction. Repetition of the reaction using NaCN, a strategy which facilitated complete chloride-cyanido exchange in [Ge(CN)$_6$]$^{2-}$, also failed to achieve any ligand substitution. The decreased reactivity of Pb(IV) versus Si$-$Sn(IV) centres towards chlorido/cyanido ligand exchange is attributed to an increased activation barrier for ligand exchange, owing to a greater overlap of the larger Pb(IV) coordination centre with the chloride ligands versus the lighter homologues. A reduction in the thermodynamic driving force for ligand exchange arises from the presence of anionic Pb(IV) in both starting material and products, in contrast to the generation of a stable salt *only* upon formation of [Sn(CN)$_6$]$^{2-}$ from Sn(CN)$_4$(L)$_2$. Both of these factors are anticipated to contribute to the difficulties in preparing [Pb(CN)$_6$]$^{2-}$. Although the thermodynamic driving force for

ligand exchange may be increased through the reaction of TMSCN and PbF$_4$, it is unclear to what extent ligand exchange could be achieved.

3.2.6 Comparison of [E(CN)$_6$]$^{2-}$ in [PPN]$_2$[E(CN)$_6$] (E = Si, Ge, Sn)

Reactivity

The [E(CN)$_6$]$^{2-}$ anions (E = Si–Pb) exhibit a decreasing trend in reactivity down group 14 (table 19). Of the four coordination centres, silicon is most predisposed towards chloride/cyanide exchange and requires only two treatments of excess [PPN]CN to achieve complete exchange.[147,169] In contrast, an extra thermodynamic driving force is required to prepare chlorine-free [Ge(CN)$_6$]$^{2-}$ and is achieved by formation of an insoluble byproduct. [PPN]$_2$[Sn(CN)$_6$] was unable to be prepared from the sole reaction of CN$^-$ with SnCl$_4$. Covalent cyanide transfer reagents were also required to impart additional (and stronger) enthalpic and entropic forces for complete ligand exchange. The trend in reactivity is concluded with E = Pb, which showed no exchange towards ionic cyanide transfer reagents.

E	Cyanido Transfer Reagent			Comments	
	Identity	**Type**	**n**		
Si	[PPN]CN	Ionic	2	Complete exchange [147,169]	Most reactive
Ge	[PPN]CN + NaCN	Ionic	3	[PPN]CN insufficient	
Sn	TMS−CN + [PPN]CN	Covalent + Ionic	1 each	[PPN]CN insufficient	
Pb	NaCN / [PPN]CN	Ionic	−	No reaction	Least reactive

Table 19. Comparison of synthetic strategies for the preparation of [PPN]$_2$[E(CN)$_6$] (E = Si, Ge, Sn, Pb). n represents the number of treatments of cyanido transfer reagent.

The air sensitivity of the complexes also increases down the group. [PPN]$_2$[Si(CN)$_6$] displays relative stability in air, whilst [PPN]$_2$[Sn(CN)$_6$] rapidly hydrolyses of upon exposure to trace amounts of moisture.[147,169] This trend in air sensitivity is reflected spectroscopically by the detection of hydrolysis products in the mass- and ^{13}C NMR spectra of [PPN]$_2$[Ge(CN)$_6$] and [PPN]$_2$[Sn(CN)$_6$], respectively. The charge-neutral complexes of Sn(IV) and Sn(II) showed the greatest sensitivity to air, to the point where complete characterisation was hindered. The more rapid decoordination of volatile ancillary ligands may contribute to a decreased air stability versus the anionic homoleptic complexes which contain less-volatile ligands.
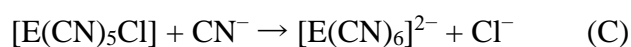
	[PPN]$_2$[E(CN)$_6$]			Sn(CN)$_4$(L)$_2$	
	Si	**Ge**	**Sn**	**L = MeCN**	**L = py**
ν(CN) / cm^{-1} [a]	2172, 2163	2164, 2159	2157, 2153, 2146	2182, 2178	2165
ν(CN) / cm^{-1} [b]	2169	2161	2157	−	−
δ(**C**N) / ppm [c]	139.9	140.0	138.5	−	113.8 [d]
Refs.	[147,169]		This work		

Table 20. Comparison of spectral data of cyanido complexes prepared in this chapter. Data for [PPN]$_2$[Si(CN)$_6$] has been provided as a comparison. [a] as nujol mull ; [b] in MeCN solution ; [c] in CD$_3$CN ; [d] in C$_5$D$_5$N.

Identity	Si	Ge	Sn
[PPN][E(CN)$_6$]$^-$	●		
[E(CN)$_6$]$^{2-}$	●		
[E(CN)$_5$]$^-$			●
[E(CN)$_3$]$^-$			●

Table 21. Summary of identity of most intense cyanido-containing fragments observed (●) in negative ion electrospray (ESI$^-$) mass spectra of [PPN]$_2$[E(CN)$_6$] (E = Si, Ge, Sn). No CN-containing fragments were observed in the mass spectrum of [PPN]$_2$[Ge(CN)$_6$].

Theoretical calculations for the mechanism of formation of [E(CN)$_6$]$^{2-}$ (E = Si−Pb) have been performed in both gas and solution phases (scheme 15) and align with the experimentally-observed outcomes of reactions between ECl$_4$ and [PPN]CN for the centres studied in this work.[169] The calculated Gibbs free energies, ΔG_{sol}, of the formation of [E(CN)$_6$]$^{2-}$ (E = Si, Ge) is lowest (and therefore most spontaneous) for the formation of the complex from [E(CN)$_5$Cl] (scheme 16). This indicates that formation proceeds by the exchange of Cl$^-$ with CN$^-$ from [E(CN)$_5$Cl] (i.e., the additional two CN ligands coordinate *prior* to full chloride/cyanido ligand exchange). In comparison, the calculated energies for E = Sn show that this mechanism is not spontaneous and is less favourable than those which begin from homoleptic Sn(CN)$_4$ (A) or [Sn(CN)$_5$]$^-$ (B) (figure 25). These calculations confirm that, in contrast to E = Si and Ge, [PPN]$_2$[Sn(CN)$_6$] cannot solely be prepared from chloride/cyanide ligand exchange. The [Pb(CN)$_6$]$^{2-}$ anion is predicted to form via the same (albeit less favourable) mechanism observed for the stannate analogue.[169] Although the initial attempts to prepare the [Pb(CN)$_6$]$^{2-}$ anion appear to align with this prediction, the inability to prepare Pb(CN)$_4$ (or adducts thereof) prevented the investigation of this methodology in more detail.

$$E(CN)_4 + CN^- \rightarrow [E(CN)_5]^- \qquad\qquad (A)$$

$$[E(CN)_5]^- + CN^- \rightarrow [E(CN)_6]^{2-} \qquad\qquad (B)$$

$$[E(CN)_5Cl] + CN^- \rightarrow [E(CN)_6]^{2-} + Cl^- \qquad (C)$$

Scheme 15. Reactions leading to formation of $[E(CN)_6]^{2-}$ investigated theoretically.[169]

$$[Si(CN)_5Cl]^{2-} + CN^- \longrightarrow [Si(CN)_6]^{2-} + Cl^-$$

$$[Ge(CN)_5Cl]^{2-} + CN^- \longrightarrow [Ge(CN)_6]^{2-} + Cl^-$$

$$Sn(CN)_4 + CN^- \longrightarrow [Sn(CN)_5]^- + CN^- \longrightarrow [Sn(CN)_6]^{2-}$$
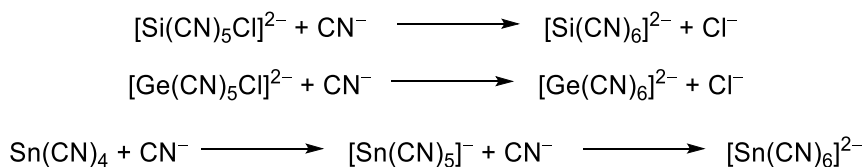
Scheme 16. Most favourable reaction pathways for the formation of $[E(CN)_6]^{2-}$ (E = Si−Sn).[169]
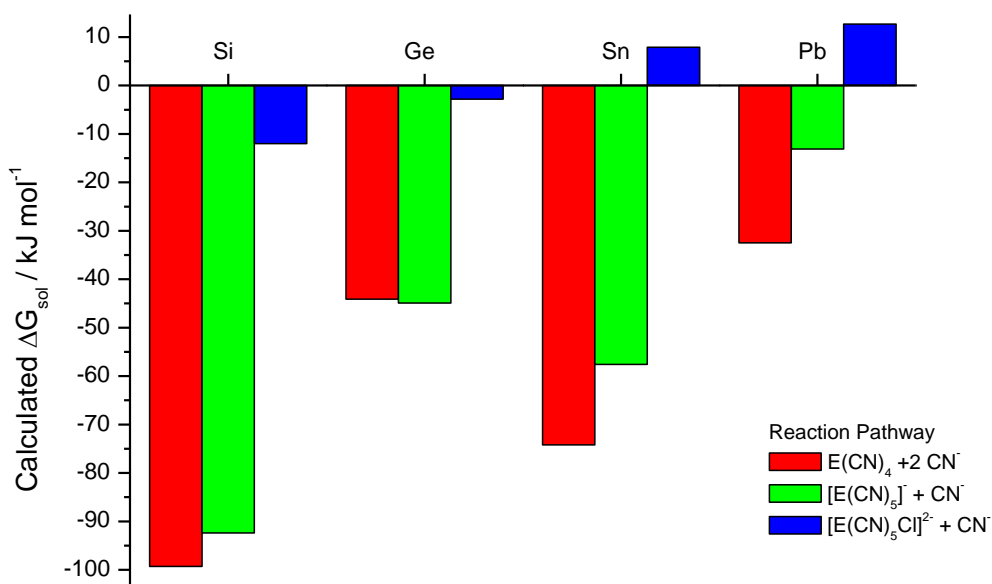
Figure 25. Solution-phase Gibbs energies calculated for the formation of $[E(CN)_6]^{2-}$ through each reaction pathway. Data obtained from reference [169].

The spectral position of a $\nu(CN)$ band decreases with increasing ionic character, as demonstrated by the respective positions of the $\nu(CN)$ band of covalent (e.g. TMS−CN, $\nu(CN)$ = 2190 cm^{-1}) versus ionic (e.g. [PPN]CN, $\nu(CN)$ = 2056 cm^{-1}) cyanide transfer reagents in the solid state.[179] The spectral position of the $\nu(CN)$ bands in the IR spectra of $[E(CN)_6]^{2-}$ decreases with increasing size and mass of the coordination centre (figure 26, table 20). The positions of the $\nu(CN)$ bands of charge-neutral $Sn(CN)_4(L)_2$ are higher than those of $[PPN]_2[Sn(CN)_6]$ (+30 cm^{-1} and +13 cm^{-1} for L = MeCN and py, respectively). This confirms that the former possess a greater degree of covalency than the anionic, hypercoordinate $[Sn(CN)_6]^{2-}$ anion and offers an explanation for the inability to decoordinate the ancillary solvent ligands in

Sn(CN)$_4$(MeCN)$_2$. In analogy to the poly(azido) complexes, the ν(CN) bands of the dicyanotin(II) adducts are observed at lower spectral positions than the Sn(IV) analogues.[102,176] However, no further conclusions can be drawn regarding the reactivity of the analogous cyanido complexes of E(II) (E = Ge, Sn) owing to their comparative infrequency and lack of characterisation data.
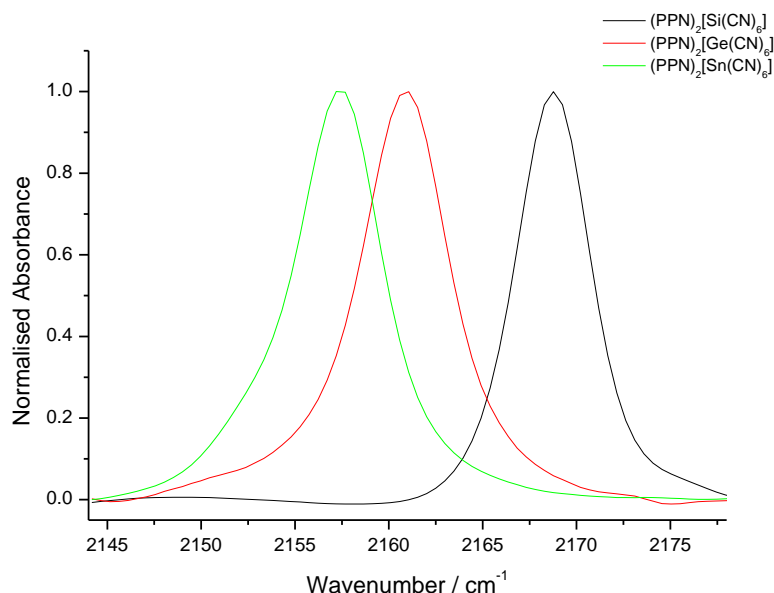
Figure 26. IR spectra of MeCN solutions of [PPN]$_2$[E(CN)$_6$] (E = Si (black line, −), Ge (green line, −), Sn (red line, −)) between 2178−2145 cm^{-1}. Each spectrum has been normalised to the most intense ν(CN) band. Data for [PPN]$_2$[Si(CN)$_6$] obtained from reference [147].

The IR spectra of all three complexes exhibit a single ν(CN) band in solution due to the adoption of perfect octahedral geometry (O$_h$ point group). An increased number of bands in the solid state occurs due to a reduction in symmetry, arising from packing arrangements and resulting in a greater number of IR-active CN stretching vibrations than in solution (tables 20, 22). The crystal structure of the [Ge(CN)$_6$]$^{2-}$ anion lacks an inversion centre and is assigned as point group C$_1$. However, the absence of IR active stretching vibrations of the CN ligands in this point group suggests that the anion instead possesses D$_{3d}$ symmetry, which contains IR active stretches. The observation of fewer ν(CN) bands than predicted is attributed to overlap of bands. The symmetry, number and location of the ν(CN) band in solution-phase IR spectra are supported by theoretical calculations.[169]

[PPN]$_2$[E(CN)$_6$]	Point Group [a]	IR active stretching vibrations	n(ν(CN)) Expected	n(ν(CN)) Observed
Si	D$_{2h}$	B$_{1u}$, B$_{2u}$, B$_{3u}$	3	2
Ge	D$_{3d}$ [b]	A$_{2u}$, 2E$_u$	3	2
Sn	D$_{2h}$	B$_{1u}$, B$_{2u}$, B$_{3u}$	3	3

Table 22. Comparison of point groups adopted in solid [PPN]$_2$[E(CN)$_6$]$^{2-}$ (E = Si, Ge, Sn) and the expected (n$_e$) number of ν(CN) bands, n{ν(CN)}, versus those observed (n$_o$). [a] deduced from crystallographic analysis; [b] Ge is considered to possess D$_{3d}$ symmetry, as discussed above.

The comparative intensities of the ν(CN) bands of [E(CN)$_6$]$^{2-}$ in solution are significantly weaker than the ν$_{as}$(N$_3$) bands of the analogous [E(N$_3$)$_6$]$^{2-}$ complexes and is attributed to the weaker dipole moment of the former anions. The relative absorbance intensities of the ν(CN) band decrease from Sn>Si>Ge, a trend which is also predicted theoretically.[169] The CN ligands of all three complexes show ^{13}C NMR resonances above those attributed to [PPN]$^+$ and shift upfield as the coordination centre changes from Si−Sn (table 23).

	[PPN]$_2$[Si(CN)$_6$]	[PPN]$_2$[Ge(CN)$_6$]	[PPN]$_2$[Sn(CN)$_6$]	[PPN]$_2$[Pb(CN)$_6$]
δ(CN) / ppm	139.9	140.0	138.5	−

Table 23. Comparison of ^{13}C NMR signals attributed to the CN ligands of [PPN]$_2$[E(CN)$_6$] (E = Si−Pb). – denotes no spectra recorded. Data for [PPN]$_2$[Si$_{(CN)6}$] obtained from reference [169].
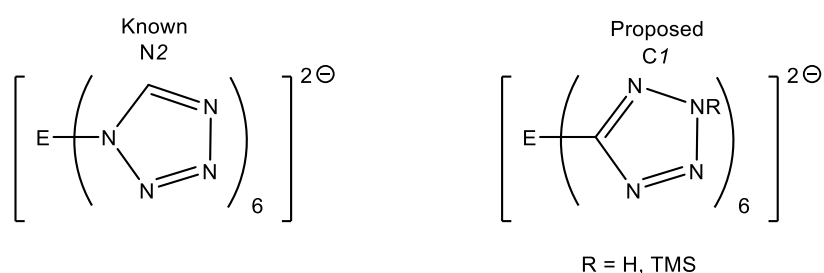
3.2.7 Cycloaddition reactions of cyano-complexes of group 14

Whilst the syntheses of the group 14 hexa(cyanido) complexes of E(IV) (E = Si−Sn) demonstrate the formation of rare or previously-unknown octahedral C-N frameworks, their low nitrogen content renders them unsuitable candidates for novel nitrogen-rich energetic materials. The [3+2] cycloaddition ('click') reaction between nitriles and azides to form tetrazoles (RCHN$_4$, scheme 17) is well-documented and similar reactions between poly(azido) silicon complexes and organic nitriles RCN (R = e.g., Me, py) were previously used to prepare substituted tetrazolato complexes.[180,181] Homoleptic hexakis(tetrazolato) complexes, prepared previously within the group, represent only the second homoleptic complexes of group 14 that contain nitrogen-rich ligands.[104] The elevated nitrogen content of tetrazolates (CHN$_4^-$ = 60% N) vs cyanides (CN$^-$ = 35% N) identifies tetrazolato complexes as potential ligand candidates in novel nitrogen-rich coordination complexes. The tetrazolato ligands in [E(CHN$_4$)$_6$]$^{2-}$

(E = Si, Ge, Sn) coordinate at the N*2* position. By contrast, a cycloaddition reaction between $[E(CN)_6]^{2-}$ and an azide group would result in a coordinatively isomeric tetrazolato ligand (figure 27). This could impact on the reactivity and properties of such complexes through alteration of packing or intermolecular interactions.
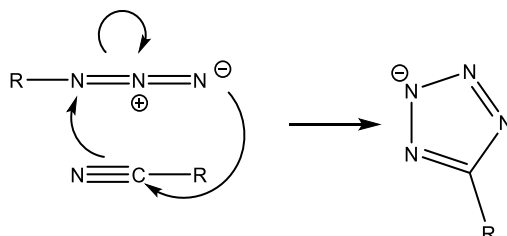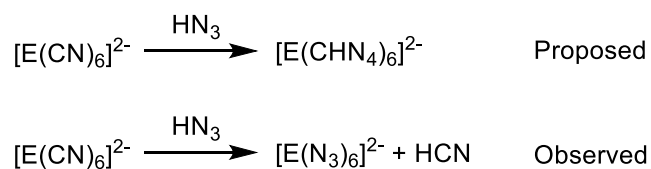

Scheme 17. Formation of a tetrazolato group by the cycloaddition reaction of a nitrile and azide.

R = H, TMS

Figure 27. Structure of known (left) and proposed (right) group 14 tetrazolato complexes. E = Si−Sn.

To test the propensity and feasibility of cycloaddition reactions involving $[E(CN)_6]^{2-}$ anions, separate samples of $[PPN]_2[Sn(CN)_6]$ were reacted with the covalent azide transfer reagents $TMSN_3$ and HN_3 (scheme 18). Tetrazolato ligands possess few characteristic IR-active stretching vibrations and the reactions were instead monitored by the disappearance of IR-active $\nu(CN)$ and $\nu_{as}(N_3)$ bands of the anion and transfer reagent, respectively, or by the spectral changes of ^1H NMR resonances associated with coordinated tetrazolato ligands, TMS−CN or $TMSN_3$. In both reactions, addition of covalent azide transfer reagent lead only to cyanido-azido ligand substitution, as observed by the growth in both the $\nu_{as}(N_3)$ bands in the spectral region of Sn(IV) poly(azido) complexes in the IR spectrum and the growth of the resonance associated with TMS−CN in the ^1H NMR spectrum. No evidence of coordinated tetrazolato ligands were observed in either reaction. It is clear from these exploratory reactions that ligand exchange occurs preferentially to cycloaddition owing to the enhanced coordination strength of the azido ligand versus the cyanido ligand towards group 14 coordination centres. These findings help to quantify the requirement for greater driving forces (longer heating times, insoluble, highly stable and/or gaseous byproducts) for the formation of homoleptic poly(cyanido) complexes.

$$[E(CN)_6]^{2-} \xrightarrow{HN_3} [E(CHN_4)_6]^{2-} \qquad \text{Proposed}$$

$$[E(CN)_6]^{2-} \xrightarrow{HN_3} [E(N_3)_6]^{2-} + HCN \qquad \text{Observed}$$

Scheme 18. Proposed versus observed reactions of $[PPN]_2[Sn(CN)_6]$ and RN_3.

3.3 Conclusions and Outlook

The use of both ionic and covalent cyanido transfers reagents has facilitated the preparation of several new poly(cyanido) complexes of germanium and tin, complementing the existing salts of $[Si(CN)_6]^{2-}$. The weakened coordination ability of the CN^- anion versus N_3^- towards the group 14 centres results in synthetic challenges in driving ligand exchange to completion versus the preparation of $[E(N_3)_6]^{2-}$ salts. The $[E(CN)_6]^{2-}$ anion in $[PPN]_2[E(CN)_6]$ (E = Ge, Sn) represents the first (E = Ge) and third (E = Sn) octahedrally coordinated $E-C_6$ bond framework. The use of several treatments of ionic cyanide transfer reagents (E = Si) or covalent cyanido transfer reagents (E = Sn) to achieve complete ligand exchange demonstrates the decreasing reactivity of ECl_4 towards cyanide salts down group 14. The isolation of $[PPN][Ag(CN)_2]\cdot MeCN$, following the use of AgCN as an ionic cyanido transfer reagent, demonstrates the unsuitability of non-innocent salts as cyanide transfer reagents. The calculated energies (and implied spontaneities) for chlorido/cyanido exchange for chlorides of Si−Pb mirror the results observed experimentally, including the lack of reactivity of $[PbCl_6]^{2-}$ towards ionic cyanide transfer reagents.

$Sn(CN)_x(L)_2$ ($x = 2$ or 4) are the first examples of charge-neutral adducted group 14 di- or tetra-cyano complexes. Whilst the coordination strength of the ancillary ligands in $Sn(CN)_4(L)_2$ is sufficient to prevent the formation of neutral $Sn(CN)_4$, the partial decoordination of one or both ancillary ligands of $Sn(CN)_2(L)_2$ demonstrates the decreased coordination strength of the cyano ligand towards Sn(II) centres than Sn(IV). This reactivity contrasts that of the neutral azido complexes of both Sn(IV) and Sn(II), where ligand decoordination is facile (and in some cases spontaneous) at ambient conditions.[102,176] The ready cyanido-azido ligand substitution reactions observed upon the reaction of $[PPN]_2[Sn(CN)_6]$ with covalent azide transfer reagents appears to limit the effectivity of the use of group 14 hexa(cyanido) complexes as precursors towards cyclisation reactions with azides.

Initial future work could focus on identification of alternative synthetic pathways to access the unisolable poly(cyanido)complexes investigated in this study. A source of analytically-pure PbF_4 is required to conclusively investigate the reactivity of the cyanido ligand towards both covalent cyanide transfer reagents and could be a route to the preparation of the unknown $[Pb(CN)_6]^{2-}$ salts (scheme 19). The syntheses of the currently-unknown $[Ge(CN)_3]^-$, and further studies on $Ge(CN)_2$, would provide further information on the coordinative behaviour of the CN ligand towards low-valent Ge(II) centres and allow comparison to the recently-studied poly(azido) complexes of the same centre (see chapter 3 and reference [182]).

$$PbF_4 + 4TMSCN \xrightarrow[\text{-4TMSF}]{\text{ex.PPNCN}} (PPN)_2[Pb(CN)_6]$$
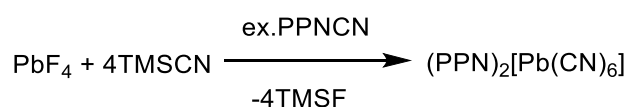
Scheme 19. Proposed formation of $[PPN]_2[Pb(CN)_6]$ from PbF_4.

Although the ancillary ligands of $Sn(CN)_4(L)_2$ have been shown to be readily displaced by other ligands such as DMF and DMSO, the increased coordinative strength and lower volatility of these ligands means that their decoordination is even less feasible than for MeCN and pyridine and $Sn(CN)_4$ remains uncharacterised. Thermogravimetric analysis (TGA) may reveal at what temperatures $Sn(CN)_4$ is formed under these conditions, if at all. The significant air-sensitivity of both adducts prepared in this work may require the syntheses of complexes containing bulkier, more strongly coordinating ancillary ligands to strike a balance between ancillary ligand volatility (to allow facile decoordination at feasible temperatures) and minimal hydrolysis. The thermal decomposition of poly(cyanido) complexes of group 14 (scheme 20) may offer promising applications in the formation of lighter group 14 carbides or carbon-nitrogen materials, similarly to those discussed later in this thesis (see chapter 3). Comprehensive characterisation of the thermal decomposition pathways, alongside careful tuning of ancillary ligands and cations, are essential for investigative work into this area.

$$E(CN)_4(L)_2 \xrightarrow[\text{-2L}]{\Delta} E(CN)_4 \xrightarrow[\text{-N}_2]{\Delta} EC_4$$

$$[E(CN)_6]^{2-} \xrightarrow[\text{-3N}_2]{\Delta} [EC_6]^{2-}$$
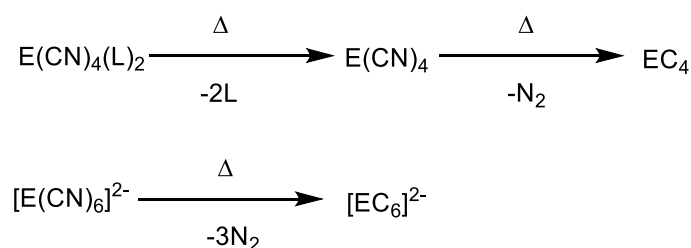
Scheme 20. Proposed thermally-induced formation of $E(CN)_4$ and EC_x (E = Ge, Sn, x = 4 or 6).

# Chapter 4. Charge-neutral, low-valent germanium azides

4.1. Introduction

4.1.1 Ge(IV) azido complexes

Homoleptic poly(azido) complexes containing Ge(IV) coordination centres are known in the form of germanium tetraazide, $Ge(N_3)_4$, and the hexa(azido)germanate anion, $[Ge(N_3)_6]^{2-}$. Both complexes are reported to be prepared from the reaction of $GeCl_4$ and NaN_3 in THF. The noticeable spectral similarities between both complexes in solution ($v_{as}(N_3) = 2133$ cm^{-1} for $Ge(N_3)_4$ vs 2123 cm^{-1} for $[Ge(N_3)_6]^{2-}$ in CCl_4 and THF, respectively) supports the hypothesis that $\{Na(THF)\}_2[Ge(N_3)_6]$ was formed instead of $Ge(N_3)_4$.[96,183] Dry $\{Na(THF)\}_2[Ge(N_3)_6]$ is friction sensitive and exploded upon grinding; although the exact identity of the sensitive component was not identified, it was speculated that loss of THF induces decomposition of $Na_2[Ge(N_3)_6]$ to $Ge(N_3)_4$. In contrast, the incorporation of phlegmatising, carbon-rich cations as $[PPN]_2[Ge(N_3)_6]$ affords energetic stability to the extent that the compound is isolable, insensitive towards energetic stimuli and melts without decomposition at elevated temperatures ($T_m = 211$ °C) (scheme 21).[96]

$$GeCl_4 \xrightarrow[\text{THF, 66 °C}]{NaN_3} \{Na(THF)\}_2[Ge(N_3)_6] \xrightarrow[\text{MeCN, rt}]{PPN(N_3)} (PPN)_2[Ge(N_3)_6]$$
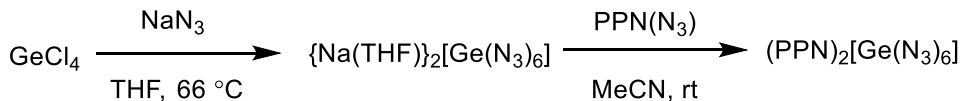
Scheme 21. Synthesis and isolation of $[PPN]_2[Ge(N_3)_6]$.[96]

$Ge(N_3)_4$ can also be stabilised by the complexation of neutral ancillary ligands. Treatment of $Na_2[Ge(N_3)_6]$ with mono- or bidentate chelating Lewis bases, i.e. bipy or py respectively, has been reported to result in the formation of charge-neutral adducts of $Ge(N_3)_4$ as $Ge(N_3)_4(L)$ (L = bipy, phen) or $Ge(N_3)_4(L)_2$ (L = py, pic) (scheme 22, figure 28).[147,167] Ancillary ligand coordination is evidenced by the formation of $v_{as}(N_3)$ bands at lower wavenumbers than that of $Na_2[Ge(N_3)_6]$ (table 24) alongside the visible elimination of NaN_3.

$$2NaN_3 + Ge(N_3)_4(L)_2 \xleftarrow{2L} \{Na(THF)\}_2[Ge(N_3)_6] \xrightarrow{L'} Ge(N_3)_4(L') + 2NaN_3$$

L =

L' =
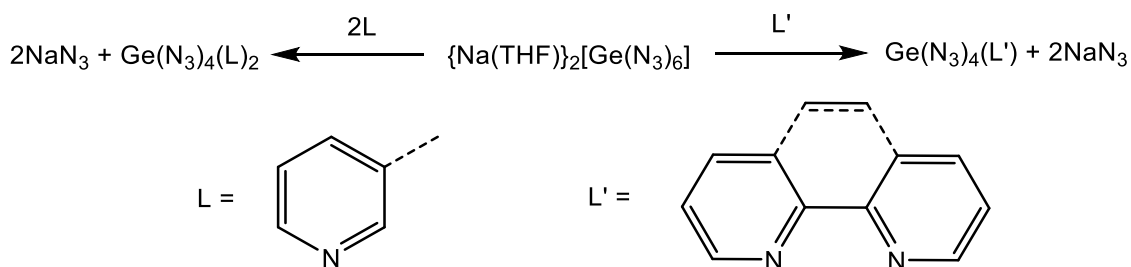
Scheme 22. Preparation of base-stabilised complexes of $Ge(N_3)_4$ from the $[Ge(N_3)_6]^{2-}$ anion.

Complex	Ancillary ligand	$\nu_{as}(N_3)$ / cm^{-1}	T$_{dec}$ / °C
Ge(N$_3$)$_4$(L)	bipy	2120, 2097, 2091	273
	phen	2120, 2093	205
Ge(N$_3$)$_4$(L)$_2$	py	2117, 2091	271
	pic	2116, 2092	256
Na$_2$[Ge(N$_3$)$_6$]	–	2123, 2089 [a]	– [b]
[PPN]$_2$[Ge(N$_3$)$_6$]	–	2083	211[c]

Table 24. Comparison of asymmetric azide bands and decomposition temperatures for base-stabilised neutral Ge(IV) tetra(azido) complexes in MeCN.[147] [a] in THF; [b] not measured ; [c] melts without decomposition.

Both the mono- and bis- adducted complexes of Ge(N$_3$)$_4$ form as crystalline solids and are rendered stable towards regular preparative handling operations, displaying high decomposition temperatures (T$_d$ = 205−271 °C) comparable to the melting point of [PPN]$_2$[Ge(N$_3$)$_6$] (T$_m$ = 211 °C).[96,147] The absence of the chelate effect leads to the formation of equilibria between the monodentate adducts and Ge(N$_3$)$_4$ in solution (scheme 23) which can be observed using IR spectroscopy.[147] No attempts to decoordinate ancillary ligands of any adduct have been reported.

$$Ge(N_3)_4(py)_2 \rightleftharpoons Ge(N_3)_4(py) + py \rightleftharpoons Ge(N_3)_4 + 2py$$
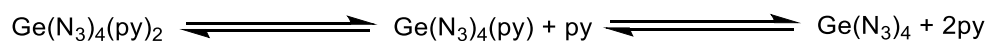
Scheme 23. Equilibrium observed between Ge(N$_3$)$_4$(py)$_2$ and Ge(N$_3$)$_4$ in solution.
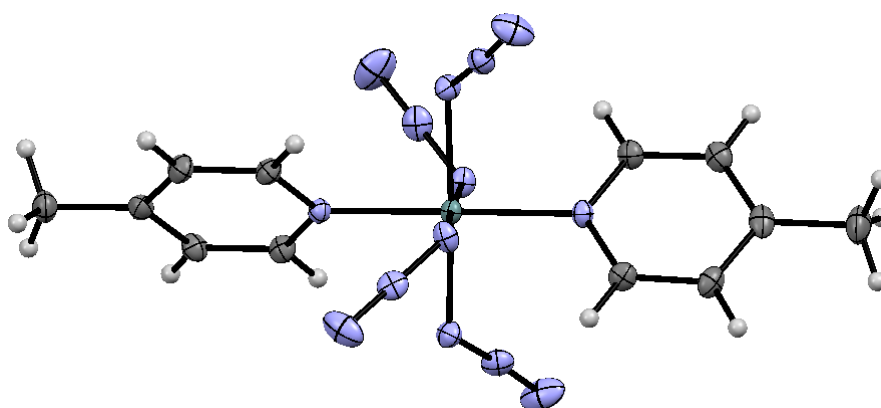
Figure 28. Crystal structure of Ge(N$_3$)$_4$(pic)$_2$. Turquoise = Ge, blue = N, grey = C. Structure generated from data from reference [147].

4.1.2 Low-valent Group 14 azido complexes: Si, Sn

Although poly(azido) coordination complexes containing group 14 E(IV) centres are extensively reported (E = Si−Sn), those containing low-valent (E(II)) central elements are less common. Si(II) dihalide complexes have been prepared through stabilisation afforded from a strongly σ-donating N-heterocyclic carbene (NHC) ligand as $(NHC)SiX_2$ (X = Cl, Br, I, figure 29).[184–186] The extremely strong ligating ability of the NHC ligand appears critical to the stabilisation of Si(II) coordination centres. However, to date all attempts to prepare Si(II) diazides (NHC-stabilised or otherwise) have been unsuccessful and $Si(N_3)_2(L)_x$ (x = 1 or 2, L = e.g. py or bipy) remain unknown.[187]
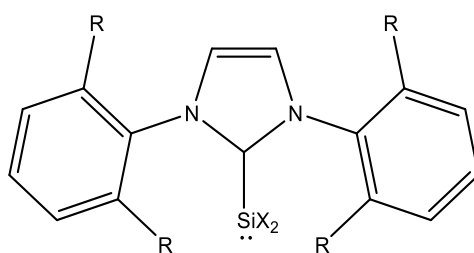
Figure 29. General structure of some NHC-stabilised Si(II) coordination complexes. When X = Cl, Br, R = ^iPr ; when X = I, R = Dipp (diisopropylphenyl). For clarity, only a single resonance form is shown. [184–186]

The additional stabilisation afforded by the coordination of strongly σ-electron donating or chelating ligands to Si(II) centres is not required for Sn(II) and di(azido) complexes of Sn(II) are easily prepared from the reaction of SnF_2 and Me_3SiN_3 (scheme 24). In analogy to the high-valent complexes, the coordination of monodentate Lewis base ligands is sufficient to allow safe isolation and handling as $Sn(N_3)_2(L)_2$ (L = py, pic, figure 30).[176] However, in ambient conditions the ancillary ligands undergo spontaneous decoordination to yield $Sn(N_3)_2$, demonstrating the decreased stabilisation effect of these weakly coordinating and volatile ancillary ligands towards Sn(II) versus Sn(IV). Decoordination can also be rapidly induced through application of high vacuum (scheme 25) and consequently the adducts are only stable in solution or when suspended in excess ligand.[176] As expected for a neutral binary azide, $Sn(N_3)_2$ is an extremely sensitive, energetic compound which may explode upon initiation through shock or electrostatic discharge.[176]

$$SnF_2 + Me_3SiN_3 \xrightarrow{L} Sn(N_3)_2(L)_2 + 4Me_3SiF$$
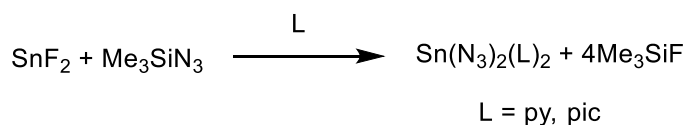
L = py, pic

Scheme 24. Synthesis of $Sn(N_3)_2(L)_2$ (L = py, pic).[176]

$$Sn(N_3)_2(py)_2 \xrightarrow[\text{2) high vacuum}]{\text{1) MeCN}} Sn(N_3)_2$$
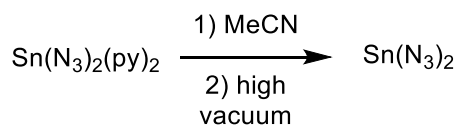
Scheme 25. Preparation of $Sn(N_3)_2$ by removal of ancillary ligands.
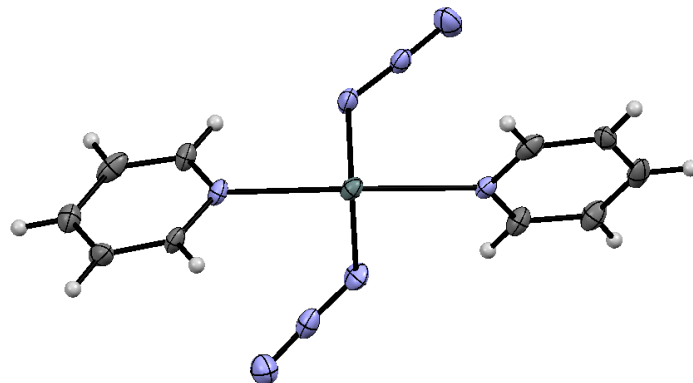
Figure 30. Crystal structure of $Sn(N_3)_2(py)_2$. Turquoise = Sn, blue = N, grey = C. Structure obtained from data from reference [176].

4.1.3 Low-valent Group 14 azido complexes: Ge

Unlike Si(II), select complexes containing Ge(II) centres can be stabilised and isolated without the requirement for a strongly coordinating NHC ligand. For example, the stabilisation of $GeCl_2$ by dioxane renders $GeCl_2(diox)$ thermally stable at room temperature. The reported syntheses of several Ge(II) pseudohalogen complexes including $Ge(NCO)_2$, $Ge(NCS)_2$ and $Ge(CN)_2$ demonstrate the capability of pseudohalide ligands to stabilise low-valent germanium centres.[155] The kinetic stabilisation of Ge(II) monoazido complexes afforded by the presence of either intramolecular, strongly-coordinating NHC or bulky chelating ligands implies that, in analogy to the as-yet unknown Si(II) diazide, a strongly coordinating and non-volatile ligand is required to stabilise a neutral Ge(II) azido complex (figure 31).[188–192]

Intramolecular stabilisation

N-heterocyclic carbene coordination

R = EtO

Bulky ligand chelation
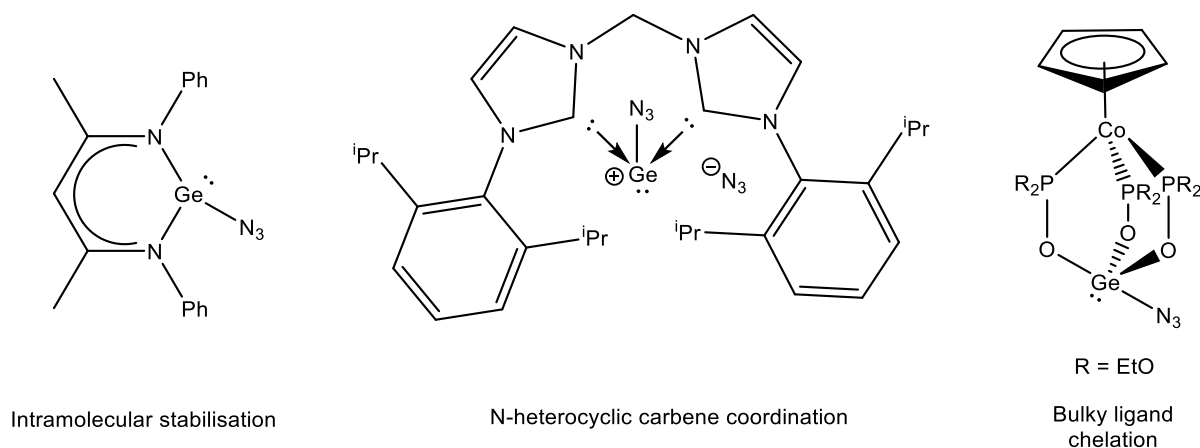
Figure 31. Structures and stabilisation strategies of three mono(azido) complexes of Ge(II).[188–192]

54

Homoleptic tri(azido)germanate salts, $[Ge(N_3)_3]^-$, are prepared directly as $(cat)[Ge(N_3)_3]$ (cat^+ = $[PPN]^+$, $[Ph_4P]^+$) from NaN_3, $[PPh_4]N_3$ and $GeCl_2(diox)$ or $[PPN][GeCl_3]$ (scheme 26, figure 32). The incorporation of a carbon-rich cation in the salt stabilises the compound towards regular preparative operations and long-term storage under inert atmospheres. To date, salts containing the $[Ge(N_3)_3]^-$ anion are the only low-valent germanium poly(azido) complex stabilised without strongly coordinating NHC ligands.[182]

$$GeCl_2(diox) \xrightarrow[\text{MeCN}]{\text{[PPN]Cl}} [PPN][GeCl_3] \xrightarrow[\text{THF}]{\text{NaN}_3} [PPN][Ge(N_3)_3] + NaCl$$
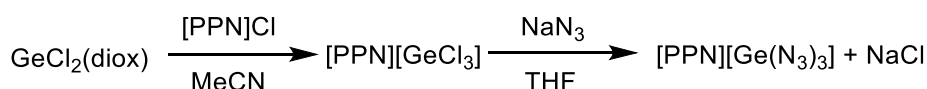
Scheme 26. Synthesis of $[PPN][Ge(N_3)_3]$.[182]
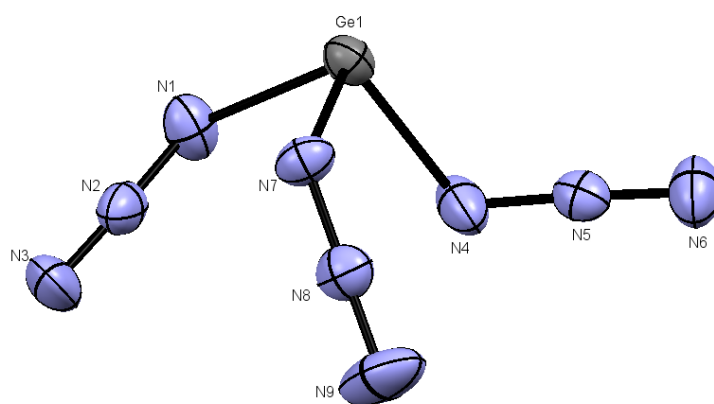
Figure 32. Molecular structure of the $[Ge(N_3)_3]^-$ anion in crystals of $[PPh_4][Ge(N_3)_3]$. Structure obtained from data from reference [182].

Germanium (II) diazide, $Ge(N_3)_2$, is unknown and consequently occupies an interesting position between the unknown $Si(N_3)_2$ and the recently-reported $Sn(N_3)_2$. In agreement with the known homoleptic, charge-neutral poly(azido) complexes such as $Si(N_3)_4$ and $Pb(N_3)_2$, the absence of phlegmatising ligands or cations means that $Ge(N_3)_2$ is predicted to be extremely unstable. $IPrGe(N_3)_2$ is the only charge-neutral di(azido) complex of germanium(II) diazide known and is prepared by ligand exchange between $IPrGeCl_2$ and NaN_3. The stabilisation afforded by the coordination of a strongly σ-electron donating NHC ligand facilitates isolation and characterisation of $IPrGe(N_3)_2$ under inert atmospheres (scheme 27).[193] No attempts to remove the NHC ligand are reported and the extremely strong coordination and low volatility of the IPr ligand is anticipated to prevent decoordination without decomposition of the entire complex. The preparation of $IPrGe(N_3)_2$ proves that Ge(II) *is* capable of coordinating two azido ligands, although it is unclear to what extent this is facilitated by the presence of a NHC ligand. Although Lewis base adducts of Ge(II) dihalides are known, no Lewis base-stabilised adducts

of Ge(N$_3$)$_2$ are reported and the stabilisation ability of volatile Lewis bases towards germanium(II) diazide is unclear. Consequently, the formation of Ge(N$_3$)$_2$ from any Ge(II) diazido complex is also unreported.
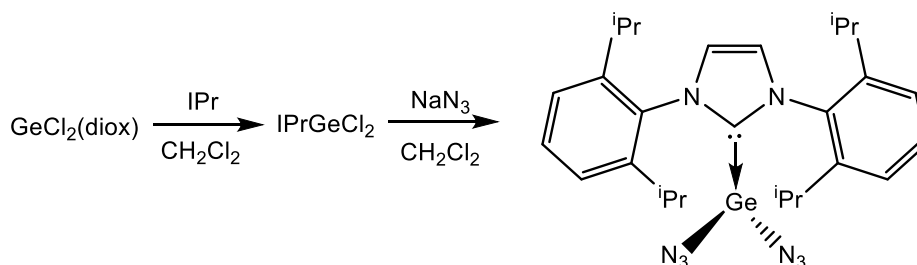
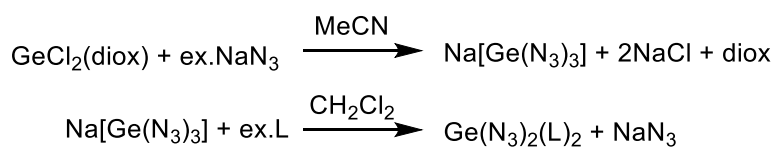**Scheme 27.** Synthesis of IPrGe(N$_3$)$_2$ from GeCl$_2$(diox) and IPr.[193]

The stabilisation of Ge(N$_3$)$_4$ afforded by coordination of labile, monodentate ligands identifies an important investigative topic to determine if Ge(N$_3$)$_2$ can be stabilised in the same fashion, as Ge(N$_3$)$_2$(L)$_2$ (L = e.g. py, pic).[147] The isolation of such complexes would allow detailed reactivity and coordination studies of neutral Ge(II) coordination centres towards azido ligands, and facilitate comparisons between the analogous low- and high- valent complexes of group 14 in the absence of strong σ-donating ligands (i.e., NHC's). The pseudohalogen concept suggests that the coordination behaviour of a pseudohalide should be analogous to other pseudohalide or halide ligands. The preparation of other bis(pseudohalogenido) complexes of Ge(II) as GeY$_2$ suggests that Ge(N$_3$)$_2$ may be accessible (albeit highly unstable, in analogy to the other binary charge-neutral group 14 azides).[155] The existence of Ge(CN)$_2$ is a particularly promising indicator that Ge(N$_3$)$_2$ is isolable, owing to the relative increase in reactivity of azido ligands versus cyanido ligands as discussed in chapter 2. Once prepared, Ge(N$_3$)$_2$(L)$_2$ could act as precursors for the preparation of Ge(N$_3$)$_2$ by facile removal of ancillary ligands under mild conditions which preserve the Ge(II) centre (scheme 28), as previously demonstrated for the preparation of Sn(N$_3$)$_2$.[176]

$$\text{Ge(N}_3\text{)}_2\text{(L)}_2 \xrightarrow{\substack{\text{high} \\ \text{vacuum}}} \text{Ge(N}_3\text{)}_2 + 2\text{L}$$
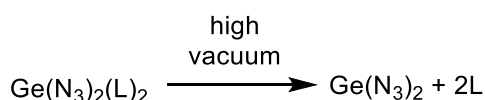
Scheme 28. Proposed removal of ancillary ligands from Ge(N$_3$)$_2$(L)$_2$ to form Ge(N$_3$)$_2$. L = volatile Lewis base, e.g. py or pic.

4.2. Results and discussion: syntheses of $Ge(N_3)_2(L)_2$ (L = py, pic, ^tBupy)

The absence of $Ge(N_3)_2$ prevented the formation of $Ge(N_3)_2(L)_2$ by direct addition of ancillary ligand, as utilised for the syntheses of $Ge(N_3)_4(L)_2$. Instead, solutions of $Na[Ge(N_3)_3]$ were treated with a Lewis base to form $Ge(N_3)_2(L)_2$ and NaN_3 (scheme 29). Three Lewis bases of varying σ-donation ability and steric bulk (L = py, pic, ^tBupy) were investigated. $Na[Ge(N_3)_3]$ was prepared from $GeCl_2(diox)$ and NaN_3 in MeCN. The residual solubility of NaN_3 in MeCN required the isolation of $Na[Ge(N_3)_3]$ from solution and the complexation of Lewis base to be performed in CH_2Cl_2. Owing to the absence of any phlegmatising cation, $Na[Ge(N_3)_3]$ was assumed to be highly unstable and explosive. Consequently, the reaction scale was restricted to small scales (i.e., less than 200 mg) to prevent the isolation of large amounts of $Na[Ge(N_3)_3]$.[182] Addition of the Lewis base to an MeCN solution of $Na[Ge(N_3)_3]$ prior to solvent removal provided additional phlegmatisation through the subsequent formation of a slurry. Despite the relatively high boiling points of the Lewis bases, care was required to ensure that significant amounts of Lewis base were not lost upon solvent removal *in vacuo*.

$$GeCl_2(diox) + ex.NaN_3 \xrightarrow{MeCN} Na[Ge(N_3)_3] + 2NaCl + diox$$

$$Na[Ge(N_3)_3] + ex.L \xrightarrow{CH_2Cl_2} Ge(N_3)_2(L)_2 + NaN_3$$

Scheme 29. Synthesis of $Na[Ge(N_3)_3]$ and subsequent reaction to form $Ge(N_3)_2(L)_2$ (L = e.g. py, pic).

Overnight stirring of suspensions of $Na[Ge(N_3)_3]$ and Lewis base in CH_2Cl_2 afforded highly turbid white suspensions due to the elimination of insoluble NaN_3. The formation of $Ge(N_3)_2(L)_2$ was signified by a decrease in the $\nu_{as}(N_3)$ bands associated with $Na[Ge(N_3)_3]$ and the concurrent growth of two new $\nu_{as}(N_3)$ bands at higher wavenumbers ($\tilde{\nu} = 2096-2097$ and $2075\ cm^{-1}$, figure 33, table 25). Bands associated with both free and coordinated ligand at ca. 1500-1650 cm^{-1} were also observed. A third azide band at 2128 cm^{-1} was attributed to $Ge(N_3)_4$, which was formed in equilibrium with $Ge(N_3)_4(L)_2$ upon unavoidable oxidation of $Ge(N_3)_2(L)_2$ during analysis (scheme 30). The same band was observed previously in samples of pure $Ge(N_3)_4(L)_2$ (L = py, pic). One $\nu_{as}(N_3)$ band of $Ge(N_3)_2(L)_2$ ($\tilde{\nu} = 2096\ cm^{-1}$) overlaps with that of $Ge(N_3)_4(L)_2$.[147] Attempts to prepare $Ge(N_3)_2(L)_2$ from $GeCl_2(diox)$ and $TMSN_3$ were unsuccessful and no evidence of ligand exchange was observed.

$$\text{Ge(N}_3)_2(L)_2 \quad + \quad HN_3 \quad \xrightarrow{-H_2} \quad \text{Ge(N}_3)_4(L)_2 \quad \rightleftharpoons \quad \text{Ge(N}_3)_4 + 2L$$

2096, 2075 cm⁻¹   2138 cm⁻¹   2114, 2096 cm⁻¹   2128 cm⁻¹

$2096, 2075\ \text{cm}^{-1}$ $\quad$ $2138\ \text{cm}^{-1}$ $\qquad$ $2114, 2096\ \text{cm}^{-1}$ $\qquad$ $2128\ \text{cm}^{-1}$
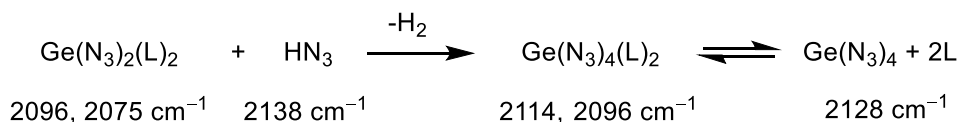
Scheme 30. Equilibrium between $Ge(N_3)_4(L)_2$, HN_3 and $Ge(N_3)_4$ in solution, with indicative $\nu_{as}(N_3)$ bands (in CH_2Cl_2, L = py,) for each.[147]

All three adducts were formed as highly air-sensitive microcrystalline solids. Although the low volatility of the excess Lewis base removed the requirement for mulling agent, paraffin oil was added to protect the samples from air exposure. The width and resolution of the $\nu_{as}(N_3)$ bands in the IR spectra of the solids was dependent on the extent to which each sample was dried.
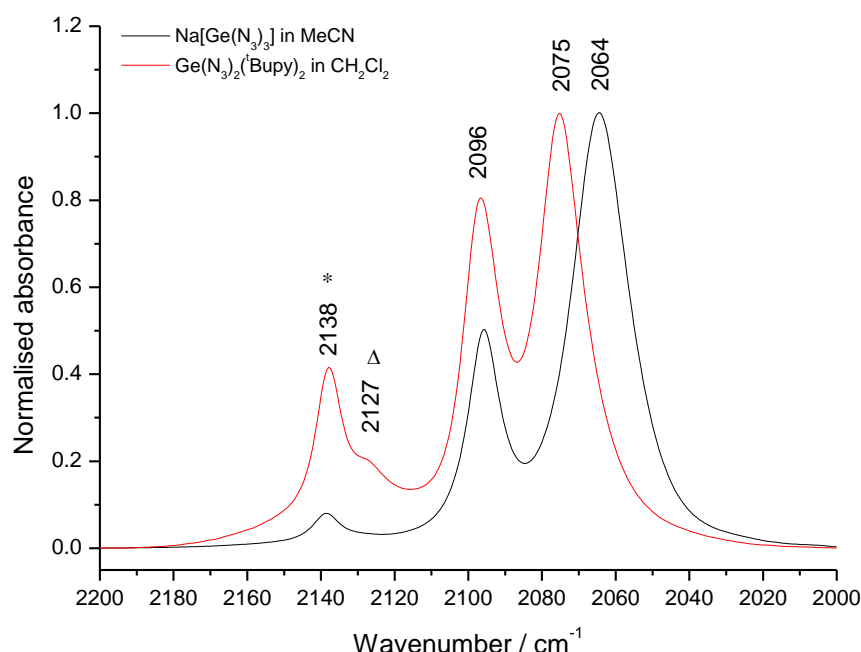
Figure 33. IR spectra of $Na[Ge(N_3)_3]$ (black, −) and $Ge(N_3)_2(^tBupy)_2$ (red, −) in CH_2Cl_2 and MeCN solutions, respectively. Both spectra have been normalised to the most intense $\nu_{as}(N_3)$ band in each spectrum. Bands marked with * and Δ are associated with HN_3 and $Ge(N_3)_4$, respectively and arise from unavoidable oxidation during analysis.

	Na[Ge(N₃)₃]	**Ge(N₃)₂(py)₂**	**Ge(N₃)₄(py)₂**	**[PPN]₂[Ge(N₃)₆]**
Oxidation state	II	II	IV	IV
Solvent	MeCN	CH_2Cl_2	CH_2Cl_2	MeCN
$\nu_{as}(N_3)$ **/ cm⁻¹**	2096, 2064	2097, 2076	2114, 2096	2083
$\nu(L)$ **/ cm⁻¹**	−	1610	1613	−
Refs.	This work	This work	[147]	[96]

Table 25. Comparison of solution-phase IR data of Ge(II) and Ge(IV) poly(azido) complexes. [a] recorded in MeCN; [b] recorded in CH_2Cl_2.

### 4.2.1 Synthesis of Ge(N₃)₂(py)₂

$Ge(N_3)_2(py)_2$ was the most air sensitive of the three adducts prepared. Even when protected under nujol, exposure of a solid sample to air for 2 minutes resulted in the almost total disappearance of both azide bands associated with the complex. After ca. 30 minutes standing at room temperature under argon atmosphere, an initially colourless solution of $Ge(N_3)_2(py)_2$ in CH_2Cl_2 rapidly became turbid and was accompanied by the disappearance of the bands associated with coordinated azide and pyridine in the solution-phase IR spectrum. The mechanism of decomposition is unclear, but is hypothesised to proceed by the oxidation of $Ge(N_3)_2(py)_2$ to the less-soluble $Ge(N_3)_4(py)_2$ (figure 34). The rate of decomposition suggests that the lifetime of $Ge(N_3)_2(py)_2$ in solution is very short and may be exceeded by the reaction time required for its quantitative formation (scheme 31), accounting for the spectroscopic detection of other azido complexes in solution. This rapid decomposition contrasts the behaviour of the high-valent analogue, $Ge(N_3)_4(py)_2$, which is stable in solution over several hours.[147]

$$Na[Ge(N_3)_3] + py \xrightarrow{k_1} Ge(N_3)_2(py)_2 \xrightarrow{k_2} \text{Decomposition products}$$

$$k_2 > k_1$$
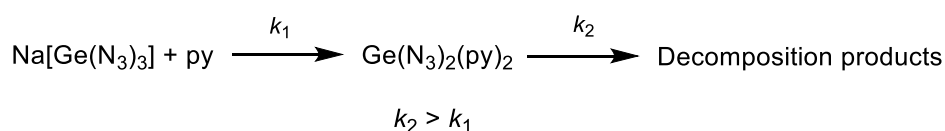
Scheme 31. Proposed competing formation and decomposition reactions of $Ge(N_3)_2(py)_2$ in solution. If the decomposition rate constant (k_2) is greater than the formation rate constant (k_1) then at no point will the reaction solution exclusively contain $Ge(N_3)_2(py)_2$.
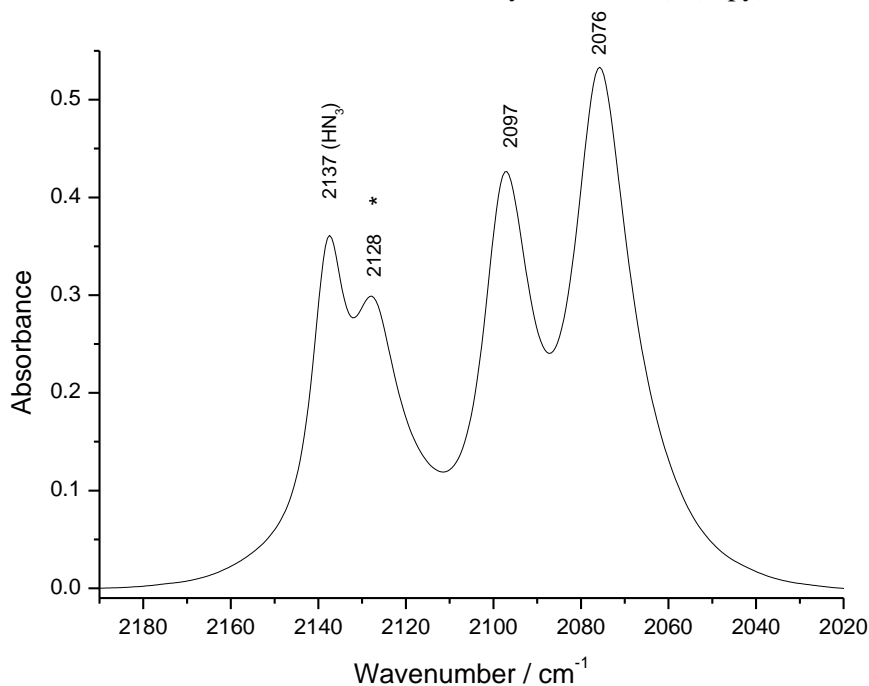

Figure 34. IR spectrum of $Ge(N_3)_2(py)_2$ in CH_2Cl_2. The band marked with an asterisk (*) is attributed to $Ge(N_3)_4$, formed in equilibrium upon oxidation of $Ge(N_3)_2(py)_2$ to $Ge(N_3)_4(py)_2$ by HN_3.

Owing to the extremely fast rate of decomposition of the complex in CH_2Cl_2, $Ge(N_3)_2(py)_2$ was not investigated further. Picoline and t-butylpyridine were examined as possible alternative Lewis bases to provide additional stabilisation of $Ge(N_3)_2$, through enhanced σ donation capability and steric bulk.
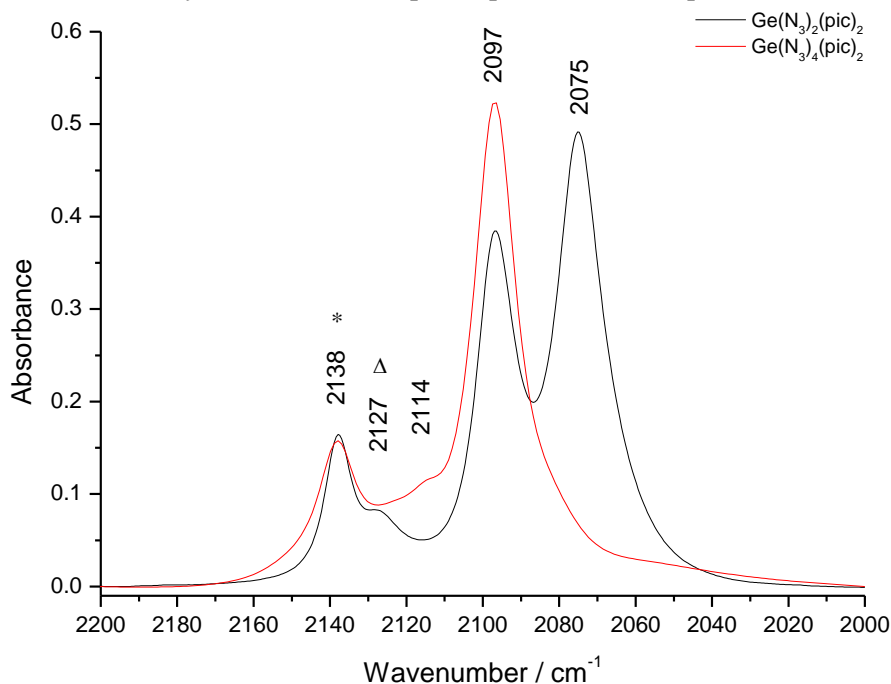
4.2.2 Synthesis of Ge(N₃)₂(pic)₂

$Ge(N_3)_2(pic)_2$ was formed upon the reaction of $Na[Ge(N_3)_3]$ with picoline. The spectral positon of the $\nu_{as}(N_3)$ bands of the complex are identical to $Ge(N_3)_2(py)_2$ in both solution and solid state IR spectra, implying that the coordinative strength of the azido ligands in both adducts are similar. The reactivity of $Ge(N_3)_2(pic)_2$ is similar to the pyridine adduct. Even when contained under nujol, crystals of $Ge(N_3)_2(pic)_2$ decomposed upon air exposure with the release of gas (figure 35). The gas is hypothesised to be HN_3 or N_2, originating from the release of azido ligands from the coordination centre. This aligns with the proposed decomposition mechanism observed in solutions of $Ge(N_3)_2(py)_2$, whereby $Ge(II)$ is oxidised to $Ge(IV)$ by HN_3. Similar spontaneous precipitation to the pyridine adduct was observed upon prolonged standing of solutions of $Ge(N_3)_2(pic)_2$ in excess picoline at room temperature. IR spectroscopic monitoring revealed an almost immediate decrease in the $\nu_{as}(N_3)$ bands of $Ge(N_3)_2(pic)_2$ upon standing, accompanied by a subsequent increase in those of $Ge(N_3)_4(pic)_2$, $Ge(N_3)_4$, $[Ge(N_3)_6]^{2-}$ and HN_3 (figure 36). Despite all attempts to control the rate of crystallisation, crystals of $Ge(N_3)_2(pic)_2$ were of insufficient size for X-ray crystallographic studies.

$$Ge(N_3)_2(pic)_2 + H_2O \longrightarrow Ge(N_3)(OH)(pic)_2 + HN_3$$

$$Ge(N_3)_2(pic)_2 + HN_3 \longrightarrow Ge(N_3)_4(pic)_2 + H_2$$
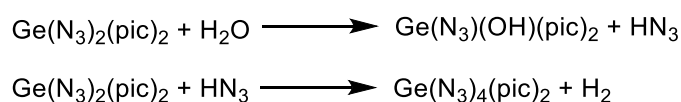
Scheme 32. Proposed hydrolysis and subsequent oxidation of $Ge(N_3)_2(pic)_2$ to $Ge(N_3)_4(pic)_2$.
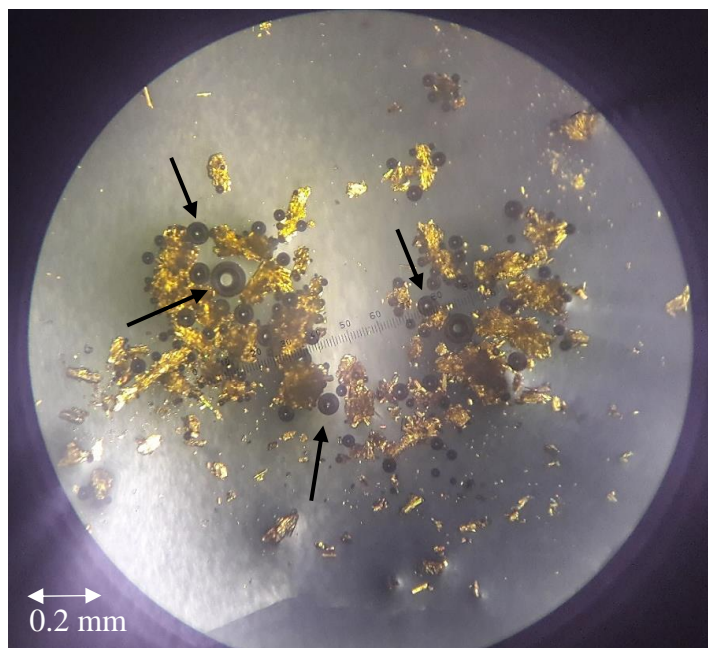
Figure 35. Microscope image showing crystals of $Ge(N_3)_2(pic)_2$ suspended in nujol. Bubbles of gas (indicated by arrows) formed upon exposure of the suspension to air.

Figure 36. IR spectrum of $Ge(N_3)_2(pic)_2$ and $Ge(N_3)_4(pic)_2$ in CH_2Cl_2. The bands marked with * and Δ are attributed to HN_3 and $Ge(N_3)_4$, respectively. The band at 2114 cm^{-1} is attributed to $[Ge(N_3)_6]^{2-}$.

4.2.3 Synthesis of $Ge(N_3)_2(^tBupy)_2$

The ^tBupy ligand was anticipated to impart additional stabilisation to the $Ge(N_3)_2$ subunit by the coordination of an even stronger σ-electron donating Lewis base than pyridine and picoline. As observed for the previous two adducts, an air-sensitive microcrystalline solid was formed which was unable to be recrystallised to afford crystals of sufficient size for crystallographic

studies. The two $\nu_{as}(N_3)$ bands were observed at almost identical positions in the IR spectrum to the other adducts in solution. However, an increasing difference in the spectral position between free and coordinated ancillary ligand (py<pic<^{t}Bupy) may reflect the increasing coordinative strength of the ancillary ligand (table 26).

	$\nu_{as}(N_3)$ / cm^{-1}	$\nu(L)$ / cm^{-1}	$\nu(free L)$ / cm^{-1}	$\Delta\nu(L)$ / cm^{-1}
Ge(N$_3$)$_2$(py)$_2$	2097, 2076	1611	1600	10
Ge(N$_3$)$_2$(pic)$_2$	2096, 2075	1627	1607	20
Ge(N$_3$)$_2$(^{t}Bupy)$_2$	2096, 2075	1621	1599	22

Table 26. Comparison of IR data for Ge(N$_3$)$_2$(L)$_2$ (L = py, pic, ^{t}Bupy) in CH$_2$Cl$_2$.

The rate of spontaneous decomposition of Ge(N$_3$)$_2$(^{t}Bupy)$_2$ in solution was much slower than the other adducts (ca. 30 h versus 30 minutes for Ge(N$_3$)$_2$(py)$_2$) and allowed more in-depth characterisation. Although no visible decomposition was observed upon exposure of a nujol suspension of the crystalline material to air (figure 37), air exposure of a CH$_2$Cl$_2$ solution still resulted in the formation of Ge(N$_3$)$_4$ and release of ^{t}Bupy (figures 38, 39).

0.2 mm
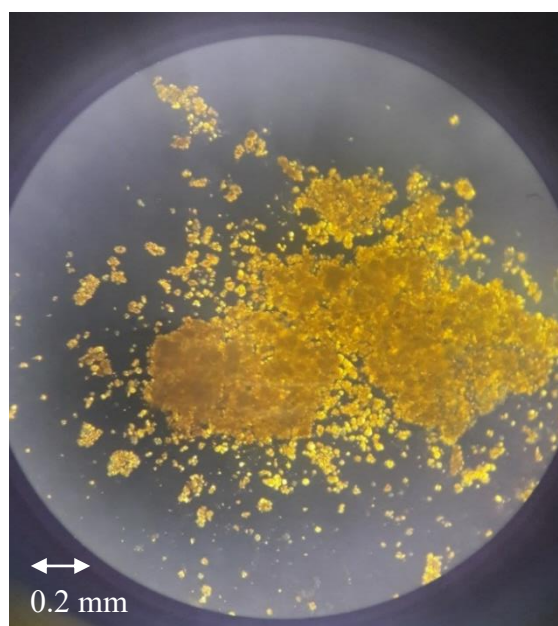
Figure 37. Microscope image of Ge(N$_3$)$_2$(^{t}Bupy)$_2$ under nujol.
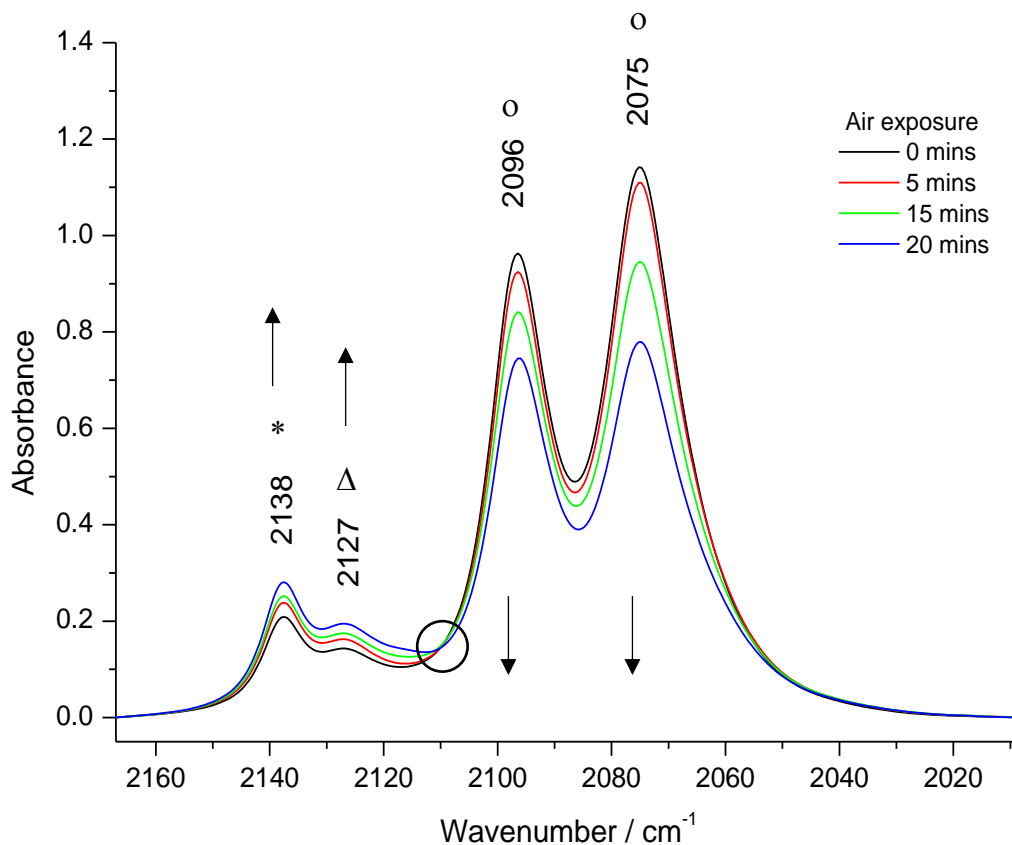
Figure 38. Spectral series of Ge(N$_3$)$_2$(^{t}Bupy)$_2$ in CH$_2$Cl$_2$ upon air exposure between 2165-2025 cm^{-1}, showing the decomposition of Ge(N$_3$)$_2$(^{t}Bupy)$_2$ (o), the formation of HN$_3$ (*) and Ge(N$_3$)$_4$ (Δ) and an isosbestic point at 2110 cm^{-1} (O).
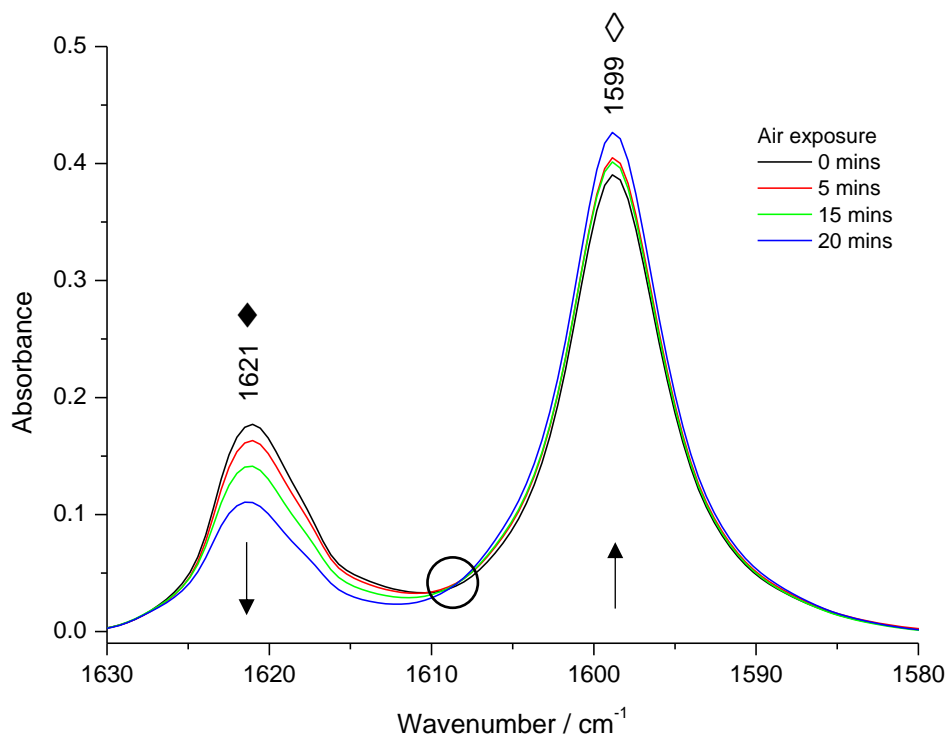
Figure 39. Spectral series of Ge(N$_3$)$_2$(^{t}Bupy)$_2$ in CH$_2$Cl$_2$ upon air exposure between 1630−1580 cm^{-1}, showing the decoordination of ^{t}Bupy ($\blacklozenge$), formation of uncoordinated ^{t}Bupy ($\lozenge$) and an isosbestic point at 1609 cm^{-1} (O).

A suspension of microcrystalline $Ge(N_3)_2({}^tBupy)_2$ in ${}^tBupy$ was investigated using powder X-ray diffraction (PXRD) (figure 40). Although the IR spectrum of the material was consistent with $Ge(N_3)_2({}^tBupy)_2$, component analysis of the obtained diffraction pattern identified two species that were each responsible for approximately half of the observed reflections (figure 41). The predicted powder pattern of $Ge(N_3)_4({}^tBupy)_2$ is in good agreement with one of these components, and occurs by oxidation of the Ge(II) coordination centre during the measurement period. Although the cause of oxidation can be explained by a poor seal of the air-sensitive sample holder, a more plausible explanation is that the Ge(II) centre has spontaneously oxidised (scheme 33) in the same fashion observed upon storage of the adducts in CH_2Cl_2 solution. The faster rate of oxidation (ca. 5h in suspension) in this study is attributed to a significant increase in the sample concentration versus CH_2Cl_2 solution (ca. 30 h). Although the component assigned as $Ge(N_3)_4({}^tBupy)_2$ could be subtracted from the dataset, the weak intensity of the remaining reflections prevented the generation of a unit cell for $Ge(N_3)_2({}^tBupy)_2$ (figure 42).
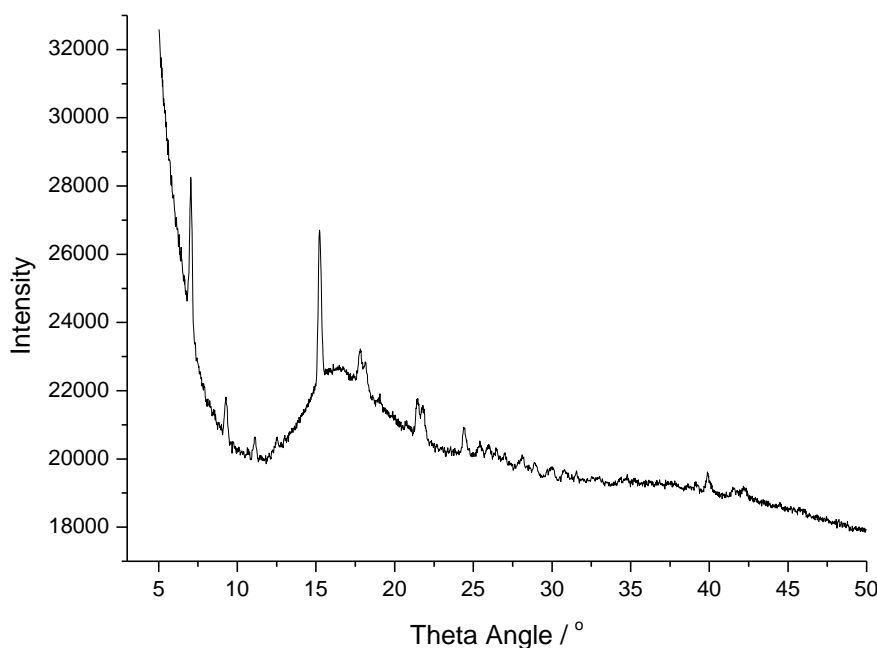
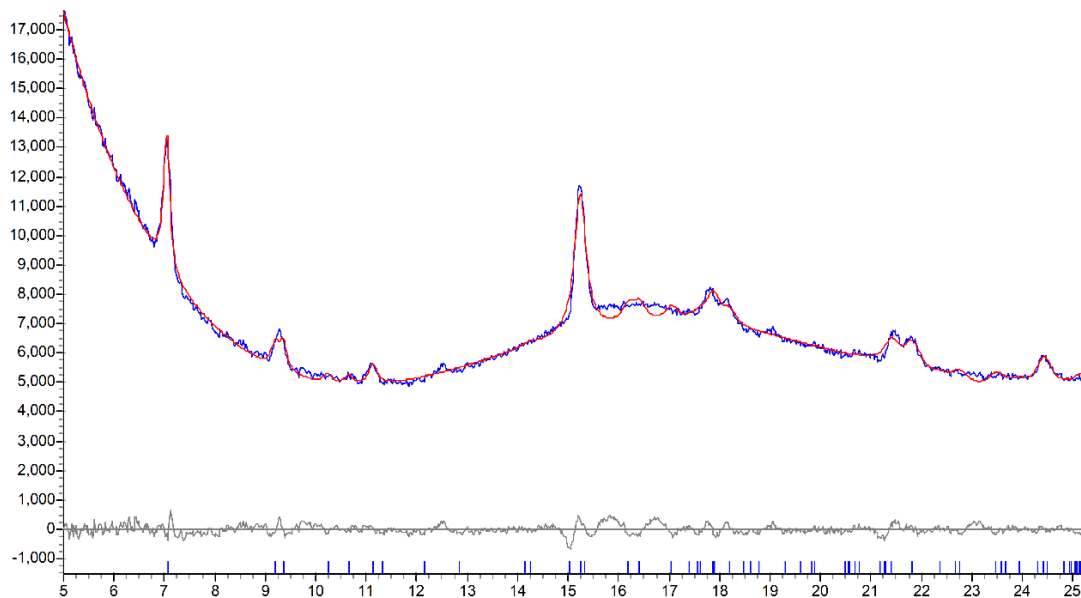**Figure 40.** Observed pattern of $Ge(N_3)_2({}^tBupy)_2$ between $3°<\theta<50°$.
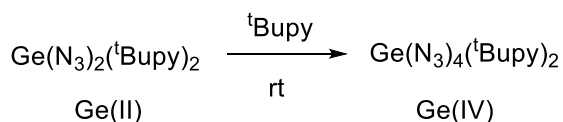
Scheme 33. Oxidation of $Ge(N_3)_2({}^tBupy)_2$ to $Ge(N_3)_4({}^tBupy)_2$.
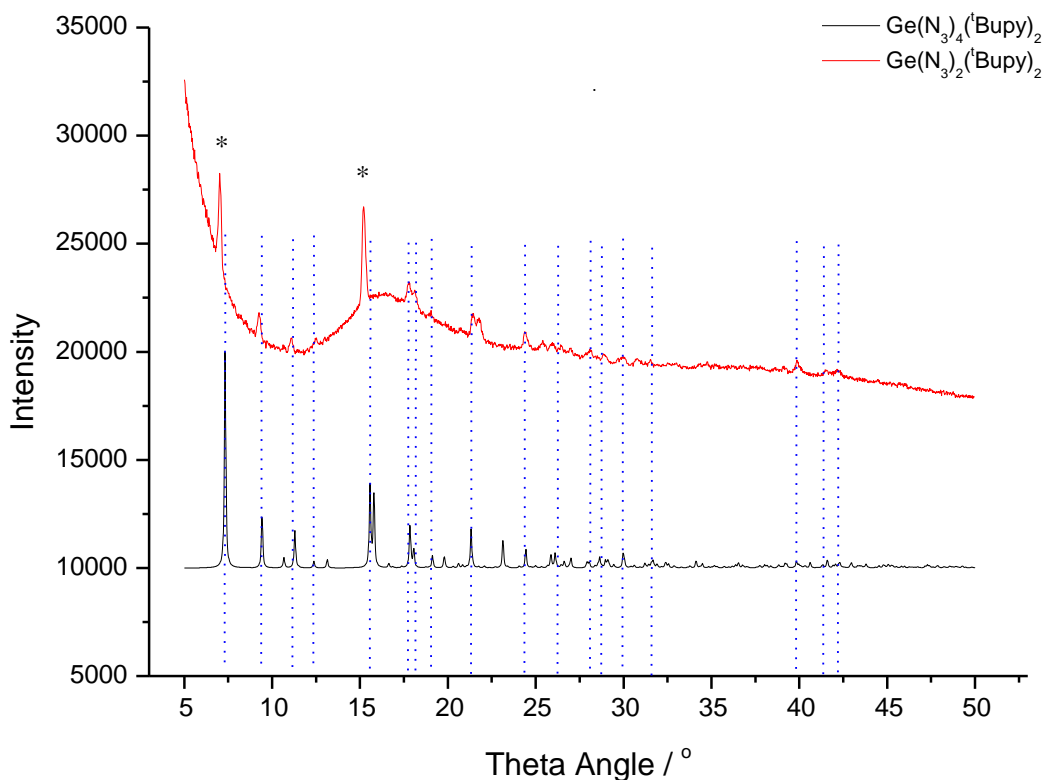
Figure 41. Overlay of powder patterns of $Ge(N_3)_4(^tBupy)_2$ (calculated, black line, −) and $Ge(N_3)_2(^tBupy)_2$ (observed, red line, −). Blue dashed lines (---) indicate reflections assigned to $Ge(N_3)_4(tBupy)_2$. Reflections marked with asterisks (*) do not directly overlap with the predicted pattern but are almost identical to reflections observed for $Ge(N_3)_4(^tBupy)_2$ and are attributed to shifts caused by differences in temperature.

Figure 42. Section of residual data (black line, −) following subtraction and Pawley refinement of predicted diffractogram of $Ge(N_3)_4(^tBupy)_2$ (red line, −) from observed pattern (blue line, −).[194]

## 4.3 Decomposition studies of Ge(N$_3$)$_2$(L)$_2$ (L = pic, ^{t}Bupy)

4.3.1 Spontaneous decomposition

A sample of Ge(N$_3$)$_2$(^{t}Bupy)$_2$ in a small amount of excess ^{t}Bupy was stood at room temperature for several days in an attempt to grow single crystals of Ge(N$_3$)$_2$(^{t}Bupy)$_2$. Instead, single crystals of the high-valent Ge(IV) analogue, Ge(N$_3$)$_4$(^{t}Bupy)$_2$ (figure 43), were formed in a red solid. IR spectroscopy showed no trace of the Ge(II) complex remained. Replication of the reaction in a glovebox eliminated the possibility of accidental oxidation through air exposure and indicated that the process appeared to be analogous to the spontaneous oxidation in solution (described above).

Ge(N$_3$)$_4$(^{t}Bupy)$_2$ crystallises as colourless blocks in space group $P\bar{1}$. All ligands are crystallographically independent and are arranged in a near-perfect octahedral GeN$_6$ geometry. The four azido ligands lie in the same equatorial plane and all six *trans* N−Ge−N bond angles in the complex are almost perfectly linear ($\angle_{\text{(N–Ge–N)}}$ = 178.27−178.65°). The Ge−N bond lengths for both ancillary ligands are slightly elongated versus those in Ge(N$_3$)$_4$(pic)$_2$ (d(Ge−N) = 2.057(5)−2.072(5) Å vs 2.0424(18)−2.0514(18) Å, respectively). The Ge−N bond lengths for the four azido ligands, however, are almost identical. The two ^{t}Bupy ligands do not line in the same plane and are rotated approximately 90° with respect to each other, presumably to minimise steric hindrance from the same ligands in adjacent molecules within the crystal lattice. The same rotational displacement of one ancillary ligand is observed in the crystal structure of Ge(N$_3$)$_4$(pic)$_2$, which crystallises with higher (P_{bca}) symmetry.[147] In further concurrence with the structure of Ge(N$_3$)$_4$(pic)$_2$, no hydrogen-bonding interactions are observed and the majority of the short-contacts observed are present between the azido ligands in one molecule and the aromatic protons of the ^{t}Bupy ligands in another.
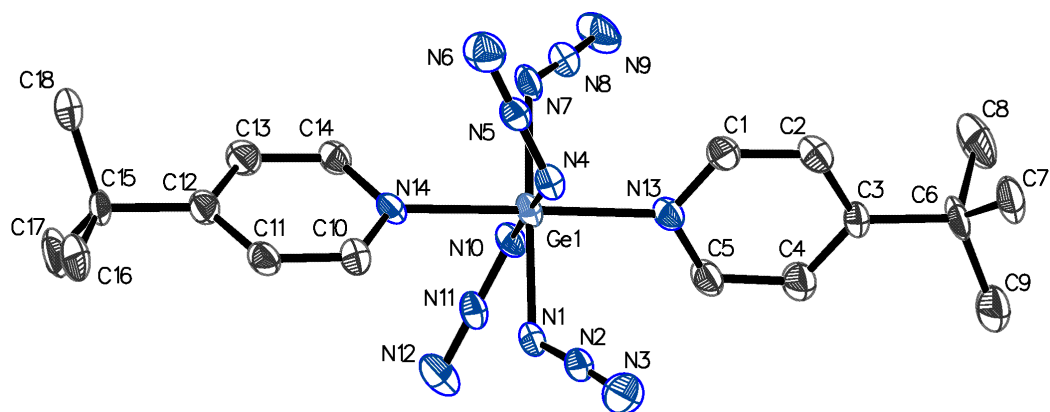
**Figure 43.** Crystal structure of $Ge(N_3)_4({}^tBupy)_2$. Hydrogen atoms omitted for clarity. Turquoise = Ge, blue = N, grey = C. Selected bond lengths (Å) and angles (°) : Ge(1)−N(14) 2.057(5) , Ge(1)−N(7) 1.934(6), Ge(1)−N(1) 1.950(6), Ge(1)−N(13) 2.072(5) , Ge(1)−N(10) 1.966(5), Ge(1)−N(4) 1.940(6), N(1)−N(2) 1.202(8) , N(2)−N(3) 1.158(9), N(4)−N(5) 1.219(8), N(5)−N(6) 1.138(9), N(7)−N(8) 1.216(8), N(8)−N(9) 1.133(9) , N(11)−N(10) 1.210(8), N(11)−N(12) 1.143(8) ; N(14)−Ge(1)−N(13) 178.58(19), N(3)−N(2)−N(1) 176.9(7) , N(6)−N(5)−N(4) 176.4(7) , N(9)−N(8)−N(7) 175.8(7) , N(12)−N(11)−N(10) 174.9(7).

To study this reaction in more detail, a sealed solution of $Ge(N_3)_2({}^tBupy)_2$ in CH_2Cl_2 was allowed to stand at room temperature in a glovebox. After ca. 36 h, colourless crystals of $Ge(N_3)_4({}^tBupy)_2$ had formed. Regular monitoring of the solution by IR spectroscopy showed a clear decrease in the $\nu_{as}(N_3)$ bands associated with $Ge(N_3)_2({}^tBupy)_2$ (figures 44, 45); the use of a spectroscopic cell with a longer path length showed four bands consistent with $Ge(N_3)_4({}^tBupy)_2$. Interestingly, despite the complete exclusion of oxygen and moisture and consistently minimal air exposure of the analyte solution during spectroscopic analysis, the band associated with HN_3 in CH_2Cl_2 was observed to grow significantly during the course of the reaction. A control reaction, where a solution of $Ge(N_3)_2({}^tBupy)_2$ was treated with dry ethereal HN_3 under inert atmospheres, showed the same spectral changes as the reaction where no HN_3 was added (figure 46). This result confirms that HN_3 *is* spontaneously formed in solution and subsequently oxidises the Ge(II) centre to Ge(IV) (scheme 34).
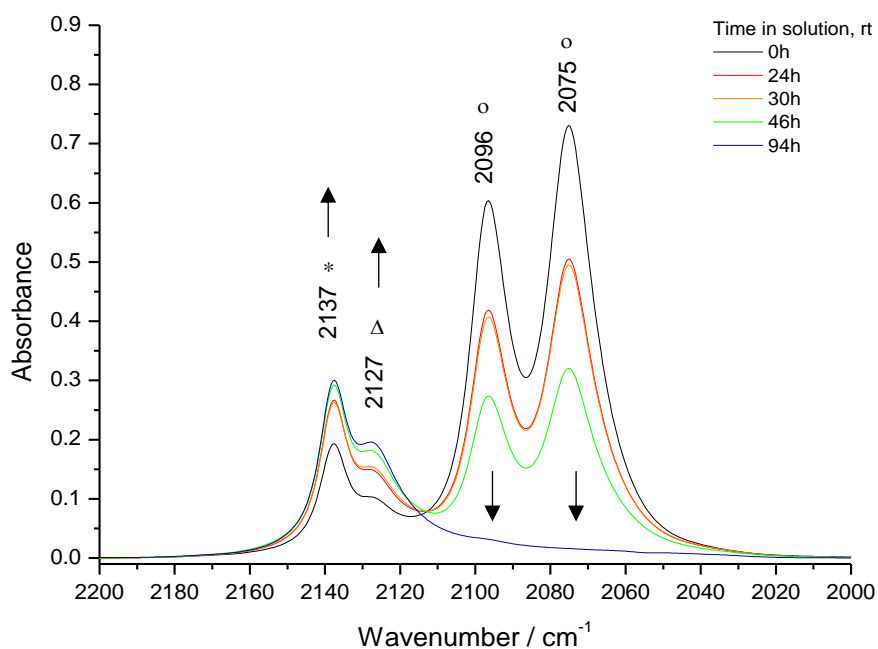
Figure 44. Spectral series showing gradual decomposition of $Ge(N_3)_2(^tBupy)_2$ (o) in CH_2Cl_2, with accompanying formation of HN_3 (*) and $Ge(N_3)_4$ (Δ).
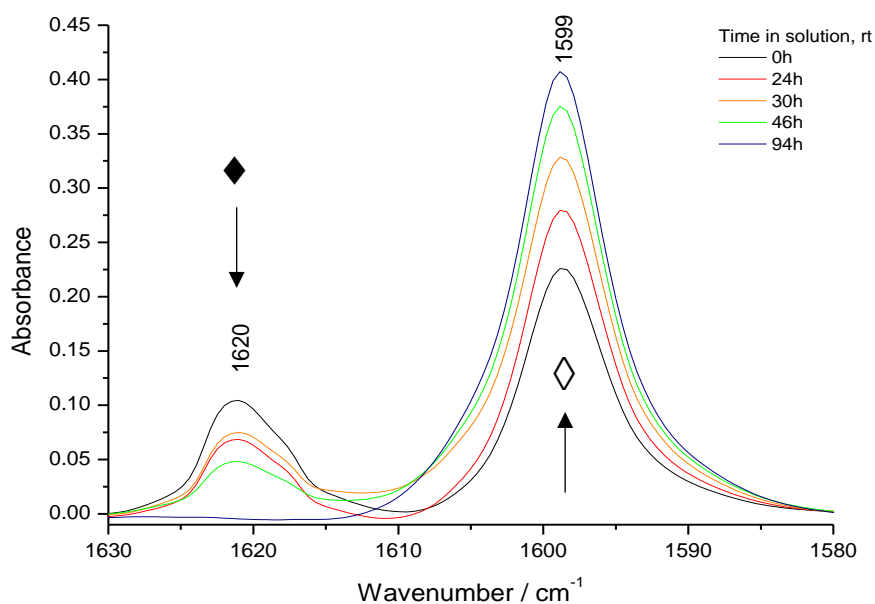
Figure 45. Spectral series showing gradual decomposition of $Ge(N_3)_2(^tBupy)_2$ in CH_2Cl_2, resulting in a decrease in coordinated ^tBupy ($\blacklozenge$) and increase in uncoordinated ^tBupy ($\lozenge$).

The cause of HN_3 generation is unclear. One hypothesis is that photolysis results in proton elimination from the CH_2Cl_2 solvent, which subsequently abstracts an azido ligand from $Ge(N_3)_4(^tBupy)_2$ to form HN_3. Regardless of mechanism, it is assumed that the same reaction occurs in solutions of $Ge(N_3)_2(py)_2$, where decomposition begins after ca. 30 minutes. However, further work is required to confirm or repute the mechanism of decomposition.

68
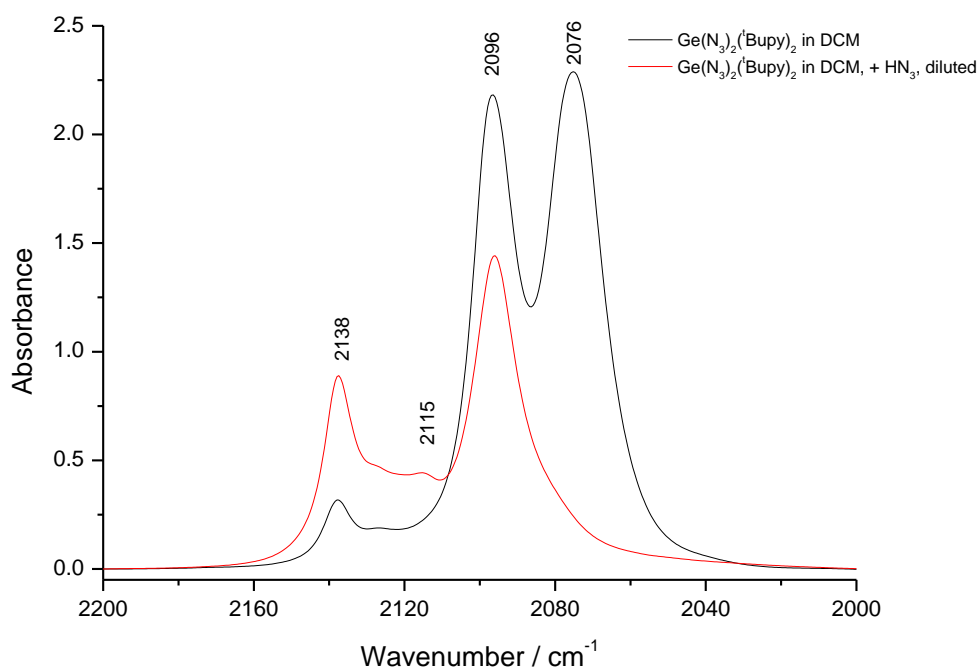
Figure 46. Spectra showing a solution of $Ge(N_3)_2({}^tBupy)_2$ in CH_2Cl_2 before (black line, $-$) and after (red line, $-$) treatment with dry, ethereal HN_3.

$$Ge(N_3)_2({}^tBupy)_2 \xrightarrow[\text{CH}_2\text{Cl}_2]{\text{HN}_3} Ge(N_3)_4({}^tBupy)_2$$
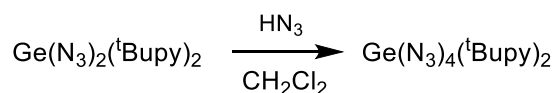
Scheme 34. Proposed decomposition of $Ge(N_3)_2({}^tBupy)_2$ into $Ge(N_3)_4({}^tBupy)_2$.

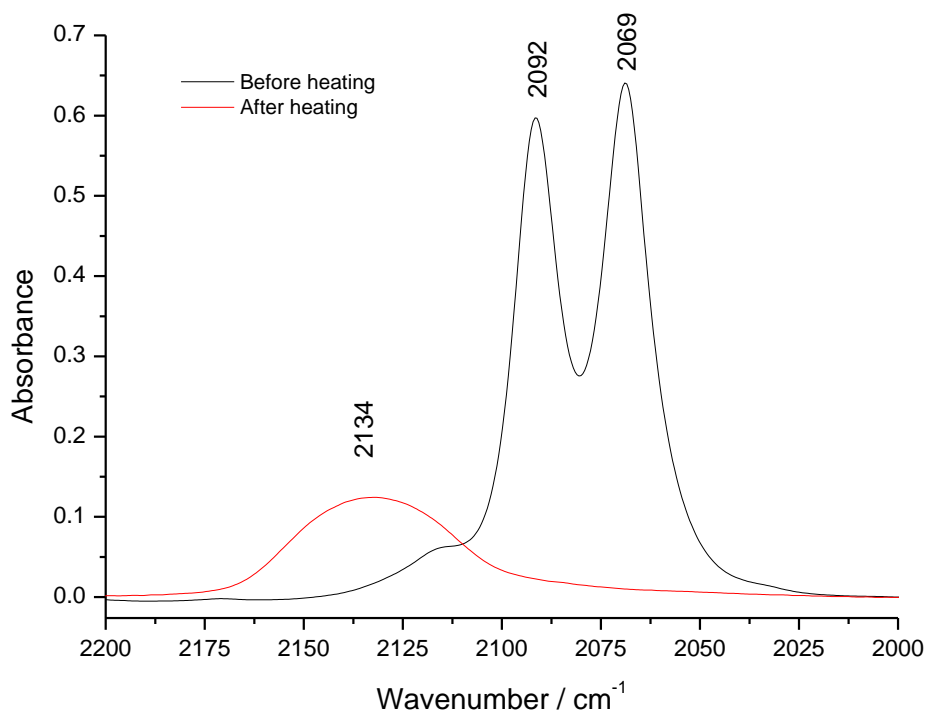### 4.3.2 Thermal decomposition

In an attempt to decoordinate both ancillary ligands and prepare $Ge(N_3)_2$, a suspension of $Ge(N_3)_2({}^tBupy)_2$ in ${}^tBupy$ was heated to 70 °C under dynamic high vacuum. Immediate heating to this temperature appeared to induce decomposition and resulted in the formation of a brown solid of unknown identity. In contrast, a gradual and regular increase in temperature over 3-4 hours formed a white solid with comparable air sensitivity to the starting material. The IR spectrum of the solid revealed that the azide bands of $Ge(N_3)_2({}^tBupy)_2$ had been replaced by a single broad band ($\tilde{v}$ = ca. 2134 cm^{-1}), located in the spectral region populated by azido complexes of Ge(IV) (figure 47).[183] The absence of bands associated with both free and coordinated ${}^tBupy$ confirmed the complete decoordination of both ancillary ligands, however, the absence of any energetic character suggests that neither $Ge(N_3)_2$ nor $Ge(N_3)_4$ were formed. Exposure to air resulted in the decomposition of the band at ca. 2134 cm^{-1} and the concurrent growth of an unidentified band at 2038 cm^{-1} (figure 48) in the spectral region similar to an azido complex of Ge(II), or an inorganic azide. The identity of this decomposition product is unclear.

69

Figure 47. IR spectra of Ge(N$_3$)$_2$(^{t}Bupy)$_2$ before (black spectrum (−), thin film) and after heating to 70°C (red spectrum (−), nujol mull).
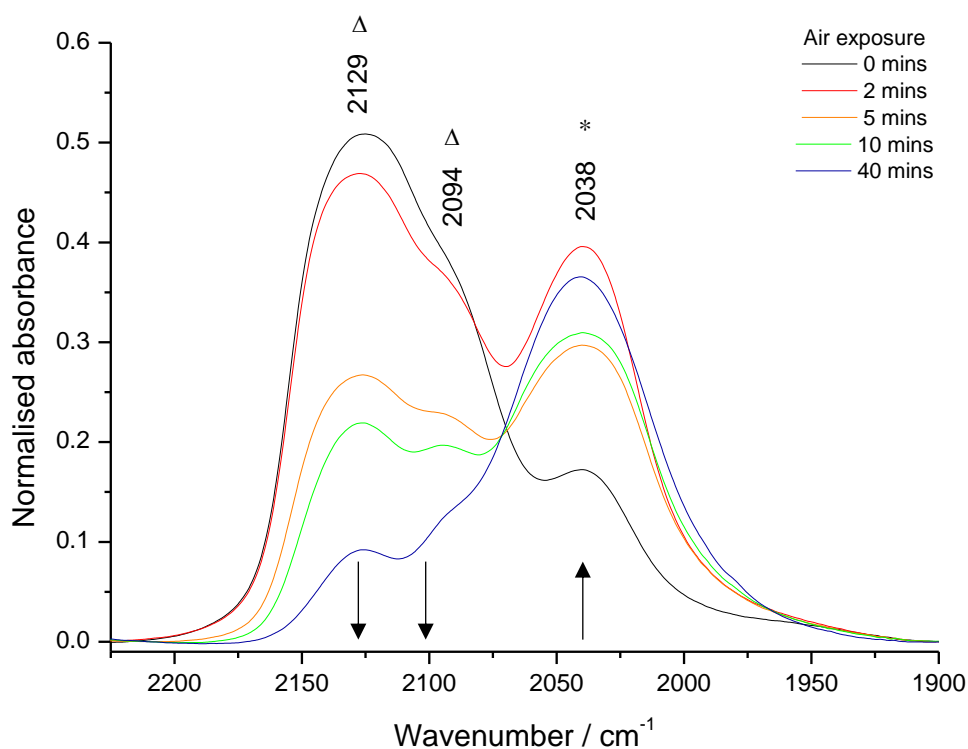
Figure 48. Normalised spectral series showing decomposition of solid Ge(N$_3$)(N) (Δ) and subsequent formation of another unknown azido species (*) upon exposure to air.

A broad band observed at ca. 800 cm^{-1} is inconsistent with azido or ^{t}Bupy ligands and is instead similar to a nitride (figure 49). This result suggests that one azido ligand has decomposed to form an azido-nitrido complex of Ge(IV) as Ge(N$_3$)$_x$N$_y$, where $x + y = 4$, accounting for the

observation of bands associated with both groups in the IR spectrum and the absence of energetic character both during and after thermal decomposition. The air stability of germanium nitride, Ge_3N_4, is inconsistent with the rapid hydrolysis observed in the thermal decomposition product and provides further evidence for the formation of an azide-nitride species. The mechanism of formation is unclear, but appears to proceed by the decoordination of both ^{t}Bupy ligands of $Ge(N_3)_2(^tBupy)_2$ to form $Ge(N_3)_2$, which rapidly rearranges by disproportionation and subsequent loss of N_2 to form $Ge(N_3)_xN_y$ (scheme 35).

high vacuum, 70 °C

$$Ge(N_3)_2(^tBupy)_2 \xrightarrow{-2^tBupy} Ge(N_3)_2 \xrightarrow{-N_2} Ge(N_3)_xN_y$$
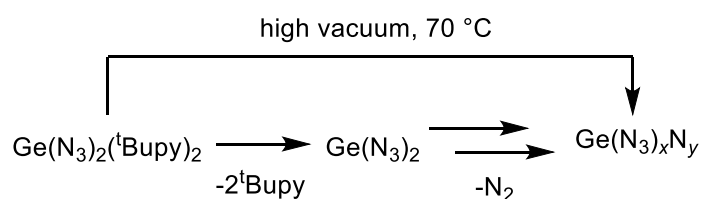
Scheme 35. Proposed formation of $Ge(N_3)_xN_y$ from $Ge(N_3)_2(^tBupy)_2$.
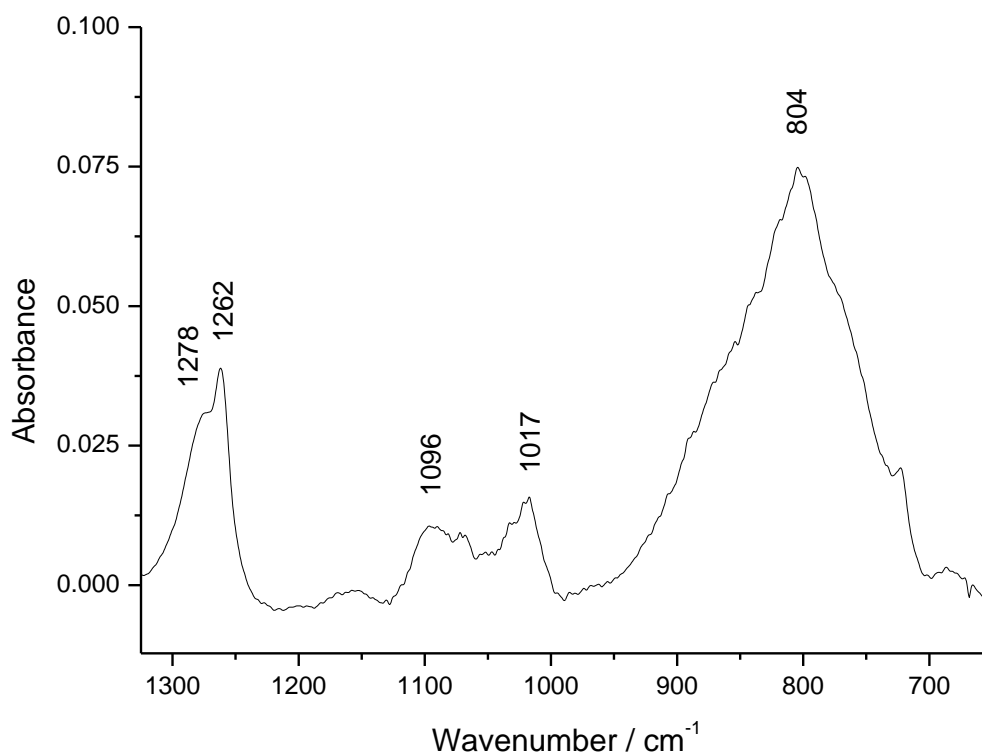
Figure 49. IR spectrum of $Ge(N_3)_2(^tBupy)_2$ after heating, fingerprint region, nujol mull.

In order to further investigate the formation of $Ge(N_3)_xN_y$, a sample of $Ge(N_3)_2(^tBupy)_2$ was analysed by thermogravimetric analysis (TGA) to quantify the changes observed in the preliminary heating studies (figures 50, 51). At approximately 301 °C, the compound exploded, resulting in the disintegration of the ceramic analysis crucible and the formation of a

71

brown/black solid hypothesised to contain elemental germanium (figure 52, scheme 36). A period of mass loss prior to decomposition approximately corresponds to the decoordination of both ^{t}Bupy ligands and loss of excess ^{t}Bupy in the analyte suspension (figure 51, table 27) or the formation of $Ge(N_3)_4$ from $Ge(N_3)_4(^tBupy)_2$. Although efforts were taken to minimise exposure to air, it is possible that spontaneous oxidation of the Ge(II) centre in the sample suspension resulted in the formation of $Ge(N_3)_4(^tBupy)_2$ during (or prior to) analysis and thus the presence of $Ge(N_3)_4$ cannot be eliminated. Therefore, the presence of excess ^{t}Bupy in the sample suspension renders mass loss as only an approximate indicator of ligand decoordination. The exact identity of the compound which decomposed could not be identified. The energetic properties of the sample are not anticipated for a stabilised complex such as $Ge(N_3)_2(^tBupy)_2$ and are instead more consistent with the behaviour expected for a binary azide such as $Ge(N_3)_4$ or $Ge(N_3)_2$.
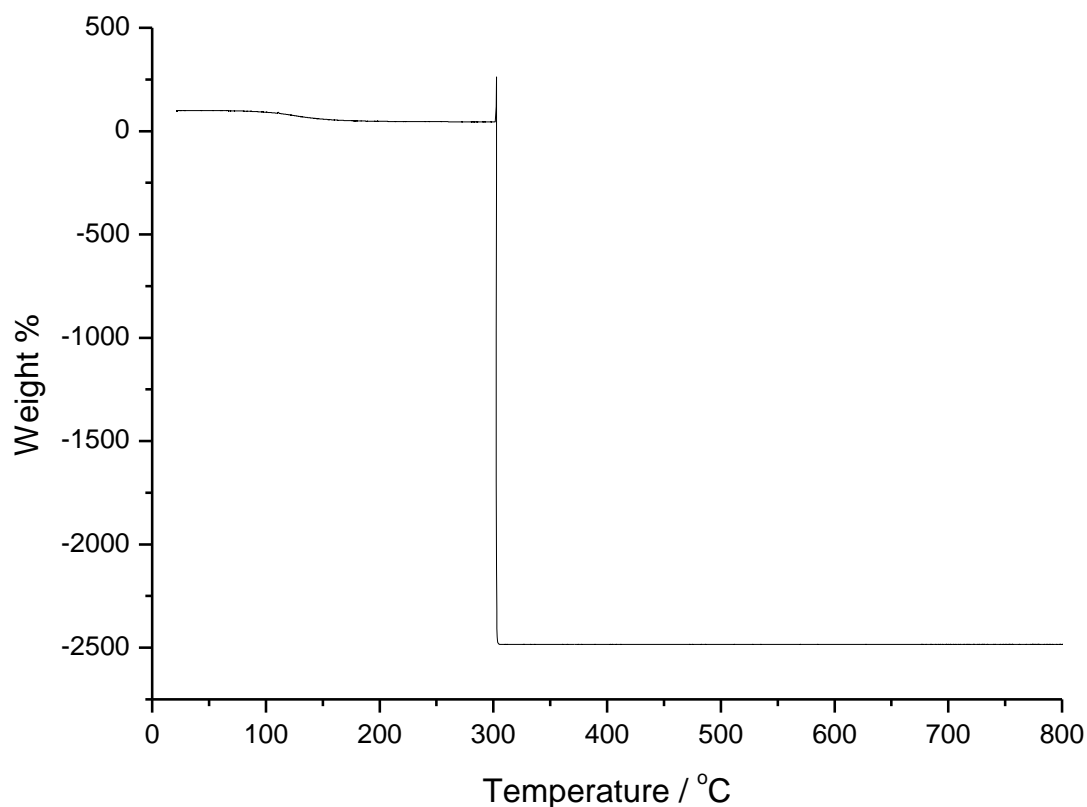
Figure 50. TGA trace of $Ge(N_3)_2(^tBupy)_2$. T_{on}(mass loss) = 41 °C, T_{dec} = 301 °C.
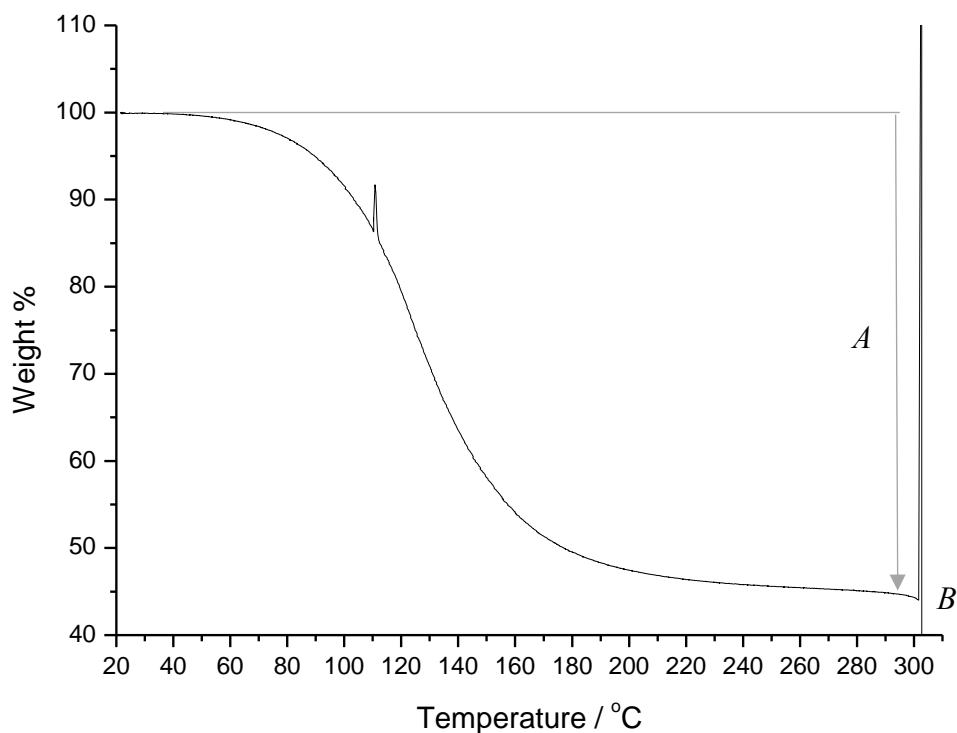
Figure 51. Expansion of thermogram between 20 °C−310 °C prior to detonation. The mass increase at T = 110 °C observed in region *A* is assigned to an anomalous mass reading from the crucible being knocked under the stream of nitrogen during analysis.

ca. 1.0 cm
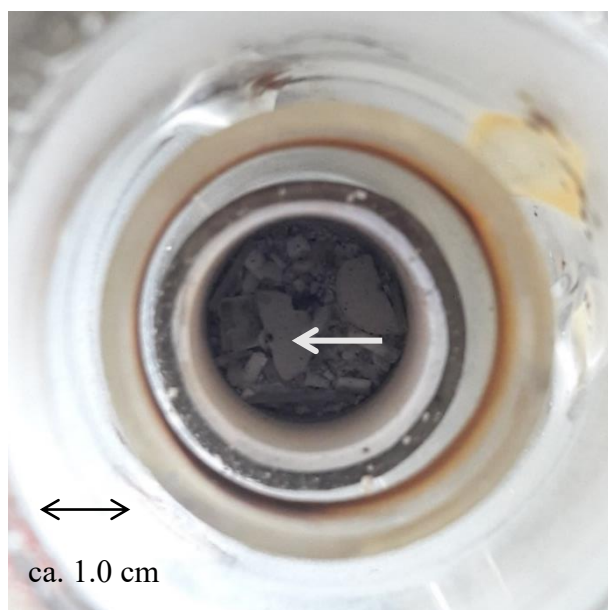
Figure 52. Photograph of broken ceramic TGA crucible (centre, indicated by arrow) contained in glass housing after explosion of compound during heating study.

$$Ge(N_3)_2 \xrightarrow{\text{T}_d} Ge + 3N_2$$
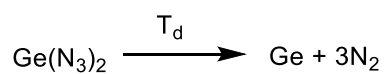
Scheme 36. Proposed decomposition pathway of $Ge(N_3)_2$ in TGA study. T_d = temperature of decomposition.

Region	Temperature Region / °C	Mass Loss / %	Comments
A	41-237 °C	−55%	Loss of ^{t}Bupy
B	301	N/A	Explosion

Table 27. Summary of mass losses observed during heating study of $Ge(N_3)_2(^tBupy)_2$. The presence of excess ancillary ^{t}Bupy in the analyte sample means that estimation of the number of ancillary ligands decoordinated from $Ge(N_3)_2(^tBupy)_2$ is only approximate.

The rate of heating in the TGA study was much faster (10 °C s^{-1}) and more consistent than the large-scale heating study at 70 °C which involved long periods at constant temperature. It is hypothesised decoordination of ^{t}Bupy forms $Ge(N_3)_2$. However, when the rate of heating is increased, as observed in the TGA study, the unstable $Ge(N_3)_2$ does not have time to undergo rearrangement into the more stable $Ge(N_3)_xN_y$ and instead induces decomposition of the complex through explosion (scheme 37). Immediate heating to 70 °C without a gradual ramp, whilst also providing insufficient time for rearrangement, is lower than the decomposition temperature of $Ge(N_3)_2$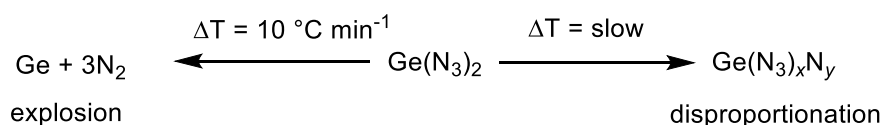 (T = 301 °C) and thus no explosion occurs. Although the precise parameters of the heating ramp are unknown, this result confirms that the rate of heating (and absence of any oxygen, or external stimuli that may induce detonation) are critical to facilitate the formation of $Ge(N_3)_xN_y$. The TGA studies meant that the rate of heating was limited to below 10 °C/min at all times in the preparation of $Ge(N_3)_xN_y$. Replication of the large-scale heating studies with $Ge(N_3)_2(pic)_2$ yielded an off-white solid that was spectroscopically identical to the ^{t}Bupy analogue and provided further evidence that all ancillary ligands were decoordinated during this process.

$$Ge + 3N_2 \quad \xleftarrow{\Delta T = 10\ °C\ min^{-1}} \quad Ge(N_3)_2 \quad \xrightarrow{\Delta T = slow} \quad Ge(N_3)_xN_y$$

explosion   disproportionation

Scheme 37. Proposed decomposition mechanisms of $Ge(N_3)_2$.

4.4 Controlled decomposition of Ge(N₃)N

4.4.1 Formation of germanium nitride?

The unexpected formation of $Ge(N_3)_xN_y$ under relatively mild conditions lead to further investigations to determine if the remaining azide ligand could also be decomposed to form germanium nitride, Ge_3N_4 (scheme 38). The controlled thermolysis of tri(azido)gallium, $[Ga(N_3)_3]_\infty$, at ca. 250−280 °C under dynamic nitrogen flow has previously been demonstrated

to form gallium nitride, GaN (scheme 39).[195] Whilst a further period of annealing at 850 °C was used to obtain phase-pure GaN, the method is a convenient and milder alternative to the high temperatures and harsh conditions of chemical vapour deposition (>950 °C, gaseous NH_3) used in conventional production of thin films of GaN. These films are commercially relevant owing to the great potential for their use in optoelectronic devices, such as blue light emitting diodes, due to the presence of a large band gap.[195,196] Despite production at much milder conditions than those used conventionally, no further research into the controlled decomposition of N-rich complexes into main group nitrides has been reported. The thermal decomposition of $Ge(N_3)_2(^tBupy)_2$ suggested that controlled decomposition of germanium(II) diazido complexes containing volatile ancillary ligands could afford germanium nitrides under mild conditions, in analogy to the process reported for $[Ga(N_3)_3]_\infty$.

$$Ge(N_3)_2 \xleftarrow[-2L]{\substack{\text{Ligand} \\ \text{decoordination}}} Ge(N_3)_2(L)_2 \xrightarrow[-N_2]{\substack{\text{Controlled} \\ \text{decomposition}}} Ge_xN_y$$
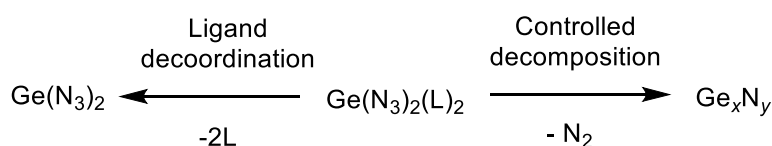
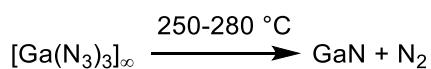**Scheme 38.** Proposed decomposition of $Ge(N_3)_2(L)_2$ to form $Ge(N_3)_2$ and Ge_xN_y.

$$[Ga(N_3)_3]_\infty \xrightarrow{250\text{-}280\ ^\circ C} GaN + N_2$$

Scheme 39. Controlled decomposition of $[Ga(N_3)_3]_\infty$ to form GaN.[195]

A sample of $Ge(N_3)_xN_y$ was analysed by TGA studies (figure 51, table 28). Unlike $Ge(N_3)_2(^tBupy)_2$, no explosions were observed, further supporting the hypothesis that the explosion observed previously originated from a binary germanium azide. A sharp loss in mass at T = 744 °C is attributed to the crucible being dislodged by fluctuations in the N_2 gas stream during analysis (region *D*). The absence of any mass increase prior to this temperature, plus the preservation of the ceramic analysis crucible, eliminated the possibility of explosion. A dark brown/grey solid was formed during analysis (figure 54).
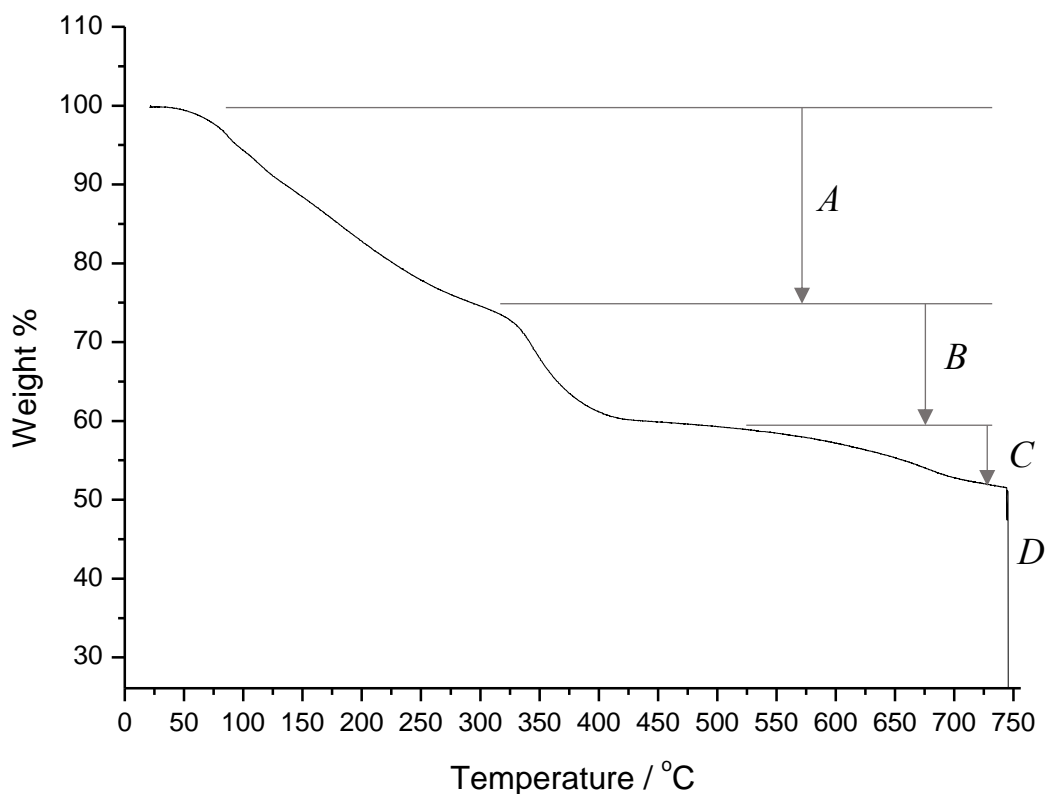
Figure 53. TGA trace of $Ge(N_3)_xN_y$, prior to sample loss at T = 744 °C.

Region	Temperature range / °C	Mass loss / %	Comments
A	42−327	27	Loss of N_2
B	327−455	13	Loss of $\frac{1}{2}N_2$
C	455−724	8	Loss of $\frac{1}{4}N_2$
D	744	−	Crucible dislodged

Table 28. Summary of mass losses observed during heating study of $Ge(N_3)_xN_y$.

The processes occurring in this heating study roughly corresponded to loss of nitrogen from a material with an average composition of $Ge(N_3)N$ to form Ge_3N_4 (scheme 40). The dark colour of the solid was attributed to trace amounts of germanium metal, formed by uneven loss of N_2, as reported previously in other preparations of Ge_3N_4.[197] Inconsistent nitrogen loss during heating indicates that a number of different nitride complexes are present which generate a product with an average composition of $Ge(N_3)N$. This accounts for the approximate correlation with the expected mass loss from $Ge(N_3)N$ into pure Ge_3N_4.
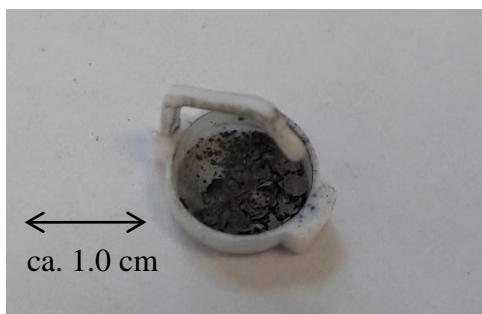
Figure 54. Photograph of crucible containing solid after TGA study.

$$3Ge(N_3)N \longrightarrow Ge_3N_4 + 4N_2$$
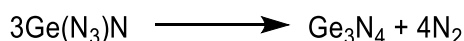
Scheme 40. Postulated decomposition of $Ge(N_3)N$ during TGA analysis.

In order to characterise the thermal decomposition product, the study was replicated on larger scale through *in situ* heating in a Schlenk tube under dynamic vacuum. The use of a tube furnace allowed large-scale slow and controlled heating (to 350 °C at a heating rate of 1 °C min^{-1}), with the preservation of an inert atmosphere. The application of dynamic vacuum also prevented any pressure increase associated with gas release during decomposition. This process resulted in the formation of an off-white, air-stable and homogenous powder which displayed an air-stability that was noticeably greater to those of the air-sensitive $Ge(N_3)N$ precursor. No azide bands were observed in the IR spectrum and the large band at ca. 800 cm^{-1} was preserved. The appearance of this band was similar to the nitride band of Ge_3N_4 reported previously.[198] Although seemingly air-stable, addition of water to a sample resulted in partial dissolution, accompanied by a strong smell of ammonia and the formation of a basic solution. This reactivity contrasts that of water-insoluble Ge_3N_4.[199]

The inconsistency of the IR spectrum of the solid with germanium oxide, GeO_2, eliminated the possibility of oxygen addition during heating (figure 55, table 29). The decomposition mechanism was proposed to proceed by the loss of all azide ligands to form a binary Ge_xN_y complex. Although the exact stoichiometry of the complex could not be confirmed, the spectral similarities suggest that the controlled decomposition of $Ge(N_3)_2(^tBupy)_2$ is capable of producing a germanium nitride as Ge_3N_y ($y = 2$ or 4). This finding also appears to confirm that the controlled thermal decomposition of gallium azides into GaN is also applicable to select germanium azides.[195]
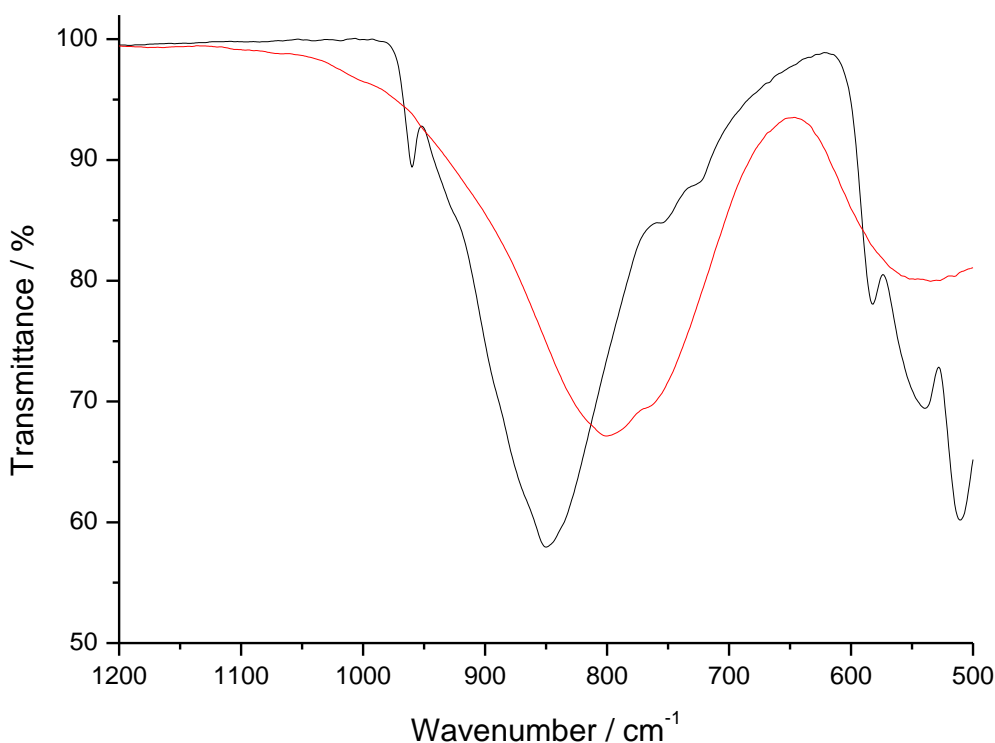
Figure 55. Baseline-corrected IR (ATR) spectral overlay of GeO_2 (black line, −) vs the compound prepared in this study (red line, −) between 1200-500 cm^{-1}.

	Key fingerprint bands / cm^{-1}	Refs
This study [a]	798, 763, 542	This work
GeO_2 [a]	961, 849, 753, 726, 582, 540, 509	This work
Ge_3N_4 [b]	904, 827, 777, 723, 546	[198]

Table 29. Summary of most intense IR fingerprint region absorbance bands for Ge_3N_4, GeO_2 and the compound prepared in this study between 1200−500 cm^{-1}; [a] recorded as ATR; [b] recorded as thin film on a CsI monocrystal (reference [198]).

Further characterisation attempts provided limited information. The amorphicity of the compound precluded PXRD studies and contrasts the syntheses and powder diffraction studies reported of phase-pure polymorphs of Ge_3N_4.[200] Microanalytical data appeared to confirm the presence of both carbon and hydrogen, despite analysis in an extended oxygen-purged atmosphere and the use of a tungsten catalyst to facilitate combustion. All microanalytical values were inconsistent with Ge_3N_4 or Ge_3N_2 (table 30). Both Ge_3N_4 and Ge_3N_2 are unlikely to combust completely and the presence of carbon and hydrogen can only arise from remaining ^{t}Bupy ligands. However, both TGA and IR studies confirmed the total loss of ancillary ligand under the conditions used and therefore it is unclear how much significance can be placed on this microanalytical data.

Conditions	Carbon / %	Hydrogen / %	Nitrogen / %
Standard [a]	3.37	1.80	8.89
Specialist [b]	**4.11**	**1.40**	**4.06**
Ge_3N_4 (expected)	**0**	**0**	**20.45**
Ge_3N_2 (expected)	**0**	**0**	**11.39**

Table 30. Microanalytical values of complex versus Ge_3N_4 and Ge_3N_2. [a] oxygen purge, no catalyst; [b] extended oxygen purge and burn time, tungsten catalyst.

Raman spectroscopy was attempted on a sample of Ge_3N_y at an excitation wavelength of 325 nm but was hindered by fluorescence (figure 56). The observation of few Raman bands is also inconsistent with previous reports of phase-pure, crystalline Ge_3N_4 (table 31). Re-analysis at the same irradiation wavelength reported in literature was also dominated by fluorescence and was inconsistent with previous reports.[201] The confirmation of amorphicity by PXRD meant that the absence of phase-pure Raman-active bands of Ge_3N_x was expected. However, the amorphicity and fluorescence of the solid, in combination with the lack of signals observed at the same irradiation wavelength as phase-pure Ge_3N_4 mean that few conclusions can be drawn. Fluorescence suppression by the use of Kerr gating would be required for future Raman spectroscopic studies.[202,203]
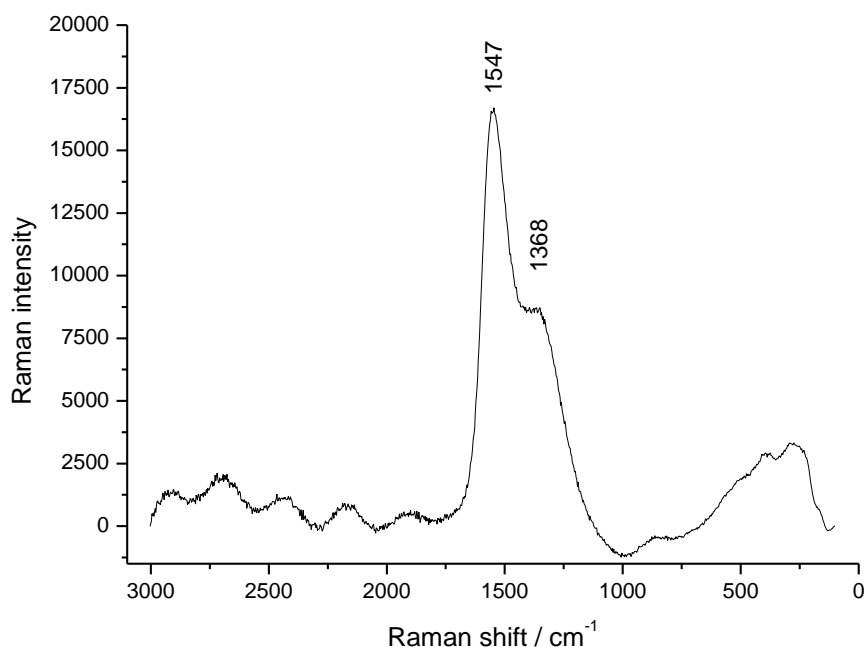
Figure 56. Baseline-corrected Raman spectrum of Ge_3N_4 at 325 nm. The changes in baseline intensities are due to sample fluorescence at the irradiation wavelength.

Phase	Raman bands / cm^{-1}	λ / nm
β	110, 115, 131, 284, 307, 377, 447, 743, 798, 813, 896	415
γ	325, 472, 593, 730, 858	415
a	1547, 1368	325

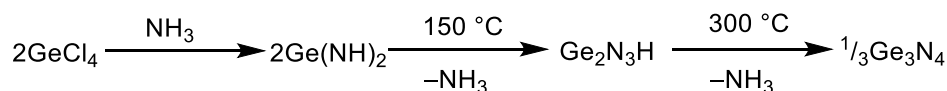**Table 31.** Comparison of Raman absorbance bands of phases of Ge$_3$N$_4$. a = amorphous, this work.[201]

4.4.2 The case for Ge$_3$N$_2$

It is reported that phase-impure Ge$_3$N$_4$, prepared through thermolysis of Ge(NH$_2$)$_2$, contains a mixture of Ge(IV) and Ge(II) nitrides.[204] Therefore, it is possible that gradual decomposition of Ge(N$_3$)$_2$(^{t}Bupy)$_2$ does not form Ge(IV) nitride (Ge$_3$N$_4$) but instead Ge(II) nitride, Ge$_3$N$_2$. Ge$_3$N$_2$ is prepared from GeNH in an analogous thermolysis method to Ge$_3$N$_4$, or by the reaction of monoatomic nitrogen with GeH$_4$, as a dark brown air-sensitive solid which decomposes with the release of NH$_3$.[199,205–207] The use of a Ge(II) precursor in this study may have resulted in the formation of a mixture of Ge(II) and Ge(IV) nitrides in the thermolysed solid. This would account for the observation of criteria inconsistent with Ge$_3$N$_4$; namely, the formation of a basic solution upon addition of water, the absence of characteristic Raman bands of any known polymorph of Ge$_3$N$_4$ and the discrepancies between the observed and calculated nitrogen content (however, the detection of carbon and hydrogen in microanalysis remains unexplained). The off-white to pale-brown appearance of the solid products in this study may be indicative of the presence of small amounts of dark-brown Ge$_3$N$_2$, in addition to Ge$_3$N$_4$. Studies on Ge$_3$N$_2$ are limited and therefore the identity and purity of the compound obtained in this work can only be speculated; consequently, although the identity of the product is suspected to be a mixture of both Ge(II) and Ge(IV) nitrides, the rest of this chapter will focus only on the formation of Ge$_3$N$_4$.

4.4.3 Significance of results

Germanium(IV) nitride is conventionally prepared by the sequential release of ammonia from germanium imide, Ge(NH)$_2$, which is in turn prepared from the reaction of GeCl$_4$ with gaseous ammonia (scheme 41).[197,199] Alternative preparations involve the reaction of germanium metal with NH$_3$ (scheme 42).[199] Strict exclusion of air and moisture is required at both stages to prevent the formation of germanium hydroxides or oxides, at temperatures no greater than ca. 700 °C to prevent decomposition into elemental Ge.[197,199] Ge$_3$N$_4$ can form as α, β (hexagonal) or γ (spinel) phases, the formation of which is influenced by the reaction conditions. For

example, the ammonolysis of germanium imide forms a mixture of α and β phases which can be converted to phase-pure hexagonal β form by controlled annealing at elevated pressures.[208] The spinel phase (γ-Ge$_3$N$_4$) can be formed from β-Ge$_3$N$_4$ under extremely high pressures and temperatures (scheme 43).[209] Commercial sources of Ge$_3$N$_4$ are stated to typically contain approximately 80% α and 20% β forms but in order to obtain compounds suitable for materials or electronics applications, complete phase purity is desired.[201]

$$2\text{GeCl}_4 \xrightarrow{\text{NH}_3} 2\text{Ge(NH)}_2 \xrightarrow[-\text{NH}_3]{150\ °\text{C}} \text{Ge}_2\text{N}_3\text{H} \xrightarrow[-\text{NH}_3]{300\ °\text{C}} {}^{1}/_{3}\text{Ge}_3\text{N}_4$$

Scheme 41. Preparation of Ge$_3$N$_4$ from GeCl$_4$.[197]

$$3\text{Ge} + 4\text{NH}_2 \xrightarrow{700\ °\text{C}} \text{Ge}_3\text{N}_4 + 6\text{H}_2$$
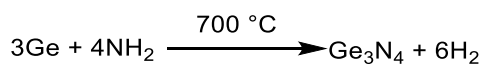
Scheme 42. Preparation of Ge$_3$N$_4$ from Ge metal.[199]

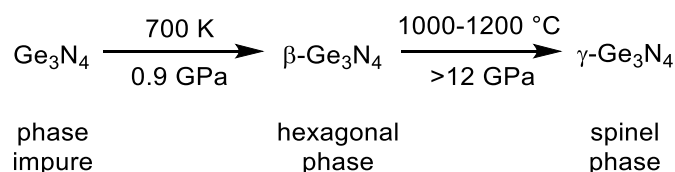$$\text{Ge}_3\text{N}_4 \xrightarrow[0.9\ \text{GPa}]{700\ \text{K}} \beta\text{-Ge}_3\text{N}_4 \xrightarrow[>12\ \text{GPa}]{1000\text{-}1200\ °\text{C}} \gamma\text{-Ge}_3\text{N}_4$$

phase   hexagonal   spinel
impure   phase   phase

Scheme 43. Preparation of Ge$_3$N$_4$ polymorphs.[208,209]

In addition to high temperatures and pressures, feasible syntheses of phase-pure Ge$_3$N$_4$ also require gaseous reagents and the careful control of synthetic conditions, depending the polymorph to be formed. The conditions required for the removal of all azide and ancillary ligands of Ge(N$_3$)$_2$(pic)$_2$ and Ge(N$_3$)$_2$(^{t}Bupy)$_2$ are much more facile than those required for the previously reported syntheses of Ge$_3$N$_4$. This result appears to be the first example of the synthesis of a completely amorphous germanium nitride, at lower temperatures than reported previously for any crystalline polymorphs. The other synthetic conditions are also significantly milder, requiring no gaseous ammonia, and reduced pressures that are easily attainable using standard high vacuum apparatus (table 32). However, careful control of the synthetic conditions is still essential to facilitate gradual decomposition.

The difficulties associated with full characterisation of the amorphous solid obtained in this work make determination of its purity very challenging. A purification process would be required to remove any trace amounts of Ge$_3$N$_2$ or other impurities that may be present. Furthermore, the lack of crystallinity of the solid could preclude its use in certain applications

such as optoelectronics. Despite these limitations, the facile preparation of amorphous Ge_3N_4 could have applications in materials sectors where amorphicity is useful, such as in environments involving high temperature and mechanical stresses where the absence of crystallinity affords additional stability.[210] Amorphous nitrides of group 14 have applications in a number of fields such as superhard coatings (silicon nitride with nanocrystalline titanium nitride), high-temperature ceramics (silicon nitride with boron) or photocatalysts (carbon nitride).[210–212] Similarly to amorphous Si_3N_4, amorphous Ge_3N_4 is reported to possess a high electrical resistance and may be of use for electrically insulating coatings or films.[213]

Phase	Description	Temperature / °C	Pressure	Comments	Ref.
'α'	phase impure	700	1 atm	From $GeCl_4 + NH_{3(g)}$	197,199
β	hexagonal	427	0.9 GPa	From 'α'-Ge_3N_4	201
γ	spinel	1000-1200	>12 GPa	From β-Ge_3N_4	214
a	**amorphous**	**350**	**ca. 5x10^{-2} mbar**	**This work**	−

Table 32. Summary of conditions for synthesis of Ge_3N_4; 'a' represents an amorphous solid.

4.4. Conclusions

The preparation of $Ge(N_3)_2(L)_2$ (L = py, pic, ^tBupy) from $Na[Ge(N_3)_3]^-$ demonstrates that di(azido) complexes containing Ge(II) coordination centres can be stabilised by the coordination of volatile, non-chelating neutral Lewis base ligands. This result is consistent with the analogous complexes of Sn(II), but contrasts those of Si(II) azido complexes of any type. The extent of stabilisation of $Ge(N_3)_2$ is less than the tin analogue and is influenced by the identity of the ancillary Lewis base in the order py<pic<^tBupy. This stabilisation is dependent on, and limited by, the σ electron donation ability and steric hindrance of the ancillary ligand. The stabilisation of the Ge(II) centre by the Lewis base ligands appears weaker than towards Sn(II) coordination centres and eventually results in spontaneous decoordination of the ancillary ligand and subsequent decomposition. This behaviour, unobserved in the Sn(II) analogues, results in oxidation of the Ge(II) centre to form Ge(IV) complexes as $Ge(N_3)_4(L)_2$. The rate of this decomposition is also dependent on the identity and coordination strength of the ancillary ligand, as demonstrated by the enhanced stability of solutions of $Ge(N_3)_2(^tBupy)_2$ versus $Ge(N_3)_2(py)_2$.

Although the decoordination of ancillary ligands occurs spontaneously, attempts to form $Ge(N_3)_2$ were unsuccessful and the compound remains unknown. The violent decomposition

of a sample upon rapid heating suggests that a binary Ge(II) or Ge(IV) azide is formed during thermal decomposition. Controlled heating and ligand decoordination forms an amorphous, azide-free solid consistent with a germanium nitride such as Ge_3N_4 or Ge_3N_2. This behaviour, also unknown for azido complexes of Sn(II), appears dependent on the volatility of the ancillary ligands and the rate of heating. Although the exact identity or mechanistic pathway for the formation of the nitride cannot be confirmed, the conditions for this formation are significantly milder than reported syntheses of Ge_3N_4 and mirror the results of controlled decomposition studies of gallium azido complexes reported previously. These findings suggest that select main-group azido complexes could act as novel precursors for the formation of main-group nitrides under mild conditions.

4.5. Future Work

In order to evaluate the impact of this work, further tests are required to accurately determine the composition and examine the material properties. This could include, for example, chemical vapour deposition (CVD) for investigation of even deposition onto surfaces (provided the compound is sufficiently volatile). Thermal annealing of the amorphous solid into one of the phase-pure crystalline polymorphs, followed by PXRD, could determine the purity of the compound and confirm if the synthesis of amorphous Ge_3N_4 could provide a new, milder synthetic route to the crystalline polymorphs. The exclusion of oxygen in this process is essential to accurately measure the purity of the amorphous precursor. Further thermal studies could identify the decomposition products and clarify what compound exploded in the TGA studies of $Ge(N_3)_2(^tBupy)_2$.

The identification of the precise decomposition products from each thermolysis is key for the determination of the oxidation state of the nitride formed in the final thermolysis step. The erroneous results obtained by elemental analysis suggest that an additional analytical method is required. Inductively-coupled plasma mass spectrometry (ICP-MS) would confirm the germanium content in the solid. However, the large sample masses needed for accurate analysis would require the preparation of large amounts of solid at once, on much larger scales (ca. 3-4 times) than are currently utilised. Prior investigation would be essential to minimise the risk posed by the spontaneous explosion of either precursor if thermal decomposition proceeds too rapidly. The combination of many smaller, separate samples invokes the assumption that the synthetic methodology produces solids of identical composition each time, which cannot currently be confirmed beyond identical IR spectroscopic data. The sparse data on Ge_3N_2

prevents direct comparison between the Ge(II) and Ge(IV) nitrides and conclusive identification of the solid nitride obtained in this work.

Once the identity of the nitride is confirmed, the reliability of the synthetic method must be tested. The slight variance in colour between samples suggests that varying amounts of elemental germanium is produced each time. This would significantly impact the yield, consistency and purity of any germanium nitride that is formed. Individual sampling of several reactions would allow for the determination of reliability of this method for the production of germanium nitrides, and possibly allow for optimisation of the reaction conditions to increase the efficiency of nitride production.

Further work could also focus on alternative ancillary ligands, which could be tailored to optimise their loss under ambient conditions whilst maintaining or enhancing the stability of the adducted complexes. Investigations into other ancillary ligands may also facilitate the formation of the still-unknown $Ge(N_3)_2$ through decoordination at a different rate, or the elusive crystallisation of compounds of $Ge(N_3)_2(L)_2$ suitable for single-crystal X-ray analysis. The latter would permit further structural comparisons between the neutral Lewis base-stabilised poly(azido) adducts of Ge(II) and Ge(IV). This strategy could subsequently be extended to investigate the preparation of other p-block nitrides from nitrogen-rich compounds (scheme 44), complementing the strategies reported here and elsewhere.[195] Of particular interest are precursor complexes that are stabilised by volatile ligands, such as those reported here.

$$E(N_3)_a(L)_b \xrightarrow[\text{H.V.}]{\Delta} E_xN_y + {}^a/_2N + bL$$
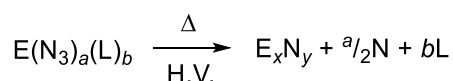
Scheme 44. General scheme for controlled decomposition of p-block poly(azido) complexes into binary p-block nitrides; $a = 2$ or 4, $b = 1$ or 2.

Chapter 5. Poly(azido) complexes of Pb(IV)

5.1. Introduction

As discussed in chapters 1 and 3, the N_3^- anion is one of the most well-defined pseudohalogens and homoleptic group 14 poly(azido) complexes containing E(IV) centres (E(IV) = Si−Sn) have been thoroughly investigated.[99] Although the low-valent complexes of the lighter elements (E(II) = Si, Ge) are comparatively infrequent, the inert pair effect renders the inverse situation true for the heavier centres (E = Sn, Pb). Consequently, complexes of Pb(II) are significantly more stable than those which contain Pb(IV).[102] This is demonstrated by the existence of low-valent neutral diazides of heavier E(II) centres (E = Sn, Pb) alongside the lighter E(IV) tetraazides (E = Si, Ge) (table 33). The requirement for base-stabilisation to isolate $Sn(N_3)_4$ and $Ge(N_3)_2$ (as $Sn(N_3)_4(L)_2$ and $Ge(N_3)_2(L)_2$, respectively) appears to represent a boundary of stability for each valency.

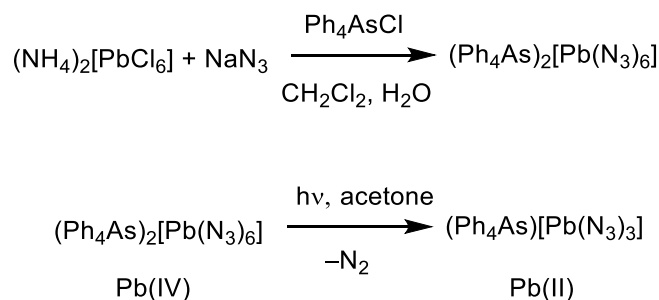|	E(IV)	E(II)
Si	$Si(N_3)_4$	−
Ge	$Ge(N_3)_4$	a
Sn	a	$Sn(N_3)_2$
Pb	−	$Pb(N_3)_2$

Table 33. Selected neutral poly(azido) complexes of E(IV) and E(II) (E = Si−Pb). Examples shaded in blue denote the valency of the more stable complex of each element. − unknown. [a] known only as base-stabilised adducts.

Lead(II) diazide, $Pb(N_3)_2$, has been known for over a century; its high energetic performance and sensitivity results in its use on industrial scales in detonators for secondary explosives.[215–217] $Pb(N_3)_2$ is prepared by the reaction of $Pb(NO_3)_2$ with NaN_3 and crystallises as one of four polymorphic forms. Each azido ligand bridges between adjacent Pb(II) centres, in analogy to the coordination behaviour observed in the lighter Sn(II) complexes of $Sn(N_3)_2(pic)_2$ and $[Sn(N_3)_3]^-$.[176,218,219] The coordination of chelating Lewis bases to $Pb(N_3)_2$ results in the formation of isolable coordination polymers with the general formula $\{Pb(N_3)_2(L)\}_n$ (L = phen, dimethylphen) which melt at temperatures (T_m = 275−283 °C) only slightly below the decomposition temperatures of $Pb(N_3)_2$ (T_{dec} = 315 °C).[220–224]

The inert pair effect means that, in stark contrast to the lighter homologues, poly(azido) complexes of Pb(IV) are extremely rare. $Ph_2Pb(N_3)_2$ is the only charge-neutral poly(azido)

complex of Pb(IV) reported to date.[225] Subsequent addition of ionic azide transfer reagents to Ph$_3$PbN$_3$ and Ph$_2$Pb(N$_3$)$_2$ forms (cat$^+$)[Ph$_3$Pb(N$_3$)$_2$] and (cat$^+$)$_2$[Ph$_2$Pb(N$_3$)$_4$], respectively (cat$^+$ = NH$_4$, Ph$_4$As).[226] Attempts to prepare Pb(N$_3$)$_4$ from the oxidation of lead(II) oxides with HN$_3$ resulted in unidentified mixtures of complexes containing Pb(II) and Pb(IV) centres.[227] Pb(N$_3$)$_4$ is unknown beyond a single theoretical study and, unlike the lighter and higher-valent analogues, no base-stabilised adducts have been prepared.[228] The closest isolable analogue to Pb(N$_3$)$_4$ is the [Pb(N$_3$)$_6$]$^{2-}$ anion, which is prepared from the reaction of [PbCl$_6$]$^{2-}$ and NaN$_3$. Ammonium hexa(azido)plumbate, (NH$_4$)$_2$[Pb(N$_3$)$_6$], is a highly explosive dark red oil.[97,227] However, the inclusion of the phlegmatising [Ph$_4$As]$^+$ cation renders the anion stable towards safe handling, characterisation and crystallisation as [Ph$_4$As]$_2$[Pb(N$_3$)$_6$], as well decreasing the moisture sensitivity reported for other hexa(azido)plumbate salts.[97,178] Hexa(azido)plumbate salts are light-sensitive and the photolytic reduction of [Ph$_4$As]$_2$[Pb(N$_3$)$_6$] in solution is reported to form the tri(azido)plumbate(II) anion, [Pb(N$_3$)$_3$]$^-$ (scheme 45).[177] To date, the photolysis of [Pb(N$_3$)$_6$]$^{2-}$ is the only reported preparation of [Pb(N$_3$)$_3$]$^-$ and is limited to IR-active ν_{as}(N$_3$) bands and microanalytical values only.[177]

$$(NH_4)_2[PbCl_6] + NaN_3 \xrightarrow[\text{CH}_2\text{Cl}_2,\ \text{H}_2\text{O}]{\text{Ph}_4\text{AsCl}} (Ph_4As)_2[Pb(N_3)_6]$$

$$\underset{\text{Pb(IV)}}{(Ph_4As)_2[Pb(N_3)_6]} \xrightarrow[-N_2]{h\nu,\ \text{acetone}} \underset{\text{Pb(II)}}{(Ph_4As)[Pb(N_3)_3]}$$

Scheme 45. Formation (top) and proposed photolytic reduction (bottom) of [Pb(N$_3$)$_6$]$^{2-}$.[97,177,178]

The trends in stability and frequency of group 14 poly(azido) complexes allow the prediction of the reactivity of azido ligands towards Pb(IV). It is unclear whether charge-neutral Pb(N$_3$)$_4$ is isolable or can be stabilised by incorporation of chelating ligands to the same extent as the lighter homologues in either oxidation state, or indeed at all. The thermodynamic driving force afforded by the formation of salt-like, insoluble Pb(N$_3$)$_2$ may be a critical factor in the reaction pathway, accessibility and stability of these complexes, possibly to a greater extent than the lighter homologues, where the neutral polyazides are less-stable, unknown or are more-soluble. The preparation of anionic and charge-neutral poly(azido) complexes of Pb(IV) would also help to determine the reactivity of pseudohalogenido complexes containing central elements in less-common valencies.
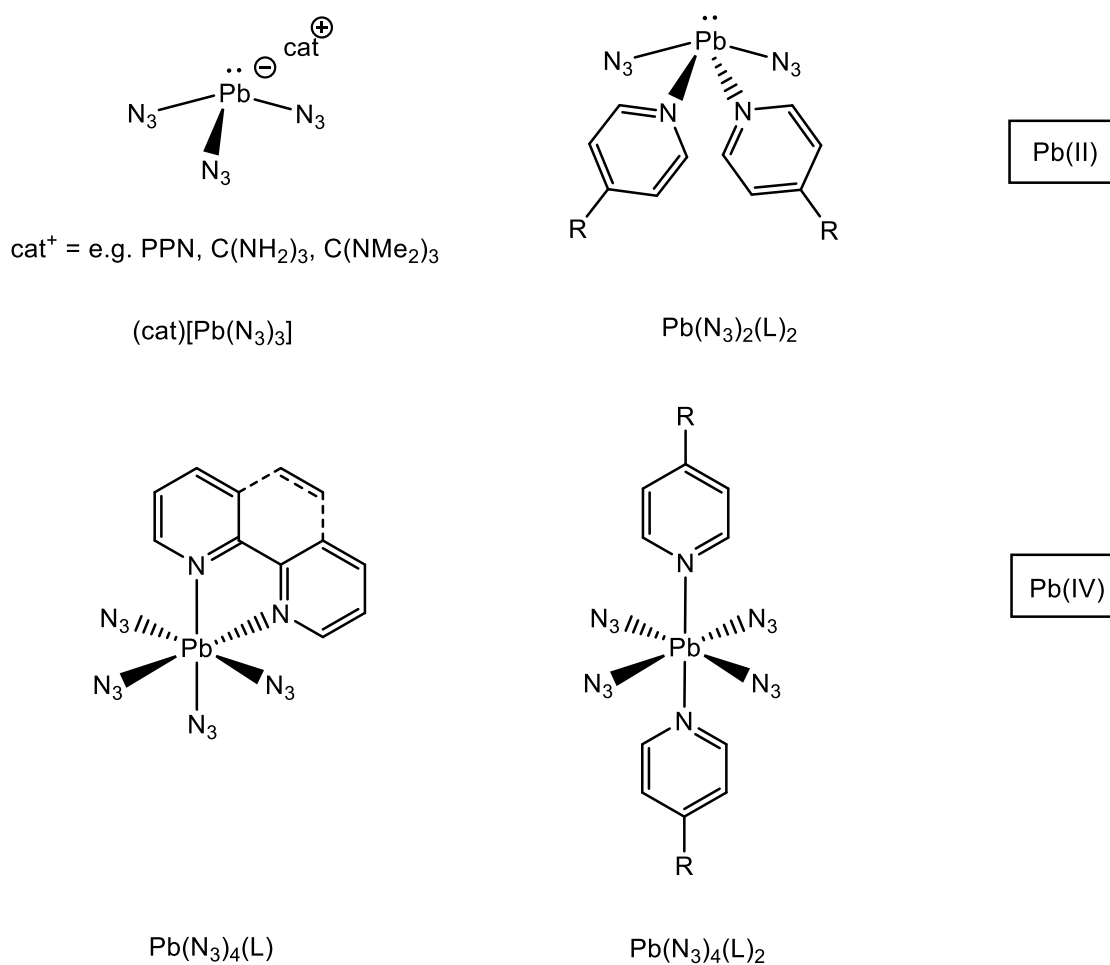
Figure 57. Proposed structures of novel Pb(II) and Pb(IV) azido complexes. R = H, Me.

The single report of $[Pb(N_3)_3]^-$ is a useful starting point to determine if, in analogy to Sn(II), Pb(II) coordination centres are capable of stabilising three azido ligands.[176] The isolation of $[Pb(N_3)_3]^-$ would represent only the second nitrogen-rich complex containing Pb(II), after $Pb(N_3)_2$, and would allow comparative studies between the two.

Further insights into the reactivity of Pb(IV) and Pb(II) towards N_3 ligands may facilitate the preparation of other nitrogen-rich lead complexes. Despite the isolation of hexakis(tetrazolato) complexes of lighter E(IV) centres (E = Si−Sn), to date no tetrazolato complexes of either Pb(IV) or Pb(II) are known and the reactivity of either centre towards this ligand is unknown.[104] The preparation of poly(tetrazolato) complexes in either valency (figure 58) would result in a new nitrogen-rich coordination complex of lead and facilitate comparisons between the two ligand types as previously investigated for the lighter complexes of group 14.[103]
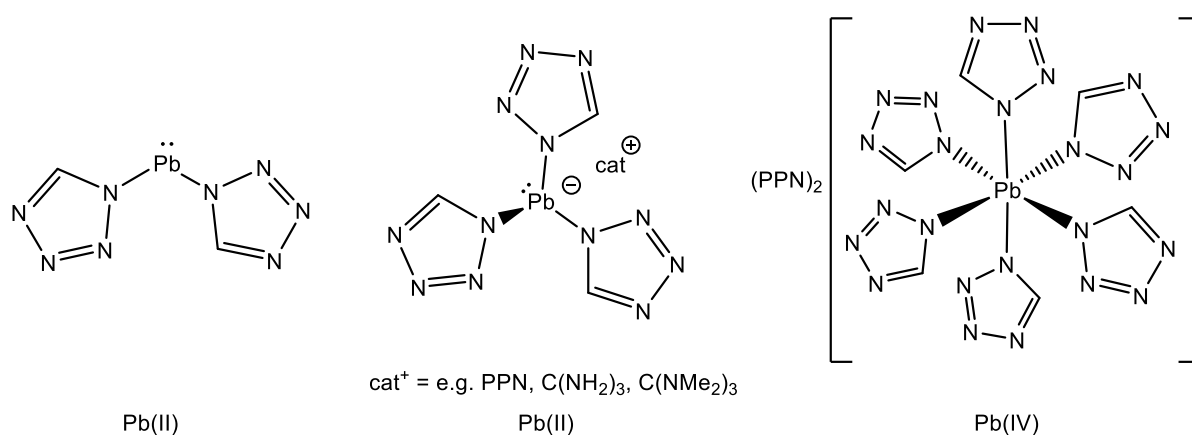
Figure 58. Proposed structures of novel tetrazolato complexes containing Pb(II) or Pb(IV) centres.

## 5.2 Results and discussion

5.2.1. The [PbCl₆]²⁻ anion

(NH₄)₂[PbCl₆] was prepared as a precursor to the [Pb(N₃)₆]²⁻ anion (scheme 46). The solid decomposed slowly in ambient conditions to form an orange solid, accompanied by the release of moisture and a chlorine-like odour. This decomposition was hypothesised to involve the gradual disproportionation of hydrated [PbCl₆]²⁻ into PbCl₂, Cl₂ and H₂O (scheme 46). A pale yellow solution of (NH₄)₂[PbCl₆] in water decolourised after several minutes, accompanied by the formation of colourless crystals. The microanalytical values of these crystals were inconsistent with either PbCl₂·HCl, NH₄Cl or (NH₄)₂[PbCl₆] and their identity remains unknown. Solid (NH₄)₂[PbCl₆] demonstrated reversible thermochromicity and turned orange upon heating under dynamic vacuum.
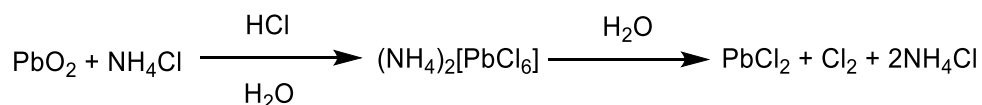

Scheme 46. Preparation and proposed decomposition of (NH₄)₂[PbCl₆].

Recrystallisation of (NH₄)₂[PbCl₆] from MeCN resulted in the formation of a coordination polymer containing Pb(II) centres in space group $P2_1/c$ (figure 59). The anomalously large thermal ellipsoid assigned to Cl(6) is not conclusively identified; it is possible that the electron density originates from adducted HCl, but proton assignment was not possible. Alternative solutions modelled as MeCN or H₂O monosolvates each resulted in a decrease in the overall quality of the structure. The presence of a 1:1 mixture of PbCl₂ and NH₄[PbCl₃] is also eliminated by the significant contraction (ca. 0.2 Å shorter) of the Pb−Cl bonds

(d = 2.860(10)− 2.990(9) Å) compared to those of [PPh$_4$][PbCl$_3$] (d = 2.596(1)−2.703(1) Å), and the low quality of the structure solution when modelled to contain NH$_4^+$ instead of HCl.[229] Therefore, at present the solution containing HCl is the most plausible. As expected, the solvate molecule occupies the voids formed upon packing (figure 59).
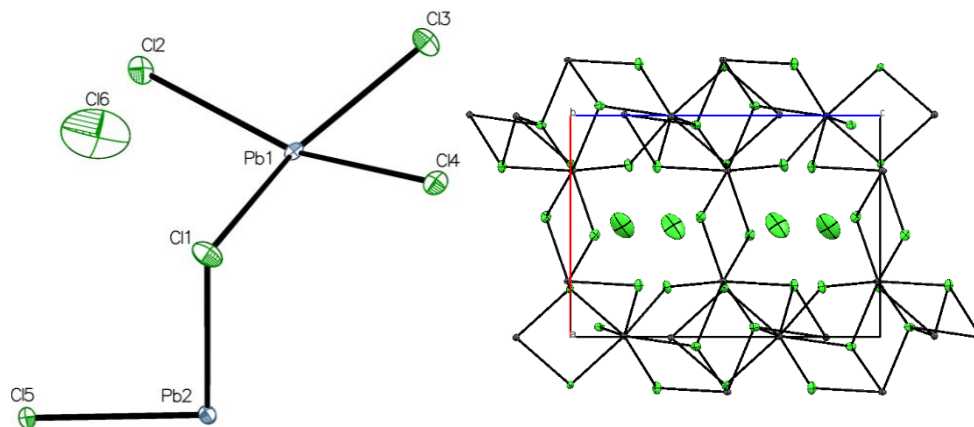
Figure 59. Left: Asymmetric unit in the crystal structure hypothesised as PbCl$_2$·HCl. Grey = Pb, green = Cl. The location of the proton in the structure could not be assigned due to disorder of the Cl atom in HCl. Selected bond distances (Å): Pb(1)−Cl(1) 2.860(10), Pb(1)−Cl(2) 2.903(10), Pb(1)−Cl(2) 2.893(9), Pb(1)−Cl(3) 2.990(9), Pb(1)−Cl(4) 2.968(9), Pb(1)−Cl(4) 2.899(9), Pb(2)−Cl(5) 2.962 (8), Pb(2)−Cl(5) 2.915(8). Right: Packing of PbCl$_2$.HCl in the crystal lattice, viewed down the crystallographic *b* axis.

The relative instability of (NH$_4$)$_2$[PbCl$_6$] and the absence of a phlegmatising cation led to the preparation of [PPN]$_2$[PbCl$_6$] as a more stable precursor for chlorido-azido ligand exchange. The salt is prepared by cation exchange between (NH$_4$)$_2$[PbCl$_6$] and [PPN]Cl. At ambient conditions, the rate of decomposition of [PPN]$_2$[PbCl$_6$] in both solid and solution was significantly slower than (NH$_4$)$_2$[PbCl$_6$]. Although solid [PPN]$_2$[PbCl$_6$] appears stable during prolonged storage periods at low temperature, gentle heating of a MeCN solution (ca. 35 °C) proved sufficient to induce decomposition to form a dark orange solution and release of gas speculated to be Cl$_2$. [PPN]$_2$[PbCl$_6$] crystallises from MeCN as yellow block-shaped crystals with space group *P*2$_1$/c (figure 60). The asymmetric unit contains three PPN cations and two [PbCl$_6$]$^{2-}$ anions, one of the latter of which is located on the crystallographic *a* axis to give an overall formula of 1.5[PPN]$_2$[PbCl$_6$] per asymmetric unit. Structural studies of [PbCl$_6$]$^{2-}$ salts are extremely sparse and occasionally without detailed bond length measurements or estimated standard deviations, i.e. (NH$_4$)$_2$[PbCl$_6$], and comparisons with other hexachloroplumbate(IV) anions are limited. The Pb−Cl bond lengths in [PPN]$_2$[PbCl$_6$] are slightly elongated versus other [PbCl$_6$]$^{2-}$ salts, and significantly so when compared to the hexachloroplumbate(II) salts (i.e., [PbCl$_6$]$^{4-}$) (table 34).[230,231]
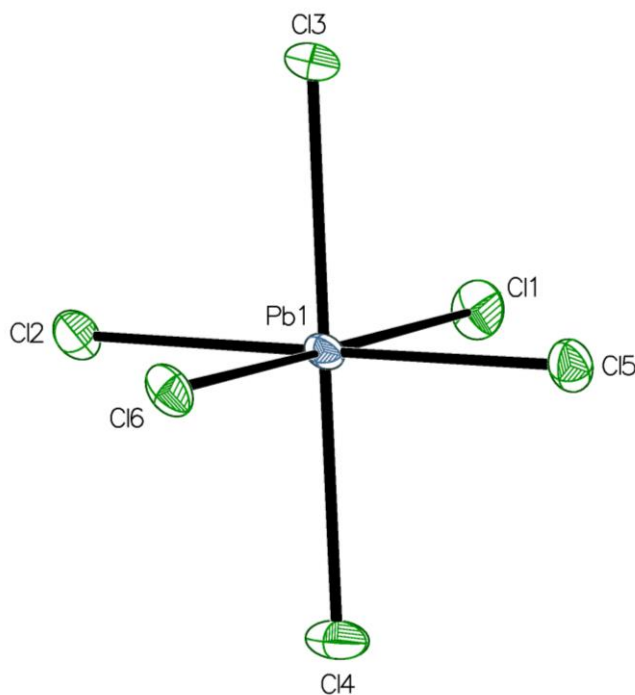
Figure 60. Crystal structure of the $[PbCl_6]^{2-}$ anion in $[PPN]_2[PbCl_6]$. Selected bond lengths (Å) and angles (°): Pb(1)−Cl(1) 2.5037(9), Pb(1)−Cl(2) 2.5287(9), Pb(1)−Cl(3) 2.5058(9), Pb(1)−Cl(4) 2.5217(9), Pb(1)−Cl(5) 2.5211(9), Pb(1)−Cl(6) 2.5249(9), Pb(2)−Cl(7) 2.5171(9), Pb(2)−Cl(8) 2.5309(9), Pb(2)−Cl(9) 2.4978(9); Cl(1)−Pb(1)−Cl(6) 179.42(4), Cl(2)−Pb(1)−Cl(4) 179.08(3), Cl(3)−Pb(1)−Cl(5) 179.19(3), Cl(7)−Pb(2)−Cl(7) 180.0, Cl(8)−Pb(2)−Cl(8) 180.0, Cl(9)−Pb(2)−Cl(9) 180.00.

Compound	Oxidation State	$d_{min,max}$(Pb−Cl) / Å	Refs.
$[PPN]_2[PbCl_6]$		2.5037(9), 2.5287(9)	This work
$(NH_4)_2[PbCl_6]$ [a]	Pb(IV)	2.488	[232]
$(Et_2N)_2[PbCl_6]$ [b]		2.460(8), 2.496(8)	[233]
$Ph_4P[PbCl_3]$ [c]		2.596(1), 2.703(1)	[229]
$(\{H_3N-C_6H_4\}_2)[PbCl_6]$	Pb(II)	2.8258(5), 2.9055(6)	[230]
$(ClC_2H_4NH_3)_6[PbCl_6] \cdot 2Cl^-$		2.850(1), 2.904(1)	[231]

Table 34. Comparison of Pb−Cl bond lengths in hexachloroplumbate salts of Pb(IV) and Pb(II). [a] no estimated standard deviations provided; [b] from powder diffraction pattern; [c] as MeCN solvate.

5.2.2. The $[Pb(N_3)_6]^{2-}$ anion

$[PPN]_2[Pb(N_3)_6]$ was formed as a deep red crystalline solid by chloro-azido ligand exchange between $[PPN]_2[PbCl_6]$ and the ionic azide transfer reagent NaN_3. The intense red colour is consistent with literature reports of other $[Pb(N_3)_6]^{2-}$ salts and is reported to arise from ligand-to-metal charge transfer interactions between the azide ligand π orbitals and the *d* orbitals of

the metal centre.[234,235] These normally symmetry-forbidden interactions are allowed due to the imperfect octahedral geometry of the complex, which decreases the energy difference between the two orbitals and allowing charge-transfer interactions which absorb in the ultra-violet to give a deep red colour (λ_{max} = 390, 318 nm in MeCN).[235] This contrasts the lighter hexa(azido) homologues of Si, Ge and Sn, which are all colourless both in solution and as solids.[95,96,102] Similar ligand-to-metal charge transfer interactions, albeit with a slightly greater energy difference, are reported as the source of the yellow colour of $(NH_4)_2[PbCl_6]$ (λ_{max} 314 and 465 nm in MeCN) and presumably account for the observation of a similar colour for $[PPN]_2[PbCl_6]$ in this work.[236]

The formation of the $[Pb(N_3)_6]^{2-}$ anion resulted in the emergence of two $\nu_{as}(N_3)$ bands in the IR spectrum (figure 61). The position of these bands are lower than those observed in the IR spectra of the lighter group 14 homologues in $[PPN]_2[E(N_3)_6]$ (E = Si−Sn), and continues the downward trend observed from Si−Sn (figures 62,63, table 35). Although the rapid hydrolysis of the $[Pb(N_3)_6]^{2-}$ anion is reported in literature, no HN_3 was observed in the IR spectra of $[PPN]_2[Pb(N_3)_6]$. This decrease in moisture sensitivity has been reported previously for the tetraphenylarsonium salt.[97] The number and intensity ratios of the azide bands in this spectral region is consistent with the increasing trend displayed down the group.
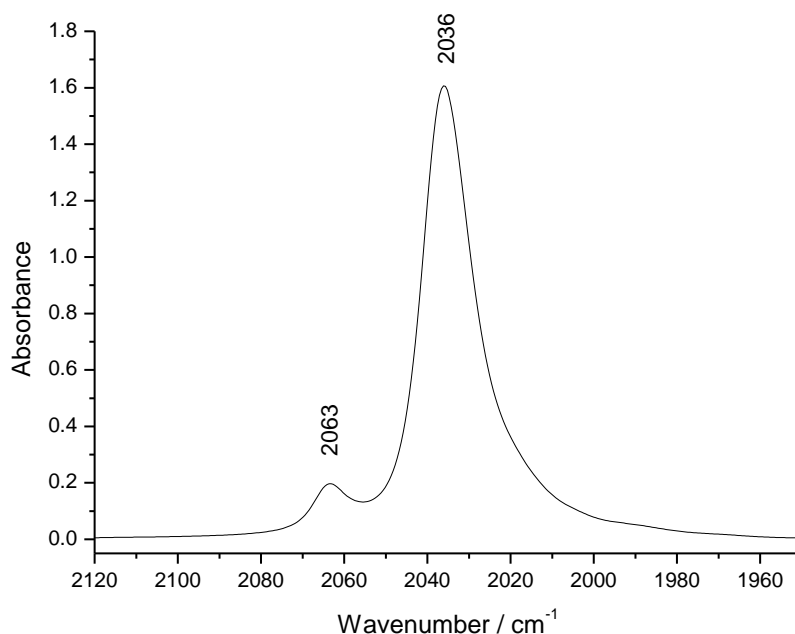

Figure 61. IR spectrum of $[PPN]_2[Pb(N_3)_6]$ in CH_2Cl_2 between 2120−1950 cm^{-1}.

Complex	$\nu_{as}(N_3)/$ cm^{-1}	Ref.
[PPN]$_2$[Si(N$_3$)$_6$]	2108	[95]
[PPN]$_2$[Ge(N$_3$)$_6$]	2083	[96]
[PPN]$_2$[Sn(N$_3$)$_6$]	2111, 2079	[102]
[PPN]$_2$[Pb(N$_3$)$_6$]	2063, 2036	This work

Table 35. Comparison of $\nu_{as}(N_3)$ bands in IR spectra of [PPN]$_2$[E(N$_3$)$_6$] (E = Si−Pb) in CH$_2$Cl$_2$.
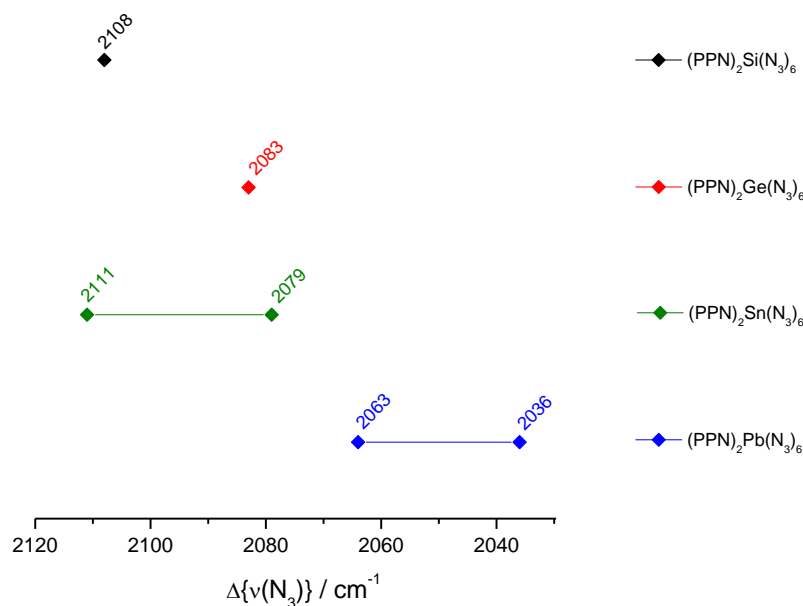
Figure 62. Graphical representation of differences between wavenumbers of $\nu_{as}(N_3)$ bands in [PPN]$_2$[E(N$_3$)$_6$] (E = Si−Pb) in CH$_2$Cl$_2$. Data for E = Si−Sn obtained from references [95,96,102].
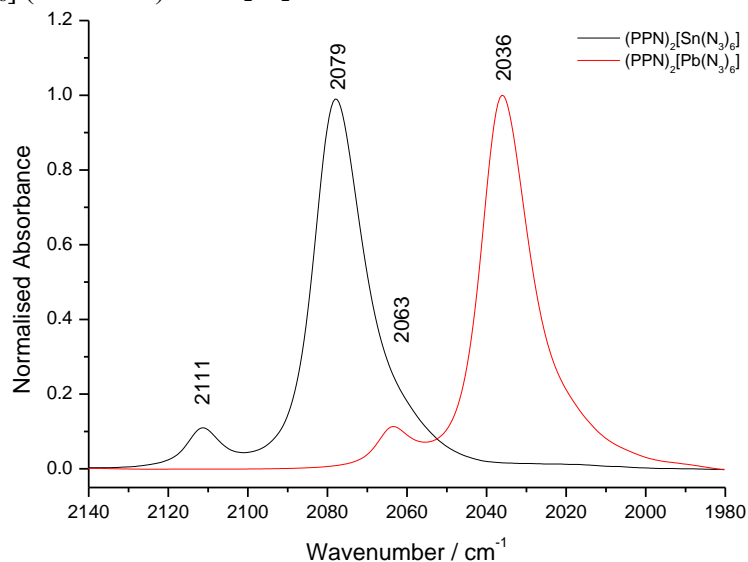
Figure 63. IR spectra of CH$_2$Cl$_2$ solutions of [PPN]$_2$[Sn(N$_3$)$_6$] (black line, −) and [PPN]$_2$[Pb(N$_3$)$_6$] (red line, −), normalised to the most intense $\nu_{as}(N_3)$ band. Data for [PPN]$_2$[Sn(N$_3$)$_6$] obtained from references [102,237].

In contrast to the hexachloroplumbate salt, neither solutions nor solid samples of [PPN]$_2$[Pb(N$_3$)$_6$] underwent noticeable decomposition at room temperature. Crystallisation from MeCN formed deep red block crystals of [PPN]$_2$[Pb(N$_3$)$_6$] in space group P_{bca} (figure 64, 65), containing one PPN cation and half of one [Pb(N$_3$)$_6$]$^{2-}$ anion lying on the crystallographic *a* axis edge (figure 66). A centre of inversion at the coordination centre results in three crystallographically independent azido ligands per anion (figure 65).
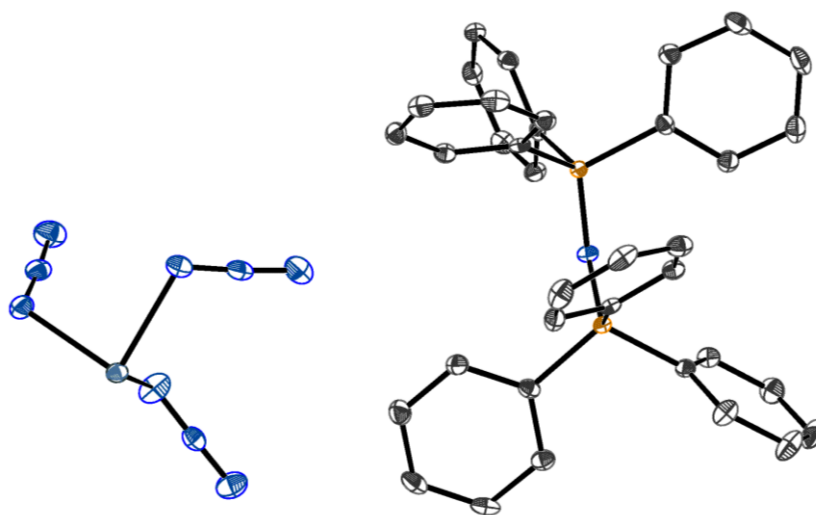
Figure 64. Asymmetric unit of [PPN]$_2$[Pb(N$_3$)$_6$]. Hydrogen atoms omitted for clarity. Grey = C, blue = N, orange = P, turquoise = Pb.
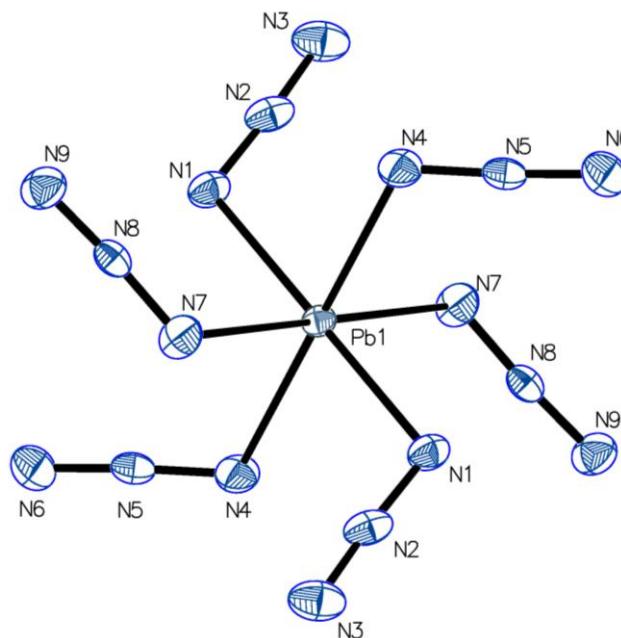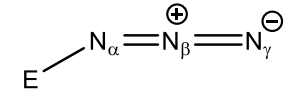
Figure 65. Crystal structure of the [Pb(N$_3$)$_6$)]$^{2-}$ anion in [PPN]$_2$[Pb(N$_3$)$_6$]. Selected bond lengths (Å) and angles (°): N(1)−Pb(1) 2.2481(17), N(4)−Pb(1) 2.2603(18), N(7)−Pb(1) 2.2649(18), N(1)−N(2) 1.222(3), N(2)−N(3) 1.147(3), N(4)−N(5) 1.201(3), N(5)−N(6) 1.155(3), N(7)−N(8) 1.200(3), N(8)−N(9) 1.150(3) ; Pb(1)−N(1)−N(2) 111.07(14), Pb−N(4)−N(5) 113.78(14), Pb(1)−N(7)−N(8) 118.33(14).
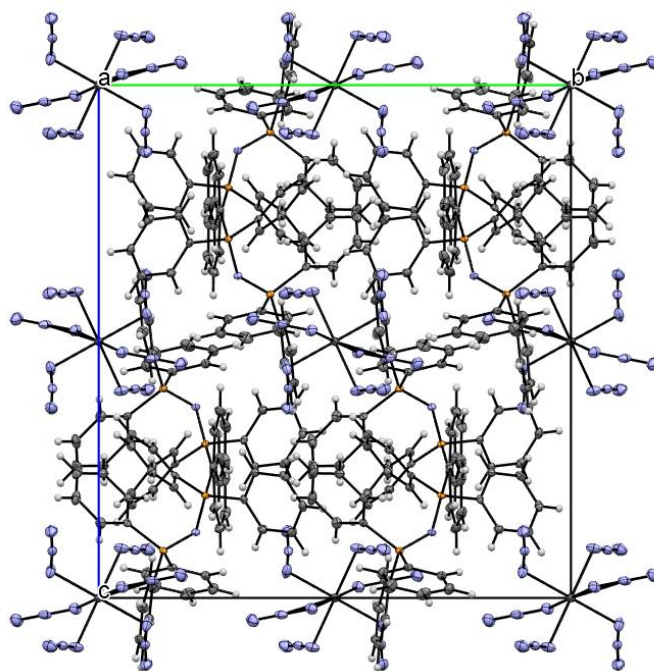
Figure 66. Packing of [PPN]$_2$[Pb(N$_3$)$_6$] in the crystal lattice, viewed down the crystallographic *a* axis.
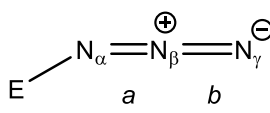
The only previous crystallographic study of the [Pb(N$_3$)$_6$]$^{2-}$ anion is of [Ph$_4$As]$_2$[Pb(N$_3$)$_6$].[177] The average N−N bond length in [PPN]$_2$[Pb(N$_3$)$_6$] is greater than that observed in the structure of [Ph$_4$As]$_2$[Pb(N$_3$)$_6$] reported previously (table 36). As the number of bonds from the coordination centre increases, the terminal N−N bond distance should decrease as the bonding approaches more singly-triply bonded sequences (E−N−N≡N) from the doubly-bonded E−N=N=N sequence.[238] This trend is observed experimentally in the crystallographic studies of the other hexa(azido) complexes of group 14 (figure 67, table 37).[95,96,102] However, only two out of the three crystallographically independent azido ligands in the reported structure of [Ph$_4$As]$_2$[Pb(N$_3$)$_6$] display this trend. The large thermal ellipsoids and higher measurement temperatures present in the structure of the latter may be responsible. Alternatively, as observed for the hexa(cyanido) complexes in chapter 2, it is possible that incomplete chlorido/azido exchange formed a mixed-ligand [Pb(N$_3$)$_{6-x}$Cl$_x$]$^{2-}$ ($x < 1$) anionic species which resulted in inconsistent bond lengths. The absence of available structure factor data for [Ph$_4$As]$_2$[Pb(N$_3$)$_6$] prevented investigation of this theory. By contrast, and in concurrence with the lighter homologues, all three crystallographically-independent azido ligands in [PPN]$_2$[Pb(N$_3$)$_6$] obey the expected trend. Microanalysis confirmed the analytical purity of the latter compound and excluded the possibility of chlorine contamination in the crystal structure. Therefore, the crystallographic study of [PPN]$_2$[Pb(N$_3$)$_6$] in this work can be considered a more accurate structural study of the [Pb(N$_3$)$_6$]$^{2-}$ anion than that of [Ph$_4$As]$_2$[Pb(N$_3$)$_6$] reported previously.

The E−N bond lengths of $[Pb(N_3)_6]^{2-}$ are longer than those in the $[Sn(N_3)_6]^{2-}$ anion, continuing the trend of increasing E−N bond lengths as the group 14 coordination centre changes from Si−Pb (table 38). The increased contraction of the N_α−N_β bonds in $[Pb(N_3)_6]^{2-}$ originates from the longer E−N bond lengths and results in a larger range of N_β−N_γ bond lengths than the lighter congeners.

$E\diagdown N_\alpha\!\!=\!\!\!\overset{\oplus}{N_\beta}\!\!=\!\!\overset{\ominus}{N_\gamma}$	[Ph₄As]₂[Pb(N₃)₆] T = 294 K	[PPN]₂[Pb(N₃)₆] T = 100 K	$\Delta(\bar{d})$/ Å
Space Group	$P\bar{1}$	P_{bca}	–
$d(N_\alpha$−$N_\beta)$ / Å	1.137−1.199	1.200(3)−1.222(3)	0.037
$d(N_\beta$−$N_\gamma)$ / Å	1.093−1.165	1.147(3)−1.155(3)	0.029
$d(Pb$−$N_\alpha)$ / Å	2.217−2.257	2.2481(17)−2.2649(18)	0.014

Table 36. Summary and comparison of average bond lengths of [cat]₂[Pb(N₃)₆] (cat = [Ph₄As]⁺, [PPN]⁺). Δ is the difference between the average bond length for each salt.

		$(a)-(b)$ / Å		
cat⁺	**1**	**2**	**3**	
[Ph₄As]⁺	0.095	-0.027	0.08	
[PPN]⁺	0.075	0.046	0.05	

$a = N_\alpha$−N_β
$b = N_\beta$−N_γ
$d(a) < d(b)$

Figure 67 (left), **table 37** (right). Pattern of bond distances expected in a coordinated azido ligand and comparison of a (N_α−N_β) and b (N_β−N_γ) bond distances in the crystal structures of (cat)₂[Pb(N₃)₆]²⁻ (cat = [Ph₄As]⁺, [PPN]⁺). **1−3** represent each of the three crystallographically independent azido ligands in the $[Pb(N_3)_6]^{2-}$ anion.[177,238]

In concurrence with the PPN salts of the lighter homologues, [PPN]₂[Pb(N₃)₆] showed no energetic decomposition towards regular preparative operations and appeared insensitive to impact on a 5 mg scale. At elevated temperatures (T = 100 °C), the solid turned black and formed a colourless liquid of unknown identity upon melting (m.p. = 169−171 °C).[239]

	[PPN]$_2$[E(N$_3$)$_6$]			
E	**Si**	**Ge**	**Sn^a**	**Pb**
T / K	180	160	100	100
Space Group	$P\bar{1}$	$P\bar{1}$	$P\bar{1}$	P_{bca}
d(E−N) / Å	1.866(1)−	1.969(2)−	2.122(2)−	2.2481(17)−
	1.881(1)	1.980(2)	2.147(2)	2.2649(18)
d(N$_\alpha$−N$_\beta$) / Å	1.198(2)−	1.210(3)−	1.206(4)−	1.200(3)−
	1.207(2)	1.214(3)	1.222(10)	1.222(3)
d(N$_\beta$−N$_\gamma$) / Å	1.144(2)−	1.143(3)−	1.128(6)−	1.147(3)−
	1.146(2)	1.152(4)	1.148(3)	1.155(3)
Refs.	[95]	[96]	[102]	This work

Table 38. Comparison of bond distances for [E(N$_3$)$_6$]$^{2-}$ anions in crystal structures of [PPN]$_2$[E(N$_3$)$_6$] (E = Si−Pb). ^{a} disordered structure.

### 5.2.3 Preparation of the [Pb(N$_3$)$_3$]$^-$ anion

The sole report of [Pb(N$_3$)$_3$]$^-$ (as [Ph$_4$As][Pb(N$_3$)$_3$]) describes its formation from photolysis of [Ph$_4$As]$_2$[Pb(N$_3$)$_6$].[177] Characterisation of the photolysis product is limited to elemental analysis and two reported ν_{as}(N$_3$) bands in the IR spectrum. However, the absence of any further reports concerning the triazidoplumbate anion mean that the reactivity and properties of the complex are unclear. Interestingly, the mass spectrum of [PPN]$_2$[Pb(N$_3$)$_6$] prepared in this study contained a fragment (m/z = 333) with an isotope pattern consistent with [Pb(N$_3$)$_3$]$^-$.[177]

In order to further investigate the synthesis and reactivity of the elusive [Pb(N$_3$)$_3$]$^-$ anion, the photolysis of [Pb(N$_3$)$_6$]$^{2-}$ described in literature was replicated to obtain [PPN][Pb(N$_3$)$_3$].[177] Several days of daylight exposure resulted in the discolouration of an initially red acetone solution of [PPN]$_2$[Pb(N$_3$)$_6$] and the precipitation of a white solid. The precipitation of solid appeared to occur both during and after the discolouration of the solution, with a negligible amount of precipitate observed immediately following discolouration and the majority of the precipitate appearing to form *after* discolouration. IR spectroscopic monitoring of the reaction solution showed the disappearance of the azide bands of the [Pb(N$_3$)$_6$]$^{2-}$ anion alongside the growth of three new, weaker bands in the spectral region typically populated by ionic azides (figure 68). The position of the band at 2030 cm^{-1} is similar to that reported for [Pb(N$_3$)$_3$]$^-$ ($\tilde{\nu}$ = 2038 cm^{-1}).[177] Two bands at 2010 and 2000 cm^{-1} arise from [PPN]N$_3$. The same spectroscopic behaviour was observed in MeCN solution (figure 70). The presence of an

isosbestic point at 2020 cm^{-1} suggests that the decomposition of [PPN]$_2$[Pb(N$_3$)$_6$] in MeCN occurs as part of the same process that results in the formation of [PPN]N$_3$.
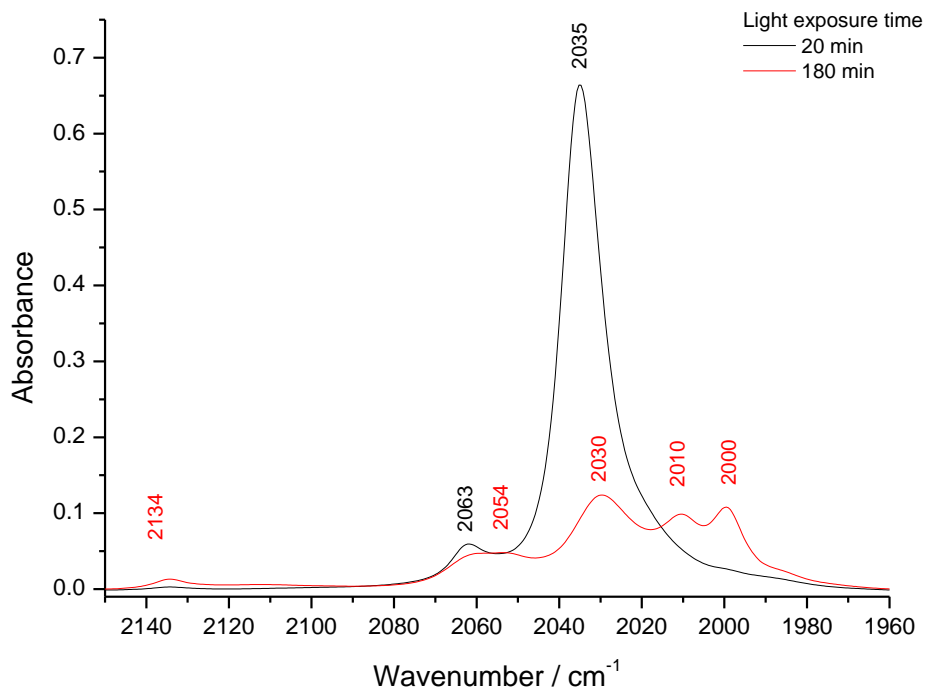
Figure 68. Spectral series showing decomposition of an acetone solution of [PPN]$_2$[Pb(N$_3$)$_6$] upon exposure to daylight for 20 mins (black line, −) and 180 mins (red line, −). The bands at 2010 and 2000 cm^{-1} are assigned to [PPN]N$_3$.
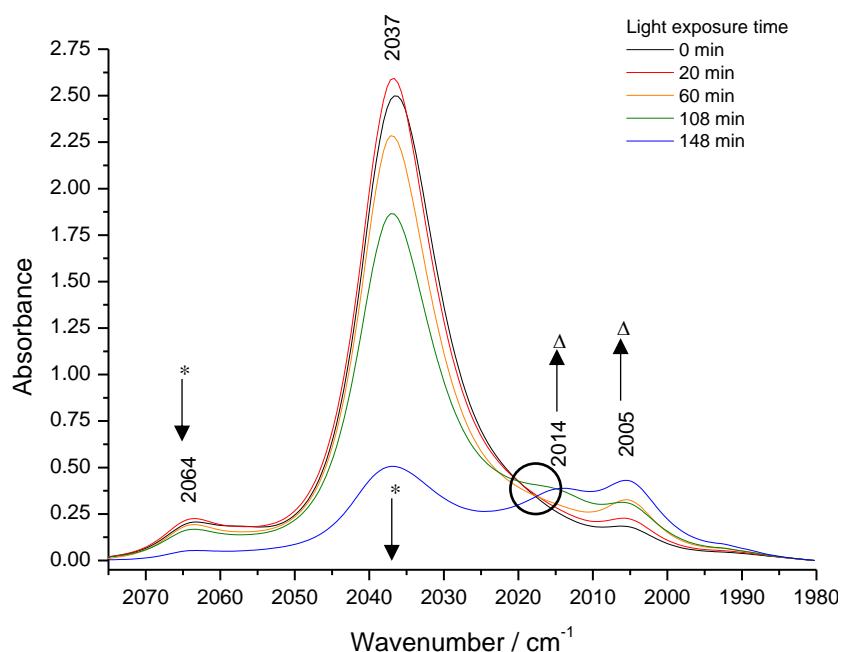

Figure 69. IR spectral series showing the decomposition of a MeCN solution of [PPN]$_2$[Pb(N$_3$)$_6$] upon light exposure, showing the decrease in bands associated with [Pb(N$_3$)$_6$]$^{2-}$ (*), an isosbestic point at 2020 cm^{-1} (O) and an increase in bands associated with [PPN]N$_3$ (Δ).

The IR spectrum of the solid precipitate obtained from the photolysis study in acetone proved spectroscopically identical to a genuine sample of $Pb(N_3)_2$. Evaporation of the supernatant acetone solution yielded a solid, the IR spectrum of which was dominated by an extremely strong azide band at 2014 cm^{-1} of almost identical shape and spectral position to the $\nu_{as}(N_3)$ band of $[PPN]N_3$ (albeit at slightly higher wavenumbers). In combination with gravimetric analysis, these findings confirm that the photolysis of $[PPN]_2[Pb(N_3)_6]$ eventually results in the formation of $Pb(N_3)_2$ and $[PPN]N_3$ (scheme 47) and that $[PPN][Pb(N_3)]$ is not stable towards prolonged storage in solution, if at all. The azide bands in the original report ($\tilde{\nu}$ = 2038 and 1309 cm^{-1}) are also extremely similar to those reported for $[Ph_4As]N_3$ in solution ($\tilde{\nu}$ = 2037 and 1314/1311 cm^{-1}) and align with the results obtained in this study (table 39).[240,241]

Compound	$\nu_{as}(N_3)$ / cm^{-1}
$[PPN]_2[Pb(N_3)_6]$	2062, 2035
$[PPN]N_3$	2010, 2000
$Pb(N_3)_2$ [a]	2112, 2000
$[Ph_4As][Pb(N_3)_3]$	2038
This study	2030, 2011, 2000

Table 39. Comparison of wavenumbers of asymmetric $\nu(N_3)$ stretching vibrations observed in IR spectra of acetone solutions of $[PPN]_2[Pb(N_3)_6]$, $Pb(N_3)_2$, $[PPN]N_3$, $[Ph_4As][Pb(N_3)_3]$ and the unknown photolysis product obtained in this study.[177] [a] recorded as a suspension.

$$(PPN)_2[Pb(N_3)_6] \xrightarrow[\text{MeCN/Me}_2\text{CO}]{h\nu,\ rt} Pb(N_3)_2 + 2PPN(N_3) + 3N_2$$
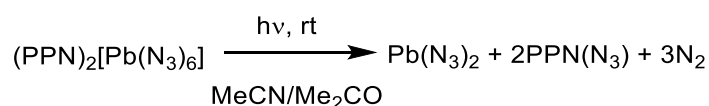
Scheme 47. Formation of $Pb(N_3)_2$ and $[PPN]N_3$ from $[PPN]_2[Pb(N_3)_6]$ in solution.

In analogy to the reported preparation of the $[PbCl_3]^-$ anion from $PbCl_2$ and a chloride salt, an acetonitrile suspension of $Pb(N_3)_2$ and $[PPN]N_3$ was monitored spectroscopically to determine if $[PPN][Pb(N_3)_3]$ could form by ligand addition.[242] Overnight stirring at room temperature resulted in the formation of a new band at 2014 cm^{-1} and a decrease in the absorbance intensity of the azide band of $[PPN]N_3$. However, after a short period of further stirring (3 h), the newly-formed band had disappeared and the azide band of $[PPN]N_3$ had returned to its original absorbance intensity. The filter residue was spectroscopically identical to $Pb(N_3)_2$ and the spectral position of the band observed in solution at $\tilde{\nu}$ = 2014 cm^{-1} was consistent with ionic azide salts. Extrapolation of IR spectral data of solutions of $[E(N_3)_3]^-$ (E = Ge, Sn) predicts both the number and position of the $\nu_{as}(N_3)$ band/s of the $[Pb(N_3)_3]^-$ anion to differ to both those

observed in this study and reported by Polborn *et al.* (table 40) and suggests that [PPN][Pb(N$_3$)$_3$] was not formed.[177,182]

Compound	Solvent	$\nu_{as}(N_3)$ / cm^{-1}
[PPN][Ge(N$_3$)$_3$]	MeCN	2095, 2064
[PPh$_4$][Sn(N$_3$)$_3$]	THF	2081, 2075, 2050
[PPN][Pb(N$_3$)$_3$]	MeCN	(ca. 2067−2061, 2050) [a], 2014 [b]
[Ph$_4$As][Pb(N$_3$)$_3$]	Acetone	2038

Table 40. Observed and predicted $\nu_{as}(N_3)$ bands in IR spectra of solutions containing the [E(N$_3$)$_3$]$^-$ anion (E = Ge−Pb).[177,182] [a] predicted ; [b] observed.

The concurrent change in intensity of the $\nu_{as}(N_3)$ band of [PPN]N$_3$ with the formation and disappearance of the unknown $\nu_{as}(N_3)$ band at 2014 cm^{-1} indicates that a reaction of some [PPN]N$_3$ does occur. The known stability of [PPN]N$_3$ in MeCN over the short reaction period precludes any reactions only involving the salt itself, and is instead more likely to involve reaction with Pb(N$_3$)$_2$ to form [Pb(N$_3$)$_3$]$^-$ as a transient species. Further reactions of both anionic and neutral complexes of Pb(II) did not form [Pb(N$_3$)$_3$]$^-$. Although the reaction of PbCl$_2$ with [PPN]N$_3$ in MeCN resulted in the formation of a turbid white suspension, no changes were observed in the IR spectrum of the supernatant solution and the IR spectrum of the solid filter residue was consistent with a mixture of [PPN]N$_3$ and Pb(N$_3$)$_2$. Combination of [PPN][PbCl$_3$] with NaN$_3$ in MeCN resulted in a suspension which contained weak $\nu(N_3)$ bands that were inconsistent to NaN$_3$ and Pb(N$_3$)$_2$, but no product was able to be isolated and the existence or extent of ligand exchange could not be determined.

The additional, unexplained azide bands observed in both photolysis of Pb(IV) and addition reaction of Pb(II) centres suggests that an additional azido species is formed in solution. The spectral position of these bands are most consistent with a Pb(II) azido complex or an ionic azide. However, [PPN][Pb(N$_3$)$_3$] was not isolated and the only confirmed formation of the [Pb(N$_3$)$_3$]$^-$ anion in this work occurs upon fragmentation of [PPN]$_2$[Pb(N$_3$)$_6$] during mass spectrometric analysis. It is possible that [Pb(N$_3$)$_3$]$^-$ exists in equilibrium with Pb(N$_3$)$_2$ which is heavily shifted to favour formation of the latter (scheme 48).

$$Pb(N_3)_2 + N_3^- \rightleftharpoons [Pb(N_3)_3]^-$$
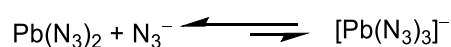
Scheme 48. Equilibrium between Pb(N$_3$)$_2$ and [Pb(N$_3$)$_3$]$^-$, shifted towards the formation of Pb(N$_3$)$_2$ and N$_3^-$.

An alternative explanation is that both the ligand addition reaction of $Pb(N_3)_2$ and the photolysis of $[Pb(N_3)_6]^{2-}$ results in the formation of $[Pb(N_3)_3]^-$ in solution, but the stability of the product is too low to allow isolation prior to decomposition. Decomposition is hypothesised to proceed by the elimination of $[PPN]N_3$ and formation of $Pb(N_3)_2$, both of which are observed in the photolytic decomposition of $[PPN]_2[Pb(N_3)_6]$ (scheme 49). The indirect formation of $Pb(N_3)_2$ also accounts for the continued formation of solid *after* the deep orange/red solutions of $[Pb(N_3)_6]^{2-}$ turned colourless in daylight. The decomposition stimuli and presence of solvent-induced stabilisation for the proposed $[Pb(N_3)_3]^-$ are unclear. The varying solvent polarities may account for the different rates of reaction of acetone and MeCN solutions, and accounts for the prolonged time period reported for the photoinduced formation of $[Ph_4As][Pb(N_3)_3]$. Further work, focusing on trapping the unstable intermediary tri(azido)plumbate anion prior to decomposition into $Pb(N_3)_2$ is required before this hypothesis can be confirmed. However, the initial evidence obtained and examined here suggests that if the $[Pb(N_3)_3]^-$ anion *can* form, its existence in solution is limited. The results of this study confirm that the photolysis of $[Pb(N_3)_6]^{2-}$ ultimately results in the formation of a mixture of $Pb(N_3)_2$ and the appropriate azide salt. A 1:1 binary mixture of $[Ph_4As]N_3$ and $Pb(N_3)_2$ would generate identical microanalytical values to those reported to arise from $[Ph_4As][Pb(N_3)_3]$ and therefore the reported preparation of $[Pb(N_3)_3]^-$ cannot be confirmed or disproved without further study.[177]

$$[cat]_2[Pb(N_3)_6] \xrightarrow[\substack{-\,[cat]N_3 \\ -\,N_2}]{h\nu} [cat][Pb(N_3)_3] \xrightarrow[-\,[cat]N_3]{} Pb(N_3)_2$$
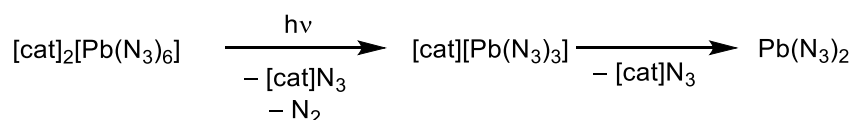
Scheme 49. Proposed formation and subsequent decomposition of $[cat]_2[Pb(N_3)_6]$ into $Pb(N_3)_2$ and $[cat]N_3$; cat = e.g. Ph_4As^+, $[PPN]^+$.

5.2.4 Charge-neutral Lewis base adducts of $Pb(N_3)_4$

Chelating Lewis bases have been demonstrated to stabilise lighter group 14 charge-neutral tetraazides as $E(N_3)_4(L)$ (E = Si, Ge, Sn, L = bipy, phen).[96,102,243] The isolation of $[Pb(N_3)_6]^{2-}$ salts demonstrates that poly(azido) complexes of Pb(IV) can be stabilised using the same strategy employed for the lighter coordination centres of group 14. However, the absence of analogous $Pb(N_3)_4(L)$ means that it is unclear if $Pb(N_3)_4$ can also be stabilised using the same strategy. To date, the only charge-neutral, base-stabilised, poly(azido) lead complexes known contain Pb(II) coordination centres as $\{Pb(N_3)_2(L)_2\}_2$ (L = $Me_2(phen)$, phen).[220–222,224,244] Consequently, the synthesis of $Pb(N_3)_4(bipy)$ was attempted to determine whether charge-

neutral and unknown $Pb(N_3)_4$ could stabilised through the same strategy proven to be successful for the lighter group 14 neutral tetraazides.

The lighter base-stabilised tetraazides are prepared from ligand exchange reactions involving chelating Lewis bases and anionic $[E(N_3)_6]^{2-}$ salts in CH_2Cl_2. The formation of $E(N_3)_4(L)$ in solution is accompanied by the precipitation of insoluble NaN_3, which provides an additional thermodynamic driving force to that afforded by ligand chelation.[96,102,243] This strategy was employed in the attempts to prepare $Pb(N_3)_4(bipy)$ from $(NH_4)_2[Pb(N_3)_6]$, prepared *in situ* by the reaction of $(NH_4)_2[PbCl_6]$ (scheme 50). Although the latter compound is water soluble, the use of aqueous conditions for the formation of the $[Pb(N_3)_6]^{2-}$ salts would remove the thermodynamic driving force afforded by the usual precipitation of NaN_3 upon bipy complexation. To overcome this, a biphasic CH_2Cl_2/H_2O solvent system, previously employed in the reported preparation of $(NH_4)_2[Pb(N_3)_6]$, was used to form $Pb(N_3)_4(bipy)$ in a separate layer to $(NH_4)_2[Pb(N_3)_6]$.[97] This strategy prevented the establishment of an equilibrium between the two complexes and facilitated the separation of both unreacted $[Pb(N_3)_6]^{2-}$ and other byproducts from both steps of the reaction. The explosive character reported for $(NH_4)_2[Pb(N_3)_6]$ meant that the compound was never isolated from solution. Light was excluded from the reaction to prevent unwanted photoreactions of any reaction intermediates (i.e., $[Pb(N_3)_6]^{2-}$) or products.

$$(NH_4)_2[PbCl_6] \xrightarrow[\text{H}_2\text{O}]{\text{NaN}_3} (NH_4)_2[Pb(N_3)_6] \xrightarrow[\text{CH}_2\text{Cl}_2]{\text{bipy}} \underset{\substack{\text{organic} \\ \text{layer}}}{Pb(N_3)_4(bipy)} + \underset{\substack{\text{aqueous} \\ \text{layer}}}{2NH_4N_3}$$
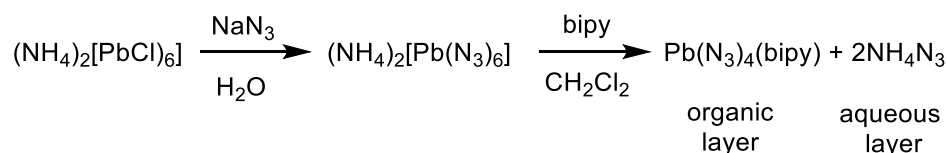
Scheme 50. Synthesis of $Pb(N_3)_4(bipy)$ from $(NH_4)_2[PbCl_6]$.

The complexation of $[Pb(N_3)_6]^{2-}$ and bipy (scheme 50) was indicated by a rapid colour change of the organic layer from colourless to orange. Two new azide bands were observed in the IR spectrum of the organic layer (figure 70) alongside bands associated with both free and coordinated bipy. An additional band at 2138 cm^{-1} arises from HN_3, which is formed upon hydrolysis of an azido complex during sample preparation. It is possible that some hydrolysis of $Pb(N_3)_4(bipy)$ occurred at the solvent interface to reform $(NH_4)_2[Pb(N_3)_6]$ in the aqueous layer, accounting for both the non-qualitative yield and the detection of HN_3 in the IR spectrum of the product solution. The hydrolysis of $(NH_4)_2[Pb(N_3)_6]$ may also be responsible. Alternatively, it is possible that HN_3 is formed upon creation of an equilibrium with ammonium azide in aqueous solution, as proposed by Möller (scheme 51).[227] The close overlap of the

$\nu_{as}(N_3)$ bands of $Pb(N_3)_4(bipy)$ and $[Pb(N_3)_6]^{2-}$ precluded detection of the latter in the analyte solution. However, the high solubility of $(NH_4)_2[Pb(N_3)_6]$ in H_2O is assumed to minimise the amount of $[Pb(N_3)_6]^{2-}$ salts present in the organic layer. The observation of bands associated with uncoordinated bipy is due to the use of a slight excess and the incomplete conversion of all $(NH_4)_2[PbCl_6]$ into $Pb(N_3)_4(bipy)$.

$$NH_4N_3 \rightleftharpoons NH_3 + HN_3$$

Scheme 51. Equilibrium between NH_4N_3 and HN_3, proposed by Möller to be present in solutions of $(NH_4)_2[Pb(N_3)_6]$.[227]
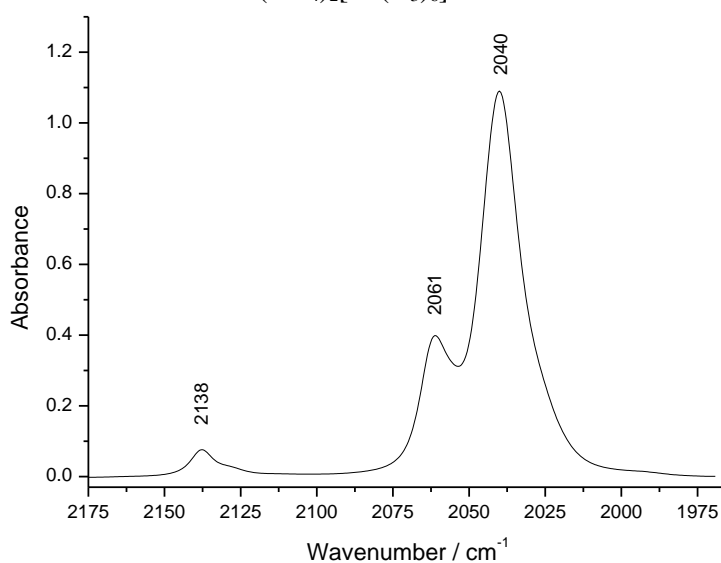
Figure 70. IR spectrum of $Pb(N_3)_4(bipy)$ in CH_2Cl_2 between $2175-1965$ cm^{-1}. The band at 2138 cm^{-1} arises from HN_3.

The removal of all solvent from solutions of $Pb(N_3)_4(bipy)$ under dynamic vacuum resulted in a dark orange/red crystalline solid. On several occasions, upon the application of minimal or no apparent stimuli (e.g. movement), the solid exploded, forming a black residue (believed to be soot and metallic lead, figure 71) and a strong odour. Decomposition of even small amounts (approx. 13 mg) was sufficient to result in the breakage of a small area of the Schlenk tube containing the compound. On one occasion, placing a spatula containing traces of crystallised material onto a bench was sufficient to induce decomposition with a loud report. Although the compound appeared extremely energetic and particularly sensitive towards impact and/or friction, precise decomposition stimuli were not determined and it is recommended that quantities no greater than 10 mg are isolated at any given time (see Experimental Section).

Figure 71. Residues following decomposition of ca. 5 mg of $Pb(N_3)_4(bipy)$ in an NMR tube under dynamic vacuum.

Several crystallographic studies were performed on single crystals of $Pb(N_3)_4(bipy)$. The rapid crystallisation of a saturated solution of $Pb(N_3)_4(bipy)$ in CH_2Cl_2 resulted in dark orange/red block crystals of $Pb(N_3)_4(bipy)$ in space group $P\bar{1}$ (figure 72). The asymmetric unit contains a single $Pb(N_3)_4(bipy)$ molecule composed of two disordered parts, each rotated approximately 30° from the other about the coordination centre. The absorption of radiation by the coordination centre led to radiative decomposition, which contributed to large amounts of disorder in the structure. Further disorder is believed to originate from the rapid rate of crystallisation that was critical to avoid decomposition in solution (see below).
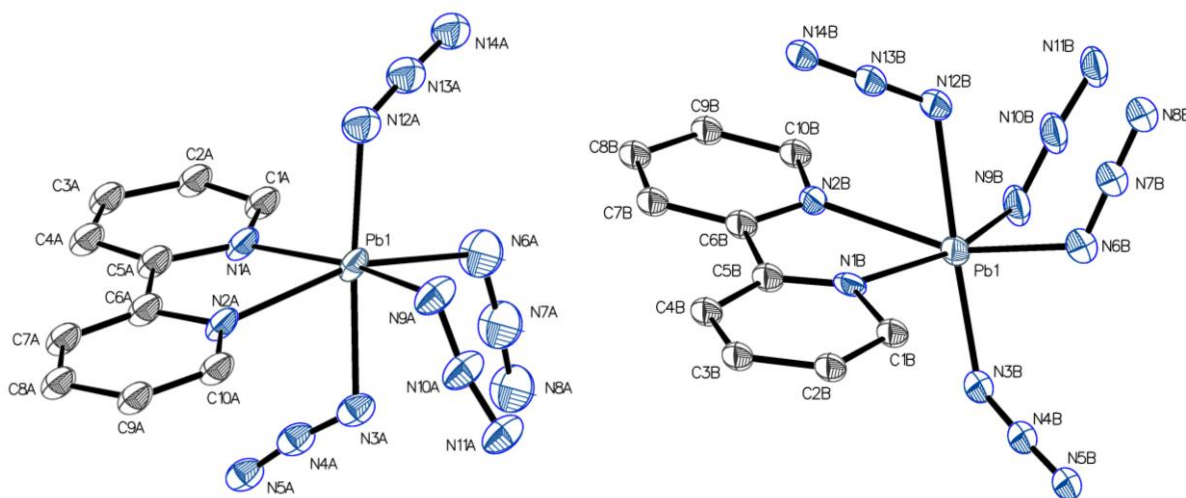
Figure 72. Crystal structure of both disordered parts of $Pb(N_3)_4(bipy)$. Hydrogen atoms omitted for clarity. The arrangement of both disordered parts in the structure is detailed in the Appendix.

All four azido ligands in both disordered parts possess N−N bond lengths comparable to those observed in the lighter homologues of $E(N_3)_4(bipy)$ (E = Si−Sn), with angles close to the planarity expected for azido ligands ($\angle_{(N–N–N)} = 170.30°−177.32°$) (table 41). Although the bond angle between each adjacent azide ligand is approximately 90°, those between opposite ligands in the same plane are significantly less than 180°, resulting in a distorted octahedral geometry (figure 73). The largest distortion from planarity occurs for the azido ligand *trans* to the bipy ring. $Pb(N_3)_4(bipy)$ is therefore a rare example of the octahedral Pb(IV)−N$_6$ coordination skeleton, alongside the $[Pb(N_3)_6]^{2-}$ and $[Pb(NH_2)_6]^{2-}$ anions.[97,245,246]
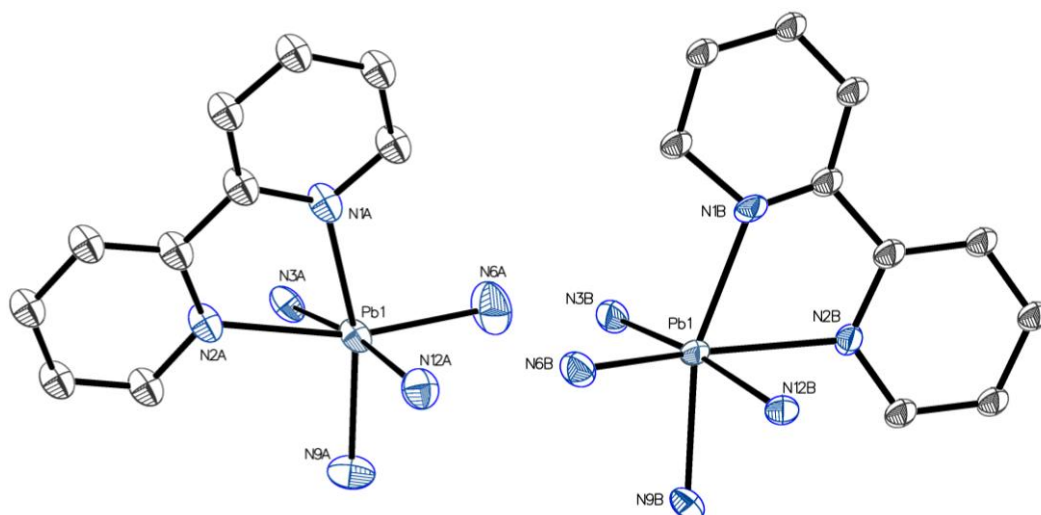
Figure 73. Distortion of Pb−N$_6$ framework from perfect octahedral geometry. For clarity, hydrogen atoms are omitted and only the ligating atom of each azido ligand in one disordered part is shown.

	Disordered Part	
Bond Sequence	**Part 1**	**Part 2**
d(Pb−N$_\alpha$) / Å	2.17(4)−2.33(5)	2.07(4)−2.37(5)
d(N$_\alpha$−N$_\beta$) / Å	1.198(18)−1.22(2)	1.20(2)−1.223(19)
d(N$_\beta$−N$_\gamma$) / Å	1.135(18)−1.15(2)	1.146(19)−1.156(19)
∠(N$_\alpha$−N$_\beta$−N$_\gamma$) / °	169(5)−176(5)	168(5)−177(5)

Table 41. Comparison of bond lengths (Å) and angles (°) of crystal structure of Pb(N$_3$)$_4$(bipy).

Despite the distortion in the coordinative framework, the other crystallographic bond lengths and angles are also similar to those observed for the lighter homologues of E(N$_3$)$_4$(bipy) (E = Si−Sn). As expected, the greatest E−N$_3$ bond length is observed when E = Pb, continuing the increasing trend observed from Si−Sn (table 42) and in analogy to [E(N$_3$)$_6$]$^{2-}$. The Pb−N$_\alpha$ bond lengths are only slightly elongated compared to those calculated for Pb(N$_3$)$_4$ (table 43).[228]

|	E(N₃)₄(bipy)			
	Si	**Ge**	**Sn**	**Pb**
Space Group	$P2_1$	$P\bar{1}$	C_c	$P\bar{1}$
T/ K	180	180	120	100
$d(E-N_\alpha)_{min, max}$ / Å	1.818(2), 1.864(2)	1.925(2), 1.972(2)	2.097(6), 2.110(5)	2.17(4), 2.33(5)
$d(E-N_{bipy})$ / Å	1.969(1), 1.943(2)	2.057(2), 2.046(2)	2.204(6), 2.211(15)	2.31(2), 2.310(18)
$d(N_\alpha-N_\beta)_{min, max}$ / Å	1.207(2), 1.220(2)	1.208(2), 1.223(2)	1.203(8), 1.228(18)	1.198(18), 1.22(2)
$d(N_\beta-N_\gamma)_{min, max}$ / Å	1.134(2), 1.142(2)	1.137(2), 1.142(3)	1.126(8), 1.150(10)	1.135(18), 1.15(2)
Refs.	[243]	[96]	[102]	This work

Table 42. Comparison of key bond lengths of E(N₃)₄(bipy) (E = Si−Pb) studied crystallographically. [a] disordered part 1 only.

Bond sequence	**Pb(N₃)₄(bipy)** [a]	**Pb(N₃)₄**	**Δ / Å**
$d(Pb-N_\alpha)$ / Å	2.17(4)−2.33(5)	2.205	0.035−0.125
$d(N_\alpha-N_\beta)$ / Å	1.198(18)−1.22(2)	1.230	0.032−0.01
$d(N_\beta-N_\gamma)$ / Å	1.135(18)−1.15(2)	1.136	0.001−0.014
Refs.	This work	[228]	−

Table 43. Comparison of Pb−N and N−N bond lengths of Pb(N₃)₄(bipy) (determined crystallographically) and Pb(N₃)₄ (predicted theoretically), and the difference between them. [a] disordered part 1 only.

Prolonged cooling of saturated solutions of Pb(N₃)₄(bipy) resulted in the spontaneous formation of deep orange/red needle crystals, similar in appearance to those discussed above. In order to avoid the radiative decomposition encountered during the crystallographic study of Pb(N₃)₄(bipy), crystallographic studies were performed using weaker-flux Cu−Kα radiation. Surprisingly, this study revealed the presence of a dimeric lead complex containing an uneven distribution of azido and bipy ligands between both coordination centres. Partial substitution of one azido ligand by chlorine generated a structure formulation of Pb(bipy)₃(N₃)₅.₂Cl₀.₈ (figure 74). Two azido ligands appear to participate in μ₁,₁ bridging interactions between the Pb centres. The arrangement of the bipy ligands prevents the formation of coordination polymers by blocking intermolecular coordination of further azido ligands to the Pb(bipy)₃ subunit. The obtained structure contrasts that of the Pb(II) analogue {Pb(N₃)₂(phen)₂}₂, which

contains an even distribution of azido and phen ligands between the two coordination centres alongside bridging interactions through one ($\mu_{1,1}$) or two ($\mu_{1,3}$) nitrogen atoms of the four azido ligands (figure 76).[244]
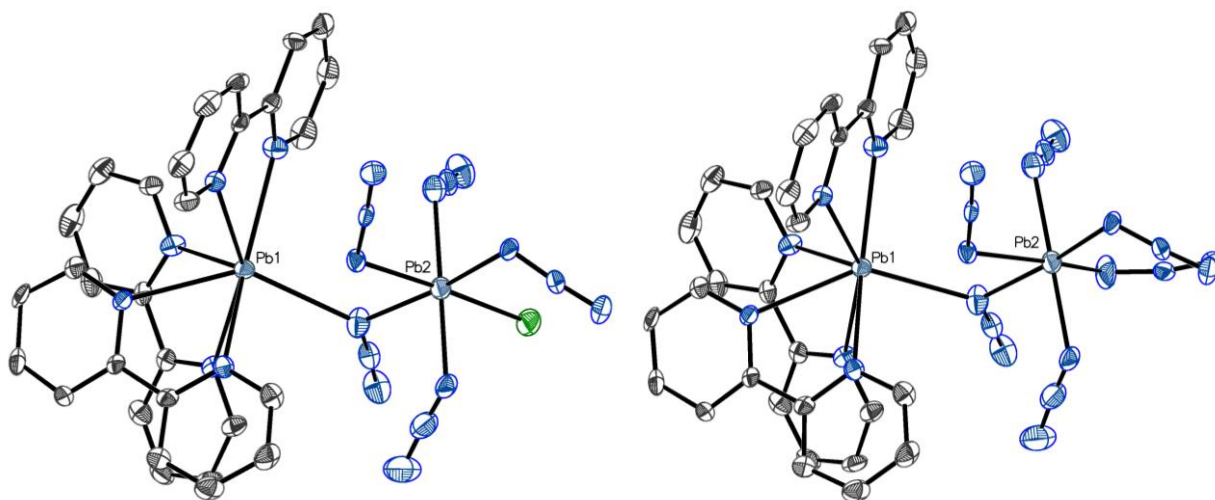
Figure 74. Structures of $Pb_2(N_3)_5(bipy)_3Cl$ (left) and $Pb_2(N_3)_6(bipy)_3$ (right) present in the crystal structure of $Pb(bipy)_3(N_3)_{5.2}Cl_{0.8}$. Hydrogen atoms omitted for clarity. Grey = C, blue = N, green = Cl. Selected bond lengths are given in table 44.
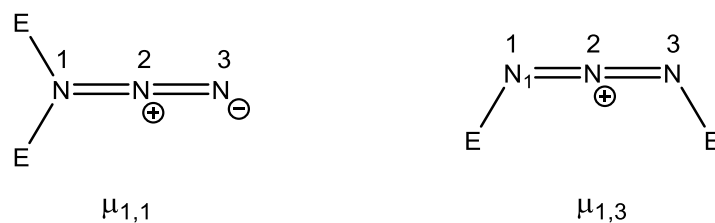
Figure 75. Bridging modes of azido ligands between two coordination centres (E).
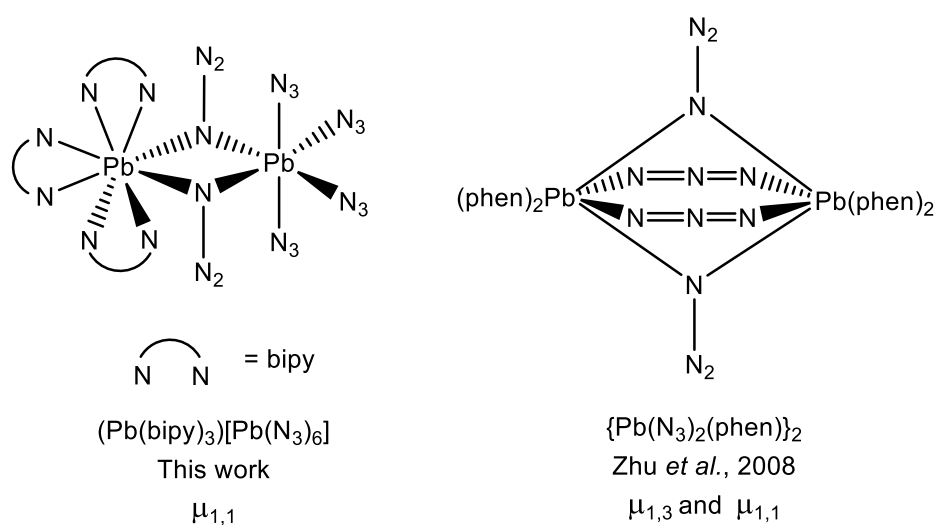
Figure 76. Structure of complex studied in this work (left) and that of $\{Pb(N_3)_2(phen)\}_2$ reported previously (right).[244] $Pb(bipy)_3[Pb(N_3)_5Cl]$ omitted for clarity.

Recrystallisation attempts from non-chlorinating solvents such as THF were restricted by the requirement of a biphasic system. Detailed crystallisation and solubility studies of both solid compounds were also limited owing to the energetic properties of the product described above. Redissolution of the solid complex in MeCN resulted in the total disappearance of the bands of coordinated bipy and a shift in $\nu_{as}(N_3)$ bands to match those of $[Pb(N_3)_6]^{2-}$, and is therefore an unsuitable recrystallisation or reaction solvent for the complex.[177]

The possibility of incomplete chlorido/azido ligand exchange in the preparation of $Pb(N_3)_4(bipy)$ was eliminated by examining the IR spectra of the latter prior to the formation of $Pb(bipy)_3(N_3)_{5.2}Cl_{0.8}$. The $\nu_{as}(N_3)$ stretching vibrations observed in the IR spectrum of $Pb(N_3)_4(bipy)$ in CH_2Cl_2 are consistent with the number and positions of the lighter $E(N_3)_4(bipy)$ homologues (E = Si−Sn). The effective C_2 symmetry predicted for $Pb(N_3)_4(bipy)$ would afford four IR-active $\nu_{as}(N_3)$ stretching vibrations, whereas the partially-substituted $Pb(N_3)_3Cl(bipy)$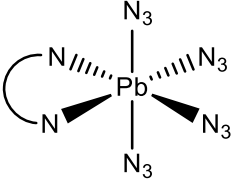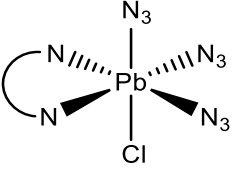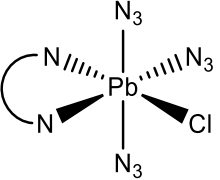 isomers would give only three (table 44). Curve-fitting analysis of the IR spectrum of the supernatant solution using Pseudo-Voigt curve profiles showed the presence of four overlapping asymmetric azide bands which appear as two broad bands in the spectrum (figure 77). This supports the hypothesis that complete chlorido/azido ligand exchange has occurred and confirms the sole presence of $Pb(N_3)_4(bipy)$ in solution.[164] These findings correlate with the obtained crystal structure of chlorine-free $Pb(N_3)_4(bipy)$. The observation of partial chlorine contamination in the crystal structure of $Pb(bipy)_3(N_3)_{5.2}Cl_{0.8}$ must therefore arise from chlorination reactions that occur during the extended crystallisation period, instead of from incomplete chlorido-azido exchange during synthesis.

Formula	$Pb(N_3)_4(bipy)$	$Pb(N_3)_3Cl(bipy)$	$Pb(N_3)_3Cl(bipy)$
Point Group	C_2	C_2	C_s
Expected $\nu_{as}(N_3)$ bands	4	3	3

Table 44. Structures, predicted point groups and expected number of $\nu_{as}(N_3)$ bands for possible products formed in solution.
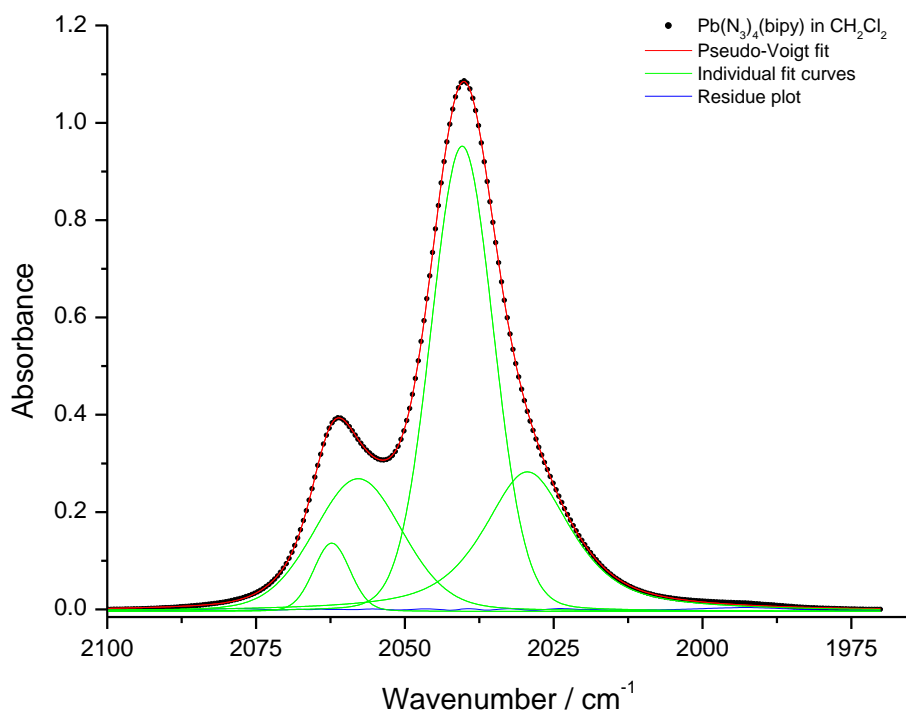
Figure 77. Pseudo-Voigt curve-fitting analysis of the IR spectrum of $Pb(N_3)_4(bipy)$ in CH_2Cl_2 versus the experimentally-determined spectral data points (•). $\nu_{calc}(N_3) = 2062, 2058, 2040, 2029$ cm^{-1}.[164]

Temporarily disregarding the chlorine impurity, it is initially unclear if the structure of $Pb_2(bipy)_3(N_3)_6$ obtained from long-term storage is truly dimeric (as $Pb_2(N_3)_6(bipy)_3$, **A**) or is, instead, salt-like (as $[Pb(bipy)_3]^{2+}[Pb(N_3)_6]^{2-}$, **B**) (figure 78). Complex **A** can be formulated as a dimeric complex containing two Pb(IV) centres as charge-neutral $Pb(N_3)_4$ and $Pb(bipy)_3(N_3)_2$ units, whilst complex **B** contains both Pb(II) and Pb(IV) coordination centres as $[Pb(bipy)_3]^{2+}$ and $[Pb(N_3)_6]^{2-}$ respectively. Solution-phase ^{207}Pb NMR spectroscopy was attempted in order to elucidate the oxidation state(s) of the lead centres present by comparison to chemical shifts of known Pb(IV) and Pb(II) complexes. However, the absence of any signals prevented the identification of oxidation states. The presence of quadrupolar ^{14}N nuclei around the ^{207}Pb nucleus is hypothesised to result in rapid relaxation of the ^{207}Pb signal, leading to an extremely broad and undetectable signal.[247] Bond length analysis was applied as an alternative strategy to identify the oxidation state(s) of the coordination centres in the crystal structure.
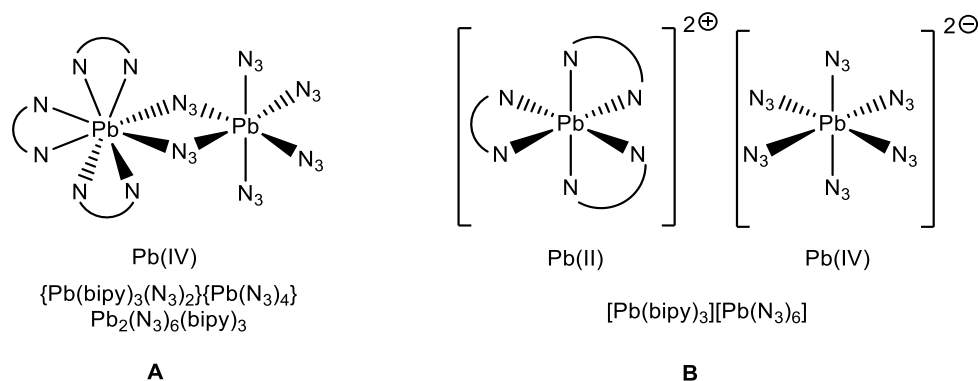
Figure 78. Proposed formulations of $Pb_2(N_3)_6$(bipy) studied crystallographically.

The lengths of the four Pb−N−Pb sequences in the structure are unequal. The shorter Pb−N bridging bonds in each sequence, in addition to those which do not participate in bridging, are consistent with those of the $[Pb(N_3)_6]^{2-}$ anion (i.e., Pb(IV)). By contrast, the longer Pb−N azido bond length originating from the central lead atom in the $Pb(bipy)_3$ subunit ($d = 2.795(5)$ Å) is more similar to those observed in the Pb(II) complex $\{Pb(N_3)_2(phen)_2\}_2$ (table 45).[220] The Pb−N bond lengths of all four bipy ligands are consistent with those observed in poly(bipyridyl) complexes of Pb(II) (table 45). [244,248,249] In the structure of $[Pb(bipy)_4][PF_6]_2$, the fourth bipy ligand is significantly removed from the coordination centre at a bond length approximately 0.2 Å greater than the other three ligands (figure 79).[248] In the structure determined in this study, the lone pairs of electrons located on the N_α atoms of the $\mu_{1,1}$ azido ligands coordinate to the Pb(II) centre (figure 79), satisfying the 18-electron rule by the formation of an extended coordination sphere similar to the $[Pb(bipy)_4]^{2+}$ cation in $[Pb(bipy)_4][PF_6]_2$.[248] These findings, together with the Pb(IV)−N_3 bond lengths observed of the second coordination centre, suggest that both oxidation states of lead are present in the structure and identifies the compound studied crystallographically as the salt-like, mixed oxidation-state compound $[Pb(bipy)_3]^{2+}[Pb(N_3)_6]^{2-}$ (**B**).

Compound	$d(Pb−N_\alpha)$ / Å	$d\{Pb−N(L)\}$ / Å	Refs.
$[PPN]_2[Pb(N_3)_6]$ [a]	2.2481(17) − 2.2649(18)	–	[d]
$[Ph_4As]_2[Pb(N_3)_6]$ [b]	2.217 − 2.257	–	[177]
$Pb_2(N_3)_{5.2}Cl_{0.8}(bipy)_3$ [a]	2.795(5) − 2.266(5)	2.638(5) − 2.712(5)	[d]
$\{Pb(N_3)_2(phen)\}_2$	2.741(7) − 2.790(7)	2.623(5) − 2.742(5)	[244]
$[Pb(bipy)_4][PF_6]$ [a]	–	2.5731(19) − 2.7602(19)	[248]
$[Pb(bipy)_4][B_{20}H_{18}]$[c]	–	2.721(2) − 2.750(2)	[249]

Table 45. Comparison of Pb−N bond lengths for the crystal structure of $Pb_2(N_3)_6(bipy)_3$. L = bipy, phen. [a] = recorded at 100 K; [b] = recorded at 294 K; [c] = recorded at 120 K; [d] = this work.
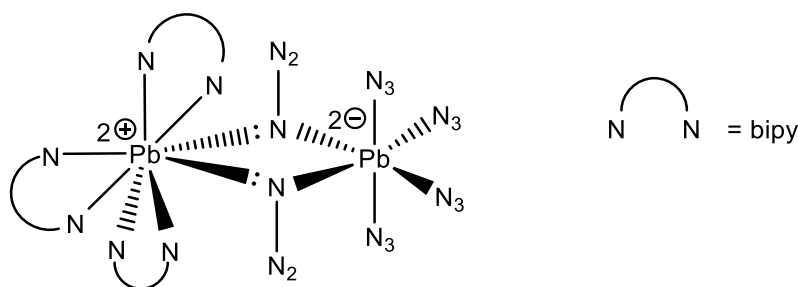
Figure 79. Bonding scheme of (Pb(bipy)$_3$)[Pb(N$_3$)$_6$] (**B**). For clarity, only the lone pairs of the bridging nitrogen atoms are shown.

The spectroscopic and crystallographic studies confirmed that neutral, monomeric Pb(N$_3$)$_4$(bipy) was formed initially and that complex **B** crystallises as a result of the complex undergoing disproportionation and ligand rearrangement in solution. The mechanism for this process is hypothesised to proceed through the reduction of Pb(N$_3$)$_4$(bipy) to the Pb(II) species Pb(N$_3$)$_2$(bipy), followed by ligand rearrangement (see below). The dimeric reaction product is less soluble than the monomeric precursor and crystallises from solution once saturation point is reached. The extended period of time prior to the commencement of crystallisation of (Pb(bipy)$_3$)[Pb(N$_3$)$_6$] as (Pb(bipy)$_3$)[Pb(N$_3$)$_{5.2}$Cl$_{0.8}$] (ca. 10 days) indicates that, as expected, the rate of reduction, rearrangement and chlorination reactions are slower at low temperatures.
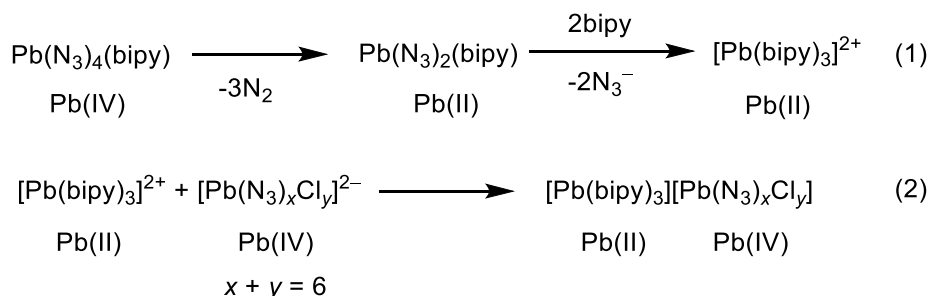
Scheme 52. Proposed reaction for formation of **B** from Pb(N$_3$)$_4$(bipy).

Storage of a CH$_2$Cl$_2$ solution of Pb(N$_3$)$_4$(bipy) at room temperature under the exclusion of light resulted in the formation of a colourless solution containing colourless shard-shaped crystals of PbCl$_2$(bipy) in space group P_{bca} (figure 80). The observed Pb−N$_{(bipy)}$ and Pb−Cl bond lengths are similar to those reported for a less-disordered structure in literature (d(Pb−Cl) = 2.767(7)−2.925(7) Å vs 2.776−2.945 Å, respectively).[250] Gradual chlorination occurs concurrently alongside the reduction of the complex in solution and confirms that the reactivity of Pb(N$_3$)$_4$(bipy) is sufficient to induce further reaction with chlorinating solvents. This process is likely to be the source of the partially disordered chlorine ligand observed in the crystal structure of [Pb(bipy)$_3$][Pb(N$_3$)$_{5.2}$Cl$_{0.8}$]. The increased extent of chlorination observed between

solutions at room temperature and low temperature confirms that the chlorination reaction is gradual and accounts for the absence of chlorine in crystals of $Pb(N_3)_4(bipy)$ when grown rapidly following complex formation.

$$6N_2 + PbCl_2(bipy) \xleftarrow[\text{3 d}]{\text{rt, }} Pb(N_3)_4(bipy) \xrightarrow[\text{10 d}]{-28\ °C} Pb_2(bipy)_3(N_3)_{6-x}Cl_x$$
$$CH_2Cl_2 \qquad 1 \le x \le 6$$
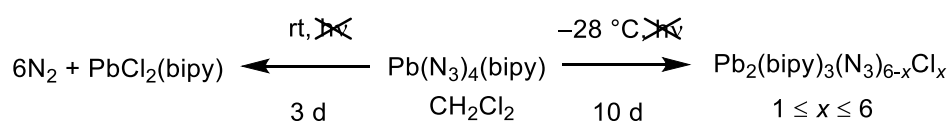
Scheme 53. Behaviour of $Pb(N_3)_4(bipy)$ in CH_2Cl_2 solution under the exclusion of light.
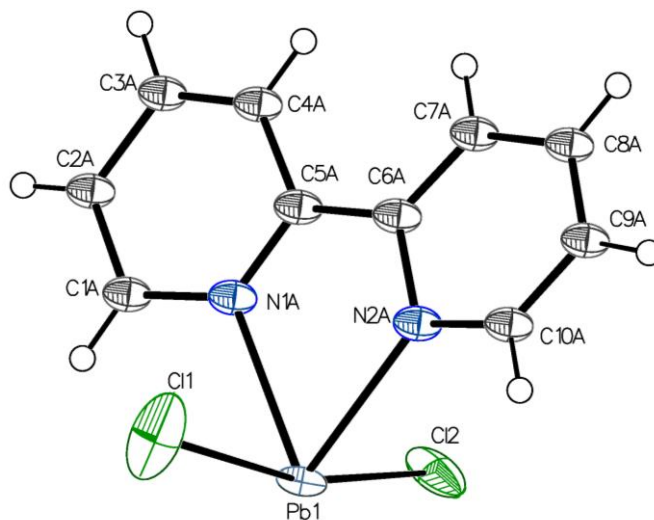
Figure 80. Crystal structure of $PbCl_2(bipy)$, formed from decomposition of $Pb(N_3)_4(bipy)$ by chlorination reaction with CH_2Cl_2. Grey = C, blue = N. For clarity, only one part of the disordered bipy ligand is displayed. Selected bond lengths (Å) and angles (°): Pb(1)−Cl(1) 2.767(7), Pb(1)−Cl(2) 2.925(7), Pb(1)−N(1A) 2.46(4), Pb(1)−N(2A) 2.44(4), Pb(1)−N(1B) 2.56(2), Pb(1)−N(2B) 2.55(2); Cl(1)−Pb(1)−Cl(2) 165.3(3).

Solutions of $Pb(N_3)_4(bipy)$ are extremely photosensitive. At room temperature, several minutes of light exposure was sufficient to induce the formation of a highly turbid solution and the precipitation of a white solid (figures 81, 82). IR spectroscopic monitoring showed the disappearance of the bands associated with coordinated azido and bipy ligands at almost identical rates (figures 83, 84), similarly to the photoinduced decomposition of $[PPN]_2[Pb(N_3)_6]$ into $Pb(N_3)_2$. The decrease in coordinated bipy was also observed using ^1H NMR spectroscopy.

| 0 mins | 10 mins | 20 mins | 40 mins | 60 mins |
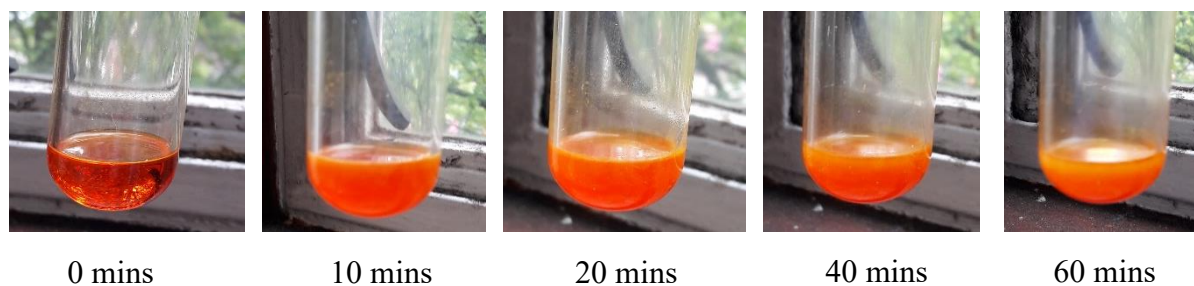
Figure 81. Solution of Pb(N$_3$)$_4$(bipy) in CH$_2$Cl$_2$ upon standing at room temperature in daylight. Irradiation times listed are approximate.
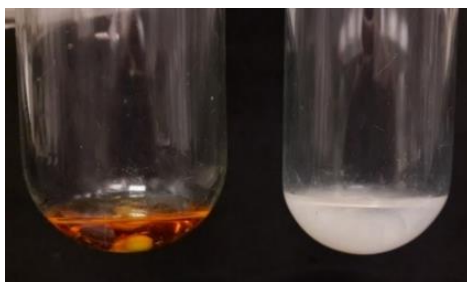
Figure 82. Solutions of Pb(N$_3$)$_4$(bipy) in CH$_2$Cl$_2$ before (left) and after (right) 3h exposure to daylight at rt.

$$Pb(N_3)_4(bipy) \xrightarrow[\text{CH}_2\text{Cl}_2,\ \text{rt}]{h\nu} Pb(N_3)_2 + bipy + N_2$$
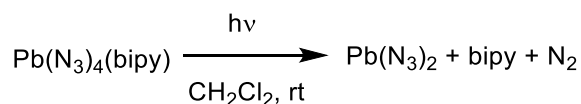
Scheme 54. Photochemically induced decomposition reaction of Pb(N$_3$)$_4$(bipy) to Pb(N$_3$)$_2$.
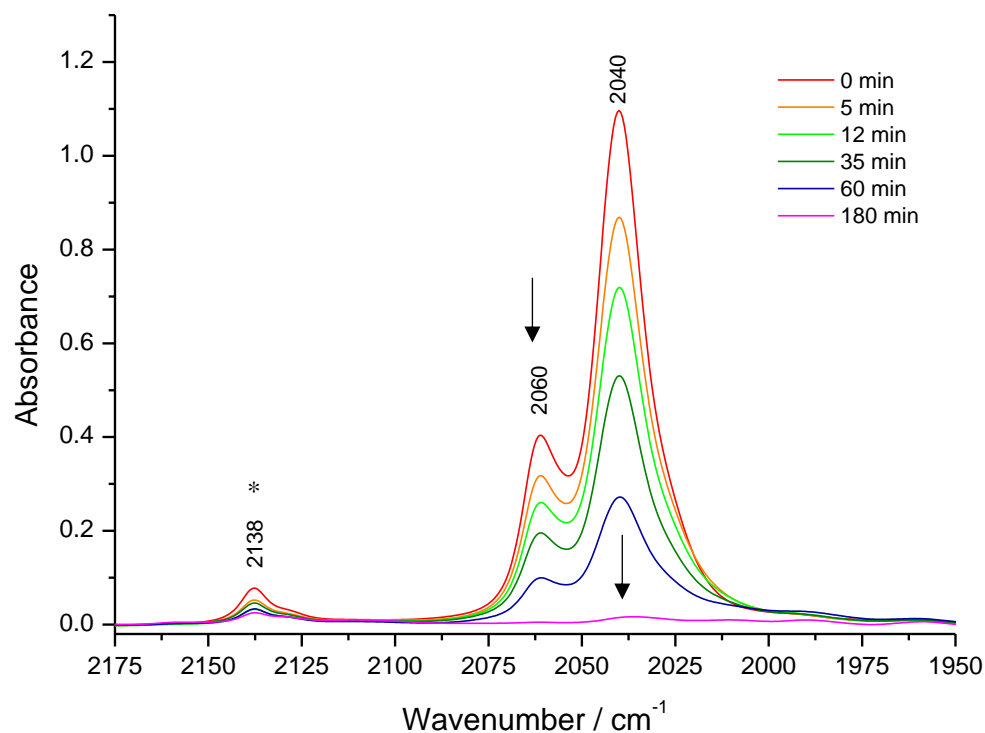
Figure 83. IR spectral series showing photoinduced decomposition of a CH$_2$Cl$_2$ solution of Pb(N$_3$)$_4$(bipy) in daylight to form Pb(N$_3$)$_2$. All times listed are approximate. The band marked with an asterisk (*) is attributed to HN$_3$ formed during decomposition.
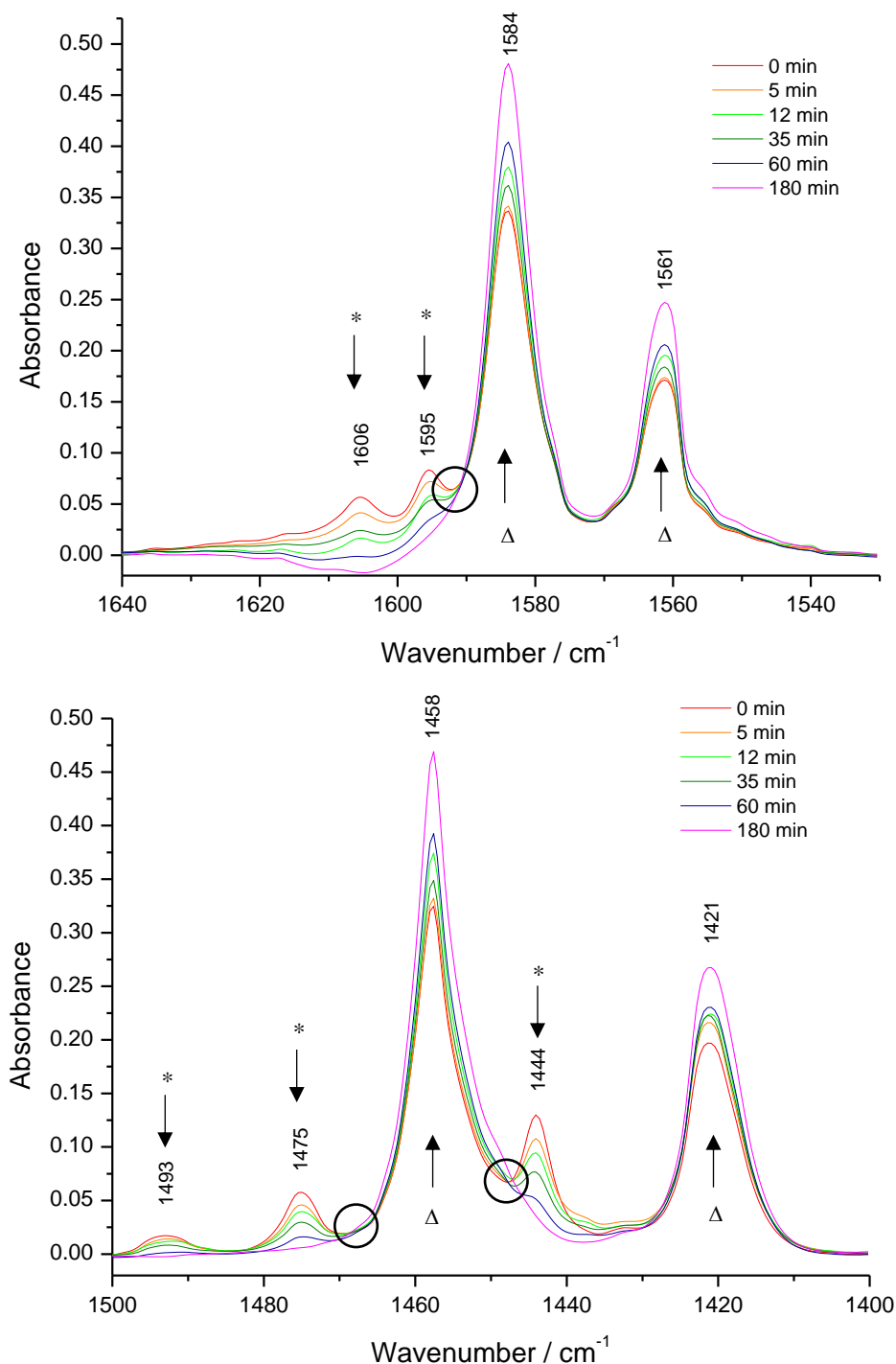
Figure 84. IR spectral series of Pb(N₃)₄(bipy) in CH₂Cl₂ solution upon light exposure between 1640−1530 cm⁻¹ (top) and 1500−1400 cm⁻¹ (bottom), showing decoordination of bipy (*), formation of uncoordinated ('free') bipy (Δ) and isosbestic points (O) at 1591, 1468 and 1448 cm⁻¹. The negative absorbances at 1595 and 1606 cm⁻¹ are artefacts arising from baseline correction.

The change in intensity of the IR absorbance bands of azido and bipy ligands during photolysis were modelled as first-order exponential functions (figures 85,86). Exponential function fitting of spectral data estimated the lifetime of Pb(N₃)₄(bipy) to be approximately 30 minutes in daylight. The consistency of the calculated lifetime values between all four bands of

coordinated bipy and azido ligands confirmed that all four arise from the same species (table 46). An approximately twofold increase in the rate of change between the bands of uncoordinated and coordinated bipy is attributed to the overlap of the bands of uncoordinated bipy with a second unidentified band to result in an inaccurate growth rate calculation.
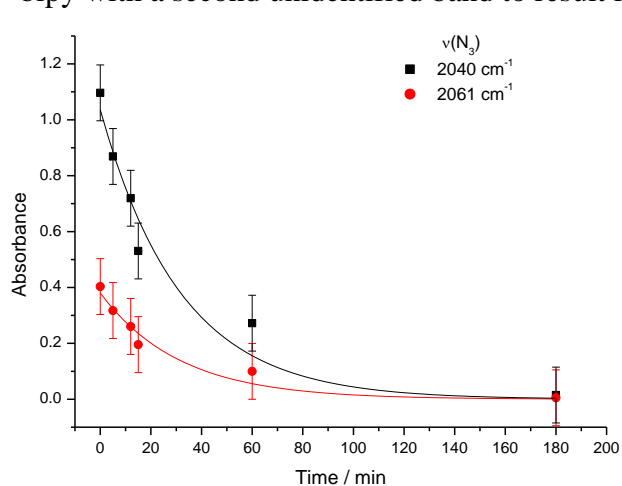
Figure 85. Exponential decrease in the absorbance of the $\nu_{as}(N_3)$ bands of $Pb(N_3)_4(bipy)$ at 2040 cm^{-1}, (■) and 2061 cm^{-1} (●) in CH_2Cl_2 at room temperature in daylight. $Y_{err} = 0.1$; $X_{err} = 1.0$.
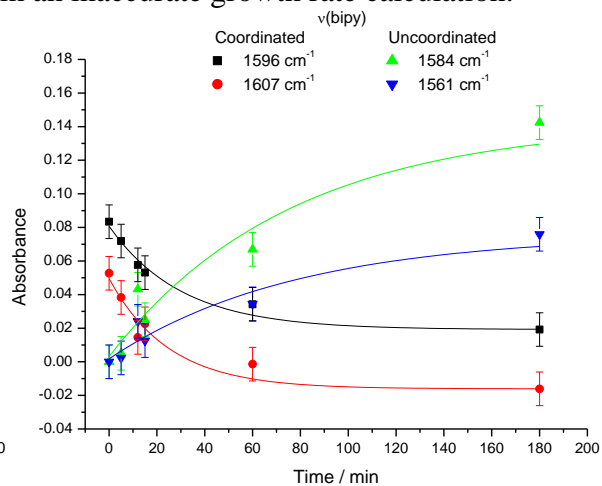
Figure 86. Exponential decreases in the intensity of the $\nu(bipy)$ bands of $Pb(N_3)_4(bipy)$ at 1596 cm^{-1}, (■) and 1607 cm^{-1} (●) alongside exponential increases in absorbance intensity of bands of uncoordinated bipy ($\tilde{\nu} = 1584$ cm^{-1}, ▲ and 1561 cm^{-1}, ▼) in CH_2Cl_2 at room temperature in daylight. $Y_{err} = 0.01$; $X_{err} = 1.0$.

bipy			N$_3$		
$\tilde{\nu}$ / cm^{-1}	Status	τ / min	$\tilde{\nu}$ / cm^{-1}	Status	τ / min
1596	Coordinated	30 ± 13	2040	Coordinated	32 ± 8
1607		25 ± 10	2061		31 ± 11
1584	Uncoordinated	75 ± 27			
1561		77 ± 52			

Table 46. Lifetimes for photoinduced exponential decomposition (coordinated bipy, N$_3$) and growth (uncoordinated bipy) observed for $Pb(N_3)_4(bipy)$ in CH_2Cl_2 solution at room temperature. All lifetimes quoted to two significant figures.

To examine if photolysis was inducing the decomposition of $Pb(N_3)_4(bipy)$, a control experiment was carried out where a solution of $Pb(N_3)_4(bipy)$ in CH_2Cl_2 was stood under the exclusion of light at room temperature. No discolouration or turbidity was observed during the experiment. However, small changes in the $\nu_{as}(N_3)$ bands were observed in solution, whereby both bands shifted to slightly lower wavenumbers that are more consistent with $[Pb(N_3)_6]^{2-}$

(figure 87, table 47). The bands associated with coordinated bipy decreased but did not reform as uncoordinated bipy. This behaviour in solution is consistent with the formation of [Pb(bipy)$_3$][Pb(N$_3$)$_6$] observed above. It is unclear to what extent, if at all, the partial chlorination observed in the crystal structure of Pb(bipy)$_3$(N$_3$)$_{5.2}$Cl$_{0.8}$ is present. However, owing to the significantly shorter storage time in this study, it is assumed that chlorination is negligible. The reactivity of Pb(N$_3$)$_4$(bipy) in CH$_2$Cl$_2$ is summarised in scheme 55.

Conditions	ν_{as}(N$_3$) / cm^{-1}	Identity
0 h	2061, 2040	Pb(N$_3$)$_4$(bipy)
3 h, daylight	2037 (w)	*[Pb(N$_3$)$_3$]$^-$*
3 h, dark	2055, 2039	[Pb(N$_3$)$_6$]$^{2-}$
[PPN]$_2$[Pb(N$_3$)$_6$]	2063, 2036	−

Table 47. Summary of ν_{as}(N$_3$) bands of Pb(N$_3$)$_4$(bipy) in CH$_2$Cl$_2$ under different conditions. 'Identity' denotes the main product present in solution in each set of conditions. 'w' denotes a weak absorbance band; *italics* denotes a speculated identity.
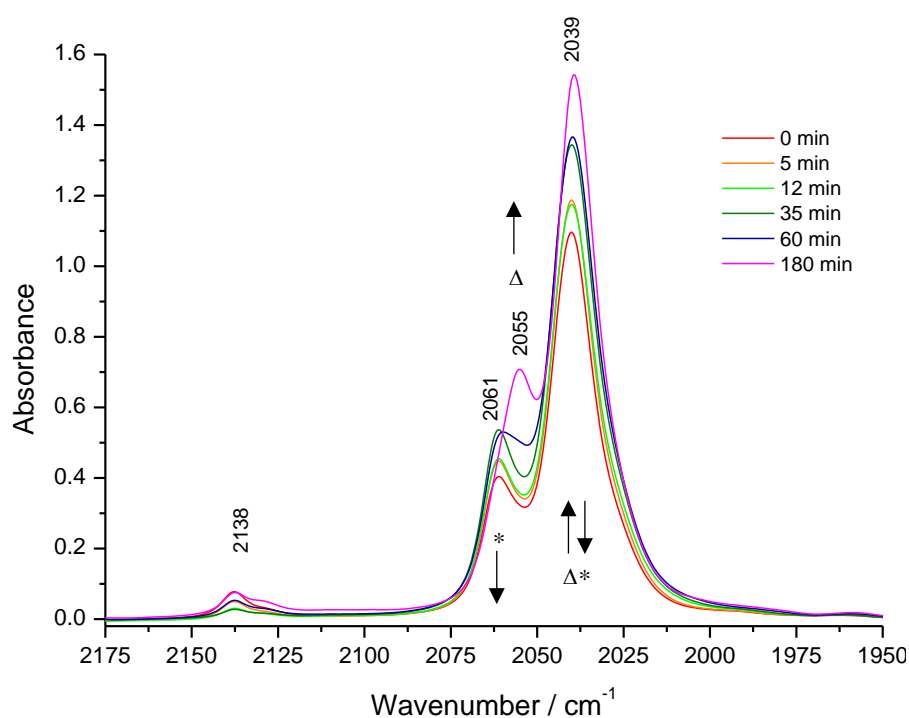
Figure 87. IR spectral series showing spontaneous decomposition of a CH$_2$Cl$_2$ solution of Pb(N$_3$)$_4$(bipy) (*) and subsequent formation of [Pb(bipy)$_3$][Pb(N$_3$)$_6$] (Δ) under the exclusion of light. All times listed are approximate. The band at 2138 cm^{-1} is attributed to HN$_3$ formed by decomposition during sample preparation.

$$[Pb(bipy)_3[Pb(N_3)_{5.2}Cl_{0.8}]$$

$$\cancel{} \quad -28\ °C,\ 10\ d$$

$$PbCl_2(bipy) \xleftarrow[\text{rt, 7d}]{\cancel{}} Pb(N_3)_4(bipy) \xrightarrow[\text{rt}]{h\nu} Pb(N_3)_2$$

$$\cancel{} \quad \text{rt, 3 h}$$

$$[Pb(bipy)_3][Pb(N_3)_6]$$
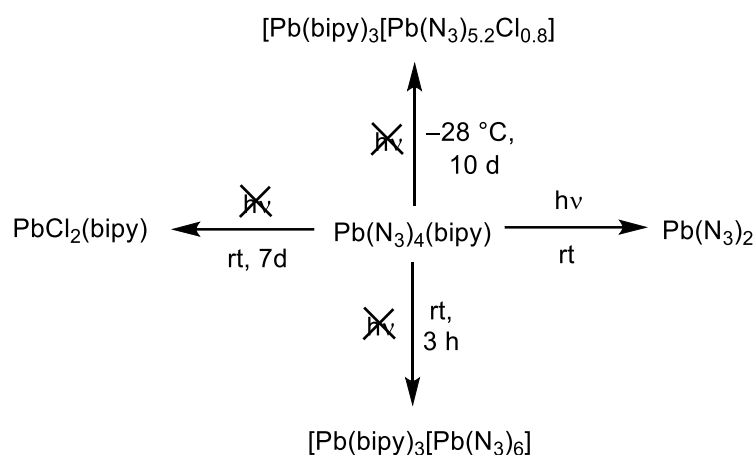
Scheme 55. Reactions observed in CH_2Cl_2 solutions of $Pb(N_3)_4(bipy)$.

Previous studies of Ph_3PbN_3 indicated that photolysis may induce the formation of radical species in solution and subsequent chlorine abstraction from CH_2Cl_2.[251] Furthermore, a previous study on the $[Pb(N_3)_6]^{2-}$ anion proposed the elimination of azide radicals prior to the release of gaseous N_2 during photolytic reduction from Pb(IV) to Pb(II).[252] This information was used here to tentatively propose several mechanisms which account for the numerous decomposition reactions observed in CH_2Cl_2 solutions of $Pb(N_3)_4(bipy)$ under varying experimental conditions (scheme 56). The photochemical formation of $Pb(N_3)_3(bipy)^\bullet$ is a critical step in these mechanisms which facilitates the subsequent reduction and chlorine abstraction reactions which afford $Pb(N_3)_2$ and $PbCl_2(bipy)$, respectively. The amount of light exposure is hypothesised to influence the reaction pathway and identity of the decomposition product in each reaction. Although efforts were made to exclude all light from the reaction which ultimately afforded $PbCl_2(bipy)$, it is possible that an initial exposure to light during sample preparation was sufficient to induce the first photolytic reduction to form $Pb(N_3)_3(bipy)^\bullet$. Once initiated, the slower chlorination reaction can occur under the exclusion of light to form $PbCl_2(bipy)$. A similar chlorine abstraction reaction is assumed to be responsible for the formation of the mixed-ligand dimeric product, specifically $[Pb(bipy)_3][Pb(N_3)_{5.2}Cl_{0.8}]$ identified by crystallographic studies. This process appears to occur at a slower rate than the formation of $Pb(N_3)_2$ through N_2 elimination, and accounts for the formation of chlorinated decomposition products only upon *prolonged* storage under the exclusion of light (see above). The varying extent of chlorination is attributed to a decreased reaction rate at lower temperatures.

The formation of anionic species containing Pb(II) and Pb(IV) is attributed to the addition of N_3^-. The azide anion is believed to be present in excess due to trace hydrolysis of $Pb(N_3)_4(bipy)$

116

in H_2O to form HN_3 and PbO_2. The latter process is hypothesised to account for the brown solid observed in the aqueous layer of the biphasic reaction solution during the synthesis of $Pb(N_3)_4(bipy)$. It is possible that additional HN_3 originates from the equilibrium of NH_4N_3 in H_2O proposed by Möller (scheme 51).[227] Excess bipy is present (and therefore capable of complexation) due to the use of an excess in the initial formation of $Pb(N_3)_4(bipy)$.
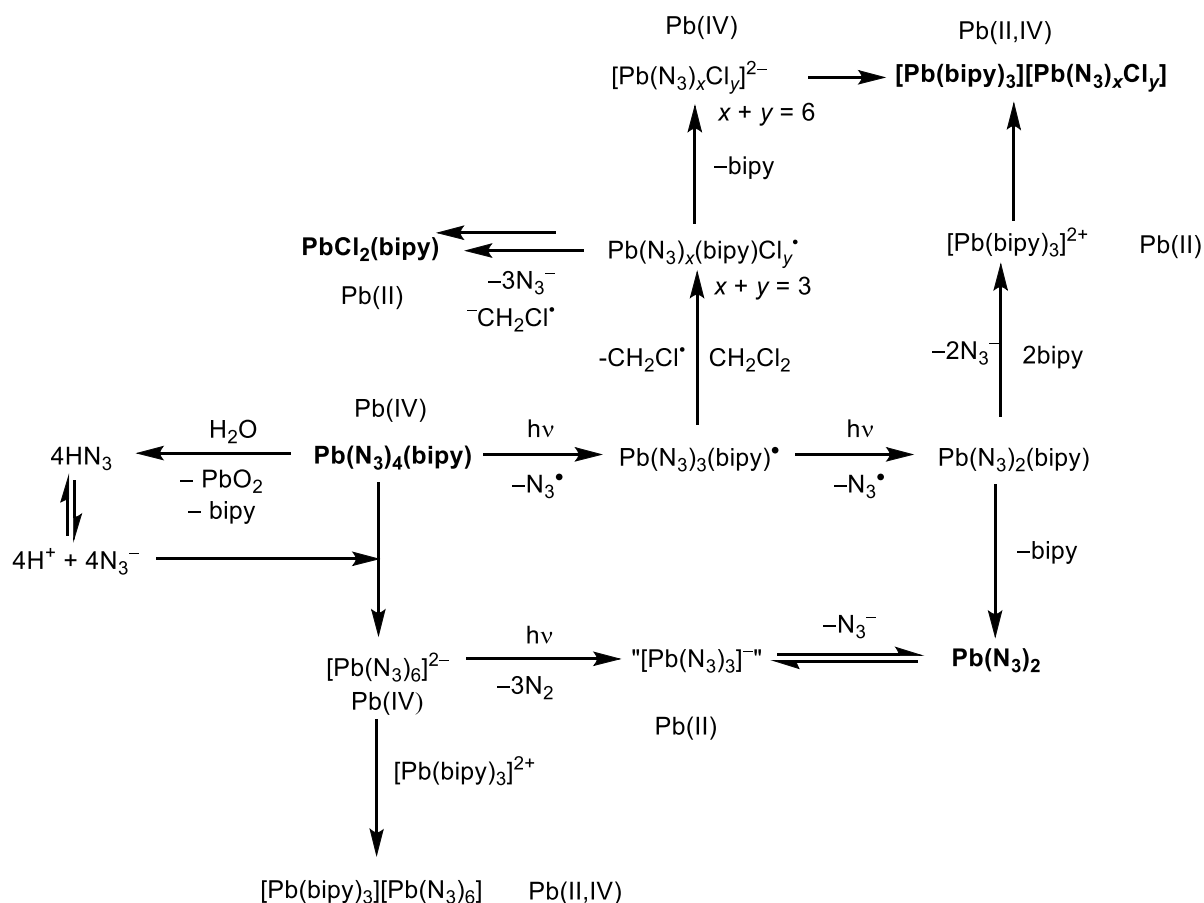
Scheme 56. Proposed reactivity of CH_2Cl_2 solutions of $Pb(N_3)_4(bipy)$. Isolated compounds are highlighted in **bold**. The generation of $[Pb(N_3)_3]^-$ is only speculated and, if formed, occurs as a transient intermediate. $[Pb(N_3)_xCl_y]^{2-}$ was not detected and has been included as a potential mechanism which accounts for the formation of $[Pb(bipy)_3][Pb(N_3)_{5.2}Cl_{0.8}]$, observed crystallographically.

Neither the exact mechanistic pathway, nor the photoproducts obtained in each reaction, can be conclusively identified and the reactions outlined above are purely speculative. The photoinduced formation of radical species such as $N_3^{\bullet}$ and $CH_3Cl^{\bullet}$ could result in azidomethane termination products with varying degrees of chlorination, such as CH_3N_3 and CH_2ClN_3. The absence of the characteristic $v_{as}(N_3)$ bands of either of these products ($\tilde{v}$ = ca. 2106 cm^{-1} and 2095 cm^{-1}, respectively) confirmed that neither product is formed in solution.[253–255] The absence of either $v(N_3)$ bands may be explained by the formation of a chloroalkane by termination of two $CH_3Cl^{\bullet}$ radicals. A broad, weak band observed at 2128 cm^{-1} during the

photolysis of $Pb(N_3)_4$(bipy) is inconsistent with either termination product. This band is hypothesised to arise from an organic azide of unknown identity, or, alternatively, occur due to the residual solubility of $Pb(N_3)_2$ in CH_2Cl_2 (which contains an azide band at 2115 cm^{-1} in the solid state). The possible overlap of the broad band with that of HN_3 ($\tilde{v} = 2138$ cm^{-1}) meant the identity of the band could not be confirmed. Diazidomethane, $CH_2(N_3)_2$, is unknown and no information regarding the spectral positon of the $v_{as}(N_3)$ band is available. An approximate extrapolation of the spectral positions of the $v_{as}(N_3)$ bands of azido- and chloroazidomethane in the same solvent ($CDCl_3$) suggests that the same asymmetric azide stretching vibration of $CH_2(N_3)_2$ would absorb at approximately 2080 cm^{-1}. A solvatochromic effect, relating increasing solvent polarity to decreasing spectral position of key stretching vibrations, well-documented in other IR-active pseudohalide reporter groups (e.g., CN, SCN), could result in a slight reduction of the position of the $v_{as}(N_3)$ band of diazidomethane ($CH_2(N_3)_2$) in CH_2Cl_2 below 2080 cm^{-1}.[256–258] This may result in an overlap with the dominant azide band of $Pb(N_3)_4$(bipy), preventing the direct observation of diazidomethane. For this reason, the possibility of double chlorine abstraction from CH_2Cl_2 (and the subsequent formation of $CH_2(N_3)_2$) cannot be eliminated without further study.

$Pb(OAc)_4$ was investigated as an alternative precursor complex for the preparation of $Pb(N_3)_4$(bipy). Although reaction of $Pb(OAc)_4$ with NaN_3 and bipy resulted in the near-immediate formation of a dark orange suspension, the IR spectrum of the supernatant solution was inconsistent with $Pb(N_3)_4$(bipy) and further characterisation was inconclusive. The disappearance of all azide bands upon further stirring of the suspension indicated that a photoreaction had taken place, similar to the reduction observed in solutions of $[PPN]_2[Pb(N_3)_6]$. Following the preparation of $Pb(N_3)_4$(bipy) from $(NH_4)_2[PbCl_6]$, the reaction of $Pb(OAc)_4$ was not investigated further.

5.2.5. Preparation of $Pb(N_3)_4$(phen)

The synthetic strategy used in the preparation of $Pb(N_3)_4$(bipy) was extended to prepare the phenanthroline adduct, $Pb(N_3)_4$(phen). The IR spectrum of the reaction solution showed similar bands, positions and intensity ratios to those observed in solutions of $Pb(N_3)_4$(bipy) (figure 88). However, the spectrum showed extremely weak bands associated with coordinated phen and noticeable similarities between the azide bands of $(NH_4)_2[Pb(N_3)_6]$ and the product ($v_{as}(N_3)$ = 2056, 2037 vs 2055, 2038 cm^{-1}, respectively).[97] Owing to the uncertain identity of the product and the difficulties encountered when handling solid samples of $Pb(N_3)_4$(bipy), the solid

complex was not isolated. Further work is required in order to investigate and compare the coordination of phen to $[Pb(N_3)_6]^{2-}$ versus bipy, especially as both adducts of the lighter homologues are isolable.[96,102,243]
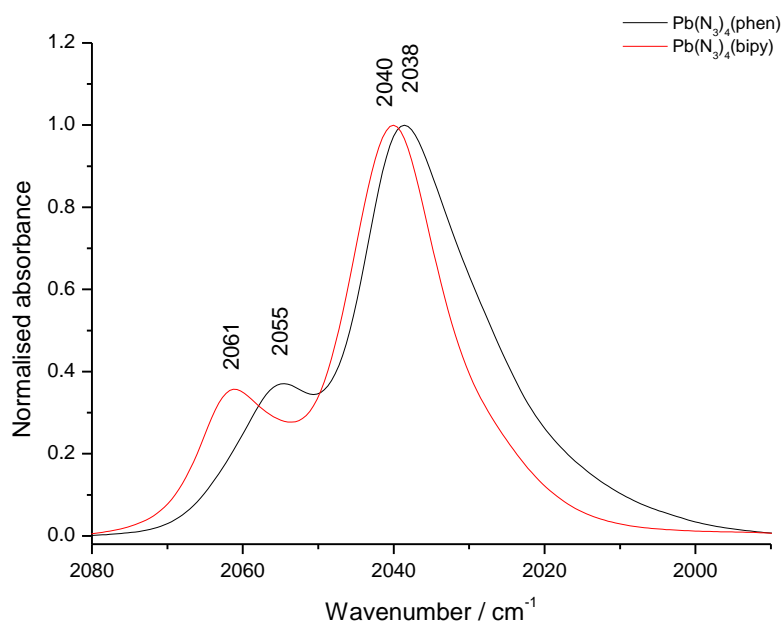
Figure 88. Normalised IR spectra of $Pb(N_3)_4(L)$ (L = bipy, phen) in CH_2Cl_2; $Pb(N_3)_4(phen)$ = black line, −; $Pb(N_3)_4(bipy)$ = red line, −.

5.2.6 Comparison of Pb(N₃)₄(bipy) to lighter homologues (E = Si−Sn)

The preparation of $Pb(N_3)_4(bipy)$ completes the set of neutral group 14 poly(azido) complexes containing E(IV) centres stabilised by Lewis bases $(E(N_3)_4(bipy)$, E = Si−Pb). Some trends in spectroscopic and reaction behaviour, previously observed for E = Si−Sn, are continued for the Pb(IV) coordination centre, although large differences in general reactivity are observed between $Pb(N_3)_4(bipy)$ and the lighter congeners. For the remainder of this discussion, the complexes will be referred to by the notation shown in figure 89.
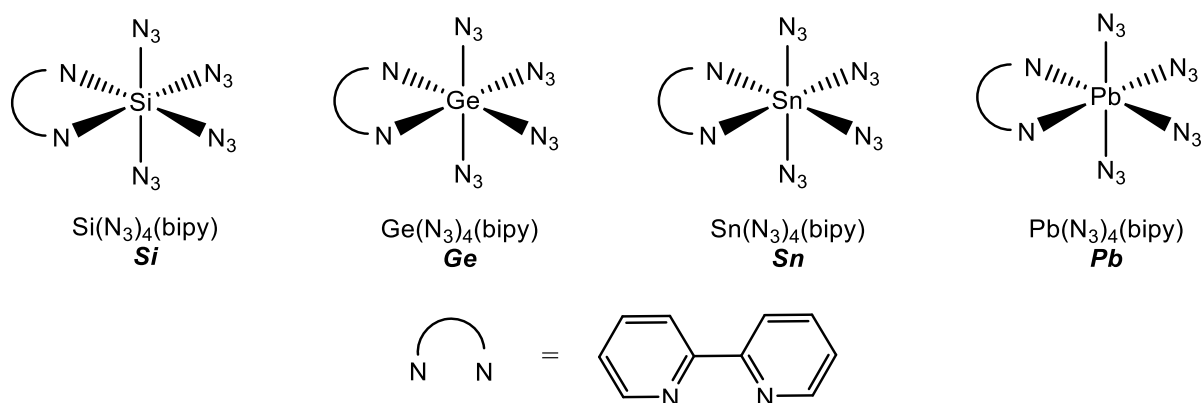
Figure 89. Simplified structures of $E(N_3)_4(bipy)$ (E = Si−Pb) and their notation for this section.

Both the spectral position and the number of $\nu_{as}(N_3)$ bands observed in the IR spectrum of ***Pb*** are lower than those of ***Si−Sn*** and continue the decreasing trend observed for the lighter homologues (table 48, figure 90). The downward trend in $\nu_{as}(N_3)$ from ***Si – Pb*** is accounted for by the decrease in coordination strength as the E−N bonds become more ionic. As the size of the coordination centre increases, the range between the highest and lowest $\nu_{as}(N_3)$ bands for each complex narrows until two of the bands converge in the spectra of ***Sn*** and ***Pb*** (figure 91). The ratio of absorbances between the two most intense $\nu_{as}(N_3)$ bands of each complex also increases from ***Si−Pb*** (figure 92).

E(N$_3$)$_4$(bipy)	ν_{as}(N$_3$) / cm^{-1}	ν(bipy) / cm^{-1}	Refs.
E = Si	2152, 2125, 2116	1623, 1614	243
E = Ge	2122, 2098, 2089	1617, 1606	96,167
E = Sn	2112, 2084	1614, 1602	102
E = Pb	2061, 2040	1606, 1596	This work

Table 48. Summary of azide bands in IR spectra of E(N$_3$)$_4$(bipy) (E = Si−Pb) in CH$_2$Cl$_2$.
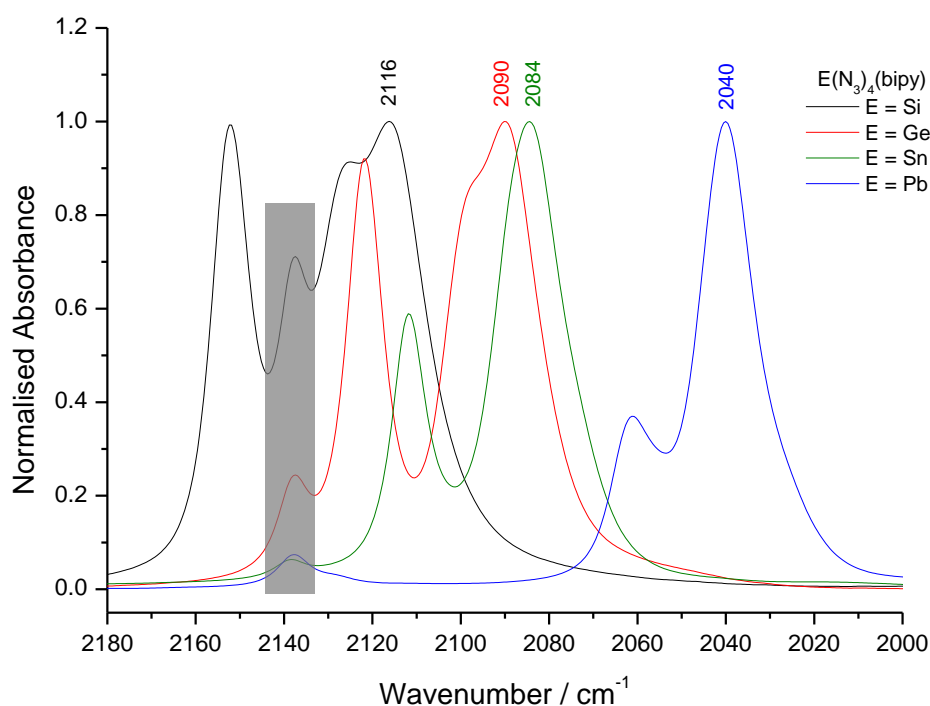
Figure 90. Comparison of ν_{as}(N$_3$) bands in solutions of ***Si−Pb*** in CH$_2$Cl$_2$. The shaded band is caused by HN$_3$, which is formed by unavoidable hydrolysis during sample preparation and acts as an internal calibrant. Data for ***Si-Sn*** obtained from references [96,102,243].
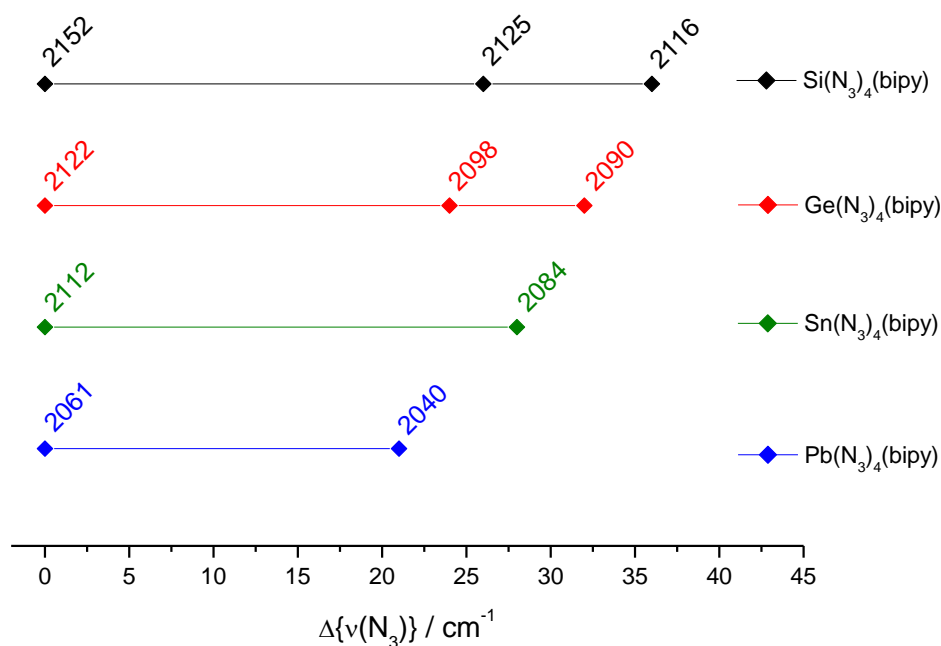
Figure 91. Differences in wavenumbers of $\nu_{as}(N_3)$ bands in CH_2Cl_2 solutions of *Si–Pb*. The highest band for each complex is set to 0 on the x-axis scale. Data for *Si-Sn* obtained from references [96,102,243].
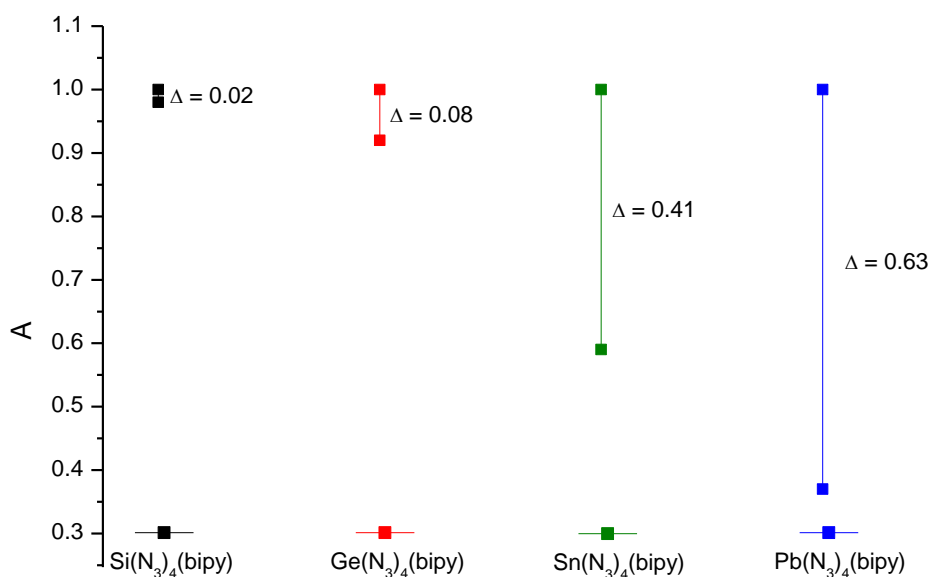
Figure 92. Absorbances of the two most intense $\nu_{as}(N_3)$ bands in CH_2Cl_2 solutions of *Si–Pb*. The most intense band for each complex is set to 1 on the y-axis scale. Data for *Si-Sn* obtained from references [102,167,243].

The Pb−N bond lengths observed in the crystal structure of *Pb* continue the trend in increasing bond lengths already observed from *Si–Sn*. Comparison of the crystallographic space groups for each complex shows that the symmetry of *Pb* ($P\bar{1}$) is the lowest of the series and particularly contrasts that of *Sn* (C_c). However, the level of disorder and radiative absorbance observed during the crystallographic studies of *Pb* limits the comparisons that can be reliably drawn. The air stability of *Pb* continues the trend of decreasing air sensitivity down the group, from rapid

121

hydrolysis in non-dry solvents (*Si*, *Ge*) to efficient preparation in aqueous conditions (*Pb*). *Pb* is also the only member of the series to display any form of energetic sensitivity to conventional preparative operations. Despite an enhanced stability to oxygen and water versus *Si*−*Sn*, solutions of *Pb* are extremely photosensitive, readily undergo reduction and is unsuitable for long-term storage even under inert conditions and low temperature.

The additional decomposition reactions observed in solutions of *Pb* occur due to the decreasing activation barrier for the reduction of Pb(IV), afforded by the enhanced stability of the low-valent oxidation state versus for the lighter homologues. This is anticipated to be the cause of the additional decomposition reactions observed in solutions of *Pb*, especially due to the additional thermodynamic driving force generated by the formation of insoluble $Pb(N_3)_2$. The lower stability of the E(II) centres in Si−Sn increases the activation barrier for their formation, rendering solutions of *Si*−*Sn* more stable towards the same conditions. The lighter homologues of $E(N_3)_4$(bipy) such as *Si* possess a greater overall stability than *Pb* in both solution and solid form. The instability of the oxidation state of a complex containing explosophoric ligands (such as *Pb*) may contribute to the energetic sensitivity of the complex. Although insufficient by itself, the combination of an unstable oxidation state with explosophoric ligands could be used as a strategy to access a new number of energetic materials, similar to the existing use of ring or cage strain as an additional approach to afford energetic character in compounds such as octanitrocubane, $\{C(NO_2)\}_8$, and HMX, $\{CN(NO_2)\}_4$.[259,260]

5.2.7. Preparation of $Pb(N_3)_x(L)_2$ (x = 2 or 4, L = py, pic)

The stabilisation of lighter group 14 tetraazides ($E(N_3)_4$, E = Si−Sn) by coordination of monodentate Lewis bases as $E(N_3)_4(L)_2$ (L = py, pic, scheme 57) was investigated to determine if stabilisation of $Pb(N_3)_4$ was feasible using the same monodentate ligands (scheme 58). Decoordination of the volatile ancillary ligands of $Pb(N_3)_4(L)_2$ could access the unknown $Pb(N_3)_4$, in a similar strategy to that investigated for the neutral Ge(II) diazido complexes discussed in chapter 3. Owing to the inexistence of $Pb(N_3)_4$, $(NH_4)_2[Pb(N_3)_6]$ was chosen as a starting material due to the proposed elimination of insoluble NH_4Cl upon ancillary ligand coordination.

$$E(N_3)_4 \xrightarrow[\text{CH}_2\text{Cl}_2]{\text{L}} E(N_3)_4(L)_2$$
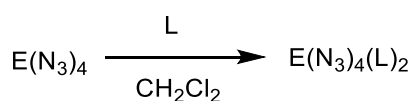
Scheme 57. Formation of $E(N_3)_4(L)_2$ (E = Si−Sn, L = py, pic).

$$(NH_4)_2[Pb(N_3)_6] \xrightarrow[CH_2Cl_2]{L} Pb(N_3)_4(L)_2 + 2NH_4Cl$$
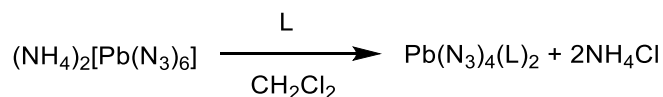
Scheme 58. Proposed formation of $Pb(N_3)_4(L)_2$ (L = py, pic).

No spectral changes were observed upon introduction of pyridine or picoline to solutions of $(NH_4)_2[Pb(N_3)_6]$. The absence of any bands associated with coordinated ancillary ligand confirms that both monodentate ligands were too weakly-coordinating to displace the azido ligands to form $Pb(N_3)_4(L)_2$. It is unclear whether either base would be capable of stabilising the $Pb(N_3)_4$ centre by direct addition to $Pb(N_3)_4$.

The stabilisation of Pb(II) azides using the same ancillary ligands was also tested (scheme 59). The absence of isolable salts of $[Pb(N_3)_3]^-$ meant alternative synthetic strategies were adopted, though the coordination of py to $Pb(N_3)_2$ or azido-chlorido ligand exchange of $PbCl_2(pic)_2$. Both strategies only afforded $Pb(N_3)_2$ and demonstrate the significant thermodynamic driving force afforded by its formation in reactions of both Pb(IV) and Pb(II) azido complexes.

$$Pb(NO_3)_2 + NaN_3 \xrightarrow{py} Pb(N_3)_2(L)_2 \xleftarrow{H_2O} PbCl_2(pic)_2 + NaN_3$$
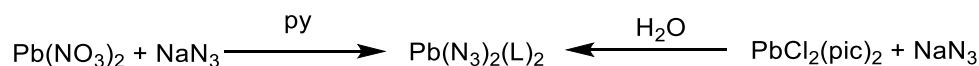
Scheme 59. Proposed formation of stabilised adducts of di(azido) complexes of Pb(II).

5.2.8. Tetrazolato complexes of Pb(IV)

Following the preparation of poly(azido) complexes of Pb(IV), the tetrazolate anion was investigated as an alternative nitrogen-rich ligand. The preparation of the hexakis(tetrazolato)plumbate anion, $[Pb(CHN_4)_6]^{2-}$, would complete the set of hexakis(tetrazolato) complexes containing group 14 centres and would allow comparison of the coordinative ability of tetrazolato and azido ligands towards Pb(IV) centres. The lighter hexakis(tetrazolato) homologues are prepared from reaction of ECl_4 with $NaCHN_4$ (E = Si, Ge) or EF_4, $NaCHN_4$ and $Me_3Si(CHN_4)$ (E = Sn).[104] However, the instability of PbF_4 and $PbCl_4$ required the use of $[PbCl_6]^{2-}$ as a starting material (scheme 60).

$$(PPN)_2[PbCl_6] \xrightarrow[MeCN]{exc.Na(CHN_4)} (PPN)_2[Pb(CHN_4)_6] + 6NaCl$$
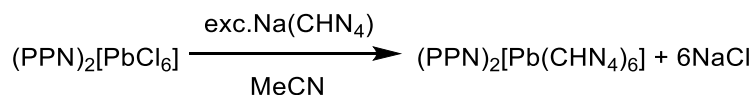
Scheme 60. Proposed formation of $[PPN]_2[Pb(CHN_4)_6]$.

The formation of an orange supernatant solution during the reaction of $[PPN]_2[PbCl_6]$ was identical to the decomposition-induced colour change of solutions of the compound in MeCN

solution. However, the formation of a white precipitate (believed to be NaCl) indicated that some ligand exchange may have occurred. An initial attempt to isolate any products from solution only resulted in the formation of an off-white foam. However, a longer stirring period under the exclusion of light and treatment with two separate batches of excess $NaCHN_4$ resulted in the isolation of a white solid from the supernatant solution. This solid contained small clusters of colourless needle-shaped crystals which were identified crystallographically as the partially-substituted product $[PPN]_2[PbCl_4(CHN_4)_2]$ (figure 93). Although the structure is solved with space group $P\bar{1}$, the structure solution and unit cell parameters initially appear consistent (but is insolvable) with space group C_2. This is consistent with a pseudosymmetric structure, where the unit cell deviates slightly to an extent sufficient to prevent solution in a higher symmetry space group.[261] The possibility of incorrect symmetry means that detailed bond length and angle analysis are not reliable and instead the structure serves only as proof of the coordination of two tetrazolato ligands to a Pb(IV) centre (scheme 61). No evidence of partially-occupied tetrazolato ligands are evident at any other coordination site.

$$(PPN)_2[PbCl_6] \xrightarrow[\text{MeCN}]{\text{exc.Na(CHN}_4)} (PPN)_2[PbCl_4(CHN_4)_2] + 2NaCl$$
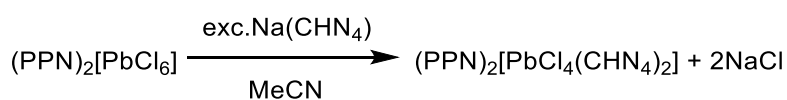
Scheme 61. Formation of $[PPN]_2[PbCl_4(CHN_4)_2]$.
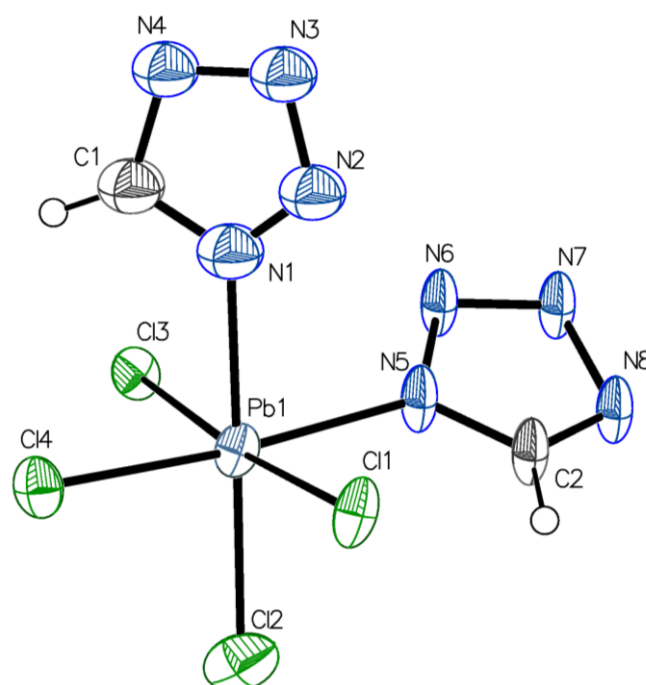
Figure 93. Molecular structure of the $[PbCl_4(CHN_4)_2]^{2-}$ anion in crystals of $[PPN]_2[PbCl_4(CHN_4)_2]$. Selected bond lengths (Å) and angles (°) : Pb(1)−Cl(1) 2.484(5), Pb(1)−Cl(2) 2.527(8), Pb(1)−Cl(3) 2.497(5), Pb(1)−Cl(4) 2.484(6), Pb(1)−N(1) 2.28(2), Pb(1)−N(5) 2.258(19) ; N(1)−Pb(1)−Cl(2 174.0(7), N(5)−Pb(1)−Cl(4 174.3(6), N(5)−Pb(1)−N(1) 85.7(9).

The tetrazolato ligands are hypothesised to coordinate in different planes in order to minimise steric hindrance. Not all solid isolated from solution is crystalline and therefore it is unclear if the bulk solid is composed of pure $[PPN]_2[PbCl_4(CHN_4)_2]$ or a mixture of partially-substituted $[PPN]_2[PbCl_x(CHN_4)_y]$ complexes, where $x + y = 6$. These findings contrast the syntheses of $[PPN]_2[Pb(N_3)_6]$, where ligand exchange is facile and proceeds to completion under similar conditions to those employed in this reaction and is consistent with the differences in experimental conditions required for the formation of homoleptic complexes of the lighter centres.[104] This confirms that the tetrazolato ligand is more weakly coordinating than N_3^- towards group 14 elements and quantifies the varying extent of ligand substitution of azido and tetrazolato complexes towards Pb(IV) centres.

The formation of $[Pb(CHN_4)_6]^{2-}$ may be prevented by increasing steric and electronic barriers. Following the substitution of two chlorido ligands, further substitution by the weakly coordinating tetrazolato ligand is not possible and no further exchange occurs. The increased steric bulk of the tetrazolato ligand versus the chlorido ligand, may also influence the extent of ligand exchange, alongside a possible decrease in solubility of the poly(tetrazolato) complexes upon further substitution of tetrazolato ligands. The requirement for the reaction to be conducted at room temperature to avoid decomposition of $[PPN]_2[PbCl_6]$ minimises the thermodynamic driving force that may be required for complete ligand exchange. In analogy to the preparation of the $[Sn(CN)_6]^{2-}$ anion, the generation of an insoluble or gaseous byproduct may be required to form a homoleptic complex. The syntheses of the lighter $[E(CHN_4)_6]^{2-}$ homologues required long periods of time at elevated temperatures to ensure complete exchange and thus the use of high reaction temperatures to increase the amount of ligand exchange, which would require a more thermally stable Pb(IV) precursor. The reported synthesis of charge-neutral $Pb(PhCHN_4)_4$ at 40 °C identifies $Pb(OAc)_4$ as a promising candidate.[262]

The large differences in reactivity of neutral Pb(IV) azido complexes versus those of E(IV) (E = Si−Sn) led to the investigation of the syntheses of neutral Pb(IV) tetrazolato complexes. The steric bulk and weaker ligating ability of the tetrazolato ligand was anticipated to account for the decreased reactivity of the ligand towards group 14 centres, as observed in the attempted synthesis of $[PPN]_2[Pb(CHN_4)_6]$ above. The Pb(IV) coordination centre was investigated to determine if an increased ionic radius and heavier, metallic coordination centre of group 14 would prove sufficient to facilitate complexation of bulky, weakly-coordinating tetrazolato

125

ligands. PbCl$_4$(bipy) was reacted with NaCHN$_4$ in DMSO-d$_6$ and monitored by NMR spectroscopy (scheme 62). Despite addition of further excesses of NaCHN$_4$ and elevated reaction temperature, no evidence of chloro-tetrazolato ligand exchange was observed. It is possible that exchange was precluded by the displacement of chlorido and tetrazolato ligands by DMSO-d$_6$. Although this effect would be negated by the use of a non-coordinating solvent, the solubility of both reagents and products were anticipated to decrease to a point where spectroscopic observation would not be possible. As such, the complexes were not investigated further.

$$\text{PbCl}_4(\text{bipy}) \xrightarrow[\text{MeCN}]{\text{ex.Na(CHN}_4)} \text{Pb(CHN}_4)_4(\text{bipy}) + 4\text{NaCl}$$
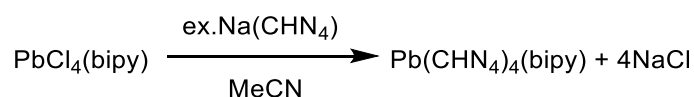
Scheme 62. Proposed formation of Pb(CHN$_4$)$_4$(bipy).

5.3. Conclusions and Outlook

The studies described in this chapter have demonstrated that although azido ligands can stabilise anionic and neutral complexes of Pb(IV) in the same fashion as the lighter group 14 centres, the extent of this stabilisation is significantly reduced versus the complexes of silicon, germanium and tin. The synthesis and characterisation of [PPN]$_2$[PbCl$_6$] facilitated the preparation of an air-stable hexa(azido)plumbate salt as [PPN]$_2$[Pb(N$_3$)$_6$]. Although energetically stable towards conventional preparative operations, the photochemically-induced decomposition in solution to form Pb(N$_3$)$_2$ represents a decrease in stability of the [Pb(N$_3$)$_6$]$^{2-}$ anion versus the hexa(azido) silicate, germanate and stannate anions. In contrast to previous reports, no evidence for the formation of [Pb(N$_3$)$_3$]$^-$ were isolated and the anion is proposed to exist only fleetingly in solution, if at all. Further attempts to prepare the salts of [Pb(N$_3$)$_3$] resulted in either no reaction or the formation of Pb(N$_3$)$_2$.

The preparation and isolation of Pb(N$_3$)$_4$(bipy) is the first example of a neutral poly(azido) complex of Pb(IV) and completes the set of neutral group 14 tetra(azido) complexes stabilised through the addition of chelating Lewis bases. Unlike the lighter homologues, Pb(N$_3$)$_4$(bipy) is characterised by energetic and photochemical instability in solution and demonstrates that the coordination of chelating Lewis bases is unable to stabilise Pb(N$_3$)$_4$ to the same extent as the lighter centres. The differing stabilities between the anionic and neutral poly(azido) complexes of Pb(IV) is consistent with the analogous chlorides, where neutral PbCl$_4$ rapidly decomposes whilst the [PbCl$_6$]$^{2-}$ anion does not.[263,264]

The instability of Pb(N$_3$)$_4$(bipy) results in many spontaneous and photoinduced decomposition reactions, the pathway of which is heavily influenced by various conditions including light, the presence of chlorinating solvent and external stimuli. Almost all of the observed reactions involve reduction of Pb(IV) to the more stable Pb(II), which is believed to contribute to the instability of Pb(N$_3$)$_4$(bipy). The formation of Pb(N$_3$)$_2$ is a key feature of many of these reactions and is likely to preclude the formation and long-term stability of novel azido complexes of Pb(IV) and Pb(II) such as Pb(N$_3$)$_4$(bipy) and [Pb(N$_3$)$_3$]$^-$. The latter of these complexes was unable to be formed from coordination complexes containing lead in either oxidation state and is only detected as a fragment in the mass spectrum of [PPN]$_2$[Pb(N$_3$)$_6$]. Pb(N$_3$)$_4$ remains unknown. Further work could focus on the detection or identification of the [Pb(N$_3$)$_3$]$^-$ anion in solution through spectroscopic methods.
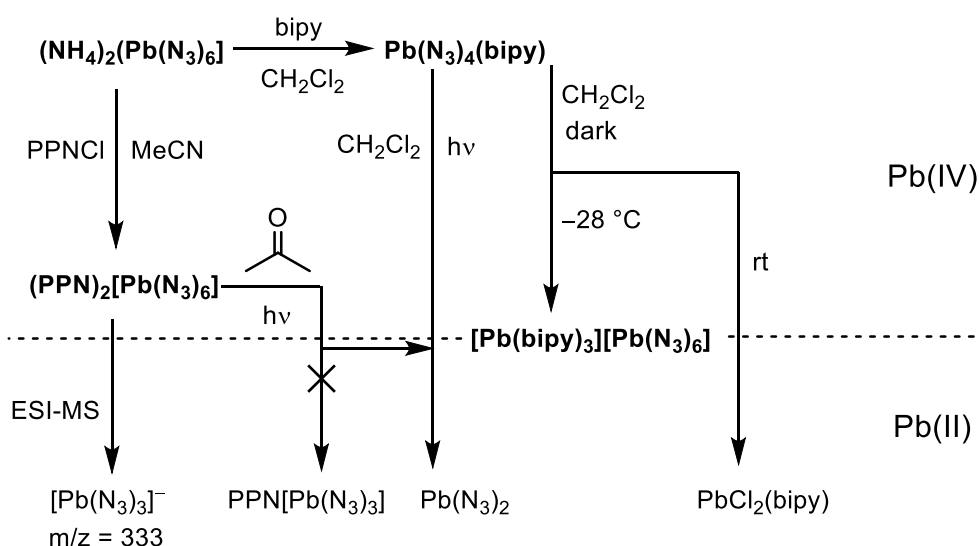
Scheme 63. Reactions involving the [Pb(N$_3$)$_6$]$^{2-}$ anion. The formation of (NH$_4$)$_2$[PbCl$_6$] has been omitted for clarity.

This work has prepared the first poly(tetrazolato) complex of Pb(IV), as [PPN]$_2$[Pb(CHN$_4$)$_2$Cl$_4$]. The limited extent of exchange between [PPN]$_2$[PbCl$_6$] and Na(CHN$_4$), in contrast to the rapid formation of [PPN]$_2$[Pb(N$_3$)$_6$], further demonstrates the decreased coordination ability of the tetrazolato versus the azido ligand. This emphasises the need for additional thermodynamic driving forces towards ligand exchange and, consequently, a thermally-stable precursor to obtain the hexakis(tetrazolato)plumbate(IV) anion. No neutral Pb(IV) complexes could be prepared and therefore Pb(CHN$_4$)$_4$ also remains unknown.

Chapter 6. Arylpentazole and the N_5^- anion

6.1. Introduction

The pentazolate anion (N_5^-) has been predicted to be one of the most stable forms of polynitrogen, owing to its proposed aromatic character.[265] The pentazole (N_5) ring has been the subject of extensive investigations and attempts to prepare N_5 rings have spanned a century. Lifschitz's 1915 report of the synthesis of an N_5 ring by ring closure of cyanotetrazole with hydrazine dihydrate was rapidly disproved by Curtius, who argued that cycloaddition instead formed bistetrazole (scheme 64).[266,267] A later study proposed the formation of a linear pentazene-type intermediate, but no N_5 species of any geometry were isolated.[268] It was not until approximately 40 years later that the first pentazoles were prepared as aromatic substituents (i.e., arylpentazoles).[269,270] The presence of an aromatic phenyl group appears critical to the stabilisation of the pentazole ring. Although theoretical studies predict methylpentazole to be one of the most stable non-aromatic pentazoles, the fleeting detection of tetrazolylpentazole (CHN_4–N_5) in a low-temperature NMR spectroscopic study is the only report of a pentazole compound which does not contain an aryl group.[269,271,272] A theoretical study predicted that the polynitrogen analogue of cyclopentadiene, $Fe(\eta^5\text{-}N_5)_2$, may be accessible.[273] Interest in arylpentazoles was recently renewed by the reported reductive cleavage of an arylpentazole precursors to produce pentazolate (N_5^-) salts on gram-scales for the first time.[76] However, the parent acid (HN_5) remains elusive and has never been isolated.[274,275] With the exception of high-pressure syntheses and despite many attempts, arylpentazoles remain the only route to obtain both anionic and charge-neutral N_5 ring systems.[276,277]
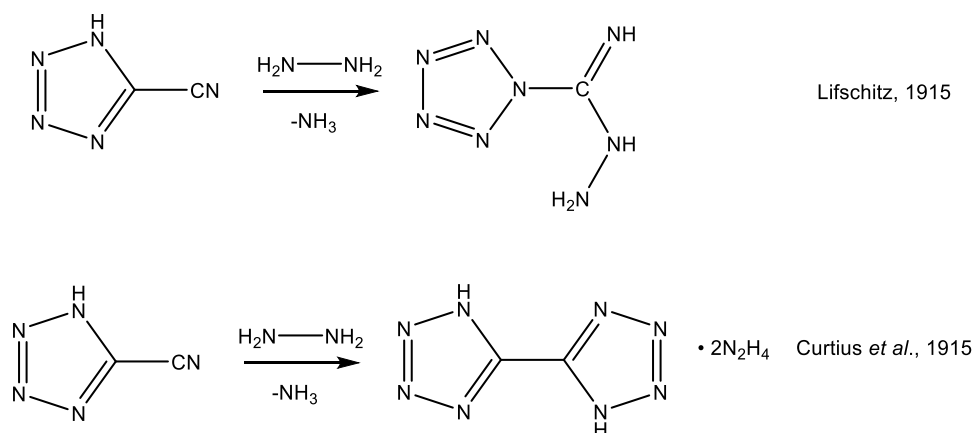
Scheme 64. Proposed synthesis of pentazole (top) by Lifschitz, later disproved by Curtius (bottom).

Arylpentazoles are prepared by the [3+2] cycloaddition reaction of an aryldiazonium salt (ArN_2^+) with an azide anion (scheme 65), in a mechanism which is analogous to the formation of tetrazoles from azides and nitriles.[269] Cycloaddition results in the formation of unstable $E-$ and $Z-$ pentazenium intermediates. Only the $Z-$ isomer is of the correct geometry to form N_5 by ring closure and the $E-$ isomer rapidly decomposes into arylazide and N_2, as indicated by gas release upon the addition of azide and diazonium salts. This results in the unavoidable contamination of arylpentazole with arylazide and further purification is a necessity to obtain analytically-pure arylpentazole.[278] Despite the stabilisation afforded by the aromatic phenyl group, arylpentazoles are characterised by thermal instability and only a single example (dimethylaminophenylpentazole, DMAP-N_5) is stable at room temperature.[279] At temperatures equal or greater than the decomposition temperature, the N_5 ring irreversibly decomposes into the corresponding arylazide and N_2 gas (see below).[278]
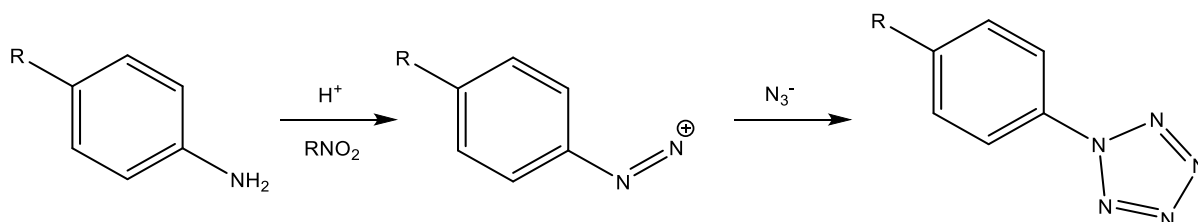
Scheme 65. Formation of arylpentazoles from diazonium salts.

The electron donation ability of the aromatic substituents play a critical role in determining the stability of arylpentazoles, the lifetime of which vary from several minutes at room temperature (DMAP-N_5) to under half a minute (C_6H_5-N_5) (table 49).[280] Although most exhibit no explosive behaviour, phenylpentazole is reported to explode upon slight impact when stored above $-10\ °C$.[270] The thermal stability of the N_5 group is proposed to stem from the strength of the $C-N$ bond between the phenyl and pentazole ring and can be quantified by the correlation of the Hammett constant of substituents in *para* and *meta* positions to the N_5 ring (σ_p and $\sigma_{m,}$ respectively).[280] A more electron donating substituent results in greater stabilisation of the N_5 resonance forms, whilst an electron-withdrawing group reduces the amount of electron density in the aromatic ring system and destabilises the N_5 ring. As a result, the lifetime of arylpentazoles is proportional to the electron-donating ability of the *para* substituent. Almost all known arylpentazoles contain a single aromatic substituent located *para* to the N_5 ring and their stability is not affected by the *meta*-substituent aromatic protons ($\sigma_{m(H)} = 0$).[281]
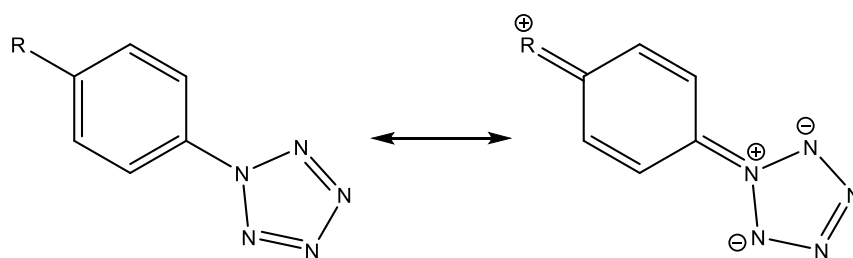
Scheme 66. Resonance forms of arylpentazoles.

Thermal decomposition of arylpentazoles proceeds by the sequential cleavage of the N(1)−N(5) and N(3)−N(4) bonds (scheme 67). The arylpentazene intermediate, formed from the first irreversible N−N bond cleavage, is analogous to that formed from the formation of the pentazole ring. Rapid decomposition of this unstable intermediate prevents reformation of the N_5 ring, instead producing N_2 gas and arylazide (scheme 68). The decomposition of the pentazene intermediate is also favoured by the entropic and enthalpic driving forces afforded by the formation of gaseous N_2.[278]
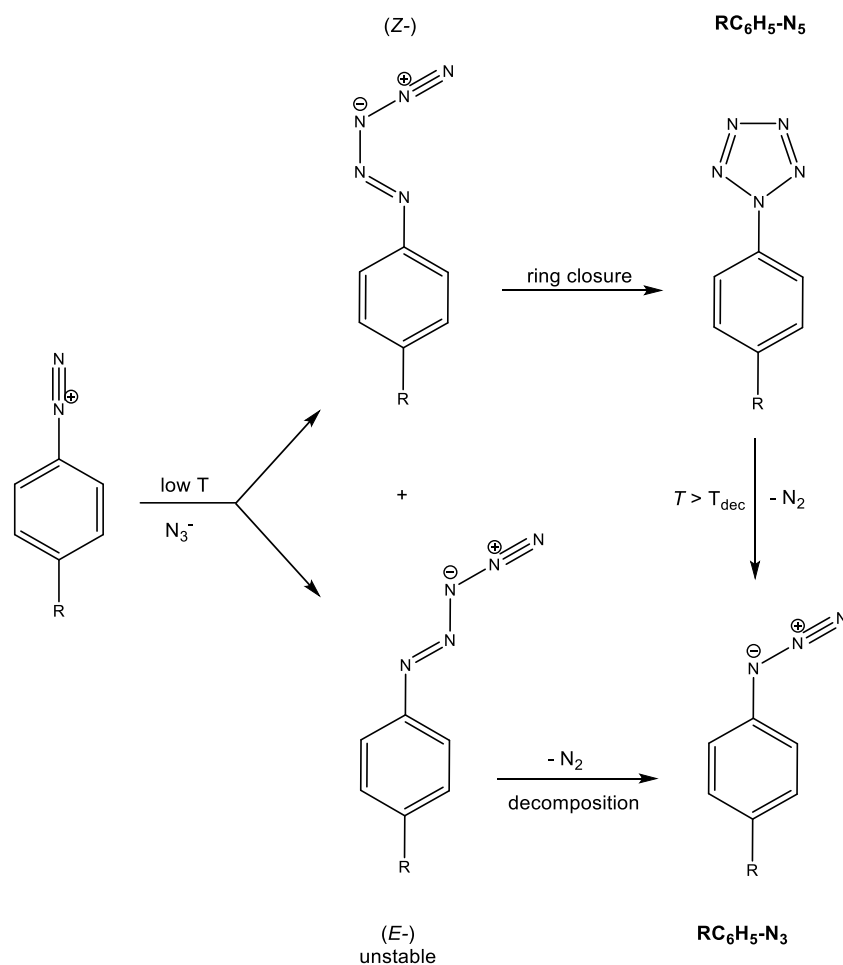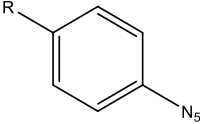
Scheme 67. Formation of arylpentazole (RC_6H_5-N_5) and arylazide (RC_6H_5-N_3) from the *Z*- and *E*-pentazenium isomers. The synthesis (T) and decomposition (T_{dec}) temperatures vary depending on the identity of the substituent R.
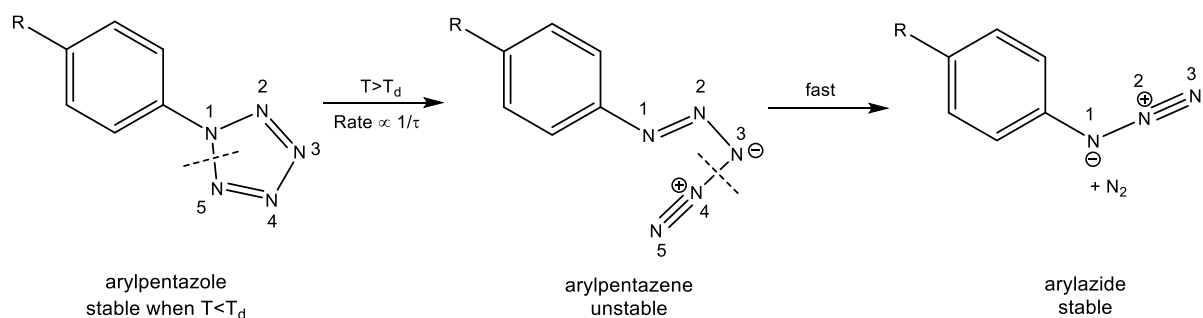
Scheme 68. Decomposition of arylpentazoles into arylazides via the unstable pentazene intermediate.

	T_d / °C	T_s / °C	Refs.
R = H	−5	−35	[270]
R = OH	+53	−15	[282]
R = NMe$_2$	+56	−35 to −60	[279]
R = MeO	−13	−35	[269]

Table 49. Decomposition (T_d) and synthesis (T_s) temperatures of selected arylpentazoles.

Despite their important status as the sole precursors to the N_5 ring system, including the N_5^- anion, synthetic and structural studies on arylpentazoles are sparse. To date, dimethylhydroxyphenylpentazole (DMHP-N_5) is the only arylpentazole that has been demonstrated to form N_5^- in bulk and it is unclear if other arylpentazoles are capable of releasing N_5^- in similar yields or though the same synthetic route (if indeed at all).[76] It is also unclear if the newly-isolated N_5^- anion can be classified as a pseudohalide in line with other nitrogen-rich ligands such as N_3^- and CHN_4^-. In this work, the stability and structure of several neutral and anionic arylpentazoles (figure 94) were studied to investigate their propensity to eliminate N_5^-.
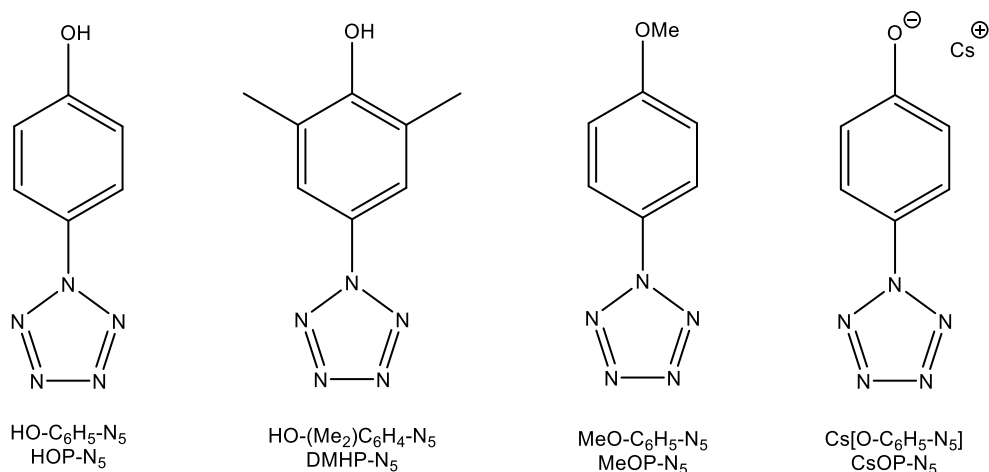
Figure 94. Arylpentazoles investigated in this study.

6.2. Results and Discussion

6.2.1. Preparation of arylpentazoles

All three neutral arylpentazoles (HOP-N_5, DMHP-N_5 and MeOP-N_5) precipitated from aqueous solution as green/grey (HOP-N_5, MeOP-N_5) or dark pink (DMHP-N_5) solids upon the addition of NaN_3. Bubbles of gas released during this addition process originated from the decomposition of the unstable *E*-pentazene isomer. The solid arylpentazoles were isolated by cold filtration and washed to remove arylazide impurities. At room temperature, colour changes were observed in solid samples of each arylpentazole. Further gas release was observed upon warming the filtrate solutions to room temperature. This is attributed to thermal decomposition of traces of arylpentazole or unreacted aryldiazonium salts remaining in the filtrate. Noticeable colour changes of the filtrate solutions of HOP-N_5 and DMHP-N_5 are attributed to side reactions of unreacted starting material or photolysis of the arylazide by nitrene formation (scheme 69).[283,284]
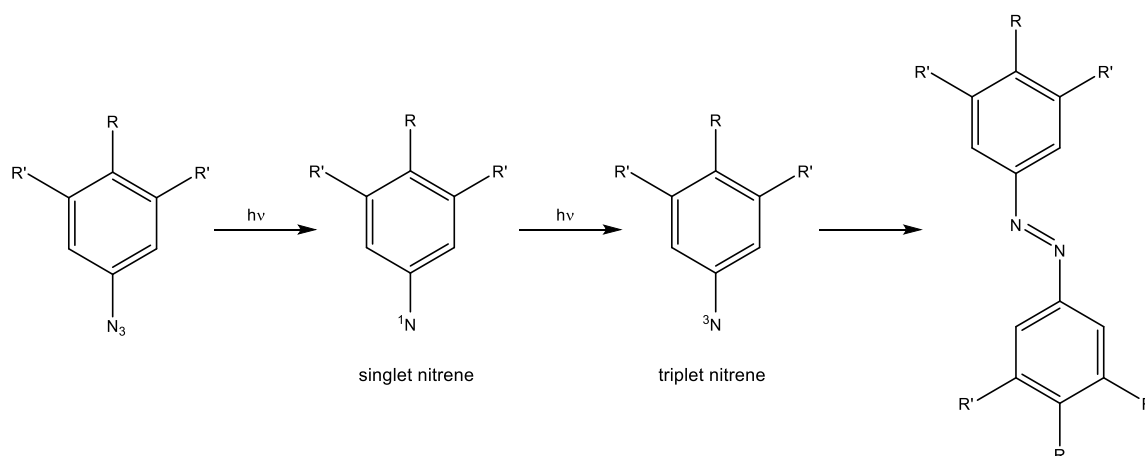
Scheme 69. Proposed photolysis reactions of arylazides into dimeric azo compounds. R = OH, OMe ; R' = Me, H.

Prolonged standing of the filtrate solution from the synthesis of DMHP-N_5 at room temperature resulted in the formation of deep red needle-shaped crystals of a dimeric quinone compound (figure 95) which crystallised as a disordered hexane solvate in space group *P*2$_1$/c. The absence of an azo bridge appears to suggest photolytic formation of a nitrene from the arylazide does not occur. Instead, the quinone is hypothesised to form by the reaction of the diazonium salt with unreacted starting material (scheme 70). Comparison to standard bond lengths rationalised the structure as a quinone-type compound containing a mixture of singly- and doubly bonded C−N and C−O sequences, as shown in figure 96.
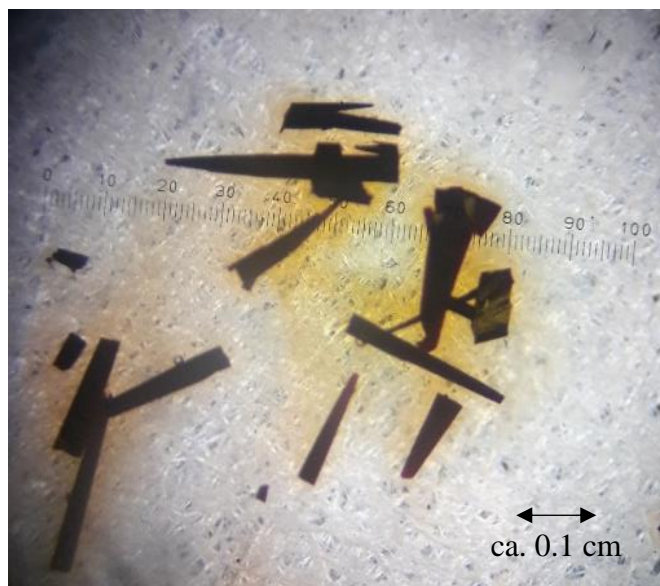
Figure 95. Photograph of single crystals of the side product of DMHP-N$_5$ in paraffin oil. Over time, the crystals began to degrade in the paraffin oil, denoted by the orange colour surrounding the crystals. The speckled background is due to paper lying underneath the microscope slide.
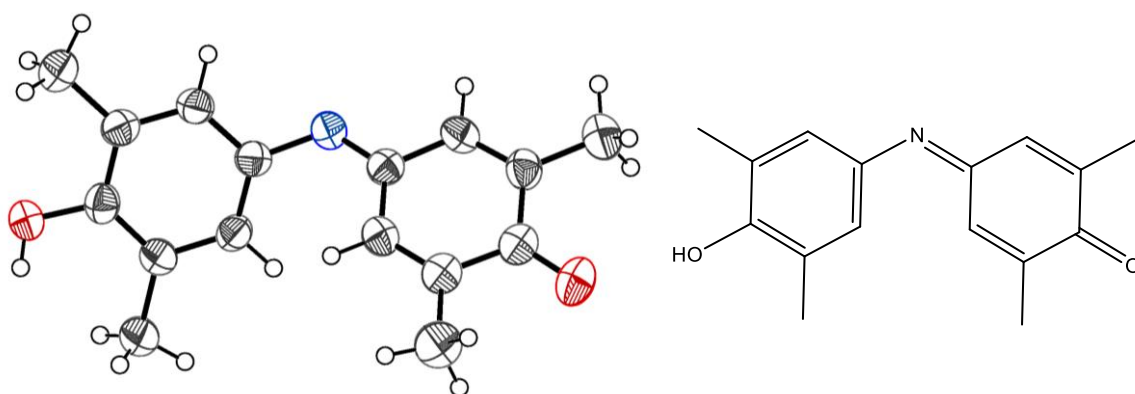
Figure 96. Structure (left) and molecular crystal structure (right) of the side product of DMHP-N$_5$. The solvent molecule has been omitted for clarity. Grey = C, white = H, red = O, blue = N.
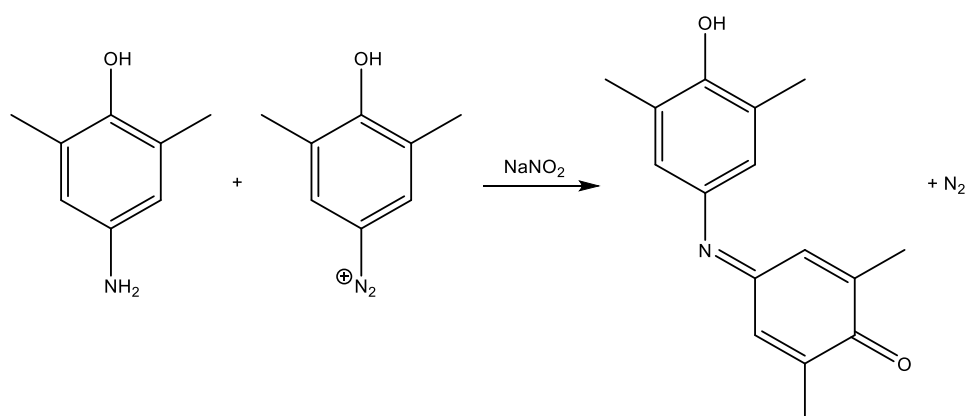
Scheme 70. Proposed formation of dimeric decomposition product of DMHP-N$_5$.

133

Caesium pentazolylphenolate, CsOP-N$_5$, was formed by the deprotonation of HOP-N$_5$ by CsOH·xH$_2$O (scheme 71).[282] The N$_5$ ring was preserved during deprotonation and crystalline CsOP-N$_5$ formed almost immediately in suspension.
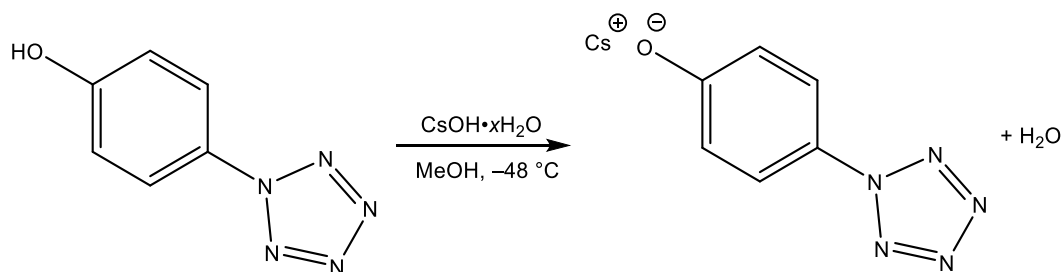
Scheme 71. Formation of CsOP-N$_5$ from HOP-N$_5$ and CsOH·xH$_2$O.

6.2.2. Thermal stability of arylpentazoles

All four compounds deflagrated during flame testing, with samples of MeOP-N$_5$ and DMHP-N$_5$ leaving dark decomposition residues. In contrast to the extremely high sensitivity reported for phenylpentazole, all four solid compounds studied appeared stable towards regular preparative handling operations, including scraping and low impacts.[270] However, the impact sensitivities of each compound were unable to be formally determined owing to their low thermal stabilities at room temperature. No explosions were observed at any point during thermal decomposition. Whilst rapid decomposition at room temperature formed the corresponding arylazides as dark, sticky solids, more controlled decomposition over the course of several days formed finely-divided, free-flowing pale powders. Both displayed identical v_{as}(N$_3$) bands and therefore the variation in colour and consistency is attributed to a small amount of a highly-conjugated product formed during rapid thermolysis. The identity of the oily impurity is not known but is speculated to be a highly-conjugated organic compound, similar to those generated by the photolysis of arylazides.[283] The mechanism of formation is unclear but appears to be influenced by the rate of decomposition, rather than light exposure.

The arylpentazoles were analysed by IR spectroscopy in an attempt to elucidate the spectral position of the v(N$_5$) bands. Despite efforts to minimise thermal decomposition prior to analysis, the preparation of each sample at room temperature resulted in unavoidable v_{as}(N$_3$) bands in the initial IR spectra of all four compounds. Although a band at 2081 cm^{-1} in HOP-N$_5$ is tentatively speculated as a v(N$_5$) band, few v(N$_5$) bands were clearly observed for the neutral arylpentazoles due to their overlap with the v_{as}(N$_3$) bands of the corresponding

arylazide. However, the spectra of CsOP-N$_5$ shows a band speculated to arise from a N$_5$ stretching vibration ($\tilde{v} = 2085$ cm^{-1}) which decreases over time at room temperature (figure 97). The decreased dipole moment of the N$_5$ ring versus the azide group may account for the weaker absorbance intensities of the corresponding bands in the spectrum of CsOP-N$_5$.

The intensity of the v_{as}(N$_3$) bands in each spectrum increased over time due to thermal decomposition of arylpentazole into arylazide at room temperature (figures 97-99). The spectral position of the v_{as}(N$_3$) bands decreases to lower wavenumbers in the order HOP-N$_5$ > CsOP-N$_5$ > DMHP-N$_5$ > MeOP-N$_5$ (table 50). The presence of more than one azide band at similar spectral positions in the IR spectra of each neutral azide is attributed to Fermi resonance and has previously been observed in the IR spectrum of DMAP-N$_3$.[285] The clearest spectral changes are observed in the spectra of CsOP-N$_5$. The growth of an additional band at 2077 cm^{-1} in this spectral series is similar to the spectral position of one band of HOP-N$_5$ or HOP-N$_3$ (table 49). The presence of water in solid CsOP-N$_5$, arising from the formation of solvated trihydrate crystals and the use of caesium hydroxide hydrate to prepare the compound, may result in the reprotonation of the hydroxide group in CsOP-N$_5$ to form HOP-N$_5$ and the band at 2085 cm^{-1} (scheme 72). It is unclear if this process occurs for both azido- and pentazolyl phenolates (i.e. CsOP-N$_3$ and CsOP-N$_5$). However, the similarities between the v_{as}(N$_3$) bands of HOP-N$_3$ and CsOP-N$_3$ prevent confirmation of this theory. The IR spectrum of DMHP-N$_5$ in THF solution at low temperature is dominated by the increase of absorbance intensity of the v_{as}(N$_3$) bands of DMHP-N$_3$ with solution temperature. A decrease in a band at 1600 cm^{-1} is consistent with the decomposition of a v(N$_5$) band (figure 100).
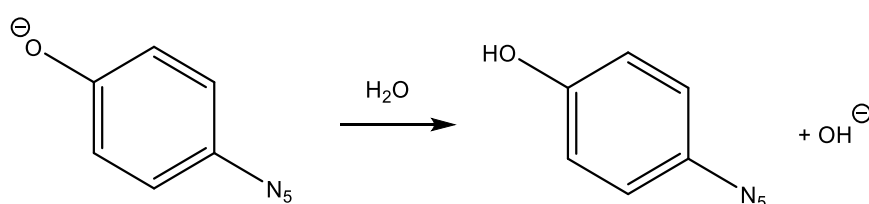
Scheme 72. Proposed formation of HOP-N$_5$ from CsOP-N$_5$ in the presence of water.

R$-$N$_5$	v(N$_5$) / cm^{-1}	v_{as}(N$_3$) / cm^{-1}
HOP	*2081*	2114[a]
DMHP	1600 [b]	2122, 2102
CsOP	2085	2116, 2076
MeOP	$-$	2134, 2103

Table 50. Key v(N$_5$) and v_{as}(N$_3$) bands of solid arylpentazoles and arylazides studied in this work. [a] broad; [b] in THF solution. The identity of bands listed in *italics* are speculated.
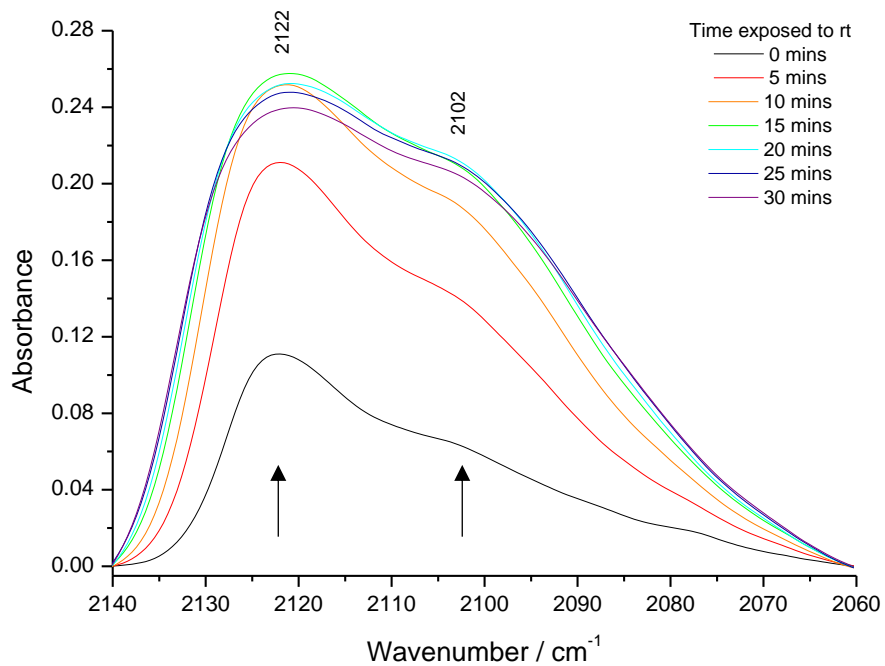
Figure 97. IR spectral series between $2140-2060$ cm^{-1} showing the thermal decomposition of solid DMHP-N$_5$ into DMHP-N$_3$ ($\uparrow$, $\nu_{as}(N_3)$ = 2122, 2102 cm^{-1}).
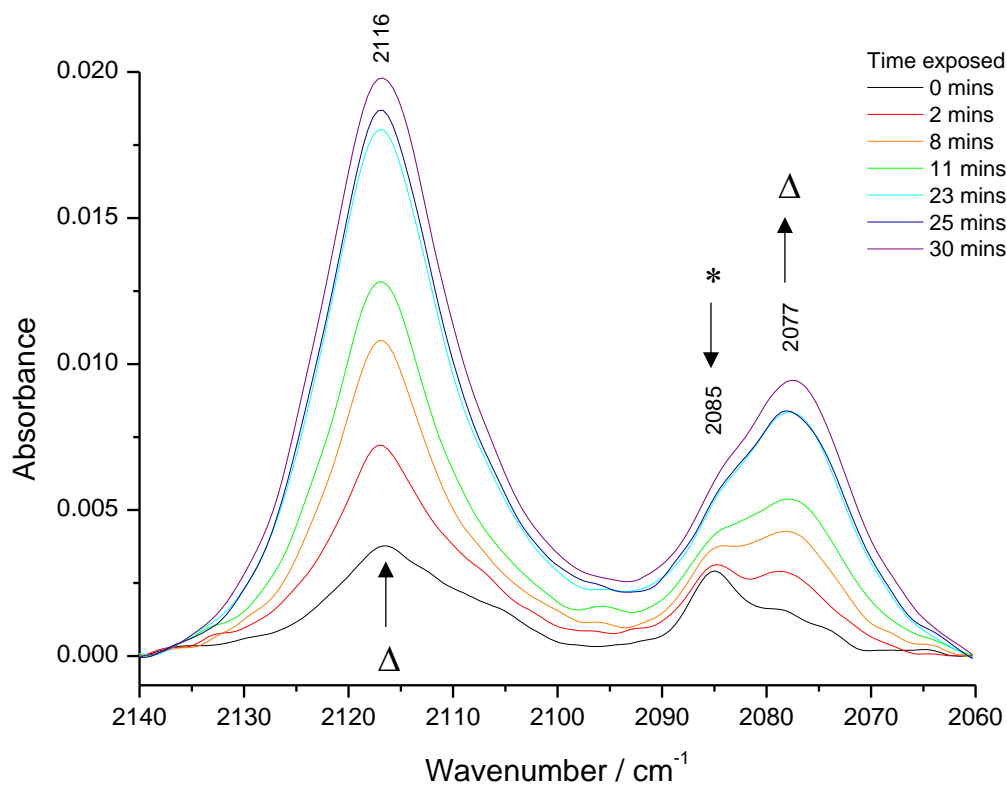
Figure 98. IR spectral series between $2140-2060$ cm^{-1} showing the decomposition ($\downarrow$) of solid CsOP-N$_5$ (*, $\nu(N_5)$ = 2085 cm^{-1}) and the concurrent formation ($\uparrow$) of CsOP-N$_3$ (Δ, $\nu_{as}(N_3)$ = 2116, 2077 cm^{-1}).
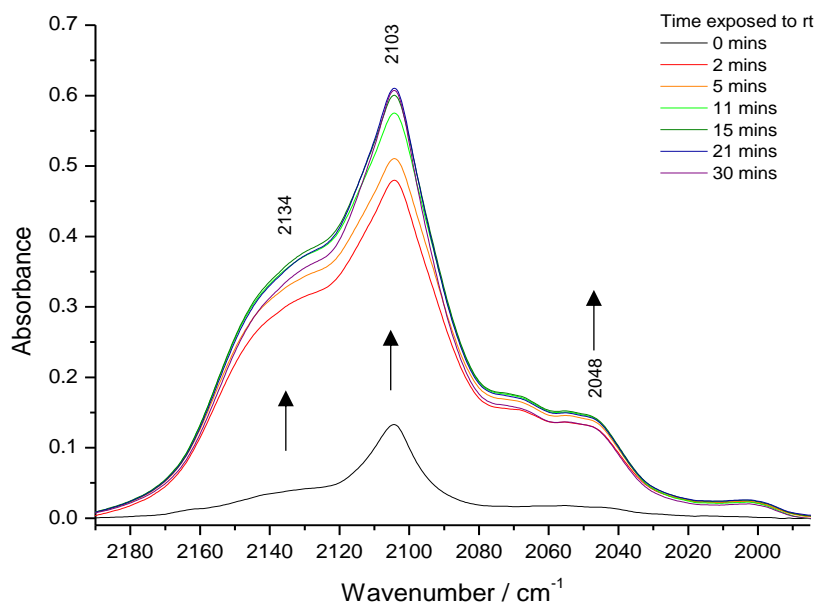
Figure 99. IR spectral series between 2140−2060 cm^{-1} showing the decomposition of solid MeOP-N$_5$ into MeOP-N$_3$ ($\uparrow$, ν_{as}(N$_3$) = 2134, 2103 cm^{-1}). It is unclear if the band at 2048 cm^{-1} arises from MeOP-N$_3$.
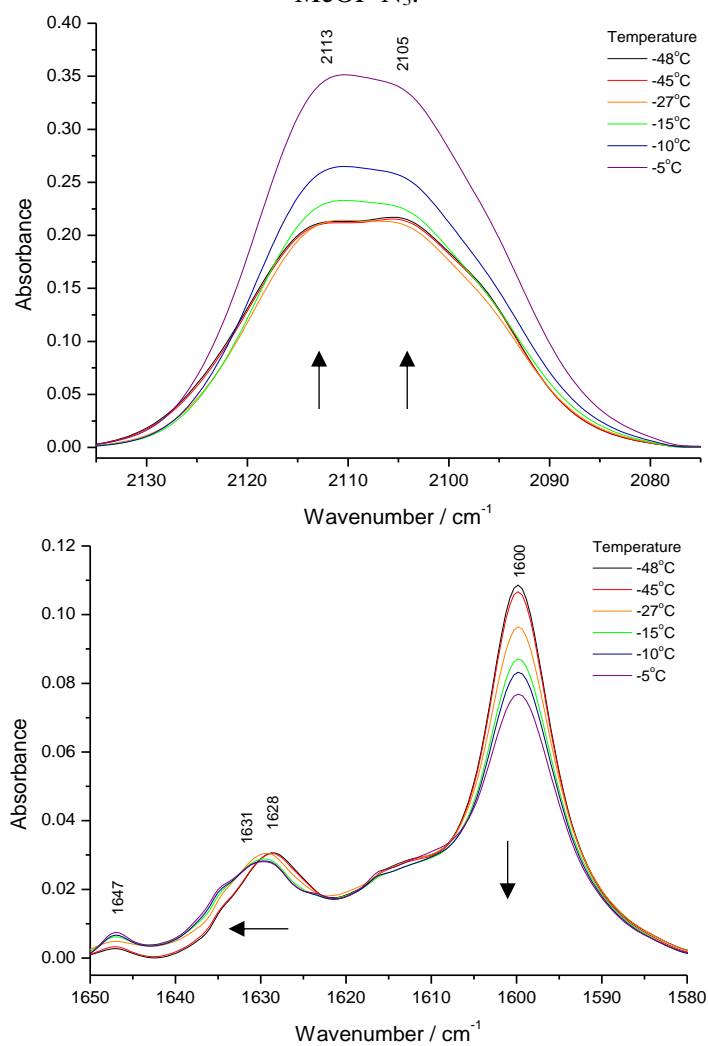
Figure 100. Decomposition of DMHP-N$_5$ in THF between −48 °C and −5 °C, showing a decrease in the ν(N$_5$) band at 1600 cm^{-1} and an increase in the ν_{as}(N$_3$) bands at 2113 and 2015 cm^{-1}.

137

The increase in intensity of azide bands associated with decomposition of arylpentazole into arylazide facilitated IR spectral monitoring of the thermal decomposition process in the solid state (figures 97−99) and an estimation of the lifetime of each arylpentazole. As decomposition proceeds, the intensity of the azide band in the IR spectrum increases exponentially until all pentazole is decomposed. Assuming a first order rate law, the rate constant for the thermal decomposition of an arylpentazole can be calculated. Calculations of the decomposition rate constants for all four arylpentazoles studied in this work showed a clear extension in the lifetime of the arylpentazole in the order $CsOP-N_5 > HOP-N_5 > DMHP-N_5 > MeOP-N_5$ (figure 101, tables 51, 52).

Compound	τ_1 / min	k / min^{-1}	$\Delta\tau_1$	Δk
$HOP-N_5$	4.40	0.23	$\pm$ 0.59	0.030
$DMHP-N_5$	3.70	0.27	$\pm$ 0.81	0.059
$MeOP-N_5$	1.50	0.67	$\pm$ 0.32	0.14
$CsOP-N_5$	19.0	0.053	$\pm$ 8.3	0.023

Table 51. Fitting model data for exponential growth curves of most intense azide absorbance band of arylazide versus time. Values are reported to 2 significant figures. τ_1 = lifetime, k = rate, $\Delta\tau_1$ = error in lifetime, Δk = error in rate.
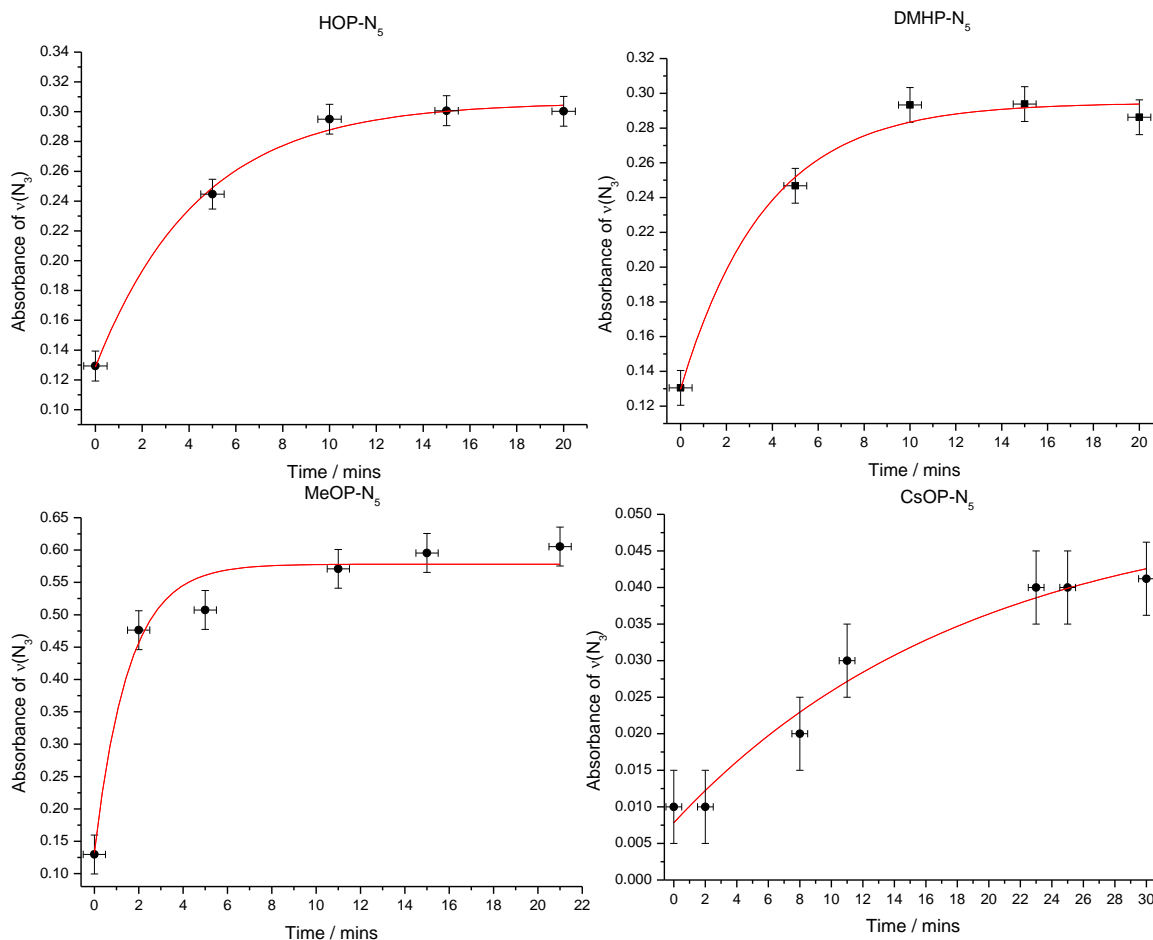
Figure 101. Exponential growth curves for the most intense azide absorbance band of the solid arylazide versus time. All spectra normalised to the most intense paraffin oil band and baseline corrected. From top, clockwise: HOP-N_5, DMHP-N_5, MeOP-N_5 and CsOP-N_5. The error bars for the x-axis (time) are set at ± 0.5 mins. The error bars for the y-axis (absorbance of $v(N_3)$) are set at ± 0.01 (HOP-N_5, DMAP-N_5), ±0.005 (CsOP-N_5) or ± 0.03 (MeOP-N_5).

The value of the lifetime of each arylpentazole can be quantified by the Hammett constants of each aromatic substituent located in *para* or *meta* positions to the pentazole ring (σ_p or σ_m respectively).[280,281] The Hammett equation shows that the Hammett constant is directly proportional to the rate constant (k) and inversely proportional to the lifetime (τ) (equation 1). Therefore, arylpentazoles containing more electron-donating *para* and *meta* substituents (and thus greater values of σ_p or σ_m) are more stable. This is exemplified by the lifetimes of $C_6H_5-N_5$ ($\sigma_p = 0$, $\tau = 1.98$ mins) versus *p*-(dimethylamino)phenylpentazole, DMAP-N_5 ($\sigma_p = -0.6$, $\tau = 10.0$ mins) at 20 °C.[280]

$$\log(k/k_0) = \rho\sigma \qquad k = 1/\tau$$
$$\text{Assuming } k_0 \text{ and } \rho \text{ are constant,}$$
$$\therefore \log(1/\tau) = a\sigma \text{ , where } a = \rho/k_0$$

Equation 1. Relationship between lifetime (τ) and the Hammett constant (σ) of arylpentazole substituents in the *para* or *meta* positions to the N_5 ring. k = rate constant, k_0 = rate constant of unsubstituted arylpentazole, ρ = reaction constant.

The *para-* aromatic substituents investigated in this work (OH, O⁻, OMe) are electron donating and therefore σ_p is always negative.[281] The lifetime of the compounds increases alongside the increasing amount of electron donation (figure 102). The previous values reported for R = *p*-OH and *p*-O⁻ in solution are in close agreement with the values for HOP-N_5 and CsOP-N_5 calculated in this study (figure 103), despite the use of approximate scaling to account for temperature differences between studies, updated Hammett constants and differences in sample form.[280,281] However, further comparisons of the stabilities in different states cannot be drawn owing to the very similar (HOP-N_5) or overlapping (CsOP-N_5) error margins between the two studies. Surprisingly, the hydrogen bonding observed in HOP-N_5 (see below) does not seem to significantly affect the stability of the compound in the solid-state versus in solution. This study does not provide evidence for any significant decrease in stability of DMHP-N_5 compared to other arylpentazoles, and therefore does not account for DMHP-N_5 role as the sole source of N_5^-.[75,76]

R−N₅	σₚ	τ / mins (ca. 20 °C)	
		This work	**Ugi *et al.***
HOP-N₅	−0.37	4.40 ± 0.59	5.21 ± 0.16
DMHP-N₅	−0.51	3.70 ± 0.81	−
CsOP-N₅	−0.81	19.0 ± 0.32	18.32 ± 0.60[a]
MeOP-N₅	−0.27	1.50 ± 8.3	−

Table 52. Comparison of calculated rate constants for the decomposition of various arylpentazoles in solid states (this work, room temperature, 2sf) and solution states (Ugi *et al.*). The values reported by Ugi *et al.* have been scaled to obtain extrapolated values for room temperature). [a] reported for ⁻OPh-N_5. The value of σ_p for DMHP-N_5 was obtained by the sum of the constants of *meta*-CH_3 and *para*-OH substituents.[280,281]
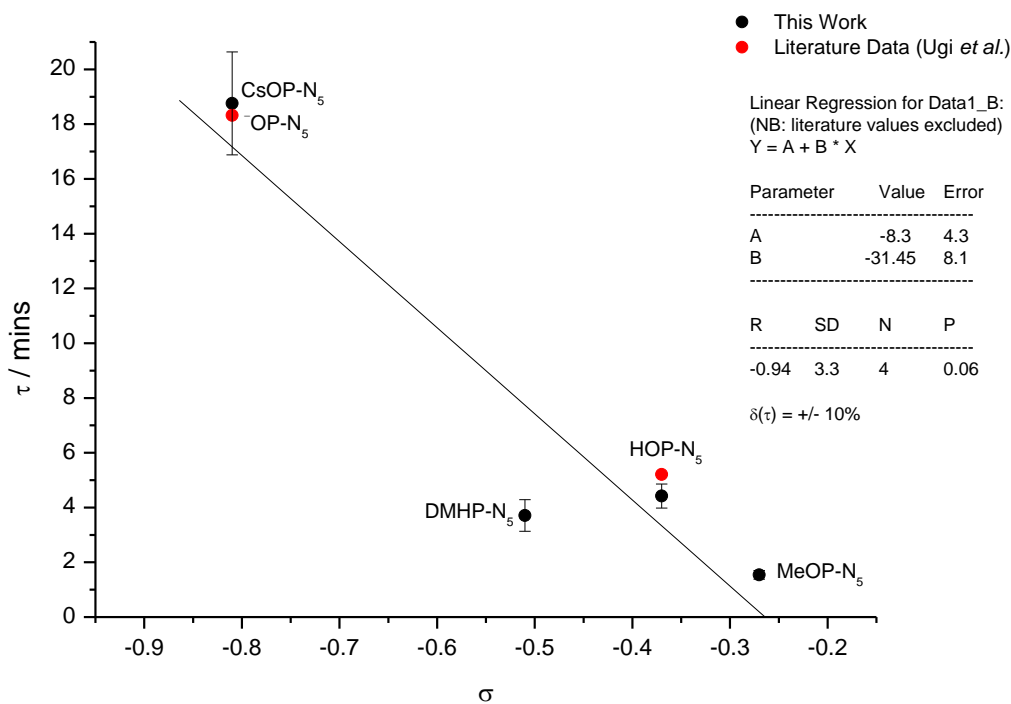
Figure 102. Correlation of Hammett constant (σ_p) versus lifetime (τ) for the arylpentazoles studied in this work and reported by Ugi *et al.*.[280,281] $R = 0.98$. The error bars for the y-axis (τ) are set at $\pm$ 10%. The literature values reported by Ugi *et al*. have been excluded from the trendline calculations.
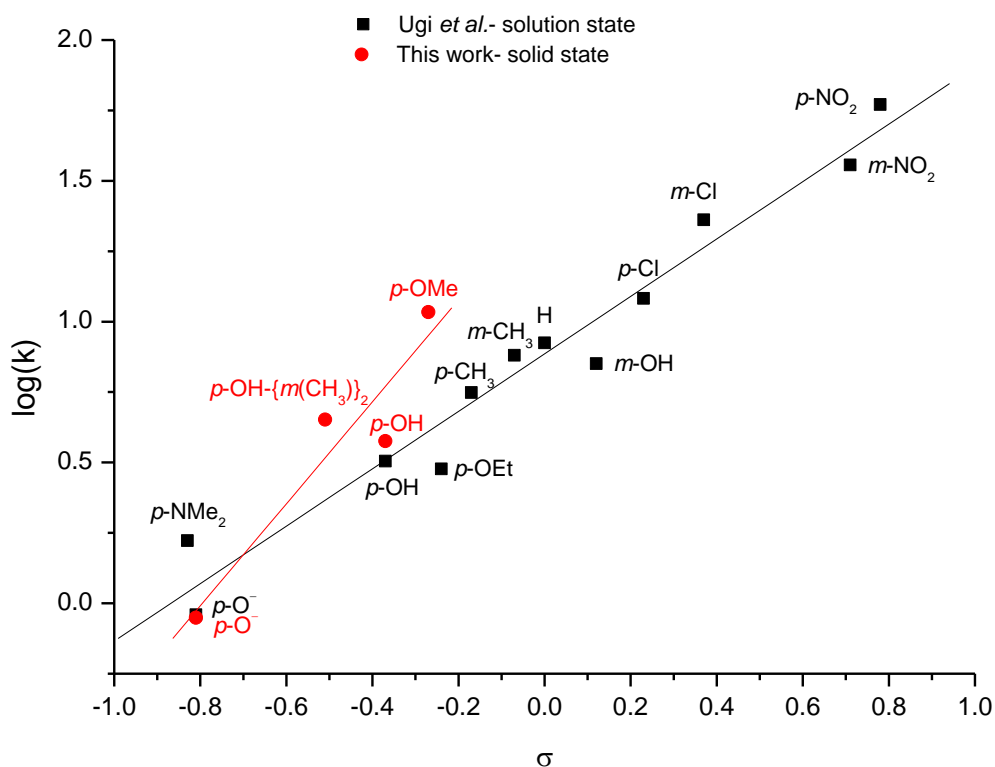
Figure 103. Comparison of Hammett constants (σ) for substituted arylpentazoles R-C$_6$H$_x$N$_5$ (x = 4 or 2) versus log of decomposition rate constants (k), for arylpentazoles studied in literature (black, ■, solution state, $R = 0.98$) and in this work (red, ●, solid state, $R = 0.95$). The label attached to each data point denotes the identity of R. k = 1/τ. NB: the σ_p value of Me$_2$N was found to be notably smaller than that used in Ugi *et al.*'s work.[280,281]

These results confirm that the amount of electron donation from substituents *para* or *meta* to the N_5 ring in arylpentazoles is critical. Although some lifetimes are predicted by Ugi, no arylpentazoles containing substituents with a σ_p value greater than that of phenylpentazole (i.e., 0) are known.[280] The findings from this work support the proposition of a tentative conditional limit for the long-term stability of arylpentazoles, that is dependent on the combined Hammett constants of the aromatic substituents (figure 104). The absence of stabilisation to the N_5 ring in unsubstituted phenylpentazole ($\sigma_p = 0$, the current upper limit) may account for the elevated energetic sensitivity versus the seemingly energetically stable compounds studied here.[270]

"For a substituted arylpentazole of general type A,
if $\sigma_p(R) + \sigma_m(Y) + \sigma_m(Z) > 0$,
the substituted arylpentazole is unlikely to be isolable"

(A)
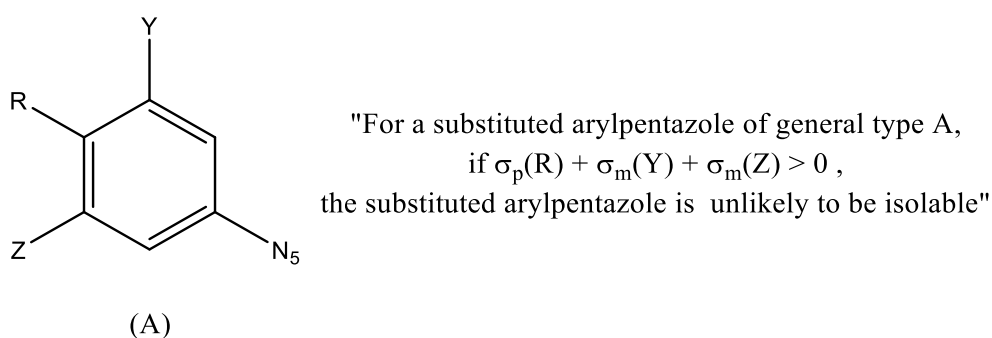
Figure 104. Proposed conditions for the hypothetical stability limit of substituted arylpentazoles. σ_p and σ_m denote the Hammett constants of *para* and *meta* substituents, respectively.

6.2.3. Crystallographic studies

Single crystals of HOP-N_5 and CsOP-N_5 were isolated from cold (-78 °C) solutions (THF and MeOH, respectively) and represent only the fourth and fifth arylpentazoles studied crystallographically. Although crystals of both compounds were stable under a liquid nitrogen cryostream (T = -173 °C), exposure to ambient temperatures during isolation and mounting induced thermal decomposition, crystal degradation and release of gas (figure 105). All attempts to crystallise MeOP-N_5 and DMHP-N_5 resulted in micro- or non-crystalline powders unsuitable for X-ray diffraction studies.
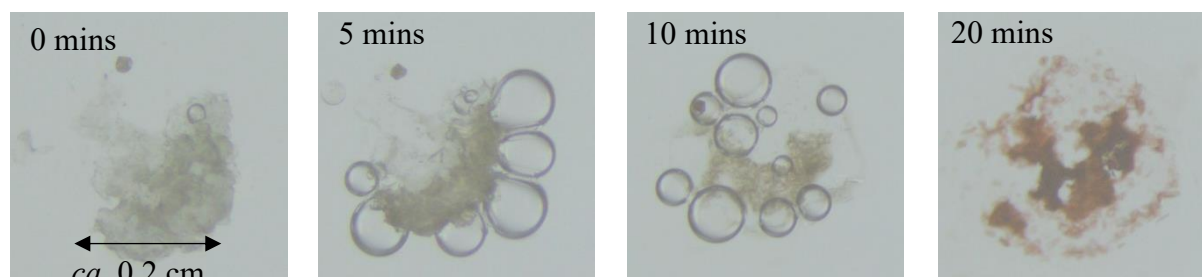
Figure 105. Microscope images of HOP-N_5 under paraffin oil at room temperature, forming HOP-N_3 and N_2. The red colour observed after 20 minutes is likely due to the presence of a highly conjugated photolysis product of HOP-N_3.

HOP-N_5 crystallises in space group $P2_1/c$ as colourless blocks (figure 106), which appear a pale grey/green colour in the bulk. The small average dihedral angle between the N_5 and phenyl ring ($-2.94°$) confirms the planarity of the compound. All five N−N bond lengths are nearly equidistant (d = 1.299−1.344 Å) and lie between the standard values for N−N single (d = 1.449 Å) and N=N double (1.252 Å) bonds expected for an aromatic ring system.[286,287] Whilst the average internal bond angles of the N_5 ring are equal to a five-membered ring (108°), the individual bond lengths vary and the N(5)−N(1)−N(2) sequence ($\angle$= 111.92°) displays the greatest deviation from the average internal angle of 108°.
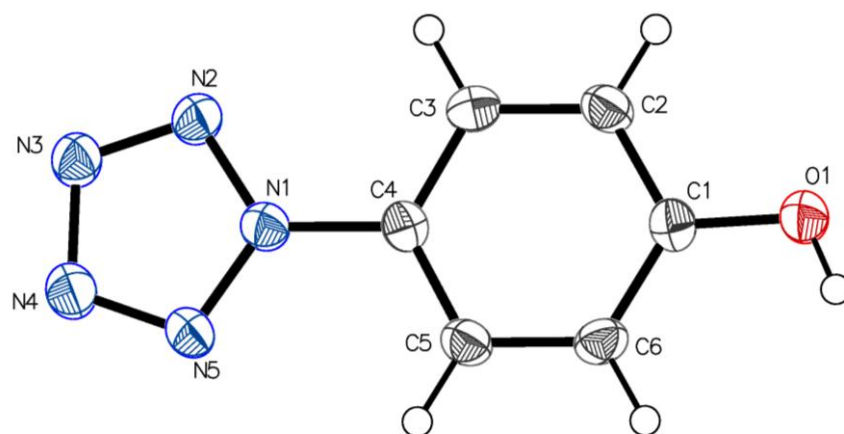
Figure 106. Crystal structure of HOP-N_5. Grey = C, blue = N, red = O, white = H. Selected bond distances (Å) and angles (°) : C(4)−N(1) 1.442(3), N(1)−N(2) 1.324(3), N(2)−N(3) 1.299(3), N(3)−N(4) 1.345(3), N(4)−N(5) 1.309(3), N(5)−N(1) 1.318(3) ; C(4)−N(1)−N(2) 123.5(2), N(1)−N(2)−N(3) 104.9(2), N(2)−N(3)−N(4) 109.58(19), N(3)−N(4)−N(5) 108.26(19), N(4)−N(5)−N(1) 105.35(19), N(5)−N(1)−N(2) 112.0(2), N(5)−N(1)−C(4) 124.6(2).

HOP-N_5 packs in offset layers where the N_5 and phenyl rings alternate positions in adjacent layers. π-stacking interactions exist between the C(3) and C(4) atoms of the phenyl groups in each layer with contact distances (d = 3.397 Å) consistent with standard π-stacking interaction distances (d = 3.30−3.80 Å) (figure 107).[288] The most notable feature is the presence of moderate-strength intermolecular hydrogen bonding interactions (d = 2.022 Å) between arylpentazole molecules in the same layer, which are not observed in any other arylpentazole studied crystallographically to date. These hydrogen bonds occur between hydroxyl protons and N(3) atoms within each layer, forming planar sheets (figure 108).[289] The H-bonding interactions are significantly shorter than those reported for DMAP-N_5 which involve weak interactions between the aromatic H atoms and the N_5 ring in separate layers of DMAP-N_5 (d = 3.090 Å).[279]
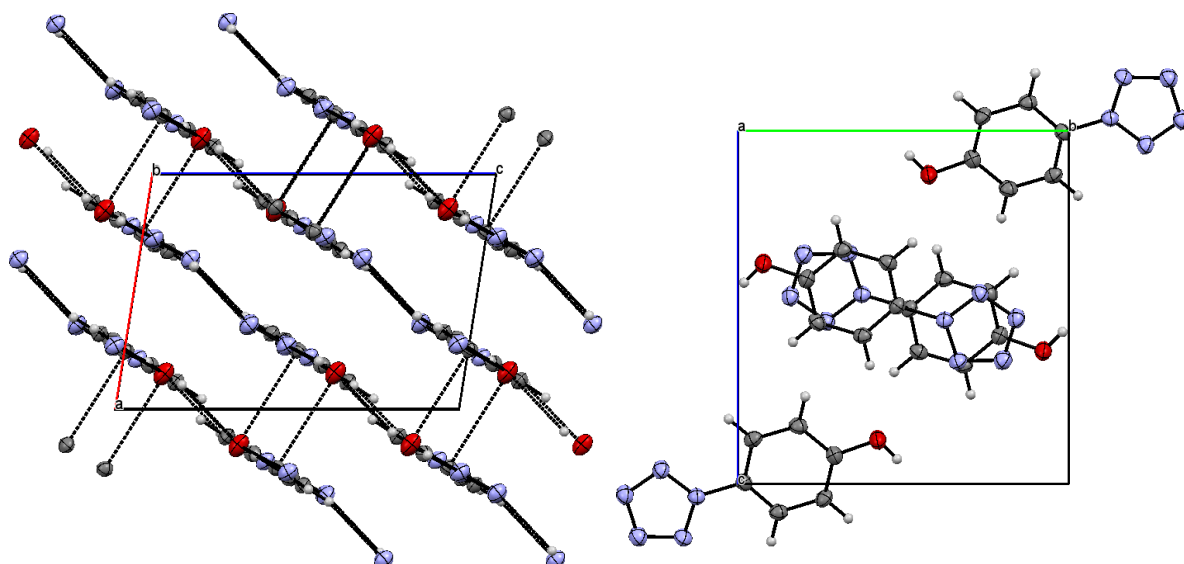
Figure 107. Short-contact and hydrogen bonding interactions (left) and offset stacking (right) of crystals of HOP-N$_5$ in the crystal lattice, viewed down the crystallographic *a* and *b* lattices respectively.
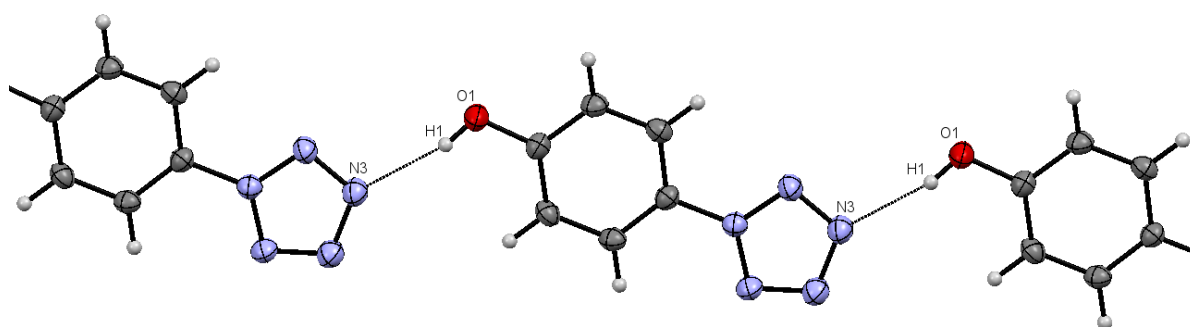
Figure 108. Hydrogen bonding interactions between OH and N$_5$ subunits in the crystal structure of HOP-N$_5$. Selected hydrogen bonding length (Å): N(3)···H(1) 2.022.

CsOP-N$_5$·3H$_2$O crystallised from cold (−78 °C) methanol solution as extremely small colourless shard-shaped crystals in space group *P*2$_1$/c (figure 109). The crystallisation of a trihydrate is likely to originate from the use of hydrated caesium hydroxide or the formation of water in the preparative procedure. CsOP−N$_5$ is only the second anionic arylpentazole to be studied crystallographically, and the first that displays coordination interactions with a metal cation. In contrast to the crystal structure of HOP-N$_5$, no hydrogen bonding is present between adjacent molecules of CsOP-N$_5$, although moderate strength hydrogen bonding is present between the phenolate group and two water molecules.[289] No additional short contacts involving the N$_5$ ring are present.
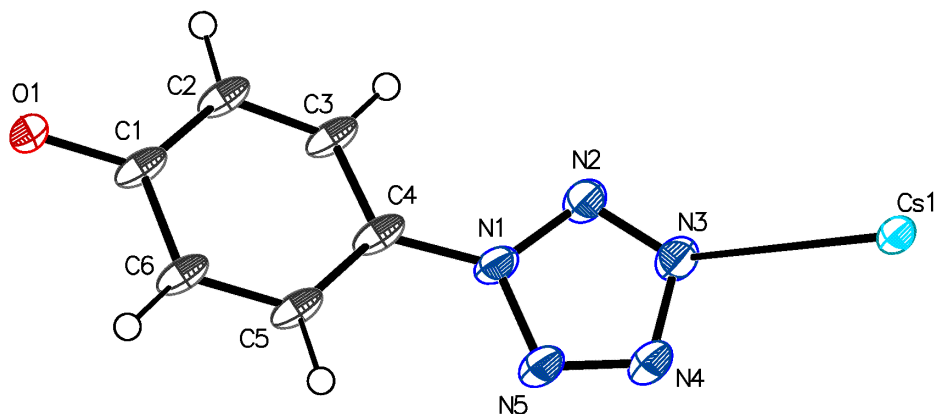
Figure 109. Crystal structure of CsOP-N$_5$ in CsOP-N$_5$·3H$_2$O. Solvent molecules omitted for clarity. Selected bond lengths (Å) and angles (°): C(4)−N(1) 1.39(2), N(1)−N(2) 1.36(2), N(2)−N(3) 1.25(2), N(3)−N(4) 1.37(2), N(4)−N(5) 1.26(2) ; N(1)−N(2)−N(3) 106.12 (16), N(2)−N(3)−N(4) 109.6 (16), N(3)−N(4)−N(5) 108.4 (15), N(4)−N(5)−N(1) 107.4 (16), N(5)−N(1)−C(4) 124.8 (16), N(2)−N(1)−C(4) 126.9 (16).

CsOP-N$_5$ packs in alternating bilayers, which are connected by interactions of the caesium cations with both the anion and solvate molecules (figure 110). In addition to the interaction with the hydroxide anion, Cs$^+$ also exhibits short contact interactions between three of the five atoms of the pentazolyl groups in the adjacent anions (N(3), N(4) and N(5)) (figure 111). The phenolate and pentazolyl groups are effectively coplanar. Although the bonding interaction between the N$_5$ and phenyl ring prevents the formation of additional short contact interactions between N(1) and Cs$^+$, it is unclear why N(2) does not participate in the same interactions as the near-symmetry equivalent N(5) atom. All of the interactions involving the Cs$^+$ cation are significantly shorter than the sum of the van der Waals' radii of the respective elements.[290] Both Cs−O and Cs−N bond lengths between the ⁻OP-N$_5$ anion and Cs$^+$ cation are comparable to those observed in caesium hydroxide and caesium hydrazinebistetrazolate anions, respectively.[31,291,292] The C−O ($d = 1.34(2)$ Å) and C−N ($d = 1.39(2)$ Å) bond lengths are most similar to standard single bonds ($d = 1.37$ and 1.46 Å, respectively).[168]
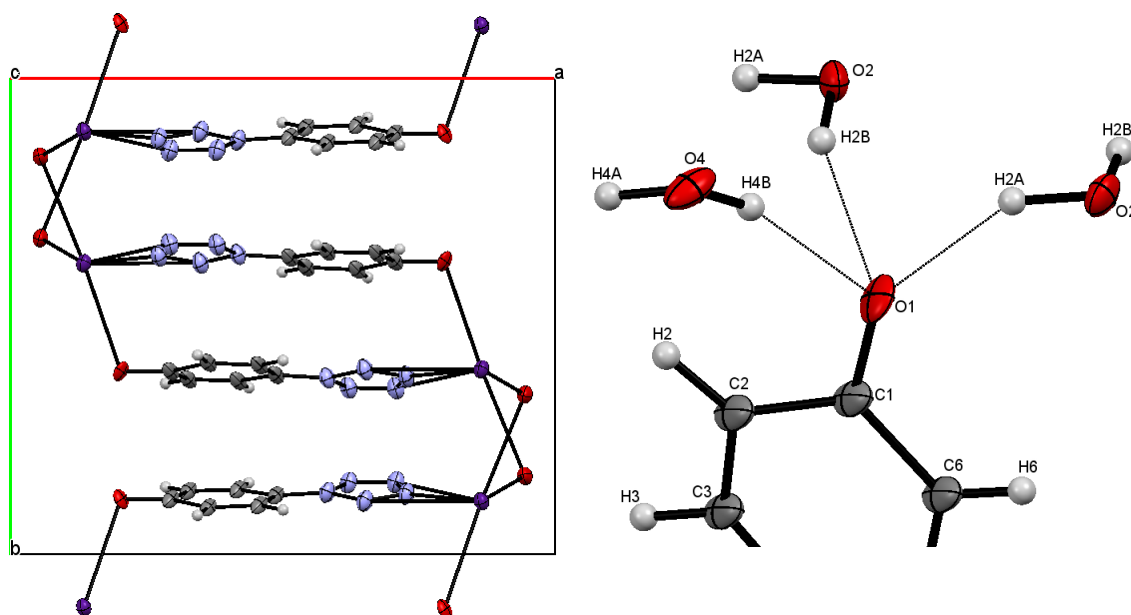
Figure 110. Left: Packing arrangement of CsOP-N$_5$ in the crystal lattice, viewed down the crystallographic *c* axis. Water molecules omitted for clarity. Right: Hydrogen bonding interactions observed between the pentazolylphenolate anion and solvate water molecules in the crystal structure of CsOP-N$_5$. Selected hydrogen bonding distances (Å): O(1)···H(2A) 1.751, O(1)···H(2B) 1.965, O(1)···H(4B) 1.781.
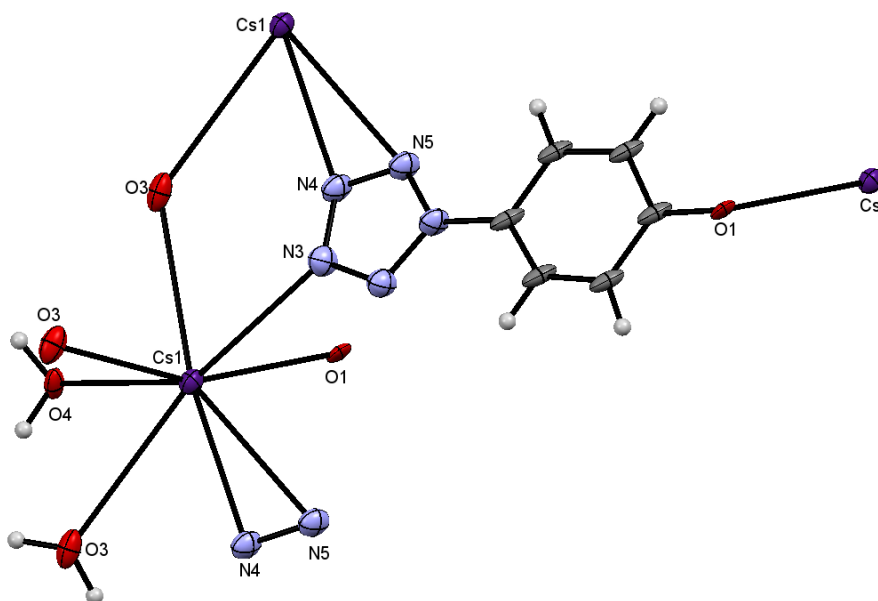
Figure 111. Coordination interactions between the Cs$^+$ cation, water solvate molecules and the pentazolylphenolate anion. Blue = N, grey = C, red = O, purple = Cs.

The influence of the substituted aryl groups results in a range of N−N bond lengths and angles in both HOP-N$_5$ and CsOP-N$_5$ that are comparable to other arylpentazoles studied crystallographically. Unsurprisingly, these values are much wider-ranging than those observed in the 'free' N$_5^-$ anion in NaN$_5$·3H$_2$O (table 53).[75] The range of N−N bond lengths in HOP-N$_5$ are greater than the other neutral arylpentazoles (figure 112). The anionic arylpentazoles

146

exhibit the largest range of bond distances by a significant margin owing to the enhanced inductive effect of the anionic versus neutral *para* substituents. The presence of the coordinating cation in CsOP-N$_5$ prevents the reliable comparison of bond lengths of the anionic pentazoles.

With the exception of DMAP-N$_5$, all arylpentazoles (studied previously and in this work) exhibit short contact interactions in the crystal lattice.[279,293] Only HOP-N$_5$ possesses hydrogen-bonding interactions directly between two arylpentazole molecules in the same layer and is only the second hydrogen-bonded arylpentazole known, after the weak interlayer interactions reported in DMAP-N$_5$.[279]

	Arylpentazole	d(N−N) / Å	Δ(N−N) / Å	d(C−N) / Å	$\angle$(N$_5$) [e] / °	T / K	Refs.
Neutral	HO−C$_6$H$_4$−N$_5$ (*HOP-N$_5$*)	1.299(3)−1.345(3)	0.046	1.442(3)	108.02	100	c
	Me$_2$N−C$_6$H$_5$−N$_5$ (*DMAP-N$_5$*)	1.3111(15)−1.344(2)	0.033	1.433	108.62	100	279
	C$_6$H$_5$−N$_5$ (*Ph-N$_5$*)[a]	1.307−1.338	0.031	1.437	108.02	173	293
Anionic	Cs[O−C$_6$H$_5$−N$_5$] (*CsOP-N$_5$*) [b]	1.25(2)−1.37(2)	0.120	1.39(2)	107.96	100	c
	[O$_3$S−C$_6$H$_5$−N$_5$] (*O$_3$SP-N$_5$*) [d]	1.211(15)−1.432(17)	0.221	1.434(14)	107.93	193	294
	NaN$_5$ [b]	1.310(3)−1.325(4)	0.015	−	108.05	170	75

Table 53. Comparison of crystallographic data of neutral arylpentazoles and NaN$_5$·3H$_2$O. [a] no error values given; [b] prepared as a trihydrate; [c] this work; [d] prepared as an 18-crown ether/THF solvate; [e] to 2dp.

Thermal decomposition of the N$_5$ ring is preceded by the elongation of two of the non-adjacent N−N bonds of the N$_5$ ring to eliminate N$_2$, alongside contraction of the remaining N−N bonds (scheme 73). Therefore, in theory, more thermally unstable arylpentazoles will possess a more accessible transition state to arylazide formation. The greater range of N−N bond lengths should permit crystallographically determined N−N bond lengths to be used as a measure of the relative thermal stability of each arylpentazole. In practice, however, the presence of a substituted phenyl ring disrupts the equivalency of the bond distances. This is demonstrated by the crystallographic analysis of CsOP-N$_5$ in this work, where the elongated β(N−N) bond distance in CsOP-N$_5$ appears to indicate that the compound is highly thermally unstable, but is

directly contradicted by lifetime measurements which show the [OP−N₅]⁻ anion to be the one of the most stable arylpentazoles known. Owing to the overlapping error margins of the crystallographically-determinned bond lengths, in addition to the lack of further crystallographic data for both arylpentazoles and arylazides, no further conclusions can be reliably drawn as to whether changes in bond lengths can be employed as an indicator of stability in these compounds.
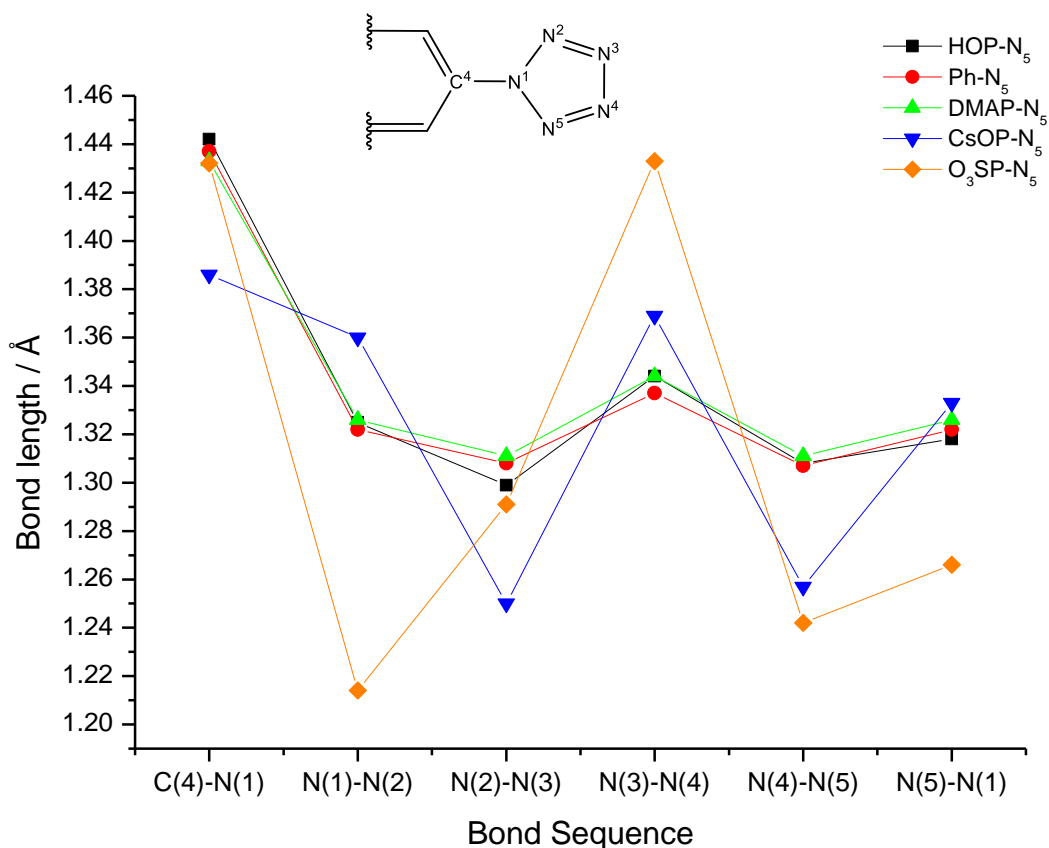
Figure 112. N−N and C−N bond distances of each bond sequence determined crystallographically for HOP−N₅ (●), Ph−N₅ (●), DMAP−N₅ (▲), CsOP−N₅ (▼) and O₃SP−N₅ (♦).
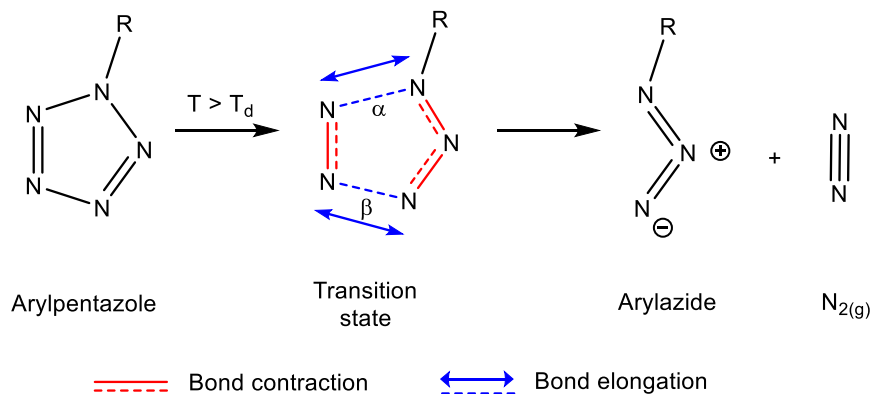
Scheme 73. Process of thermal decomposition of an arylpentazole to arylazide. R = aryl.

148

6.3. Arylpentazoles as precursors to the N_5^- anion: electrochemical reduction of arylpentazoles

Preparation of the N_5^- anion by electrochemical cleavage of the C−N bond has been reported in both electrospray ionisation (ESI) and laser-desorption ionisation (LDI) mass spectrometric studies of pentazolylphenolate ($^-$OP−N_5) and dimethylaminophenylpentazole (DMAP-N_5).[295,296] The identity and stability of the fragment can be confirmed by ^{15}N isotopic labelling and time-of-flight (TOF) mass spectroscopic measurements, respectively. These reports provide evidence that electrochemical reduction of arylpentazoles facilitates the release of N_5^-. Larger-scale electrochemical cleavage reactions have also previously been investigated. Spectroelectrochemical studies of solutions of DMAP-N_5 showed an irreversible reductive wave which corresponded to the release of N_5^-, but further analysis was hindered by passivation of the cell electrodes upon reduction. Accompanying oxidative waves corresponded to the formation of [DMAP-N_5]$^+$ and [DMAP-N_3]$^+$.[285] A further study indicates that similar behaviour occurs in the reduction of MeOP-N_5, although the absence of spectroscopic analysis precludes confirmation of this theory.[297]

Despite this evidence suggesting N_5^- can be generated from electrochemical reduction of arylpentazoles, further spectroscopic evidence is limited. For this reason, DMHP-N_5 and MeOP-N_5 were investigated in this work in order to determine if the N_5^- anion could be generated in bulk through electrochemical reduction methods (scheme 74). The electrochemical behaviour of DMHP-N_5 is of particular interest, as its role in syntheses of N_5^- salts already confirms that N_5^- elimination from the compound is both feasible and favourable.
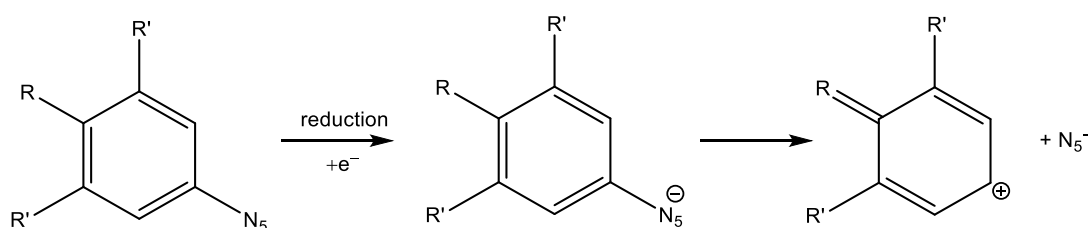
Scheme 74. Proposed formation of N_5^- from electrochemical reduction of arylpentazoles. R = OH, MeO, R$^{'}$ = H, Me.

Preliminary cyclic voltammetry studies were performed on cold (−25 to −40 °C) solutions of arylpentazole in THF, CH$_2$Cl$_2$ or butyronitrile (PrCN) with positive sweeps (i.e., to higher applied potential) first, unless solely reductive process were investigated. Two waves, attributed to the oxidation and reduction of the arylpentazole species, were observed in the

cyclic voltammogram of DMHP-N$_5$. The disappearance of the reversible reductive wave at −1.59 V upon analysis at room temperature confirmed the wave arises solely from DMHP-N$_5$ (figure 113, left). A reversible oxidative wave at ca. 0.75 V (figure 113, right) from the oxidation of the hydroxyl substituent on the aromatic ring, obscured any oxidative waves originating from the pentazole ring (scheme 75).
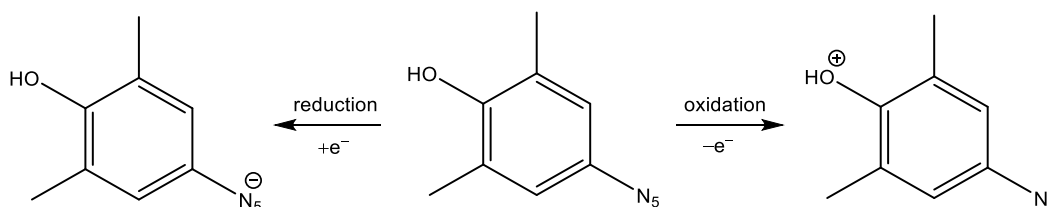
Scheme 75. Oxidation and reduction reactions observed in cyclic voltammetry studies of DMHP-N$_5$.
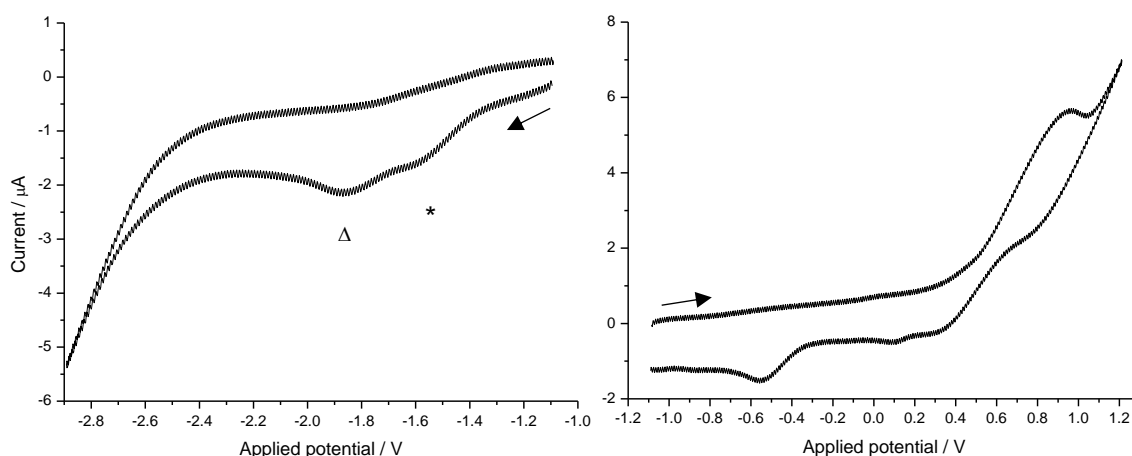
Figure 113. Cyclic voltammogram of full range (left) and isolated irreversible reductive wave (right, *, E_{cell} = −1.59 V) of DMHP-N$_5$ in THF at −45 °C, referenced to Fc/Fc$^+$. The reductive wave at −1.89 V (Δ) is attributed to the reduction of dissolved oxygen in the analyte solution.

The oxidation of the hydroxyl substituent rendered DMHP-N$_5$ and DMHP-N$_3$ unsuitable for spectroelectrochemical studies and neither compound was investigated further. However, the use of DMHP-N$_5$ to obtain gram-scale quantities of pentazolate salts, coupled with the observation of an irreversible reductive wave at a similar potential to DMAP-N$_5$, provides tentative evidence to suggest that the reductive wave observed in both DMHP-N$_5$ (this study) and DMAP-N$_5$ (previous work) may correspond to the release of N$_5^-$.[75,285] Further studies are required to prove this theory.

MeOP-N$_5$ contains no additional redox-active aromatic substituents in the scan region. Although the electrochemical behaviour of MeOP-N$_5$ has been investigated previously, beyond the presence of a reversible reductive wave in unknown conditions, the conclusions are unclear

and characterisation information is limited.[297] Therefore, the electrochemistry of MeOP-N$_5$ was investigated to examine the electrochemical behaviour of the N$_5$ ring (figure 114).
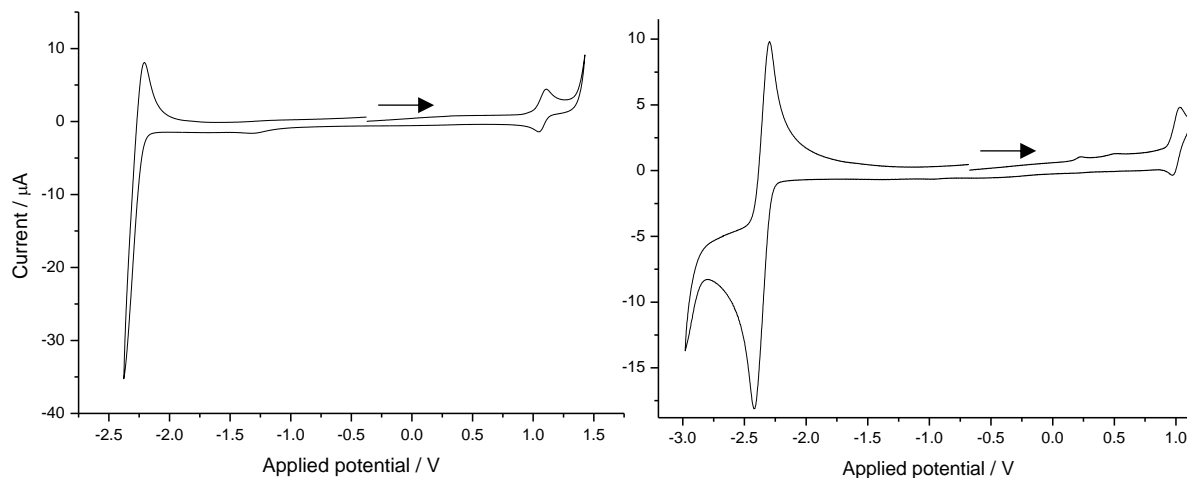
Figure 114. Cyclic voltammogram of MeOP-N$_5$ in CH$_2$Cl$_2$ (left) and PrCN (right) at −43 °C.

The observation of a reversible oxidative wave at 1.09 V was identical to that observed for the oxidation of MeOP-N$_3$ to [MeOP-N$_3$]$^+$ under the same conditions. No other oxidative processes were observed. The proximity of a reductive wave at −2.20 V to the lower scan limits in CH$_2$Cl$_2$ prevented determination of the reversibility in this solvent, but the disappearance of this wave at room temperature (producing a voltammogram identical to MeOP-N$_3$) confirmed that the wave originated from the N$_5$ ring. Replication in PrCN allowed extension of the scan limits and confirmed the reversibility of the reductive wave of MeOP-N$_5$ (figure 115). At room temperature, the wave was replaced by an irreversible reductive wave consistent with MeOP-N$_3$ (E_{cell} = −2.55 V). The preservation of the oxidative wave at 1.09 V at low and ambient temperatures identified contamination of MeOP-N$_5$ by MeOP-N$_3$ (figure 116). This was not unexpected, owing to the inevitable formation of both during arylpentazole syntheses.
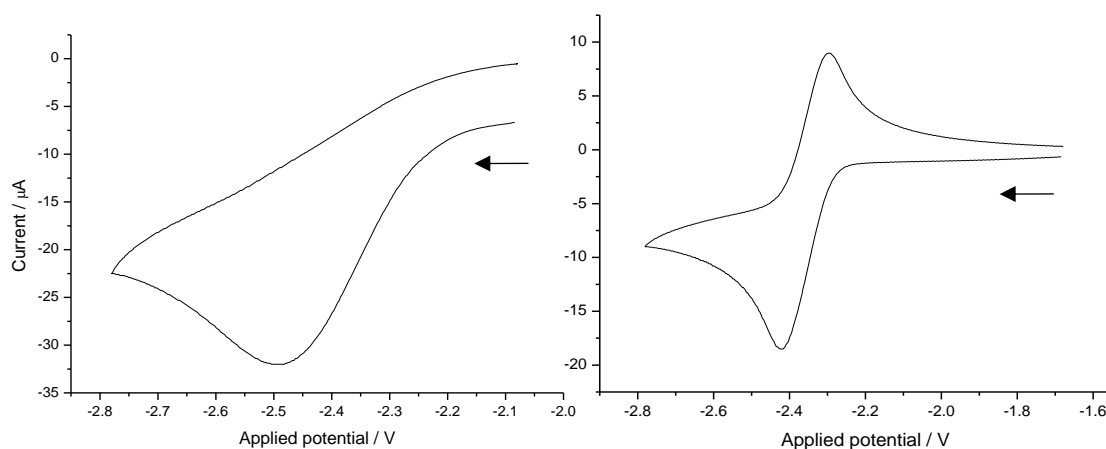
Figure 115. Isolation of reductive irreversible wave of MeOP-N$_3$ (left, E_{cell} = −2.55 V) and reversible wave of MeOP-N$_5$ (right, E_{cell} = −2.34 V) in PrCN.

151
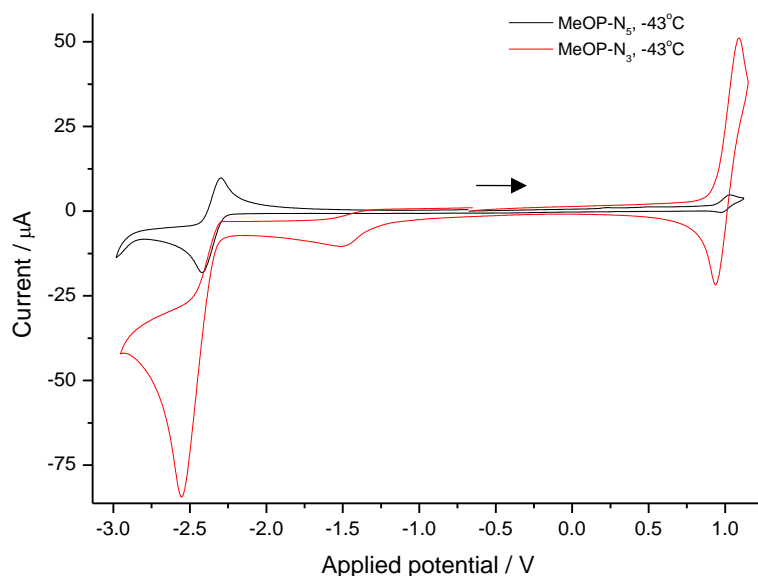
Figure 116. Overlay of cyclic voltammograms of MeOP-N$_5$ (black line, −) and MeOP-N$_3$ (red line, −) in PrCN at −43 °C.

	Compound	E_{red} / V	Comments	E_{ox}/ V	Comments	Solvent
Ar−N$_5$	DMHP-N$_5$	−1.59	Irreversible	0.63	Irreversible	THF
	DMAP-N$_5$	−2.68	Irreversible	0.67	Irreversible	CH$_2$Cl$_2$
	MeOP-N$_5$	−2.20 / −2.34	Reversible	−	−	CH$_2$Cl$_2$ / PrCN
Ar−N$_3$	DMHP-N$_3$	−2.19	Irreversible	−0.12	Reversible	THF
	DMAP-N$_3$	−	−	0.32	Reversible	CH$_2$Cl$_2$
	MeOP-N$_3$	−2.55[a]	Irreversible	1.09[b]	Reversible	CH$_2$Cl$_2$ / PrCN

Table 54. Comparison of reductive (E_{red}) and oxidative (E_{ox}) potentials of three arylpentazoles and the corresponding arylazides.[285] [a] recorded in PrCN. [b] recorded in CH$_2$Cl$_2$. Data for DMAP-N$_5$ and DMAP-N$_3$ obtained from reference [285].

Although both DMHP-N$_5$ and MeOP-N$_5$ were observed to undergo reductive electrochemical processes in solution, the identity of the products were unclear. Low-temperature Optically Transparent Thin-Layer Electrochemistry (OTTLE) spectroelectrochemistry studies were performed on solutions of MeOP-N$_3$ to identify the products formed from oxidation. The spectra of MeOP-N$_3$ in CH$_2$Cl$_2$ showed a decrease in the parent azide bands at 2108 and 2136 cm^{-1} with increasing oxidative potential, accompanied by the concurrent formation of two product bands at 2163 and 2086 cm^{-1} (figure 117). The same behaviour was observed in PrCN (figure 118). In the latter, three bands (ν_{as}(N$_3$) = 2139, 2107 and 2116 cm^{-1}) displayed concurrent changes in absorbance intensity and were identified as originating from the parent azide, whilst a further two bands with a larger rate of change (ν_{as}(N$_3$) = 2085 and 2170 cm^{-1})

152

were attributed to the product azide (figure 119). Scaled subtraction of the parent and product azide bands in both solvents confirmed that the oxidation of MeOP-N_3 results in the formation of two new azide bands of an oxidised product, believed to be [MeOP-N_3]$^+$ (figure 120). The formation of this oxidised product resulted in electrode passivation and affected the absorbance intensities of the final spectra.
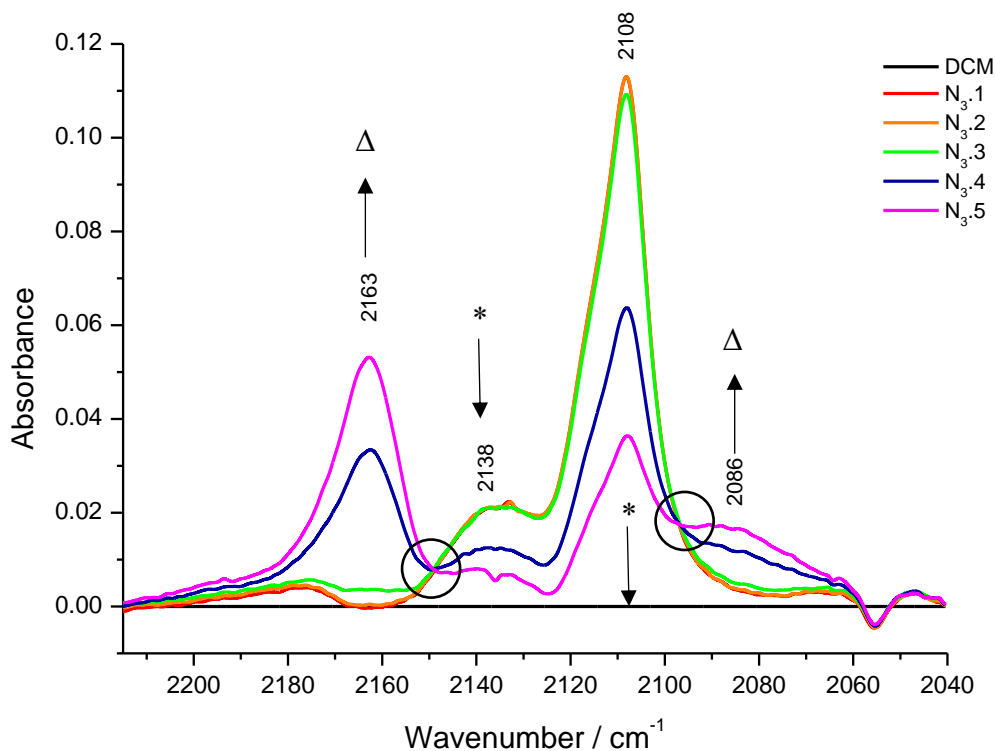
Figure 117. IR spectral series between 2220−2040 cm^{-1} of MeOP-N_3 at 1.80 V in CH$_2$Cl$_2$ at −40 °C, showing the decomposition of the parent azide bands (*), concurrent increase in azide bands of the oxidised product (Δ) and isosbestic points at 2148 cm^{-1} and 2095 cm^{-1} (O). All spectra solvent subtracted, 10-point adjacent averaged and baseline corrected.
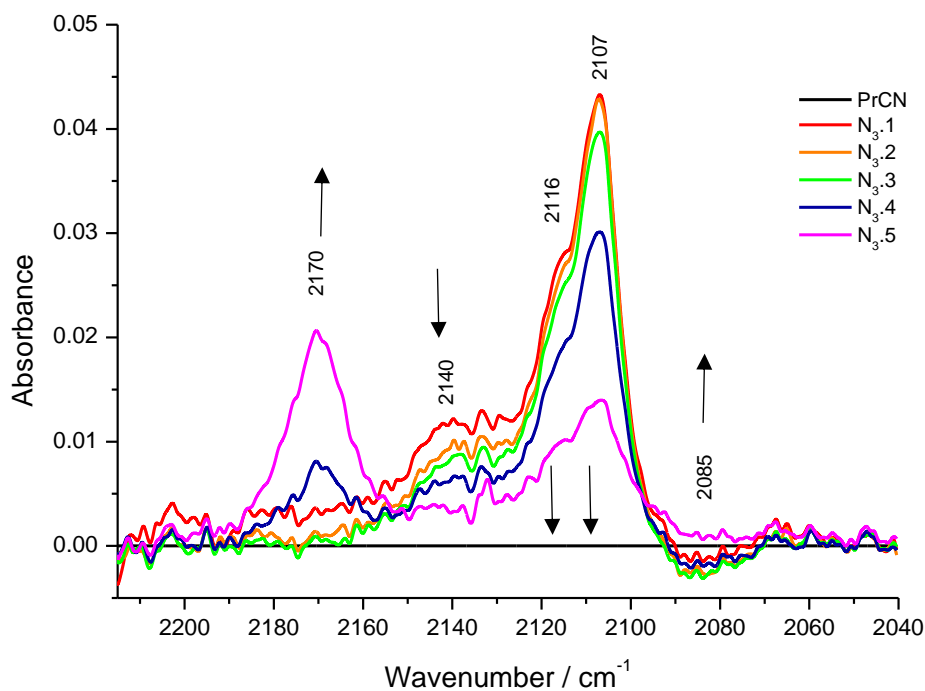
Figure 118. IR spectral series between 2220−2040 cm^{-1} of MeOP-N$_3$ at 1.80 V in PrCN at −50 °C, showing the decomposition of the parent azide bands (*) and concurrent increase in azide bands of the oxidised product (Δ) with increasing oxidative potential. All spectra solvent subtracted, 10-point adjacent averaged and baseline corrected.
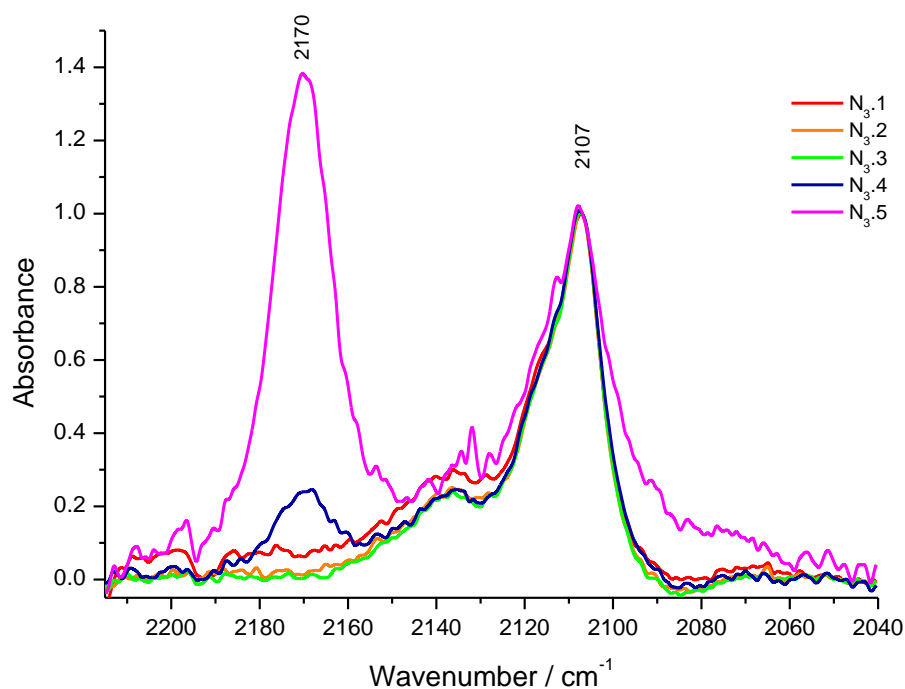
Figure 119. Normalised IR spectral series between 2220−2040 cm^{-1} of MeOP-N$_3$ with increasing oxidative potential at 1.80 V in PrCN at −50 °C. All spectra solvent subtracted, 10-point adjacent averaged and baseline corrected.
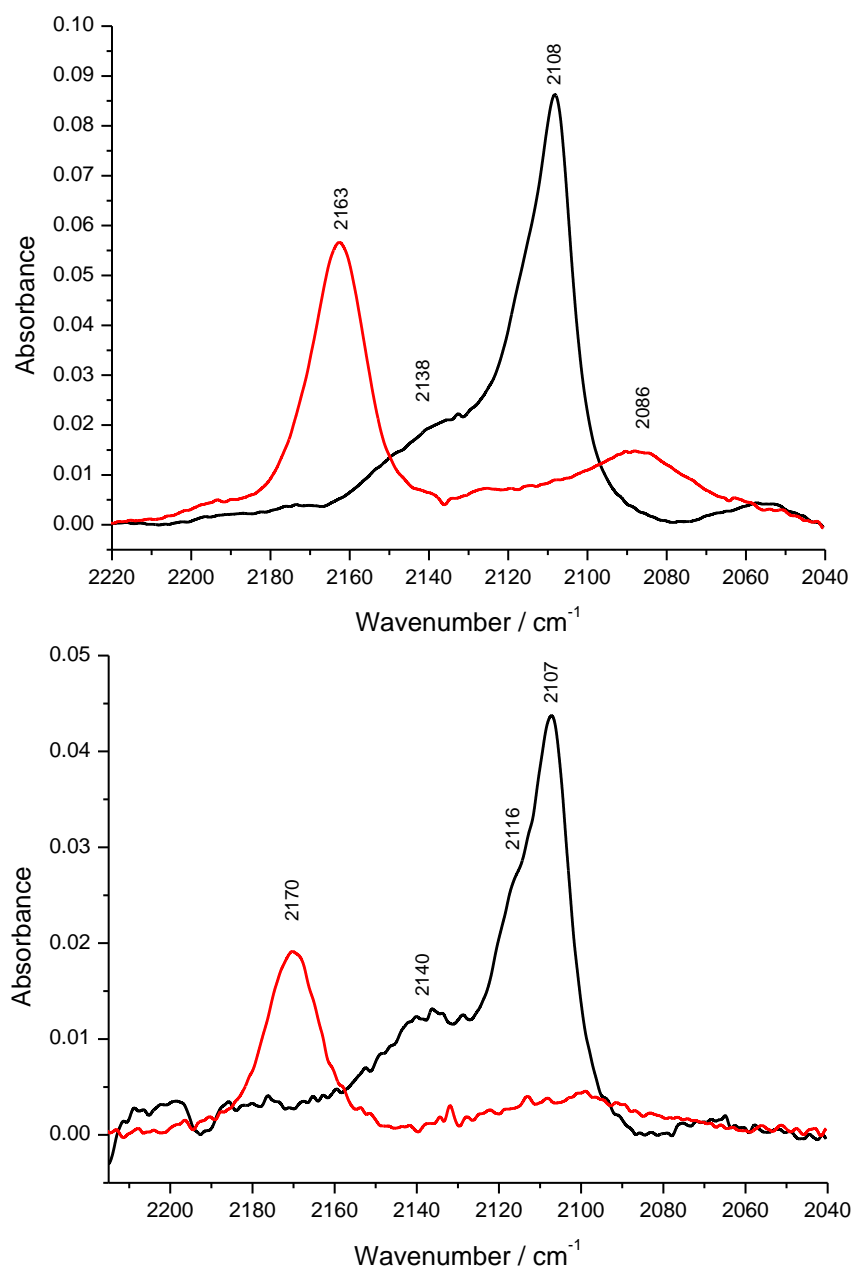
Figure 120. Scaled subtracted spectra of MeOP-N$_3$ in CH$_2$Cl$_2$ (top) and PrCN (bottom) at 1.80 V, showing the decrease in parent azide bands (black line, —) and increase in product azide bands (red line, —).[298]

The oxidative behaviour of MeOP-N$_3$ is consistent with that of DMAP-N$_3$. Previous studies of the latter showed that an increase in oxidation potential resulted in the formation of the oxidised arylpentazole [DMAP-N$_3$]$^+$ and the generation of an unknown, further oxidised azido compound as a secondary reaction product. The fewer number of azide bands observed in this study (MeOP-N$_3$), versus those for DMAP-N$_3$ reported previously (table 55), suggests that the oxidation of MeOP-N$_3$ is both non-destructive and selective towards the formation of [MeOP-N$_3$]$^+$. Further reaction and formation of secondary products, such as that observed in the study

of DMAP-N$_3$, may be precluded in this work by electrode passivation or by an enhanced stability of the first oxidation product versus [DMAP-N$_3$]$^+$.

Compound	$v_{as}(N_3)$ / cm^{-1}	T / K
MeOP-N$_3$	2108, 2117, 2138	233
[MeOP-N$_3$]$^+$	2163, 2086	233
DMAP-N$_3$	2128, 2096, 2017	226
[DMAP-N$_3$]$^{+\ a}$	2146, 2124, 2106	226
[DMAP-N$_3$]$^{+\ b}$	2140, 2128, 2115	273

Table 55. Asymmetric azide bands of MeOP-N$_3$, DMAP-N$_3$ and related oxidation products in CH$_2$Cl$_2$ at 1.80V. ^{a} = first oxidation product; ^{b} = second oxidation product. Data for DMAP-N$_3$ obtained from reference [285].

6.4. Conclusions and Future Work

The bonding, reactivity and decomposition rate of four arylpentazoles have been studied, with the thermal decomposition rates of two (MeOP-N$_5$ and DMHP-N$_5$) determined for the first time. The decomposition rates of all four compounds studied are in good agreement with those values predicted or reported in literature, despite differences in analysis state, and support the notion of a theoretical stability limit for isolable arylpentazoles (where σ_p <0). Both HOP-N$_5$ and CsOP-N$_5$·3H$_2$O have been studied crystallographically for the first time and represent only the fourth and second crystallographic studies of neutral and anionic arylpentazoles, respectively. The presence of intraplanar hydrogen-bonding (HOP-N$_5$) and metal coordination (CsOP-N$_5$·3H$_2$O) interactions in these structures have not been observed in any other arylpentazoles to date and may afford additional stability to the N$_5$ ring. However, the presence of external interactions between adjacent arylpentazole or solvent molecules precluded the analysis of N−N or C−N bond lengths as an indicator of the degree of thermal stability in each species.

Although a reversible reductive process was observed in cyclic voltammetry studies of DMHP-N$_5$, the presence of a redox-active hydroxyl group meant that no conclusion could be drawn regarding this process resulted in elimination of N$_5^-$. Tentative evidence suggests that the same reductive process occurred in previous studies of DMAP-N$_5$ and that this may correspond to the release of N$_5^-$. Cyclic voltammetry studies of MeOP-N$_5$ suggest that its reduction may result in *reversible* release of N$_5^-$, in contrast to the *irreversible* reductive behaviour observed

in the previous studies of DMAP-N$_5$.[285] OTTLE spectroelectrochemical studies of the oxidation of MeOP-N$_3$ confirmed that [MeOP-N$_3$]$^+$ was formed, similarly to the oxidation of DMAP-N$_3$ studied previously.[285] However, unlike DMAP-N$_3$ and for reasons unclear, the formation of [MeOP-N$_3$]$^+$ is non-destructive and appears more stable than [DMAP-N$_3$]$^+$ (scheme 76).[285] No information from the oxidative OTTLE studies of MeOP-N$_3$ can be extrapolated to the electrochemical reduction behaviour of MeOP-N$_5$ and further studies on this behaviour are of critical interest to determine if the latter species is a feasible precursor for the electrochemical synthesis of N$_5^-$. OTTLE spectroelectrochemical measurements of MeOP-N$_5$ could also aid in the identification of the reduction mechanism and reaction products, which may include MeOP-N$_3$, N$_5^-$, or an alternative reduction product (scheme 77).

$$MeOP\text{-}N_3 \longrightarrow [MeOP\text{-}N_3]^+ + e^-$$

$$\nu_{as}(N_3) = 2163,\ 2086\ \text{cm}^{-1}$$

$$DMAP\text{-}N_3 \longrightarrow [DMAP\text{-}N_3]^+ + e^- \longrightarrow [R^-N_3]^+$$

$$\nu_{as}(N_3) = 2146,\ 2124,\ 2106\ \text{cm}^{-1} \qquad \nu_{as}(N_3) = 2140,\ 2128,\ 2115\ \text{cm}^{-1}$$
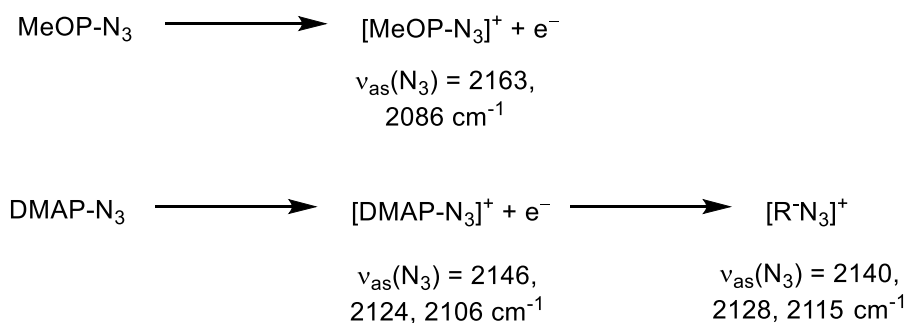
Scheme 76. Oxidation products and $\nu_{as}(N_3)$ bands of MeOP-N$_3$ (top) and DMAP-N$_3$ (bottom), with $\nu_{as}(N_3)$ bands for each in CH$_2$Cl$_2$.

$$MeOP\text{-}N_5 \xrightarrow{e^-}
\begin{cases}
[MeOP]^+ + N_5^- \\
[MeOP\text{-}N_2]^+ + N_3^- \\
[MeOP]^+ + N_3^- + N_2
\end{cases}$$
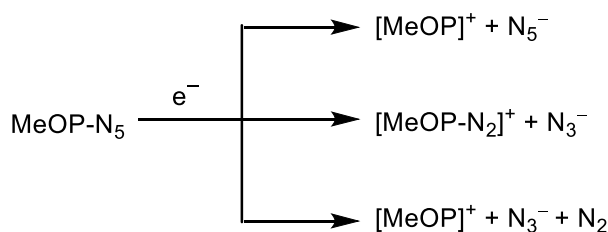
Scheme 77. Reduction pathways of MeOP-N$_5$ proposed for OTTLE studies.

Chapter 7. Routes towards the N_5^- anion

7.1. Introduction

The pentazolate anion (N_5^-) has been an attractive target ever since the syntheses of the first arylpentazoles. Efforts to prepare N_5^- have focused on three main synthetic strategies (scheme 78), which afford varying degrees of scale and purity:

High-pressure synthesis involving N_3^- and N_2

$$N_3^- + N_2 \xrightarrow{\text{P > ca. 60 GPa}} N_5^-$$

Electrochemical reduction of arylpentazoles

$$RN_5 \xrightarrow{e^-} N_5^- + R^+$$

Chemical cleavage of arylpentazoles

$$RN_5 \xrightarrow{[CA]} N_5^- + R'$$

[CA] = cleaving agent
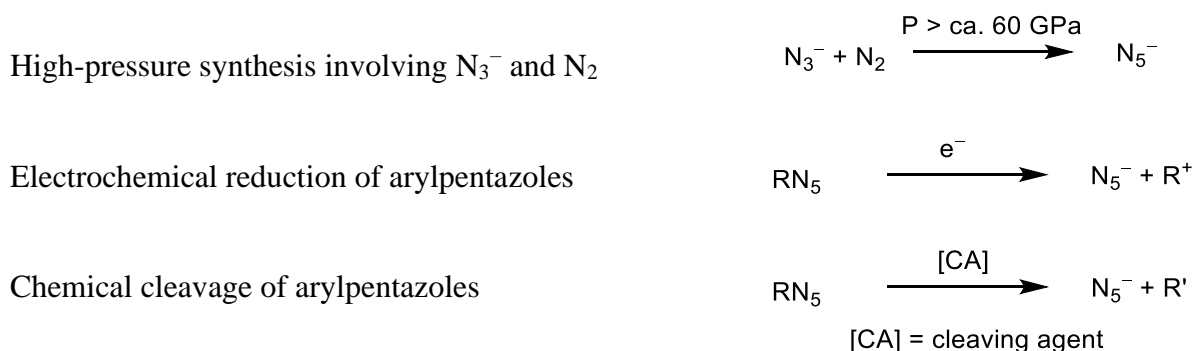
Scheme 78. Synthetic routes towards the N_5^- anion.

The formation of pentazolate salts through high pressure cyclisation reactions is an emerging field in the last few years.[276] Caesium pentazolate, CsN_5, was the first pentazolate salt prepared from CsN_3 and N_2 at high pressure. At ambient conditions, the compound loses crystallinity but is otherwise stable.[276,277] A high pressure study of NaN_3 some 12 years prior details the formation of an unidentified compound above 50 GPa, which is assigned to the previously-observed polymeric nitrogen.[69,299] A later study instead proposed the compound as NaN_5, but did not provide complete confirmation.[300] At similar pressures or higher (>60 GPa), several stable pentazolate salts such as NH_4N_5 and KN_5 are predicted, as well as HN_5.[301,302] However, the stability of these compounds under ambient conditions is not known.[301] This work in this study focused on the preparation of N_5^- from arylpentazoles and therefore this synthetic strategy was not investigated.

The other two strategies are performed at ambient pressure and utilise arylpentazoles as N_5^- precursors. Careful choices of reagent and synthetic conditions are essential to facilitate selective cleavage of the C−N bond and preserve the N_5 ring.

7.1.1. Chemical reduction of arylpentazoles and the first preparation of N_5^- in bulk

The first attempts of arylpentazole reduction were reported only three years after the pioneering syntheses of arylpentazoles. The reaction of phenylpentazole with sodium or lithium metal in liquid ammonia did not result in N_5^- but instead formed aniline and N_2 due to the over-reduction and destruction of the N_5 ring. Ozonolytic reduction of DMAP-N_5 resulted in the decomposition of the phenyl ring and N_5^- was not obtained.[303]

It was not until after the first mass spectrometric detection of N_5^- that chemical strategies to prepare the anion were outlined. The reduction of MeOP-N_5 was attempted by Butler *et al.* using a mild oxidising agent (ceric ammonium nitrate, $(NH_4)_2[Ce(NO_3)_6]$ or CAN) in order to preserve the N_5 ring and prevent the over-reduction observed previously upon the use of alkali metals or ozone.[274,303] Reduction was performed in the presence of $Zn(NO_3)_2$ to complex any N_5^- formed as $Zn(N_5)_x$. ^{15}N NMR spectroscopy following reduction of isotopically labelled arylpentazoles showed a signal which was assigned to complexed N_5^- in $Zn(N_5)Cl$. The similarities between the chemical shifts observed experimentally and the value of $Zn(N_5)_2$ predicted theoretically ($\delta = -17.5$ vs -16.6 ppm, respectively) supported this assignment.[304] Raising the temperature of the solution resulted in the formation of two other ^{15}N resonances, attributed to the thermal decomposition of N_5^- into N_3^-, followed by the total disappearance of both signals at higher temperatures. The formation of a signal inconsistent with arylpentazole but similar to that expected to $Zn(N_5)_x$, alongside the accompanied formation of a benzoquinone byproduct, lead the authors to propose this methodology as the first chemical synthesis of N_5^-.[304] A replication study by a different research group challenged this finding, claiming the three signals were from NO_3^-, N_3^- and MeOP-N_3, instead of arising from the generation of N_5^- (scheme 79).[305] Re-evaluation of the debated claim by the original authors maintained that the reduction of MeOP-N_5 *did* result in C−N bond cleavage, but concluded N_5^- was *not* detected and was too unstable to be observed under the experimental conditions used.[275]
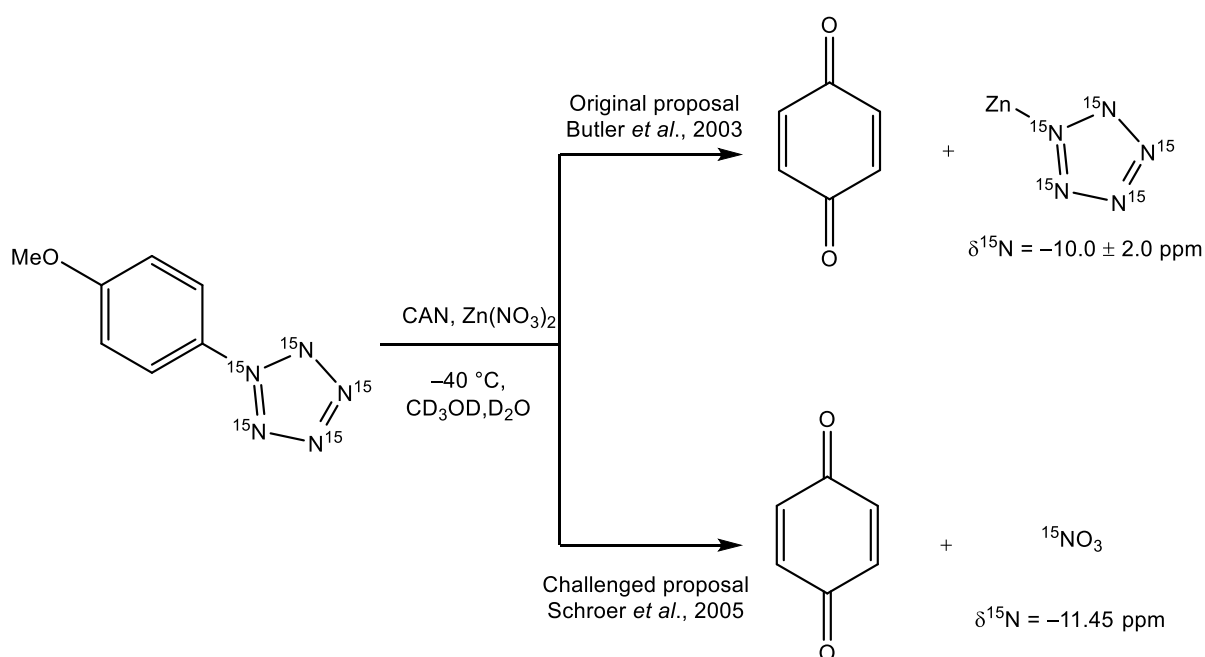
Scheme 79. Proposed reduction of MeOP-N$_5$ with CAN as proposed (top) and later challenged (bottom).[274,305]

The alkali metal-induced reduction of phenylpentazole was revisited in 2009, nearly 50 years after the original report by Ugi and Huisgen.[303,306] Whilst treatment of phenylpentazole with lithium or sodium metal in liquid ammonia lead to decomposition of the N$_5$ ring, reduction of the same compound by sodium or potassium in THF solution for ca. 10 days lead to the detection of a signal at m/z = 70 in the mass spectrum of the reaction solution.[306] Replication of the study with isotopically-labelled phenylpentazole lead to the observation of the corresponding isotopic signals concurrent with singly- or doubly-labelled N$_5^-$. The authors proposed the elimination of N$_5^-$ occurred by formation of a radical N$_5^{·-}$ anion as a thermally unstable intermediate which subsequently decomposed at room temperature to form N$_5^-$ (scheme 80). The anion appeared indefinitely stable at low temperature but decomposed after several minutes at room temperature. Despite this, extension of the strategy towards DMAP-N$_5$ did not form N$_5^-$. The authors later clarified that the use of *passivated* alkali metal is critical for the formation of N$_5^-$ due to its role as a weaker reducing agent that preserves the N$_5$ ring. This accounts for the absence of over-reduction in the first studies which contrasted the observations of the reduction attempts reported some 55 years prior.[303,306,307]
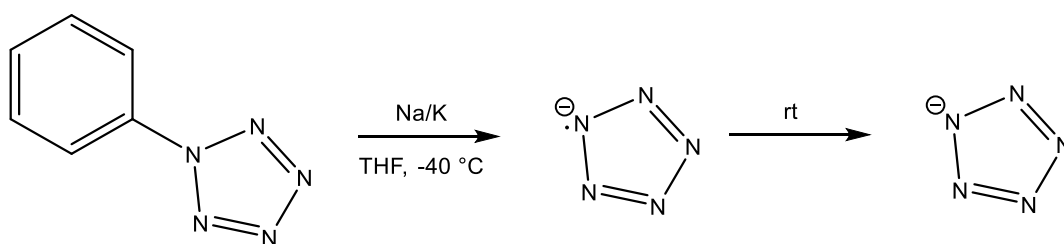
Scheme 80. Reduction of phenylpentazole to form N_5^- via a thermally-unstable $N_5^{\cdot-}$ radical anion intermediate.[306]

Despite evidence supporting the preparation and stability of N_5^- at low temperatures, a preparative procedure to prepare pentazolate salts on larger scales remained elusive. Very recently, the first preparation of the N_5^- anion on gram-scales was reported. The pentazolate salts (initially $(NH_4)_4(H_3O)_3(N_5)_6Cl$ and later $NaN_5 \cdot 3H_2O$) were formed through C−N bond cleavage of DMHP-N_5 by meta-chloroperbenzoic acid (*m*CPBA) and ferrous glycinate $(Fe(gly)_2)$ (scheme 81).[75,76] The formation of N_5^- is believed to proceed by the oxidative cleavage of the C−N bond in the dimethylpentazolylphenolate anion to release N_5^-. $Fe(gly)_2$ is claimed to stabilise the pentazolate anion, but it is unclear if the radical anion pathway proposed in earlier reductive studies of arylpentazoles is present in this work.[76] The precise mechanism of formation is unknown and a detailed mechanistic pathway has not been proposed. The variation of the stoichiometry of NaN_3 in the initial formation of DMHP-N_5 appears to be the influential difference between the formation of $(NH_4)(H_3O)(N_5)(Cl)$ and $NaN_5 \cdot 3H_2O$.
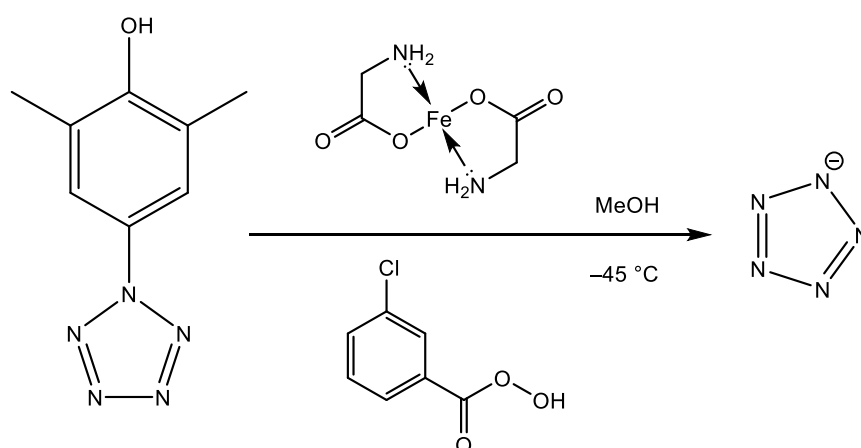
Scheme 81. Formation of N_5^- from DMHP-N_5 as $(NH_4)_4(H_3O)_3(N_5)_6Cl$ or $NaN_5 \cdot 3H_2O$.

Unlike the arylpentazoles, both pentazolate salts are stable at temperatures well above room temperature (T_d = 117 °C and 111 °C for $(NH_4)(H_3O)(N_5)(Cl)$ and $NaN_5 \cdot 3H_2O$ respectively), in complete contrast to the extremely high thermal sensitivities and energetic character of the

pentazenium (N_5^+) salts reported some 10 years prior (prepared at -64 °C). Although the formation of N_5^- by reduction of arylpentazoles supports the detection of N_5^- upon reduction of arylpentazoles using passivated sodium, the long term stability of the pentazolate salts first isolated by Zhang *et al.* are much greater than the N_5^- fragment detected in the latter which disappeared after only several minutes at room temperature.[306] Extensive hydrogen-bonding is observed between the N_5 ring and water molecules in both $(NH_4)(H_3O)(N_5)(Cl)$ and $NaN_5 \cdot 3H_2O$ and is hypothesised to contribute to their high thermal stability, which is so extensive that solid NaN_5 is stable even when heated to 60 °C for 30 minutes.[75] The formation and stability of the N_5^- anion is proposed to originate from 'dual aromaticity' of the ring system, comprised of both conventional π aromaticity and aromaticity afforded by overlap between filled σ^* orbitals and vacant π orbitals (so-called "σ aromaticity").[308] These 'σ aromatic' contributions mean the overall aromaticity of the N_5^- ring is calculated to slightly exceed that of benzene despite a decreased π aromaticity versus the latter.[309] Further theoretical calculations predict that the degree of protonation of the N_5 ring in DMHP-N_5 is critical to the formation and yield of the N_5^- anion. An increased acidity has been predicted to result in enhanced N−N bond strengths through hydrogen bonding or protonation, and that N_5^- release would only occur when the strength of all five N−N bonds exceeded that of the C−N bond (achieved through a three- to four-fold relative increase in acidity versus N_5^-). Consequently, the same authors proposed that an acidity approximately three- to four times greater than the concentration of N_5^- to be formed is critical for the formation N_5^- prepared by the reduction of arylpentazoles.[309]

The crystallographic studies of the N_5^- anion in $(NH_4)_4(H_3O)_3(N_5)_6Cl$ generated considerable debate about the degree of protonation and whether the N_5^- anion is, in fact, the previously-unknown HN_5.[310,311] Recent theoretical studies identified the presence of an equilibrium between protonated and deprotonated pentazole (scheme 82) where proton coordination is minimal at the low temperatures used in both synthesis and crystallographic measurements.[312] It is therefore assumed that the N_5 compounds synthesised in the bulk *are* anionic, supporting the claims of the original authors who prepared the N_5^- salts as well as the hypothesis proposed 16 years prior that HN_5 is too unstable to exist at room temperature for extended periods.[274] HN_5 remains unisolable.

$$HN_5 \rightleftharpoons N_5^- + H^+$$
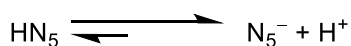
Scheme 82. The proposed equilibrium between N_5^- and HN_5.[312]

NaN$_5$ is an important synthon for the synthesis of other pentazolate compounds and its preparation lead to a rapid series of reports detailing the isolation of a number of pentazolate salts, complexes and coordination polymers (figure 121), several of which are formed as hydrates.[105,106,313–315] A number of energetic, nitrogen-rich N$_5^-$ salts have been prepared (figure 122), some of which are stabilised by the inclusion of hydrogen-bonding energetic cations such as DABTT (figure 123).[316] The recent isolation of NH$_4$N$_5$ complements the previous preparation of the compound using high pressure methods, and is the first example of a pentazolate salt prepared using two synthetic methodologies (i.e., high-pressure and cation exchange, notwithstanding the unconfirmed synthesis of NaN$_5$ by the former method).[66,301] N$_5^+$N$_5^-$, a close analogue to N$_\infty$, is unknown and predictions anticipate the stability of the compound to be even lower than the known all-nitrogen salt N$_5^+$N$_3^-$.[317]

cat$^\oplus$ = NH$_4^+$, Na$^+$ [Co(N$_5$)$_2$(H$_2$O)$_4$]   (NaN$_5$)$_2$(C$_2$H$_4$N$_4$)]$_n$

Salts   Monomeric coordination compounds   Coordination polymers
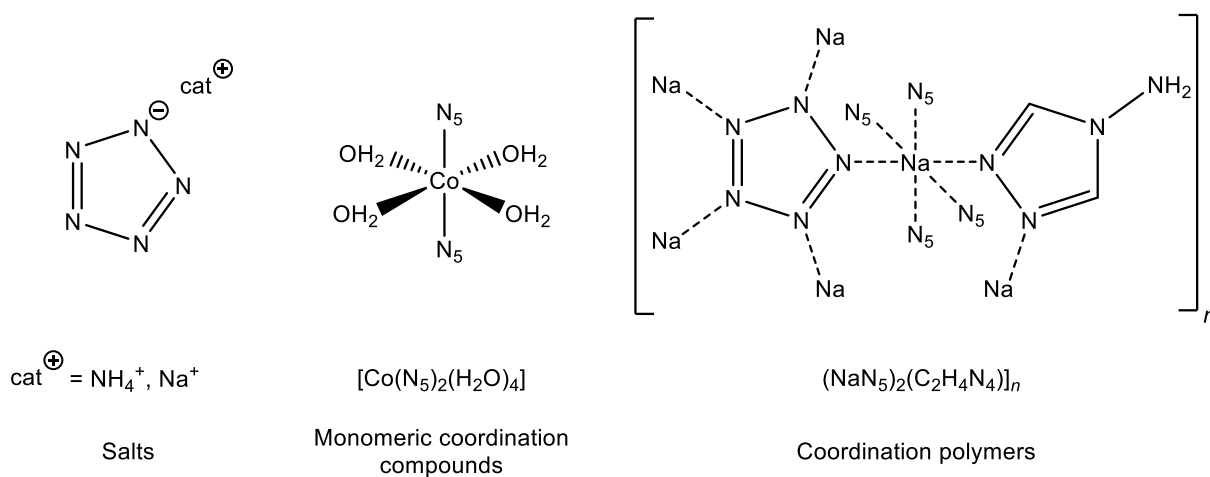
Figure 121. Examples of salts, monomeric coordination compounds and coordination polymers containing N$_5^-$.[75,76,105,108]

cat$^+$ = TABT
C$_4$H$_9$N$_{15}$
%N = 79%

cat$^+$ = GU
C$_2$H$_7$N$_9$O
%N = 73%

cat$^+$ = oxalohydrazinium (oxahy)
C$_2$H$_7$N$_9$O$_2$
%N = 67%
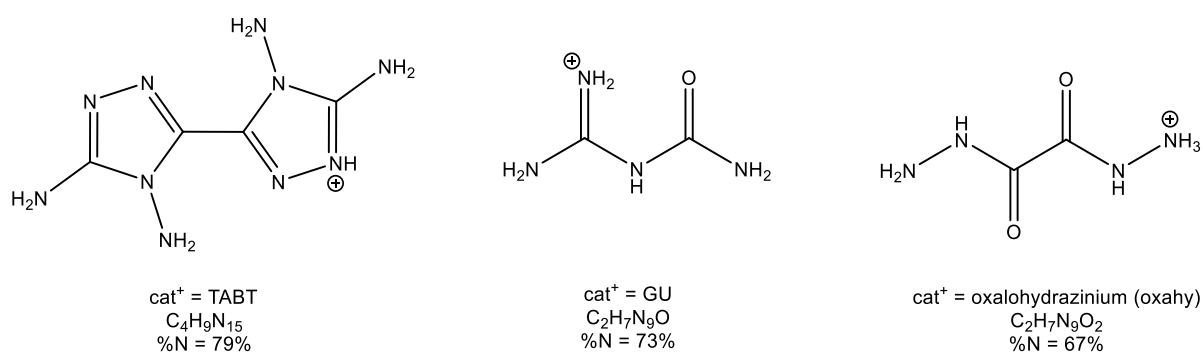
Figure 122. Examples and nitrogen content of some known energetic N$_5^-$ salts (cat$^+$N$_5^-$).[314,316]
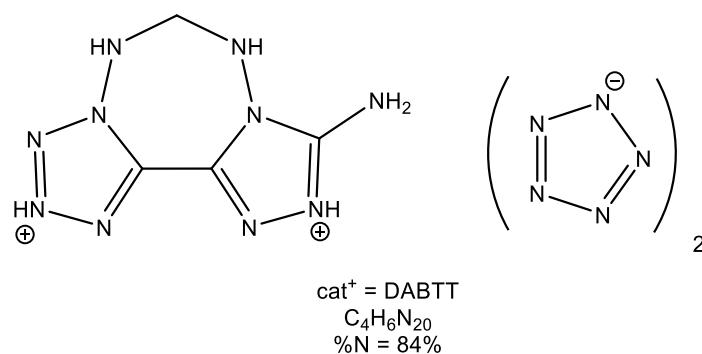
Figure 123. Structure and nitrogen content of the hydrogen-bonded energetic pentazolate salt (DABTT)(N$_5$)$_2$.[314]

Despite the recent rapid advances in preparation of numerous pentazolate salts, few anhydrous non-energetic N$_5^-$ salts have been synthesised and no main-group pentazolato complexes have been prepared to date. Anhydrous pentazolato transfer reagents are required to facilitate investigations into the coordination ability of N$_5^-$, in order to prevent hydrolysis of precursors such as SiCl$_4$. In this work, the synthesis of the N$_5^-$ anion was replicated in order to prepare two new, anhydrous pentazolato salts, [PPN]N$_5$ and AgN$_5$ for investigations into the reactions of ionic pentazolato transfer reagents towards main group coordination centres.[i]

7.2. Results and Discussion

7.2.1. Formation of N$_5^-$ by reduction of DMHP-N$_5$ with Na

Owing to the proven ability of DMHP-N$_5$ to generate N$_5^-$ in bulk, a solution of DMHP-N$_5$ in liquid ammonia was treated with sodium metal in a replication of the method reported by Ugi. IR spectra of the solid product showed no ν_{as}(N$_3$) bands either before or after several minutes at room temperature and confirmed that all DMHP-N$_5$ was consumed in the reaction. The absence of characteristic ν(N$_5$) bands at ca. 1200−1250 cm^{-1} also established that neither NaN$_5$ (ν(N$_5$) = 1219, 1246 cm^{-1}), nor any other N$_5^-$ salt, were formed.[75] It is plausible that DMHP-N$_5$ was over-reduced into aniline (scheme 83), supporting the findings of Ugi regarding the reduction of Ph-N$_5$ under the same conditions, and infers that the reduction potential of metallic sodium is also too great to facilitate selective C−N bond cleavage in DMHP-N$_5$.[303] This finding is supported by the later report of N$_5^-$ generation by reduction using *passivated* sodium metal.[307] Therefore, subsequent investigations focused on the proven reductive elimination of N$_5^-$ from DMHP-N$_5$.[75]

---

[i] At the same time as this work was undertaken, the syntheses of both AgN$_5$ and other silver pentazolato complexes were reported.[313] These are discussed later in this chapter.
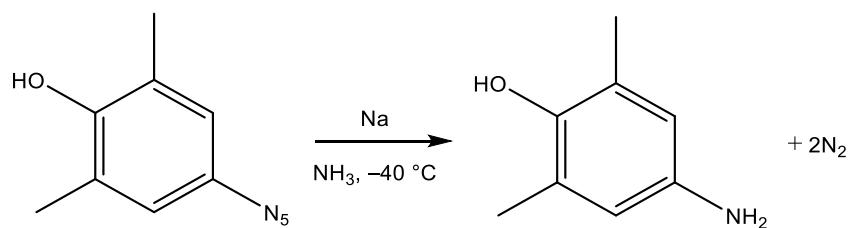
Scheme 83. Formation of dimethylhydroxyaniline from reduction of DMHP-N$_5$.[303]

7.2.2. Bulk Synthesis of N$_5^-$ from chemical cleavage of DMHP-N$_5$

The recent preparation of NaN$_5$·3H$_2$O from DMHP-N$_5$ was replicated in order to investigate ion and ligand exchange reactions involving N$_5^-$. Mass spectroscopic analysis of the crude reaction product revealed a signal at m/z = 70 which confirmed that the preparative procedure had produced N$_5^-$. Several additional signals were observed including two fragments corresponding to *m*-chlorobenzoate (m/z = 155) and chlorobenzene (m/z = 111) (scheme 84, table 56). These latter two signals were also observed in the mass spectrum of a genuine sample of *m*CPBA and arise from the use of an approximately fourfold excess of *m*CPBA in the reduction of DMHP-N$_5$. Additional signals at m/z = 69, 93, 213 (pre-HPLC) and 77, 86 and 93 (post-HPLC) could not be identified conclusively. On one occasion, a signal at m/z = 141 was also observed, which corresponds to [H(N$_5$)$_2$]$^{\bullet-}$.
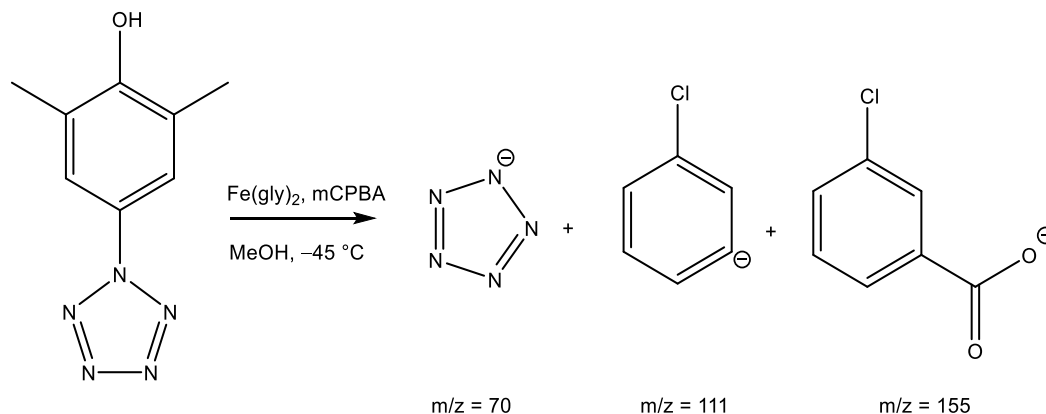
Scheme 84. Main products formed from reduction of DMHP-N$_5$ with *m*CPBA. The two carbon-based fragments (m/z = 111 and 155) arise from the fragmentation of *m*CPBA.

Separation by the gradient-elution column chromatographic method described in the original report proved challenging and preparative reverse-phase high-performance liquid chromatography (HPLC) was used instead to isolate N$_5^-$. Mass spectrometric analysis identified the three main products had been separated using this method, whilst the retention of fragments containing N$_5^-$ (including the main N$_5^-$ signal at m/z = 70) confirmed the stability of the anion towards separation at ambient conditions.

Pre-HPLC			Post-HPLC	
m/z	Identity		m/z	Identity
69	*Unknown*		70*	N_5^-
70	N_5^-		77	*Unknown*
93	*Unknown*	HPLC	86	*Unknown*
102	$[N_5 \cdot MeOH]^-$	→	93	*Unknown*
111	$[ClC_6H_4]^-$		102	$[N_5 \cdot MeOH]^-$
155*	$[ClC_6H_4COO]^-$		113	$[H(N_5)(N_3)]^-$
213	*Unknown*			

Table 56. Hypothesised identities of fragments observed in crude (left) and chromatographically separated (right) fractions obtained from replication of synthesis of $NaN_5 \cdot 3H_2O$. * denotes the most intense fragment observed in each spectrum Analysis solvent: 30:70 H_2O:MeOH.

The lower detection limit of the mass spectrometer prevented the observation of N_3^- or HN_3 and therefore the relative stability of the N_5^- anion can only be estimated by the absence of solvated N_3^- fragments (*i.e.* $[H(N_5)(N_3)]^-$). A separate replication of the procedure using optimised conditions (more effective stirring and an increased surface area of $Fe(gly)_2$) resulted in the absence of any major fragments of *m*CPBA and an increased intensity of the N_5^- signal in the mass spectrum.[318] Owing to the use of relative intensity scales in each mass spectrometric analyses, it is unclear if the optimised conditions increase the yield of N_5^- or if the removal of the most intense signal (m/z = 155) merely distorts the intensity of the remaining fragments.

Despite careful replication of the reported procedure and the mass spectrometric detection of N_5^- in the previous step, crystallisation of $NaN_5 \cdot 3H_2O$ was not successful. Although the mass spectrum was dominated by the signal arising from N_5^- (m/z = 70), a sticky, dark brown solid was produced which contrasted the described appearance of $NaN_5 \cdot 3H_2O$ as a colourless microcrystalline solid.[75] The absence of significant impurities in the mass spectrum indicates that the unknown brown impurity is likely to be non-volatile; a possible candidate is FeO_2, which could originate from inadvertent oxidation of $Fe(gly)_2$. The presence of an unknown impurity prevented the determination of the yield, purity or identity of the N_5^- salt in the reaction product. A single band in the IR spectrum ($\tilde{v} = 1256$ cm^{-1}) is similar to the highest $v(N_5)$ band of $NaN_5 \cdot 3H_2O$ ($v(N_5) = 1246, 1219$ cm^{-1}). The second band may have been masked by the unknown impurity in the product. Both the appearance and IR spectrum of the product

were inconsistent with $(N_5)_6(H_3O)_3(NH_4)_4Cl$ ($\nu(N_5) = 1224$ cm^{-1}), confirming that although N_5^- was formed, further purification is required to obtain the solid in useable quantities.

It is unclear why the reaction was not reproducible. The formation of *m*-chlorobenzoic acid from *m*CPBA may have affected the acidity of the reaction solution, and thus the ease of separation and yield of the product.[319] The report discussing the critical acidity of solutions containing N_5^- (see above) only appeared after this synthetic work was undertaken and therefore the acidity of the reaction solution was not considered at the time, beyond replication of the scales and stoichiometries reported in the original syntheses which produce N_5^-.[309] Although the presence of a pentazolate salt was confirmed by mass spectrometry, the inability to obtain pure $NaN_5 \cdot 3H_2O$ prevented further investigations towards the formation of main-group pentazolato complexes. However, detection of N_5^- signals in the mass spectrum did facilitate mass spectrometric investigations into the formation of new N_5^- salts, [PPN]N$_5$ and AgN$_5$, by cation exchange.

7.2.3. Formation of novel pentazolate salts I: synthesis of [PPN]N$_5$

PPN salts are prepared by the reaction of [PPN]Cl and a salt containing the desired anion, e.g. NaN$_3$.[320] The phlegmatisation afforded by PPN cations and the facile preparation and crystallisation of water-free compounds render PPN salts an ideal transfer reagent for the preparation of nitrogen-rich main group coordination complexes, such as $[E(N_3)_6]^{2-}$ (E = Si−Pb).[95,96,102] The same strategy was extended to a sample of "$NaN_5 \cdot 3H_2O$" described above (scheme 85) to attempt to prepare [PPN]N$_5$.

$$NaN_5 + ex.PPNCl \xrightarrow{H_2O} PPN(N_5) + NaCl$$
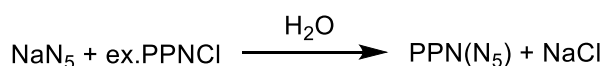
Scheme 85. Preparation of [PPN]N$_5$.

An off-white solid immediately precipitated upon the combination of hot (60 °C) aqueous solutions of [PPN]Cl and NaN$_5$. Previous investigations of sodium pentazolate have reported the compound to be stable at this temperature for 30 minutes and thus degradation of the N_5^- anion at this temperature within the reaction time (several minutes) is unlikely.[75] The mass spectrum (ESI$^-$) of the colourless filtrate contained only signals consistent with fragments of [PPN]$^+$ and confirmed that all N_5^- had been removed from solution (table 57). The precipitate was recrystallised from MeCN to remove excess [PPN]Cl. The mass spectrum of the recrystallised solid still contained fragments of both [PPN]$^+$ and N_5^- (table 59). Although colourless needle crystals were obtained, the size was insufficient for crystallographic studies.

Storage of a solution of [PPN]N$_5$ at ambient conditions for 2 weeks did not result in the disappearance of the signal associated with N$_5^-$, stability which is in agreement with that of NaN$_5$·3H$_2$O (table 59). The disappearance of the fragment at m/z = 106 (N$_5^-$·3H$_2$O) is attributed to water loss during evaporation. An increase in the intensity of the N$_5^-$ signal (relative to the PPN cation fragments) in the recrystallised solid versus the crude product arises from the removal of excess [PPN]Cl and is solely subjective owing to the use of relative scales for each mass spectrum. The inability to obtain crystals suitable for crystallographic studies precluded investigations into the presence and contribution of hydrogen bonding on the N$_5^-$ anion and also prevented confirmation of the identities of the fragments tentatively assigned in the mass spectra. Therefore, although mass spectrometric data suggests that cation exchange is feasible and has occurred, further work is required to reliably confirm this result and optimise the process for large-scale syntheses.

Filtrate (H$_2$O)			Recrystallised Solid (MeCN)		
m/z	Identity	Number	m/z	Identity	Number
69	[PH$_2$·H$_2$O]$^-$	1	69	[PH$_2$·H$_2$O]$^-$	1
72	[Cl$_4$H$_2$]$^{2-}$	3	**70**	**N$_5^-$**	**2**
77	*Unknown*	4	89	[P(MeCN)(OH)]$^-$	6
86	*Unknown*	5	102	[(NH$_3$)$_5$·OH]$^-$	8
93	[NaClOH.H$_2$O]$^-$	7	**106**	**[N$_5$·2H$_2$O]$^-$**	**9**
102	[(NH$_3$)$_5$·OH]$^-$	8	113	[P$_2$O$_3$H$_3$]$^-$	10
113	[P$_2$O$_3$H$_3$]$^-$	10	539	[PPN]$^+$	18
119	*Unknown*	11	555	[PPN]$^+$·H$_2$O	19
141	[Cl(NH$_3$)$_2$·4H$_2$O]$^-$	12			
152	[NH$_3$·H$_2$O·(MeCN)$_2$Cl]$^-$	14			
161	[Cl$_2$(NH$_4$)·4H$_2$O]$^-$	16			
198	[Cl$_2$(NH$_4$)·6H$_2$O]$^-$	17			
539	[PPN]$^+$	18			

Table 57. Main signals (ESI$^+$ and ESI$^-$) observed in the mass spectrum of the filtrate of [PPN]Cl + NaN$_5$ in aqueous solution (left, analysis solvent: H$_2$O) and of the recrystallised product "[PPN]N$_5$" (right, analysis solvent: MeCN). Fragments arising from N$_5^-$ are highlighted in **bold**. The absence of any signals containing N$_5^-$ in the filtrate solution confirms all N$_5^-$ was removed from solution upon reaction with [PPN]Cl.

	1	2	6	8	9	10	13	15	18*	19*	Notes
m/z	69	70	89	102	106	113	145	159	539	555	
B	●	●	●	●	●	●			●	●	Supernatant recryst. soln.
C	●	●	●	●			●	●	−	−	After redissolution, 3w
D	●		●			●			●		[PPN]Cl

Table 58. Summary of fragments (ESI$^-$ and ESI$^+$) observed (●) in mass spectrometric studies of recrystallised [PPN]N$_5$ before redissolution and after 3 weeks in solution. Analysis solvent: MeCN. Fragments observed only in the mass spectrum of the aqueous filtrate have been omitted for clarity. Green shading denotes N$_5^-$ containing fragments; blue shading denotes fragments arising from [PPN]$^+$. − = not measured; * = ESI$^+$.

			Observed	
m/z	Identity	Number	Before Evaporation	After Redissolution
69	[PH$_2$·H$_2$O]$^{-\,a}$	1	●	●
70	**N$_5^-$**	**2**	●	●
89	[P(MeCN)(OH)]$^{-\,a}$	6	●	●
102	[(NH$_3$)$_5$·OH]$^-$	8	●	●
106	**[N$_5$·2H$_2$O]$^-$**	**9**	●	
113	[P$_2$O$_3$H$_3$]$^{-\,a}$	10	●	
145	*Unknown*	13		●
159	[N$_3$·2MeCN·Cl]$^-$	15		●

Table 59. Comparison of fragments observed (●) in mass spectrum of [PPN]N$_5$ before and after solvent evaporation and redissolution. Fragments arising from N$_5^-$ are highlighted in **bold**. Analysis solvent: MeCN. [a] observed in the mass spectrum of [PPN]Cl in MeCN.

IR spectroscopic studies showed minimal variation between [PPN]N$_5$ and [PPN]Cl (figure 124), which is expected due to the small number of expected bands for the N$_5^-$ anion (versus none observed for Cl$^-$). The extensive spectroscopic similarities between [PPN]N$_5$ and [PPN]Cl render definitive characterisation of the former compound difficult and evaluation of purity impossible. Although mass spectrometric data confirmed that both N$_5^-$ and [PPN]$^+$ ions were present in the analyte solution, the possibility of contamination through further excess [PPN]Cl cannot be excluded; furthermore, the presence of a signal attributed to a chlorine-containing fragment at m/z = 159 showed that crystallisation of analytically-pure '[PPN]N$_5$' was not achieved. As encountered during the synthesis of NaN$_5$·3H$_2$O, the analysis limits of the mass spectrometer prevented detection of N$_3^-$ (m/z = 42), which would be formed by decomposition of [PPN]N$_5$. However, the continued detection of the signal at m/z = 70 is a promising indicator that the N$_5^-$ anion was preserved during cation exchange. The detection of

trace impurities by mass spectrometry further complicated the ability to isolate and determine the purity of any [PPN]N$_5$ formed. Additionally, the extremely low yield of "NaN$_5$·3H$_2$O" in the previous step introduced further difficulties in crystallisation, characterisation and reactivity studies. In order for [PPN]N$_5$ to be prepared in practical quantities, the synthesis of NaN$_5$ must first be optimised to increase the yield and purity to levels suitable for use in further investigations.
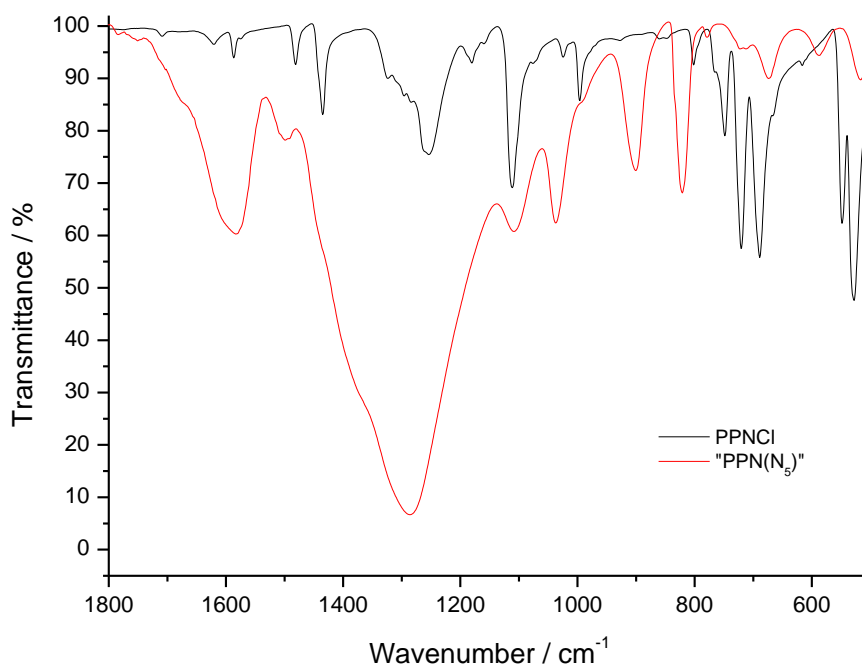
Figure 124. ATR-IR spectral overlay of [PPN]Cl (black line, −) and "[PPN]N$_5$" (red line, −).

7.2.4. Formation of novel pentazolate salts II: synthesis of AgN$_5$

AgN$_3$ is a particularly effective azide transfer reagent owing to the formation of insoluble silver salt byproducts in ligand exchange reactions. The synthesis of AgN$_5$ (scheme 86) was investigated to prepare of a new anhydrous pentazolate transfer reagent that could facilitate alternative or a larger number of ligand exchange reactions than acetonitrile-soluble [PPN]N$_5$.

$$NaN_5 + Ag(NO_3) \xrightarrow{H_2O} Ag(N_5) + AgNO_3$$
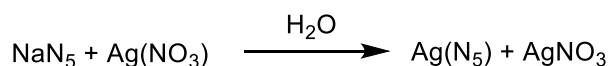
Scheme 86. Synthesis of AgN$_5$.

The combination of aqueous solutions of NaN$_5$ and AgNO$_3$ resulted in the immediate precipitation of a white solid. The detection of N$_5^-$ in the filtrate solution by mass spectrometry is attributed to the addition of insufficient AgNO$_3$ for complete cation exchange. Treatment of the filtrate solution with further AgNO$_3$ resulted in negligible precipitation and the

disappearance of the N_5^- signal from the mass spectrum of the filtrate, accompanied by the formation of several other signals corresponding to fragments of $AgNO_3$ (tables 60, 61).

Before				After		
m/z	Identity	Number		m/z	Identity	Number
70	N_5^-	1		131	$[NaNO_3 \cdot NO_2]^-$	3
120	$[N_3 \cdot HN_3 \cdot Cl]^-$	2		147	*Unknown*	4
131	$[NaNO_3 \cdot NO_2]^-$	3	$AgNO_3$	216	$[Ag_2]^-$	5
147	$[Na(NO_3)_2]^-$	4		230	$[Ag(NO_3)_2]^-$	6
				317	$[Ag_3(NO_3)_5]^-$	7
				366	*Unknown Ag fragment*	8
				402	$[Ag_2(NO_3)_3]^-$	9

Table 60. Signals observed in mass spectrum of filtrate solution of AgN_5, before (left) and after (right) addition of further $AgNO_3$. Analysis solvent: H_2O.

Owing to the inability to obtain analytically pure NaN_5, trace chlorine contaminants may have reacted preferentially with $AgNO_3$ to precipitate $AgCl$ instead of (or in addition to) AgN_5. The negligible amount of solid formed upon the second addition of $AgNO_3$ was insufficient for IR spectroscopic analysis and the identity of the second precipitate is therefore inconclusive. These preliminary studies indicated that AgN_5 can be prepared from NaN_5, but the purity and yield are currently unknown. It is also unclear if the presence of $AgNO_3$ oxidised the N_5^- anion. In order to confirm that AgN_5 is formed and that the presence of excess $AgNO_3$ does not oxidise the N_5^- anion in solution, larger-scale studies are required once a bulk-scale synthesis of analytically pure NaN_5 is optimised.

		Number of treatments with AgNO$_3$	
Number	**m/z**	**1**	**2**
1	70	●	
2	120	●	
3	131	●	●
4	147	●	●
5	230		●
6	230		●
7	317		●
8	366		●
9	402		●

Table 61. Comparison of signals observed (●) in mass spectrum of AgN$_5$ filtrate solution, before and after treatment with further AgNO$_3$. Rows shaded in green correspond to N$_5^-$ fragments. Rows shaded in blue correspond to fragments from NaNO$_3$.

At the same time as this work was being undertaken, the synthesis of AgN$_5$ from [Mg(H$_2$O)$_6$][(N$_5$)$_2$(H$_2$O)] was reported (scheme 87).[313] The reason for the use of the magnesium salt instead of NaN$_5$ is not discussed. Treatment of AgN$_5$ with NH$_3$ solution forms [Ag(NH$_3$)$_2$][Ag$_3$(N$_5$)$_4$] as colourless crystals. The IR spectra of both solvated and non-solvated silver salts are reported to contain strong, sharp bands indicative of a ν(N$_5$) stretching vibration at 1234 and 1213 cm^{-1} for AgN$_5$ and [Ag(NH$_3$)$_2$][Ag$_3$(N$_5$)$_4$], respectively. Both of the reported bands are similar to the reported ν(N$_5$) bands of NaN$_5$·3H$_2$O (ν(N$_5$) = 1246, 1219 cm^{-1}).[75] Both compounds display few bands in the fingerprint region of the IR spectrum.[313]

$$[Mg(H_2O)_6][(N_5)_2(H_2O)] \xrightarrow[\text{MeOH}]{\text{ex.AgNO}_3} AgN_5 + Mg(NO_3)_2$$
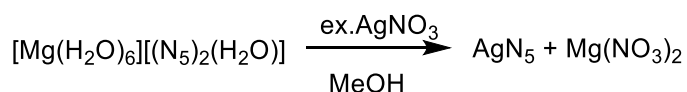
Scheme 87. Synthesis of AgN$_5$ as reported by Sun *et al.*[313]

Comparison of the IR spectra of the product obtained in this study to that reported for AgN$_5$ showed that the number of bands observed in the former was higher than reported. The spectrum obtained in this work is inconsistent with AgNO$_3$ or NaCl (both of which are anticipated to remain in solution if formed) but displays similarities to AgCl. A band in the ν(N$_5$) region (1264 cm^{-1}) is identical to that of AgCl, whilst the band reported for AgN$_5$ in literature (ṽ = 1246 cm^{-1}) is absent (figure 125).[313] However, a sharp band at 693 cm^{-1}, observed in the IR spectrum of the product obtained in this study, is absent in AgCl and is almost identical to that reported for [Ag(NH$_3$)$_2$][Ag$_3$(N$_5$)$_4$] (table 62). These similarities suggest

that in this work, an AgN$_5$-containing complex *and* AgCl may have precipitated from solution. However, the preparation of both the reaction product and genuine AgCl using the same synthetic method means that the presence of the same contaminant in both solids cannot be excluded. A more likely explanation is that the presence of chloride (and thus the formation of AgCl) originates from the initial synthesis of NaN$_5$, either through incomplete purification or the inadvertent formation of (NH$_4$)$_4$(H$_3$O)$_3$(N$_5$)$_6$Cl (scheme 88). The similarities in isotope patterns of chlorine and silver fragments made conclusive identification of any chlorine impurities challenging. As concluded for the [PPN] salts, the isolation of analytically pure material is required before the identity of the chlorine impurity (and indeed the product) can be confirmed.

$$N_5^- + Cl^- \quad \xrightarrow{\quad Ag^+ \quad} \quad AgCl + AgN_5$$
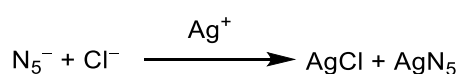
Scheme 88. One possible formation of AgCl and AgN$_5$ from a product mixture containing both N$_5^-$ and Cl$^-$ anions. The inability to identify the composition of the starting material means other anions may be present and may also react with Ag$^+$.
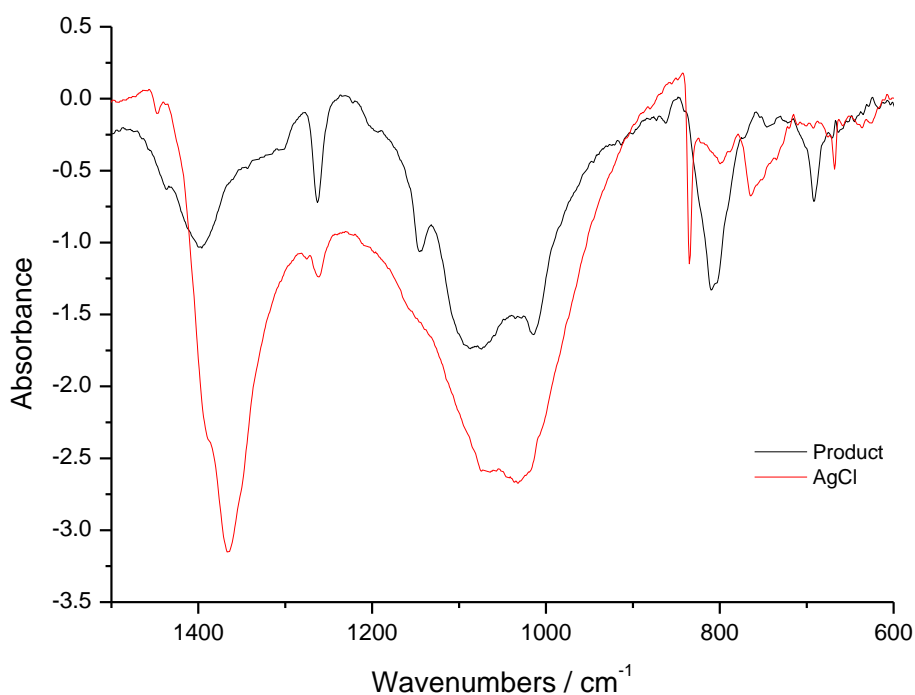
Figure 125. ATR-IR spectra of the reaction product hypothesised as 'AgN$_5$' (black line, −) and AgCl (red line, −).

Compound	$\tilde{\nu}$ / cm^{-1} (1500−600 cm^{-1})							
This work [a]	1438	1397	1264	1087	1016	808		693
AgCl [a]	1449	1367	1263	1063	1033	835	766	668
AgN$_5$ [b]		1361	1234					
[Ag(NH$_3$)$_2$][Ag$_3$(N$_5$)$_4$]			1213					688
NaN$_5$·3H$_2$O			1246, 1219					

Table 62. Comparison of selected IR bands of pentazolate compounds and AgCl between 1500−600 cm^{-1}.[75,313] Values shaded in green denote the region of the ν(N$_5$) stretching vibration.

7.2.5. Is N$_5^-$ a pseudohalide?

The recent literature studies concerning the N$_5^-$ anion allowed the determination of pseudohalide character for the first time. As discussed in chapter 1, the concept of pseudohalogen character is defined by criteria involving reactions of the candidate species. The isolation of coordination complexes, binary salts and a water-insoluble silver salt are all demonstrated by N$_5^-$, whilst the unconfirmed detection of HN$_5$ and the absence of (N$_5$)$_2$ represent unfulfilled criteria. Comparison with other ligands studied in this work shows that although the number of pseudohalide criteria met by the pentazolate anion is currently less than the cyanide and azide anions, it is comparable to those displayed by the dicyanamide anion (table 63). Given the recent isolation of N$_5^-$ in bulk quantities, it is anticipated that other reactivity criteria may be achieved in the near future (in particular the formation of radicals) and therefore the N$_5^-$ anion can be classified as a pseudohalide.

Criterion	Description	N$_5^-$	[N(CN)$_2$]$^-$
		Example	Example
A	Formation of radicals	−	[N(CN)$_2$]$^\bullet$
B	Existence of anions	NaN$_5$	NaN(CN)$_2$
C	Formation of insoluble Ag/Pb salts	AgN$_5$	AgN(CN)$_2$
D	Formation of coordination complexes	[Co(N$_5$)$_2$(H$_2$O)$_4$]^a	Co{N(CN)$_2$}$_2$
E	Existence of protonated form	*HN$_5$*	*HN(CN)$_2$*
F	Existence of dimers	−	−
G	Interpseudohalide compounds	−	−

Table 63. Criteria and examples of fulfilment of pseudohalide character for N$_5^-$. *italics* denote an unknown compound. [a] as [Co(N$_5$)$_2$(H$_2$O)$_4$]·4H$_2$O.[105] − = unknown.

7.3. Conclusions and Outlook

It can be concluded that replication of the *m*CPBA-induced C−N bond cleavage of DMHP-N$_5$ did result in the formation of the N$_5^-$ anion. However, the preparation of analytically pure N$_5^-$ salts on the scales reported in literature was unsuccessful, for reasons which are still not known. In lieu of standard column chromatography, preparative HPLC was demonstrated to efficiently separate three main reaction products, one of which was shown to contain N$_5^-$ by mass spectrometry. The reaction mechanism for the formation of N$_5^-$ remains unclear and the solid compound obtained from this replication study is inconsistent with NaN$_5$. Mass spectrometry confirmed the stability of the N$_5^-$ anion, including towards separation. The inability to prepare N$_5^-$ salts on larger scales prevented further confirmation of identity or purity and thus detailed coordination or reactivity studies are not currently possible.

Only limited conclusions can be drawn concerning the reactions occurring in these studies owing to the low scale and purity of the NaN$_5$ precursor. Despite this, mass spectrometric studies of the salt metathesis reactions between NaN$_5$ and Ag$^+$ or PPN$^+$ appear to provide evidence for the formation of [PPN]N$_5$ and Ag(N$_5$). The persistence of the N$_5^-$ signal at m/z = 70 in [PPN]N$_5$ implies that the salt is stable at room temperature, in analogy to NaN$_5 \cdot 3$H$_2$O. The disappearance of the N$_5^-$ signal in the supernatant solution of NaN$_5$ and AgNO$_3$, accompanied by precipitation of an insoluble solid, suggests that this reaction may be an alternative preparation of AgN$_5$ to that described recently.[313] Both reactions provide proof-of-concept for the preparation of anhydrous pentazolato salts, which could be used in the preparation of novel main group poly(pentazolato) complexes. However, owing to the factors described above, beyond the maintenance or disappearance of the N$_5^-$ anion upon reaction, the identity or purity of the compounds formed cannot yet be confirmed. Despite these issues, the pseudohalide character of the N$_5^-$ anion is demonstrated. Before these important pentazolato transfer reagents are studied further, the synthesis of NaN$_5$ requires optimisation to afford the higher yields and analytically pure material reported in literature. The large-scale use of analytically pure NaN$_5$ in these salt metathesis reactions will allow complete determination of both the identity and purity of the products. This is an essential step in the preparation of useable quantities of water-free pentazolate salts before coordination studies are commenced.

7.4. Further Work

The bulk syntheses of analytically pure, thermally stable pentazolate salts allows the investigation of many new pentazolate compounds and, consequently, a greater understanding of polynitrogen chemistry. Some relevant theses are outlined below:

i. How does the behaviour of N_5^- compare to other pseudohalogens?

ii. Can HN_5 be conclusively prepared and isolated? Does the experimental data match that observed in the challenged report of the synthesis of HN_5, published prior to the synthesis of NaN_5?

iii. How does the N_5^- anion compare in reactivity to the N_3^- anion?

iv. Can poly(pentazolato) complexes of non-metallic elements (e.g. Si, Ge) be prepared, and how do their syntheses and reactivity compare to other nitrogen-rich silicate and germanate anions known (e.g., $[E(N_3)_6]^{2-}$ and $[E(CHN_4)_6]^{2-}$)?

The first of these theses has been partially answered in the discussion above. However, the existence of the protonated parent acid HN_5 remains unclear. Limited *in situ* NMR studies towards HN_5 were conducted some 20 years prior to the synthesis of NaN_5, and the conclusions were the subject of contentious debate. Despite the recent isolation of N_5^- in several pentazolate salts, no further experimental work towards HN_5 has been reported.[76,274,305] The recent theoretical study proposing a low-temperature equilibrium between protonated and deprotonated forms of HN_5 would be a key point of interest which could be investigated through temperature-dependent spectroscopic methods. However, analytically pure NaN_5 or another pentazolate salt is required before further work into HN_5 could be performed.

The preparation of anhydrous pentazolate salts such as $[PPN]N_5$ described above will allow the investigation of the propensity of the N_5^- anion to coordinate to non-metallic centres such as main group elements (e.g., figure 126). The formation of group 14 pentazolato complexes wouldallow comparison with the analogous azido and tetrazolato complexes $[E(N_3)_6]^{2-}$ and $[E(CHN_4)_6]^{2-}$, especially with respect to the differences in ligating ability between the three nitrogen-rich ligands. The preparation of anionic or neutral poly(pentazolato) complexes of silicon, germanium, tin and/or lead would be only the third example of a nitrogen-rich homoleptic group 14 coordination complex and would provide further insight into the use of N_5^- as a new nitrogen-rich pseudohalide ligand (table 64). A theoretical study calculates the N_5 group to behave similarly to the CN group in terms of electron withdrawing effects and

therefore the reactivity of the N_5 ligand may be similar to that observed in the preparation of hexa(cyanido) complexes of the same elements (see chapter 2).[148,169,321] Experimental investigations into the coordination ability of the N_5 group are critical to allow the evaluation of this prediction and its extension to other pseudohalides.

$$ECl_4 \xrightarrow[\text{MeCN}]{\text{PPN}(N_5)} (PPN)_2[E(N_5)_6] + 4PPNCl$$
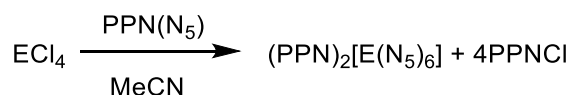
Scheme 89. Proposed formation of $[PPN]_2[E(N_5)_6]$ (E = Si−Sn) by ligand exchange with a water-free pentazolate salt, *cf.* the preparation of $[PPN]_2[E(N_3)_6]$.
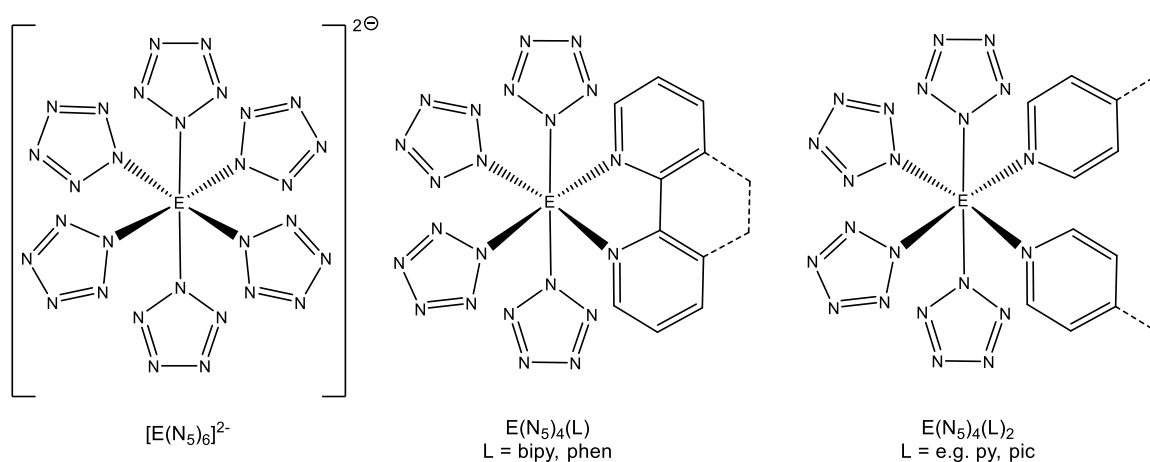
Figure 126. Proposed structure of poly(pentazolato) complexes of Si−Sn.

Ligand	Complex (E = Si−Sn)	Nitrogen Content (wt%)	Refs.
N_5	$E(N_5)_6]^{2-}$	94−78	−
	$E(N_5)_4(bipy)$	66−56	−
	$E(N_5)_4(py)_2$	66−55	−
N_3	$[E(N_3)_6]^{2-}$	90−68	95,96,322
	$E(N_3)_4(bipy)$	56−44	96,102,243
	$E(N_3)_4(py)_2$	55−44	102,147

Table 64. Comparison of nitrogen contents of poly(pentazolato) and poly(azido) complexes of Si, Ge and Sn.

Chapter 8. Dicyanamido complexes containing group 14 centres

8.1. Introduction

The dicyanamide anion, $[N(CN)_2]^-$, was one of the first pseudohalogens reported and fulfils almost all of the pseudohalide classification criteria (figure 127).[1] Several attempts to form $HN(CN)_2$ (figure 128) through acidification of $AgN(CN)_2$ resulted in crystalline solids of unknown composition. The protonated dicyanamide is described as stable in aqueous solution but decomposes rapidly when isolated; although the compound is reported to be highly acidic, this has not been quantified experimentally and studies concerning $HN(CN)_2$ are extremely limited.[4,5,323] Despite a theoretical study predicting the stability of one isomeric form, no dicyanamide dimers $[\{N(CN)_2\}_2]$ are known (figure 128).[324] Organodicyanamides such as $MeN(CN)_2$ and $PhN(CN)_2$ are known, with the latter reported to display bonding isomerism congruent with the varying resonance structures of the anionic form.[325–327]
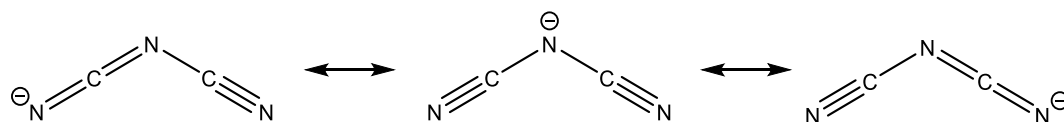
Figure 127. Resonance forms of the dicyanamide anion.

protonated form   dimeric form
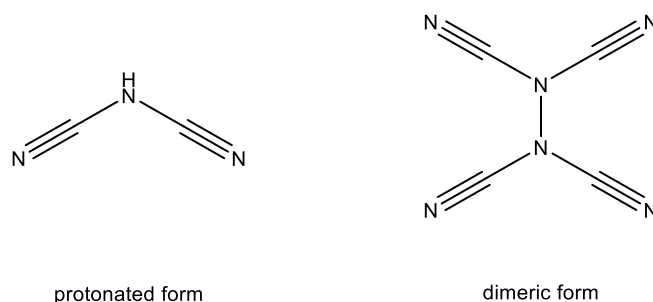
Figure 128. Proposed structures of protonated (left) and dimeric form (right) of dicyanamide. The dimeric structure shown has been predicted to be stable by theoretical studies.[324]

The dicyanamide anion is capable of forming coordination compounds containing *d-*, *p-* and *f-*block coordination centres. Homoleptic poly(dicyanamido) complexes containing transition metal centres are plentiful and have been extensively reviewed.[328,329] Coordination of dicyanamide ligands in these complexes is usually achieved by ligand exchange of metal chlorides or nitrates with ionic dicyanamido exchange reagents to form neutral (e.g. $M\{N(CN)_2\}_2$, M = Co, Cr, Cu, Fe, Mn, Zn) or anionic (e.g. $[M\{N(CN)_2\}_4]^{2-}$, M = Pd, Pt, Co) complexes.[330,331] The multiple coordination sites of the dicyanamide anion results in a number of mono-, bi- and tri-dentate coordination modes (figure 129, table 65) which vary by

coordination number and centre identity.[330,332,333] The majority of homoleptic poly(dicyanamido) transition metal complexes contain bidentate bridging dicyanamido ligands (form III) and form as coordination polymers or extended networks. The monodentate dicyanamido ligands of forms I and II often require sterically-hindering ligands or saturated coordination centres to prevent the formation of coordination polymers.[334] Homoleptic tris(dicyanamido) complexes containing *f*-block centres as [M{N(CN)$_2$}$_3$] (M = La−Nd, Sm, Eu, Tb) have also been reported with tridentate dicyanamido ligands (form V).[335,336] The applications of dicyanamido coordination complexes are varied. Select transition metal dicyanamido complexes, M{N(CN)$_2$}$_2$ (M = Co, Cr, Mn) display weak ferromagnetic behaviour at low temperatures and tris(dicyanamido) europium and terbium luminesce in the red and green regions, respectively.[331,335–337]
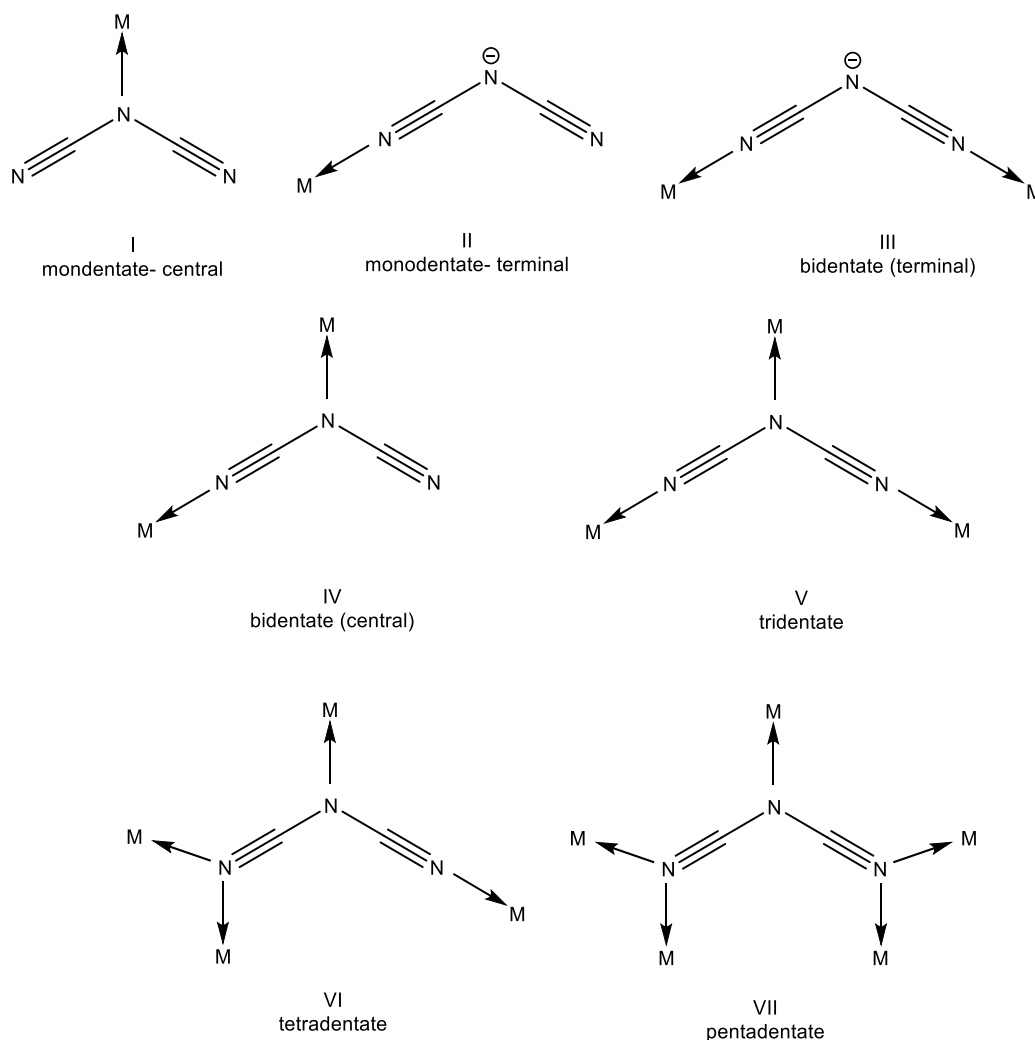
Figure 129. Coordination modes (forms I−VII) of the dicyanamido ligand.

I	II	III	IV	V	VI
$Co(R)_2(N(CN)_2)_2$	$Zn\{N(CN)_2\}_2(OH_2)R_2$	$[M^1\{N(CN)_2\}_3]^-$	$Me_2TlN(CN)_2$	$M^4\{N(CN)_2\}_2$	$Pb\{N(CN)_2\}_2$
		$[M^2\{N(CN)_2\}_4]^-$			
		$[M^3\{N(CN)_2\}_3]$			
		$Me_2Sn\{N(CN)_2\}_2$			
338	334	137,339–342	343	330	344

Table 65. Examples of transition metal dicyanamido complexes containing coordination forms I−VI described above. R = H$_2$BzIm (BzIm = benzylimidazole) ; R = bispyridylaminotriazole ; M^1 = Ni, Co, Mn ; M^2 = Pd, Pt ; M^3 = V, Ti ; M^4 = Mn, Fe, Co, Ni, Cu, Cd.

Reports of *p*-block dicyanamido complexes are much rarer. The sole homoleptic dicyanamido complex of group 14 is $Pb\{N(CN)_2\}_2$, which forms as a crosslinking coordination polymer in two polymorphs which contain dicyanamido ligands in the rare forms VI and VII.[344,345] To date, no homoleptic poly(dicyanamido) coordination complexes of silicon, germanium or tin are known. Dicyanamido complexes of lighter group 14 centres are restricted to non-homoleptic organometallic complexes, with the general formula $R_xE\{N(CN)_2\}_y$ (R = Me or Ph, E = Si−Pb, x = 1 or 2, $x + y$ = 4), prepared from the respective group 14 organochlorides with $AgN(CN)_2$.[340,341,346,347] Although some are stable at room temperature (E = Sn or R = Ph), the methylsilane or -germane derivatives rapidly polymerise at room temperature to form dark-coloured solids that are likely to be coordination polymers.[346]

The preparation of coordination complexes by ligand substitution demonstrates that ionic dicyanamido transfer reagents are capable of displacing halide ligands from group 14 coordination complexes, in analogy to the cyanido and azido pseudohalides discussed in previous chapters. However, it is less clear if electronic or steric hindrance prevents the formation of homoleptic dicyanamido complexes. The preparation of anionic hexakis(dicyanamido) complexes containing silicon, germanium and tin centres would provide more insight into the coordination ability of an additional pseudohalogen towards these sparsely-studied hypercoordinate centres (figure 130). Once prepared, the reactivity of these complexes could be investigated towards HN$_3$ to prepare novel N-rich bis(tetrazolato) ligands *in situ* (scheme 90).

$$ECl_4 + ex.cat[N(CN)_2] \longrightarrow cat_2[E\{N(CN)_2\}_6] + 4catCl$$
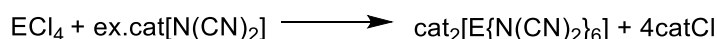
Scheme 90. Proposed synthesis of hexakis(dicyanamido) complexes of group 14 elements. E = Si−Sn, cat$^+$ = e.g. [PPN]$^+$.
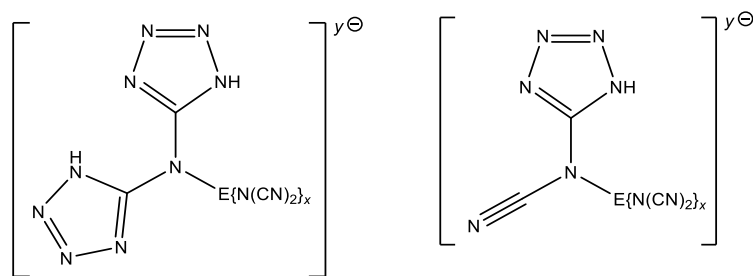
Figure 130. Proposed structures of ligands prepared from reaction of group 14 homoleptic dicyanamido complexes with azide groups. E = Si−Sn, x = 4 or 6, y = 4-x.

8.2. Results and Discussion

8.2.1. Synthesis of [PPN][N(CN)$_2$]

Following the success in the use of other PPN pseudohalide salts as ionic ligand transfer reagents towards group 14 chlorides, [PPN][N(CN)$_2$] was synthesised to prepare an ionic dicyanamido transfer reagent. [PPN][N(CN)$_2$] was prepared from Na[NCN)$_2$] and [PPN]Cl. The compound crystallises from hot MeCN as colourless block crystals in space group $P2_1$/c (figure 131) and contains two anions and two cations per unit cell. Both C−N−C bond angles are similar to the 120° angle expected for a trigonal planar complex and both C−N bonds are effectively linear, with comparable bond distances and angles to other dicyanamide salts (table 66). The significant elongation of the thermal ellipsoid of the central nitrogen atom arises from a swinging-type motion of the anion about the terminal nitrogen atoms. The same phenomenon is also observed in the structure of Ph$_4$P[N(CN)$_2$].[348] Both the terminal and central C−N bond lengths are similar to standard C≡N (d = 1.14 Å) and C=N bonds (d = 1.26 Å).[168] The absence of any bond lengths comparable to C−N single bonds (d = 1.51 Å) confirms the presence of a resonance hybrid structure in the anion.[168] Both C−N bonds are shorter than those observed in the crystal structure of Me$_2$Sn{N(CN)$_2$}$_2$ (table 67).[341]
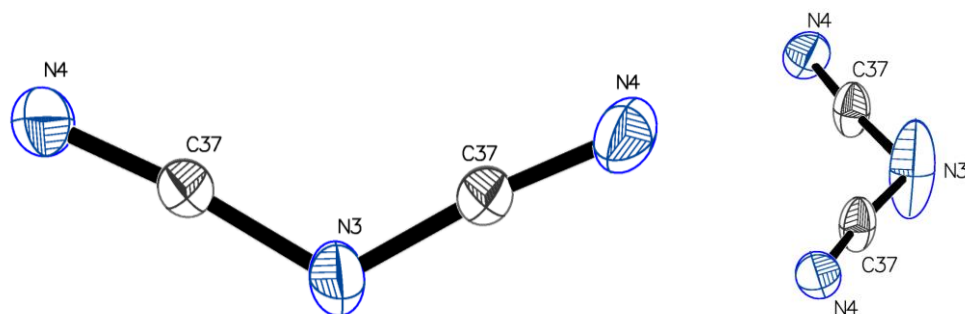
Figure 131. Molecular structure of one of the [N(CN)$_2$]$^-$ anions in the asymmetric unit of [PPN][N(CN)$_2$]. Left: vertical projection, right: lateral projection. Selected bond lengths (Å) and angles (°) : N(3)−C(37) 1.292(9), N(5)−C(38) 1.289(10), N(4)−C(37) 1.154(9), C(38)−N(6) 1.169(11) ; C(37)−N(3)−C(37) 119.0(10), C(38)−N(5)−C(38) 121.7(10), N(4)−C(37)−N(3) 173.9(8), N(6)−C(38)−N(5) 173.5(9).

cat$^+$	d(C−N$_t$) / Å	d(C−N$_c$) / Å	∠(C−N−C) / °	∠(N−C−N) / °	T / K	Refs.
Cs$^+$	1.126, 1.177	1.256, 1.310	123.94	171.74, 172.76	295	[349] [a]
NH$_4$$^+$	1.149(2), 1.156(2)	1.305(2), 1.319(2)	120.67(15)	173.12(18), 173.83(19)	200	[350]
PPh$_4$$^+$	1.1497(18), 1.1532(18)	1.3091(18), 1.3112(18)	119.60(12)	173.19(15), 173.28(15)	100	[348]
PPN$^+$	1.154(9), 1.169(11)	1.289(10), 1.292(9)	119.0(10), 121.7(10)	173.5(9), 173.9(8)	100	this work

Table 66. Comparison of crystallographically studied bond lengths and angles of the [N(CN)$_2$]$^-$ anion in cat$^+$[N(CN)$_2$]$^-$. N$_t$ and N$_c$ denote terminal and central nitrogen atoms, respectively. [a] no estimated standard deviations given.

cat$^+$	d(C−N$_t$) / Å	d(C−N$_c$) / Å	T / K	Refs.
[PPN][N(CN)$_2$]	1.154(9), 1.169(11)	1.289 (10), 1.292(9)	100	this work
Me$_2$Sn{N(CN)$_2$}$_2$	1.138(9), 1.125(7)	1.281(10), 1.297(8)	295	[341]

Table 67. Comparison of the [N(CN)$_2$]$^-$ anion in [PPN][N(CN)$_2$] with the dicyanamide ligand in Me$_2$Sn{N(CN)$_2$}$_2$.

The C-N bonds present in the dicyanamide anion are effective IR reporter groups and allow spectral analysis through the number and spectral position of bands associated with the C−N, C=N and C≡N stretching vibrations. Based on the trigonal planar geometry (and therefore C$_{2v}$ symmetry) of the dicyanamide anion observed in crystallographic studies, four IR-active CN stretching vibrations are predicted. The IR spectrum of [PPN][N(CN)$_2$] contains three intense bands in the spectral region populated by C≡N stretching vibrations (ν(CN) = 2228, 2188, 2128 cm^{-1}) and additional weak bands at 2168 and 2098 cm^{-1}. The identity of the highest band in this spectral region, assigned previously as the ν_{as}(C−N) + ν_s(C−N) combination band in other dicyanamide salts, could not be confirmed.[4] The observation of three ν(CN) bands is consistent with the reported spectra of NaN(CN)$_2$ (ν(CN) = 2285, 2232, 2166 cm^{-1}), where the fourth band assumed to converge with another (table 68).[4] The observation of a split band in the spectrum of NaN(CN)$_2$ recorded in this study ($\tilde{\nu}$ = 2234, 2229 cm^{-1}) is likely to arise from the resolution of the fourth additional band predicted from group theory. The asymmetric ν_{as}(C−N) stretching vibration for the dicyanamide anion, reported at 1344 cm^{-1} for NaN(CN)$_2$,

is masked by the characteristic bands of the $[PPN]^+$ cation in $[PPN][N(CN)_2]$. Two bands are observed in the region of the symmetric $\nu_s(C-N)$ vibrational band ($\tilde{\nu}$ = 906, 899 cm^{-1}), in a similar spectral position to the single $\nu_s(C-N)$ band observed in $NaN(CN)_2$ ($\tilde{\nu}$ = 930 cm^{-1}). An explanation or assignment of both bands are unclear. The presence and absence of spectral bands associated with C−N and C=N stretching vibrations, respectively, contrasts the bond lengths observed crystallographically and confirms the presence of a resonance-hybridised structure of $[N(CN)_2]^-$ in $[PPN][N(CN)_2]$.

$\tilde{\nu}$ / cm^{-1}			Assignment [4]
NaN(CN)$_2$ [4]	NaN(CN)$_2$ [a]	[PPN][N(CN)$_2$]	
2286	2285	−[b]	$\nu_{as}(C-N) + \nu_s(C-N)$
2232	2229, 2234	2228	$\nu_{as}(C\equiv N)$
2179	2183	2188	$\nu_s(C\equiv N)$
1344	1343	−	$\nu_{as}(C-N)$
930	930	906, 899	$\nu_s(C-N)$

Table 68. Summary of symmetric and asymmetric C−N bond stretching vibrations observed in the IR spectra of NaN(CN)$_2$ and [PPN][N(CN)$_2$]. [a] this work. [b] the position of the $\nu_{as}(C-N) + \nu_s(C-N)$ combination band could not be confirmed. – not observed.

8.2.2. Reaction of SiCl$_4$ with [N(CN)$_2$]$^-$

The reaction of SiCl$_4$ with $[N(CN)_2]^-$ was trialled to determine if any chloro-dicyanamido ligand exchange would occur on the silicon centre without the presence of stabilising and electron donating methyl or phenyl ligands. The reaction of SiCl$_4$ and NaN(CN)$_2$ resulted in the formation of a yellow suspension, indicative of a coordination polymer, and was not investigated further. Replication of the reaction with [PPN][N(CN)$_2$], instead of NaN(CN)$_2$, also formed a yellow suspension. The removal of all solvent from the yellow supernatant solution formed a sticky foam, which afforded [PPN][N(CN)$_2$] upon recrystallisation from MeCN. Recrystallisation of the yellow solid from CH$_2$Cl$_2$ formed a glassy yellow solid that was unsuitable for X-ray diffraction studies. Two weak $\nu(CN)$ bands were observed in the IR spectrum of the solid product which were inconsistent with [PPN][N(CN)$_2$]. A band at 1438 cm^{-1} was hypothesised to originate from a C=N bond, formed during the formation of a coordination polymer assumed to be of the type shown below (figure 132). However, the identity of the complex was unable to be determined further. Despite the prediction that the formation of insoluble AgCl would provide an additional thermodynamic driving force towards complete ligand exchange, the reaction between SiCl$_4$ and AgN(CN)$_2$ also formed a thick

yellow oil. Curiously, the IR spectrum of this product showed no bands associated with C=N bonds. However, the intense colour of the complex is consistent with the other silicon coordination polymers obtained and is indicative of a highly conjugated compound.

Each of the yellow intractable oils and solids are believed to be coordination polymers that contain bridging dicyanamido ligands between two or three coordination centres (forms III-VII), similar to those frequently observed in transition metal dicyanamido complexes. The intractable nature of the oil prevented further characterisation beyond IR spectroscopy and therefore the identity of the compound is unclear. Consequently, although an oligomeric structure can be proposed, no evidence is available to confirm or refute the accuracy of the proposition, including the number, bridging mode or denticity of the dicyanamido ligand/s. The formation of coordination polymers is analogous to the reported spontaneous oligomerisation of organodicyanamidosilanes, e.g. $Me_3SiN(CN)_2$, which forms a yellow coordination polymer at room temperature.[346]
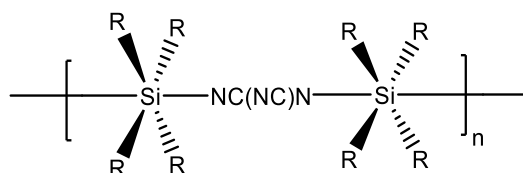
Figure 132. Proposed structure of dicyanamidosilane oligomers formed upon reaction of $SiCl_4$ with $[N(CN)_2]^-$. R = Cl or $N(CN)_2$.

$$SiCl_4 + ex.AgN(CN)_2 \xrightarrow{MeCN} \!\!\!\!\!\!\!/\!\!\!/\longrightarrow Si\{N(CN)_2\}_4 + 4AgCl$$

$$SiCl_4 + ex.AgN(CN)_2 \xrightarrow{MeCN} [Si\{N(CN)_2\}]_n + 4AgCl$$
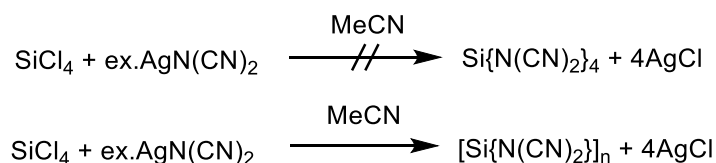
Scheme 91. Formation of silicon-dicyanamido coordination polymer from the reaction between $SiCl_4$ and $AgN(CN)_2$ in MeCN.

8.2.3. Attempted preparation of $Sn\{N(CN)_2\}_4$

The reaction of $Me_3SiN(CN)_2$ with SnF_4 appeared to be a promising synthetic strategy for the formation of dicyanamido tin complexes, owing to the large enthalpic and entropic driving force afforded by the formation of Si−F bonds in Me_3SiF. The analogous reactions between SnF_4 and trimethylsilylpseudohalides (TMS-Y) are key synthetic strategies to access neutral poly(pseudohalogenido) complexes of Sn(IV) as $Sn(Y)_4(py)_2$ (Y = N_3 or CN) and allows the preparation of anionic homoleptic poly(pseudohalogenido) stannates as $[Sn(Y)_6]^{2-}$ (Y = N_3, CN, CHN_4) through further reaction with ionic ligand transfer reagents.[102,103,169] Consequently, trimethyl- and triphenylsilyldicyanamide ($Me_3SiN(CN)_2$ and $Ph_3SiN(CN)_2$, respectively) were

prepared to investigate their reactivity towards SnF_4 as covalent dicyanamido transfer reagents (scheme 92) and compare their coordination ability to other pseudohalides.

$$SnF_4 + R_3SiN(CN)_2 \xrightarrow[\text{- }4R_3SiF]{} Sn\{N(CN)_2\}_4 \xrightarrow{PPN[N(CN)_2]} (PPN)_2[Sn\{N(CN)_2\}_6]$$

Scheme 92. Proposed formation of $[PPN]_2[Sn\{N(CN)_2\}_6]$ from $R_3SiN(CN)_2$ (R = Me, Ph) and SnF_4.

$Me_3SiN(CN)_2$ is reported as thermally unstable, polymerising at temperatures above -20 °C. By contrast, $Ph_3SiN(CN)_2$ is described as more stable at room temperature, presumably owing to the enhanced steric bulk of the aromatic aryl groups hindering oligomerisation.[346] Triphenylsilyldicyanamide was prepared as a colourless solid but turned pale yellow during prolonged storage under inert conditions, indicating that the thermal stability of the compound is limited even at ambient temperatures. Melting point studies exacerbated this colour change, in alignment with literature reports of the thermal instability of monomeric dicyanamidosilanes. The formation of a yellow solid at room temperature identified the oligomerisation of the dicyanamido ligand as the source of the yellow intractable products obtained from the reaction of $[N(CN)_2]^-$ with $SiCl_4$ described above. Oligomerisation resulted in the observation of additional $\nu(C\equiv N)$ bands in the IR spectrum versus literature values (table 69), further supporting the presence of coordination polymers containing dicyanamido ligands in varying multidentate coordination modes.[346] Recrystallisation afforded a colourless glassy solid unsuitable for crystallographic studies and the solid was unable to be investigated further.

	Observed (this work)	**Reported** [a]
$\nu(C\equiv N)$ / cm^{-1}	2256, 2228, 2188, 2106	2284, 2200

Table 69. Comparison of observed and reported $\nu(CN)$ bands of $Ph_3SiN(CN)_2$, recorded as nujol mulls.[a] reference [346].

The reaction of SnF_4 with both methyl- and phenyl-dicyanamido derivatives formed insoluble precipitates which displayed several $\nu(C\equiv N)$ bands in the IR spectrum that were similar to those reported for neutral $Me_2Sn\{N(CN)_2\}_2$.[341] Although IR spectroscopy confirmed that ligand exchange had occurred, inconsistencies in the position and number of $\nu(C\equiv N)$ bands suggested that the extent of ligand exchange varied between the two reactions and are hereby described as $SnF_n\{N(CN)_2\}_{4-n}$, where $n = 0-3$. The use of low temperatures for the reaction of $Me_3SiN(CN)_2$ may account for reduced ligand exchange versus the reaction of $Ph_3SiN(CN)_2$ performed at room temperature. The solid formed from the reaction of $Ph_3SiN(CN)_2$ was extremely insoluble in hot MeCN, THF and CH_2Cl_2 and appeared to decompose in hot ethanol.

In analogy to the preparation of $Sn(CN)_4(MeCN)_2$ from SnF_4 and TMSCN (see chapter 2), the low solubility of both complexes prevented further characterisation or determination of the extent of ligand exchange. The product obtained from the reaction with $Ph_3SiN(CN)_2$ was treated with $[PPN][N(CN)_2]$, in an attempt to prepare $[PPN]_2[Sn\{N(CN)_2\}_6]$ and indirectly confirm the formation of $Sn\{N(CN)_2\}_4$ in the previous step. However, no further reaction was observed and both the anion and the identity of the products formed from the reaction of the organodicyanamidosilanes with SnF_4 remain unknown.

8.2.4. Reaction of SnCl₄ with [PPN][N(CN)₂]

Owing to the enhanced stability of the organodicyanamido complexes of heavier group 14 coordination centres, an analogous reaction was attempted between $SnCl_4$ and $[PPN][N(CN)_2]$ to obtain $[PPN]_2[Sn\{N(CN)_2\}_6]$. A colourless, crystalline solid was isolated from solution, indicative of a monomeric complex instead of the brightly coloured oligomeric products obtained from the analogous reaction of $SiCl_4$. The IR spectrum of the crystalline solid contained three $\nu(C\equiv N)$ bands, all three of which were located at a lower spectral position than the $[N(CN)_2]^-$ anion. This is attributed to a reduction of electron density of the $C\equiv N$ bond in question, resulting in a weaker bond and a corresponding decrease in spectral position versus the uncoordinated dicyanamide anion. By contrast, coordination results in a slight decrease in the stretching frequency of the central $\nu(C-N)$ bands and hence these bands shift to higher spectral positions upon coordination. The same phenomenon has previously been observed in both transition metal and other main group (Pb, Sn) dicyanamido complexes of varying denticity.[4] The shift in spectral position of the $C-N$ and $C\equiv N$ stretching vibrations is more pronounced than observed in neutral $Me_2Sn\{N(CN)_2\}_2$ and is attributed to the formation of an anionic coordination complex (table 70). It is expected that the position of the stretching vibrations is affected by the coordination mode of the dicyanamido ligand, although this was unable to be quantified directly.

Assignment	$[PPN]_2[SnCl_4\{N(CN)_2\}_2]$	$Me_2Sn\{N(CN)_2\}_2$	$[PPN][N(CN)_2]$
$\nu_s(C-N)$ + $\nu_{as}(C-N)$ / cm^{-1}	2228 [a]	2290	– [a]
$\nu(C\equiv N)$ / cm^{-1}	2168, 2123	2210, 2170	2228, 2188
$\nu_{as}(C-N)$ / cm^{-1}	1438	1370	–
$\nu_s(C-N)$ / cm^{-1}	915	930	906, 899

Table 70. Summary of $\nu(CN)$ bands observed in the IR spectra of $[PPN]_2[SnCl_4\{N(CN)_2\}_2]$, $Me_2Sn\{N(CN)_2\}_2$ and $[PPN][N(CN)_2]$. Data for $Me_2Sn\{N(CN)_2\}_2$ obtained from reference [340]. [a] The location of the $\nu_s(C-N)$ + $\nu_{as}(C-N)$ combination band cannot be confirmed; – not observed.

Recrystallisation from acetonitrile afforded single crystals of the Lewis base adduct [PPN]$_2$[SnCl$_4$\{N(CN)$_2$\}$_2$]·MeCN as colourless blocks in space group *P*2$_1$/n (figure 133). A centre of inversion is located at the coordination centre and each anion contains a single crystallographically independent dicyanamido ligand. Attempts to prepare [PPN]$_2$[Sn\{N(CN)$_2$\}$_6$] through additional ligand exchange between [PPN]$_2$[SnCl$_4$\{N(CN)$_2$\}$_2$]·MeCN and [PPN][N(CN)$_2$] was unsuccesful. The reactivity and propensity of the dicyanamido ligand towards ligand exchange (or lack thereof) contrasts the azido, tetrazolato and cyanido complexes of Sn(IV), where ligand exchange can be driven to completion by treatment with an excess of ligand transfer reagent.[102,103,169] The absence of further reactivity confirmed that the dicyanamido ligand is weakly coordinating (and is indeed the weakest of the pseudohalides studied in this work) towards Sn(IV). Despite these synthetic challenges, the preparation of [PPN]$_2$[SnCl$_4$\{N(CN)$_2$\}$_2$] is the first example of a hypercoordinate poly(dicyanamido) complex of Sn(IV).
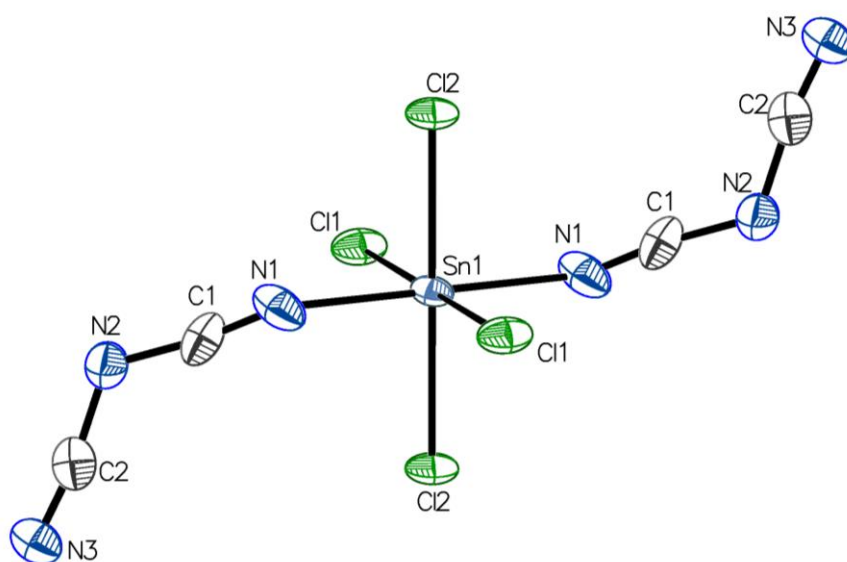
Figure 133. Crystal structure of the [SnCl$_4$\{N(CN)$_2$\}$_2$]$^{2-}$ anion in [PPN]$_2$[SnCl$_4$\{N(CN)$_2$\}$_2$]·MeCN. Selected bond lengths (Å) and angles (°) : Sn(1)−N(1) 2.170(3), N(1)−C(1) 1.094(4), N(2)−C(1) 1.315(5), N(2)−C(2) 1.348(5), N(3)−C(2) 1.130(4) ; C(1)−N(1)−Sn(1) 143.4(3), C(1)−N(2)−C(2) 123.0(3), N(1)−C(1)−N(2) 172.7(4), N(3)−C(2)−N(2) 172.0(4).

Interestingly, and in contrast to the majority of poly(dicyanamido) complexes containing transition metal centres, each dicyanamido ligand is monodentate and coordinates through a single terminal nitrogen atom (i.e., form II). This is in contrast to both Me$_2$Sn\{N(CN)$_2$\}$_2$ and also the majority of transition metal homoleptic dicyanamido complexes reported, which form as coordination polymers through bridging interactions of the dicyanamido ligands (i.e., form III in Me$_2$Sn\{N(CN)$_2$\}$_2$).[341] The presence of large, bulky cations adjacent to the

$[SnCl_4\{N(CN)_2\}_2]^{2-}$ anion precluded the formation of any dicyanamido bridging interactions through steric hindrance. The saturated Sn(IV) coordination centre, surrounded by ligands which are too strongly coordinated to be displaced by the weakly coordinating dicyanamido ligand, is an additional barrier to the formation of bridging interactions. Both the central nitrogen atom and non-coordinating CN group display interactions with the aromatic protons of $[PPN]^+$ (figure 134) but no short contact interactions invoving the tin centre are observed.
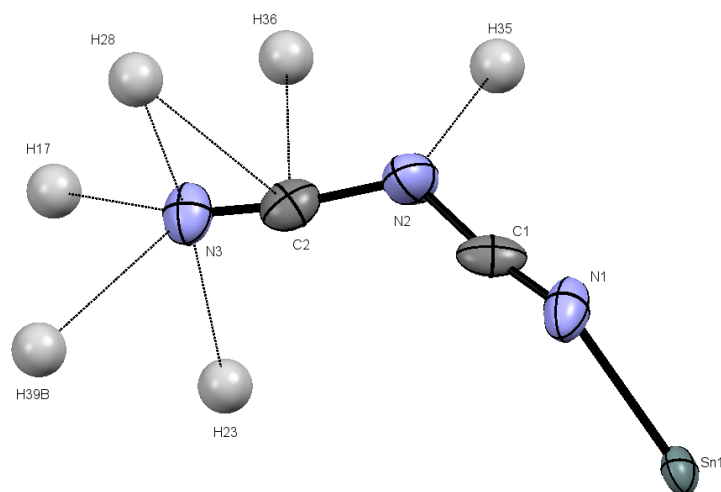
Figure 134. Short contacts between the dicyanamido ligand of $[Sn\{N(CN)_2\}_2Cl_4]^{2-}$ and the aromatic protons of $[PPN]^+$. All interactions shown are shorter than the sum of the van der Waal's radii for the respective atom pairs. All other atoms have been removed for clarity.

Analysis of the C−N bond lengths in the dicyanamido ligand allows the determination of the resonance form present in each ligand. The C−N bond of the coordinating CN group is shorter than that of the non-coordinating group in $[PPN][N(CN)_2]$. The bond lengths of both terminal and ligating CN bonds are consistent with a C≡N triple bond, whilst the central C−N bond lengths are more similar to a C=N double bond.[168] The range of bond lengths confirms the presence of a doubly- and triply-bonded resonance hybrid in each dicyanamido ligand (figure 135). The larger range of C−N bond lengths than both neutral $[Me_2Sn\{N(CN)_2\}_2]$ and the $[N(CN)_2]^-$ anion imply that the dicyanamido ligands in $[Sn\{N(CN)_2\}_2Cl_4]^{2-}$ are less hybridised. The Sn−N bonds in the $[Sn\{N(CN)_2\}_2Cl_4]^{2-}$ anion prepared in this work are shorter than those observed in the structure of $Me_2Sn\{N(CN)_2\}_2$ (d = 2.170(3) Å vs 2.289(5)−2.289(6) Å, respectively), whilst the Sn−Cl bonds (d = 2.3944(8)−2.4023(9) Å) are comparable to other hexachlorostannate anions in $(cat)_2[SnCl_6]$ (cat^+ = Ph_3PCl^+, d = 2.434 Å, cat^+ = NMe_4^+, d = 2.425 Å) recorded at higher temperatures (T = 203 K and 160 K, respectively).[351,352] Both N−C−N and C−N−C bond angles are comparable to those of the dicyanamide anion in $[PPN][N(CN)_2]$. These findings are summarised in table 71.
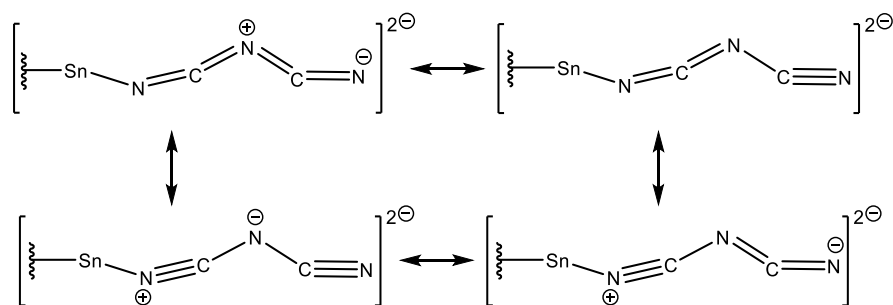
Figure 135. Schematic showing resonance forms of dicyanamido ligands in $[Sn\{N(CN)_2\}_2Cl_4]^{2-}$.

Bond Sequence	[PPN][N(CN)$_2$]	$[Sn\{N(CN)_2\}_2Cl_4]^{2-}$	$[Me_2Sn\{N(CN)_2\}_2]_n$
T / K	100	100	195
d(C$-$N$_t$) / Å	1.154(9), 1.169(11),	1.094(4), 1.130(4)	1.125(7), 1.138(9)
d(C$-$N$_c$) / Å	1.289 (10), 1.292(9)	1.315(5), 1.348(5)	1.281(10), 1.297(8)
Δd(C$-$N) / Å	0.120$-$0.138	0.185$-$0.254	0.143$-$0.172
$\angle$(C$-$N$-$C) / °	119.0(10), 121.7(10)	123.0(12)	124.2(8)
$\angle$(N$-$C$-$N) / °	173.5(9), 173.9(8)	172.0(4), 172.7(4)	171.8(7), 172.8(8)
Refs.	This work		[341]

Table 71. Comparison of bond distances in neutral, anionic and binary compounds containing the [N(CN)$_2$] unit. N$_t$ and N$_c$ denote terminal and central nitrogen atoms, respectively.

8.3. Conclusions and Outlook

The reactivity and coordination behaviour of the dicyanamido ligand varies widely between coordination centres of group 14. No homoleptic poly(dicyanamido) complexes of Si(IV) or Sn(IV) were formed. For the lighter silicon centre, the attempted preparation of hexakis(dicyanamido) silicate resulted only in intractable yellow oils consistent with oligomeric poly(dicyanamido)silanes of unknown identity. The ambidentate nature of the ligand appears to preclude the possibility of formation of a discrete, monomeric complex. Reaction with sterically hindered dicyanamido transfer reagents at low temperatures appears to negate this oligomerisation but no discrete complexes could be isolated. In contrast, the extremely weak coordination ability of the dicyanamido ligand towards Sn(IV) results in the formation of a monomeric Lewis base adduct which does not participate in ligand exchange. The weak coordination ability of the dicyanamido ligand, in combination with the presence of coordinatively saturated centres, appears to prevent bridging interactions of the dicyanamido ligands between adjacent coordination centres.

189

The variation in coordination behaviour of the ligand, in particular the weakly coordinating behaviour towards heavier centres of group 14, precluded further investigations into the formation of homoleptic dicyanamido coordination complexes. This work concludes that the dicyanamido group may be more suitable for cyclisation or derivatisation studies as an uncoordinated anion or functional group, instead of as a ligand in *p*-block coordination complexes.

Chapter 9. Conclusions

This work has investigated the coordination chemistry and reactivity of several known (CN^-, N_3^-, $[N(CN)_2]^-$) and unconfirmed (N_5^-) pseudohalides towards *p*-block coordination centres, specifically those of group 14 elements. The variation in reactivity and stability of the complexes investigated shows that despite the fulfilment of criterion as a critical requirement for classification as a pseudohalide, wide disparities in the chemical behaviour of different pseudohalides exist.

This work shows that of the pseudohalides studied, the azide anion is by far the strongest coordinating ligand, reacting readily with coordination centres in both high- and low-valent states. The many possible coordination modes of the dicyanamido ligand are anticipated to be responsible for the decreased reactivity towards the centres studied in this work versus the other pseudohalides. As such, studies concerning the group 14 dicyanamido coordination complexes remain more limited in comparison to the azido and cyanido analogues. The syntheses of novel poly(pseudohalogen) complexes provides further information about the reactivity of pseudohalides towards *p*-block coordination centres, similarly to the extensive investigations that exist for the *d*-block. An approximate series of coordination ability can be proposed for the pseudohalides studied in this work, where the azido ligand is observed to be the most likely to coordinate to the central elements investigated in this work and the dicyanamide anion the weakest (figure 136). The coordination ability of the N_5^- anion was unable to be investigated towards *p*-block centres owing to the inability to prepare analytically pure pentazolate salts. However, tentative identification of the N_5^- anion as a pseudohalide offers great potential for the preparation of new, metal-free nitrogen-rich complexes of *p*-block elements to complement the poly(azido) complexes already known.

$$N_3^- > CN^- > CHN_4^- > N(CN)_2^-$$

Strongly coordinating → Weakly coordinating
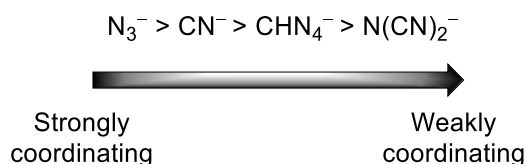
Figure 136. Approximate series ranking the coordination strength and ability of the pseudohalides studied in this work. As no *p*-block complexes containing N_5 ligands have been prepared, the position of N_5^- is unknown.

The choice of coordination centre also affects the reactivity and behaviour of the complexes. The formation of homoleptic complexes containing coordination centres in less-stable oxidation states, e.g. Pb(IV) and Ge(II), can facilitate further reactions which form unexpected

or unknown decomposition products. These products can be selectively formed through careful control of experimental conditions or ligand identities, e.g. exclusion of light or rate of heating. These studies provide further information about the reactivity of combinations of ligands and coordination centres. The preparation of $Pb(N_3)_4(bipy)$ demonstrates that the identity and oxidation state of the coordination centre can also influences the stability of a complex, including its sensitivity towards energetic stimuli, and demonstrates the varying effectiveness of stabilisation strategies towards pseudohalide complexes down group 14. In the case of the azido complexes of Ge(II), careful control of these conditions has proven beneficial through the apparent formation of compounds which conventionally require harsh synthetic conditions. These findings demonstrate that the enhanced reactivity of certain pseudohalide/coordination centre combinations can be advantageous in the formation of novel compounds, or afford desirable properties to others.
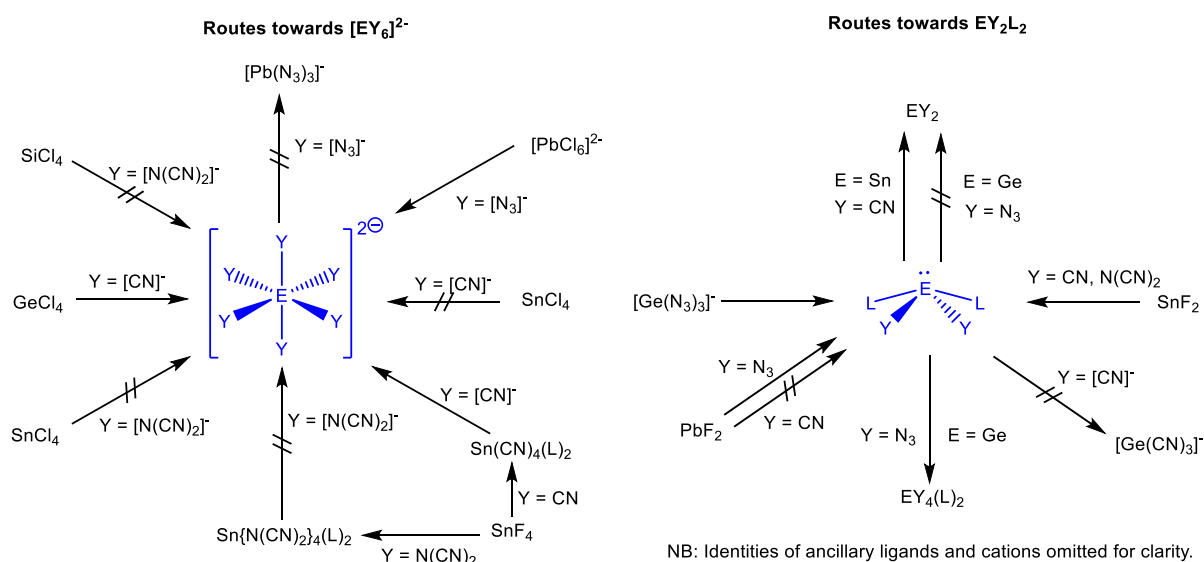
Scheme 93. Reactivity of pseudohalide ligands (Y) towards centres of E(IV) (top) and E(II) (bottom) investigated in this work. $Y = CN, N_3, N(CN)_2$; $E = Si-Pb$.

Anion	Criterion						
	A	**B**	**C**	**D**	**E**	**F**	**G**
CN^-	●	●	●	●	●	●	●
N_3^-	●	●	●	●	●		●
$[N(CN)_2]^-$	●	●	●	●	○		
N_5^-		●	●	●	○		

Table 72. Summary of criteria fulfilment (●) for the known and speculated pseudohalides featured in this work. ○ = unconfirmed compound.
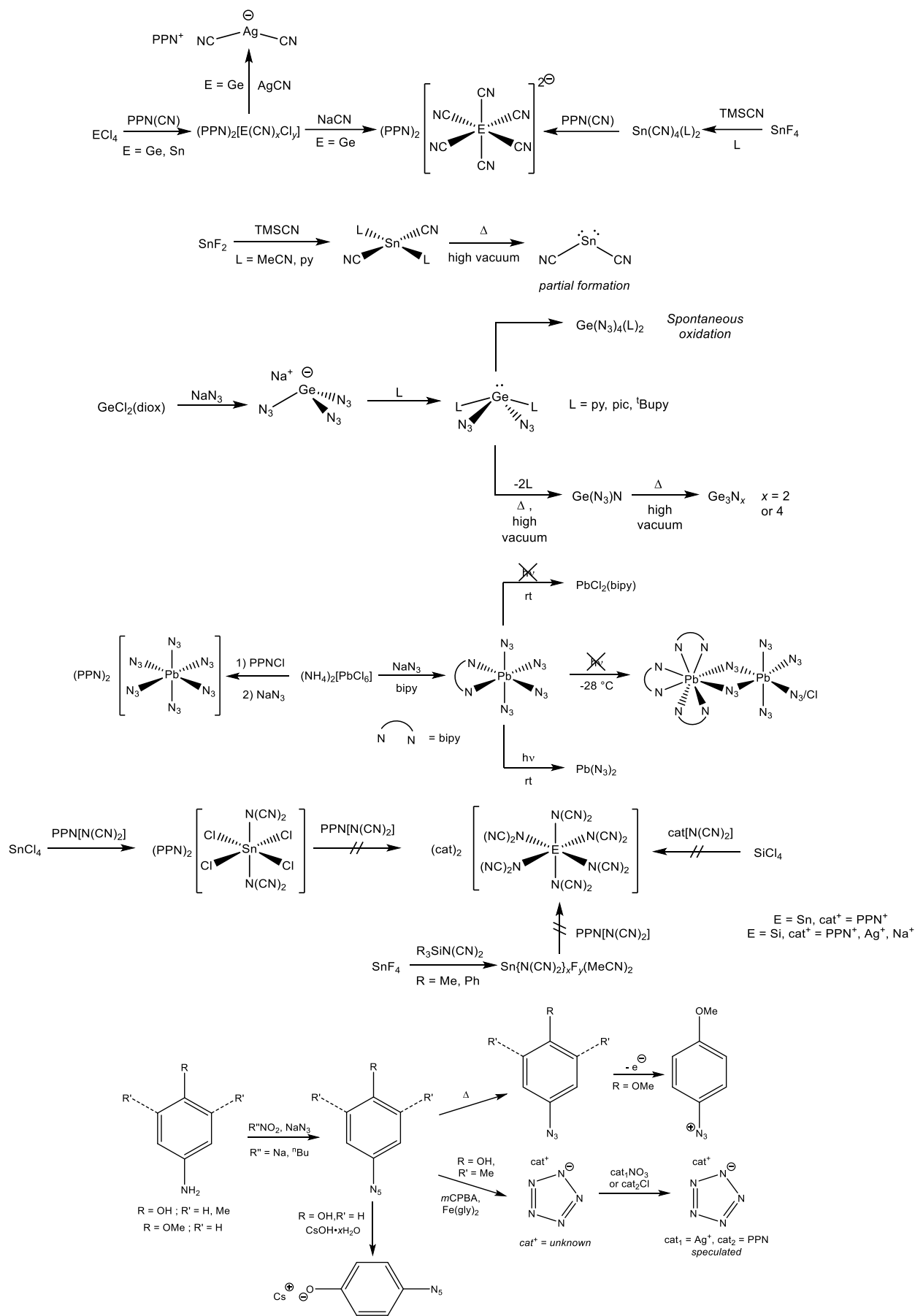
Scheme 94. Key syntheses undertaken in this work.

Chapter 10. Experimental Section

10.1. General Experimental Information

Unless otherwise stated, all reagents were purchased from commercial sources and used as received without further purification. All solvents were purchased from commercial sources and dried over CaH_2 (with the exception of MeOH, which was dried over sodium metal) before being trap-to-trap condensed into ampoules equipped with a Young's tap and stored under argon. Acetone was not dried before use and was degassed only. Deuterated solvents for NMR were dried and stored in the same fashion, apart from DMSO-d_6 which was used as received (VWR, sealed ampoules, 99.8% D, <0.02% H_2O). $SiCl_4$ (99%, Aldrich), $GeCl_4$ (99.9999% metals basis, Alfa Aesar) and $SnCl_4$ (99%, Aldrich) were dried over Na_2CO_3 and trap-to-trap condensed in the same fashion as the dry solvents. TMSCN (98%, Fluorochem) was recondensed into an ampoule before use and stored under the exclusion of light to prevent formation of a yellow impurity. NaN_3, AgCN, NaCN, KCN, SnF_2, $PbCl_2$, PbF_2 and PbF_4 and SnF_4 were dried at a minimum of 110 °C for a minimum of 3h under dynamic high vacuum before use. 2,2'-bipridyl (bipy) and 1,10-phenanthroline (phen) were purified by sublimation before use. TMS-N_3,[353] $Si(N_3)_4$(bipy),[243] [PPN]N_3,[320] $Pb(N_3)_2$ [218] and [PPN]CHN_4 [103] were prepared according to previously reported procedures. Ethereal HN_3 was prepared by Dr Rory Campbell.[237] Dry, ethereal HN_3 for reaction with $Ge(N_3)_2$(^{t}Bupy)$_2$ was dried over sicapent (P_2O_5 with indicator) and recondensed (under dynamic vacuum, at temperatures no higher than rt) into an ampoule before use. Solutions and samples for storage and crystallisation were cooled to −28 °C in a freezer or −10 °C in a fridge. The purities and sources of all reagents are listed in the appendix.

Unless otherwise stated, standard Schlenk technique was applied throughout, including use of high vacuum (ultimate vacuum ca. 4.0×10^{-2} mbar) and cylinder-grade argon. All solids were handled in an argon-filled glovebox. Transfer of solutions and filtrations were performed using stainless steel cannulas under positive argon pressure. Volumetric pipettes were used for addition of liquid reagents. Low temperature syntheses were performed using a cold bath filled with isopropanol/liquid N_2 or isopropanol/solid CO_2 mixtures in a Dewar flask, unless otherwise stated. Filtration of temperature sensitive samples was performed using a filter stick surrounded by a jacket containing cold solvent (figure 137, left). Solid samples were transferred using precooled spatulas and solutions were transferred by decantation using precooled volumetric pipettes. All manipulations were conducted under gentle argon flow to minimise

water condensation onto the samples. Thermally sensitive samples were stored in a Dewar vessel filled with dry ice or, alternatively, in a −80 °C freezer.

Analyte solutions of thermally-sensitive arylpentazoles (for IR/UV-visible spectroscopy) were prepared using precooled Schlenk tubes and dry solvent under argon flow to prevent condensation of water into the system. Cold solvent was transferred using precooled volumetric pipettes. Low-temperature spectra were recorded using a Specac cold cell, equipped with KBr cell windows and encased in an evacuated metal shroud containing NaCl windows (figure 137, right). The cell was cooled using dry ice in ^{i}PrOH. Background spectra were recorded using solvent cooled to the same temperature as the analyte solution. Once a solvent background had been recorded, a precooled syringe equipped with a Luer lock needle was used to draw up an aliquot of the analyte solution under argon flow. The needle was removed and the solution immediately pushed into the cell to displacing the solvent background solution, until the analyte was observed to flow out of the other side of the cell. At this point, the cell was sealed and quickly analysed with constant measurement and maintenance of internal cell temperature throughout. When measurements at higher temperatures were required, the cell was allowed to warm to these temperatures naturally to prevent thermal shock. The vacuum of the external shroud was periodically refreshed to prevent moisture condensation on the outer windows.

Unless otherwise stated, analyses were performed in air at room temperature. IR spectra were recorded with 8 scans per sample at 2 cm^{-1} resolution, between NaCl (solid) windows or a CaF$_2$ solution cell sealed with Teflon inserts, using a Bruker Tensor 27 FT-IR spectrometer operated by OPUS software. Unless otherwise stated, spectra of solid samples were recorded as a paraffin mull to improve spectral quality and prevent decomposition through air exposure. ATR-IR spectra were recorded with 4 scans per sample at a spectral resolution of 4 cm^{-1}, using a PerkinElmer UATR Two spectrometer equipped with PerkinElmer Spectrum software. Samples of air-sensitive solids were prepared in a glovebox. IR spectra of air-sensitive solutions were recorded by extraction of an aliquot of the analyte solution using a volumetric pipette under argon flow, followed by immediate transfer into an argon-filled spectroscopic solution cell. All paraffin mulling agent (hereby described as nujol) was stored over sodium. Nujol used for spectroscopy of air-sensitive samples was stored over sodium in a glovebox. IR spectra were visualised using Origin 6.0. Bands are described as s (sharp), br (broad), st (strong), sh (shoulder) and w (weak).

NMR spectra were recorded using a Bruker AV 400MHz, AVIIIHD 400 MHz or AVIIIHD 500 MHz spectrometers forming part of the NMR spectroscopy service at The University of Sheffield. ^1H and ^{13}C spectra were calibrated with respect to the residual solvent signals; ^{19}F, ^{14}N and ^{31}P NMR spectra are uncalibrated.[174,354] ^{119}Sn solution-state NMR spectroscopy was calibrated to a sample of $SnEt_4$ prior to measurement. The chemical shift of MeOD was used to check the operating temperature of the spectrometer prior to low-temperature measurements. Solid-state MAS NMR spectra were recorded on samples contained within a restricted rotor, exposed to air only during sample packing, using an AVIIIHD 500 MHz spectrometer at 500.13 MHz (^{13}C = 125.76 MHz) using a 4mm HX broadband MAS probe. ^{119}Sn solid-state NMR spectroscopy was performed on the same spectrometer with acquisition of 29200 scans and calibrated to a solid sample of commercial $SnCl_2$ (99%, Sigma-Aldrich). NMR spectra were visualised using TopSpin. The NMR spectra of $Pb(N_3)_4(bipy)$ in CH_2Cl_2 were recorded using an external lock solvent of DMSO-d_6, contained in a sealed NMR tube within the sample. Signals are described as s (singlet), d (doublet), m (multiplet) or combinations thereof.

Single crystal X-ray diffraction studies were undertaken at the X-ray Crystallography Service at The University of Sheffield. Studies were performed using a Bruker D8 Venture diffractometer equipped with a cooled (−15 °C) Photon 100 CMOS detector and a CuKα microfocus X-ray source. Alternatively, structures were recorded using a Bruker SMART APEX-II or Kappa diffractometer equipped with a cooled (−50 °C) CCD detector and MoKα radiation from a sealed tube X-ray source. All measurements were carried out following cooling of the crystal, mounted on a MiTiGen microloop, using a cryogenic N_2 gas stream set to 100 or 296 K. Crystals for studies were picked from solution in an argon gas stream and immediately immersed into paraffin oil on a glass slide, or transferred into paraffin oil on a glass slide in a glovebox. Particularly air-sensitive crystals were transferred to the mounting area in an argon-filled container to minimise hydrolysis. Crystals of thermally sensitive arylpentazoles were transferred directly onto a glass slide containing Fomblin-Y (L-Vac) oil that had been precooled by solid CO_2 contained in a Petri dish (figure 138) for mounting. An LED polarising light microscope was used for thermally sensitive crystals in order to reduce the amount of local heating on the slide. In all cases, mounted crystals were immediately transferred to the goniometer to prevent degradation by air exposure or thermal decomposition. Data was processed using shelxtl and Olex2-1.2 and visualised using Mercury 4.1.0 and Olex2-1.2, with all ellipsoids plotted at 50% probability.[2-4,8] Data was corrected for absorption using empirical methods (SADABS) based on symmetry equivalent reflections combined with

measurements at different azimuthal angles.[5,6] The crystal structures were solved and refined against F^2 values using shelxt for solution and shelxl for refinement, accessed *via* the Olex2 or shelxtl programmes.[2,3,7,8] Non-hydrogen atoms were refined anisotropically. Hydrogen atoms were placed in calculated positions with idealized geometries and then refined by employing a riding model and isotropic displacement parameters. Short-contact and hydrogen bonding interactions were calculated using the standard definitions in Mercury 4.1.0. The standard definition for a short contact in the programme is defined as an interaction distance which is shorter than the sum of the van der Waal's radii, i.e. $d < \Sigma_r(vdW)$. A hydrogen bond is defined as a donor-acceptor distance that is shorter than the sum of the van der Waal's radii by 5.00 Å, i.e. $\Sigma_r(vdW)-5.00$ Å. The crystallographic datasets of $[PPN]_2[Ge(CN)_6]$, $[PPN]_2[Sn(CN)_6]$ and $[PPN][Ag(CN)_2]\cdot MeCN$ have been deposited in the Cambridge Crystallographic Structural Database with deposition numbers 1820360, 1820145 and 1856451, respectively. A discussion of the treatment of disordered structures can be found in the Appendix.

Powder X-ray diffraction data of $Ge(N_3)_2(^tBupy)_2$ was recorded on a Rigaku Miniflex benchtop powder diffractometer equipped with a Mo-K$_\alpha$ radiation source. The sample was loaded and sealed into an air-sensitive sample holder in a glovebox, then transferred to the diffractometer. Analysis was performed at room temperature between $3°<\theta<50°$ at a step angle of $2°$. The obtained data was prepared as input files using jEdit and Pawley fitting performed using TOPAS.[355–357] The unit cell parameters obtained from the crystallographic analysis of $Ge(N_3)_4(^tBupy)_2$ were used as a starting point. This refinement used 445 parameters (12 background, 1 zero error, 5 profile, 6 unit cell and 421 reflections), resulting in weighted R-factors (R_{wp} and $R_{wp'}$) of 0.0178 and 0.1085, respectively.[194] The powder pattern of $Ge(N_3)_4(^tBupy)_2$ was predicted from the crystallographic dataset using Mercury 3.10.3.

Raman spectra were recorded using a Renishaw inVia Raman microscope equipped with a ca. 3 μm diffraction grating. Samples were analysed with a 325 nm, 2 mW laser with an accumulation time of 30 s and 10 accumulations. Further analysis at 514.5 nm was recorded using a 1 mW laser with 30 accumulations with an accumulation time of 30 s. UV-visible absorption spectra were recorded at room temperature, unless otherwise stated, using a Cary 50 Bio instrument and an approximate sample concentration of ca. 1 mmol mL^{-1}. Low temperature measurements were recorded using the same instrument. Elemental analysis for detection of C, H and N was performed at The University of Sheffield using an Elementar Vario MICROcube CHN/S analyser. Air-sensitive samples were analysed immediately

following sample preparation, in order to minimise air exposure. Analysis of $Ge(N_3)N$ was performed using the same analyser with an oxygen purge and the use of a tungsten catalyst to ensure complete combustion. Chlorine determination was performed by hand using Schöniger analysis. Thermogravimetric (TGA) studies were performed using a PerkinElmer Pyris 1 combustion analyser equipped with a ceramic crucible. Samples were loaded and analysed under a stream of N_2 at an approximate flow rate of 60 mL min^{-1}. Preparative HPLC was performed using a Varian Prostar setup, equipped with an autosampler, visualiser, pumps and fraction collector (models 410, 320, 210 and 701, respectively). A Waters XBridge Prep C18 5μm column (ø = 19 mm, l = 250 mm) was used for all samples and the chromatogram outputs visualised at 365 nm. The setup was purged with 3:1 MeOH:H_2O prior to use. Melting points were recorded on a Büchi melting point apparatus and are uncalibrated. A Carbolite tube furnace was used for the controlled heating of samples of $Ge(N_3)N$. Mass spectrometry was performed at the Chemistry Mass Spectrometry Facility at The University of Sheffield. Samples for ESI−TOF measurements were introduced via direct infusion into a Micromass LCT spectrometer. Accurate mass spectrometry was performed using an Agilent Technologies 6530 Accurate Mass Q-TOF LC/MS instrument and the sample introduced using a loop injector at an approximate flow rate of 20 μL min^{-1}. Solvents used for analysis are stated alongside the data for each compound in question. All mass spectral data is reported to 0 decimal places.

Cyclic voltammetry was performed using an Autolab galvanostat and a PGSTAT100 differential electrometer amplifier. The electrochemical cell was equipped with a glassy carbon working electrode, Pt wire counter electrode and an Ag wire reference electrode. Ferrocene was added at the end of each analysis as an internal calibrant and all electrochemical potentials and voltammograms discussed here are referenced to Fc/Fc$^+$. All voltammograms in this work were recorded using oxidative sweeps (i.e., to positive voltages first) at a scan rate of 100 mV s^{-1} on sample solutions of ca. 5 mM concentration. All solvents used for electrochemistry were dried in the same fashion as described above, before being exposed to air and moisture only for analysis. All samples were prepared under inert conditions in order to minimise the amount of water and oxygen present. Twice-recrystallised and dried $NH_4[PF_6]$ was used as the electrolyte, which was dried in an oven immediately prior to use. Cylinder-grade oxygen-free nitrogen was used as a purge gas and passed through a bubbler containing the appropriate analysis solvent before reaching the cell. Voltammograms were recorded using NOVA 1.10 software.

Spectroelectrochemistry was performed at Reading University using a Bruker 70v FT-IR spectrometer connected to an external Bio-Rad FTS 60 MCT detector. Electrolysis was controlled using a PalmSens EmStat3 potentiostat. Spectra and voltammograms were visualised using Bruker OPUS and PSTrace software, respectively. The samples were contained in a cryostatted low-temperature Optically Transparent Thin-Layer Electrochemistry (OTTLE) cell (Spectroelectrochemistry Reading), containing platinum minigrid working and counter electrodes and a silver wire pseudo-reference electrode, between CaF_2 windows.[358] Samples were prepared at an approximate concentration of 4 mM (PrCN) or 9 mM (CH_2Cl_2), in ca. 6 mL of solvent and an approximate electrolyte concentration of 0.5 mmol mL^{-1}. CH_2Cl_2 and PrCN were dried over CaH_2 or sodium wire, respectively, prior to use. The electrolyte, $NH_4[PF_6]$, was twice-recrystallised from absolute ethanol before being dried under vacuum at 80 °C overnight before use. All measurement temperatures are stated in the discussion of data.
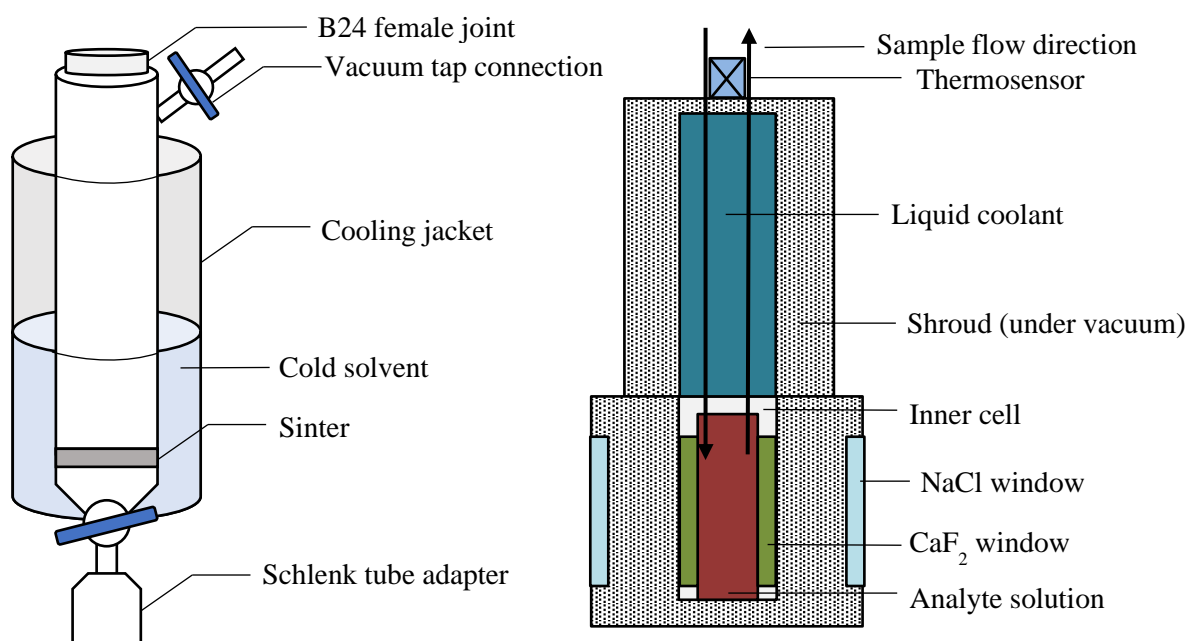
Figure 137. Schematic showing setup for cold filtrations (left) and IR/UV-visible solution spectroscopic analysis (right) of thermally sensitive arylpentazoles.
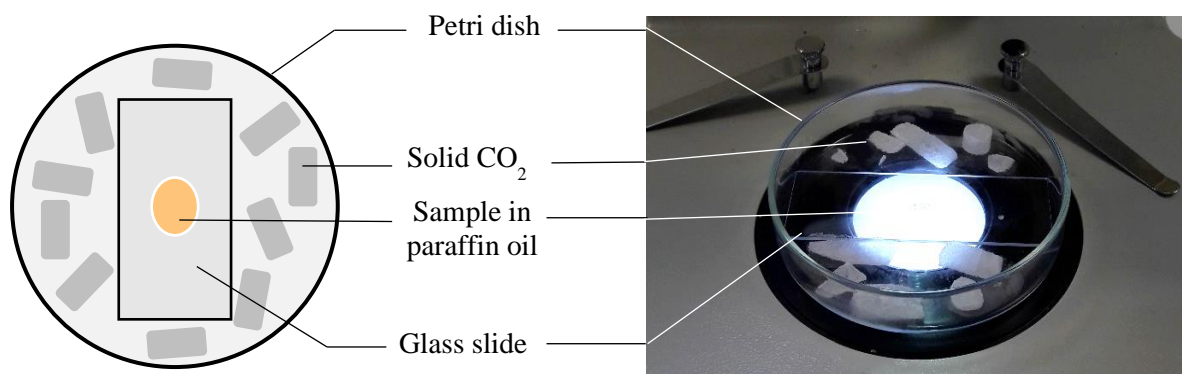
Figure 138. Schematic (left) and photograph (right) of setup for mounting of thermally sensitive crystals.

10.2. Group 14 cyanido complexes

10.2.1. [PPN]Cl

Adapted from a preparative procedure by Martinsen and Songstad.[320]

In a three-necked flask connected to distillation apparatus, triphenylphosphine (196.456 g, 0.75 mol, 1.44 eqs) was suspended in 1,1,2,2-tetrachloroethane (310 mL) and the resulting suspension stirred for 20 mins at rt, resulting in the complete dissolution of all solid. The flask was immersed into an oil bath and heated to 50 °C. PCl_5 (109.068 g, 0.52 mol, 1.00 eq) was added to the reaction solution in portions over the course of 10 minutes, allowing for complete dissolution of each portion before the addition of the next. During addition, the temperature of the solution increased to 68 °C. Once addition was complete, the solution was heated to 115 °C, resulting in the formation of a dark brown solution, and the apparatus connected to a high vacuum line to remove PCl_3 by distillation under static vacuum at a solution temperature of 109 °C and a head temperature of 81°C. After the collection of ca. 50 mL of distillate some 30 mins later, a visible change in the density of the solution entering the trap signified the conclusion of PCl_3 distillation. The distillation sump was allowed to cool to 65 °C and the distillation apparatus exchanged for a reflux condenser connected to a three-away adapter attached to an argon inlet and two water-filled Dreschel bottles. $NH_2OH \cdot HCl$ (18.286 g, 0.27 mmol, 0.51 eqs) was added, the system purged with argon and the orange suspension heated to 160 °C for 8 h. The resulting dark orange/red suspension was allowed to cool to rt and decanted into a beaker of hexane (1.5 L), resulting in the formation of a pale yellow turbid organic layer and a dark orange aqueous layer. The aqueous layer was separated and quickly extracted with hexane (3 x 100 mL); this extraction step results in the rapid formation of precipitate, hindering separation. The solid was treated with hexane:ethyl acetate (6:1, 720 mL total), manually stirred and filtered. The filter residue was washed with ethyl acetate (3 x 120 mL) and hexane (3 x 100 mL) and dried on the filter. The off-white filter residue was subsequently dissolved in 250 mL hot (85 °C) water, the solution heated to 80 °C and treated with 50 mL 35% HCl to induce precipitation. The suspension was allowed to cool, the filter residue isolated by filtration and the filtrate discarded. The filtrate was washed with HCl (35%, 3 x 15 mL) and H_2O (3 x 50 mL), dried for 10 minutes. The cream solid was washed further with diethyl ether (3 x 50 mL) and dried on the filter for a further 50 minutes. This gave crude [PPN]Cl as a cream solid.

The crude product was dissolved in 100 mL boiling CH_2Cl_2 and treated with THF (1 L). The solution was cooled to −28 °C for 17 h, resulting in the formation of colourless crystals contained in an orange solution. The crystals were isolated by filtration, washed with ice-cold

THF (3 x 50 mL) and dried on the filter for 10 mins and in air for a further 1h. The semi-dry solid was transferred into two Schlenk tubes, immersed into an oil bath heated to 150 °C and dried under dynamic high vacuum for 17 h. This gave [PPN]Cl (86.365 g, 56%) as a cream solid. M.p. = 266-269 °C. IR(nujol, cm^{-1}) $\tilde{v}$ = 3638, 3052, 2711, 2023, 2009, 1989, 1975, 1921, 1898, 1836, 1816, 1799, 1776, 1691, 1617, 1591, 1577, 1486, 1441, 1313, 1278, 1190, 1116, 1071, 1028, 994, 943, 861, 753, 696 . NMR (^{1}H, CDCl$_3$, ppm) δ = 7.85-7.31 (m, [PPN]$^+$). NMR (^{13}C, CDCl$_3$, ppm) δ = 134.0 (s), 132.0 (m), 129.6 (m), 129.7 (dd) {all [PPN]$^+$}. NMR (^{31}P, CDCl$_3$, ppm) δ = 21.02 ({Ph$_3$$P$}$_2$N).

10.2.2. [PPN]CN

Adapted from a preparative procedure by James.[147]

[PPN]Cl (10.546g, 18.37 mmol, 1.00 eq) was dissolved in 20 mL dry MeOH with stirring and heated to 45 °C to aid dissolution. The solution was cooled to rt and transferred into a Schlenk tube containing KCN (1.997g, 32.20 mmol, 1.75 eqs) suspended in MeOH (10 mL). A white solid is observed upon addition of [PPN]Cl to the suspension. The Schlenk tube was immersed into an oil bath and heated with stirring at 45 °C for 10 mins, then cooled in ice for 1 h. This yielded a white solid contained in a brown supernatant solution. The supernatant solution was filtered onto a fresh portion of KCN (0.897 g, 14.47 mmol, 1.27 eqs), heated to 45 °C for a further 10 mins and cooled in ice for 45 mins. The white solid precipitate was subsequently isolated by filtration and discarded. The pale brown filtrate was dried under dynamic vacuum at rt to remove all solvent, forming a white solid which was redissolved in degassed acetone (20 mL). The addition of diethyl ether counter-solvent (ca. 50 mL) resulted in the precipitation of a white solid. When substantial solid precipitation was observed, trituration was halted and the suspension was cooled to −28 °C for 17 h. The white crystalline solid was isolated by filtration. The Schlenk tube containing the filter residue was immersed into an oil bath set to 65 °C and dried under dynamic vacuum for 5.5 h. This yielded [PPN]CN (8.814 g, 85%) as a white solid. Treatment of the isolated filtrate with further acetone, followed by cooling to −28 °C for 17 h, can result in further crops of [PPN]CN (0.786 g, 7.6%) that are spectroscopically identical to the first. IR (nujol, cm^{-1}) $\tilde{v}$ = 3169, 3146, 3049, 2803, 2056, 1901, 1824, 1776, 1587sh, 1577 1481, 1435, 1264, 1179, 1168, 1113, 1057, 1040sh, 1025sh, 996sh, 801, 767, 748, 691, 550. IR (MeCN, cm^{-1}) $\tilde{v}$ = 2058w (v(CN)).

10.2.3. [PPN]$_2$[Ge(CN)$_x$(CN)$_y$] $(x + y) = 6$

[PPN]CN (3.368 g, 5.97 mmol, 6.80 eqs) was dissolved in 15 mL MeCN and GeCl$_4$ (0.10 mL, 0.88 mmol, 1.00 eq) added. This addition resulted in the almost instantaneous precipitation of white solid from the previously clear solution. The suspension was stirred at rt for 17 h, resulting in a thicker white suspension. The white solid (0.692 g) was isolated by filtration, dried under vacuum and combined with a fresh portion of [PPN]CN (2.466 g, 4.37 mmol, 5.0 eqs) and the mixture resuspended in 10 mL MeCN. The suspension was immersed into an oil bath and heated to 60 °C for 68 h, upon which almost all solid dissolved after ca. 10 minutes. The solution was allowed to cool to rt and the white solid (ca. 1.86 g) isolated by filtration and recrystallised from the minimum volume (ca. 20 mL) of warm MeCN. Slow cooling to −28 °C in a Dewar flask containing ^{i}PrOH resulted in colourless block crystals, which were isolated by filtration. This intermediary complex was reacted with further [PPN]CN (1.647 g, 2.92 mmol, 2.05 eqs with respect to the intermediary compound) following the same procedure described above, with heating for 96 h. This gave large block-shaped crystals of [PPN]$_2$[Ge(CN)$_x$Cl$_y$] $(x + y = 6$, 0.845 g). Microanalysis for the compound correlates closest to [PPN]$_2$[Ge$_{0.07}$(CN)$_{0.74}$Cl$_{0.52}$(MeCN)$_{0.89}$]; Elem. Anal. Cald C, 74.91; H, 5.33; N, 5.98; Cl, 2.98% ; found C, 74.87; H, 5.48; N, 5.94 ; Cl, 2.95%. IR (nujol cm^{-1}) $\tilde{\nu}$ = 3175, 3157, 3146, 3077, 3064, 3055, 3037, 3023, 3013, 2992, 2799, 2293, 2248, 2215br, 2161, 2155, 2053, [1977, 1922, 1906, 1827, 1779, 1687, 1616]br, 1588, 1574, 1481, 1457, 1437, 1435, 1261, 1184, 1164, 1113, 1055, 1027, 998, 938, 850, 797, 759, 748, 690, 664, 616, 550, 530. NMR (^{1}H, CD$_3$CN, ppm) δ = 7.69-7.64 (m), 7.61-7.55 (m), 7.50-7.45 (m). NMR (^{13}C, CD$_3$CN, ppm) δ = 141.7 (s, CN), 140.2 (s, CN), 134.5 (s, PPN), 133.2 (m, PPN), 130.3 (m, PPN), 128.2 (dd, PPN).

10.2.4. Attempted preparation of Ge(CN)$_4$

To a solution of GeCl$_4$ (0.1 mL, 0.88 mmol, 1.00 eq) in MeCN (15 mL), TMSCN (0.44 mL, 3.47 mmol, 3.94 eqs) was added and the solution stirred for 17 h at rt. A further 0.04 mL of TMSCN was added. The Schlenk tube was immersed into an oil bath set to 60 °C and heated for a further 31.5 h. IR spectroscopy of the resulting yellow solution showed no change in the concentration of TMSCN nor the formation of new ν(CN) bands associated with complex formation, and the reaction was discarded.

10.2.5. [PPN]$_2$[Ge(CN)$_6$]

A solid mixture of [PPN]$_2$[Ge(CN)$_x$Cl$_y$] $(x + y = 6)$, [PPN]CN and [PPN]Cl (0.459 g, max. 0.35 mmol of [PPN]$_2$[Ge(CN)$_x$Cl$_y$] {assuming $x = 5$}) was combined with NaCN (0.186 g, 3.80

mmol, 10.86 eqs) and suspended in 15 mL MeCN. The resulting suspension was immersed into an oil bath and heated to 65 °C for 196 h, forming a white suspension which was filtered. The filter residue, assumed to be NaCl, was discarded and the filtrate concentrated under dynamic vacuum. At the onset of precipitation, the suspension was warmed in hot air to redissolve the precipitate then cooled to −28 °C. This gave colourless block-shaped crystals of similar appearance to the [PPN]$_2$[Ge(CN)$_x$Cl$_y$] precursor, contained in a pale yellow solution. The crystals were isolated by filtration to give analytically pure [PPN]$_2$[Ge(CN)$_6$] (0.196 g, 82% with respect to GeCl$_4$) as colourless block-shaped crystals. M.p. 188 °C (decomp.). Elem. Anal. Cald. for C$_{78}$H$_{60}$N$_8$P$_4$Ge (1305.92 g mol^{-1}) C, 71.74; H, 4.63; N, 8.58; Cl, 0%. Found C, 71.37; H, 4.66; N, 8.63; Cl, <0.3 %. IR (nujol, cm^{-1}) $\tilde{v}$ = 3173, 3145, 3079, 3063, 2251(br), 2217(br), 2165, 2159, 1985, 1918, 1906, 1824, 1780, 1684, 1613, 1588, 1575, 1482, 1439, 1436, 1316, 1301, 1284, 1265, 1185, 1162, 1116, 1109, 1073, 1027, 997, 795, 757, 750, 695, 689, 663, 617, 550, 534. IR (MeCN, cm^{-1}) v(CN) = 2161. NMR (^{1}H, CD$_3$CN, ppm) δ = 7.45-7.71 (m, PPN). NMR (^{13}C, CD$_3$CN, ppm) δ = 128.2 (d, PPN), 130.3 (m, PPN), 133.2 (m, PPN), 134.6 (s, PPN), 140. 0 (s, CN). ^{73}Ge NMR spectra were unable to be recorded owing to the lack of sensitivity of the spectrometer probe for this nucleus. MS (ESI$^-$, MeCN) m/z = 245 (100%), 141 (81%), 123 (17%), all hydroxy-germanium decomposition products; no signals attributed to [PPN]$_2$[Ge(CN)$_6$] observed. MS (ESI$^+$, MeCN), m/z = 538 ([PPN]$^+$, 100%).

10.2.6. [PPN][Ag(CN)$_2$]

[PPN]$_2$[Ge(CN)$_x$Cl$_y$] (ca. 0.633 g, 0.48 mmol assuming x = 5, 1.00 eq) was combined with AgCN (0.574 g, 4.29 mmol, 4.89 eqs). The mixture was suspended in 20 mL MeCN and the Schlenk tube immersed into an oil bath and heated to 65 °C for ca. 10 h. During this time, the white suspension became more finely divided. Once cooled to rt, the colourless supernatant solution was isolated and the solid filter residue discarded. The filtrate solution was concentrated under dynamic vacuum until the onset of precipitation (ca. 5 mL), the precipitate redissolved by warming in hot air. Cooling to −28 °C resulted in colourless block-shaped crystals of [PPN]$_2$[Ag(CN)$_2$]·MeCN (0.448 g) which were isolated by filtration. IR (nujol, cm^{-1}) $\tilde{v}$ = 3058, 2326, 2291, 2250, 2217, 2169 (MeCN), 2159 (v(CN)), 2148 (MeCN), 2135 (v(CN)), 2052, 1986, 1913br, 1824br, 1779, 1680br, 1617br, 1588, 1574, 1482, 1434, 1315, 1297, 1282, 1248, 1179,1 163, 1115, 1100, 1074, 1070, 1026, 997, 977, 933, 917, 846, 840, 805, 797, 761, 750, 745, 690, 667, 616, 553, 550, 533.

10.2.7. Sn(CN)₄(L)₂ (L = MeCN, py)

SnF_4 (1.00 eq) was suspended in 15 mL ancillary ligand (MeCN or py) and TMSCN (4.00 eqs) added by volumetric pipette. The suspension was stirred for 17 h at rt, resulting in a noticeably thicker suspension. The cream solid was isolated by filtration and the filtrate discarded. The filter residue was dried under vacuum to give $Sn(CN)_4(L)_2$ (78−82%) as highly air-sensitive cream solids. Exposure to air results in an immediate discolouration to a yellow solid and the release of HCN and ancillary ligand. The extreme air sensitivity of the solid precluded reliable elemental analyses.

Sn(CN)₄(MeCN)₂: 0.261 g, 1.34 mmol of SnF_4, 0.67 mL, 5.36 mmol , 4.00 eqs TMSCN gives $Sn(CN)_4(MeCN)_2$ (0.234 g, 78%). IR (nujol, cm⁻¹) $\tilde{\nu}$ = 3320br, 2320, [2290, 2241br (MeCN)], 2182 ν(CN), 1593br, 1260, 1207, 1169, 844, 804. Elem. Anal. Cald. for $C_8H_6N_6Sn$ (304.78 g mol⁻¹) C, 31.50; H, 1.98; N, 27.57 %. Found C, 5.46; H, 0; N, 5.41.

Sn(CN)₄(py)₂: 0.270 g, 1.39 mmol of SnF_4, 0.72 mL, 5.68 mmol, 4.09 eqs TMSCN gives $Sn(CN)_4(py)_2$ (0.434 g, 82%). M.p. 270 °C (decomp.). IR (nujol, cm⁻¹) $\tilde{\nu}$ = 3335br, 3221, 3119, 3110, 3093, 3080, 3053, 3033, 2165 (ν(CN)), 2025, 1989, 1954, 1918, 1880, 1842, 1808, 1704, 1699, 1671, 1629, 1610, 1601, 1572, 1485, 1447, 1396, 1353, 1299, 1251, 1210, 1157, 1150, 1091, 1061, 1046, 1018, 1011, 868, 760, 705, 689, 648. NMR (¹H, DMSO-d₆, ppm) δ = 8.57 (m, py), 7.78(m, py), 7.38 (m, py), 6.38 (s, attributed to *H*CN). NMR (¹³C, DMSO-d₆, ppm) δ = 149.6 (s, py), 136.2 (s, py), 124.0 (s, py), 113.8 (s, *C*N). NMR (¹⁹F, DMSO-d₆, ppm) no resonance observed. A recrystallisation attempt from DMF resulted in the complete dissolution of all solid and no crystalline material could be isolated.

10.2.8. Attempted preparation of Sn(CN)₄

$Sn(CN)_4(MeCN)_2$ (164 mg) was placed into a Schlenk tube and placed under dynamic vacuum at rt until a constant pressure was achieved (2.5×10^{-2} mbar). The tube was then immersed into an oil bath and heated under dynamic vacuum at 45 °C for 5.5 h. No decrease in mass was observed and the IR spectrum of the solid remained unchanged.

10.2.9. [PPN]₂[Sn(CN)ₓ(CN)ᵧ] (x + y) = 6

$SnCl_4$ (0.1 mL, 0.88 mmol, 1.00 eqs) was added to a solution of [PPN]CN (3.488 g, 6.17 mmol, 7.01 eqs) in 15 mL MeCN. The solution was immersed into an oil bath and heated to 60 °C for 133 h, resulting in a pale brown solution. The solution was concentrated under dynamic vacuum until the onset of precipitation, warmed in hot air to redissolve all precipitate, then cooled to −28 °C. This gave colourless crystals contained in a pale brown supernatant solution,

which were isolated by filtration and the filtrate discarded. Recrystallisation from the minimum volume of MeCN (ca. 10 mL) by cooling to −28 °C in a Dewar flask filled with ^{i}PrOH, gave colourless block-shaped crystals of [PPN]$_2$[Sn(CN)$_6$] and [PPN]$_2$[Sn(CN)$_5$Cl]. Microanalysis for the compound correlates closest to [PPN]$_2$[Sn(CN)$_{5.55}$Cl$_{0.45}$] ; Elem. Anal. Cald. for C$_{77.5}$H$_{60}$Cl$_{0.45}$N$_{7.55}$Sn (1356.21 g mol^{-1}) C, 68.68; H, 4.46; N, 7.80; Cl, 1.18%; found C, 68.52; H, 4.52; N, 7.53; Cl, 1.00%. IR (nujol, cm^{-1}) ṽ = 3175, 3143, 3081, 3064, 3057, 3038, 3025, 2792, 2786, 2251, 2218, 2157, 2152, 2050(br), 1985, 1915, 1898, 1833, 1806, 1694, 1615, 1588, 1575, 1483, 1439, 1318, 1308, 1294, 1276, 1260, 1253, 1186, 1181, 1171, 1165, 1114, 1069, 1028, 998, 797, 755, 692, 664, 616, 550, 531. NMR (^{1}H, CD$_3$CN, ppm) δ = 8.05-7.11 (m, PPN). NMR (^{13}C, CD$_3$CN, ppm) δ = 134. 7 (s, PPN), 133.3 (m, PPN), 130.4 (m, PPN), 128.3 (dd, PPN), 139.6 (s, *C*N), 138.6 (s, *C*N).

10.2.10. [PPN]$_2$[Sn(CN)$_6$]

In a Schlenk tube, Sn(CN)$_4$(MeCN)$_2$ (0.209 g, 0.67 mmol, 1.00 eq) and [PPN]CN (1.262 g, 2.24 mmol, 3.27 eqs) were suspended in MeCN (15 mL). The tube was immersed into an oil bath and heated to 60 °C for 21 h before being cooled to rt. The pale brown solution was filtered in order to remove a small amount of undissolved solid, which was discarded. The filtrate was concentrated under dynamic vacuum until the onset of precipitation, redissolved by warming in hot air, then cooled to −28 °C. This gave pale yellow block-shaped crystals contained in a yellow solution. The crystals were isolated by filtration and the filtrate concentrated further under vacuum. Repetition of the same cooling process gave a further crop of block-shaped crystals which were shown to be spectroscopically identical to the first. Both crops were combined to give analytically pure [PPN]$_2$[Sn(CN)$_6$] (0.914 g, 98% with respect to Sn(CN)$_4$) as colourless crystals which appear pale yellow in the bulk. M.p. = 271−275 °C. Elem. Anal. Cald. for C$_{78}$H$_{60}$N$_8$P$_4$Sn (1351.99 g mol^{-1}) C, 69.30; H, 4.47; N, 8.29; Cl, 0%; found C, 68.74; H, 4.54; N, 8.04; Cl, <0.3%. IR (nujol, cm^{-1}) ṽ = 3173, 3146, 3081, 3064, 3039, 3025, 2794, 2787, 2696, 2252, 2218br, 2157, 2153, 2049br, 1985, 1915, 1833, 1616, 1588, 1575, 1482, 1439, 1436, 1260, 1252, 1186, 1179, 1114, 1069, 1028, 1020, 998, 941, 929, 924, 864, 797, 755, 695, 691, 664, 616, 550, 532. IR (MeCN, cm^{-1}), ν(CN) = 2157, 2153(sh), 2135. NMR (^{1}H, CD$_3$CN, ppm) δ = 7.89-7.22 (m, PPN). NMR (^{13}C, CD$_3$CN, ppm) δ = 128.2 (d, PPN), 130.3 (m, PPN), 133.2 (m, PPN), 134.6 (s, PPN), 138.5 (s, *C*N), 139.5 (s, cyanostannate decomposition product). NMR (^{119}Sn, CD$_3$CN, ppm) δ = −879.46 ([Sn(CN)$_6$]$^{2-}$), −850.17 (Sn-containing hydrolysis product). NMR (^{119}Sn, MAS, ppm) δ = −871.46 ([Sn(CN)$_6$]$^{2-}$). MS (ESI$^-$, MeCN) m/z = 283 ([((NC)$_2$C$_3$N$_3$)$_2$Na]$^-$, 100%), 250 ([Sn(CN)$_5$]$^-$, 33%), 198

([Sn(CN)$_3$]$^-$, 20%), 194 ([((NC)$_2$C$_3$N$_3$)Na(MeCN)]$^-$, 22%), 142 ([(C$_3$N$_3$)Na(MeCN)]$^-$, 23%).
MS (ESI$^+$, MeCN) m/z = 538 [PPN]$^+$, 100%).

10.2.11. Sn(CN)$_2$(MeCN)$_2$

SnF$_2$ (0.277 g, 1.77 mmol, 1.00 eq) was suspended in 15 mL MeCN and TMSCN (0.45mL, 3.55 mmol, 2.01 eqs) added. The suspension was stirred at rt for a total of 18.5 h, resulting in a very thick suspension. The white solid was isolated by filtration and dried under dynamic vacuum at rt to give Sn(CN)$_2$(MeCN)$_2$ (0.336 g, 75%) as an extremely air-sensitive white solid. Exposure to air results in the immediate formation of a yellow solid and the release of HCN and MeCN. The extreme air-sensitivity of the complex prevented reliable elemental analyses results from being recorded. M.p. 270 °C (decomp.). IR (nujol, cm^{-1}) ṽ = 3200, 3166, {2291, 2254} (MeCN)), [2162, 2155 ν(CN)], 1381, 1261, 2151, 1032, 922, 871, 838, 803, 754. Elem. Anal. Cald. for C$_6$H$_6$N$_4$Sn (252.84 g mol^{-1}) : C,28.50; H,2.39; N,22.15 %. Found C, 5.46; H,0; N,5.41 %. NMR (^{1}H, C$_5$D$_5$N, ppm) δ = 8.71 (s, py), 7.56 (s, py), 7.19 (s, py), 1.84 (s, possibly MeCN). NMR (^{13}C, C$_5$D$_5$N, ppm) δ = 149.8 (t, py), 135.5 (t, py), 123.5 (t, py). NMR (^{19}F, C$_5$D$_5$N, ppm) δ = no signal.

10.2.12. Sn(CN)$_2$(py)$_2$

SnF$_2$ (0.297 g, 1.90 mmol, 1.00 eq) was dissolved in 15 mL py and TMSCN (0.48 mL, 3.79 mmol, 2.00 eqs) added. The bright yellow solution was stirred for 20 h at rt. After 1 h, the solution became paler. The solution was concentrated under dynamic vacuum until the onset of precipitation (ca. 11 mL) and cooled to −28 °C. This gave a yellow solid contained in a pale yellow solution, which was isolated by filtration and dried under dynamic vacuum to give Sn(CN)$_2$(py)$_2$ (0.353 g, 56%) as a pale yellow, extremely air-sensitive crystalline solid. The extreme air-sensitivity of the complex prevented reliable elemental analyses results from being recorded. M.p. 127−134 °C (decomp.). Elem. Anal. Cald. for C$_{12}$H$_{10}$N$_4$Sn (304.93 g mol^{-1}) C,43.82; H,3.06; N,17.03 %. Found C, 30.12; H,2.59; N,11.62 %. IR (nujol, cm^{-1}) ṽ = 3099, 3086, 3065, 3032, 2998, 2139sh (ν(CN)), 2001w, 1990, 1950w, 1934, 1881w, 1865w, {1627, 1597, 1588, 1571sh} (ν(py)), 1488, 1443, 1308br, 1237, 1218sh, 1153sh, 1071sh, 1033sh, 1002, 952, 758, 697. 618. NMR (^{13}C, C$_5$D$_5$N, ppm) δ = 149.8 (t, py), 143.8 (s, *C*N), 135.5 (t, py), 123.5 (t, py). Additional resonances at 150.2 (s), 136.0 (s) and 124.0 (s) are attributed to coordinated py.

10.2.13. Attempted preparation of Sn(CN)$_2$

Sn(CN)$_2$(MeCN)$_2$ (165 mg) was placed into a Schlenk tube and immersed into an oil bath set to 60 °C. The solid was heated under dynamic vacuum until constant mass was achieved (ca.145 mg). IR spectroscopy of the dried solid still showed the presence of coordinated MeCN, but also confirmed the emergence of two new ν(CN) bands at 2173 and 2163 cm^{-1} consistent with Sn(CN)$_2$. IR (nujol, cm^{-1}) $\tilde{\nu}$ = 3163br, [2291, 2251 (MeCN)], 2187w, [2173, 2163 ν(CN)], 2143w, 1367, 1261, 1095br, 1062br, 866, 804.

10.2.14. Attempted preparation of Pb(CN)$_4$(MeCN)$_2$

PbF$_4$ (0.215 g, 0.76 mmol, 1.00 eq) was suspended in 10 mL MeCN and TMSCN (0.39 mL, 3.08 mmol, 4.05 eqs) added. Stirring of the suspension at rt for 6.5 h did not result in any change in the intensity of the ν(CN) band of TMSCN. Owing to the high possibility of the decomposition of PbF$_4$ prior to analysis, the reaction was halted.

10.2.15. Attempted preparation of Pb(CN)$_4$(py)$_2$ from PbF$_4$

PbF$_4$ (0.287 g, 1.01 mmol, 1.00 eq) was suspended in 15 mL py. TMSCN (0.52 mL, 4.10 mmol, 4.06 eqs) was added and the brown suspension stirred vigorously at rt for 21 h. The suspension was allowed to settle and the brown solid isolated by filtration. This gave an unknown cyanido lead complex (0.313 g) which contains coordinated pyridine and mulls poorly. The solid is hypothesised to be Pb(CN)$_4$(py)$_2$, although the identity could not be confirmed. IR (nujol, cm^{-1}) $\tilde{\nu}$ = 3146, 3101, 3047, 3032, 2998, 2472, 2222, 2151, 2123sh, 2006, 1989, 1949, 1932, 1887, 1875, 1886, 1872, 1836, 1702, 1625, 1236, 1222, 1148sh, 1074sh, 1031, 999, 950, 758sh, 616sh.

10.2.16. Attempted preparation of [PPN]$_2$[Pb(CN)$_6$]

"Pb(CN)$_4$(py)$_2$" (max.0.313 g, 1.01 mmol, 1.00 eq) was combined with [PPN]CN (1.075 g, 1.90 mmol, minimum of 1.89 eqs) and suspended in 15 mL py. The Schlenk tube was immersed into an oil bath and heated to 65 °C for 43.5 h, then allowed to cool. A small amount of brown solid was removed by filtration and the dark brown filtrate dried under dynamic vacuum to form a brown sticky foam. Freeze pumping gave a brown solid (1.253 g) which is inconsistent with either starting material. The conclusive identity of the compound could not be determined. IR (nujol, cm^{-1}) $\tilde{\nu}$ = 3172, 3146, 2697, [2214, 2146, 2131] (ν(CN)), 2038, 1981, 1912, 1821, 1779, 1563, 1483, 1438sh, 1284, 1247, 1190, 1116sh, 1068, 1028, 997, 946, 926, 880, 858, 792, 764, 747, 690, 619, 605sh.

10.2.17. Attempted preparation of Pb(CN)$_4$(py)$_2$ from Pb(OAc)$_4$

AgCN (0.869 g, 6.49 mmol, 4.16 eqs) was placed into a Schlenk tube, immersed into an oil bath heated to 110 °C and dried under dynamic vacuum for 2.5 h. Once cool, the dry solid was combined with solid Pb(OAc)$_4$ (0.691 g, 1.56 mmol, 1.00 eq) in a glovebox. The tube was removed from the glovebox, a stirrer bar added under argon flow and the solid suspended in 15 mL pyridine. This resulted in almost complete dissolution of all solid and the formation of a yellow solution. The solution was stirred at rt for 1.5 h, after which time a white solid contained in an orange solution had formed. The suspension was stirred for a further 48 h and the orange supernatant solution isolated by filtration. The filtrate was concentrated under vacuum and cooled to −28 °C, resulting in a bright orange crystalline solid. Recrystallisation from hot py did not yield single crystals of Pb(CN)$_4$(py)$_2$ but instead Pb(OAc)$_4$(py)$_2$, despite the observation of a strong ν(CN) band in the IR spectrum. IR (nujol, cm^{-1}) $\tilde{\nu}$ = 3146, 3081, 3038, 2143s (ν(CN)), 2131, 2012, 1992, 1955, 1929sh, 1890, 1867, 1711, 1591s, 1480s, 1443s, 1338, 1233, 1213sh, 1150sh, 1068, 1031, 1005, 932,753, 704s, 670, 616.

10.2.18. Preparation of Pb(CN)$_2$(py)$_2$

PbF$_2$ (0.251 g, 1.02 mmol, 1.00 eq) was suspended in dry py (ca. 20 mL) and TMSCN (0.26 mL, 2.05 mmol, 2.01 eqs) added, immediately resulting in a thickening of the white suspension. The suspension was stirred at rt for 24 h, after which time the supernatant solution had turned pale yellow. The white solid was isolated by filtration and dried under vacuum to give Pb(CN)$_2$(py)$_2$ (0.358 g, 90%) as a white solid. M.p. 143−145 °C. Elem. Anal. Cald. for C$_{12}$H$_{10}$N$_4$Pb (417.44 g mol^{-1}) C, 34.51, H, 2.42, N, 13.42 ; Found C, 32.54, H, 2.22, N, 12.77 %. IR (nujol, cm^{-1}) $\tilde{\nu}$ = 3112, 3098, 3089, 3050, 3032, 3015, 2998, 2474, 2123s (ν(CN)), 2073w, 2003, 1990, 1948, 1932, 1887, 1873, 1704, 1652, 1646, 1626, 1594, 1587, 1572, 1487, 1457, 1440, 1223, 1221, 1147, 1074, 1031sh, 1001, 950sh, 756sh, 697sh, 617sh. NMR (^{1}H, DMSO-d$_6$, ppm) δ = 8.58 (dt, py), 7.78 (tt, py), 7.38 (dd, py). No signals associated with coordinated py were observed. NMR (^{13}C, DMSO-d$_6$, ppm) δ = 149.6 (s, py), 136.0 (s, py), 123.9 (s, py). NMR (^{19}F, DMSO-d$_6$, ppm) δ = no signal.

10.2.19. Preparation of Pb(CN)$_2$

Pb(CN)$_2$(py)$_2$ (ca.0.358 g, 0.86 mmol, 1.00 eq) was placed into a Schlenk tube. The tube was immersed into an oil bath and heated to 80 °C under dynamic vacuum until constant mass was achieved. This gave a lead-cyanido complex (ca. 0.318 g, >100% w.r.t. Pb(CN)$_2$) speculated to be Pb(CN)$_2$; the inaccurate mass balance suggests that pyridine removal is incomplete. IR

(nujol, cm^{-1}) $\tilde{\nu}$ = 3175w, [2145, 2121] (s, ν(CN)), [1624, 1595, 1551, 1302, 1260, 1219, 1170, 1150, 1076,1067, 1032, 1003, 757, 700]w.

10.2.20. Attempted [2+3] cycloaddition reaction between [PPN]$_2$[Sn(CN)$_6$] and TMSN$_3$

A solution of TMSN$_3$ (0.1 mL, 0.75 mmol, 6.25 eqs) in dry MeCN (20 mL) was added to a suspension of [PPN]$_2$[Sn(CN)$_6$] (0.156 g, 0.12 mmol, 1.00 eq) in MeCN (5 mL), resulting in the immediate dissolution of all solid. The reaction was stirred at rt for a total of 50 h. IR spectroscopic monitoring showed the decrease of the ν(N$_3$) band of TMSN$_3$ at 2140 cm^{-1} and the increase of bands associated with an azidostannate complex ($\tilde{\nu}$ = 2074 cm^{-1}) and TMSCN ($\tilde{\nu}$ = 2089 cm^{-1}, w). Repetition of the reaction on smaller scales in CD$_3$CN, with heating to 65 °C for 16 h followed by further heating at 100 °C for 60 h, showed the disappearance of the signal associated with TMSN$_3$ (δ = 0.27 ppm), accompanied by the formation of TMSCN (δ = 0.35 ppm) and the extremely slow formation of TMSCHN$_4$ (δ = 0.59 ppm).

10.2.21. Attempted [2+3] cycloaddition reaction between [PPN]$_2$[Sn(CN)$_6$] and HN$_3$

Ethereal HN$_3$ (0.28 mL, ca. 3.3 mmol mL^{-1}, 0.92 mmol, 6.13 eqs)[237] was added to a solution of [PPN]$_2$[Sn(CN)$_6$] (0.208 g, 0.15 mmol, 1.00 eq) in 15 mL MeCN and the solution stirred at rt for 1 h 40 min. Spectroscopic monitoring showed the decrease in the ν(N$_3$) bands associated with HN$_3$ ($\tilde{\nu}$ = 2138 cm^{-1}) and [Sn(CN)$_6$]$^{2-}$ ($\tilde{\nu}$ = 2158 cm^{-1}) and the increase in bands associated with an azidostannate ($\tilde{\nu}$ = 2074 cm^{-1}) and TMSCN ($\tilde{\nu}$ = 2090 cm^{-1}). A band observed at 2190 cm^{-1} could not be identified.

10.3. Ge(II) azides

10.3.1. Synthesis of GeCl$_2$(diox)

Adapted from a preparative procedure by Portius.[164,359]

To a Schlenk tube containing a previously-prepared stock solution of GeCl$_4$, LiAlH$_4$, Et$_3$SiH, toluene and dioxane, dry dioxane (2.24 mL, 26.29 mmol, 1.00 eqs), dry GeCl$_4$ (3.00 mL, 26.30 mmol, 1.00 eq) and Et$_3$SiH (used as received, 8.41 mL, 52.65 mmol, 2.00 eqs) were added under argon flow. A reflux condenser was baked out in vacuo in hot air and connected to the Schlenk tube and a mercury bubbler. The pale yellow solution was immersed into an oil bath set to 140-145 °C and heated to reflux for ca. 3.5 h. During reflux, the system was periodically purged with argon. Reflux was observed to begin at a bath temperature of 106 °C. At a bath temperature of 130 °C, bubbles of gas were observed to be released from the solution. After ca. 1 h of reflux, gas release ceased for 45 mins. After a total reflux time of 3.5 h, large amounts

of pale yellow solid precipitated rapidly from solution. The Schlenk tube was immediately cooled in ice to rt, then disconnected from the reflux apparatus under argon flow and cooled to −28 °C for 1.5 h. The resulting pale yellow crystalline solid was isolated by filtration and dried under dynamic vacuum at rt for 1 h 15 mins. This gave $GeCl_2(diox)$ (4.026 g, 66%) as fibrous yellow crystals. The colourless filtrate can be stored under argon at −28 °C and used in subsequent preparations of $GeCl_2(diox)$ as a stock solution. IR (nujol, cm^{-1}) $\tilde{v}$ = 2984, 1446, 1332, 1286, 1253, 1216, 1105, 1074, 1034, 1011, 895, 841, 747, 623.

NB: If the reaction solution is not cooled immediately upon precipitation of $GeCl_2(diox)$, a dark orange solid forms. This solid is isolated by filtration, resuspended in CH_2Cl_2 and stirred vigorously for 20 minutes. The orange solid contaminant, believed to contain germanium sub-halides, is removed by filtration and discarded. Removal of all solvent from the pale yellow filtrate solution yields $GeCl_2(diox)$ in comparable purity and decreased yield (i.e., 44% vs 66%) to the standard procedure detailed above.

10.3.2. Synthesis of Na[Ge(N₃)₃]

Adapted from a preparative procedure by Peerless *et al.*[182]

$GeCl_2(diox)$ (0.164 g, 0.71 mmol, 1.00 eq) and NaN_3 (0.274 g, 4.21 mmol. 5.93 eqs) were combined in a Schlenk tube and suspended in ca. 20 mL of MeCN. The yellow suspension was stirred rapidly at rt for 3.5 h. After ca. 0.5 h stirring, the suspension became darker and highly turbid.[a] The brown suspension was allowed to settle, the supernatant solution containing $Na[Ge(N_3)_3]$ carefully removed by decantation and the brown filter residue discarded. Owing to the high energetic sensitivity predicted for $Na[Ge(N_3)_3]$, solid material was isolated only on small scales (i.e., <200 mg) when contained in excess ancillary ligand (for preparation of $Ge(N_3)_2(L)_2$, see below) and was not handled directly. IR (MeCN, cm^{-1}) $\tilde{v}$ = 2139 (HN_3), 2096, 2064.[ii]

10.3.3. Preparation of Ge(N₃)₂(L)₂ (L = py, pic, ᵗBupy)

To a solution of $Na[Ge(N_3)_3]$ in MeCN, ancillary ligand L (L = py, pic, ᵗBupy, typically 0.13−0.23 mL, ca. 2.5 eqs with respect to $GeCl_2(diox)$) was added by pipette. The suspension was stirred for several minutes before all MeCN was removed under vacuum at temperatures equal or below room temperature to avoid loss of ancillary ligand. MeCN removal was

---

[ii] NB: The colour of the suspension varies between dark orange and brown, depending on the amount of germanium sub-halides present in $GeCl_2(diox)$. These solid impurities are easily removed by filtration.

indicated by the observation of little to no change between static and dynamic vacuum pressures. The white solid was then resuspended in CH_2Cl_2 (25 mL), ensuring that almost all solid on the walls of the flask was covered.[iii] The suspension was stirred for a further 17 h at rt, forming a noticeably thicker white suspension after ca. 2 h. The suspension was allowed to settle, the supernatant solution isolated by filtration and the white filter residue is discarded. The colourless supernatant solution was concentrated under vacuum until the onset of precipitation, initially via the formation of a colourless to pale yellow oil. This formed $Ge(N_3)_2(L)_2$ as colourless microcrystalline solids, contained in excess ancillary ligand.[iv] Determination of precise yields are difficult to owing to the presence of excess ancillary ligand in the product mixture. Further crystallisation can be induced by cooling the solution to −28 °C. Prolonged storage results in discolouration of the microcrystalline solids from colourless to yellow. Prolonged storage in CH_2Cl_2 results in the spontaneous formation of $Ge(N_3)_4(L)_2$.

$Ge(N_3)_2(py)_2$: py = 0.13 mL, 1.64 mmol, 2.52 eqs. IR (nujol, cm^{-1}) $\tilde{v}$ = 3183br, 2725, 2670, [2100, 2066] ($v_{as}(N_3)$), 1611, 1597, 1293br, 1213, 1168, 1156, 1068, 1045,1017, 824br, 693. IR (CH_2Cl_2, cm^{-1}) $v_{as}(N_3)$ = 2097, 2076, v(py) = 1611 (coordinated), 1600 (free). Elem. Anal. Cald. for $C_{10}H_{10}N_8Ge$ (286.86 g mol^{-1}) C, 38.13, H, 3.20, N, 35.59, Cl, 0 ; Found C, 27.72, H, 2.88, N, 43.34, Cl, <0.3%.

$Ge(N_3)_2(pic)_2$: pic = 0.23 mL, 1.44 mmol, 2.51 eqs. IR (nujol, cm^{-1}) $\tilde{v}$ = 3405, 3367, 3141, 3106, 2728, 2632, 2578, 2515, [2154, 2089, 2063] $v_{as}(N_3)$, 1949, 1853, 1687, 1628, 1605, 1563, 1506, 1458, 1364, 1332, 1296, 1284, 1261, 1233, 1208, 1183, 1125, 1095, 1065, 1033, 873, 861, 819, 808, 801, 718, 677, 594, 554. IR (CH_2Cl_2, cm^{-1}) $v_{as}(N_3)$ = 2097, 2075, v(pic) = 1627 (coordinated), 1607 (free). NMR (^{1}H, CD_2Cl_2, ppm) δ = 8.94 (d, C*H*), 7.59 (d, C*H*), 7.32 (s), 2.58 (s, C*H$_3$*). Signals consistent with uncoordinated pic at δ [ppm] = 8.42 (d, C*H*), 7.13 (d, C*H*) and 2.35 (s, C*H$_3$*) are also observed. NMR (^{13}C, CD_2Cl_2, ppm) δ = 126.9 (s, *C*H). No signals associated with the other carbon environments present in coordinated pic are observed; however, signals consistent with uncoordinated pic at δ [ppm] = 149.7 (s, *C*H), 145.8 (s, *C*H), 125.0 (s, *C*H), 20.9 (s, *C*H$_3$*) are present in the spectrum.

[iii] Under solution, solid can be removed from the walls of the vessel by gentle agitation of the stirrer bar using a magnet.
[iv] The extent of drying affects the shape and width of the $v_{as}(N_3)$ bands in IR spectra of the solid product. As such, it is difficult to obtain spectra at comparable drying stages for each adduct.

Ge(N$_3$)$_2$(^{t}Bupy)$_2$: ^{t}Bupy = 0.25 mL, 1.71 mmol, 2.55 eqs. IR (CH$_2$Cl$_2$, cm^{-1}) ν_{as}(N$_3$) = 2096, 2075, ν(^{t}Bupy) = 1621 (coordinated), 1599 (free). IR (nujol, cm^{-1}) $\tilde{\nu}$ = 3368s, 3135, 3078, 3024, 2362, 2566, 2521, [2154, 2126, 2091, 2060]s (ν_{as}(N$_3$)), 1945, 1844, 1694, 1622, 1600, 1557, 1546, 1497, 1409, 1338, 1293, 1273, 1224sh, 1205sh, 1122sh, 1071, 1037, 1028, 994, 821, 667, 593, 571, 548. IR (thin film in ^{t}Bupy, cm^{-1}) $\tilde{\nu}$ = 3078, 3027, 2967, 2907, 2870, [2092, 2067] (ν_{as}(N$_3$)), 1597s, 1557, 1546, 1495, 1472, 1409sh, 1367, 1276, 1227, 1205, 1077, 997sh, 846, 823sh, 750, 712, 571sh, 531. NMR (^{1}H, CD$_2$Cl$_2$, ppm) δ = 8.98 (d, CH_2), 7.76 (d, CH_2), 1.46 (s, {CH_3}$_3$). Signals consistent with uncoordinated ^{t}Bupy at δ = 8.47 (d), 7.29 (d), and 1.31 (s) ppm are also observed. NMR (^{13}C, CD$_2$Cl$_2$, ppm) δ = 146.0 (s, CH_2), 123.3 (s, CH_2). The signals associated with i-C$_6$H$_4$N or C{CH$_3$}$_3$ are not observed. Signals consistent with uncoordinated ^{t}Bupy at δ [ppm] = 149.9 (s, CH_2), 121.1 (s, CH_2), 30.6 (s, {CH_3}$_3$) are also observed. ^{73}Ge NMR spectra were unable to be recorded owing to the lack of sensitivity of the spectrometer probe for this nucleus.

10.3.4. Spontaneous decomposition of Ge(N$_3$)$_2$(^{t}Bupy)$_2$ to form Ge(N$_3$)$_4$(^{t}Bupy)$_2$

A solution of Ge(N$_3$)$_2$(^{t}Bupy)$_2$ in CH$_2$Cl$_2$ was allowed to stand at rt in a glovebox. After ca. 24 h, the turbidity of the solution had increased. After ca. 36 h, colourless crystals of Ge(N$_3$)$_4$(^{t}Bupy)$_2$ formed, contained in a colourless supernatant solution. Colourless crystals of the same compound are obtained when oils of Ge(N$_3$)$_2$(^{t}Bupy)$_2$ are stored under the same conditions, contained in a red solid of unknown identity. IR (nujol, cm^{-1}) $\tilde{\nu}$ = 3078, 3024, [2131, 2089]br (ν_{as}(N$_3$)), 1932, 1639, 1624, 1598, 1556, 1545, 1495, 1410, 1396, 1294br, 1275, 1226, 1203, 1107br, 1075, 1020br, 997, 843, 819, 712, 569.

10.3.5. Oxidation study of Ge(N$_3$)$_2$(py)$_2$ to Ge(N$_3$)$_4$(py)$_2$ using HN$_3$

A single drop of dry ethereal HN$_3$ (ca. 0.02 mL, max. concentration ca.1.58−1.68 mmol mL^{-1}, 0.03 mmol)[360] was added by Pasteur pipette to a solution of Ge(N$_3$)$_2$(py)$_2$ in CH$_2$Cl$_2$. The reaction solution was swirled by hand and stood for 5 mins at rt. After this time, a crystalline solid had formed on the walls of the tube. An aliquot of the solution was taken for IR spectroscopy and examined after 5 and 10 minutes in $situ$ in the spectrometer. The band of Ge(N$_3$)$_2$(py)$_2$ at 2075 cm^{-1} was observed to decrease between analyses. The bands associated with HN$_3$ and Ge(N$_3$)$_4$(py)$_2$ remained approximately constant. This spectral change is consistent with the oxidation of Ge(N$_3$)$_2$(py)$_2$ to Ge(N$_3$)$_4$(py)$_2$ by HN$_3$. IR (CH$_2$Cl$_2$, cm^{-1}), ν_{as}(N$_3$) = 2138 (HN$_3$), 2115 ([Ge(N$_3$)$_6$]$^{2-}$), 2096 (Ge(N$_3$)$_4$(py)$_2$).

10.3.6. Attempted synthesis of Ge(N₃)₂(diox) using TMS−N₃

GeCl$_2$(diox) (40 mg, 0.17 mmol, 1.00 eq) was dissolved in 15 mL MeCN and cooled in ice. TMS-N$_3$ (0.27 mL, 2.15 mmol, 4.89 eqs) was added and the solution stirred in ice for 5 mins before being allowed to warm to rt. After 25 h stirring at rt, a white solid contained in a colourless solution had formed. The suspension was filtered and the filtrate cooled to −28 °C for several days, resulting in the formation of colourless crystals of dioxane which melted upon rewarming to rt. No ν(N$_3$) bands associated with coordinated azido ligands were observed in the filtrate and the reaction was discarded.

10.3.7. Preparation of Ge(N₃)ₓNᵧ

A sample of Ge(N$_3$)$_2$(L)$_2$ (L = pic, ^{t}Bupy) in a Schlenk tube was immediately immersed into a water bath and heated in stages to 70 °C under high vacuum, dwelling at each intermediary temperature for ca. 45-60 mins. Typical intermediary temperatures chosen were rt (ca. 20 °C), 30 °C, 40 °C, 50 °C and 70 °C. The formation of Ge(N$_3$)$_x$N$_y$ was deemed complete when the mass at 70 °C became constant, and was accompanied by the formation of a finely-divided, white, highly air-sensitive solid. IR (nujol, cm^{-1}) $\tilde{\nu}$ = 3356w, 2134br, 1366, 1278br, 1262, 1096w, 1017w, 804br. Rapid heating from rt to 70 °C resulted in decomposition to form a brown solid of unknown identity.

10.3.8. Heating of Ge(N₃)ₓNᵧ

A Schlenk tube containing typically ca. 100 mg of Ge(N$_3$)$_x$N$_y$ was placed under high vacuum at rt. Once an acceptable vacuum pressure had been achieved (typically 6 x10^{-2} mbar or below), the Schlenk tube was inserted into a tube furnace and connected to a vacuum pump. The tubing connecting the pump to the vessel was degassed under dynamic vacuum for ca. 10 mins prior to heating. Once degassed, the Schlenk tube was opened to dynamic vacuum and the solid was heated to 350 °C from room temperature at a set rate of 1 °C/min. The maximum temperature was maintained for 4 h, then allowed to cool to rt naturally over the course of ca. 10 h. This gives a white to pale brown, air stable, amorphous solid speculated to be Ge$_3$N$_x$ (x = 2 or 4) (ca. 69 mg). Addition of water to this solid results in near-complete dissolution, forming a basic solution and a strong smell of NH$_3$. The use of a liquid N$_2$ cold trap between the Schlenk tube and vacuum pump during heating did not appear to affect the outcome of the reaction. IR (nujol, cm^{-1}) $\tilde{\nu}$ = 3467 br, 3249br, 2728w, 1642, 1608, 1506, 1341, 1266br, 1208br, 1160br, 829br, 573br. IR (ATR, cm^{-1}) $\bar{\nu}$ = 3326br, 1642, 1612, 1430br, 1262, 798, 763, 542. Raman (solid

state, rt, 325 nm, cm^{-1}) $\tilde{\nu}$ = 1547, 1368. If the heating ramp rate is too rapid, uncontrolled decomposition occurs and a dark brown/black solid is formed.

10.4. Pb(IV) azido complexes

10.4.1. Cautionary note on Pb azides

Caution! Several of the azido complexes prepared as part of this work are extremely energetically sensitive and decompose violently. The $[Pb(N_3)_6]^{2-}$ anion was only isolated in the form of the stable $[PPN]_2[Pb(N_3)_6]$ salt; $(NH_4)_2[Pb(N_3)_6]$, required for the synthesis of $Pb(N_3)_4(bipy)$, was prepared *in situ* and was not isolated at any point. On several occasions, attempts to isolate $Pb(N_3)_4(bipy)$ resulted in decomposition, accompanied by a loud report and the generation of soot. The causes of decomposition are unclear but appear to include impact. On another occasion, the compound decomposed without any apparent external stimulation. The energetic sensitivity of $[Pb(bipy)_3][Pb(N_3)_6]$ and any partially-chlorinated derivatives such as $[Pb(bipy)_3][Pb(N_3)_{5.2}Cl_{0.8}]$ are assumed to be similar to that of $Pb(N_3)_4(bipy)$. Many of the attempts to prepare $[PPN][Pb(N_3)_3]$ resulted in the formation of $Pb(N_3)_2$, a primary explosive of which the high energetic sensitivity is well-reported.[361] Extreme caution must be exercised when preparing or handling any of the azido complexes mentioned in this chapter, particularly for $Pb(N_3)_4(bipy)$ and its decomposition products, and the standard preparative precautions for work involving energetic materials (i.e., working on scales no greater than 100 mg and with the use of a blast shield, Kevlar gloves, safety glasses and face shield) must be used. Wherever possible, studies should be undertaken in solution.

10.4.2. $(NH_4)_2[PbCl_6]$

Adapted from a preparative procedure by Pant.[362]

HCl (35%, 150 mL) was placed into a 250 mL round-bottomed flask and cooled to 0 °C. PbO$_2$ (22.950 g, 0.10 mmol, 1.0 eqs) was added slowly in portions to ensure the solution temperature was maintained at 0 °C, forming a black solid suspended in a yellow-green solution. The suspension was stirred at this temperature for 30 mins before a cold solution of NH$_4$Cl (10.839 g, 0.20 mol, 2.00 eqs) in 35 mL H$_2$O was added in portions over 30 minutes. The addition of this solution formed a yellow precipitate, which was isolated by filtration, washed with Et$_2$O (4x50 mL) and dried in air. This gave $(NH_4)_2[PbCl_6]$ (37.575 g, 82%) as a bright yellow powder which smells strongly of chlorine. IR (nujol, cm^{-1}) $\tilde{\nu}$ = 3226br, 1409s, 772w, 738, 664. m.p. 262 °C (decomp.). Elem. Anal. Cald. for H$_8$N$_2$PbCl$_6$ (455.98 g mol^{-1}) expected C = 1.77, N = 6.14, Cl = 46.65; found C = 2.21, N = 6.13, Cl = 40.90. The deviations from the expected

C,H,Cl values are attributed to incomplete combustion of the sample during analysis. TOF-MS (MeCN, ESI$^-$) m/z = 385 ([PbCl$_5$]$^-$), 313 ([PbCl$_3$]$^-$). Prolonged exposure to air results in discolouration of the solid to dark orange and the release of colourless liquid.

10.4.3. [PPN]$_2$[PbCl$_6$]

A suspension of (NH$_4$)$_2$[PbCl$_6$] (4.723 g, 0.01 mol, 1.00 eq) in 200 mL MeCN was combined with a solution of [PPN]Cl (11.912 g, 0.02 mol, 2.00 eqs) in 60 mL MeCN. The resulting suspension was stirred at rt for 1 h, forming a white solid suspended in a pale yellow solution. The solid was isolated by filtration and discarded. The filtrate was cooled to -28 °C for 17 h, resulting in the formation of yellow block crystals which were isolated by filtration. Concentration of the resulting filtrate by approximately half *in vacuo* and cooling to -28 °C resulted in a further crop of yellow crystals which were shown to be spectroscopically identical to the first. Both crops were combined, dissolved in 180 mL MeCN, a small amount of white solid removed by filtration and the filtrate cooled to -28 °C for 17 h. This gave analytically pure [PPN]$_2$[PbCl$_6$] (9.191 g, 61%) as yellow block crystals. M.p. 244$-$250 °C (decomp. 260 °C). Elem. Anal. Cald. for C$_{72}$H$_{60}$P$_4$N$_2$Cl$_6$Pb (m/z/ = 1497.06 g mol^{-1}) expected C = 57.74, H = 4.04, N = 1.87, Cl = 14.22 ; found C = 57.02, H = 4.16, N = 1.94, Cl = 13.92 %. IR (nujol, cm^{-1}) $\tilde{\nu}$ = 3175, 3072, 2003, 1978, 1927, 1904, 1827, 1779, 1682, 1588sh, 1574sh, 1480, 1438, 1261, 1182, 1165sh, 1111, 1028sh, 999sh, 934, 855, 798sh, 749, 693, 694, 616.

10.4.4. [PPN]$_2$[Pb(N$_3$)$_6$]

[PPN]$_2$[PbCl$_6$] (0.487 g, 0.33 mmol, 1.00 eq) was placed into a Schlenk tube and dissolved in ca.20 mL dry MeCN. The resulting yellow solution was transferred into a Schlenk tube containing NaN$_3$ (0.228 g, 3.51 mmol, 10.64 eqs) and the suspension stirred at rt for 24 h. The resulting orange suspension was filtered and the white filter residue discarded. The filtrate was concentrated under vacuum until the onset of precipitation, redissolved at room temperature and slowly cooled to -28 °C in an ^{i}PrOH-filled Dewar flask for 17 h. This gave [PPN]$_2$[Pb(N$_3$)$_6$] (0.246g, 45%) as deep red block crystals. M.p. 169$-$171 °C. Elem. Anal. Calcd. For C$_{72}$H$_{60}$P$_2$N$_{20}$Pb (m/z = 1368.40 g mol^{-1}) expected C = 56.26, H = 3.94, N = 18.24, Cl = 0; found C = 56.42, H = 3.41, N = 18.02, Cl = <0.3 %. IR (nujol, cm^{-1}) $\tilde{\nu}$ = 3311, 3266, 3058, 2026s, 1588, 1574, 1486, 1438, 1315, 1284, 1264, 1182, 1162, 1119, 1077, 1025, 997, 798sh, 741, 690, 616, 599, 551. IR (MeCN, cm^{-1}) $\tilde{\nu}$ = 2064, 2037, 2005. IR (CH$_2$Cl$_2$, cm^{-1}) ν_{as}(N$_3$) = 2063, 2036. IR (acetone, cm^{-1}) ν_{as}(N$_3$) = 2062, 2035. TOF-MS (MeCN, ESI$^-$) m/z = 334 ([Pb(N$_3$)$_3$]$^-$), 255 (Pb-containing, unknown). MS (MeCN, ESI$^+$) m/z = 538 ([PPN]$^+$).

10.4.5. Attempted preparation of [PPN][Pb(N₃)₃] from [PPN]₂[Pb(N₃)₆]

Based on a preparative procedure by Polborn *et al.*[177]

A solution of [PPN]₂[Pb(N₃)₆] (0.03 g, 0.02 mmol) in acetone (5 mL) was stood in daylight at rt. After ca. 2.5 h, the orange solution had become colourless and a white solid had precipitated. The colourless supernatant solution was decanted, leaving a white solid filter residue. The filter residue was characterised by IR spectroscopy as $Pb(N_3)_2$. The filtrate was evaporated to dryness at rt, yielding a white solid. IR (acetone, cm^{-1}) $\nu_{as}(N_3)$ = 2134, 2054br, 2030, {2010, 2000 [PPN]N₃}. IR (nujol, cm^{-1}) $\tilde{\nu}$ = 3351br, 3058, [2023, 2014 s] ($\nu(N_3)$), 1436, 1296, 1260, 1217, 1187, 1174, 1163, 1113, 1026, 996, 931, 854, 845, 758, 748, 690, 550, 529.

10.4.6. Analytical data for Pb(N₃)₂

Based on a preparative procedure by Kreißl *et al.*[218] which gave $Pb(N_3)_2$ (50 mg, 50%) as a white solid which mulls extremely poorly and possesses large solid state effects in the IR spectrum. IR (nujol, cm^{-1}) $\tilde{\nu}$ = 3326, [2116, 2042, 2001] ($\nu(N_3)$), 1347, 1342, 1330, 1263, 1258, 1214, 654, 651, 634, 624, 614, 610, 607, 601. Flame testing of the solid gave an extremely loud report.

10.4.7. Attempted preparation of [PPN][Pb(N₃)₃] from Pb(N₃)₂

$Pb(N_3)_2$ (52 mg, 0.18 mmol, 1.00 eq) was combined with [PPN]N₃ (0.223 g, 0.38 mmol, 2.11 eqs) and suspended in 20 mL non-dry MeCN. The suspension was stirred at rt under argon for 17 h, forming a finely divided off-white solid. A band at 2014 cm^{-1} in the IR spectrum of the supernatant solution is observed to form alongside a decrease in intensity of the band associated with [PPN]N₃ ($\tilde{\nu}$ = 2006 cm^{-1}). A further period of stirring at rt (ca. 3 h) resulted in the disappearance of the band at 2014 cm^{-1}. The pale brown supernatant solution was removed and discarded. The filter residue was dried under vacuum to give 49 mg of a cream solid, shown to be $Pb(N_3)_2$ by IR spectroscopy.

10.4.8. Preparation of [PPN][PbCl₃]

Based on a preparative procedure by Crozier.[103]

A suspension of PbCl₂ (0.164 g, 0.59 mmol, 1.02eqs) in hot (60°C) H₂O (10 mL) was combined with a solution of [PPN]Cl (0.333 g, 0.58 mmol, 1.00eq) in 10 mL H₂O at the same temperature. After combination, a colourless solution formed, which precipitated a white solid upon cooling to rt. The suspension was cooled in ice, filtered and washed with H₂O (4 x 5 mL) to give an off-white filter residue (0.280 g). Recrystallisation from the minimum volume of hot MeCN

yielded [PPN][PbCl$_3$] (0.163 g, 33%) as colourless needle crystals. The similarities between [PPN]Cl and [PPN][PbCl$_3$] in the IR spectrum precluded definite characterisation of the reaction product.

10.4.9. Attempted preparation of [PPN][Pb(N$_3$)$_3$] from [PPN][PbCl$_3$]

[PPN][PbCl$_3$] (0.098 g, 0.12 mmol, 1.00eq) and NaN$_3$ (0.042 g, 0.65 mmol, 5.42 eqs) were combined and suspended in MeCN (15 mL), resulting in the rapid dissolution of some solid. The suspension was stirred at rt for 2.5 h. IR spectroscopy of the supernatant solution showed ν(N$_3$) bands consistent with [PPN]N$_3$ and Pb(N$_3$)$_2$. IR (MeCN, cm^{-1}) ν(N$_3$) = 2044 (Pb(N$_3$)$_2$), 2005 ([PPN]N$_3$).

10.4.10. Attempted preparation of [PPN][Pb(N$_3$)$_3$] from PbCl$_2$

PbCl$_2$ (0.129 g, 0.46 mmol, 1.00eq) and [PPN]N$_3$ (0.797 g, 1.37 mmol, 2.98 eqs) were combined and suspended in 15 mL MeCN. The suspension was stirred rapidly at rt for 5 h 40 mins, after which time the IR spectrum of the supernatant solution showed a decrease in the ν(N$_3$) band of [PPN]N$_3$. A solution of [PPN]N$_3$ (0.104 g, 0.18 mmol, 0.39 eqs) in MeCN was added and the suspension stirred for a further 16 h at rt, resulting in a white solid contained in a pale orange suspension. The supernatant solution was isolated by filtration and the white solid filter residue discarded. IR spectroscopy of the filtrate showed ν(N$_3$) bands consistent with [PPN]N$_3$, Pb(N$_3$)$_2$ and an unknown band at 2031 cm^{-1}. IR (MeCN, cm^{-1}) ν(N$_3$) = 2044, 2031, 2005. Removal of all solvent under dynamic vacuum resulted in a white solid (0.893 g) which was almost spectroscopically identical to [PPN]N$_3$ and Pb(N$_3$)$_2$.

10.4.11. Pb(N$_3$)$_4$(bipy)

Based on a preparative procedure by Beck *et al.*[97]

NaN$_3$ (0.137 g, 2.10 mmol, 9.54 eqs) was dissolved in 10 mL H$_2$O. A solution of bipy (0.073 g, 0.47 mmol, 2.14 eqs) in dichloromethane (10 mL) was added, resulting in a colourless solution containing two layers. To this solution, solid (NH$_4$)$_2$[PbCl$_6$] (0.099 g, 0.22 mmol, 1 eq) was added, resulting in the immediate formation of an orange biphasic solution. The reaction mixture was stirred under the exclusion of light for 1 h 10 mins at rt. This resulted in an orange organic layer and a brown aqueous suspension, containing a dark brown solid at the phase boundary. A filter stick, containing ca.1 cm depth celite, was connected to a Schlenk tube, baked out in hot air under dynamic vacuum then refilled with argon.

Once the stirring period was complete, the organic (lower) layer was separated and the aqueous layer neutralised and discarded. The organic layer was rapidly filtered through the celite into

the Schlenk tube, the filtration apparatus disassembled and the dark orange solution concentrated under dynamic vacuum until the onset of precipitation. The resulting orange suspension was warmed gently back to rt in warm air, placed in a Dewar containing isopropanol and cooled in a freezer. This resulted in a small number of very small orange crystals and a dark orange solid. The supernatant solution was removed by cannula filtration to give $Pb(N_3)_4(bipy)$ as an orange solid (5 mg, 22%). IR (nujol, cm^{-1}) $\tilde{\nu}$ = 3086, 3076, 3064, 3054, 2058 (sh, $\nu_{as}(N_3)$), 2026 ($\nu_{as}(N_3)$), 1966(sh), 1591(sh), 1585, 1558, 1557, 1489, 1458, 1434, 1418, 1367, 1312, 1256,1250, 1212, 1172, 1154, 1148,1138, 1114, 1100 (sh), 1089, 1084, 1064, 1040, 1007, 993, 975, 893,806, 755, 734, 656, 652, 641, 620, 594. IR (CH$_2$Cl$_2$, cm^{-1}) $\nu_{as}(N_3)$ = 2138 (HN$_3$), 2128sh, 2061, 2040, ν(bipy) = [1606, 1595, 1493, 1475, 1444] (coordinated), [1584, 1561, 1458, 1421] (free). An aliquot of the reaction solution was transferred into an NMR tube, all solvent carefully removed under vacuum and CDCl$_3$ added for NMR studies. NMR (^{1}H, CDCl$_3$, ppm), δ = 9.52 (d, bipy), 8.63 (d, bipy), 8.34 (d, bipy), 8.26 (m, bipy). Signals associated with uncoordinated bipy at δ [ppm] = 8.72 (s), 8.42 (d), 7.86 (m) and 7.35 (s) are also observed.[v] NMR (^{1}H, DMSO-d$_6$, ppm) δ = 8.10 (d, bipy), 7.85 (d, bipy), 7.27 (t, bipy), 6.76 (m, bipy), 4.76 (t, CH_2Cl$_2$), 3.32 (s, H_2O), 1.45 (unknown).[vi] NMR (^{13}C, DMSO-d$_6$, ppm) δ = 148.0 (s, bipy), 135.9 (s, bipy), 122.8 (s, bipy), 119.8 (s, bipy), 52.8 (s, CH$_2$Cl$_2$). NMR (^{207}Pb, DMSO-d$_6$, ppm), δ = no signal.

Crystals of $Pb(N_3)_4(bipy)$ suitable for X-ray diffraction studies were grown by concentration of a CH$_2$Cl$_2$ solution of the compound under dynamic vacuum, promptly followed by cooling to -28 °C for ca. 2 h. This process was performed immediately following isolation of the product in solution to avoid decomposition through unwanted photolysis and chlorination reactions. After 2 h, dark orange/ruby red crystals had formed in an orange solution. A sample of these crystals were picked from solution and immediately carefully mounted onto a goniometer. Owing to the energetic sensitivity of the complex, microanalysis was not performed.

---

[v] The solution of $Pb(N_3)_4(bipy)$ in CH$_2$Cl$_2$ was stood for 3 h in the dark prior to analysis. Therefore, the exact identity of the compound in solution cannot be confirmed and the NMR spectra obtained may in fact be [Pb(bipy)$_3$][Pb(N$_3$)$_6$] or a partially-chlorinated derivative, *cf.* [Pb(bipy)$_3$][Pb(N$_3$)$_{5.2}$Cl$_{0.8}$]. This NMR data provides spectroscopic evidence only for the coordination of bipy ligands. All other attempts to record NMR data in CDCl$_3$ showed only signals consistent with uncoordinated bipy. The reasons for this are unclear.

[vi] Spectroscopic studies in CH$_2$Cl$_2$/DMSO-d$_6$ external lock solvent showed a single set of signals; the absence of additional, smaller signals slightly up- or downfield suggests these signals arise from uncoordinated bipy also.

10.4.12. Decomposition studies of Pb(N$_3$)$_4$(bipy) (light and dark)

A solution of Pb(N$_3$)$_4$(bipy) in CH$_2$Cl$_2$ was freshly prepared and placed into a Schlenk tube. The tube was placed into direct sunlight at rt and aliquots removed at regular intervals for IR spectroscopy. Within ca. 10 minutes of light exposure, an orange solid had formed in suspension. IR spectroscopy revealed the decrease in bands associated with Pb(N$_3$)$_4$(bipy) in solution. As the exposure time increased, the solid rapidly turned white and was identified as Pb(N$_3$)$_2$ by IR spectroscopy.

A separate solution of Pb(N$_3$)$_4$(bipy) in CH$_2$Cl$_2$ was stood at rt under the exclusion of light. Spectroscopic monitoring showed the formation of v(N$_3$) bands consistent with [Pb(N$_3$)$_6$]$^{2-}$ (v_{as}(N$_3$) = 2055, 2039 cm^{-1}). No suspension was observed to form and the colour of the solution remained almost unchanged.

10.4.13. [Pb(bipy)$_3$][Pb(N$_3$)$_{5.2}$Cl$_{0.8}$]

A solution of Pb(N$_3$)$_4$(bipy) in CH$_2$Cl$_2$ was prepared and immediately stored at −28 °C under the exclusion of light. After ca. 10 days, dark red block crystals had formed, contained in a yellow supernatant solution. Single crystal X-ray diffraction studies confirmed the identity of the crystals as [Pb(bipy)$_3$][Pb(N$_3$)$_6$], containing a disordered N$_3$/Cl unit. The crystals mull poorly. Owing to the energetic sensitivity of the complex, microanalysis was not performed. IR (nujol, cm^{-1}) $\tilde{v}$ = 3067w, 3058w, 2062, 2040, 2022, 2011, 1591, 1488, 1457, 1437, 1314, 1252, 1173, 1005, 757, 738, 669, 648, 636, 620.

10.4.14. PbCl$_2$(bipy) from Pb(N$_3$)$_4$(bipy)

A solution of Pb(N$_3$)$_4$(bipy) in CH$_2$Cl$_2$ was prepared. Storage at rt under the exclusion of light for several hours resulted in the formation of a small amount of microcrystalline solid which mulls poorly and displays very few bands in the IR spectrum. IR spectroscopy confirmed the solid did not contain coordinated bipy. IR (nujol, cm^{-1}) $\tilde{v}$ = 2228, 2128, 2018br, 757. After ca. 7 days resulted in a colourless solution containing colourless block-shaped crystals which were confirmed as PbCl$_2$(bipy) by single crystal X-ray diffraction studies. The supernatant solution was shown by IR spectroscopy to contain v(N$_3$) bands, hypothesised to arise from a Pb(IV) azido complex of unknown identity. IR (CH$_2$Cl$_2$, cm^{-1}) v(N$_3$) = 2161, 2138, 2128.

10.4.15. Pb(N$_3$)$_4$(bipy) from Pb(OAc)$_4$

Pb(OAc)$_4$ (0.092 g, 0.21 mmol, 1.00 eq), NaN$_3$ (0.082 g, 1.26 mmol, 6.00 eqs) and bipy (0.092 g, 0.59 mmol, 2.80 eqs) were combined and suspended in 15 mL CH$_2$Cl$_2$. After ca. 5

mins stirring at rt, a pale-yellow solution had formed. Further stirring at rt for 3 h resulted in a thicker suspension and the formation of a dark orange solid similar in appearance to the residue formed from the preparation of $Pb(N_3)_4(bipy)$ from $(NH_4)_2[PbCl_6]$. IR spectroscopy of the reaction solution showed no bands associated with coordinated bipy and a $\nu(N_3)$ band inconsistent with $Pb(N_3)_4(bipy)$ described above and the reaction was discarded. IR (CH_2Cl_2, cm^{-1}) $\nu(N_3) = 2048$.

10.4.16. Pb(N₃)₄(phen)

The same procedure used for the preparation of $Pb(N_3)_4(bipy)$ was adapted for the preparation of the phenanthroline adduct. The coordination of phenanthroline ligands to the coordination centre could not be clearly identified and the $\nu(N_3)$ bands of the reaction solution were observed to be almost identical to the reported bands of $(NH_4)_2[Pb(N_3)_6]$ in the same solvents ($\tilde{\nu} = 2055$, $2038 \ cm^{-1}$).[97] As such, it is unclear if $Pb(N_3)_4(phen)$ had formed and the reaction was discarded. IR (CH_2Cl_2, cm^{-1}) $\nu(N_3) = 2138$ (HN_3), 2131, 2055, 2039.

10.4.17. Attempted preparation of Pb(N₃)₄(L)₂ (L = py, pic)

L = py: $(NH_4)_2[PbCl_6]$ (0.083 g, 0.18 mmol, 1.00 eq) and NaN_3 (0.126 g, 1.94 mmol, 10.78 eqs) were combined and suspended in 10 mL CH_2Cl_2. The addition of pyridine (0.1 mL, 1.24 mmol, 6.89 eqs) immediately resulted in the formation of a dark red suspension. The suspension was stirred at 3 h at rt under the exclusion of light, resulting in a white solid suspended in an orange solution. IR spectroscopy showed no evidence of coordinated pyridine. Further stirring under the same conditions for 19 h did not result in any further change and the solution was discarded. IR (CH_2Cl_2, cm^{-1}) $\nu(N_3) = 2138$ (HN_3), 2128, 2059, 2041.

L = pic: $(NH_4)_2[PbCl_6]$ (0.086 g, 0.19 mmol, 1.00 eq) and NaN_3 (0.136 g, 2.10 mmol, 11.05 eqs) were combined and suspended in picoline (10 mL). The suspension was stirred under the exclusion of light for ca. 2 h. IR (pic, cm^{-1}) $\nu(N_3) = 2121$, 2054, 2047, 2034. The latter three $\nu(N_3)$ bands are similar to those observed in the attempted preparation of $Pb(N_3)_4(py)_2$, which showed no pyridine coordination, and as such the reaction was halted.

10.4.18. Attempted preparation of Pb(N₃)₂(py)₂ from Pb(N₃)₂

$Pb(N_3)_2$ (61 mg max.) was prepared from $Pb(NO_3)_2$ (69 mg, 0.21 mmol, 1.00 eq) and NaN_3 (27 mg, 0.42 mmol, 2.00 eqs) following the procedure detailed above and washed with H_2O, EtOH and Et_2O (1 x 5 mL each). The dry white solid was contained in a Schlenk tube immersed in water throughout. The solid was resuspended in py (10 mL) and stirred at rt for 1.5 h. No

change was observed in the suspension and IR spectroscopy showed no evidence of coordinated py. IR (py, cm^{-1}) $\tilde{\nu}$ = 2038, 2020, 2000. Replication of the reaction on similar scales with picoline (ca. 69 mg Pb(N$_3$)$_2$ and 10 mL pic) also showed no ancillary ligand coordination.

10.4.19. Preparation of [PPN]$_2$[PbCl$_4$(CHN$_4$)$_6$] from attempted preparation of [PPN]$_2$[Pb(CHN$_4$)$_6$]

[PPN]$_2$[PbCl$_6$] (0.218 g, 0.15 mmol, 1.00 eq) and NaN$_4$CH (0.195 g, 2.12 mmol, 14.10 eqs) were suspended in 20 mL MeCN and stirred at rt for 72 h under the exclusion of light, forming an orange suspension. The colourless supernatant solution was filtered onto a fresh portion of NaN$_4$CH (0.133 g, 1.45 mmol, 9.67 eqs) and the orange filter residue discarded. The suspension was stirred vigorously under the exclusion of light for a further 8.5 h at rt, forming a pale orange solid suspended in a colourless supernatant solution. The filter residue was isolated by filtration and discarded. Colourless crystals, observed to form in the filtrate solution after several minutes, were redissolved by warming in hot air and cooled to −28 °C for several days. This did not afford [PPN]$_2$[Pb(CHN$_4$)$_6$] but instead gave colourless cuboidal crystals of [PPN]$_2$[PbCl$_4$(CHN$_4$)$_2$] (84 mg, 33%).

10.5. Arylpentazoles

10.5.1. Hydroxyphenylpentazole, HOP−N$_5$

Based on a preparative procedure by Ek *et al.*[282]

A solution of 4-hydroxyaniline (2.620 g, 24.93 mmol, 1.33 eqs) in 45 mL H$_2$O was cooled to −3°C. Ice-cold HCl (35%, 3.07 mL) was added to the solution. NaNO$_2$ (1.351 g, 19.58 mmol, 1.04 eqs) was added in portions over 8 minutes, ensuring that the temperature of the reaction solution did not exceed −3 °C. The addition of NaNO$_2$ caused the solution to change colour from pale grey to deep red/purple. The solution was stirred at −3 °C for 10 mins before an ice-cold solution of NaN$_3$ (1.224 g, 18.83 mmol, 1.00 eq) in H$_2$O (7 mL) was added in one portion. Upon addition, a dark green suspension formed immediately, accompanied by the release of gas. The suspension was stirred at 0 °C for a further 10 minutes. The solid material was isolated by filtration using a cold filter stick pre-cooled to (−5 to −10 °C) and washed with 2 x 5 mL ice-cold H$_2$O. The dark green filtrate changes colour and releases gas when warmed to rt and was discarded. The pale grey-green filter residue was dried on the filter stick at the same temperature under dynamic vacuum until no change in pressure was observed between static and dynamic vacuum. The solid was then rapidly transferred to a pre-cooled (−20 °C) Schlenk

tube. This gave hydroxyphenylpentazole, HOP−N$_5$ (0.470 g, 16%) as a pale grey/green solid. Single crystals of HOP−N$_5$ were obtained by dissolving a solid sample in ca. 2 mL of cold (−20 °C) THF in a Schlenk tube, followed by cooling to −78 °C by storage in a Dewar flask filled with dry ice for ca. 3 h. After this time, colourless needle crystals were observed to form, contained in a pale green supernatant solution. The supernatant solution can be isolated using a pre-cooled filter cannula but is more easily and rapidly removed by careful decantation using a pre-cooled volumetric pipette. IR (nujol, cm^{-1}) ṽ = 3523, 3316br, 3126, 3095, 3084, 3050, 2734, 2663, 2572, 2436, 2231, 2197, 2120, 2081 ν(N$_5$), 1912sh, 1665, 1614sh, 1597s, 1514, 1466, 1358, 1352, 1287, 1230, 1222, 1174, 1132, 1120, 1105, 983, 947, 843, 826, 771, 740, 718, 708, 628. NMR (CD$_3$CN, −20 °C, ^{1}H, ppm) δ = 8.03 (s), 7.95 (d, C*H*), 7.22 (s), 7.06 (d, C*H*), 2.49 (s, O*H*). NMR (CD$_3$CN, −20 °C, ^{13}C, ppm) δ = 160.0 (s, *C*−OH), 126.6 (s, *C*H), 123.5 (s, *C*H), 120.5 (s, *C*H), 116.9 (s, *C*−N$_5$). NMR (CD$_3$CN, −20 °C, ^{14}N, ppm) δ = −135.86 (s, N$_5$). NMR signals at δ = 6.89, 6.78 ppm (^{1}H, −20 °C) and the IR band at 2120 cm^{-1} are attributed to HOP−N$_3$.

10.5.2. Hydroxyphenylazide, HOP−N$_3$

A solid sample of HOP−N$_5$ was allowed to warm to rt in the dark. A dark red sticky oil is formed which contains HOP−N$_3$. Slower thermal decomposition at −10 °C for ca. 24 h results in a grey solid that is almost spectroscopically identical to the red oil. IR (nujol, cm^{-1}) ṽ = 3523, 3419, 3317br, 3129, 3092, 3050, 2571, 2433, 2259, 2225, 2200, [2114br, 2077s] (ν(N$_3$)), 1912 (ν(N$_5$)), 1881, 1665, 1614, 1591s, 1511, 1466, 1314 (ν(N$_5$)), 1287, 1259, 1230, 1173, 1133, 1119, 1105, 1067, 983, 949, 846, 829, 775, 741, 718, 710, 630br, 525. NMR (^{1}H, CD$_3$CN, ppm) δ = 6.98 (s), 6.92 (d, C*H*), 6.83 (d, C*H*), 2.19 (s, O*H*). NMR (^{13}C, CD$_3$CN, ppm) δ = 155.3 (s, *C*−OH), 132.3 (s,*C*H), 121.0 (s), 117.4 (s, *C*−N$_5$).

10.5.3. Caesium pentazolylphenolate, CsOP−N$_5$

Based on a preparative procedure by Ek *et al.*[282]

Crude HOP-N$_5$ (0.356 g, 2.39 mmol if all solid is assumed to be HOP-N$_5$, 1.00 eq) was placed into a precooled (−45 °C) Schlenk tube and dissolved in 4 mL cold (−45 °C) degassed MeOH, forming a dark yellow/brown solution. A −45 °C solution of CsOH.H$_2$O (0.487 g, 2.90 mmol, 1.21 eqs) in 4 mL degassed MeOH was added steadily to the solution containing HOP-N$_5$ over the course of 5 minutes. The solution was allowed to warm to −20 °C over the course of 2h with stirring, then concentrated under dynamic vacuum at the same temperature to approximately ¼ of the original volume (ca. 2 mL). This resulted in the precipitation of a

crystalline cream solid contained in a brown supernatant solution. The solid was isolated by cold filtration using a precooled (-30 °C) filter stick, washed with degassed acetone (-50 °C, 2 x 2 mL) and dried at the same temperature under dynamic vacuum on the filter. Once dry, as evidenced by the absence of a pressure change between static and dynamic vacuum, the solid was transferred to a precooled (-30 °C) Schlenk tube in the same method used for the transfer of solid HOP$-$N$_5$. This gave CsOP$-$N$_5$ (0.143 g, 20%) as a crystalline cream solid. Attempts to grow single crystals from cold solutions of MeOH were unsuccessful; crystals suitable for X-ray diffraction studies were obtained from the crystalline bulk solid. IR (nujol, cm^{-1}) $\tilde{\nu}$ = 3396br (MeOH), 2231br, 2216 (ν(N$_3$)), 2085 (ν(N$_5$)), 2076 (ν(N$_3$)), 1889 (ν(N$_5$)), 1593, 1573, 1511, 1457, 1343, 1320, 1298, 1212, 1177, 1116, 1102, 1001, 991, 950, 934, 838, 744, 642.

10.5.4. Dimethylhydroxyaniline

Based on a preparative procedure by Alisi *et al*.[363]

Sulphanilic acid (7.833 g, 45.23 mmol, 1.08 eqs) was almost completely dissolved in 50 mL H$_2$O. Na$_2$CO$_3$ (2.201 g, 20.77 mmol, 0.49 eqs) was added to the suspension with stirring, resulting in the release of gas and the dissolution of almost all solid, and stirred for a further 15 mins at rt. Stirring for a further 15 mins did not increase the amount of dissolution of the solid. The suspension was then cooled to 10 °C and 13.5 mL of an ice-cold aqueous NaNO$_2$ solution (4.658 g in 13.5 mL H$_2$O, 5 M, 67.5 mmol, 1.61 eqs) was added dropwise over the course of 10 minutes, forming a pale brown solution. The solution was then cooled to 0 °C in ice and decanted into a beaker containing ice-cold HCl (9 mL, 12 M, 35%, 0.11 mmol, 0.002 eqs), forming a peach-coloured precipitate (suspension *A*) which was stirred vigorously at 0 °C for 50 mins.

In a separate flask, NaOH (9.002 g, 22.51 mmol, 0.54 eqs) was dissolved in 50 mL H$_2$O whilst being cooled in ice. The solution was warmed to rt and dimethylphenol (5.133 g, 42.02 mmol, 1.00 eq) was added to form a dusky-pink solution. This solution was cooled to 5°C in ice and suspension *A* was added steadily in 5 mL portions, immediately forming an intense red solution. Care was taken to ensure the reaction temperature did not exceed 5°C during addition. The solution was stirred at 0 °C for 1 h before being heated to 80 °C and Na$_2$S$_2$O$_4$ (20.01 g, 0.11 mmol, 2.60 eqs) added at this temperature over 5 minutes, with stirring. After ca. 15 g of Na$_2$S$_2$O$_4$ had been added, the reaction solution lightened in colour to form an intense yellow solution which appears red in the bulk, alongside the formation of a precipitate. Once addition was complete, the solution was allowed to cool to rt with stirring, resulting in the formation of

further precipitate. The red/yellow solid was isolated by filtration and washed with a saturated solution of $Na_2S_2O_4$ (5 x 10 mL), resulting in the solid becoming pale pink. The solid was dried on the filter to give dimethylhydroxyaniline (3.281 g, 57%) as a pale pink solid. IR (nujol, cm^{-1}) ṽ = 3359, 3291, 2080br, 1918, 1890, 1739, 1699, 1608br, 1386, 1338, 1290, 1207, 1159, 1028, 971, 952, 898br, 849, 758, 701, 593sh, 579sh. NMR (^{1}H, DMSO-d$_6$, ppm) δ = 7.14 (s, C*H*), 6.16 (s, C*H*), 4.26 (s, O*H*), 3.33 (H_2O), 2.02 (s, C*H$_3$*). NMR (^{13}C, DMSO-d$_6$, ppm) δ = 143.9 (s, *C*−OH), 140.8 (s, *C*−NH), 125.2 (s, *C*−H), 114.3 (s, *C*−CH$_3$), 16.8 (s, *C*H$_3$).

10.5.5. Dimethylhydroxyphenylpentazole, DMHP−N$_5$

Based on a preparative procedure by Zhang *et al.*[364]

Dimethylhydroxyaniline (0.687 g, 5.01 mmol, 1.00 eq) was suspended in THF (2mL) in a Schlenk tube. HCl (35%, 0.79 mL, 8.95 mmol, 1.79 eqs) was added. The red/purple suspension was cooled to −5 °C in a cold bath and an ice-cold solution of $NaNO_2$ (0.359 g, 5.20 mmol, 1.04 eqs) in the minimum volume of H_2O (0.67 mL) was added dropwise. The suspension was stirred at this temperature for 30 mins then cooled to −40 °C. A cold (−5 °C) 1:2 mixture of MeOH (6 mL) and 60-80 petroleum ether (12 mL) was added, forming a colourless upper layer and a dark red lower layer. An ice-cold solution of NaN_3 (0.338 g, 5.20 mmol, 1.04 eqs) in 1 mL H_2O was added by volumetric pipette to the lower layer, resulting in the immediate formation of a suspension and gas release. The suspension was stirred vigorously at −40 °C for 15 minutes before the solid was isolated by cold filtration (−40 °C) and the dark red filtrate was discarded. The solid was washed with −40 °C MeOH (4 x 5 mL) and dried under dynamic vacuum on the filter at temperatures not exceeding −30 °C. This gave dimethylhydroxyphenylpentazole, DMHP−N$_5$ (0.133 g, 14%) as a dark pink solid. IR (nujol, cm^{-1}) ṽ = 3353, 3382br, 3065, 2734, 2430, 2231, 2188, 2123, 1910, 1770, 1753, 1742, 1614, 1594, 1495s, 1484, 1431, 1387, 1345, 1312, 1255, 1233, 1206, 1139, 1123, 1114, 1085, 1070, 1036, 971, 946, 886, 876, 735, 716, 591. IR (THF, −48 °C) v(N_3) = 2113, 2105, v(N_5) = 1600. UV (THF, −45 °C, nm) λ = 221, 286.

10.5.6. Dimethylhydroxyphenylazide, DMHP−N$_3$

A solid sample of DMHP−N$_5$ was warmed to rt under the exclusion of light, resulting in a dark red sticky solid. Prolonged storage of DMAP−N$_5$ for several months at −28 °C also forms DMAP−N$_3$ as a pale grey solid. IR (nujol, cm^{-1}) ṽ = 3573, 3553, 3385, [2122, 2102br v(N_3)], 1614, 1596, 1494, 1485, 1436, 1344, 1335, 1313, 1255, 1233, 1205, 1114, 1085, 1032, 1001,

972, 945, 883, 875, 860, 850, 774, 734, 698, 637, 590. IR (MeCN, cm^{-1}) ν(N$_3$) = 2117br. IR (THF, cm^{-1}) ν(N$_3$) = 2109. UV (THF, −15 °C, nm) λ = 238, 245, 279.

10.5.7. Methoxyphenylpentazole, MeOP−N$_5$

Based on a preparative procedure by Geiger and Haas.[365]

p-anisidine (0.400 g, 3.25 mmol, 1.00 eq) was dissolved in 2.05 MeOH and cooled to −5 °C. Ice-cold HCl (37%, 0.53 mL, 6.35 mmol, 1.95 eqs) was added dropwise to the solution over the course of 5 mins, resulting in a colour change from dark yellow to dark purple approximately halfway through addition. Cold (−5 °C) butylnitrite (0.42 mL, 3.59 mmol, 1.10 eqs) was added dropwise over the course of 5 minutes, resulting in a further colour change to deep red ca. 5 minutes post-addition. The solution was stirred between −10 and −5 °C for 30 minutes, then cooled to −30 °C. A cold (−30 °C) solution of MeOH:H$_2$O (1:1, 5.60 mL total) was added, followed by 45 mL cold (−35 °C) hexane, resulting in the formation of a biphasic solution containing a colourless organic (upper) layer and a dark red aqueous (lower) layer. A cold (−30 °C) solution of NaN$_3$ (0.228g, 3.51 mmol, 1.08 eqs) in MeOH:H$_2$O (2:3, 1.8 mL total) was added directly to the lower layer. This addition immediately causes gas release and the formation of a pale pink/purple solid in the aqueous layer. The suspension was stirred at −35 °C for 30 minutes before the solid was isolated by cold filtration at −35 °C. The pale pink filter residue was washed with precooled (−78 °C) MeOH:H$_2$O (2:3, 2 x 15 mL total) then MeOH at the same temperature, then dried at −35°C on the filter under dynamic vacuum until the pressure is near-constant (ca. 6.5−5.2x10^{-2} mbar). This gave MeOP−N$_5$ (0.087 g, 15%) as a pale grey/green solid. Cooling of cold (−35 °C) saturated CH$_2$Cl$_2$ or THF solutions of MeOP−N$_5$ to −78 °C did not result in crystallisation. IR (nujol, cm^{-1}) $\tilde{\nu}$ = 3425br, 3121, 3092, 3081, 3061, 3021, [2134, 2103] (ν(N$_3$)), 2048br, 1901, 1651, 1607, 1596, 1507, 1466, 1438, 1344 ν(N$_5$), 1306, 1288, 1260 ν(N$_5$), 1247, 1210 ν(N$_5$), 1180, ,1174, 1148, 1127, 1120 ν(N$_5$), 1103, 1024, 959 ν(N$_5$), 940, 835 ν(N$_5$), 827, 819, 803, 754, 717 ν(N$_5$), 636, 618 ν(N$_5$).

10.5.8. Methoxyphenylazide, MeOP−N$_3$

A solid sample of MeOP−N$_5$ was stored at −10 °C for ca. 24 h, resulting in MeOP−N$_3$ as a pale grey solid. IR (nujol, cm^{-1}) $\tilde{\nu}$ = 3425br, 2262, [2134, 2106, 2052 ν(N$_3$)], 1875, 1640, 1585, 1509, 1304, 1294, 1285, 1247, 1181, 1172, 1151w, 1131, 1110, 1040, 1027, 827, 809w, 794w, 756, 642, 626.

10.6. Pentazolate (N_5^-) salts

10.6.1. Reaction of DMAP-N₅ with Na

In a glovebox, solid sodium (11 mg, 0.48 mmol, 1.20 eqs) was cut into small pieces and placed into an ampoule equipped with a Teflon Young's tap that had previously been thoroughly baked out under dynamic vacuum. The ampoule was removed from the glovebox and connected to a cylinder of ammonia using Teflon tubing and a Suba seal connection to the ampoule. The transfer line was gently baked out under argon before the ampoule was immersed into a -65 °C cold bath (^{i}PrOH/liquid N_2). The cylinder was opened and approximately 4 mL of NH_3 was condensed into the ampoule, forming an intense deep blue solution. The cylinder was disconnected, the ampoule refilled with argon and solid DMAP-N₅ (044 mg, 0.40 mmol, 1.00 eq) was quickly transferred into the solution under argon flow. Almost immediately, the blue colour disappeared and a pale brown solution was formed. The solution was allowed to warm to -35 °C over the course of 1 h with stirring, before the ampoule was connected to a bubbler and purged with argon for several minutes. The bath temperature was raised to -30 °C to evaporate the remaining NH_3. This formed a colourless, acrystalline solid (ca. 40 mg) which smelt strongly of an amide compound. No azide bands are observed, even when the solid is warmed to rt. The colour of the solid varied between colourless and brown between preparations. IR (nujol, cm^{-1}) $\tilde{v} = 3638, 3575, 3257, 3209, 2725, 2671, 1516, 1367, 812, 774$.

10.6.2. Iron(II) glycinate

Based on a preparative procedure by Fitzsimmons *et al.*[366]

In a Schlenk tube, a mixture of $LiOH \cdot H_2O$ (4.247 g, 0.10 mol, 2.00 eqs) and glycine (7.598 g, 0.10 mol, 2.00 eqs) was suspended in 80 mL degassed MeOH. A large stirrer bar is required for effective stirring; occasionally, manual agitation is required under argon flow to allow the mixture to stir. The suspension was heated and stirred vigorously in a steam bath set to 95 °C for 1 h. The resulting thick white suspension was allowed to settle and the supernatant solution filtered into a solution of $FeCl_2 \cdot 4H_2O$ in 25 mL degassed MeOH. Upon addition of the filtrate solution, the pale green solution containing $FeCl_2$ became darker in colour and a precipitate formed. The suspension was stirred at rt for a further 1 h, forming a finely-divided solid which results in long filtration times. The supernatant solution was removed by filtration and discarded. The grey-green filter residue was washed with a further 25 mL degassed MeOH, with manual stirring under argon flow, and dried under high vacuum. This gave Fe(gly)₂ as a finely-divided, pale grey solid (4.417 g, 43%) which mulls poorly. Air exposure results in an immediate discolouration to a brown solid consistent with iron oxides and consequently all

manipulations and weighing operations involving Fe(gly)$_2$ were performed in a glovebox. IR (nujol, cm^{-1}) $\tilde{\nu}$ = 3332, 3277, 3183, 1613, 1332, 1185, 1089, 1020, 937, 906.

10.6.3. 'NaN$_5$·3H$_2$O'

Based on a preparative procedure by Xu *et al.*[75]

2,6-dimethylhydroxyphenylpentazole, DMHP-N$_5$ (0.260 g, 1.36 mmol, 1.00 eq) was placed into a precooled (−45 °C) Schlenk tube and suspended in cold (−45°C) degassed MeCN:MeOH (1:1, 40 mL total). To this pink suspension, an ice-cold solution of Fe(gly)$_2$ (0.694 g, 3.40 mmol, 2.5 eqs) in degassed H$_2$O (5 mL) was added, resulting in the immediate formation of a white precipitate. The suspension was cooled to −45 °C by the use of a cryostat and stirred at this temperature for 0.5 h. After this time, a green/blue solid had formed, contained in a pale yellow solution. A cold (−45 °C) solution of mCPBA (0.952 g, 5.52 mmol, 4.06 eqs) in 7 mL degassed MeOH was added. After ca. 5 mins stirring, the suspension had turned dark brown. The suspension was stirred at this temperature for 25 h, then filtered at the same temperature using a cold filter stick. Both the filtrate and filter residue were dark brown. The filter residue was discarded and all solvent was removed from the filtrate under dynamic vacuum at −35 °C over the course of 3 days. This gave a dark brown solid (3.729 g) shown by mass spectrometry to contain N$_5^-$.

The brown solid was suspended in ca. 50 mL H$_2$O, stirred at rt for 30 mins and filtered. The filter residue was discarded and the filtrate dried *in vacuo* to form a brown solid which contains signals at m/z = 70 (N$_5^-$), 111 ([ClC$_6$H$_5$]$^-$) and 155 ([ClC$_6$H$_4$COO]$^-$). Separation by reverse-phase HPLC in batches results in three components, the first of which are collected and combined with the same fractions in each batch. The second and third components, in order of elution, are consistent with chlorobenzene and *m*-chlorobenzoate, respectively. Removal of all solvent *in vacuo* gives a brown solid (ca. 73 mg from 200 mg starting material), the mass spectrum of which is dominated by a signal consistent with N$_5^-$. The exact identity of the compound could not be determined and was termed 'NaN$_5$·3H$_2$O'. IR (nujol, cm^{-1}) $\tilde{\nu}$ = 3399br, 3212br, 3035br, 2040br, 1625s, 1446, 1409, 1332, 1256, 1034, 991, 920, 898, 676, 590. MS (ESI$^-$, MeOH:H$_2$O (70%:30%)) m/z = 69 (9%, unknown), 70 (100%, N$_5^-$), 77 (8%, unknown), 86 (12%, unknown), 93 (38%, unknown), 102 (12%, [N$_5$·MeOH)]$^-$), 113 (37%, [H(N$_5$)N$_3$)]$^-$). On one occasion, an additional fragment at m/z = 141 ([H(N$_5$)$_2$]$^{\cdot-}$) was observed.

The brown solid can also be separated by the use of cold silica column chromatography, eluted with 10:1 EtOAc:EtOH at ca. −35 °C. At a column width and height of ca. 3 x 10 cm, elution

gives three distinct bands visualised under UV light. Separation obtains three fractions. The first fraction, a pale yellow solid, was dried under vacuum and gave negligible mass insufficient for characterisation (i.e., <5 mg). The second and third fractions form dark brown oils which do not undergo noticeable decomposition upon warming to rt. Although cold column chromatography was used in this instance, it appears separation at rt would obtain the same results.

10.6.4. '[PPN]N$_5$'

A sample of 'NaN$_5$·3H$_2$O' (86 mg, max. 0.67 mmol, 4.50 eqs) was dissolved in 4 mL H$_2$O. In a separate flask, [PPN]Cl (85 mg, 0.15 mmol, 1.00 eq) was suspended in 8 mL H$_2$O. Both solutions were heated to 60 °C, forming clear colourless ([PPN]Cl) and pale brown (NaN$_5$) solutions. Addition of the [PPN]Cl solution to the solution containing NaN$_5$ at the same temperature resulted in the immediate precipitation of a white solid. The suspension was allowed to cool to rt for 5 mins, with stirring, before being cooled in ice. The very pale brown solid (58 mg, 64%) was isolated by filtration, washed with ice-cold H$_2$O (3 x 3 mL) and dried on the filter. IR (nujol, cm^{-1}) $\tilde{\nu}$ = 3374br, 3052, 2012, 1972, 1910, 1827, 1776, 1637br, 1588sh, 1347, 1298, 1259, 1219, 1187, 1173, 1114, 1023, 997sh, 932, 855, 849, 750, 690, 616, 531. MS (ESI$^-$, MeCN) m/z = 69 ([PH$_2$.H$_2$O]$^-$ or [NaNO$_2$]$^-$, 25%), 70 ([N$_5$]$^-$, 38%), 89 ([P(MeCN)(OH)]$^-$, 5%), 102 ([(NH$_3$)$_5$·OH]$^-$, 4%), 106 ([N$_5$·2H$_2$O]$^-$, <1%), 113 ([P$_2$O$_3$H$_3$]$^-$, 0.1%), 145 (unknown, 12%). An additional fragment at m/z = 159 ([N$_3$·2MeCN·Cl]$^-$, 100%) is present. MS (ESI$^+$, MeCN) m/z = 538 ([PPN]$^+$, 100%).

10.6.5. 'AgN$_5$'

A solution of AgNO$_3$ (0.98 mg, 0.58 mmol, 1.00 eq) in 1 mL H$_2$O was added to a solution of 'NaN$_5$·3H$_2$O' (81 mg, 0.63 mmol, 1.09 eqs) in 5 mL H$_2$O. A white suspension formed immediately, which was stirred at rt for 5 mins under the exclusion of light. The white solid was isolated by filtration, washed with H$_2$O (3 x 2 mL) and Et$_2$O (4 x 2 mL) and dried on the filter under the exclusion of light. This gave 'AgN$_5$' (48 mg, 47%) as a free-flowing white solid. IR (ATR, cm^{-1}) $\tilde{\nu}$ = 1641, 1620, 1438, 1397, 1264, 1147, 1087, 1016, 808, 693. MS (ESI$^-$, H$_2$O) m/z = 70 ([N$_5$]$^-$, 18%), 120 ([N$_3$·HN$_3$·Cl]$^-$, 5%). Additional impurity fragments are observed at m/z = 131 ([NaNO$_3$·NO$_2$]$^-$, 92%) and 147 ([Na(NO$_3$)$_2$]$^-$, 100%). The brown filtrate solution was allowed to evaporate to dryness at rt and redissolved in 3 mL H$_2$O. Treatment of the colourless filtrate with further AgNO$_3$ (100 mg, 0.59 mmol, 1.02 eqs) in 1 mL H$_2$O resulted in the immediate formation of a small amount of white precipitate, which was removed by filtration. Mass spectrometry of the filtrate solution showed no signals associated

with N_5; MS (ESI$^-$, H_2O) m/z = 131 ([NaNO$_3$·NO$_2$]$^-$, 12%), 147 ([Na(NO$_3$)$_2$]$^-$, 25%), 216 ([Ag$_2$]$^-$, <1%), 232 ([Ag(NO$_3$)$_2$]$^-$, 100%), 317 ([Ag$_3$(NO$_3$)$_5$]$^-$, <1%), 366 (unknown Ag-containing fragment, 2%), 402 ([Ag$_2$(NO$_3$)$_3$]$^-$, <1%).

10.7. Dicyanamides

10.7.1. [PPN][N(CN)$_2$]

Based on a preparative procedure by Köhler *et al.*[339]

A solution of NaN(CN)$_2$ (0.526 g, 5.91 mmol, 2.04 eqs) in 30 mL hot (60 °C) water was added to a solution of [PPN]Cl (1.66 g, 2.89 mmol, 1.00 eq) in 30 mL hot water at the same temperature. Upon combination, a large amount of white precipitate immediately formed. The suspension was stirred at rt for 15 minutes before the precipitate was isolated by filtration and dried in air. The colourless filtrate was discarded. Once dry, the solid filter residue was recrystallised at −28 °C from 15 mL hot MeCN. This gave [PPN][N(CN)$_2$] (0.935 g, 53%) as colourless block crystals. IR (nujol, cm^{-1}), $\tilde{\nu}$ = 3485, 3135, 3061, 3015, [2228, 2188, 2128]s (ν(CN)), 2168w, 2098w, 1588, 1574, 1486, 1438, 1304, 1179, 1116, 1028, 997, 906, 899, 798, 764, 744, 690, 548, 531. IR (MeCN, cm^{-1}) ν(CN) = 2228, 2193, 2132. IR (THF, cm^{-1}) ν(CN) = 2220w, 2126w. IR (CH$_2$Cl$_2$, cm^{-1}) ν(CN) = 2231, 2191, 2131. NMR (^{1}H, CDCl$_3$, ppm) δ = 7.90-7.37 (m, PPN). NMR (^{13}C, CDCl$_3$, ppm) δ =133.4 (s, PPN), 132.2 (m, PPN), 129.7 (m, PPN), 127.0 (dd, PPN), 120.3 (s, [N(CN)$_2$]$^-$). NMR (^{31}P, CDCl$_3$, ppm) δ = 21.11 (s, PPN).

10.7.2. AgN(CN)$_2$

Adapted from a preparative procedure by Li *et al.*[367]

AgNO$_3$ (5.89 g, 34.67 mmol, 1.00 eq) was dissolved in 25 mL H$_2$O under the exclusion of light. The solution was combined with a solution of NaN(CN)$_2$ (3.089 g, 34.70 mmol, 1.00 eq) in 25 mL H$_2$O, resulting in the immediate precipitation of a white solid. The solid was isolated by filtration and the filtrate discarded. The filter residue was dried in air for 20 mins under the exclusion of light, before being transferred to a Schlenk tube, immersed into an oil bath set to 80 °C and heated under dynamic vacuum for 17 h. This yielded AgN(CN)$_2$ (5.751 g, 95%) as a pale grey solid. Exposure to daylight results in discolouration of the solid from pale to extremely dark grey, as observed with other silver salts. IR (nujol, cm^{-1}) $\tilde{\nu}$ = 3601s, 3521, 3232, 3175, 3087, 2736, 2412, 2372, 2308, 2291 (MeCN), 2251 (MeCN), 2187, 2021w, 1416, 1150, 1008, 932s, 655.

10.7.3. Attempted preparation of [PPN]₂[Si{N(CN)₂}₆] from SiCl₄ + [PPN][N(CN)₂]

SiCl₄ (0.1 mL, 0.87 mmol, 1 eq) added to a suspension of [PPN][N(CN)₂] (1.096 g, 1.81 mmol, 2.07 eqs) in MeCN (10 mL). The resulting yellow solution was stirred at rt for 19 h, after which time a small amount of yellow solid had formed on the walls of the Schlenk tube. The solution was cooled to −28 °C for 2 d, forming a glassy yellow solid (0.150 g). Concentration of the filtrate solution under dynamic vacuum resulted in the formation of a yellow oil, which became a foam upon further drying. Resuspension of the foam in MeCN, followed by filtration and cooling of the filtrate solution to −28 °C, resulted in a yellow solid containing glassy crystals which were unsuitable for single crystal X-ray diffraction studies. The identity of the reaction product is inconclusive but is hypothesised to be a silicon-dicyanamido oligomer (0.370 g). Both crops of solid are spectroscopically identical. IR (nujol, cm^{-1}) $\tilde{\nu}$ = 3052, 2248, 2191, 2177, 1438, 1284, 1267, 1185, 1162, 1114, 1025, 997, 795, 750, 690, 616. Further concentration of the filtrate solution resulted in crystals of [PPN][N(CN)₂] only.

10.7.4. Attempted preparation of [PPN]₂[Si{N(CN)₂}₆] from SiCl₄ + NaN(CN)₂

Dry NaN(CN)₂ (1.026 g, 11.52 mmol, 4.13 eqs) was suspended in MeCN (25 mL) and SiCl₄ (0.32 mL, 2.79 mmol, 1 eq) added, resulting in the formation of a pale yellow solution containing a white solid in suspension. The suspension was stirred at rt for 41 h, by which point the suspension had become too thick to stir. All solvent was removed under dynamic vacuum and the solid freeze-dried to give 1.543 g of a yellow solid, believed to be an oligomeric dicyanamidosilane. The solid is insoluble in MeCN and CH₂Cl₂. IR (nujol, cm^{-1}) $\tilde{\nu}$ = 3691, 3316, 3203, 3166, 3116, 2377, 2271, 2203, 1032, 944, 919, 793br, 749, 653.

10.7.5. Reaction of SiCl₄ + AgN(CN)₂

AgN(CN)₂ (0.609 g, 3.50 mmol, 4.02 eqs) was suspended in 20 mL MeCN. SiCl₄ (0.1 mL, 0.87 mmol, 1.00 eq) was added and the suspension stirred at rt for 17 h under the exclusion of light. A colourless solution was formed, containing a white solid suspended above a pale grey solid. Careful filtration of the pale grey solid gave an off-white suspension, which was filtered further to yield an off-white filter residue inconsistent with AgN(CN)₂. Further reaction with [PPN][N(CN)₂] did not result in any further reaction. IR (nujol, cm^{-1}) $\tilde{\nu}$ = 3706, 3337br, 3206br, 2447, 2387, [2291s, 2156] (MeCN)}, 2219s, 1074br, 963, 784, 655, 536, 522.

10.7.6. Me₃SiN(CN)₂

Based on a preparative procedure by Köhler and Maushake.[346]

$AgN(CN)_2$ (2.993 g, 17.21 mmol, 1.51 eqs) was suspended in dry Et_2O (25 mL) and cooled to −25 °C in a cold bath and cold (−25 °C) TMSCl (1.45 mL, 11.42 mmol, 1.00 eq) was added. The suspension immediately became much finer in appearance. The suspension was stirred at −25 to −35 °C for 3 h and allowed to settle before the supernatant solution was filtered into a precooled (−25 °C) Schlenk tube. The grey solid filter residue was discarded and all solvent removed from the filtrate under dynamic vacuum to give $Me_3SiN(CN)_2$ (1.293 g, 81%) as a white crystalline solid which melts at temperatures above −25 °C (ρ = ca. 1.052 g cm^{-3}). IR (nujol, cm^{-1}) $\tilde{v}$ = 3701, 3308br, 3197br, 3138br, 2700, 2660, 2441, 2387, 2254, [2225, 2143, 2114] (ν(CN)), 2026, 1969, 1890, 1259, 1057, 1006, 932, 846, 767, 650.

10.7.7. Reaction of Me₃SiN(CN)₂ and SnF₄

$Me_3SiN(CN)_2$ (0.5 mL, 0.526 g, 3.78 mmol, 4.06 eqs) was transferred into an ice-cold Schlenk tube and dissolved in MeCN (20 mL). The solution was cooled in ice and transferred into a Schlenk tube containing SnF_4 (0.181 g, 0.93 mmol, 1.00 eq) and stirred for a total of ca. 87 h in ice. After ca. 45 mins, the intensity of the ν(CN) band at 2118 cm^{-1} had decreased and remained constant for the rest of the stirring period. The suspension was filtered and the filtrate discarded. The filter residue was dried to give a white solid, hypothesised as $SnF_n\{N(CN)_2\}_{4-n}$ (n = 0−3, 0.256 g, 72% if n = 0) as a white solid which mulls poorly. IR (nujol, cm^{-1}) $\tilde{v}$ = 3225br, 2438, 2353, [2245, 2197]br (ν(CN)), 1307, 1256, 1168, 886, 852.

10.7.8. Ph₃SiN(CN)₂

Based on a preparative procedure by Köhler and Maushake.[346]

Triphenylchlorosilane (0.911 g, 3.09 mmol, 1.00 eq) and $AgN(CN)_2$ (0.804 g, 4.62 mmol, 1.50 eqs) were suspended in 15 mL THF and stirred at rt for 2.5 h. The pale grey solid was isolated by filtration and discarded. The colourless filtrate was concentrated under vacuum until the onset of crystallisation was observed on the sides of the flask, then cooled to −28 °C for 2 days. This gave $Ph_3SiN(CN)_2$ (0.322 g, 32%) as colourless glassy crystals contained in a pale yellow solution, which were isolated by filtration. Prolonged storage at rt under inert atmosphere for several days results in the discolouration of the crystals to pale yellow, believed to be due to slow oligomerisation. This discolouration is accelerated by heating. Crystallographic studies were not possible owing to the glassy nature of the solid. M.p. = 127−129 °C. Elem. Anal. Cald. for $C_{20}H_{15}N_3Si$ (325.45 g mol^{-1}) C, 73.82, H, 4.65, N, 12.91, Cl, 0 % ; found C, 73.39,

H, 4.76, N, 12.90, Cl, <0.3 %. IR (nujol, cm^{-1}) $\tilde{\nu}$ = 3732, 3183, 3137, 3072, 3055, 3013, 2073, 2450, 2401, 2256s, 2228, 2188, 2106, 1986, 1969, 1918, 1901, 1830, 1782, 1674, 1591sh, 1586, 1486, 1429sh, 1386, 1338, 1313, 1187, 1162, 1116sh, 1102, 1003sh, 917, 747sh, 716sh, 701sh, 681sh, 622. IR (THF, cm^{-1}) ν(CN) = 2257, 2250, 2205, 2196, 2139. NMR (^{1}H, CDCl$_3$, ppm) δ = 7.59 (m, Ph), 7.49 (m, Ph). NMR (^{13}C, CDCl$_3$, ppm) δ = 135.2 (s, Ph) 131.8 (s, Ph), 129.4 (s, Ph), 128.8 (s, Ph), 106.6 (s, N(CN)$_2$).

10.7.9. Attempted preparation of Sn{N(CN)$_2$}$_4$ and [PPN]$_2$[Sn{N(CN)$_2$}$_6$]

A solution of Ph$_3$SiN(CN)$_2$ (0.788 g, 2.42 mmol, 4.00 eqs) in 10 mL THF was transferred onto SnF$_4$ (0.117 g, 0.60 mmol, 1.00 eq) cooled in ice. The solution was allowed to warm to rt and stirred for 70 mins, forming a cream suspension which was isolated by filtration. The filtrate was discarded and the filter residue washed with THF. This gave a pale-yellow solid which is hypothesised to be SnF$_n${N(CN)$_2$}$_{4-n}$ (0.183g, n = 0−3, 80% if n = 0). The insolubility of the solid in hot THF, MeCN and CH$_2$Cl$_2$ precluded detailed analysis. IR (nujol, cm^{-1}) $\tilde{\nu}$ = 3254br, 3072, 3052, 2433br, 2293, 2200br, 1648br, 1429, 1261, 1187, 1122, 997, 849, 738, 718, 609, 616. Stirring a suspension of the solid product (0.183 g, 0.48 mmol, 1.00 eq) and [PPN][N(CN)$_2$] (0.991 g, 1.64 mmol, 3.43 eqs) in 20 mL MeCN for 3 d at rt showed no reaction and [PPN]$_2$[Sn{N(CN)$_2$}$_6$] was not formed.

10.7.10. [PPN]$_2$[SnCl$_4${N(CN)$_2$}$_2$]

To a solution of [PPN][N(CN)$_2$] (3.199 g, 5.29 mmol, 6.22 eqs) in MeCN (30 mL), SnCl$_4$ (0.1 mL, 0.85 mmol, 1.00 eq) was added. The solution was stirred overnight at rt, then concentrated under dynamic vacuum until the onset of precipitation, rewarmed in hot air and cooled to −28 °C. This resulted in colourless crystals of [PPN][N(CN)$_2$], which were isolated by filtration. The filtrate was concentrated again using the same procedure and rewarmed in hot air. Slow cooling to −28 °C in a Dewar flask filled with isopropanol resulted in white crystals of [PPN]$_2$[Sn{N(CN)$_2$}Cl$_4$] (1.024 g, 83%).). IR (nujol, cm^{-1}) $\tilde{\nu}$ = 3612, 3177w, 3058, 2728, 2697, 2401, 2305br, 2228, 2168, 2123, 2049, 1975, 1901, 1824, 1776, 1591, 1483, 1438, 1244br, 1185, 1108, 1028, 1000, 915, 849, 806, 744, 690, 670, 647, 616. NMR (^{1}H, CDCl$_3$, ppm) δ = 7.67-7.58 (m, PPN), 7.50-7.42 (m, PPN). NMR (^{13}C, CDCl$_3$, ppm) δ = 134.0 (s, PPN), 132.2 (m, PPN), 129.7 (m, PPN), 127.0 (dd, PPN), 116.6 (s, [Sn{N(CN)$_2$}$_2$Cl$_4$]$^{2-}$. NMR (^{31}P, CDCl$_3$, ppm) δ = 21.18 (s, PPN).

Chapter 11. References

1   L. Birckenbach and K. Kellermann, *Ber. Dtsch. Chem. Ges.*, 1925, **58**, 786–794.

2   A. M. Golub, H. Köhler and V. V Skopenko, *Chemistry of Pseudohalides*, Elsevier, Amsterdam, 1986.

3   H. Brand, A. Schulz and A. Villinger, *Z. Anorg. Allg. Chem.*, 2007, **633**, 22–35.

4   M. Kuhn and R. Mecke, *Chem. Ber.*, 1961, **94**, 3010–3015.

5   W. Madelung and E. Kern, *Justus Liebigs Ann. Chem.*, 1922, **427**, 1–26.

6   R. Warrington, *Q. Rev. Chem. Soc.*, 1849, **1**, 117–121.

7   F. Kröhnke and B. Sander, *Z. Anorg. Allg. Chem.*, 1964, **235**, 66–71.

8   F. D. Marsh, *J. Org. Chem.*, 1972, **37**, 2966–2969.

9   A. M. Golub, V. V Skopenko and H. Köhler, in *Chemistry of Pseudohalides*, Elsevier, Braunschweig, 1986, pp. 36–37.

10   C. E. Housecroft and A. G. Sharpe, in *Inorganic Chemistry*, Pearson/Prentice Hall, Harlow, 3rd edn., 2008, p. 406.

11   F. A. Cotton and G. Wilkinson, in *Advanced Inorganic Chemistry*, Wiley Interscience, New York, 5th edn., p. 248.

12   F. A. Cotton and G. Wilkinson, in *Advanced Inorganic Chemistry*, Wiley Interscience, New York, 5th edn., 1988, pp. 571–572.

13   A. M. Golub, H. Köhler and V. V Skopenko, in *Chemistry of Pseudohalides*, Elsevier, 1986, pp. 413–433.

14   A. M. Golub, H. Köhler and V. V Skopenko, in *Chemistry of Pseudohalides*, Elsevier, 1986, pp. 364–412.

15   M. J. Crawford, T. M. Klapötke, P. Klüfers, P. Mayer and P. S. White, *J. Am. Chem. Soc.*, 2000, **122**, 9052–9053.

16   A. Hantzsch and A. Rinckenberger, *Ber. Dtsch. Chem. Ges.*, 1899, **32**, 628–641.

17   M. Göbel, T. M. Klapötke and P. Mayer, *Z. Anorg. Allg. Chem.*, 2006, **632**, 1043–1050.

18   T. Austad, J. Songstad and K. Åse, *Acta Chem. Scand.*, 1971, **25**, 331–333.

19   N. N. Greenwood, R. Little and M. J. Sprague, *J. Chem. Soc.*, 1964, **1**, 1292–1295.

20   H. Köhler, B. Eichler and R. Salewski, *Z. Anorg. Allg. Chem.*, 1970, **379**, 183–192.

21   A. M. Golub, H. Köhler and V. V Skopenko, in *Chemistry of Pseudohalides*, Elsevier, 1986, pp. 465–469.

22   H. Brand, J. F. Liebman, A. Schulz, P. Mayer and A. Villinger, *Eur. J. Inorg. Chem.*, 2006, 4294–4308.

23   S. Trofimenko and B. C. McKusick, *J. Am. Chem. Soc.*, 1962, **84**, 3677–3678.

24   W. Will, *Ber. Dtsch. Chem. Ges.*, 1914, **47**, 961–965.

25   S. Trofimenko, E. L. Little and H. F. Mower, *J. Org. Chem.*, 1962, **27**, 433–438.

26   G. S. Hammond, W. D. Emmons, C. O. Parker, B. M. Graybill, J. H. Waters and M. F. Hawthorne, *Tetrahedron*, 1963, **19**, 177–195.

27   H. Köhler and B. Seifert, *Z. Naturforsch.*, 1967, **22b**, 238–241.

28   G. Bélanger-Chabot, M. Rahm, R. Haiges and K. O. Christe, *Angew. Chem. Int. Ed.*, 2013, **52**, 11002–11006.

29   E. Mayer, *Monatsh. Chem.*, 1969, **100**, 462–468.

30   R. Haiges and K. O. Christe, *Inorg. Chem.*, 2013, **52**, 7249–7260.

31   M. Ebespächer, T. M. Klapötke and C. M. Sabaté, *New J. Chem.*, 2009, **33**, 517–527.

32   T. Fendt, N. Fischer, T. M. Klapötke and J. Stierstorfer, *Inorg. Chem.*, 2011, **50**, 1447–58.

33   T. M. Klapötke, M. Stein and J. Stierstorfer, *Z. Anorg. Allg. Chem.*, 2008, **634**, 1711–1723.

34   P. L. Franke and W. L. Groeneveld, *Transit. Met. Chem.*, 1980, **5**, 240–244.

35   N. Fischer, T. M. Klapötke, S. Rappenglück and J. Stierstorfer, *Chempluschem*, 2012, **77**, 877–888.

36   T. M. Klapötke and C. M. Sabaté, *Chem. Mater.*, 2008, **20**, 3629–3637.

37   R. Schlodder, S. Vogler and W. Beck, *Z. Naturforsch.*, 1972, **27b**, 463–465.

38   G. Oskam, B. V. Bergeron, G. J. Meyer and P. C. Searson, *J. Phys. Chem. B*, 2001, **105**, 6867–6873.

39   V. Vreshch, B. Nohra, C. Lescop and R. Réau, *Inorg. Chem.*, 2013, **52**, 1496–1503.

40   S. R. Batten and K. S. Murray, *Coord. Chem. Rev.*, 2003, **246**, 103–130.

41   T. M. Klapötke, in *Chemistry of High-Energy Materials*, De Gruyter, Berlin/Boston, 3rd edn., 2015, p. 42.

42   T. M. Klapötke, in *Chemistry of High-Energy Materials*, De Gruyter, Berlin/Boston, 3rd edn., 2015, pp. 49–52.

43   T. M. Klapötke, in *Chemistry of High-Energy Materials*, De Gruyter, Berlin/Boston, 3rd edn., 2015, p. 173.

44   M. B. Talawar, R. Sivabalan, T. Mukundan, H. Muthurajan, A. K. Sikder, B. R. Gandhe and A. S. Rao, *J. Hazard. Mater.*, 2009, **161**, 589–607.

45   T. M. Klapötke, P. C. Schmid, S. Schnell and J. Stierstorfer, *J. Mater. Chem. A*, 2015, **3**, 2658–2668.

46   M. Sućeska, *Propellants, Explos. Pyrotech.*, 1999, **24**, 280–285.

47   G. Steinhauser and T. M. Klapötke, *Angew. Chem. Int. Ed.*, 2008, **47**, 3330–3347.

48   J. M. Samet, F. Dominici, F. C. Curriero, I. Coursac and S. L. Zeger, *N. Engl. J. Med.*, 2000, **343**, 1742–1749.

49   C. A. Pope, M. Ezzati and D. W. Dockery, *N. Engl. J. Med.*, 2009, **360**, 376–386.

50   D. J. Seidel and A. N. Birnbaum, *Atmos. Environ.*, 2015, **115**, 192–198.

51   G. Steinhauser, J. H. Sterba, M. Foster, F. Grass and M. Bichler, *Atmos. Environ.*, 2008, **42**, 8616–8622.

52   P. Kumarathilaka, C. Oze, S. P. Indraratne and M. Vithanage, *Chemosphere*, 2016, **150**, 667–677.

53   R. C. Pleus and L. M. Corey, *Toxicol. Appl. Pharmacol.*, 2018, **358**, 102–109.

54   R. T. Wilkin, D. D. Fine and N. G. Burnett, *Environ. Sci. Technol.*, 2007, **41**, 3966–3971.

55   O. Fleischer, H. Wichmann and W. Lorenz, *Chemosphere*, 1999, **39**, 925–932.

56   J. J. Sabatini, J. C. Poret and R. N. Broad, *Angew. Chem. Int. Ed.*, 2011, **50**, 4624–4626.

57   C. E. Housecroft and A. G. Sharpe, in *Inorganic Chemistry*, Pearson/Prentice Hall, Harlow, 3rd edn., 2008, p. 439.

58   C. E. Housecroft and A. G. Sharpe, in *Inorganic Chemistry*, Pearson/Prentice Hall, Harlow, 3rd edn., 2008, p. 382.

59   M. H. V Huynh, M. A. Hiskey, T. J. Meyer and M. Wetzler, *Proc. Natl. Acad. Sci. U. S. A.*, 2006, **103**, 5409–5412.

60   J. J. Sabatini, A. V. Nagori, G. Chen, P. Chu, R. Damavarapu and T. M. Klapötke, *Chem. Eur. J.*, 2012, **18**, 628–631.

61   M. A. Hiskey, N. Goldman and J. R. Stine, *J. Energ. Mater.*, 1998, **16**, 119–127.

62   N. Fischer, D. Izsák, T. M. Klapötke, S. Rappenglück and J. Stierstorfer, *Chem. Eur. J.*, 2012, **18**, 4051–62.

63   M.-X. Zhang, P. E. Eaton and R. Gilardi, *Angew. Chem. Int. Ed.*, 2000, **39**, 401–404.

64   T. M. Klapötke, B. Krumm and C. C. Unger, *Inorg. Chem.*, 2019, **58**, 2881–2887.

65   N. Fischer, D. Fischer, T. M. Klapötke, D. G. Piercey and J. Stierstorfer, *J. Mater. Chem.*, 2012, **22**, 20418–20422.

66   C. Yang, C. Zhang, Z. Zheng, C. Jiang, J. Luo, Y. Du, B. Hu, C. Sun and K. O. Christe, *J. Am. Chem. Soc.*, 2018, **140**, 16488–16494.

67   B. Khasainov, M. Comet, B. Veyssiere and D. Spitzer, *Propellants, Explos. Pyrotech.*, 2017, **42**, 547–557.

68   J. Stierstorfer, T. M. Klapötke, A. Hammerl and R. D. Chapman, *Z. Anorg. Allg. Chem.*, 2008, **634**, 1051–1057.

69   M. I. Eremets, A. G. Gavriliuk, I. A. Trojan, D. A. Dzivenko and R. Boehler, *Nat. Mater.*, 2004, **3**, 558–563.

70   E. M. Benchafia, Z. Yao, G. Yuan, T. Chou, H. Piao, X. Wang and Z. Iqbal, *Nat. Commun.*, 2017, **8**, 1–6.

71   B. Hirshberg, R. B. Gerber and A. I. Krylov, *Nat. Chem.*, 2014, **6**, 52–56.

72   T. Curtius, *Ber. Dtsch. Chem. Ges.*, 1890, **23**, 3023–3033.

73   K. O. Christe, W. W. Wilson, J. A. Sheehy and J. A. Boatz, *Angew. Chem. Int. Ed.*, 1999, **40**, 2947.

74   R. Haiges, S. Schneider, T. Schroer and K. O. Christe, *Angew. Chem. Int. Ed.*, 2004, **43**, 4919–4924.

75   Y. Xu, Q. Wang, C. Shen, Q. Lin, P. Wang and M. Lu, *Nature*, 2017, **549**, 78–81.

76   C. Zhang, C. Sun, B. Hu, C. Yu and M. Lu, *Science*, 2017, **355**, 374–376.

77   T. M. Klapötke and J. Stierstorfer, *J. Am. Chem. Soc.*, 2009, **131**, 1122–1134.

78   K. Banert, Y.-H. Joo, T. Rüffer, B. Walfort and H. Lang, *Angew. Chem. Int. Ed.*, 2007, **46**, 1168–1171.

79   T. Curtius and A. Darapsky, *J. Prakt. Chem.*, 1900, **61**, 408–422.

80   N. Fischer, T. M. Klapötke, K. Peters, M. Rusan and J. Stierstorfer, *Z. Anorg. Allg. Chem.*, 2011, **637**, 1693–1701.

81   T. M. Klapötke, M. Rusan and V. Sproll, *Z. Anorg. Allg. Chem.*, 2014, **640**, 1892–1899.

82   D. Fischer, T. M. Klapötke and J. Stierstorfer, *Angew. Chem. Int. Ed.*, 2014, **53**, 8172–8175.

83   P. S. Dendage, D. B. Sarwade, S. N. Asthana and H. Singh, *J. Energ. Mater.*, 2001, **19**, 41–78.

84   J. Musher, *Angew. Chem. Int. Ed.*, 1969, **8**, 54–68.

85   R. Gillespie and E. Robinson, *Inorg. Chem.*, 1995, **34**, 978–979.

86   C. E. Housecroft and A. G. Sharpe, in *Inorganic Chemistry*, Pearson/Prentice Hall, 3rd edn., 2008, p. 41.

87   W. Kutzelnigg, *Angew. Chem. Int. Ed.*, 1984, **23**, 272–295.

88   K. Y. Akiba, M. Yamashita, Y. Yamamoto and S. Nagase, *J. Am. Chem. Soc.*, 1999, **121**, 10644–10645.

89   R. R. Maar, S. D. Catingan, V. N. Staroverov and J. B. Gilroy, *Angew. Chem. Int. Ed.*, 2018, **57**, 9870–9874.

90   R. J. P. Corriu, *J. Organomet. Chem.*, 1990, **400**, 81–106.

91   S. Noury, B. Silvi and R. J. Gillespie, *Inorg. Chem.*, 2002, **41**, 2164–2172.

92   O. J. Curnow, *J. Chem. Educ.*, 1998, **75**, 3–8.

93   A. Khan and D. Foucher, *Coord. Chem. Rev.*, 2016, **312**, 41–66.

94   A. E. Reed and P. V. R. Schleyer, *J. Am. Chem. Soc.*, 1990, **112**, 1434–1445.

95   A. C. Filippou, P. Portius and G. Schnakenburg, *J. Am. Chem. Soc.*, 2002, **124**, 12396–12397.

96   A. C. Filippou, P. Portius, D. U. Neumann and K.-D. Wehrstedt, *Angew. Chem. Int. Ed.*, 2000, **39**, 4333–4336.

97   W. Beck, W. P. Fehlhammer, P. Pöllmann, E. Schuierer and K. Feldl, *Chem. Ber.*, 1967, **100**, 2335–2361.

98   W. P. Fehlhammer and W. Beck, *Z. Anorg. Allg. Chem.*, 2013, **639**, 1053–1082.

99   P. Portius and M. Davis, *Coord. Chem. Rev.*, 2013, **257**, 1011–1025.

100   B. E. Liljedahl, U. Qvarfort, R. Berglind and J. Sjöström, *WIT Trans. Biomed. Heal. Environ. Heal. Biomed.*, 2011, **15**, 291–306.

101   R. A. Goyer, *Environ. Health Perspect.*, 1993, **100**, 177–187.

102   R. Campbell, M. F. Davis, M. Fazakerley and P. Portius, *Chem. Eur. J.*, 2015, 18690–18698.

103   B. Crozier, PhD Thesis, The University of Sheffield, 2016.

104 Z. Smallwood, B. Crozier, L. James, M. Davis and P. Portius, *Unpublished Work*.

105 C. Zhang, C. Yang, B. Hu, C. Yu, Z. Zheng and C. Sun, *Angew. Chem. Int. Ed.*, 2017, **56**, 4512–4514.

106 W. Zhang, K. Wang, J. Li, Z. Lin, S. Song, S. Huang, Y. Liu, F. Nie and Q. Zhang, *Angew. Chem. Int. Ed.*, 2018, **57**, 2592–2595.

107 Y. Xu, P. Wang, Q. Lin, X. Mei and M. Lu, *Dalton Trans.*, 2018, **47**, 1398–1401.

108 P. C. Wang, Y. G. Xu, Q. Wang, Y. L. Shao, Q. H. Lin and M. Lu, *Sci. China Mater.*, 2018, **62**, 1–8.

109 Q. Yang, X. Song, G. Zhao, G. Yang, L. Yang, Q. Wei, G. Xie, S. Chen and S. Gao, *Eur. J. Inorg. Chem.*, 2016, **2016**, 5052–5056.

110 S. Li, Y. Wang, C. Qi, X. Zhao, J. Zhang, S. Zhang and S. Pang, *Angew. Chem. Int. Ed.*, 2013, **52**, 14031–14035.

111 W. Li, K. Wang, X. Qi, Y. Jin and Q. Zhang, *Cryst. Growth Des.*, 2018, **18**, 1896–1902.

112 X. Qu, Q. Yang, J. Han, Q. Wei, G. Xie, S. Chen and S. Gao, *RSC Adv.*, 2016, **6**, 46212–46217.

113 J. Di Lin, Y. H. Li, J. G. Xu, F. K. Zheng, G. C. Guo, R. X. Lv, W. C. He, Z. N. Huang and J. F. Liu, *J. Solid State Chem.*, 2018, **265**, 42–49.

114 A. M. Golub, H. Köhler and V. V Skopenko, in *Chemistry of Pseudohalides*, Elsevier, Amsterdam, 1986, pp. 77–185.

115 K. R. Dunbar and R. A. Heintz, *Prog. Inorg. Chem.*, 1997, **45**, 283–391.

116 S. Chorazy, J. J. Zakrzewski, M. Reczyński and B. Sieklucka, *Chem. Commun.*, 2019, **55**, 3057–3060.

117 S. Tanase and J. Reedijk, *Coord. Chem. Rev.*, 2006, **250**, 2501–2510.

118 S. S. Kaye and J. R. Long, *J. Am. Chem. Soc.*, 2005, **127**, 6506–6507.

119 M. Chaigneau, *C. R. Hebd. Seances Acad. Sci.*, 1954, **239**, 1220–1222.

120 D. Williams, B. Pleune, J. Kouvetakis, M. D. Williams and R. A. Andersen, *J. Am. Chem. Soc.*, 2000, **122**, 7735–7741.

121 E. Bernhardt, G. Henkel and H. Willner, *Z. Anorg. Allg. Chem.*, 2000, **626**, 560–568.

122 K. Bläsing, S. Ellinger, J. Harloff, A. Schulz, K. Sievert, C. Täschler, A. Villinger and C. Zur Täschler, *Chem. Eur. J.*, 2016, **22**, 4175–4188.

123 E. Bernhardt, V. Bernhardt-Pitchougina, H. Willner and N. Ignatiev, *Angew. Chem. Int. Ed.*, 2011, **50**, 12085–12088.

124 J. Landmann, J. A. P. Sprenger, R. Bertermann, N. Ignat'ev, V. Bernhardt-Pitchougina, E. Bernhardt, H. Willner and M. Finze, *Chem. Commun.*, 2015, **51**, 4989–4992.

125 J. Landmann, J. A. P. Sprenger, M. Hailmann, V. Bernhardt-Pitchougina, H. Willner, N. Ignat'ev, E. Bernhardt and M. Finze, *Angew. Chem. Int. Ed.*, 2015, **54**, 11259–11264.

126 G. Wittig and H. Bille, *Z. Naturforsch.*, 1951, **6b**, 226–227.

127 DE2222172, 1972, 35.

128   T. Sommerfeld and B. Bhattarai, *Phys. Chem. Chem. Phys.*, 2011, **13**, 18393–18397.

129   L. C. Brousseau, D. Williams, J. Kouvetakis and M. O'Keeffe, *J. Am. Chem. Soc.*, 1997, **119**, 6292–6296.

130   R. Haiges, P. Deokar, M. Vasiliu, T. H. Stein, D. A. Dixon and K. O. Christe, *Chem. Eur. J.*, 2017, **23**, 1–14.

131   P. L. Goggin, I. J. McColm and R. Shore, *J. Chem. Soc. Sect. A*, 1966, 1314–1317.

132   J. Blixt, B. Györi and J. Glaser, *J. Am. Chem. Soc.*, 1989, **111**, 7784–7791.

133   J. Blixt, J. Glaser, J. Mink, I. Persson, P. Persson and M. Sandström, *J. Am. Chem. Soc.*, 1995, **117**, 5089–5104.

134   P. L. Goggin and I. J. McColm, *J. Less-Common Met.*, 1966, **11**, 292–294.

135   T. A. Bither, W. H. Knoth, R. V. Lindsey, Jr. and W. H. Sharkey, *J. Am. Chem. Soc.*, 1958, **80**, 4151–4153.

136   K. Emerson, PhD Thesis, University of Minnesota, 1961.

137   H. Köhler, M. Jeschke and H. Wusterhausen, *Z. Anorg. Allg. Chem.*, 1987, **549**, 199–203.

138   B. Jürgens, E. Irran and W. Schnick, *J. Solid State Chem.*, 2001, **157**, 241–249.

139   A. Schmidpeter, F. Zwaschka and W. S. Sheldrick, *Chem. Ber.*, 1985, **118**, 1078–1085.

140   W. S. Sheldrick, J. Kroner, F. Zwaschka and A. Schmidpeter, *Angew. Chem. Int. Ed. Engl.*, 1979, **18**, 934–935.

141   S. Arlt, J. Harloff, A. Schulz, A. Stoffers and A. Villinger, *Inorg. Chem.*, 2016, **55**, 12321–12328.

142   J. Bresien, S. Ellinger, J. Harloff, A. Schulz, K. Sievert, A. Stoffers, C. Täschler, A. Villinger and C. Zur Täschler, *Angew. Chem. Int. Ed.*, 2015, **54**, 4474–4477.

143   T. Soltner, J. Häusler and A. J. Kornath, *Angew. Chem. Int. Ed.*, 2015, **54**, 13775–13776.

144   K. Banert, M. Chityala, M. Hagedorn, H. Beckers, T. Stüker, S. Riedel, T. Rüffer and H. Lang, *Angew. Chem. Int. Ed.*, 2017, **56**, 9582–9586.

145   E. Pohland, *Z. Anorg. Allg. Chem.*, 1931, **201**, 265–281.

146   J. Howdeshell, PhD Thesis, University of Wyoming, 1973.

147   L. James, PhD Thesis, The University of Sheffield, 2014.

148   J. Harloff, D. Michalik, S. Nier, A. Schulz, P. Stoer and A. Villinger, *Angew. Chem. Int. Ed.*, 2019, 5452–5456.

149   W. Menzer, *Angew. Chem.*, 1958, **70**, 656.

150   S. Jung, F. Renz, M. Klein, M. Menzel, R. Boča and R. Stößer, in *Journal of Physics: Conference Series*, 2010, vol. 217, p. 012027.

151   F. Renz, S. Jung, M. Klein, M. Menzel and A. F. Thünemann, *Polyhedron*, 2009, **28**, 1818–1821.

152   K. B. Dillon and A. Marshall, *J. Chem. Soc. Dalt. Trans.*, 1987, 315–317.

153   US2674519, 1954.

154 P. G. Harrison and S. R. Stobart, *J. Chem. Soc. Dalt. Trans.*, 1967, 940–943.

155 M. Onyszchuk, A. Castel, P. Riviere and J. Satge, *J. Organomet. Chem.*, 1986, **317**, C35–C37.

156 T. Küppers, E. Bernhardt, H. Willner, H. W. Rohm and M. Köckerling, *Inorg. Chem.*, 2005, **44**, 1015–1022.

157 E. Bernhardt, M. Finze and H. Willner, *Z. Anorg. Allg. Chem.*, 2003, **629**, 1229–1234.

158 K. Bläsing, S. Ellinger, J. Harloff, A. Schulz, K. Sievert, C. Täschler, A. Villinger and C. Zur Täschler, *Eur. J. Inorg. Chem.*, 2016, 1175–1183.

159 J. H. Enermark and R. H. Holm, *Inorg. Nucl. Chem. Lett.*, 1964, **3**, 1516–1521.

160 F. A. Miller, S. G. Frankiss and O. Sala, *Spectrochem. Acta*, 1965, **21**, 775–781.

161 K. Emerson and D. Britton, *Acta Cryst.*, 1964, **17**, 1134–1139.

162 K. Emerson and D. Britton, *Acta Cryst.*, 1963, **16**, 113–118.

163 S. Arlt, J. Harloff, A. Schulz, A. Stoffers and A. Villinger, *Inorg. Chem.*, 2016, **55**, 12321–12328.

164 P. Portius, *Private Communication*.

165 B. O. Pray, L. H. Sommer, G. M. Goldberg, G. T. Kerr, P. A. Di Giorgio and F. C. Whitmore, *J. Am. Chem. Soc.*, 1948, **70**, 433–434.

166 Ē. Kupče and E. Lukevics, *J. Magn. Reson.*, 1988, **79**, 325–327.

167 P. Portius, PhD Thesis, Humboldt-Universität zu Berlin, 2000.

168 S. Marriott and R. D. Topsom, *J. Mol. Struct.*, 1984, **110**, 337–340.

169 Z. M. Smallwood, M. F. Davis, J. G. Hill, L. J. R. James and P. Portius, *Inorg. Chem.*, 2019, **58**, 4583–4591.

170 T. M. Klapötke, B. Krumm and M. Scherr, *J. Am. Chem. Soc.*, 2009, **131**, 72–74.

171 O. H. Ellestad, P. Klæboe, E. E. Tucker and J. Songstad, *Acta Chem. Scand.*, 1972, **26**, 3579–3592.

172 M. Carcelli, C. Ferrari, C. Pelizzi, G. Pelizzi, G. Predieri and C. Solinas, *J. Chem. Soc. Dalt. Trans.*, 1992, **26**, 2127–2128.

173 M. Jaafar, X. Liu, F. Dielmann, F. E. Hahn, K. Al-Farhan, A. Alsalme and J. Reedijk, *Inorg. Chim. Acta*, 2016, **443**, 45–50.

174 H. E. Gottlieb, V. Kotlyar and A. Nudelman, *J. Org. Chem.*, 1997, **3263**, 7512–7515.

175 I. Schrader, K. Zeckert and S. Zahn, *Angew. Chem. Int. Ed.*, 2014, **53**, 13698–13700.

176 R. Campbell, S. Konar, S. Hunter, C. Pulham and P. Portius, *Inorg. Chem.*, 2018, **57**, 400–411.

177 K. Polborn, E. Leidl and W. Beck, *Z. Naturforsch.*, 1988, **43b**, 1206–1208.

178 W. Beck, E. Schuierer, P. Pöllmann and W. P. Fehlhammer, *Z. Naturforsch.*, 1966, **21b**, 811–812.

179 M. R. Booth and S. G. Frankiss, *Spectrochim. Acta A*, 1970, **26**, 859–869.

180 H. C. Kolb, M. G. Finn and K. B. Sharpless, *Angew. Chem. Int. Ed.*, 2001, 40, 2004–2021.

181 P. Portius and M. Davis, *Dalton Trans.*, 2016, **45**, 17141–17152.

182 B. Peerless, T. Keane, A. J. H. M. Meijer and P. Portius, *Chem. Commun.*, 2015, **51**, 7435–7438.

183 J. E. Drake and R. T. Hemmings, *Can. J. Chem.*, 1973, **51**, 302–311.

184 R. S. Ghadwal, H. W. Roesky, S. Merkel, J. Henn and D. Stalke, *Angew. Chem. Int. Ed.*, 2009, **48**, 5683–5686.

185 A. C. Filippou, O. Chernov and G. Schnakenburg, *Angew. Chem. Int. Ed.*, 2009, **48**, 5687–5690.

186 A. C. Filippou, Y. N. Lebedev, O. Chernov, M. Straßmann and G. Schnakenburg, *Angew. Chem. Int. Ed.*, 2013, **52**, 6974–6978.

187 B. Peerless, PhD Thesis, The University of Sheffield, 2017.

188 M. Veith and A. Rammo, *Z. Anorg. Allg. Chem.*, 2001, **627**, 662–668.

189 A. C. Filippou, P. Portius and G. Kociok-Köhn, *Chem. Commun.*, 1998, 2327–2328.

190 A. Jana, H. W. Roesky and C. Schulzke, *Dalton Trans.*, 2010, **39**, 132–138.

191 A. C. Filippou, P. Portius, G. Kociok-Köhn and V. Albrecht, *J. Chem. Soc. Dalt. Trans.*, 2000, 1759–1768.

192 Y. Xiong, S. Yao and M. Driess, *Chem. Commun.*, 2014, **50**, 418–420.

193 B. Lyhs, D. Bläser, C. Wölper, S. Schulz, R. Haack and G. Jansen, *Inorg. Chem.*, 2013, **52**, 7236–7241.

194 T. Roseveare, *Private Communication*.

195 R. A. Fischer, A. Miehr, E. Herdtweck, M. R. Mattner, O. Ambacher, T. Metzger, E. Born, S. Weinkauf, C. R. Pulham and S. Parsons, *Chem. Eur. J.*, 1996, **2**, 1353–1358.

196 I. Akasaki, H. Amano, H. Murakami, M. Sassa, H. Kato and K. Manabe, *J. Cryst. Growth*, 1993, **128**, 379–383.

197 R. Schwarz and P. W. Schenk, *Chem. Ber.*, 1930, **63**, 296–300.

198 M. I. Baraton, R. Marchand and P. Quintard, *J. Mol. Struct.*, 1986, **143**, 9–12.

199 W. C. Johnson, *J. Am. Chem. Soc.*, 1930, **52**, 5160–5165.

200 S. N. Ruddlesden and P. Popper, *Acta Cryst.*, 1958, **11**, 465–468.

201 S. K. Deb, J. Dong, H. Hubert, P. F. McMillan and O. F. Sankey, *Solid State Commun.*, 2000, **114**, 137–142.

202 P. Matousek, M. Towrie, A. Stanley and A. W. Parker, *Appl. Spectrosc.*, 1999, **53**, 1485–1489.

203 P. Matousek, M. Towrie, C. Ma, W. M. Kwok, D. Phillips, W. T. Toner and A. W. Parker, *J. Raman Spectrosc.*, 2001, **32**, 983–988.

204 I. Chambouleyron and A. R. Zanatta, *J. Appl. Phys.*, 1998, **84**, 1–30.

205 L. Gmelin, in *Gmelin Handbuch der Anorganischen Chemie, System-Nummer 45: Germanium Ergänzungsband*, Springer-Verlag, Berlin, 8th edn., 1958, p. 507.

206 W. C. Johnson and G. H. Ridgely, *J. Am. Chem. Soc.*, 1934, **56**, 2395–2397.

207 R. Storr, A. N. Wright and C. A. Winkler, *Can. J. Chem.*, 1962, **40**, 1296–1301.

208 P. F. McMillan, S. K. Deb and J.-J. Dong, *J. Raman Spectrosc.*, 2003, **34**, 567–577.

209   K. Leinenweber, M. O'Keeffe, M. Somayazulu, H. Hubert, P. F. McMillan and G. H. Wolf, *Chem. Eur. J.*, 1999, **5**, 3076–3078.

210   H.-P. Baldus and M. Jansen, *Angew. Chem. Int. Ed.*, 1997, **36**, 328–343.

211   S. Veprěk and S. Reiprich, *Thin Solid Films*, 1995, **268**, 64–71.

212   Y. Kang, Y. Yang, L. C. Yin, X. Kang, G. Liu and H. M. Cheng, *Adv. Mater.*, 2015, **27**, 4572–4577.

213   H. Nagai and T. Niimi, *J. Electrochem. Soc.*, 1968, **115**, 671–672.

214   G. Serghiou, G. Miehe, O. Tschauner, A. Zerr and R. Boehler, *J. Chem. Phys.*, 1999, **111**, 4659–4662.

215   L. Wöhler, *Abstract of Chem. Zeit.*, 1912, **35**, 1096.

216   L. Wöhler and W. Krupko, *Ber. Dtsch. Chem. Ges.*, 1913, **46**, 2045–2057.

217   T. M. Klapötke, in *Chemistry of High-Energy Materials*, De Gruyter, Berlin/Boston, 2nd edn., 2012, p. 58.

218   F. R. Kreißl and O. Krätz, in *Feuer und Flamme, Schall und Rauch: Schauexperimente und Chemiehistorisches*, Wiley-VCH, Weinheim, 2nd edn., 2008, pp. 111–112.

219   C. S. Choi and H. P. Boutin, *Acta Crystallogr. Sect. B*, 1969, **25**, 982–987.

220   F. Marandi, B. Mirtamizdoust, A. A. Soudi and H.-K. Fun, *Inorg. Chem. Commun.*, 2007, **10**, 174–177.

221   B. Shaabani, B. Mirtamizdoust, M. Shadman and H.-K. Fun, *Z. Anorg. Allg. Chem.*, 2009, **635**, 2642–2647.

222   B. Mirtamizdoust, S. Ali-Asgari, S. W. Joo, E. Maskani, Y. Hanifehpour and T. H. Oh, *J. Inorg. Organomet. Polym. Mater.*, 2013, **23**, 751–757.

223   T. M. Klapötke, in *Chemistry of High-Energy Materials*, Wiley-VCH, Berlin/Boston, 3rd edn., 2015, p. 39.

224   Y. Hanifehpour, B. Mirtamizdoust and S. W. Joo, *J. Inorg. Organomet. Polym. Mater.*, 2012, **22**, 916–922.

225   E. Lieber, C. N. R. Rao and F. M. Keane, *J. Inorg. Nucl. Chem.*, 1963, **25**, 631–635.

226   N. Bertazzi, G. Alonzo, G. C. Stocco and L. Pellerito, *J. Organomet. Chem.*, 1974, **80**, 225–228.

227   H. Möller, *Z. Anorg. Allg. Chem.*, 1949, **260**, 249–254.

228   Q. S. Li and H. X. Duan, *J. Phys. Chem. A*, 2005, **109**, 9089–9094.

229   W. Czado and U. Müller, *Z. Anorg. Allg. Chem.*, 1998, **624**, 925–926.

230   S. A. Bourne and Z. Mangombo, *CrystEngComm*, 2004, **6**, 437–442.

231   M. Geselle and H. Fuess, *Acta Cryst. C*, 2002, **51**, 242–244.

232   G. Engel, *Z. Kristallogr.*, 1935, **90**, 341–373.

233   A. Ouasri, A. Rhandour, S. Schloots and G. J. Reiss, *J. Chem. Crystallogr.*, 2017, **47**, 173–181.

234   P. N. Schatz, P. J. Stephens, G. N. Henning and A. J. McCaffery, *Inorg. Chem.*, 1968, **7**, 1246–1248.

235   A. Vogler, C. Quett, A. Paukner and H. Kunkely, *J. Am. Chem. Soc.*, 1986, **108**, 8263–8265.

236   R. A. Walton, R. W. Matthews and C. K. Jørgensen, *Inorg. Chim. Acta*, 1967, **1**, 355–359.

237   R. Campbell, PhD Thesis, The University of Sheffield, 2016.

238   Z. Dori and R. F. Ziolo, *Chem. Rev.*, 1973, **73**, 247–254.

239   G. Szolin-Jones, *Private Communication*.

240   R. Haiges, T. Schroer, M. Yousufuddin and K. O. Christe, *Z. Anorg. Allg. Chem.*, 2005, **631**, 2691–2695.

241   M.-J. Crawford and T. M. Klapötke, *Heteroat. Chem.*, 1999, **10**, 325–329.

242   W. Czado and U. Müller, *Z. Anorg. Allg. Chem.*, 1998, **624**, 925–926.

243   P. Portius, A. C. Filippou, G. Schnakenburg, M. Davis and K.-D. Wehrstedt, *Angew. Chem. Int. Ed.*, 2010, **49**, 8013–6.

244   L. H. Zhu, M.-H. Zeng, X.-C. Shen and S. W. Ng, *Main Group Met. Chem.*, 2008, **31**, 103–104.

245   O. Schmitz-Du Mont and W. Jansen, *Angew. Chem. Int. Ed.*, 1968, **7**, 950–951.

246   O. Schmitz-Du Mont and W. Jansen, *Z. Anorg. Allg. Chem.*, 1970, **375**, 98–102.

247   S. van Meurs, *Private Communication*.

248   M. Kadarkaraisamy, D. P. Engelhart, P. N. Basa and A. G. Sykes, *J. Coord. Chem.*, 2010, **63**, 2261–2267.

249   V. V Avdeeva, M. I. Buzin, A. O. Dmitrienko, P. V Dorovatovskii, E. A. Malinina, N. T. Kuznetsov, E. D. Voronova, Y. V Zubavichus and A. V Vologzhanina, *Chem. Eur. J.*, 2017, **23**, 16819–16828.

250   G. Bowmaker, J. M. Harrowfield, H. Miyamae, T. H. Shand, B. W. Skelton, A. A. Soudi and A. H. White, *Aust. J. Chem.*, 1996, **49**, 1089–1097.

251   J. Jappy and P. N. Preston, *Inorg. Nucl. Chem. Lett.*, 1968, **4**, 503–506.

252   W. Beck and K. Schorpp, *Angew. Chem. Int. Ed.*, 1970, **9**, 735–735.

253   F. A. Miller and D. Bassi, *Spectrochim. Acta*, 1963, **19**, 565–573.

254   D. T. Durig, M. S. Durig and J. R. Durig, *Spectrochim. Acta A*, 2005, **61**, 1287–1306.

255   K. Banert, Y. H. Joo, T. Rüffer, B. Walfort and H. Lang, *Tetrahedron Lett.*, 2010, **51**, 2880–2882.

256   W. R. Fawcett, G. Liu and T. E. Kessler, *J. Phys. Chem.*, 1993, **97**, 9293–9298.

257   N. M. Levinson, S. D. Fried and S. G. Boxer, *J. Phys. Chem. B*, 2012, **116**, 10470–10476.

258   L. J. G. W. Van Wilderen, D. Kern-Michler, H. M. Müller-Werkmeister and J. Bredenbeck, *Phys. Chem. Chem. Phys.*, 2014, **16**, 19643–19653.

259   M. H. V. Huynh, M. D. Coburn, T. J. Meyer and M. Wetzler, *Proc. Natl. Acad. Sci. U. S. A.*, 2006, **103**, 10322–10327.

260   T. M. Klapötke, in *Chemistry of High-Energy Materials*, De Gruyter, Berlin/Boston, 2nd edn., 2012, p. 153.

261 P. H. Zwart, R. W. Grosse-Kunstleve, A. A. Lebedev, G. N. Murshudov and P. D. Adams, *Acta Crystallogr. Sect. D*, 2007, **64**, 99–107.

262 I. F. Cottrell, A. R. Cowley, L. J. Croft, L. Hymns, M. G. Moloney, E. J. Nettleton, H. K. Smithies and A. L. Thompson, *Tetrahedron*, 2009, **65**, 2537–2550.

263 W. Biltz and E. Meinecke, *Z. Anorg. Allg. Chem.*, 1923, **131**, 1–21.

264 E. W. Abel, in *The Chemistry of Germaniun, Tin and Lead*, Pergamon Press, Braunschweig, 1975, p. 136.

265 M. N. Glukhovtsev, H. Jiao and P. V. R. Schleyer, *Inorg. Chem.*, 1996, **35**, 7124–7133.

266 J. Lifschitz, *Ber. Dtsch. Chem. Ges.*, 1915, **48**, 410–420.

267 T. Curtius, A. Darapsky and E. Müller, *Ber. Dtsch. Chem. Ges.*, 1915, **48**, 1614–1634.

268 K. Clusius and H. Hürzeler, *Helv. Chim. Acta*, 1954, **37**, 798–804.

269 R. Huisgen and I. Ugi, *Chem. Ber.*, 1957, **90**, 2914–2927.

270 I. Ugi, H. Perlinger and L. Behringer, *Chem. Ber.*, 1958, **91**, 2324–2329.

271 A. Hammerl, T. M. Klapötke and P. Schwerdtfeger, *Chem. Eur. J.*, 2003, **9**, 5511–5519.

272 A. Hammerl and T. M. Klapötke, *Inorg. Chem.*, 2002, **41**, 906–912.

273 M. Lein, J. Frunzke, A. Timoshkin and G. Frenking, *Chem. Eur. J.*, 2001, **7**, 4155–4163.

274 R. N. Butler, J. C. Stephens and L. A. Burke, *Chem. Commun.*, 2003, **2**, 1016–1017.

275 R. N. Butler, J. M. Hanniffy, J. C. Stephens and L. A. Burke, *J. Org. Chem.*, 2008, **73**, 1354–1364.

276 B. A. Steele, E. Stavrous, V. B. Prakapenka, H. Radousky, J. Zaug, J. C. Crowhurst and I. I. Oleynik, *AIP Conf. Proc.*, 2017, **1793**, 040016.

277 B. A. Steele, E. Stavrou, J. C. Crowhurst, J. M. Zaug, V. B. Prakapenka and I. I. Oleynik, *Chem. Mater.*, 2017, **29**, 735–741.

278 R. N. Butler, A. Fox and L. A. Burke, *J. Chem. Soc., Perk. Trans. 2*, 1998, 2243–2247.

279 Y. Yang, Y. Li, R. Zhang, C. Sun and S. Pang, *RSC Adv.*, 2014, **4**, 57629–57634.

280 I. Ugi and R. Huisgen, *Chem. Ber.*, 1958, **91**, 531–537.

281 C. Hansch, A. Leo and R. W. Taft, *Chem. Rev.*, 1991, **91**, 165–195.

282 S. Ek, S. Rehn, L. Y. Wahlström and H. Östmark, *J. Heterocycl. Chem.*, 2013, **50**, 263–267.

283 N. P. Gritsan and M. S. Platz, *Chem. Rev.*, 2006, **106**, 3844–3867.

284 N. P. Gritsan, D. Tigelaar and M. S. Platz, *J. Phys. Chem. A*, 1999, **103**, 4465–4469.

285 P. Portius, M. Davis, R. Campbell, F. Hartl, Q. Zeng, A. J. H. M. Meijer and M. Towrie, *J. Phys. Chem. A*, 2013, **117**, 12759–12769.

286 Y. Morino, T. Ijima and Y. Murata, *Bull. Chem. Soc. Jpn.*, 1959, **33**, 46–48.

287 M. Carlotti, J. W. C. Johns and A. Trombetti, *Can. J. Phys.*, 1974, 340.

288 C. Janiak, *J. Chem. Soc. Dalt. Trans.*, 2000, 3885–3896.

289 T. Steiner, *Angew. Chem. Int. Ed.*, 2002, **41**, 49–76.

290 S. Alvarez, *Dalton Trans.*, 2013, **42**, 8617–8636.

291   A. Leclaire, *J. Solid State Chem.*, 2008, **181**, 2338–2345.

292   R. Marx, *Z. Naturforsch.*, 1988, **43b**, 521–524.

293   F. Biesemeier, U. Müller and W. Massa, *Z. Anorg. Allg. Chem.*, 2002, **628**, 1933–1934.

294   F. Biesemeier, K. Harms and U. Müller, *Z. Anorg. Allg. Chem.*, 2004, **630**, 787–793.

295   A. Vij, J. G. Pavlovich, W. W. Wilson, V. Vij and K. O. Christe, *Angew. Chem. Int. Ed.*, 2002, **41**, 3051–3054.

296   H. Östmark, S. Wallin, T. Brinck, P. Carlqvist, R. Claridge, E. Hedlund and L. Yudina, *Chem. Phys. Lett.*, 2003, **379**, 539–546.

297   S. Wallin, H. Östmark, T. Brinck, M. Norrefeldt and S. Rehn, *Novel high energetic materials: Calculations and synthesis attempts of metal pentazolates by electrochemistry*, Tumba, 2006.

298   F. Hartl, *Private Communication*.

299   M. I. Eremets, M. Y. Popov, I. A. Trojan, V. N. Denisov, R. Boehler and R. J. Hemley, *J. Chem. Phys.*, 2004, **120**, 10618–10623.

300   B. A. Steele and I. I. Oleynik, *Chem. Phys. Lett.*, 2016, **643**, 21–26.

301   B. A. Steele and I. I. Oleynik, *J. Phys. Chem. A*, 2017, **121**, 1808–1813.

302   B. A. Steele and I. I. Oleynik, *J. Phys. Chem. A*, 2017, **121**, 8955–8961.

303   I. Ugi, *Angew. Chem.*, 1961, **73**, 172.

304   L. A. Burke, R. N. Butler and J. C. Stephens, *J. Chem. Soc. Perkin Trans. 2*, 2001, 1679–1684.

305   T. Schroer, R. Haiges, S. Schneider and K. O. Christe, *Chem. Commun.*, 2005, 1607–1609.

306   B. Bazanov, U. Geiger, R. Carmieli, D. Grinstein, S. Welner and Y. Haas, *Angew. Chem. Int. Ed.*, 2016, **55**, 13233–13235.

307   B. Bazanov, U. Geiger, D. Grinstein, S. Welner and Y. Haas, *J. Phys. Chem. A*, 2017, **121**, 6727–6731.

308   A. Göller and T. Clark, *J. Mol. Model.*, 2000, **6**, 133–149.

309   L. Zhang, C. Yao, Y. Yu, S. Jiang, C. Q. Sun and J. Chen, *J. Phys. Chem. Lett.*, 2019, **10**, 2378–2385.

310   R. Huang and H. Xu, *Science*, 2018, **359**, eeao3672.[vii]

311   C. Jiang, L. Zhang, C. Sun, C. Zhang, C. Yang, J. Chen and B. Hu, *Science*, 2018, **359**, eaas8953.[viii]

312   H. Huang, J. Zhong, L. Ma, L. Lv, J. S. Francisco and X. C. Zeng, *J. Am. Chem. Soc.*, 2019, **141**, 2984–2989.

[vii] Technical Comment, published regarding the article by Zhang *et al.* detailed in reference 76. Full title: *Comment on "Synthesis and characterization of the pentazolate anion cyclo-N_5^- in $(N_5)_6(H_3O)_3(NH_4)_4Cl$"*.

[viii] Technical Response to the Comment by Huang and Xu detailed in reference 310. Full title: *Response to Comment on "Synthesis and characterization of the pentazolate anion cyclo-N_5^- in $(N_5)_6(H_3O)_3(NH_4)_4Cl$"*.

313   C. Sun, C. Zhang, C. Jiang, C. Yang, Y. Du, Y. Zhao, B. Hu, Z. Zheng and K. O. Christe, *Nat. Commun.*, 2018, **9**, 1269.

314   Y. Xu, L. Tian, P. Wang, Q. Lin and M. Lu, *Cryst. Growth Des.*, 2019, **19**, 1853–1859.

315   P. Wang, Y. Xu, Q. Lin and M. Lu, *Chem. Soc. Rev.*, 2018, **47**, 7522–7538.

316   Y. Xu, Q. Lin, P. Wang and M. Lu, *Chem. Asian J.*, 2018, **13**, 924–928.

317   D. A. Dixon, D. Feller, K. O. Christe, W. W. Wilson, A. Vij, V. Vij, H. D. B. Jenkins, R. M. Olson and M. S. Gordon, *J. Am. Chem. Soc.*, 2004, **126**, 834–843.

318   B. Westwater, *Private Communication*.

319   R. N. McDonald, R. Steppel and J. E. Dorsey, *Org. Synth.*, 1970, **50**, 15.

320   A. Martinsen and J. Songstad, *Acta Chem. Scand. A*, 1977, **31**, 645–650.

321   P. Carlqvist, H. Östmark and T. Brinck, *J. Phys. Chem. A*, 2004, **108**, 7463–7467.

322   E. Wiberg and H. Michaud, *Z. Naturforsch.*, 1954, **9b**, 500–501.

323   W. L. Burdick, *J. Am. Chem. Soc.*, 1925, **47**, 1485–1490.

324   C. F. Wilcox and S. H. Bauer, *J. Mol. Struct. THEOCHEM*, 2003, **625**, 1–8.

325   H. Brand, J. Martens, P. Mayer, A. Schulz, M. Seibald and T. Soller, *Chem. Asian J.*, 2009, **4**, 1588–1603.

326   H. Köhler and L. Jäger, *Z. Chem.*, 1988, **28**, 305–306.

327   J. Biechler, *C. R. Hebd. Seances Acad. Sci.*, 1935, **200**, 141–143.

328   A. M. Golub, H. Köhler and V. V Skopenko, in *Chemistry of Pseudohalides*, Elsevier, Berlin, 1986, pp. 444–450.

329   J. Kohout, L. Jäger, M. Hvastijová and J. Kožíšek, *J. Coord. Chem.*, 2000, **51**, 169–218.

330   H. Köhler, A. Kolbe and G. Lux, *Z. Anorg. Allg. Chem.*, 1977, **428**, 103–112.

331   J. L. Manson, C. R. Kmety, A. J. Epstein and J. S. Miller, *Inorg. Chem.*, 1999, **38**, 2552–2553.

332   P. M. van der Werff, S. R. Batten, P. Jensen, B. Moubaraki, K. S. Murray and J. D. Cashion, *Cryst. Growth Des.*, 2004, **4**, 503–508.

333   Z. Setifi, D. Geiger, C. Jelsch, T. Maris, C. Glidewell, M. Mirzaei, M. Arefian and F. Setifi, *J. Mol. Struct.*, 2018, **1173**, 697–706.

334   X.-Y. Wang, X. Zhu, X. Lu and J.-Q. Wang, *Z. Krist. New Cryst. Struct.*, 2018, **233**, 85–86.

335   A. Nag, P. J. Schmidt and W. Schnick, *Chem. Mater.*, 2006, **18**, 5738–5745.

336   B. Jürgens, E. Irran and W. Schnick, *J. Solid State Chem.*, 2005, **178**, 72–78.

337   L. Jäger, C. Wagner, M. Korabik, A. Zygmunt and J. Mroziński, *J. Mol. Struct.*, 2001, **570**, 159–164.

338   S. R. Marshall, C. D. Incarvito, W. W. Shum, A. L. Rheingold and J. S. Miller, *Chem. Commun.*, 2002, **21**, 3006–3007.

339   H. Köhler, H. Hartung and A. M. Golub, *Z. Anorg. Allg. Chem.*, 1974, **44**, 41–44.

340   H. Köhler, R. Menzel, F. Mandl and L. Jäger, *Z. Anorg. Allg. Chem.*, 1987, **551**, 173–178.

341   Y. M. Chow, *Inorg. Chem.*, 1971, **10**, 1938–1942.

342   H. Köhler, P. Laub and A. Frischkorn, *J. Less-Common Met.*, 1970, **3**, 171–175.

343   Y. M. Chow and D. Britton, *Acta Cryst. B* , 1975, **31**, 1934–1937.

344   Y.-J. Shi, X.-T. Chen, Y.-Z. Li, Z. Xue and X.-Z. You, *New J. Chem.*, 2002, **26**, 1711–1713.

345   B. Jürgens, H. A. Höppe and W. Schnick, *Solid State Sci.*, 2002, **4**, 821–825.

346   H. Köhler and K. H. Maushake, *J. Organomet. Chem.*, 1968, **14**, 103–107.

347   H. Köhler and W. Beck, *Z. Anorg. Allg. Chem.*, 1968, **237**, 241–245.

348   I. Ling, Y. Alias, A. N. Sobolev and C. L. Raston, *CrystEngComm*, 2010, **12**, 4321.

349   P. Starynowicz, *Acta Cryst. C*, 1991, **47**, 2198–2199.

350   B. Jürgens, H. A. Höppe, E. Irran and W. Schnick, *Inorg. Chem.*, 2002, **41**, 4849–4851.

351   E. Rentschler and K. Dehnicke, *Z. Kristallogr. Cryst. Mater.*, 1994, **209**, 89.

352   K. Nielsen and R. Willestofte Berg, *Acta Chem. Scand.*, 1980, **34a**, 153–154.

353   L. Birkofer and P. Wegner, *Org. Synth.*, 1970, **50**, 107.

354   N. H. Sherden, J. E. Bercaw, A. J. M. Miller, H. E. Gottlieb, B. M. Stoltz, A. Nudelman, G. R. Fulmer and K. I. Goldberg, *Organometallics*, 2010, **29**, 2176–2179.

355   G. S. Pawley, *J. Appl. Crystallogr.*, 1981, **14**, 357–361.

356   A. A. Coelho, *Topas Academic Version 4.1, see http//www.topas-academic.net*.

357   A. A. Coelho, J. Evans, I. Evans, A. Kern and S. Parsons, *Powder Diffr.*, 2011, **26**, S22–S25.

358   T. Mahabiersing, H. Lyuten, R. C. Nieuwendam and F. Hartl, *Collect. Czech. Chem. Commun.*, 2003, **68**, 1687–1709.

359   EP0568074A1, 1993.

360   R. Campbell, *Private Communication*.

361   T. M. Klapötke, in *Chemistry of High-Energy Materials*, De Gruyter, Berlin/Boston, 3rd edn., 2015, p. 32.

362   DE2043906, 1969.

363   M. A. Alisi, M. Brufani, N. Cazzolla, F. Ceccacci, P. Dragone, M. Felici, G. Furlotti, B. Garofalo, A. La Bella, O. Lanzalunga, F. Leonelli, R. Marini Bettolo, C. Maugeri, L. M. Migneco and V. Russo, *Tetrahedron*, 2012, **68**, 10180–10187.

364   C. Zhang, C. Sun, B. Hu and M. Lu, *J. Energ. Mater.*, 2016, **34**, 103–111.

365   U. Geiger and Y. Haas, *J. Phys. Chem. B*, 2015, **119**, 7338–7348.

366   B. W. Fitzsimmons, A. Hume, L. F. Larkworthy, M. H. Turnbull and A. Yavari, *Inorg. Chim. Acta*, 1985, **106**, 109–114.

367   P. Li, D. R. Paul and T. Chung, *Green Chem.*, 2012, **14**, 1052–1063.

Appendix

Contents

A1. Abbreviations and Symbols

$\angle$	bond angle
ø	diameter
Ak	alkyl group
Ar	aryl group
Bipy	2,2'-bipyridyl
b.p.	boiling point
^{n}Bu	n-butyl group
ca.	approximately
cf.	similar to
CsOP-N$_3$	caesium azidophenolate
CsOP-N$_5$	caesium pentazolylphenolate
CV	Cyclic Voltammetry
δ	NMR chemical shift
d	bond length
D	detonation velocity
DCM	dichloromethane
DMAP-N$_3$	dimethylaminophenylazide
DMAP-N$_5$	dimethylaminophenylpentazole
DMF	dimethyformamide
DMHP-N$_3$	dimethylhydroxyphenylazide
DMHP-N$_5$	dimethylhydroxyphenylpentazole
DMSO	dimethylsulphoxide
ESI-MS	Electrospray Ionisation Mass Spectrometry
EtOH	ethanol
Fe(gly)$_2$	iron(II) bisglycinate
G	guanidinium, $C(NH_2)_3^+$
HEDM	High Energy Density Material
HPLC	High Performance Liquid Chromatography
HOP-N$_3$	*para*-hydroxyphenylazide
HOP-N$_5$	*para*-hydroxyphenylpentazole
hν	daylight
^{i}PrOH	isopropanol
IR	Infra-red
MAS	Magic-Angle Spinning
*m*CPBA	*meta*-chloroperbenzoic acid

MeCN	acetonitrile
MeOH	methanol
MeOP-N_3	*para*-methoxyphenylazide
MeOP-N_5	*para*-methoxyphenylpentazole
m.p.	melting point
μ	bridging interaction
$\tilde{\nu}$	wavenumber
ν	stretching vibration
ν_{as}	asymmetric stretching vibration
ν_s	symmetric stretching vibration
NMR	Nuclear Magnetic Resonance
OAc	acetate
OTTLE	Optically Transparent Thin-Layer Electrochemistry
Ph	phenyl
Ph-N_3	phenylazide
Ph-N_5	phenylpentazole
phen	phenanthroline
pic	picoline
PrCN	butyronitrile
PPN	bis(triphenylphosphine)iminium, $\{(Ph_3)_4P\}_2N^+$
PXRD	Powder X-Ray Diffraction
py	pyridine
R	functional group of varying identity
rt	room temperature
sf	significant figures
^{t}Bupy	4-tert-butylpyridine
TGA	Thermogravimetric Analysis
THF	tetrahydrofuran
TMS	trimethylsilyl, Me_3Si
TNT	trinitrotoluene
TOF	Time of Flight

A2. Key Structural Abbreviations
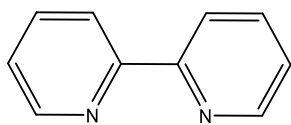
bipy
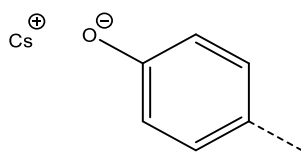
CsOP
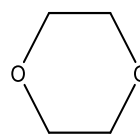
diox
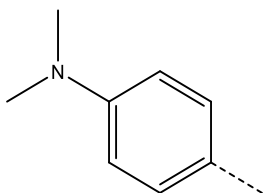
DMAP
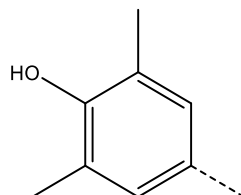
DMHP
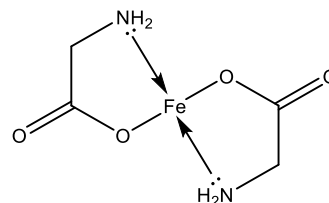
Fe(gly)$_2$
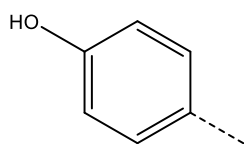
HOP
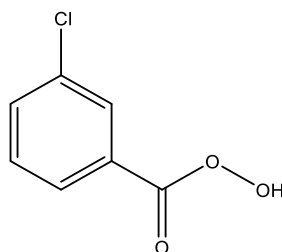
*m*CPBA
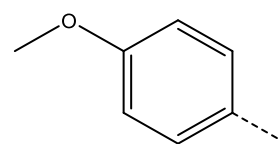
MeOP
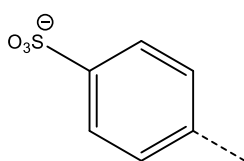
O$_3$SP
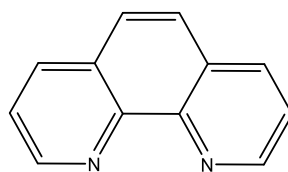
phen
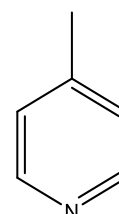
pic
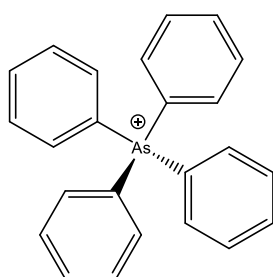
[Ph$_4$As]$^+$

[PPh$_4$]$^+$

[PPN]

PrCN

py
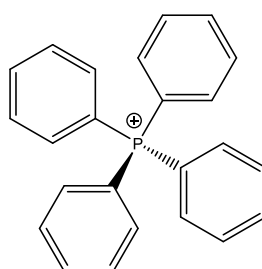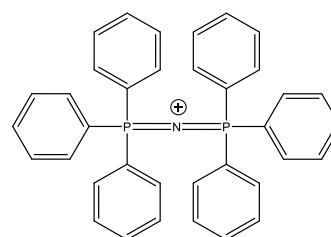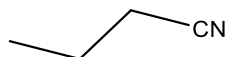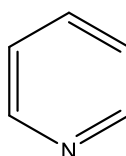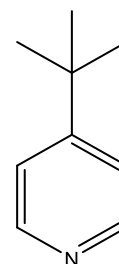
^{t}Bupy

A3. Reagent Sources and Purities

Compound	Source	Purity
1,1,2,2-tetrachloroethane	Sigma-Aldrich	99%
40-60 petroleum ether	VWR	≤0.001% hydrocarbons
Acetone	Fisher Scientific	≥99%
AgCN	Acros Organics	99%
AgNO$_3$	Fisher Scientific	Analytical Reagent Grade
2,2'bipyridyl	Sigma-Aldrich	≥99%
Butyronitrile	Acros Organics	99%
C$_5$D$_5$N	Sigma-Aldrich	99.50%
CDCl$_3$	VWR	99.80%D, <0.01% H$_2$O
CD$_2$Cl$_2$	Cambridge Isotope Laboratories	99.9%D
CD$_3$CN	Aldrich	≥99%, ≥99.8%D
Celite	Alfa Aesar	–
CH$_2$Cl$_2$	VWR	100%
CsOH·H$_2$O	Aldrich	99.95%
D$_2$O	Aldrich	99%, 99%D
Dimethyl-hydroxyaniline	Acros	99%
Dimethylphenol	Aldrich	99%
DMF	Fisher Scientific	>99%
DMSO-d$_6$	VWR	99.8%D, <0.02% H$_2$O
Et$_2$O	Honeywell	≥99.8%
EtOAc	Merck	≥99.7%

Compound	Source	Purity
EtOH	Honeywell	≥99.8%
FeCl$_2$·4H$_2$O	Alfa Aesar	98%
GeCl$_4$	Alfa Aesar	100.00%
Glycine	Fisons	≥99.0%
HCl	Fisher Scientific	~37%
Hexane	Honeywell	≥97.0%
Hydroxyaniline	Aldrich	≥98%
KCN	Sigma-Aldrich	≥97.0%
LiOH·H$_2$O	Fluka	>98%
mCPBA	Sigma-Aldrich	≤77%
Me$_3$SiCN	Fluorochem	98%
MeCN	Fisher Scientific	≥99%
MeOD	Aldrich	99.8%D
MeOH	Fisher Scientific	≥99.8%
Na metal	Sigma-Aldrich	99%, in kerosene
Na$_2$S$_2$O$_4$	Fisher Scientific	≥85%
NaCN	Alfa Aesar	98%
NaN(CN)$_2$	Aldrich	96%
NaN$_3$	Merck Millipore	≥99.0
NaNO$_2$	Fisons	≥96%

Compound	Source	Purity
n-butylnitrite	Aldrich	95%
NH$_2$OH·HCl	Fluka	≥99.0%
NH$_{3\,(g)}$	Air Liquide	Anhydrous
NH$_4$Cl	Fisher Scientific	>99%
p-anisidine	Alfa	99%
PbCl$_2$	Merck Millipore	≥98.0%
PbF$_2$	Alfa Aesar	≥99%
PbF$_4$	Alfa Aesar	99%
Pb(NO$_3$)$_2$	BDH	≥99.5%
N,N'dimethyl-p-phenylenediamine	Aldrich	–
Picoline	Aldrich	98%
1,10-phenantholine	Acros	99.9%
Pyridine	Fisher Scientific	99.80%
SiCl$_4$	Aldrich	99%
SnCl$_4$	Aldrich	99%
SnF$_2$	Aldrich	99%
SnF$_4$	Alfa Aesar	99%
Sulphanilic acid	Acros Organics	ACS Reagent Grade
^{t}Bupy	Fluorochem	97%
THF	VWR	≥99.7%

– = no purity stated.

251

A4. Key compounds prepared in this work
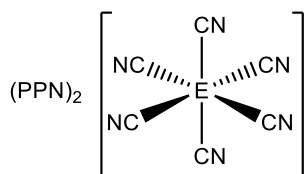
[PPN]$_2$[E(CN)$_6$]
(E = Ge, Sn)
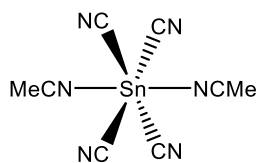
Sn(CN)$_4$(L)$_2$
(L = MeCN, py)
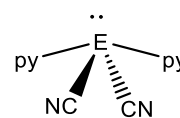
E(CN)$_2$(py)$_2$
(E = Sn, Pb)
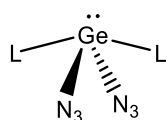
Ge(N$_3$)$_2$(L)$_2$
(L = py, pic, ^{t}Bupy)

Ge(N$_3$)N

Ge$_3$N$_x$
(x = 2 or 4)
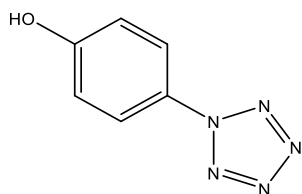
HOP-N$_5$
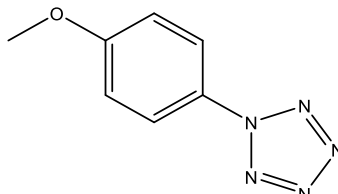
MeOP-N$_5$
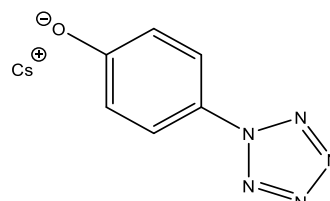
CsOP-N$_5$
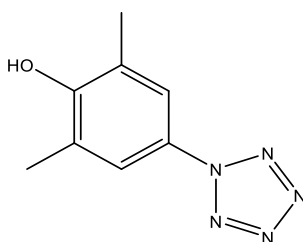
DMHP-N$_5$
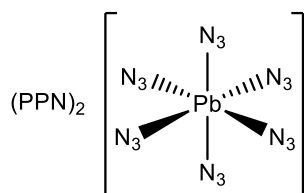
[PPN]$_2$[Pb(N$_3$)$_6$]
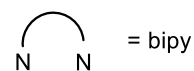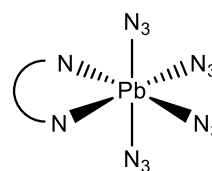
Pb(N$_3$)$_4$(bipy)
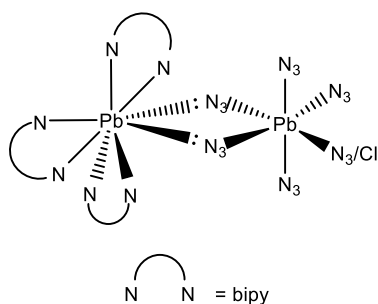
[Pb(bipy)$_3$][Pb(N$_3$)$_{5.2}$Cl$_{0.8}$]
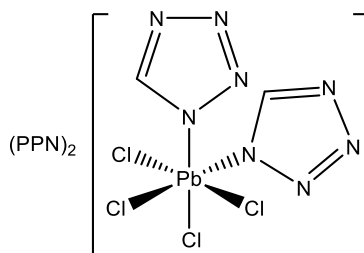
[PPN]$_2$[PbCl$_4$(CHN$_4$)$_2$]
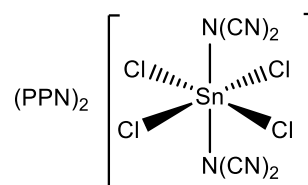
[PPN]$_2$[SnCl$_4${N(CN)$_2$}$_2$]

A5. Discussion of Crystallographic Disorder

Some of the crystallographic datasets presented in this work contain. A list of these, and a brief explanation of the treatment applied to each, is outlined below.

A5.1 [PPN]$_2$[Pb(CHN$_4$)$_2$Cl$_4$] (ch1ppx373)

Although the unit cell parameters and initial structure solution suggest a structure in space group C$_2$, all attempts to generate a structure solution were unsuccessful, and instead a structure could only be generated when solved in triclinic symmetry (space group $\bar{P}$1). It is possible that the structure is pseudosymmetric and only *appears* to possess higher symmetry. The space group shown here serves only as proof that two tetrazolato ligands have coordinated to the Pb(IV) centre and further analysis of bond lengths, distances and interactions cannot be relied upon. The thermal ellipsoids were restrained using EADP to generate an average thermal ellipsoid based on the others of the same atom type.

A5.2 Pb(N$_3$)$_4$(bipy) (ch1ppx393)

The strong absorbing nature of the Pb coordination centre lead to gradual crystal decomposition time over the analysis window, in part due to the high flux of the Cu-K$_\alpha$ radiation used for diffraction studies. To account for this, only the first five of nine runs were used, which generated a trial structure containing low completeness (ca. 91%) due to the absence of a full dataset.

The high levels of disorder in the structure are attributed to the rapid crystallisation conditions, required to obtain monomeric, chlorine-free Pb(N$_3$)$_4$(bipy), and the radiative decomposition of the crystal during analysis The structure is rotationally disordered about the Pb coordination centre, with each disordered part containing four azido ligands and one bipy ligand. The two parts were freely refined using the PART command, with the sum of the occupancies set to 1. The coordination centre was refined as PART 0. Each disordered part has a single azido ligand which undergoes interactions with the bipy ligand of an adjacent molecule; to avoid this, the bond distance between the terminal nitrogen atom of the azide group in question and the carbon atom of the bipy ring in both parts (N11−C9) were elongated and restrained using DFIX (d = ca. 1.75 ± 0.02 Å). This allowed the two atoms to be positioned at a distance greater than any C−N bond, and the generation of a chemically sensible structure. The thermal ellipsoids in both parts were restrained using EADP and the bond lengths of each azide ligand restrained using DFIX to distances approximately similar to those observed in the analogous E(N$_3$)$_4$(bipy)

complexes of the other group 14 elements Si−Sn (d = 1.21 ± 0.02 Å and 1.15 ± 0.05 Å for N$_\alpha$−N$_\beta$ and N$_\beta$−N$_\gamma$, respectively). The bipy ring in the second disordered part was restrained using the FLAT command.
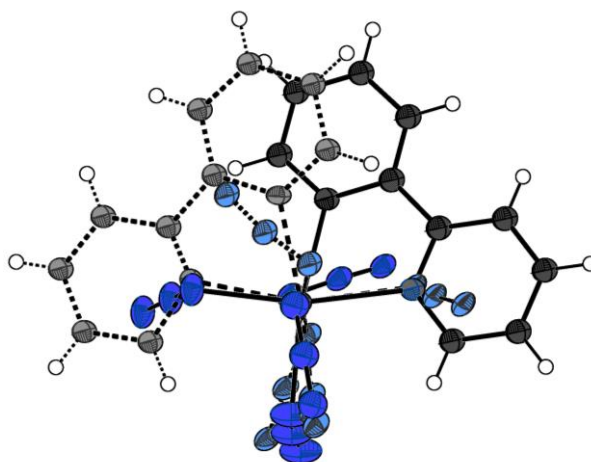
Figure 139. Structure of Pb(N$_3$)$_4$(bipy), showing both disordered parts. Atoms in light grey/light blue with dashed bonds (---) are assigned to the second disordered part.

A5.3 PbCl$_2$(bipy) (ch1ppx394)

The thermal ellipsoids of each heavy atom in the bipy ligand were restrained with SIMU and EADP. The bipy ring was split into two disordered parts of equal occupancy.

A5.4 [Pb(bipy)$_3$][Pb(N$_3$)$_6$] (ch1ppx396)

The collected dataset is incomplete owing to a failure of one quadrant of the charge-coupled detector (CCD) prior to analysis. Consequently, only three-quarters of the generated data was able to be used in the structure solution. Prior to solving, a mask was applied to the data in order to cover the area failed by the faulty detector quadrant. This appears to increase the completeness of the data collected and allows a better refinement. The resolution was set to 0.84 Å to obtain a better structure solution, instead of the 0.77 Å diffractometer resolution limit.

The partially occupied chlorine ligand on the Pb(2) atom is modelled as a separate part to the azido ligand in the same position using the PART command. The sum of occupancies of both parts was set to 1. The occupancy of the chlorine atom (ca. 0.82) was determined by free refinement. The occupancies of the chlorine and azido ligands were subsequently fixed and refined at 0.82 and 0.18, respectively.

Several of the aromatic carbon atoms and oxygen molecules were disordered and were NPD. The ellipsoids of each aromatic carbon atom in the phenyl ring were restrained using EADP. The ellipsoids of each N atom in the N$_5$ ring were restrained using SIMU and DELU. The two water molecules containing O(2) and O(3) were restrained to fixed O−H bond lengths (d = 0.96 Å) using the DFIX command. These disorder modelling restraints are anticipated to be the cause of the low precision in the crystallographic bond lengths.

A6. Discussion of curve fitting of IR spectra using Pseudo-Voigt curve function

In order to determine the true number of bands present in regions of solution-phase IR spectra, curve fitting can be used to model each curve as a converged series of smaller overlapping bands. Each curve was modelled as a Pseudo-Voigt curve function using Origin6.0, defined as:

$$Y = Y_0 + A \left(m_u \left(\frac{2}{\pi} \right) \right) \left(\left(\frac{w}{(4(x - x_c)^2 + w^2)} \right) \right) + (1 - m_u) \left(\frac{\sqrt{4 \ln 2}}{\sqrt{\pi} w} \right) e^{-\left(\frac{4 \ln 2}{w^2} \right)(x - x_c)^2}$$

Where: Y = intensity of the curve,

Y_0 = baseline intensity,

A = area under the curve,

m_u = constant of proportionality between Lorentzian and Gaussian curves ($0 \leq m_u \leq 1$). Solely Lorentzian and Gaussian curves will have m_u values of 0 and 1, respectively.

w = curve width,

x = observed curve position (i.e., the wavenumber),

and x_c = calculated curve position.

All variables were freely refined and the value of m_u restrained between 0 and 1.

A7. Crystallographic Data Tables

A7.1 [PPN]$_2$[Ge(CN)$_6$]

Table 1 Crystal data and structure refinement for ch1ppx359.

Identification code	ch1ppx359
Empirical formula	$C_{78}H_{60}GeN_8P_4$
Formula weight	1305.81
Temperature/K	100(2)
Crystal system	monoclinic
Space group	$P2_1/c$
a/Å	25.2314(8)
b/Å	13.1344(4)
c/Å	20.6130(6)
α/°	90
β/°	107.5545(11)
γ/°	90
Volume/Å^3	6513.0(3)
Z	4
ρ_{calc}g/cm^3	1.332
μ/mm^{-1}	1.974
F(000)	2704.0
Crystal size/mm^3	$0.3 \times 0.29 \times 0.11$
Radiation	CuKα (λ = 1.54178)
2Θ range for data collection/°	3.672 to 133.494
Index ranges	$-29 \leq h \leq 30$, $-15 \leq k \leq 15$, $-24 \leq l \leq 24$
Reflections collected	88733
Independent reflections	11500 [R_{int} = 0.0279, R_{sigma} = 0.0155]
Data/restraints/parameters	11500/0/820
Goodness-of-fit on F^2	1.060
Final R indexes [I>=2σ (I)]	R_1 = 0.0261, wR_2 = 0.0693
Final R indexes [all data]	R_1 = 0.0283, wR_2 = 0.0708
Largest diff. peak/hole / e Å^{-3}	0.35/-0.51

A7.2 [PPN]$_2$[Sn(CN)$_6$]

Table 1 Crystal data and structure refinement for ch1ppx330_0m.

Identification code	ch1ppx330_0m
Empirical formula	C$_{78}$H$_{60}$N$_8$P$_4$Sn
Formula weight	1351.91
Temperature/K	100(2)
Crystal system	monoclinic
Space group	P2$_1$/n
a/Å	10.4512(2)
b/Å	24.5682(6)
c/Å	13.2178(3)
α/°	90
β/°	102.2838(10)
γ/°	90
Volume/Å^3	3316.20(13)
Z	2
ρ_{calc}g/cm^3	1.354
μ/mm^{-1}	4.376
F(000)	1388.0
Crystal size/mm^3	0.300 × 0.250 × 0.200
Radiation	CuKα (λ = 1.54178)
2Θ range for data collection/°	7.196 to 133.37
Index ranges	-12 ≤ h ≤ 12, -29 ≤ k ≤ 29, -15 ≤ l ≤ 15
Reflections collected	46511
Independent reflections	5872 [R$_{int}$ = 0.0425, R$_{sigma}$ = 0.0215]
Data/restraints/parameters	5872/0/412
Goodness-of-fit on F^2	1.071
Final R indexes [I>=2σ (I)]	R$_1$ = 0.0258, wR$_2$ = 0.0595
Final R indexes [all data]	R$_1$ = 0.0300, wR$_2$ = 0.0612
Largest diff. peak/hole / e Å^{-3}	0.56/-0.42

A7.3 [PPN][Ag(CN)$_2$]·MeCN

Table 1 Crystal data and structure refinement for ch1ppx350_0m.

Identification code	ch1ppx350_0m
Empirical formula	C$_{40}$H$_{33}$AgN$_4$P$_2$
Formula weight	739.51
Temperature/K	99.98
Crystal system	monoclinic
Space group	P2$_1$/n
a/Å	9.4853(3)
b/Å	20.0306(7)
c/Å	19.0715(6)
α/°	90
β/°	102.969(2)
γ/°	90
Volume/Å^3	3531.1(2)
Z	4
ρ$_{calc}$g/cm^3	1.391
μ/mm^{-1}	5.695
F(000)	1512.0
Crystal size/mm^3	0.21 × 0.19 × 0.13
Radiation	CuKα (λ = 1.54178)
2Θ range for data collection/°	6.488 to 133.718
Index ranges	-11 ≤ h ≤ 11, -23 ≤ k ≤ 23, -22 ≤ l ≤ 22
Reflections collected	46631
Independent reflections	6255 [R$_{int}$ = 0.1787, R$_{sigma}$ = 0.0907]
Data/restraints/parameters	6255/0/425
Goodness-of-fit on F^2	1.038
Final R indexes [I>=2σ (I)]	R$_1$ = 0.0623, wR$_2$ = 0.1113
Final R indexes [all data]	R$_1$ = 0.1067, wR$_2$ = 0.1261
Largest diff. peak/hole / e Å^{-3}	0.55/-0.63

A7.4 $Ge(N_3)_4(^tBupy)_2$

Table 1 Crystal data and structure refinement for ch1ppx432.

Identification code	ch1ppx432
Empirical formula	$C_{18}H_{26}GeN_{14}$
Formula weight	511.12
Temperature/K	100.0
Crystal system	triclinic
Space group	P-1
a/Å	10.183(2)
b/Å	10.4099(18)
c/Å	12.527(2)
α/°	74.876(6)
β/°	80.391(7)
γ/°	67.346(6)
Volume/Å^3	1179.8(4)
Z	2
ρ_{calc}g/cm^3	1.439
μ/mm^{-1}	2.076
F(000)	528.0
Crystal size/mm^3	$0.5 \times 0.5 \times 0.4$
Radiation	CuKα (λ = 1.54178)
2Θ range for data collection/°	9.428 to 134.366
Index ranges	$-12 \leq h \leq 11$, $-12 \leq k \leq 12$, $-14 \leq l \leq 14$
Reflections collected	14931
Independent reflections	4036 [R_{int} = 0.0638, R_{sigma} = 0.0558]
Data/restraints/parameters	4036/0/304
Goodness-of-fit on F^2	1.063
Final R indexes [I>=2σ (I)]	R_1 = 0.0967, wR_2 = 0.2649
Final R indexes [all data]	R_1 = 0.1025, wR_2 = 0.2705
Largest diff. peak/hole / e Å^{-3}	2.43/-1.90

A7.5 PbCl$_2$·HCl

Table 1 Crystal data and structure refinement for ch1ppx364_0m.

Identification code	ch1ppx364_0m
Empirical formula	Cl$_6$H$_8$N$_2$Pb
Formula weight	455.97
Temperature/K	296.15
Crystal system	monoclinic
Space group	P2$_1$/c
a/Å	8.983(4)
b/Å	7.909(3)
c/Å	12.429(5)
α/°	90
β/°	90.057(8)
γ/°	90
Volume/Å^3	883.0(6)
Z	4
ρ$_{calc}$g/cm^3	3.430
μ/mm^{-1}	20.844
F(000)	824.0
Crystal size/mm^3	0.20 × 0.10 × 0.10
Radiation	MoKα (λ = 0.71073)
2Θ range for data collection/°	4.534 to 55.244
Index ranges	-11 ≤ h ≤ 11, -9 ≤ k ≤ 10, -16 ≤ l ≤ 15
Reflections collected	6135
Independent reflections	2046 [R$_{int}$ = 0.0447, R$_{sigma}$ = 0.0505]
Data/restraints/parameters	2046/0/73
Goodness-of-fit on F^2	1.248
Final R indexes [I>=2σ (I)]	R$_1$ = 0.0863, wR$_2$ = 0.2010
Final R indexes [all data]	R$_1$ = 0.0970, wR$_2$ = 0.2139
Largest diff. peak/hole / e Å^{-3}	8.08/-11.72

A7.6 [PPN]$_2$[PbCl$_6$]

Table 1 Crystal data and structure refinement for ch1ppx366monop_a.

Identification code	ch1ppx366monop_a
Empirical formula	C$_{72}$H$_{60}$Cl$_6$N$_2$P$_4$Pb
Formula weight	1496.99
Temperature/K	100(2)
Crystal system	monoclinic
Space group	P2$_1$/c
a/Å	28.3905(7)
b/Å	13.1442(3)
c/Å	27.0563(7)
α/°	90
β/°	107.5090(10)
γ/°	90
Volume/Å^3	9628.8(4)
Z	6
ρ$_{calc}$g/cm^3	1.549
μ/mm^{-1}	8.700
F(000)	4500.0
Crystal size/mm^3	0.11 × 0.07 × 0.07
Radiation	CuKα (λ = 1.54178)
2Θ range for data collection/°	6.528 to 133.53
Index ranges	-28 ≤ h ≤ 33, -15 ≤ k ≤ 15, -32 ≤ l ≤ 32
Reflections collected	162295
Independent reflections	16979 [R$_{int}$ = 0.0896, R$_{sigma}$ = 0.0390]
Data/restraints/parameters	16979/0/1150
Goodness-of-fit on F^2	1.029
Final R indexes [I>=2σ (I)]	R$_1$ = 0.0325, wR$_2$ = 0.0611
Final R indexes [all data]	R$_1$ = 0.0487, wR$_2$ = 0.0656
Largest diff. peak/hole / e Å^{-3}	1.75/-0.98

A7.7 [PPN]$_2$[Pb(N$_3$)$_6$]

Table 1 Crystal data and structure refinement for ch1ppx371_0m.

Identification code	ch1ppx371_0m
Empirical formula	C$_{72}$H$_{60}$N$_{20}$P$_4$Pb
Formula weight	1536.47
Temperature/K	100(2)
Crystal system	orthorhombic
Space group	Pbca
a/Å	17.8629(5)
b/Å	18.6463(6)
c/Å	20.2757(6)
α/°	90
β/°	90
γ/°	90
Volume/Å^3	6753.4(4)
Z	4
ρ$_{calc}$g/cm^3	1.511
μ/mm^{-1}	6.236
F(000)	3096.0
Crystal size/mm^3	0.30 × 0.20 × 0.10
Radiation	CuKα (λ = 1.54178)
2Θ range for data collection/°	8.124 to 133.484
Index ranges	-21 ≤ h ≤ 21, -22 ≤ k ≤ 21, -24 ≤ l ≤ 24
Reflections collected	98697
Independent reflections	5969 [R$_{int}$ = 0.0385, R$_{sigma}$ = 0.0127]
Data/restraints/parameters	5969/0/439
Goodness-of-fit on F^2	1.054
Final R indexes [I>=2σ (I)]	R$_1$ = 0.0198, wR$_2$ = 0.0467
Final R indexes [all data]	R$_1$ = 0.0245, wR$_2$ = 0.0488
Largest diff. peak/hole / e Å^{-3}	0.34/-0.90

A7.8 PbCl$_2$(bipy)

Table 1 Crystal data and structure refinement for ch1ppx394_p21c.

Identification code	ch1ppx394_p21c
Empirical formula	C$_{10}$H$_8$Cl$_2$N$_2$Pb
Formula weight	434.27
Temperature/K	296.15
Crystal system	monoclinic
Space group	P2$_1$/c
a/Å	15.073(12)
b/Å	9.416(7)
c/Å	8.150(6)
α/°	90
β/°	91.483(12)
γ/°	90
Volume/Å^3	1156.3(16)
Z	4
ρ$_{calc}$g/cm^3	2.495
μ/mm^{-1}	15.019
F(000)	792.0
Crystal size/mm^3	0.33 × 0.13 × 0.10
Radiation	MoKα (λ = 0.71073)
2Θ range for data collection/°	2.702 to 55.896
Index ranges	-19 ≤ h ≤ 19, -10 ≤ k ≤ 12, -10 ≤ l ≤ 10
Reflections collected	11857
Independent reflections	2776 [R$_{int}$ = 0.1458, R$_{sigma}$ = 0.1123]
Data/restraints/parameters	2776/0/88
Goodness-of-fit on F^2	1.089
Final R indexes [I>=2σ (I)]	R$_1$ = 0.0824, wR$_2$ = 0.1917
Final R indexes [all data]	R$_1$ = 0.1254, wR$_2$ = 0.2220
Largest diff. peak/hole / e Å^{-3}	4.50/-5.34

A7.9 Pb(N$_3$)$_4$(bipy)

Table 1 Crystal data and structure refinement for ch1ppx393_1-5.

Identification code	ch1ppx393_1-5
Empirical formula	C$_{10}$H$_8$N$_{14}$Pb
Formula weight	531.49
Temperature/K	100.0
Crystal system	triclinic
Space group	P-1
a/Å	9.1452(9)
b/Å	9.3594(10)
c/Å	11.1979(13)
α/°	94.010(7)
β/°	112.408(7)
γ/°	114.073(7)
Volume/Å^3	779.65(15)
Z	2
ρ$_{calc}$g/cm^3	2.264
μ/mm^{-1}	21.324
F(000)	496.0
Crystal size/mm^3	0.15 × 0.1 × 0.1
Radiation	CuKα (λ = 1.54178)
2Θ range for data collection/°	8.864 to 133.416
Index ranges	-10 ≤ h ≤ 10, -11 ≤ k ≤ 11, -13 ≤ l ≤ 13
Reflections collected	3520
Independent reflections	2506 [R$_{int}$ = 0.0572, R$_{sigma}$ = 0.1035]
Data/restraints/parameters	2506/447/173
Goodness-of-fit on F^2	1.088
Final R indexes [I>=2σ (I)]	R$_1$ = 0.0943, wR$_2$ = 0.2344
Final R indexes [all data]	R$_1$ = 0.1127, wR$_2$ = 0.2480
Largest diff. peak/hole / e Å^{-3}	10.10/-2.22

A7.10 $[Pb(bipy)_3][PbCl_{0.8}(N_3)_{5.2}]$

Table 1 Crystal data and structure refinement for ch1ppx396_084_po.

Identification code	ch1ppx396_084_po
Empirical formula	$C_{30}H_{24}Cl_{0.8}N_{21.6}Pb_2$
Formula weight	1129.85
Temperature/K	100.0
Crystal system	orthorhombic
Space group	Pbca
a/Å	11.4283(2)
b/Å	20.3633(4)
c/Å	31.2223(5)
α/°	90
β/°	90
γ/°	90
Volume/Å^3	7266.0(2)
Z	8
ρ_{calc}g/cm^3	2.066
μ/mm^{-1}	9.373
F(000)	4262.0
Crystal size/mm^3	$0.22 \times 0.19 \times 0.16$
Radiation	MoKα ($\lambda = 0.71073$)
2Θ range for data collection/°	4 to 50.048
Index ranges	$-10 \leq h \leq 13, -19 \leq k \leq 16, -36 \leq l \leq 36$
Reflections collected	46853
Independent reflections	5671 [$R_{int} = 0.0498$, $R_{sigma} = 0.0466$]
Data/restraints/parameters	5671/540/517
Goodness-of-fit on F^2	1.044
Final R indexes [I>=2σ (I)]	$R_1 = 0.0332$, $wR_2 = 0.0535$
Final R indexes [all data]	$R_1 = 0.0585$, $wR_2 = 0.0601$
Largest diff. peak/hole / e Å^{-3}	1.80/-1.23

A7.11 [PPN]$_2$[PbCl$_4$(CHN$_4$)$_2$]

Table 1 Crystal data and structure refinement for shelx.

Identification code	shelx
Empirical formula	C$_{74}$H$_{63}$Cl$_4$N$_{10}$P$_4$Pb
Formula weight	1565.21
Temperature/K	100.0
Crystal system	triclinic
Space group	P-1
a/Å	17.5572(4)
b/Å	17.6301(4)
c/Å	23.4670(6)
α/°	96.662(2)
β/°	96.768(2)
γ/°	104.505(2)
Volume/Å^3	6902.9(3)
Z	4
ρ_{calc}g/cm^3	1.506
μ/mm^{-1}	7.458
F(000)	3148.0
Crystal size/mm^3	0.17 × 0.11 × 0.08
Radiation	CuKα (λ = 1.54178)
2Θ range for data collection/°	5.238 to 133.746
Index ranges	-20 ≤ h ≤ 19, -20 ≤ k ≤ 21, -27 ≤ l ≤ 27
Reflections collected	104487
Independent reflections	24241 [R$_{int}$ = 0.1396, R$_{sigma}$ = 0.1017]
Data/restraints/parameters	24241/0/841
Goodness-of-fit on F^2	1.255
Final R indexes [I>=2σ (I)]	R$_1$ = 0.1627, wR$_2$ = 0.3625
Final R indexes [all data]	R$_1$ = 0.1949, wR$_2$ = 0.3758
Largest diff. peak/hole / e Å^{-3}	14.83/-4.37

A7.12 HOP−N$_5$

Table 1 Crystal data and structure refinement for ch1ppx385_0m.

Identification code	ch1ppx385_0m
Empirical formula	C$_6$H$_5$N$_5$O
Formula weight	163.15
Temperature/K	100(2)
Crystal system	monoclinic
Space group	P2$_1$/c
a/Å	7.1685(5)
b/Å	9.5944(6)
c/Å	10.3321(7)
α/°	90
β/°	98.962(5)
γ/°	90
Volume/Å^3	701.94(8)
Z	4
ρ$_{calc}$g/cm^3	1.544
μ/mm^{-1}	0.975
F(000)	336.0
Crystal size/mm^3	0.10 × 0.06 × 0.03
Radiation	CuKα (λ = 1.54178)
2Θ range for data collection/°	12.5 to 133.418
Index ranges	-8 ≤ h ≤ 8, -11 ≤ k ≤ 11, -12 ≤ l ≤ 10
Reflections collected	9325
Independent reflections	1242 [R$_{int}$ = 0.0806, R$_{sigma}$ = 0.0448]
Data/restraints/parameters	1242/0/113
Goodness-of-fit on F^2	1.059
Final R indexes [I>=2σ (I)]	R$_1$ = 0.0502, wR$_2$ = 0.1216
Final R indexes [all data]	R$_1$ = 0.0780, wR$_2$ = 0.1354
Largest diff. peak/hole / e Å^{-3}	0.20/-0.26

A7.13 DMHP−N($C_6H_2Me_2O$)

Table 1 Crystal data and structure refinement for ch1ppx424_0m.

Identification code	ch1ppx424_0m
Empirical formula	$C_{19}H_{24}NO_2$
Formula weight	298.39
Temperature/K	100.0
Crystal system	monoclinic
Space group	$P2_1/c$
a/Å	8.0016(17)
b/Å	18.434(4)
c/Å	11.888(3)
α/°	90
β/°	98.137(15)
γ/°	90
Volume/Å^3	1735.8(7)
Z	4
ρ_{calc}g/cm^3	1.142
μ/mm^{-1}	0.073
F(000)	644.0
Crystal size/mm^3	$0.65 \times 0.18 \times 0.11$
Radiation	MoKα ($\lambda = 0.71073$)
2Θ range for data collection/°	4.106 to 55.33
Index ranges	$-10 \leq h \leq 10, -23 \leq k \leq 23, -15 \leq l \leq 15$
Reflections collected	45386
Independent reflections	3978 [$R_{int} = 0.1417$, $R_{sigma} = 0.0814$]
Data/restraints/parameters	3978/73/233
Goodness-of-fit on F^2	1.049
Final R indexes [I>=2σ (I)]	$R_1 = 0.0889$, $wR_2 = 0.2401$
Final R indexes [all data]	$R_1 = 0.1703$, $wR_2 = 0.2909$
Largest diff. peak/hole / e Å^{-3}	0.63/-0.35

A7.14 CsOP−N₅·3H₂O

Table 1 Crystal data and structure refinement for ch1ppx390_0ma_a.

Identification code	ch1ppx390_0ma_a
Empirical formula	$C_6H_5CsN_5O$
Formula weight	296.06
Temperature/K	100(2)
Crystal system	monoclinic
Space group	$P2_1/c$
a/Å	14.6203(10)
b/Å	12.4834(9)
c/Å	6.2739(4)
α/°	90
β/°	102.229(4)
γ/°	90
Volume/Å³	1119.07(13)
Z	4
ρ_{calc}g/cm³	1.757
μ/mm⁻¹	25.633
F(000)	556.0
Crystal size/mm³	$0.10 \times 0.08 \times 0.07$
Radiation	CuKα (λ = 1.54178)
2Θ range for data collection/°	6.186 to 133.652
Index ranges	$-17 \leq h \leq 17, -14 \leq k \leq 14, -7 \leq l \leq 7$
Reflections collected	22883
Independent reflections	1990 [R_{int} = 0.2689, R_{sigma} = 0.0929]
Data/restraints/parameters	1990/44/128
Goodness-of-fit on F^2	1.129
Final R indexes [I>=2σ (I)]	R_1 = 0.0938, wR_2 = 0.2095
Final R indexes [all data]	R_1 = 0.1223, wR_2 = 0.2219
Largest diff. peak/hole / e Å⁻³	3.01/-2.18

A7.15 [PPN][N(CN)$_2$]

Table 1 Crystal data and structure refinement for CH1PPX237_0m.

Identification code	CH1PPX237_0m
Empirical formula	C$_{38}$H$_{30}$N$_4$P$_2$
Formula weight	604.60
Temperature/K	100(2)
Crystal system	monoclinic
Space group	P2/c
a/Å	11.8137(7)
b/Å	16.4149(9)
c/Å	15.8689(10)
α/°	90
β/°	92.645(3)
γ/°	90
Volume/Å^3	3074.0(3)
Z	4
ρ$_{calc}$g/cm^3	1.306
μ/mm^{-1}	1.547
F(000)	1264.0
Crystal size/mm^3	0.450 × 0.400 × 0.400
Radiation	CuKα (λ = 1.54178)
2Θ range for data collection/°	5.384 to 133.634
Index ranges	-14 ≤ h ≤ 13, -19 ≤ k ≤ 19, -18 ≤ l ≤ 18
Reflections collected	29748
Independent reflections	5377 [R$_{int}$ = 0.0552, R$_{sigma}$ = 0.0386]
Data/restraints/parameters	5377/0/399
Goodness-of-fit on F^2	1.144
Final R indexes [I>=2σ (I)]	R$_1$ = 0.1048, wR$_2$ = 0.2749
Final R indexes [all data]	R$_1$ = 0.1154, wR$_2$ = 0.2806
Largest diff. peak/hole / e Å^{-3}	2.05/-0.61

A7.16 [PPN]$_2$[SnCl$_4$\{N(CN)$_2$\}$_2$]

Table 1 Crystal data and structure refinement for ch1ppx265_0m.

Identification code	ch1ppx265_0m
Empirical formula	$C_{40}H_{33}Cl_2N_5P_2Sn_{0.5}$
Formula weight	775.90
Temperature/K	296.15
Crystal system	monoclinic
Space group	P2$_1$/n
a/Å	16.0229(15)
b/Å	15.0858(13)
c/Å	16.6183(14)
α/°	90
β/°	111.970(5)
γ/°	90
Volume/Å^3	3725.2(6)
Z	4
ρ_{calc}g/cm^3	1.383
μ/mm^{-1}	0.624
F(000)	1588.0
Crystal size/mm^3	$0.2 \times 0.1 \times 0.1$
Radiation	MoKα ($\lambda = 0.71073$)
2Θ range for data collection/°	3.778 to 55.254
Index ranges	$-20 \leq h \leq 20$, $-19 \leq k \leq 19$, $-21 \leq l \leq 21$
Reflections collected	63042
Independent reflections	8593 [$R_{int} = 0.1003$, $R_{sigma} = 0.0774$]
Data/restraints/parameters	8593/0/449
Goodness-of-fit on F^2	1.020
Final R indexes [I>=2σ (I)]	$R_1 = 0.0465$, $wR_2 = 0.0925$
Final R indexes [all data]	$R_1 = 0.0920$, $wR_2 = 0.1081$
Largest diff. peak/hole / e Å^{-3}	1.04/-0.59

A8. IR Spectra
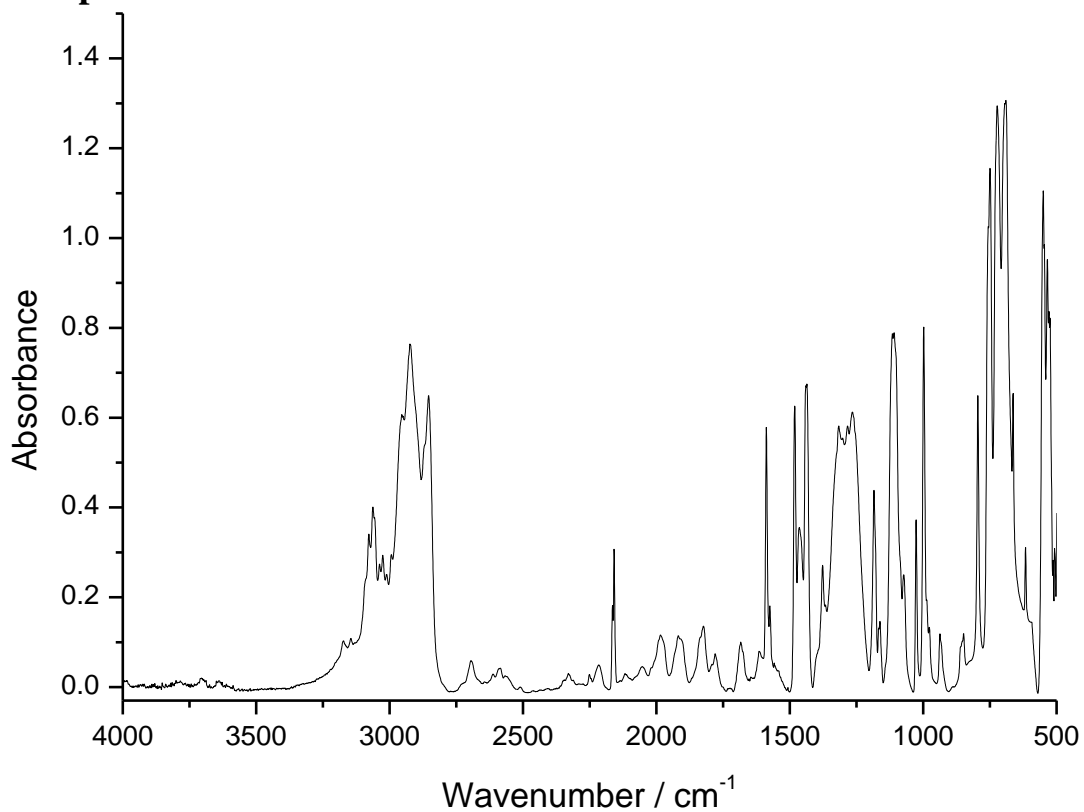
Figure A8.1. FT-IR spectrum of [PPN]$_2$[Ge(CN)$_6$], nujol mull.
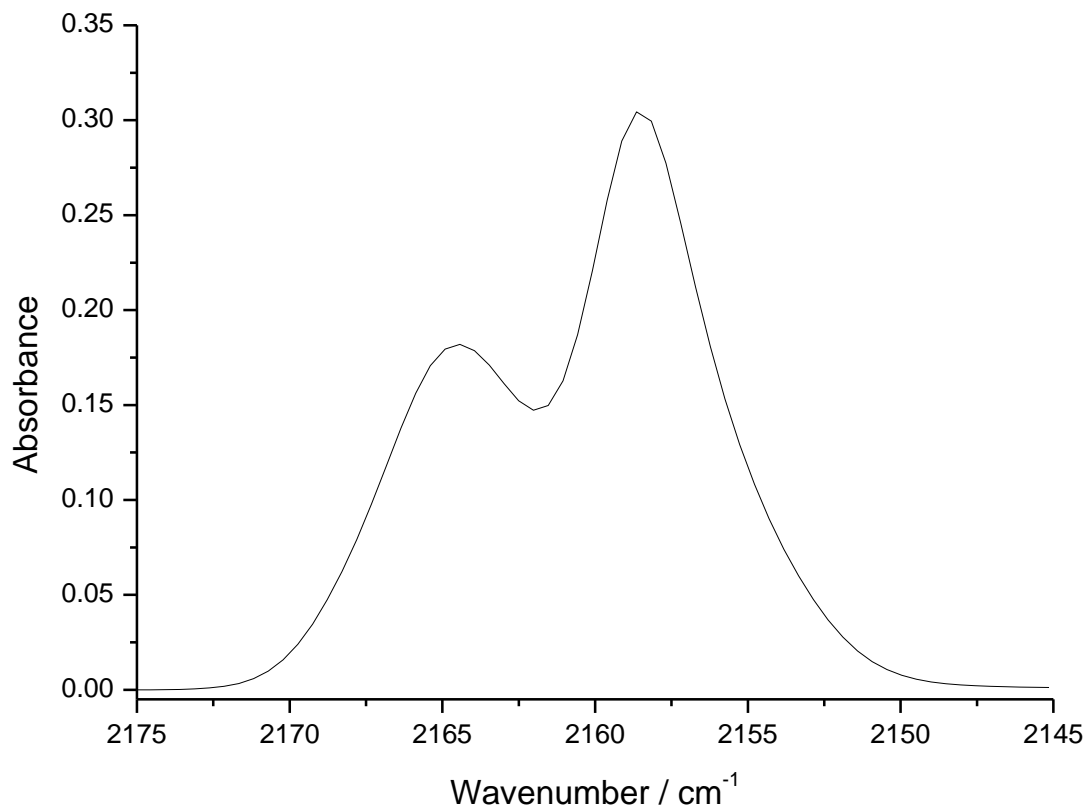
Figure A8.2. Expansion of FT-IR spectrum (nujol mull) of [PPN]$_2$[Ge(CN)$_6$] (figure 8.1) between 2175−2145 cm^{-1}, showing the ν(CN) bands.
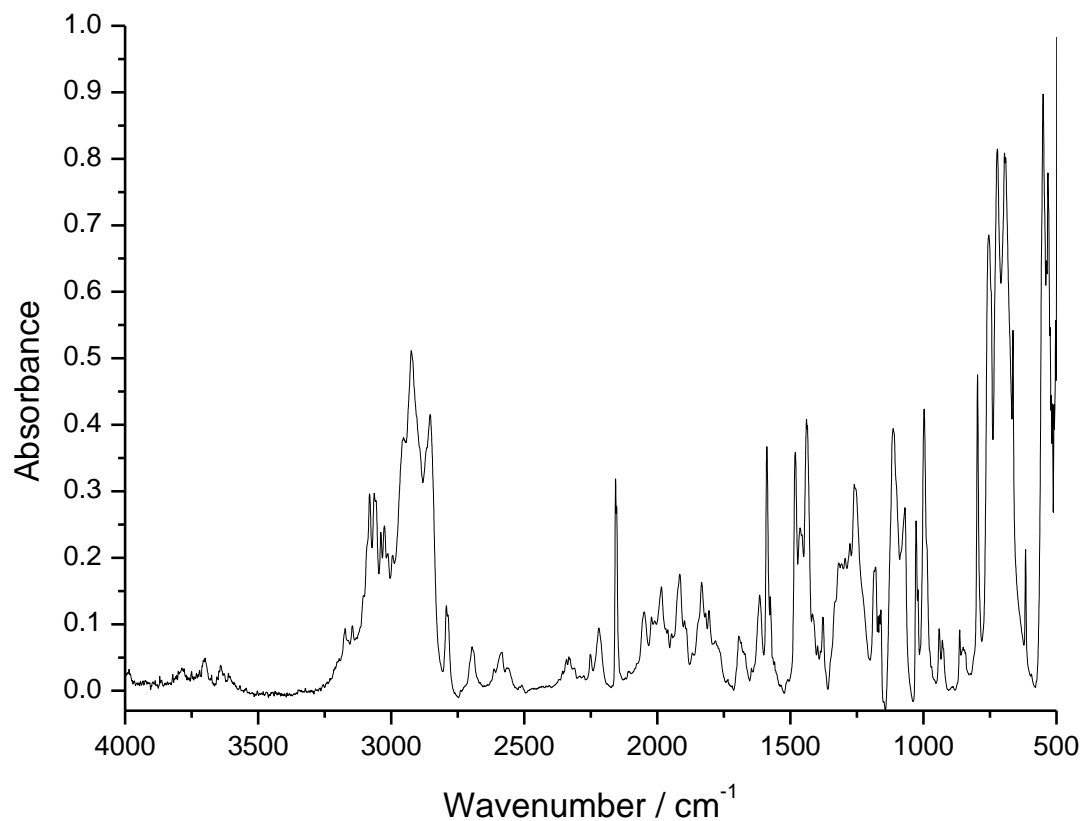
Figure A8.3. FT-IR spectrum of [PPN]$_2$[Sn(CN)$_6$], nujol mull.
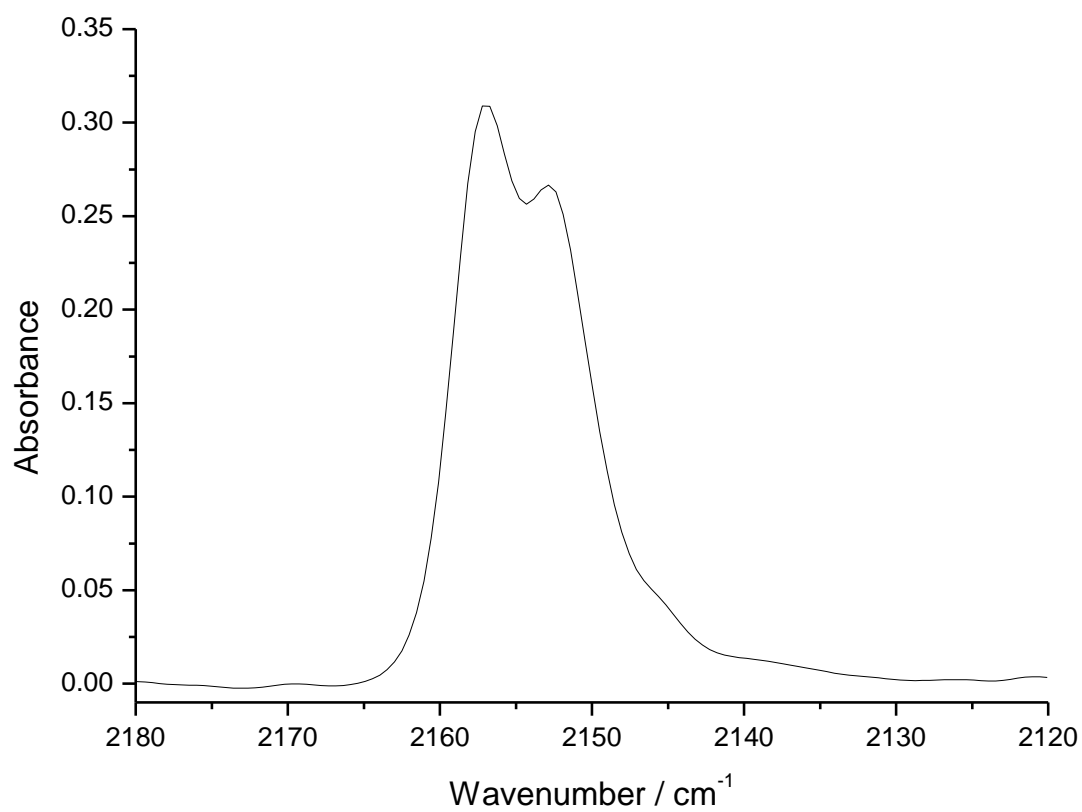
Figure A8.4. Expansion of FT-IR spectrum (nujol mull) of [PPN]$_2$[Sn(CN)$_6$] (figure 7.3) between 2180−2120 cm^{-1}, showing the ν(CN) bands.
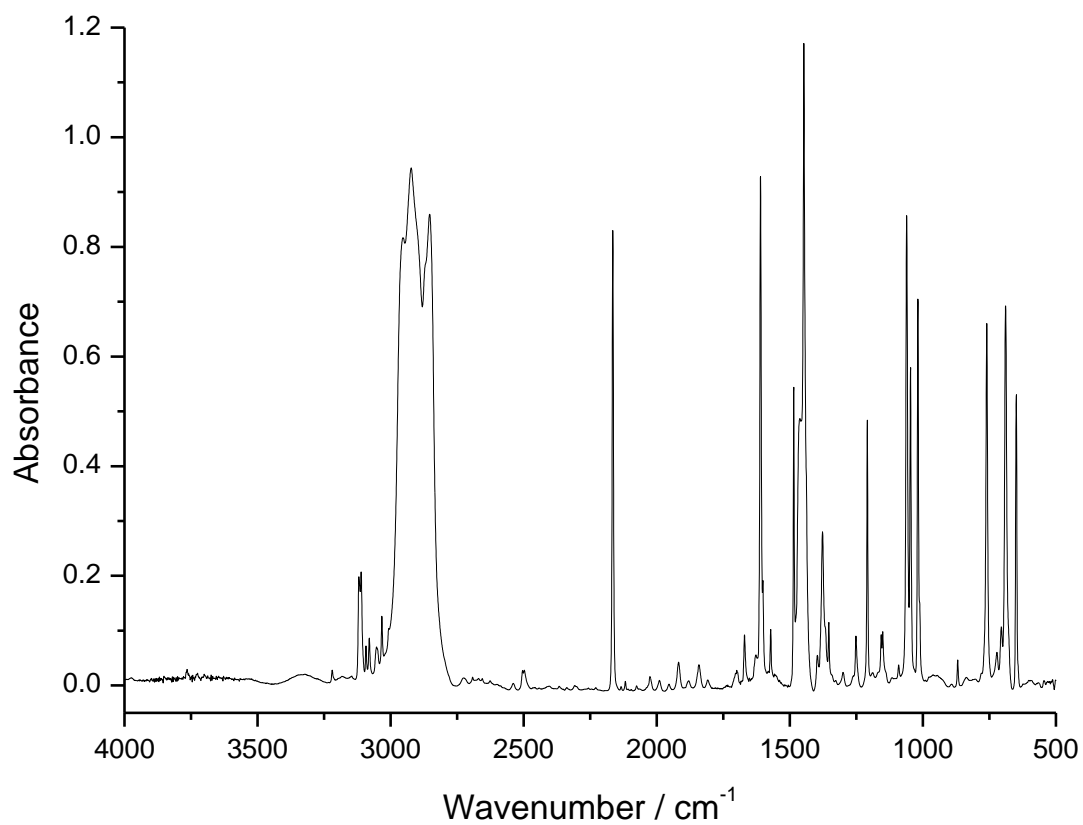
Figure A8.5 FT-IR spectrum of Sn(CN)$_4$(py)$_2$, nujol mull.
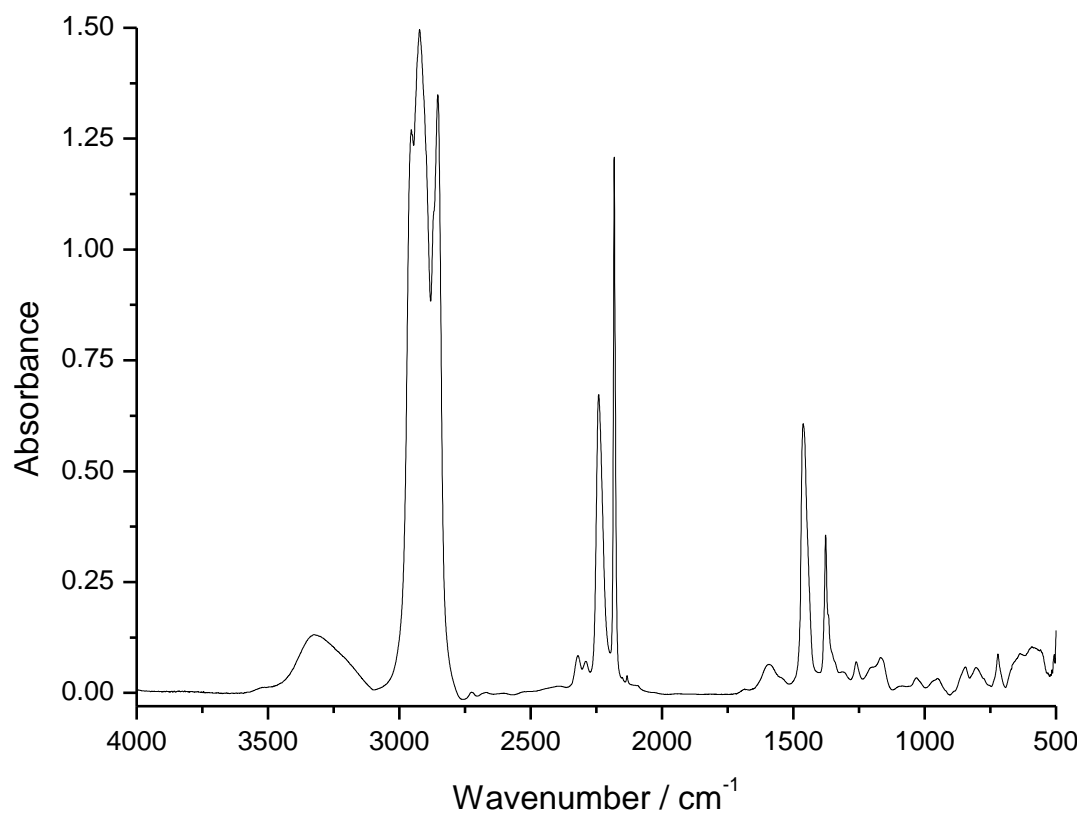
Figure A8.6. FT-IR spectrum of Sn(CN)$_4$(MeCN)$_2$, nujol mull.
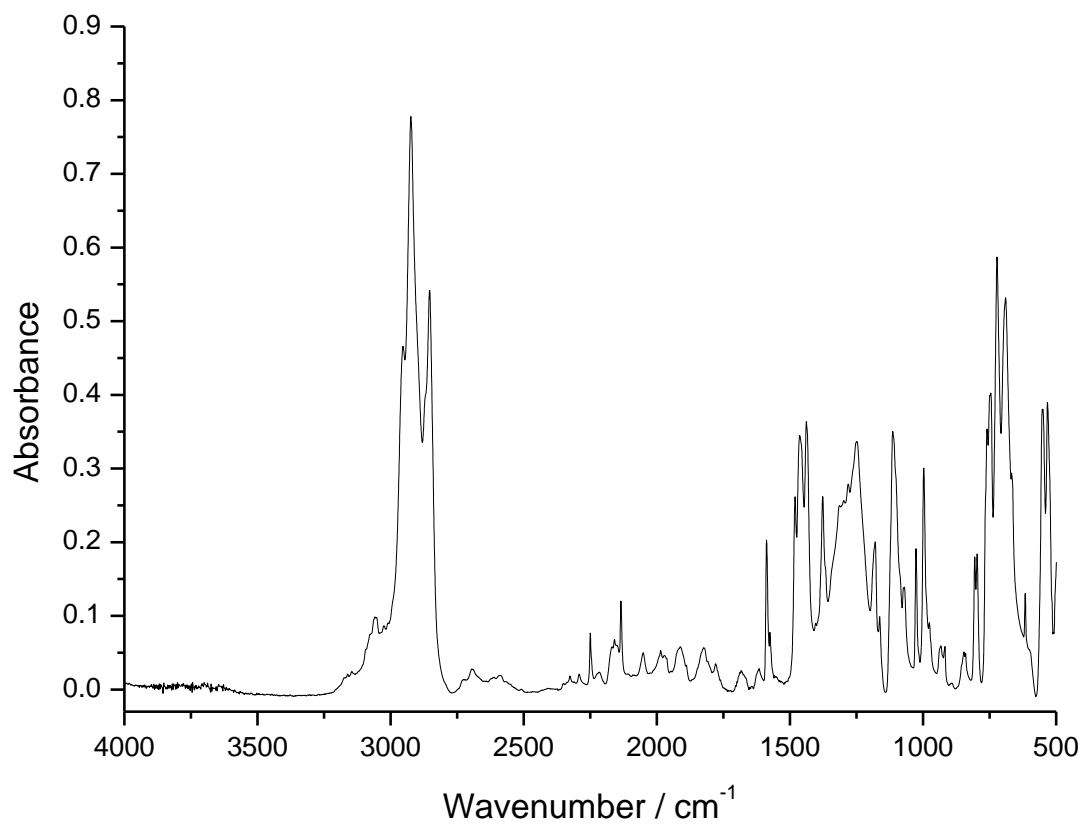
Figure A8.7. FT-IR spectrum of [PPN][Ag(CN)$_2$]·MeCN, nujol mull.
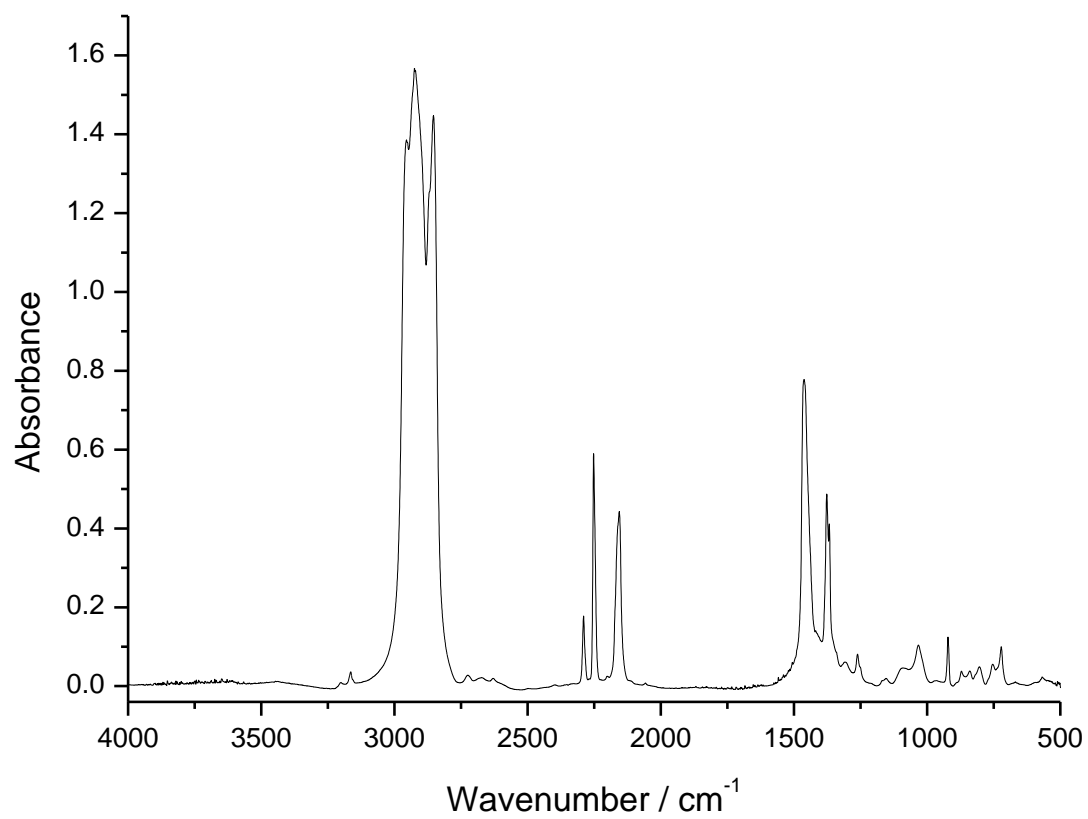
Figure A8.8. FT-IR spectrum of Sn(CN)$_2$(MeCN)$_2$, nujol mull.
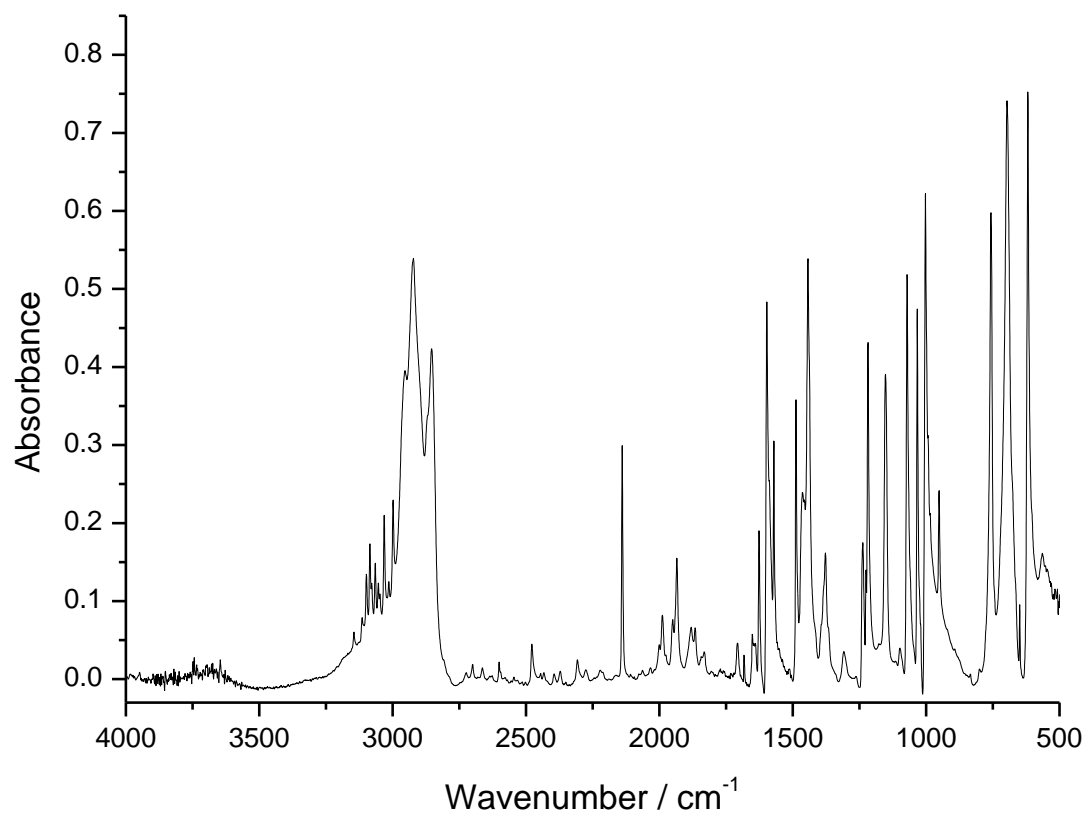
Figure A8.9. FT-IR spectrum of Sn(CN)$_2$(py)$_2$, nujol mull.
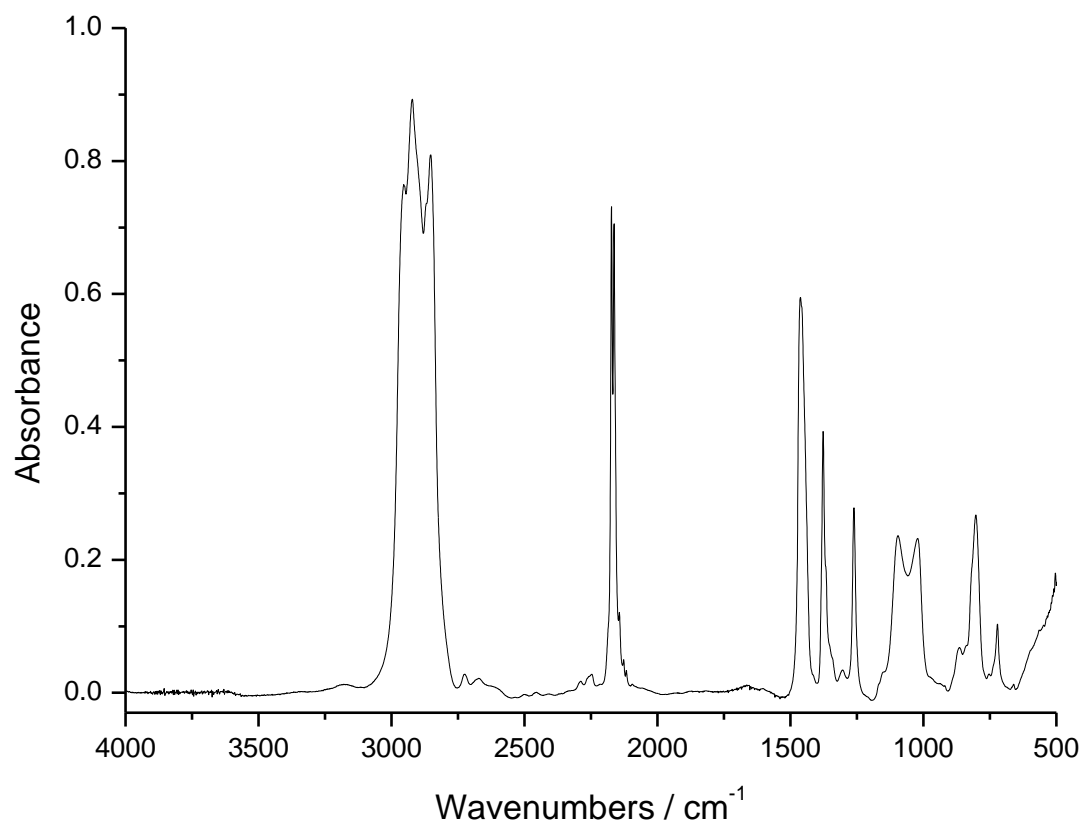
Figure A8.10. FT-IR spectrum of Sn(CN)$_2$, nujol mull.
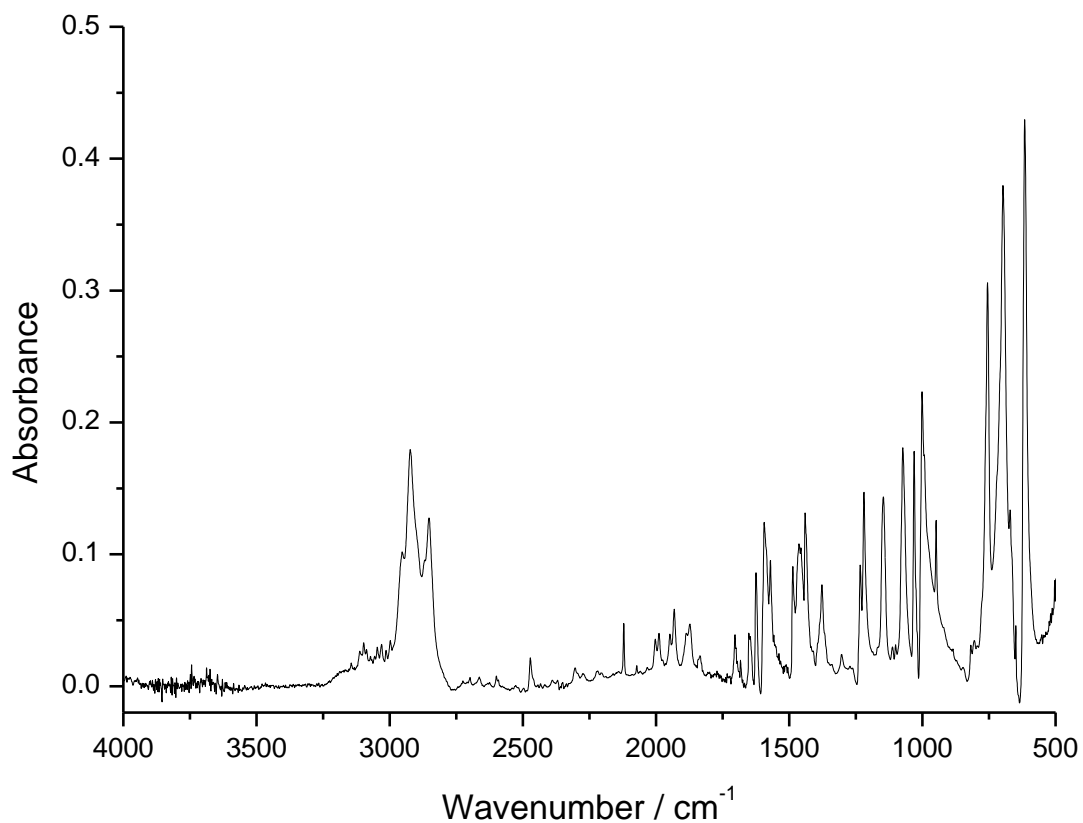
Figure A8.11. FT-IR spectrum of Pb(CN)$_2$(py)$_2$, nujol mull.
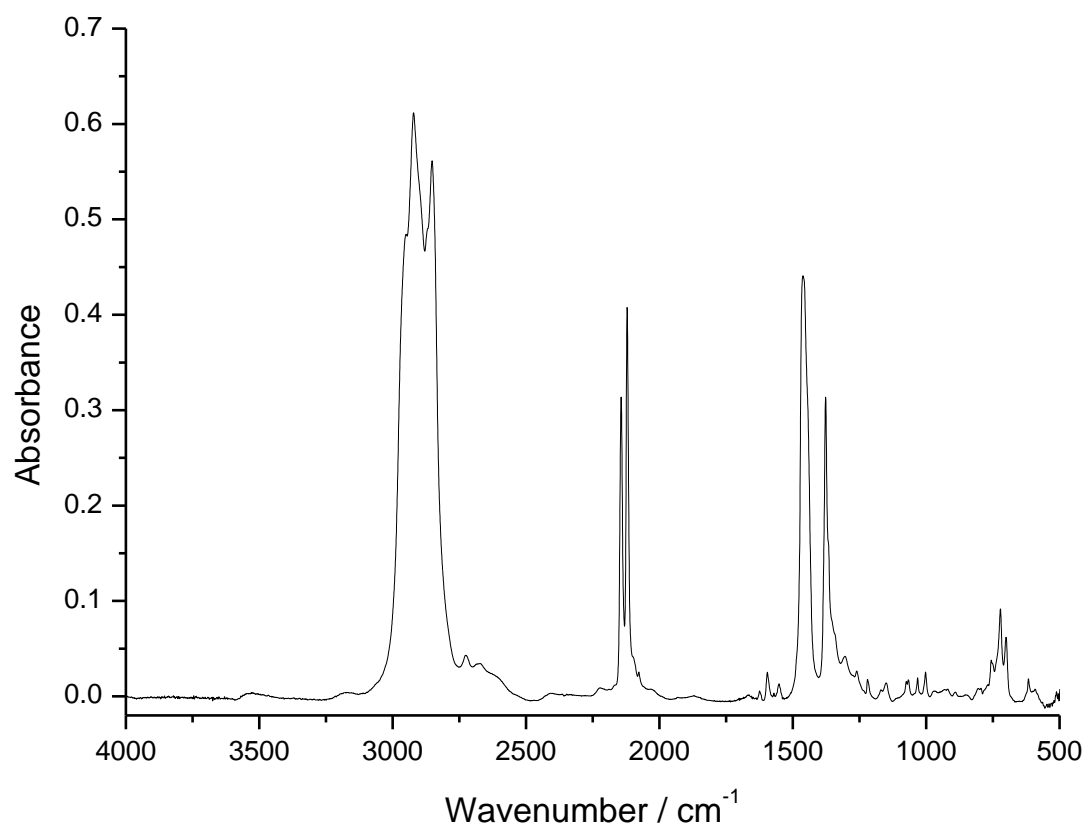
Figure A8.12. FT-IR spectrum of Pb(CN)$_2$, nujol mull.

277
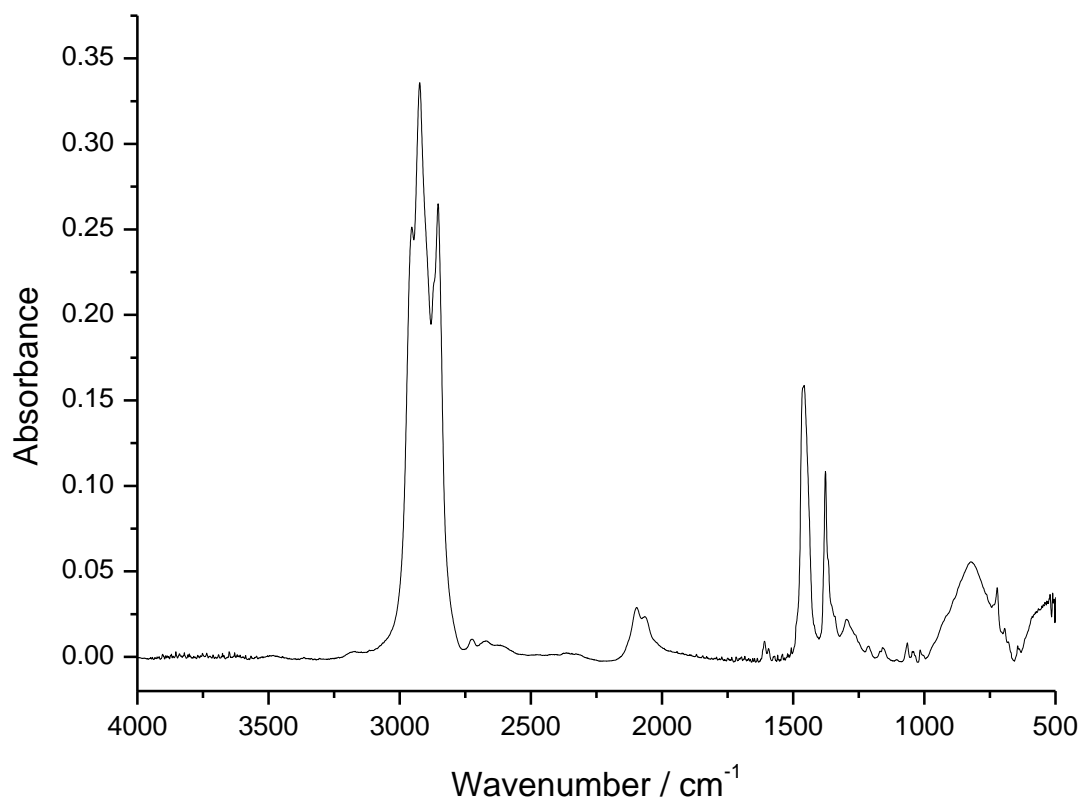
Figure A8.13. FT-IR spectrum of Ge(N$_3$)$_2$(py)$_2$, nujol mull.
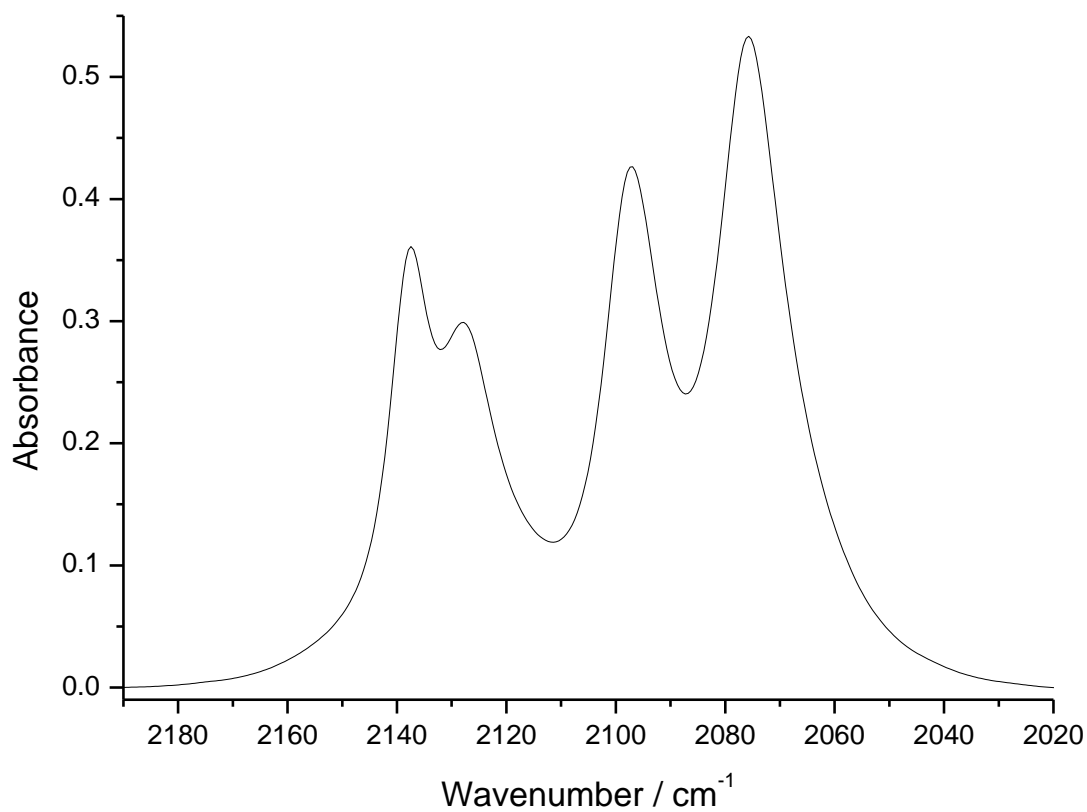
Figure A8.14. Expansion of nujol mull FT-IR spectrum of Ge(N$_3$)$_2$(py)$_2$ (figure 8.13) between 2190-2020 cm^{-1}, showing the ν_{as}(N$_3$) bands.
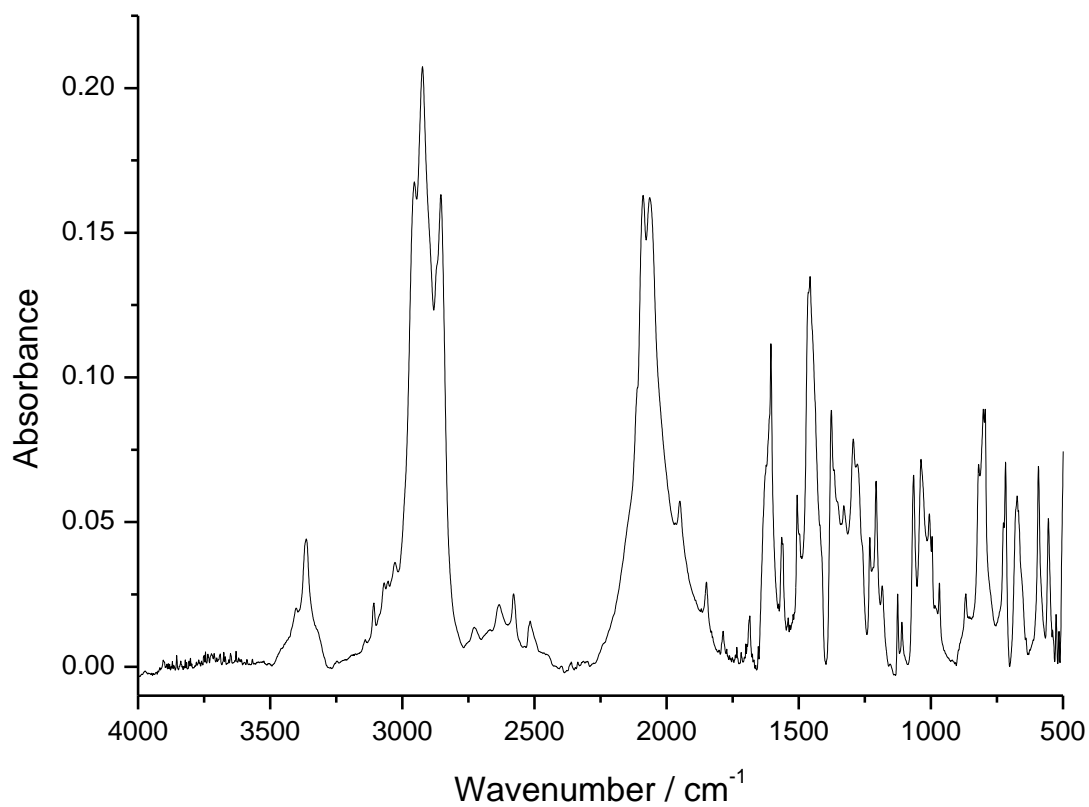
Figure A8.15. FT-IR spectrum of Ge(N$_3$)$_2$(pic)$_2$, nujol mull.
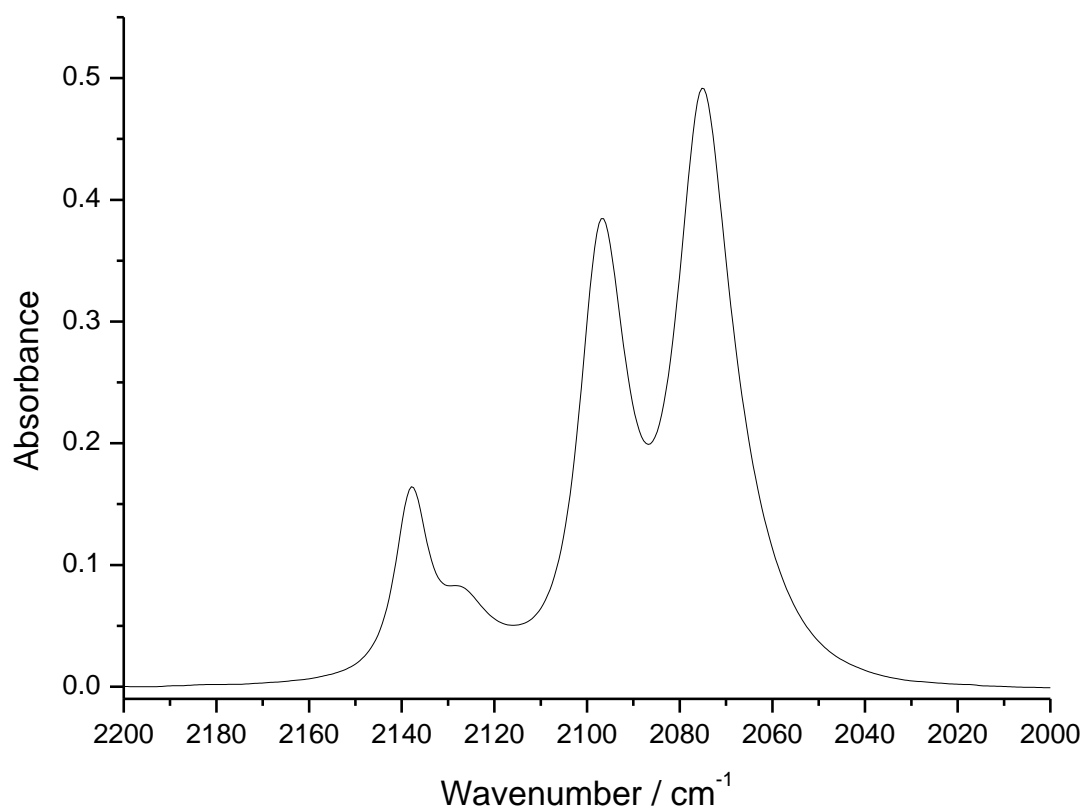
Figure A8.16. Expansion of nujol mull FT-IR spectrum of Ge(N$_3$)$_2$(pic)$_2$ (figure 8.15) between 2200-2000 cm^{-1}, showing the ν_{as}(N$_3$) bands.
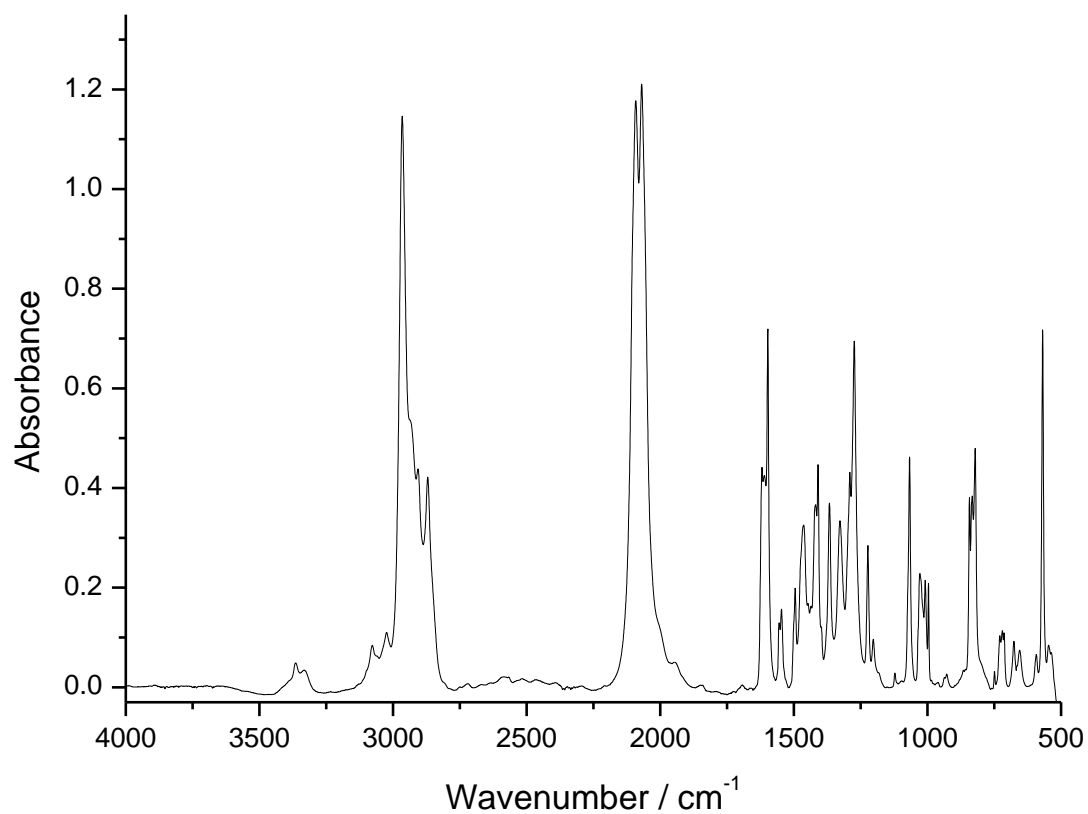
Figure A8.17. FT-IR spectrum of Ge(N$_3$)$_2$(^{t}Bupy)$_2$, thin film in ^{t}Bupy.
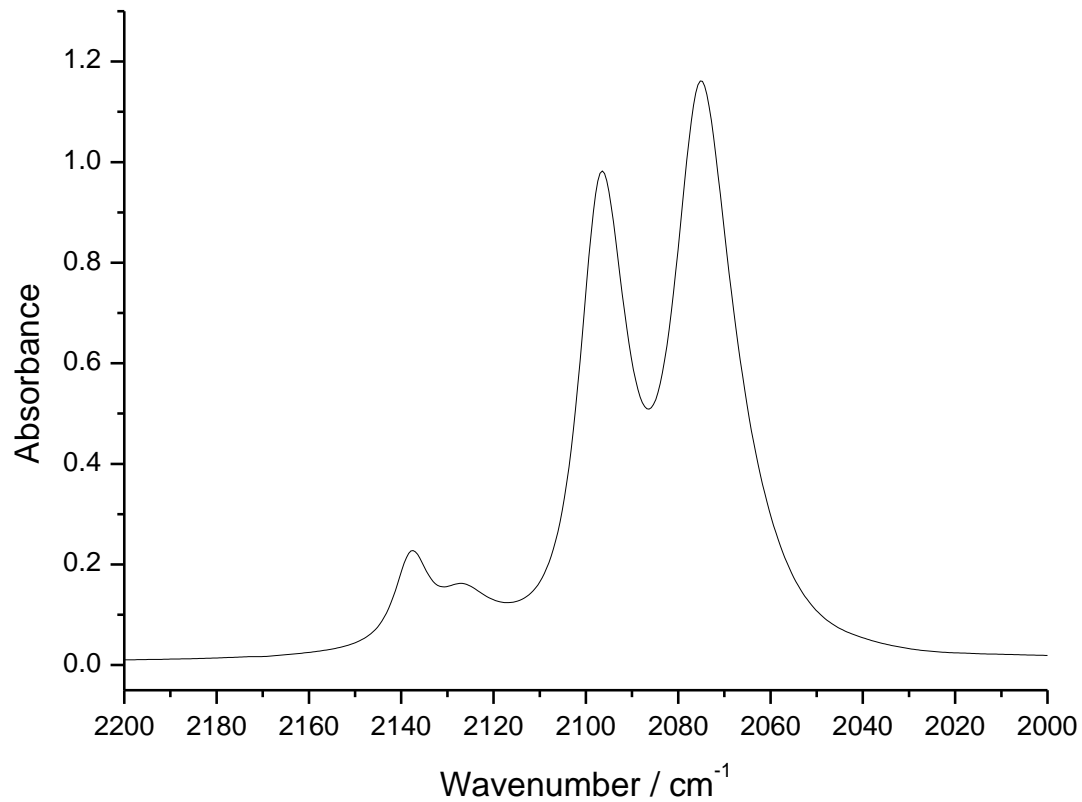
Figure A8.18. Expansion of thin film FT-IR spectrum of Ge(N$_3$)$_2$(^{t}Bupy)$_2$ (figure 8.17) between 2200-2000 cm^{-1}, showing the ν_{as}(N$_3$) bands.
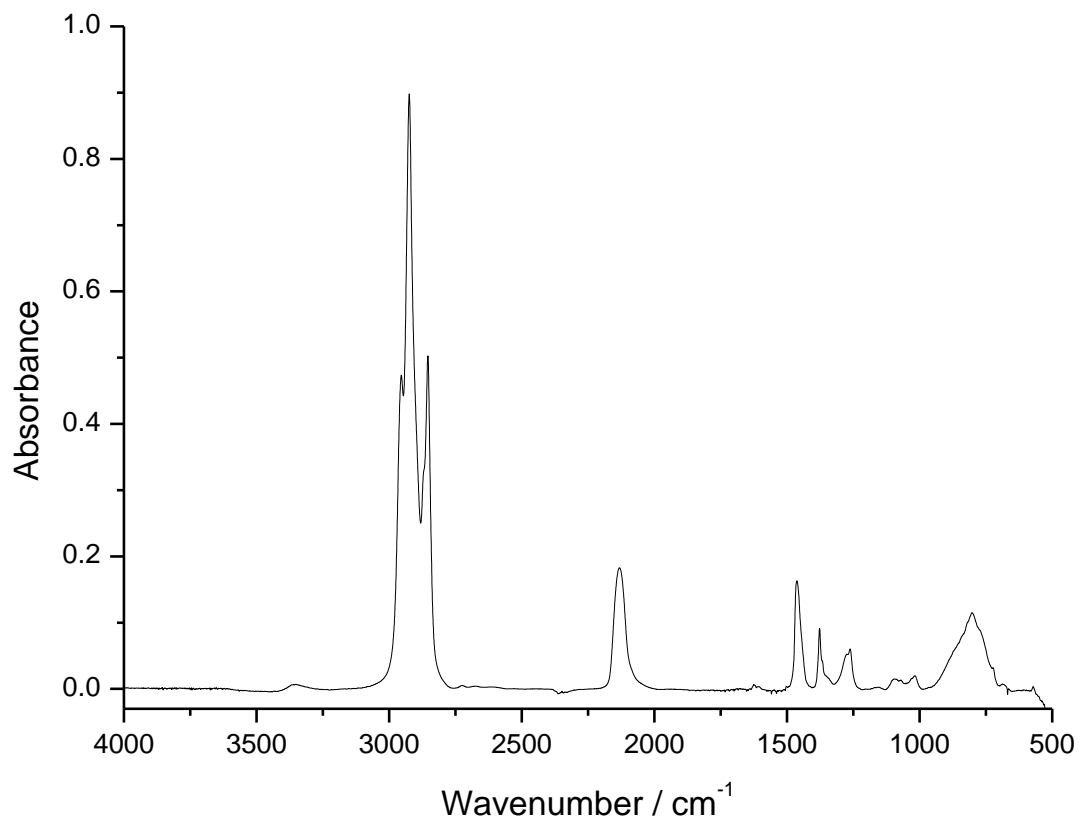
Figure A8.19. FT-IR spectrum of Ge(N$_3$)N, nujol mull.
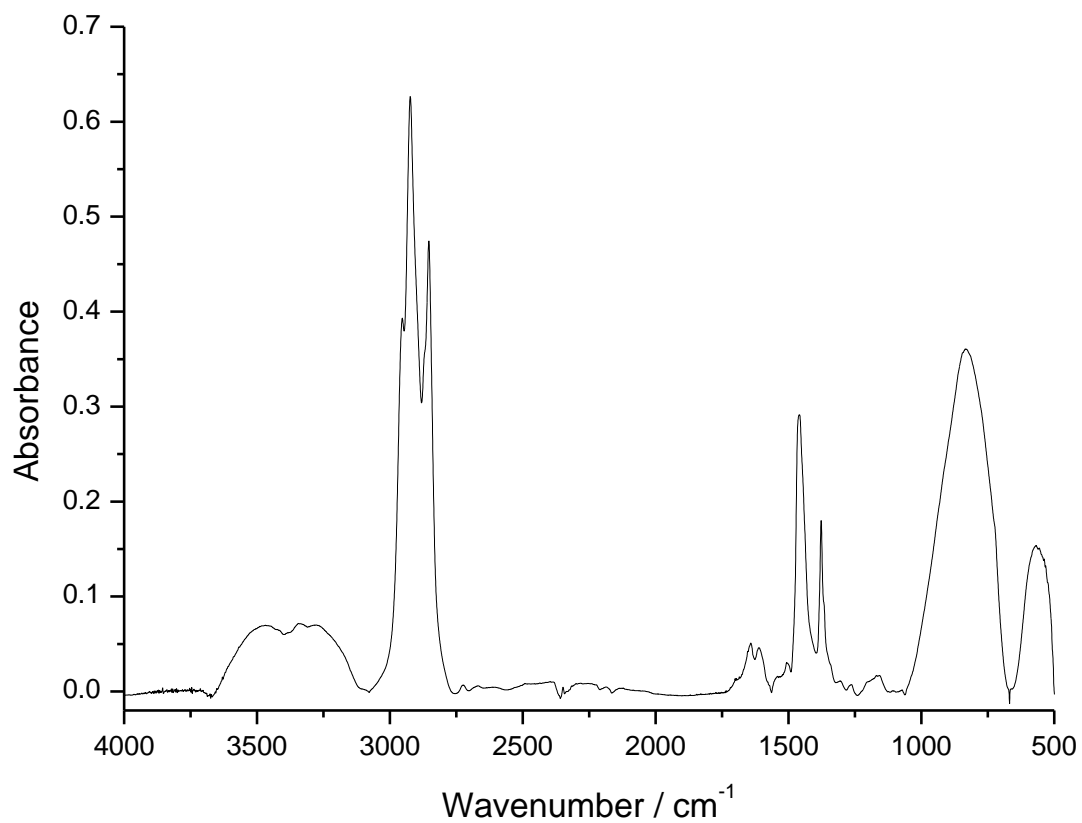
Figure A8.20. FT-IR spectrum of product obtained from further heating of Ge(N$_3$)N, believed to be Ge$_3$N$_x$ (x = 2 or 4), nujol mull.
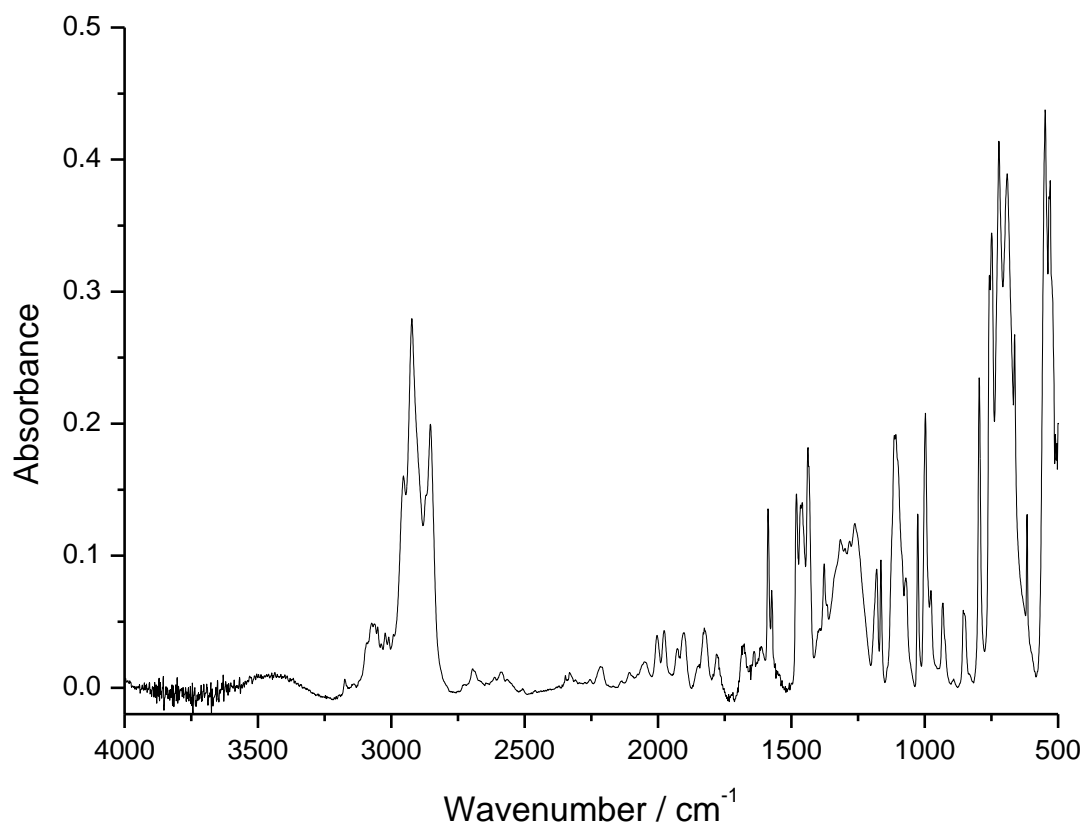
Figure A8.21. FT-IR spectrum of [PPN]$_2$[PbCl$_6$], nujol mull.
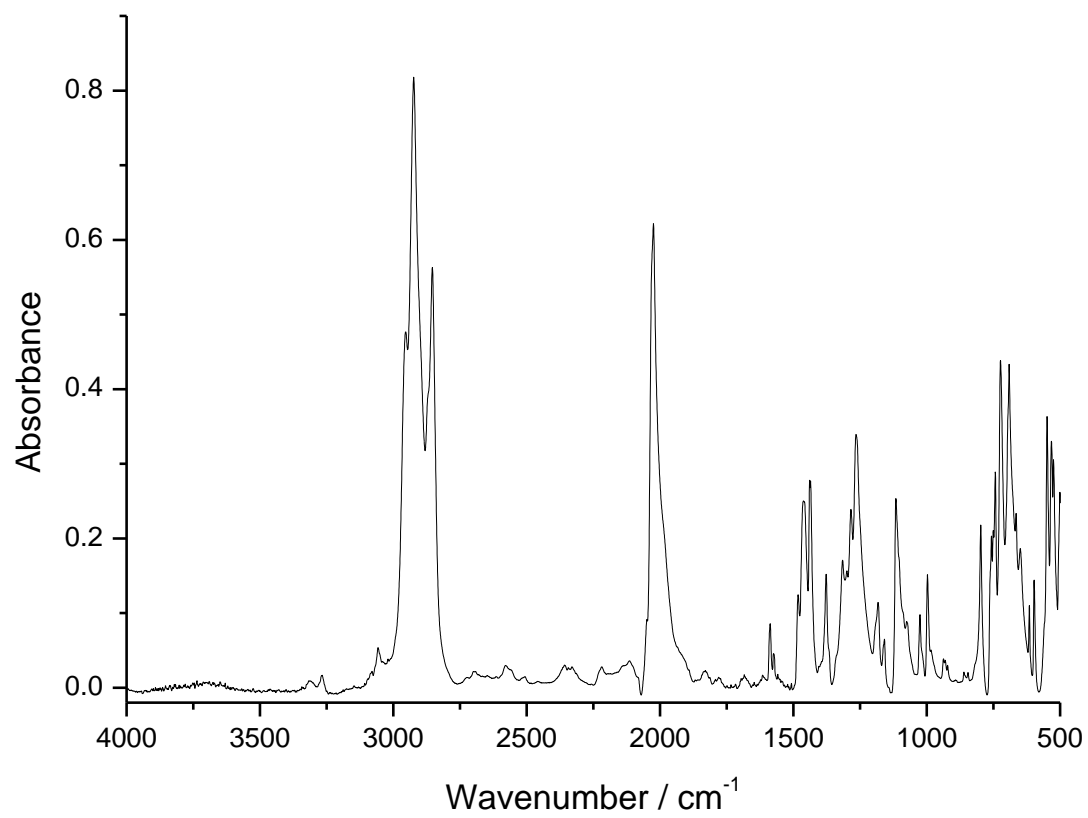
Figure A8.22. FT-IR spectrum of [PPN]$_2$[Pb(N$_3$)$_6$], nujol mull.
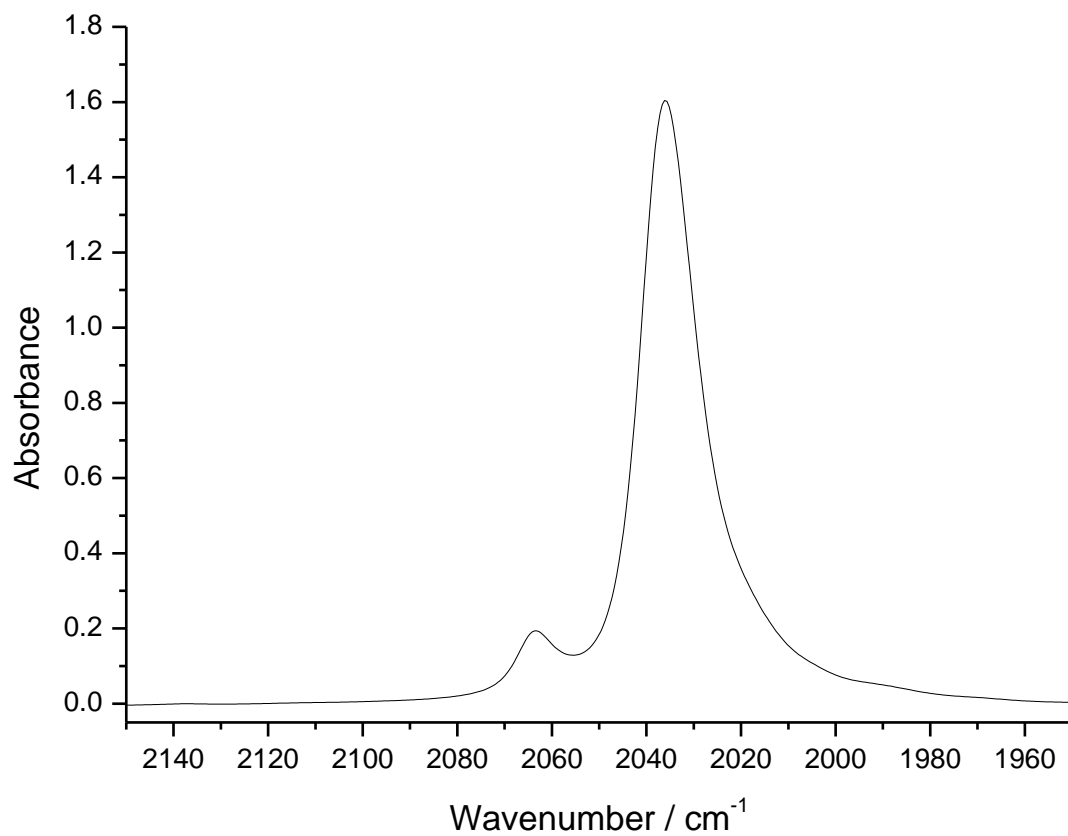
Figure A8.23. FT-IR spectrum of [PPN]$_2$[Pb(N$_3$)$_6$] in CH$_2$Cl$_2$ solution.
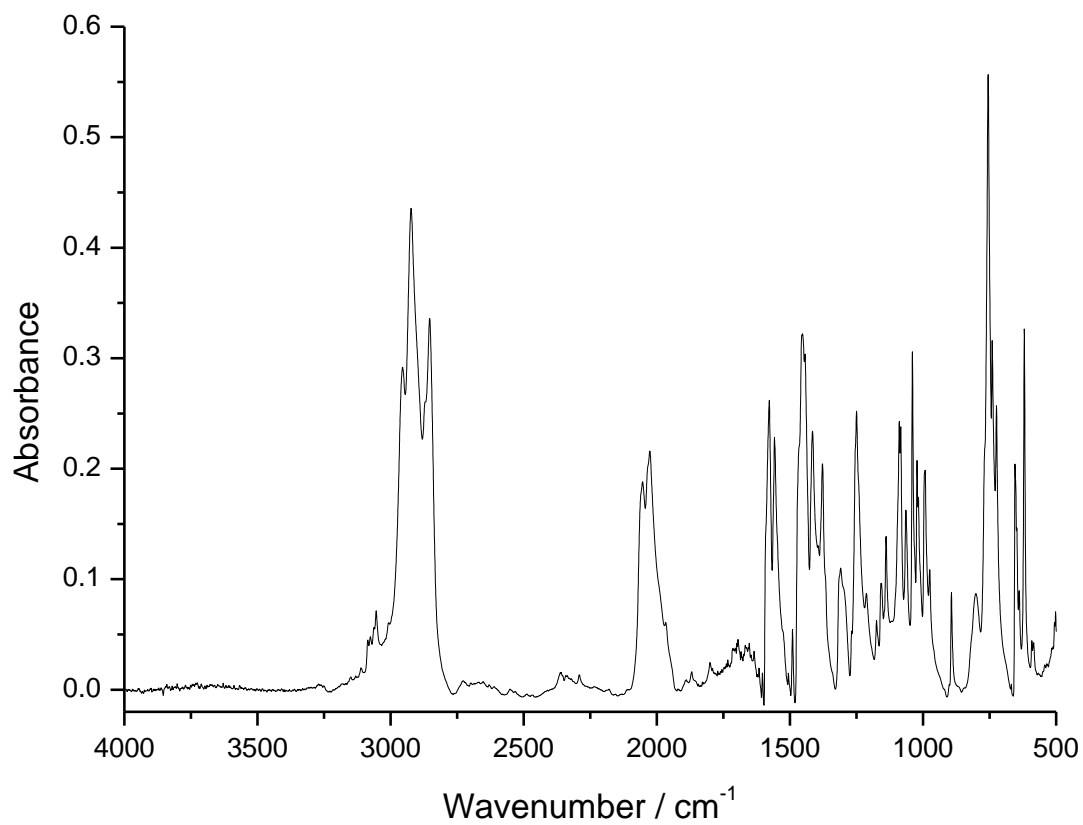
Figure A8.24. FT-IR spectrum of Pb(N$_3$)$_4$(bipy), nujol mull.
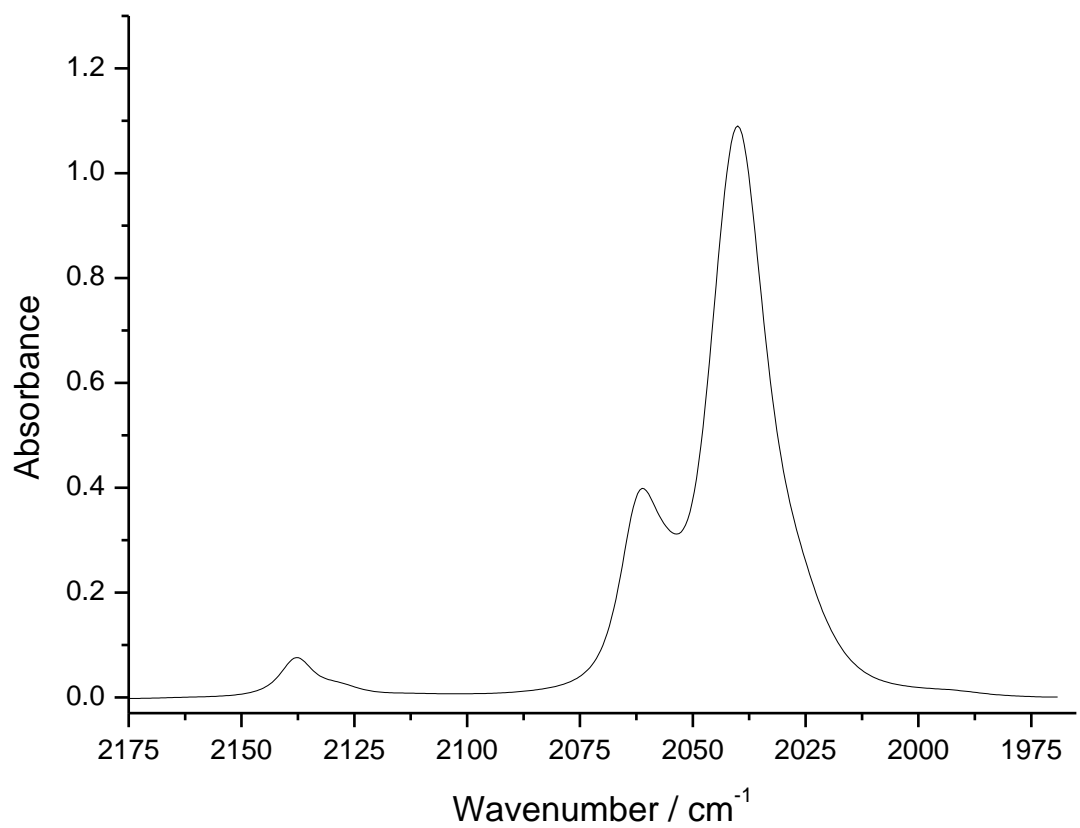
Figure A8.25. FT-IR spectrum of Pb(N$_3$)$_4$(bipy) in CH$_2$Cl$_2$ solution.
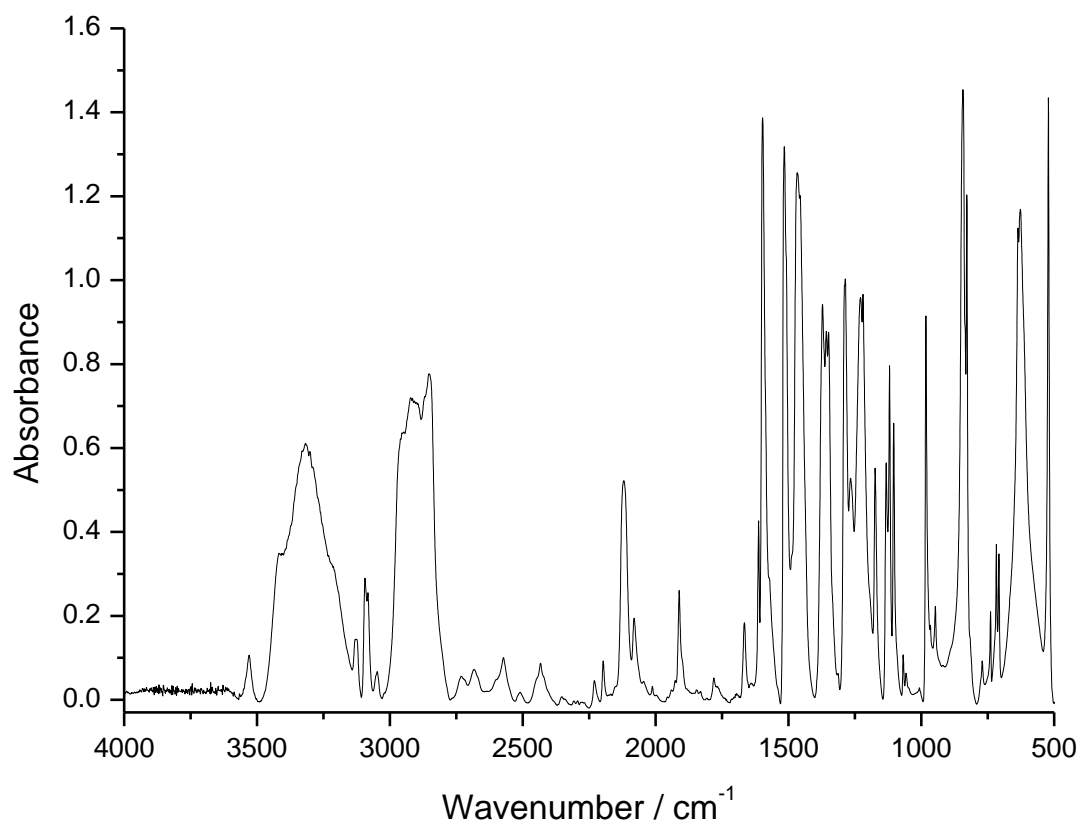
Figure A8.26. FT-IR spectrum of HOP−N$_5$, nujol mull.
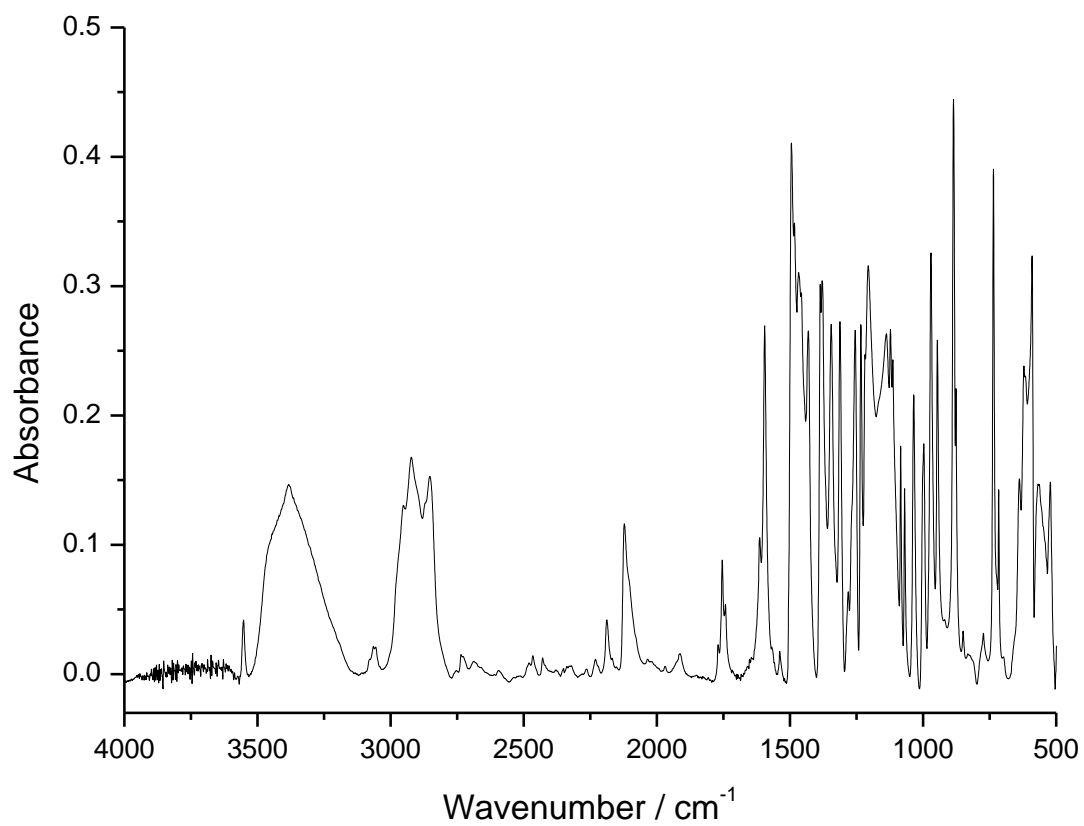
Figure A8.27. FT-IR spectrum of DMHP−N$_5$, nujol mull.
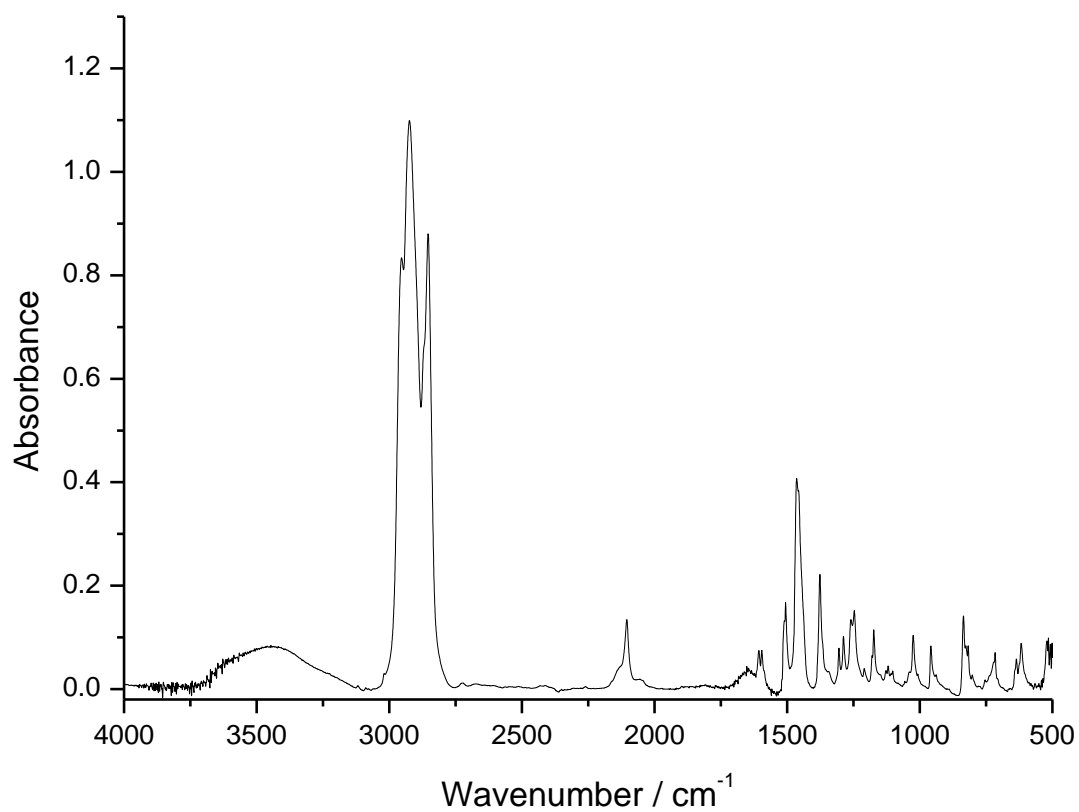
Figure A8.28. FT-IR spectrum of MeOP−N$_5$, nujol mull.
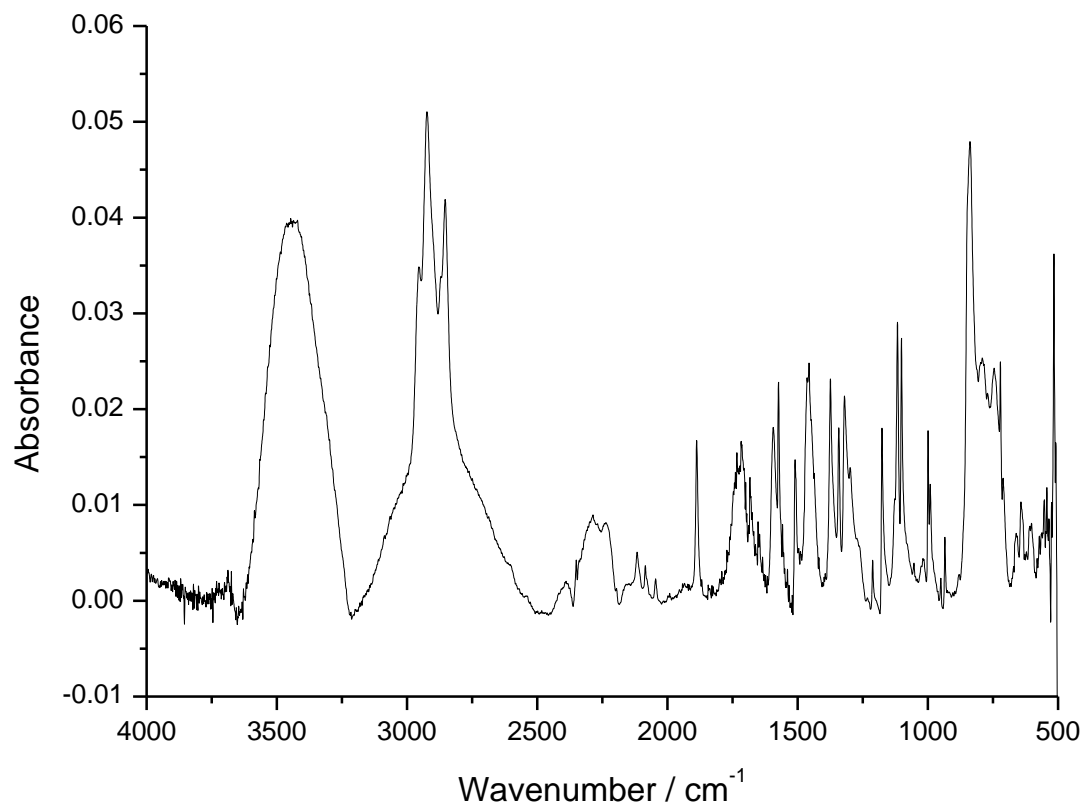
Figure A8.29. FT-IR spectrum of CsOP−N$_5$, nujol mull.
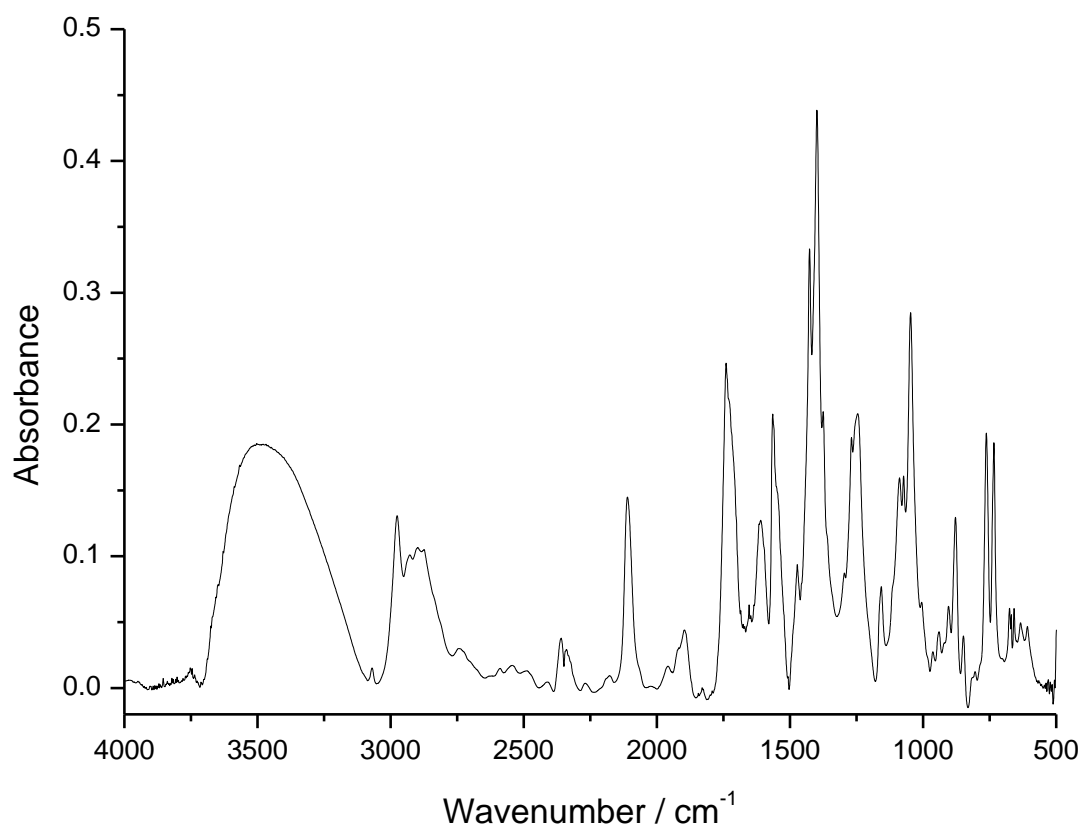
Figure A8.30. FT-IR spectrum of 'NaN$_5$·3H$_2$O', nujol mull.
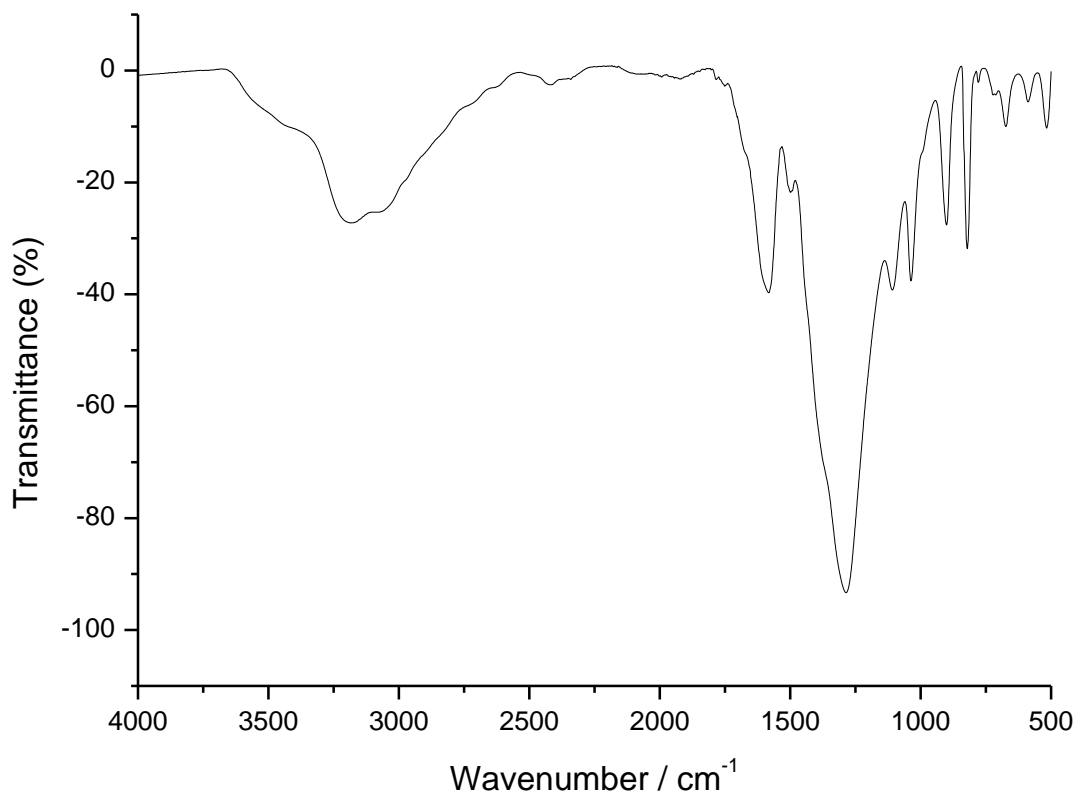
Figure A8.31. ATR-IR spectrum of '[PPN]N$_5$'.
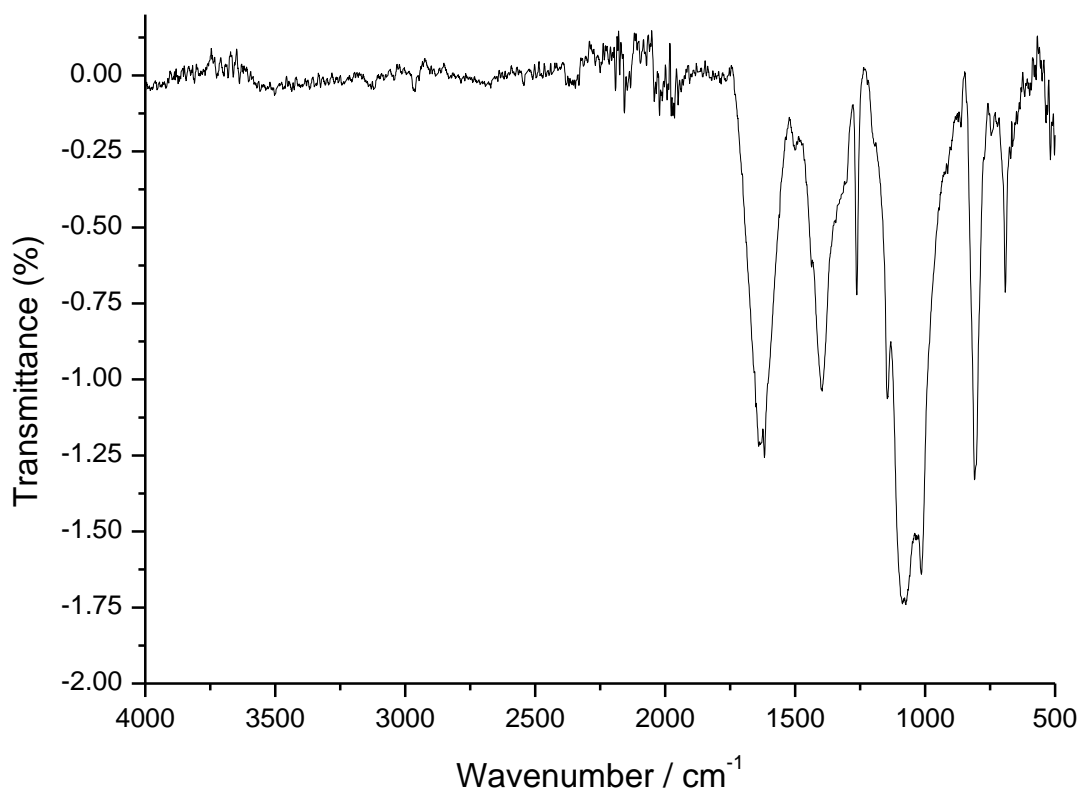
Figure A8.32. ATR-IR spectrum of 'AgN$_5$'.
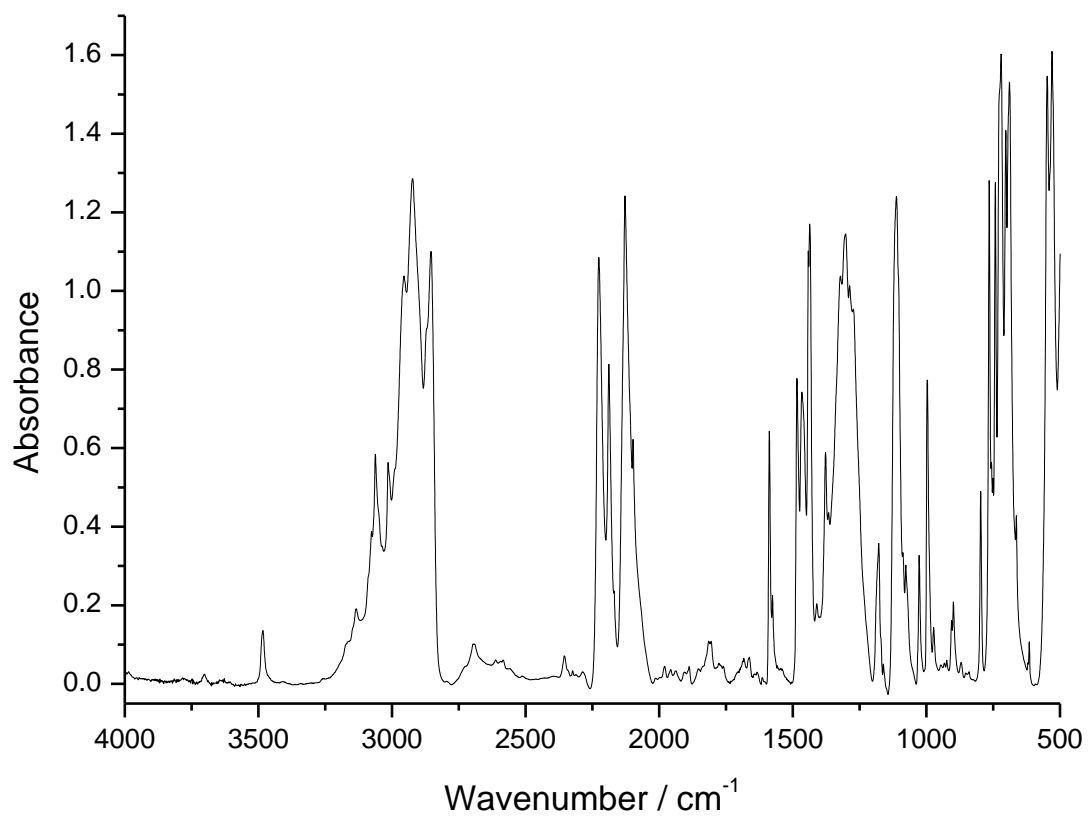
Figure A8.33. FT-IR spectrum of [PPN][N(CN)$_2$], nujol mull.
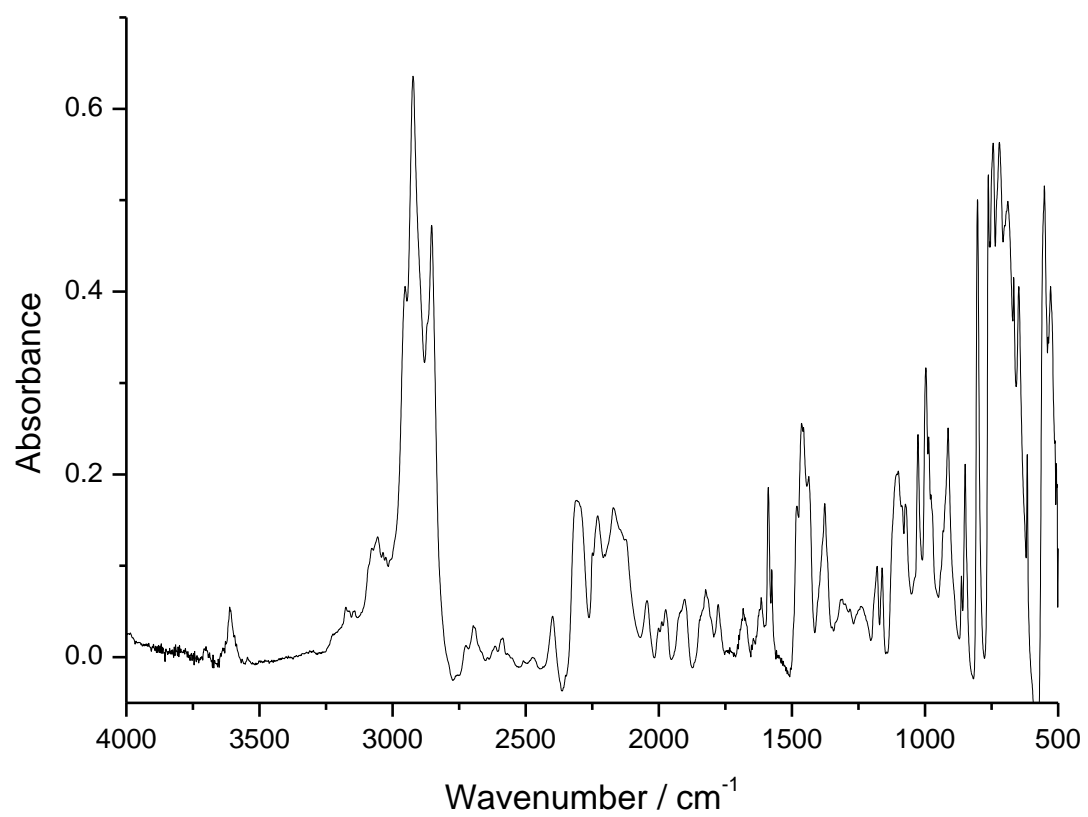
Figure A8.34. FT-IR spectrum of [PPN]$_2$[SnCl$_4${N(CN)$_2$}$_2$], nujol mull.

A9. NMR Spectra

ZS135
C13CPD250PPM CD3CN {C:\06Jun2016} ch3ppx 33
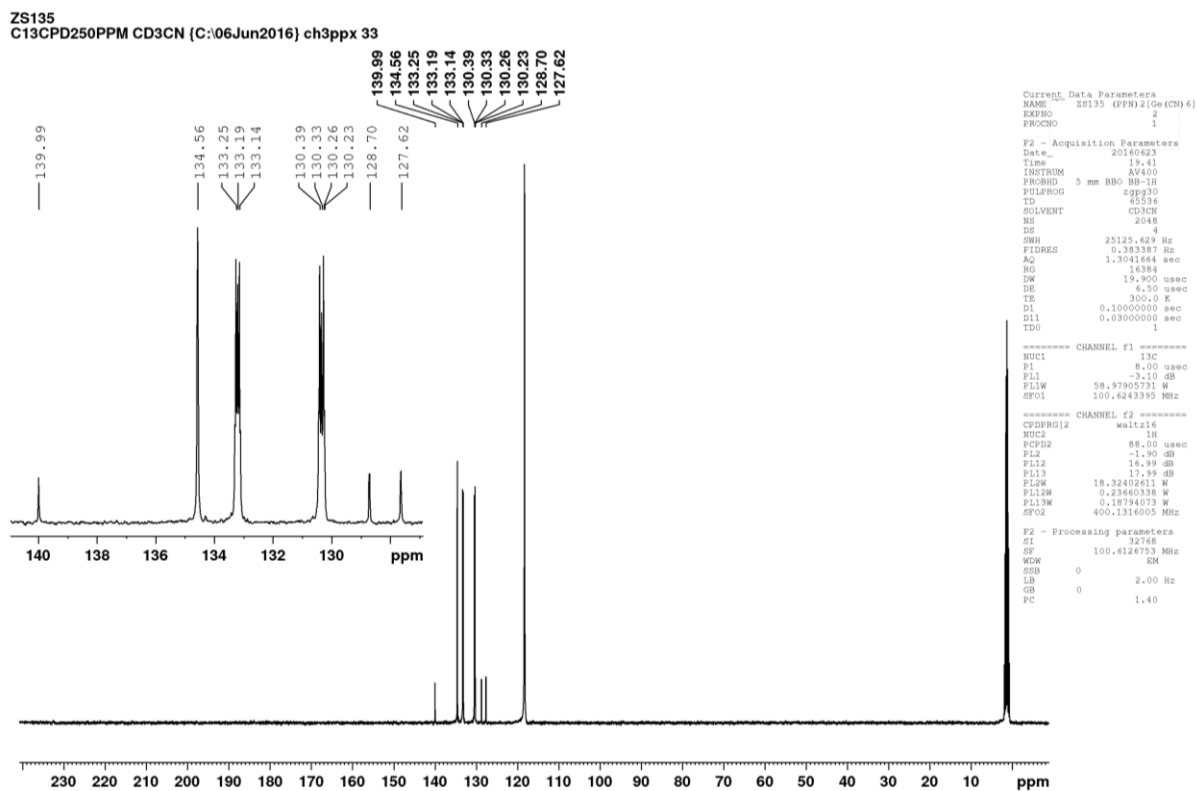
Figure A9.1. ^{13}C NMR spectrum of $[PPN]_2[Ge(CN)_6]$ in CD_3CN.

ZS85
PRO DMSO {C:\NMRData\11Nov2015} ch3ppx 60
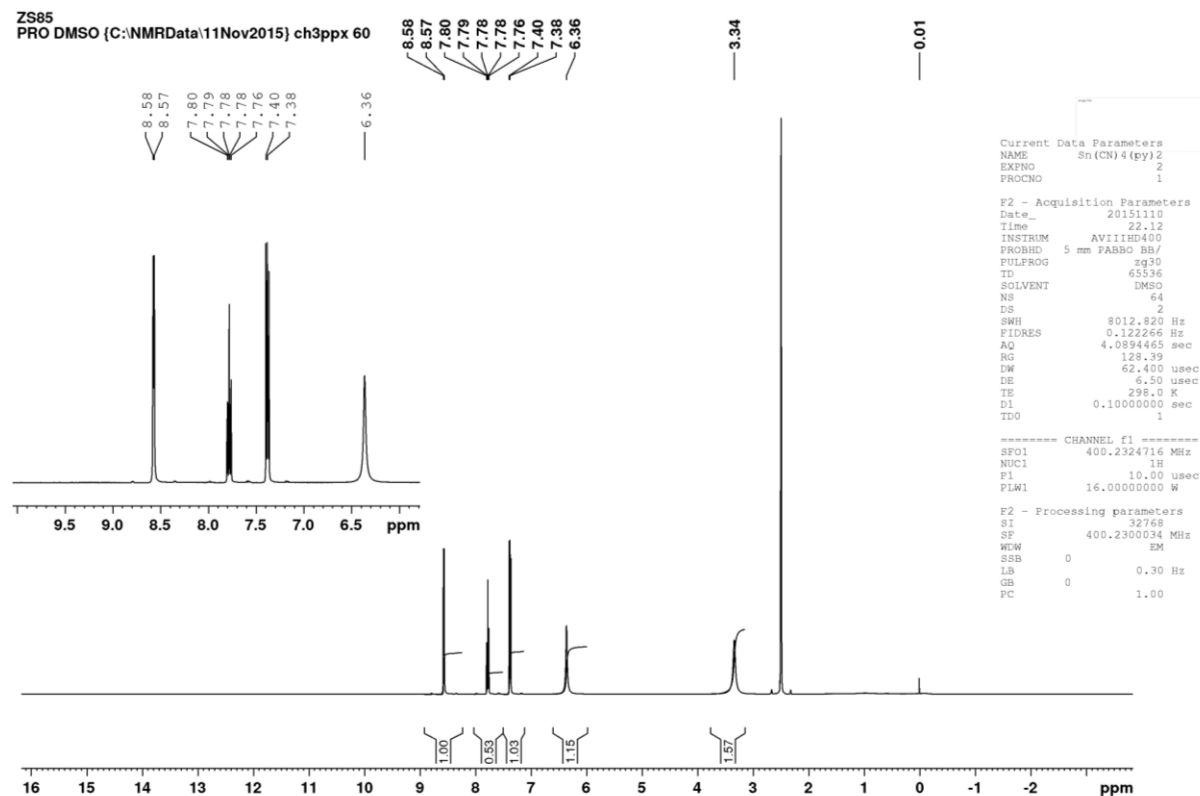
Figure A9.2. ^1H NMR spectrum of $Sn(CN)_4(py)_2$ in DMSO-d_6. The signals at δ = 6.36 ppm and 3.34 ppm are attributed to HCN and H_2O, respectively.

289
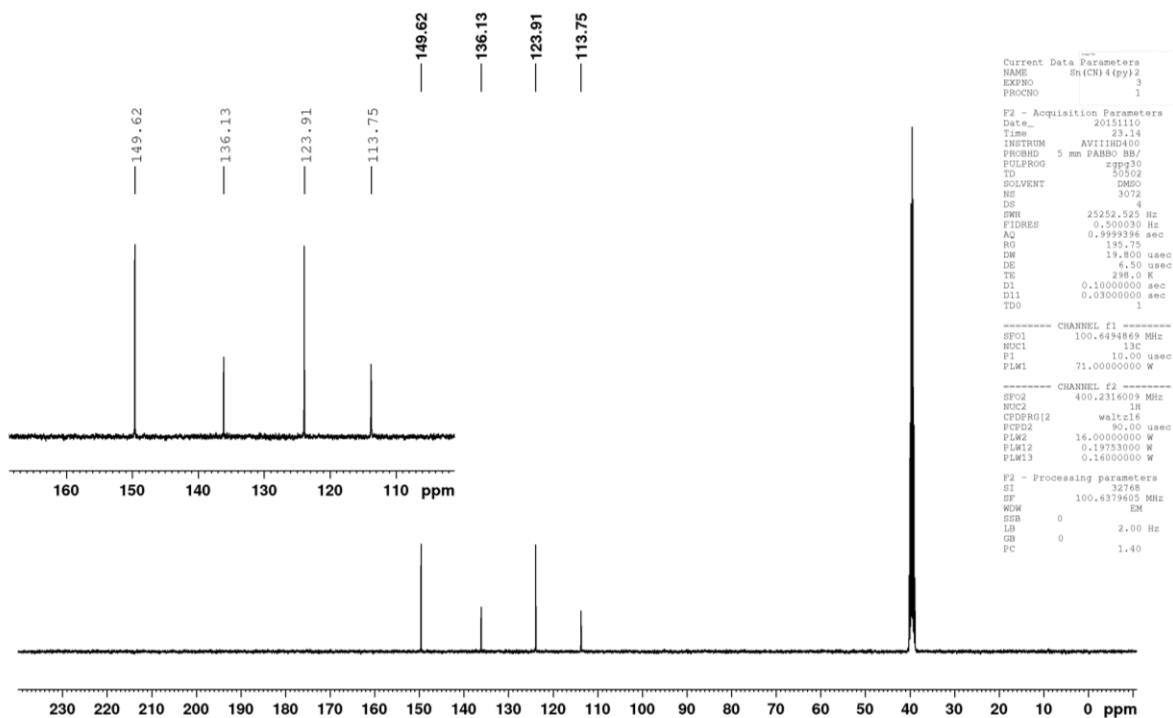
Figure A9.3. ^{13}C NMR spectrum of Sn(CN)$_4$(py)$_2$ in DMSO-d$_6$.

.
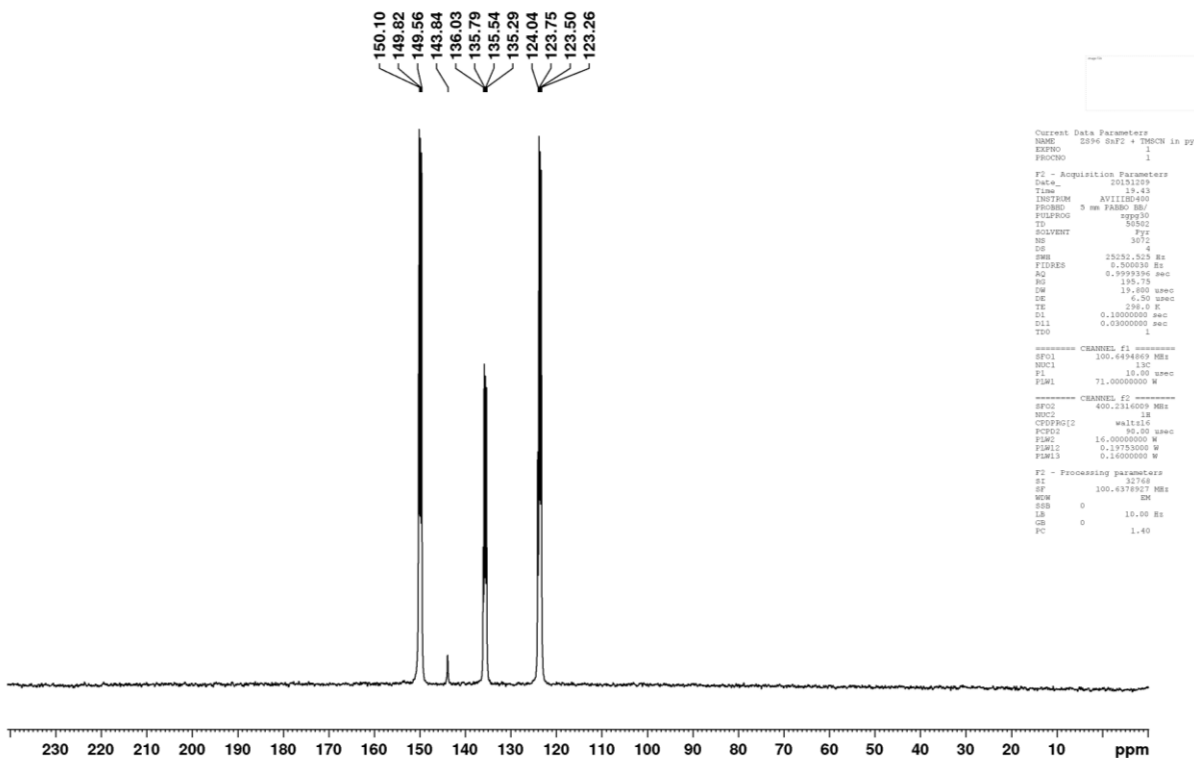
Figure A9.4. ^{13}C NMR spectrum of Sn(CN)$_2$(py)$_2$ in pyridine-d$_5$.

290
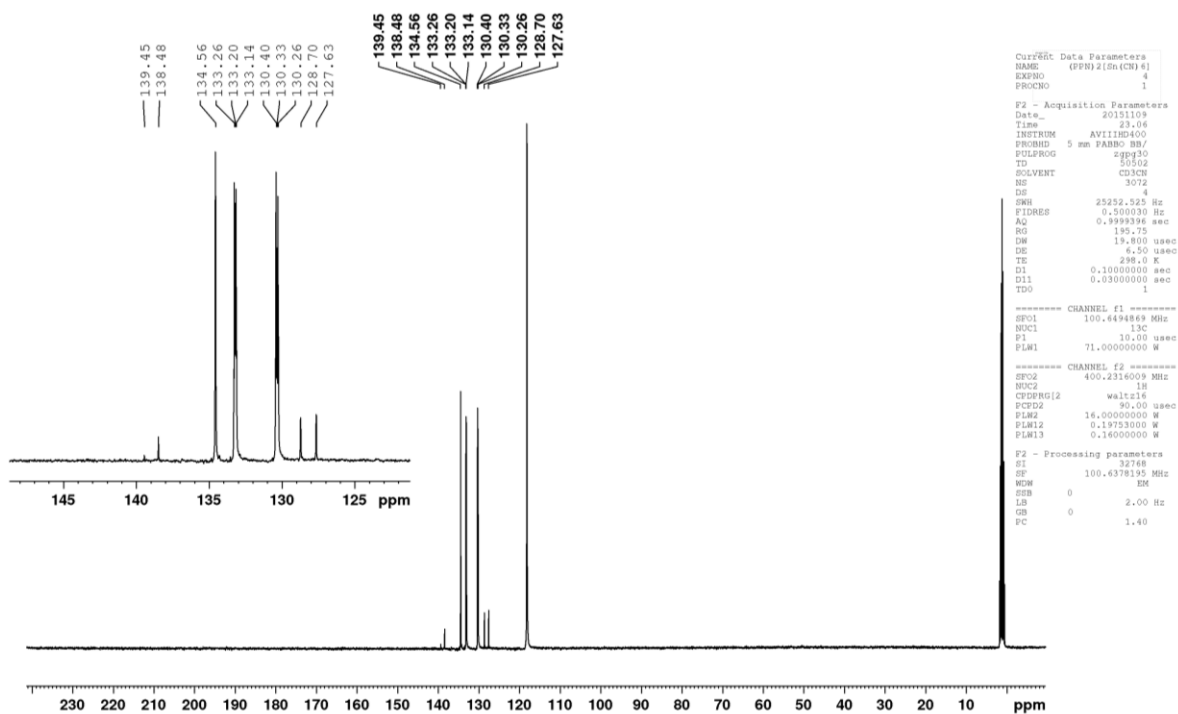
Figure A9.5. ^{13}C NMR spectrum of [PPN]$_2$[Sn(CN)$_6$] in CD$_3$CN. The signal at δ = 138.5 ppm is attributed to an unknown tin-based hydrolysis product.
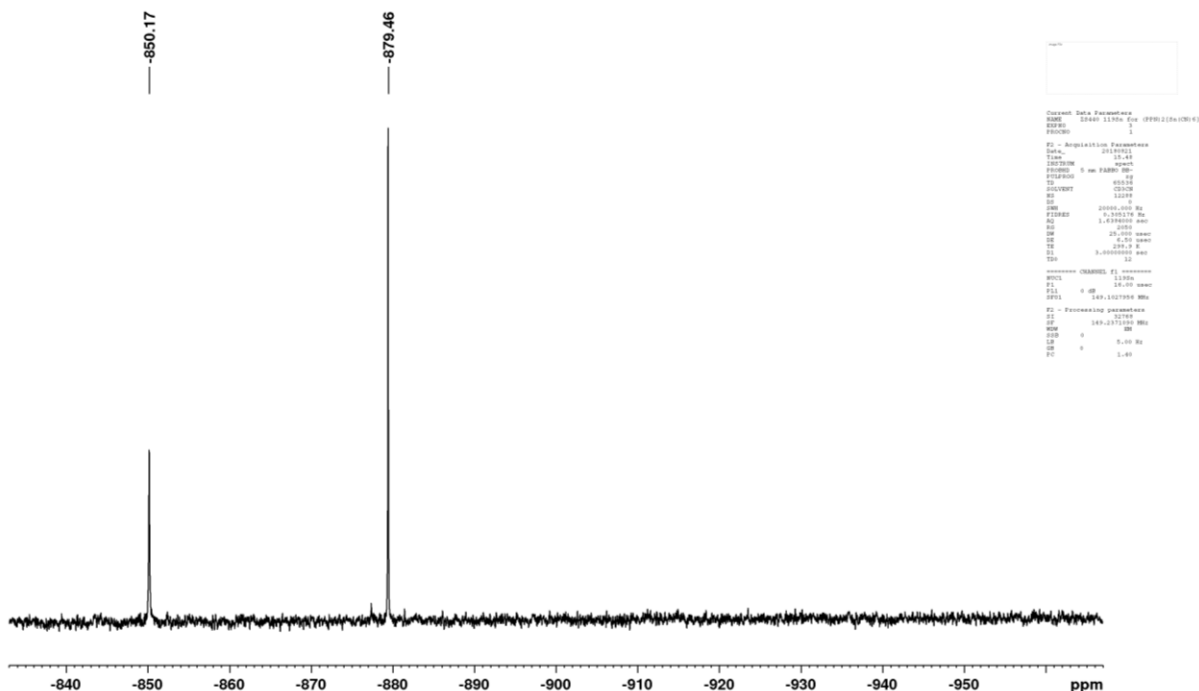
Figure A9.6. ^{119}Sn NMR spectrum of [PPN]$_2$[Sn(CN)$_6$] in CD$_3$CN. The signal at δ = −850.17 ppm is attributed to an unknown tin-containing hydrolysis product.

291
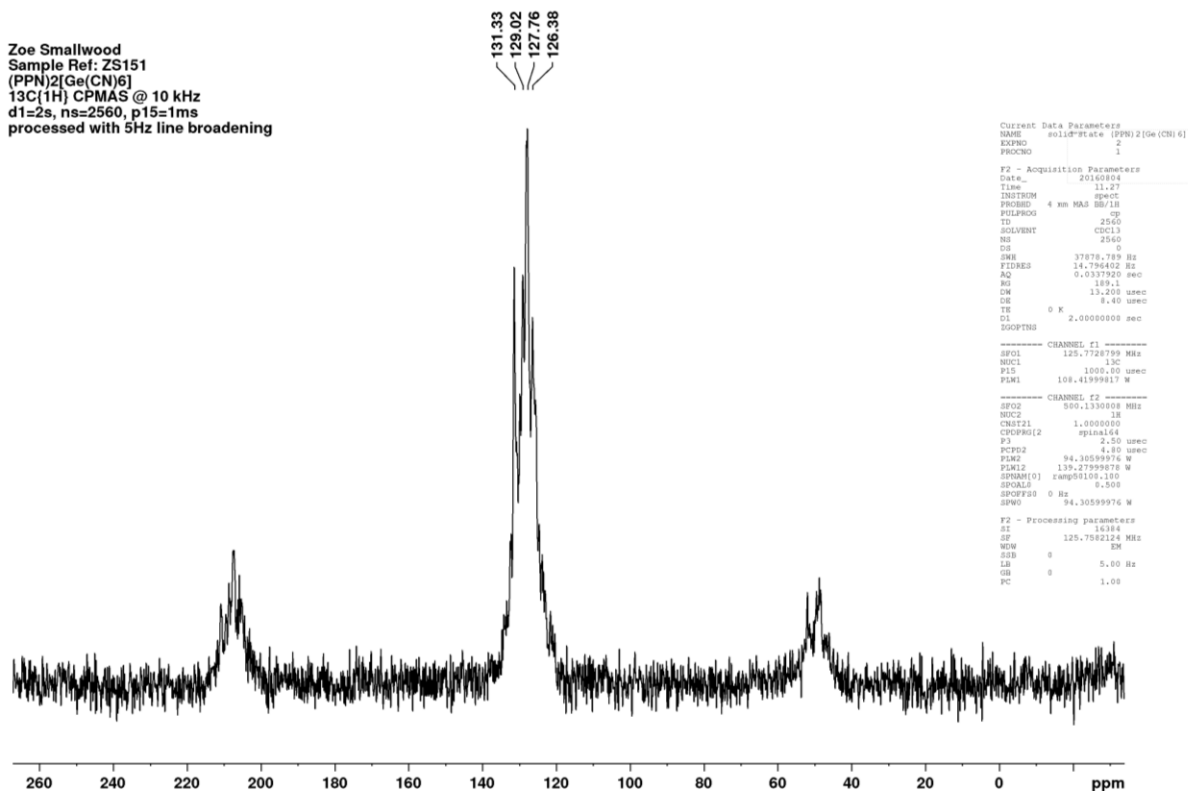
Figure A9.7. ^{13}C MAS NMR spectrum of [PPN]$_2$[Ge(CN)$_6$]. The two smaller bands either side of the main signal are attributed to spinning side-bands.
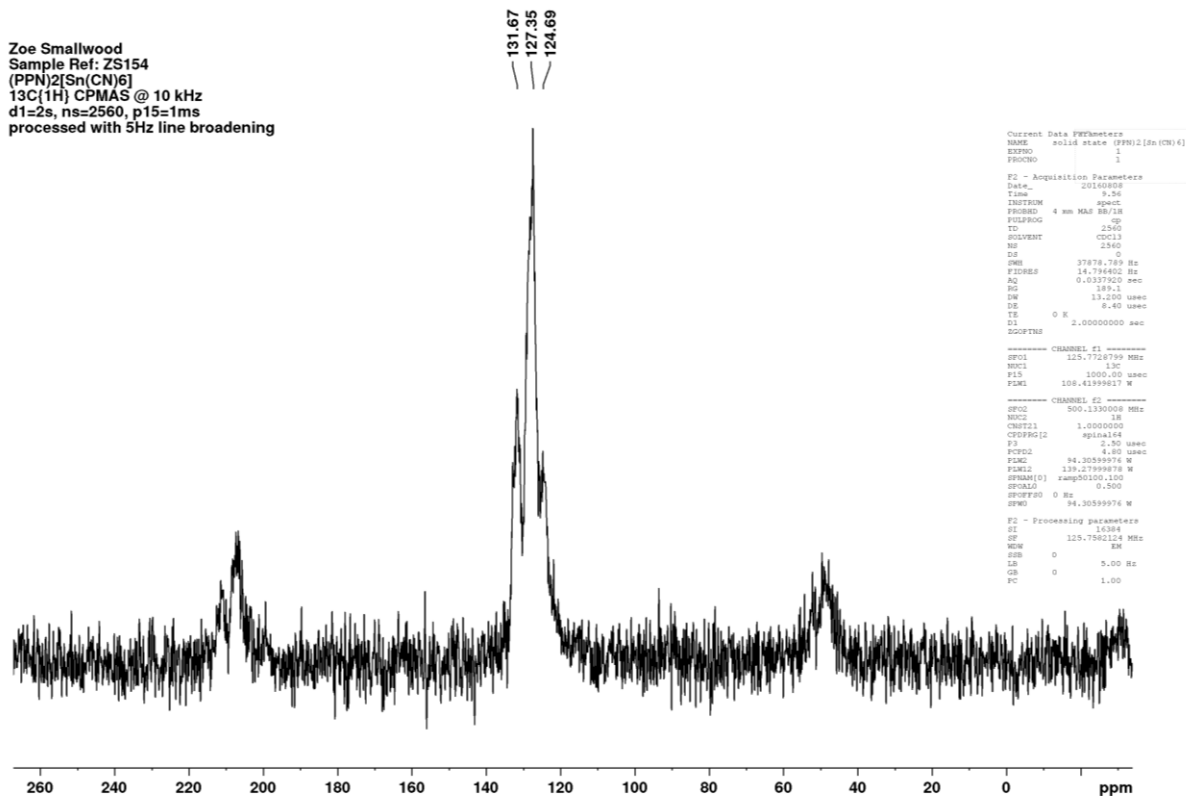
Figure A9.8. ^{13}C MAS NMR spectrum of [PPN]$_2$[Sn(CN)$_6$]. The two smaller bands either side of the main signal are attributed to spinning side-bands.
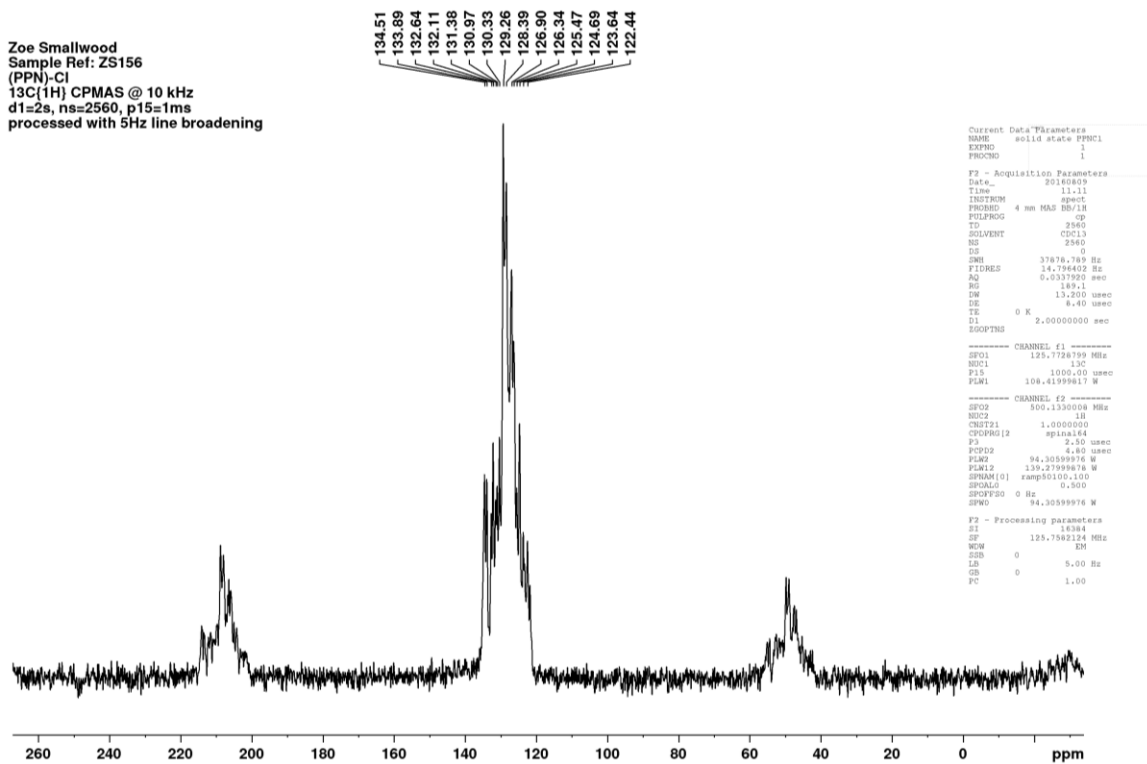
Figure A9.9. ^{13}C MAS NMR spectrum of [PPN]Cl. The two smaller bands either side of the main signal are attributed to spinning side-bands.
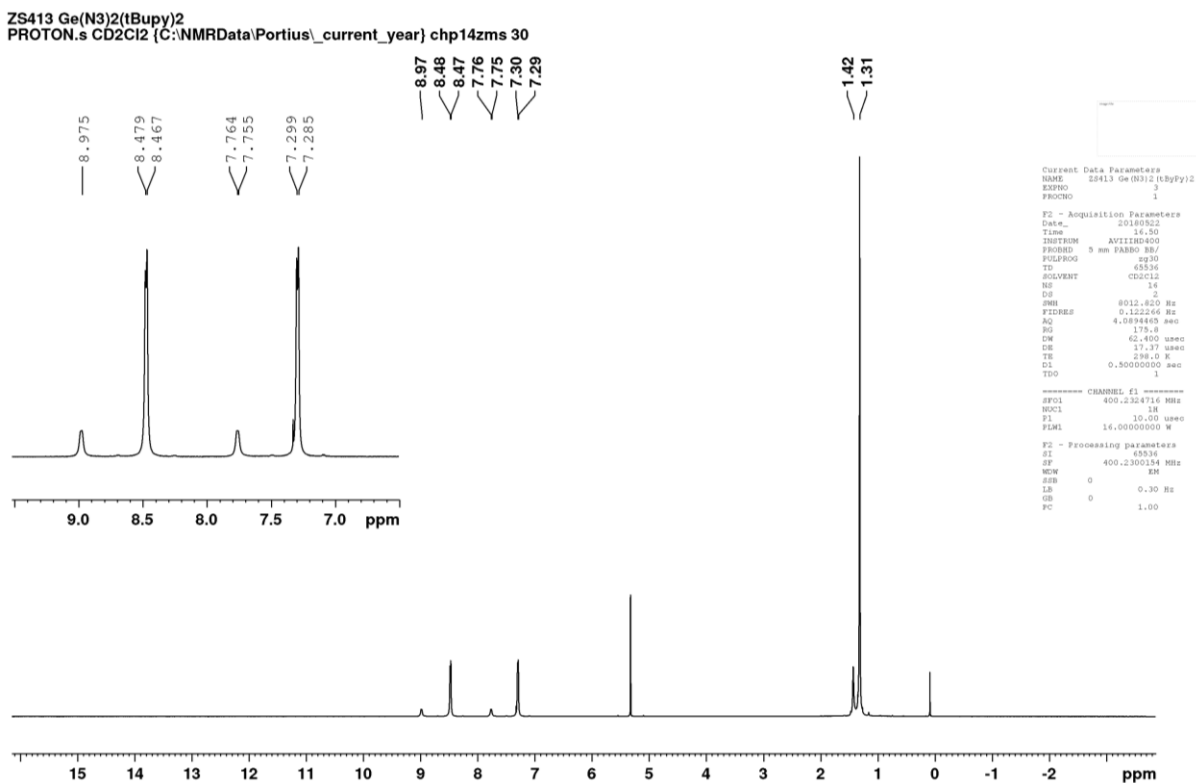
Figure A9.10. ^1H NMR spectrum of Ge(N$_3$)$_2$(^{t}Bupy)$_2$ in CD$_2$Cl$_2$. The signals at δ = 8.47, 7.29 and 1.31 ppm are attributed to uncoordinated ^{t}Bupy.
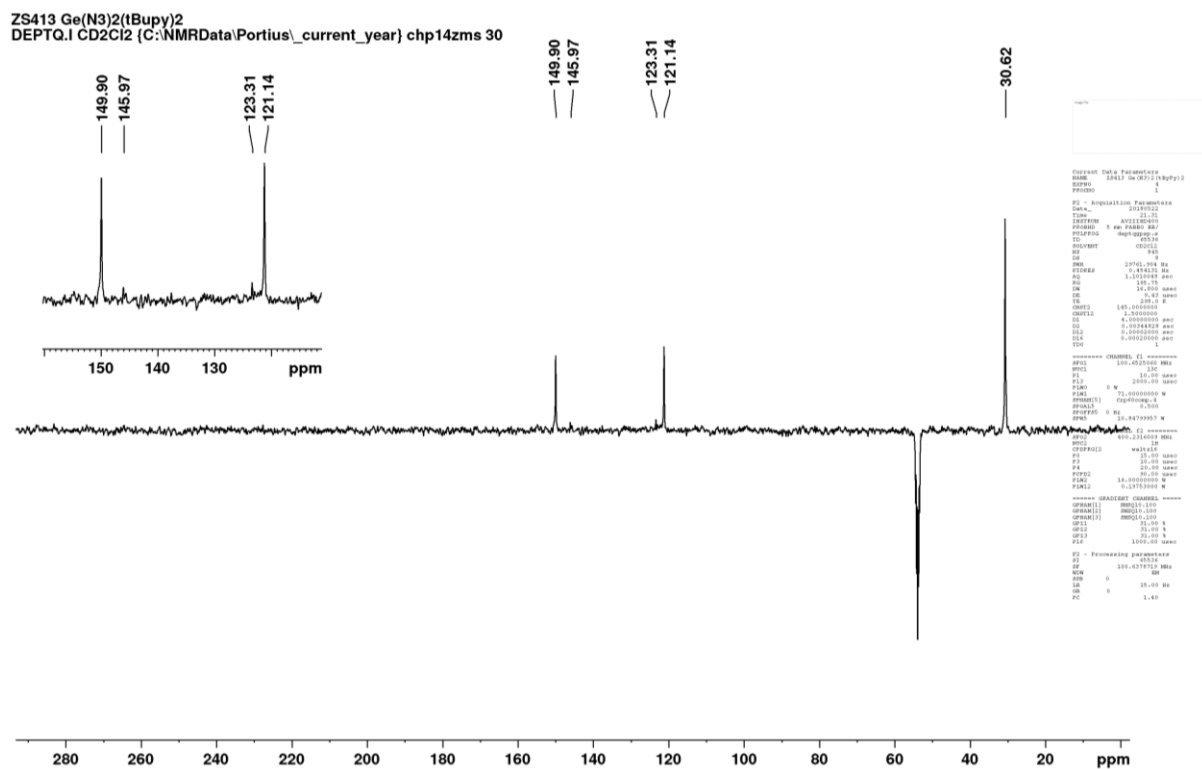
Figure A9.11. ^{13}C NMR spectrum of Ge(N$_3$)$_2$(^{t}Bupy)$_2$ in CD$_2$Cl$_2$. The signals at δ = 148.9, 121.1 and 30.5 ppm are attributed to uncoordinated ^{t}Bupy.
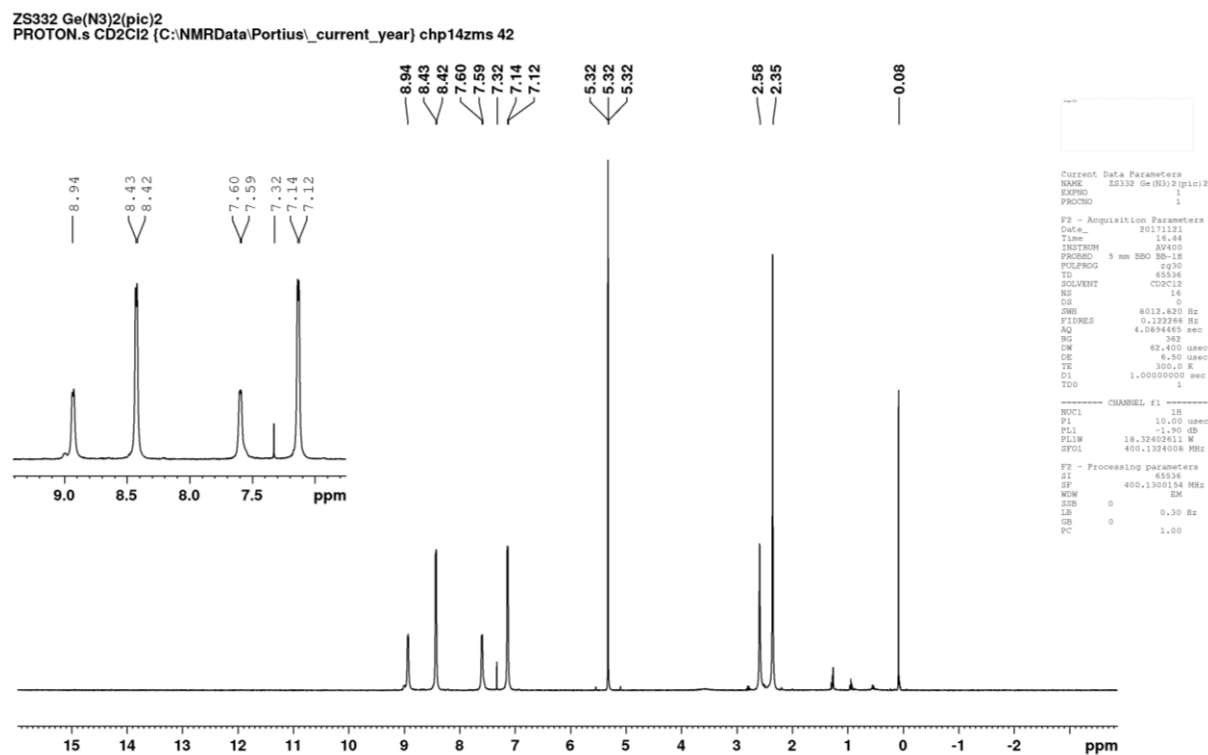
Figure A9.12. ^{1}H NMR spectrum of Ge(N$_3$)$_2$(pic)$_2$ in CD$_2$Cl$_2$. The signals at 8.42, 7.13 and 2.35 ppm are attributed to uncoordinated pic. The signal at δ = 7.32 ppm arises from CHCl$_3$ and is an impurity.

294

ZS332 Ge(N3)2(pic)2
DEPTQ.s CD2Cl2 {C:\NMRData\Portius_current_year} chp14zms 42
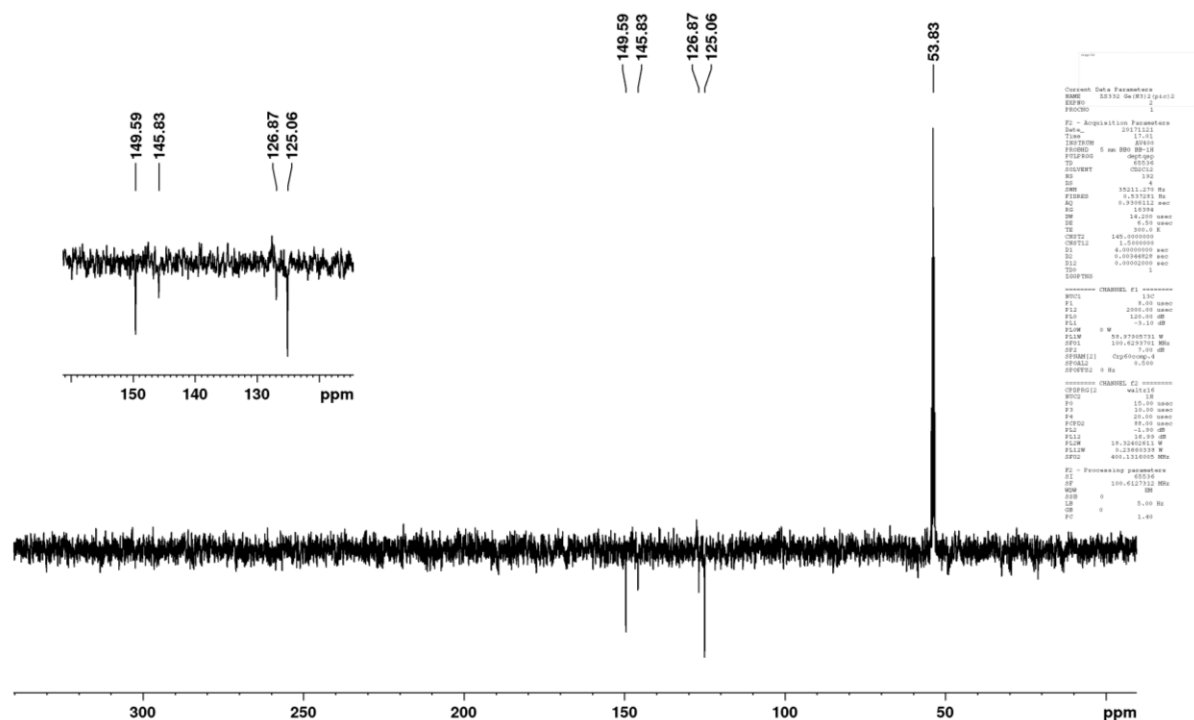
Figure A9.13. ^{13}C NMR spectrum of Ge(N$_3$)$_2$(pic)$_2$ in CD$_2$Cl$_2$. The signals at δ = 149.6 and 125.0 are attributed to uncoordinated pic.

ZS289 Pb(N3)4(bipy) in CDCl3, after 3h in dark
PROTON.s CDCl3 {C:\NMRData\Portius_current_year} chp14zms 16
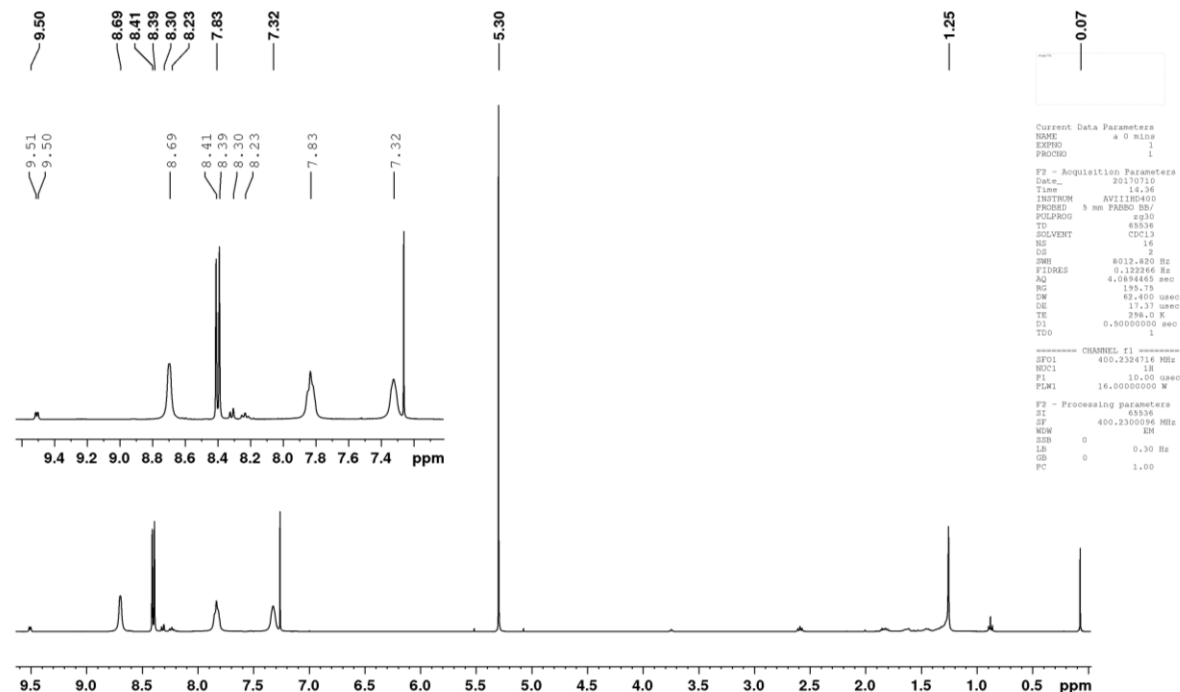
Figure A9.14. ^1H NMR spectrum of Pb(N$_3$)$_4$(bipy) in CDCl$_3$. The signals at δ = 8.69, 8.40, 7.83 and 7.32 ppm are attributed to uncoordinated bipy. NB: the exact identity of the compound was unable to be determined owing to the rapid reactivity of Pb(N$_3$)$_4$(bipy) in solution and the delay between preparation and analysis (see experimental section for more information).

295

Figure A9.15. ^{1}H NMR spectrum of Pb(N$_3$)$_4$(bipy) in CH$_2$Cl$_2$, DMSO-d$_6$ external lock. The signals at δ = 8.10, 7.85, 7.27, 6.76 ppm are attributed to bipy; the signals at δ = 4.76 and 3.32 are attributed to CH$_2$Cl$_2$ and H$_2$O, respectively. The bipy signals are assumed to arise from uncoordinated bipy, owing to the absence of any other signals shifted slightly up- or downfield.
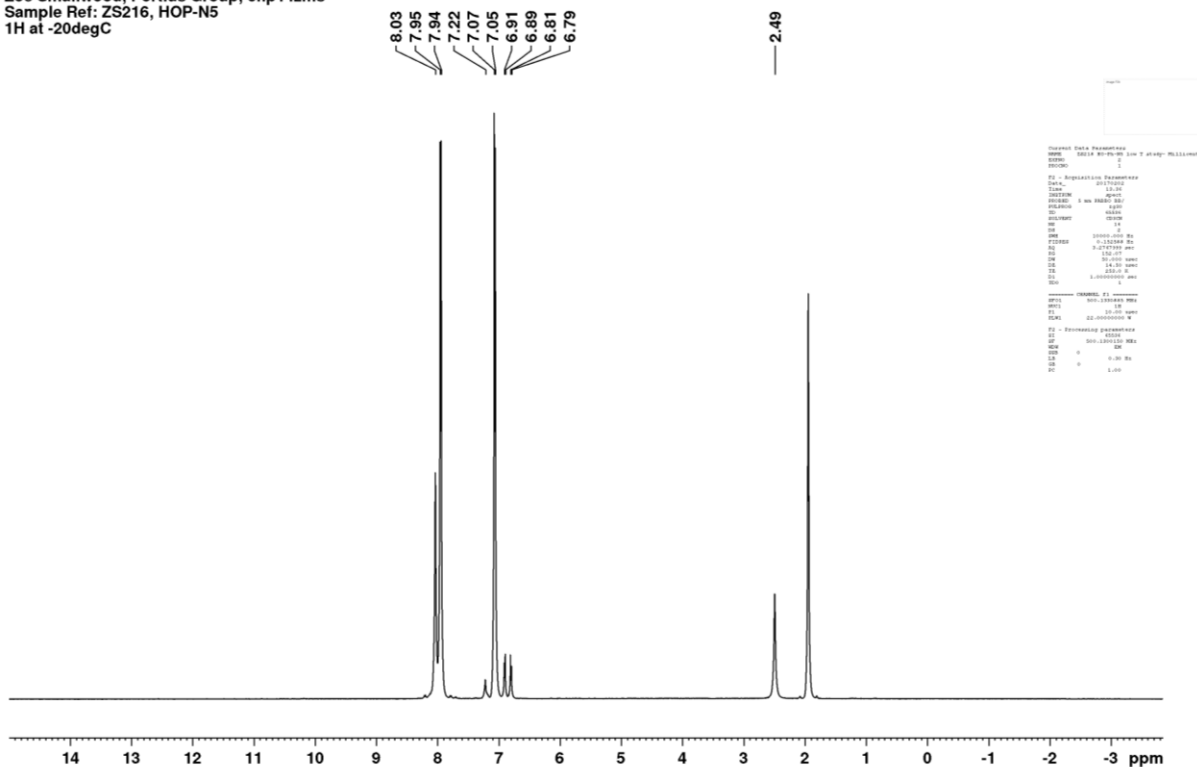
Figure A9.16. ^{1}H NMR spectrum of HOP−N$_5$ at −20 °C in CD$_3$CN. The signals at δ = 6.81 and 7.79 ppm are attributed to HOP−N$_3$.

296

160.07

126.60
123.54
120.51
116.90

126.60
123.54
120.51
116.90

128   126   124   122   120   118   116   ppm

155   150   145   140   135   130   125   120   115   110   105   100   95   ppm
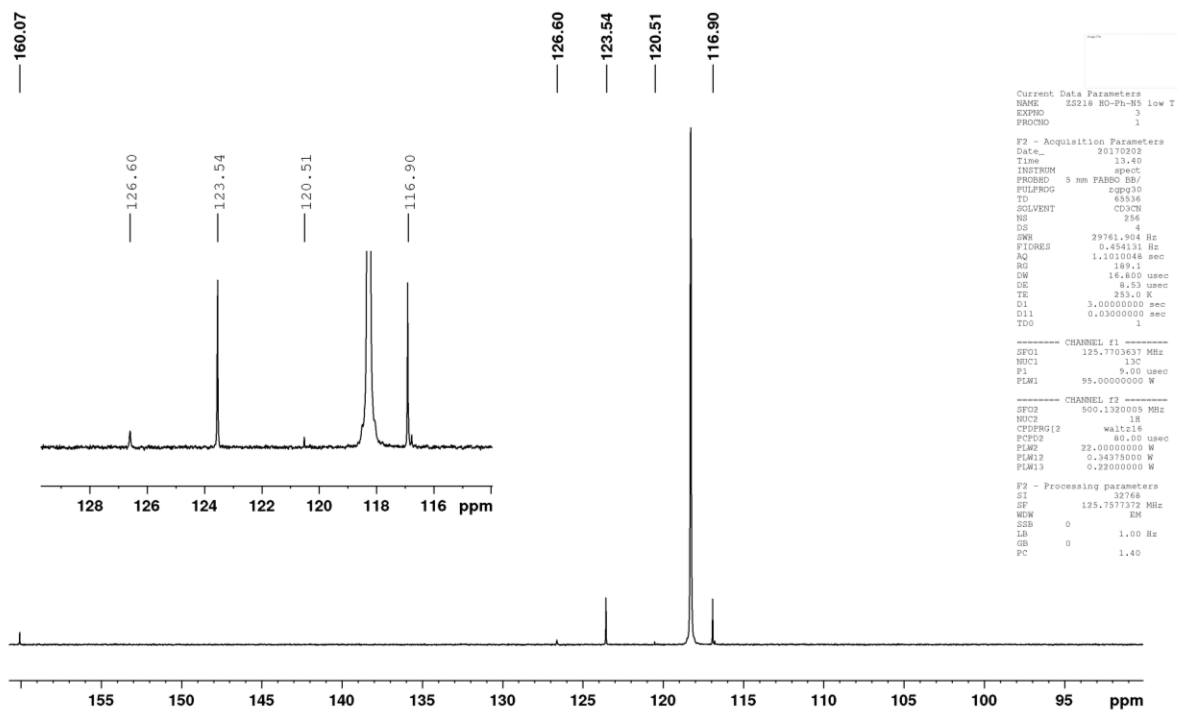
Figure A9.17. ^{13}C NMR spectrum of HOP−N$_5$ at −20 °C in CD$_3$CN. The signals at δ = 126.6 and 121.5 ppm are attributed to HOP−N$_3$.

-135.86

50   0   -50   -100   -150   -200   -250   -300   ppm
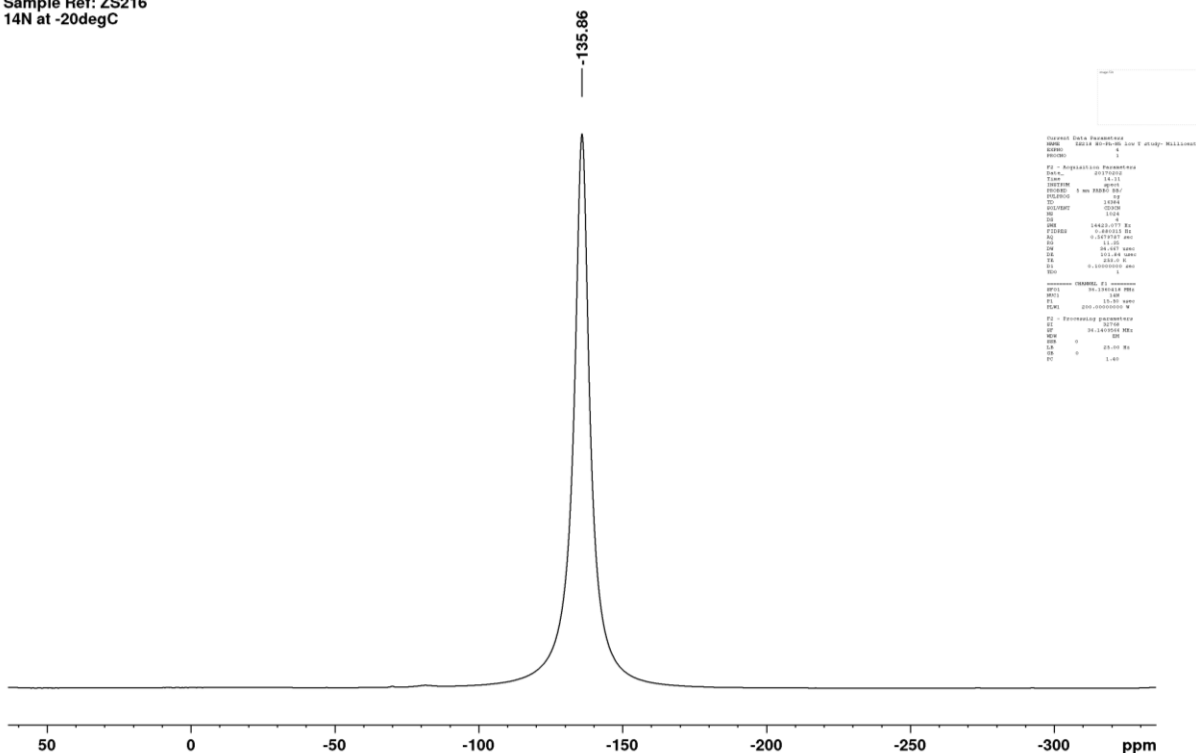
Figure A9.18. ^{14}N NMR spectrum of HOP−N$_5$ at −20 °C in CD$_3$CN.

6.98
6.91
6.84

6.98
6.91
6.84

2.19
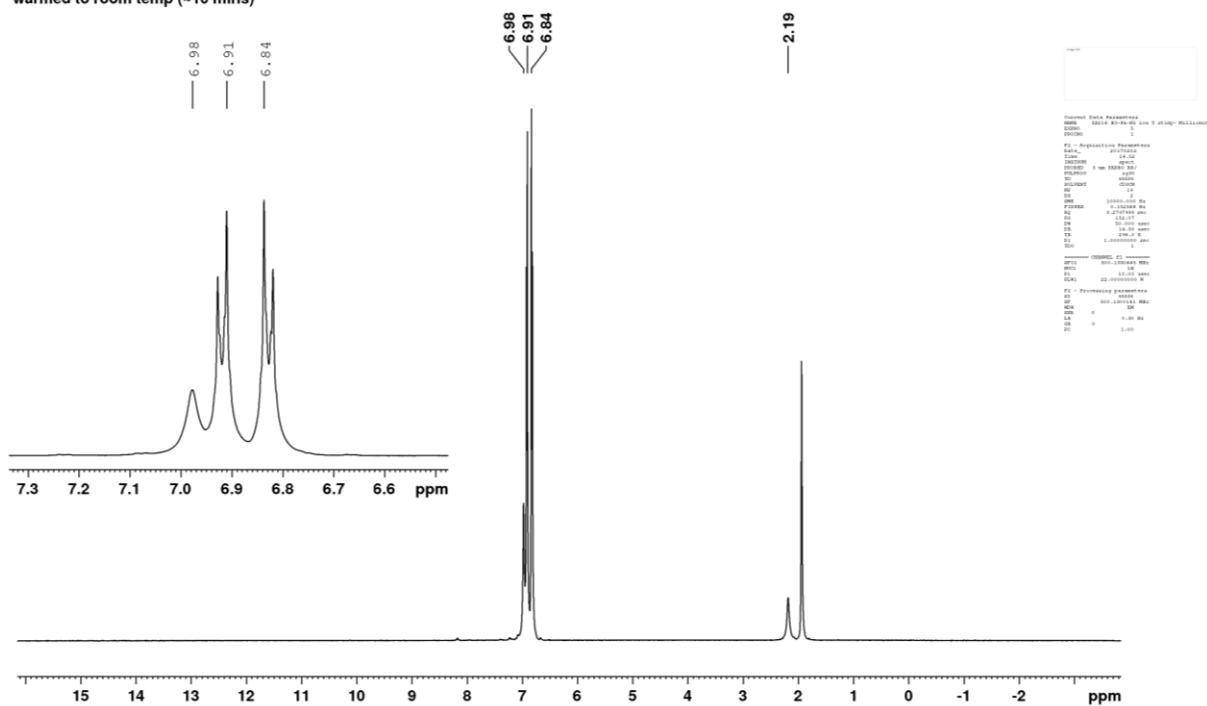
Figure A9.19. ^{1}H NMR spectrum of HOP-N$_3$ at room temperature in CD$_3$CN.

155.34
132.31
121.04
117.43
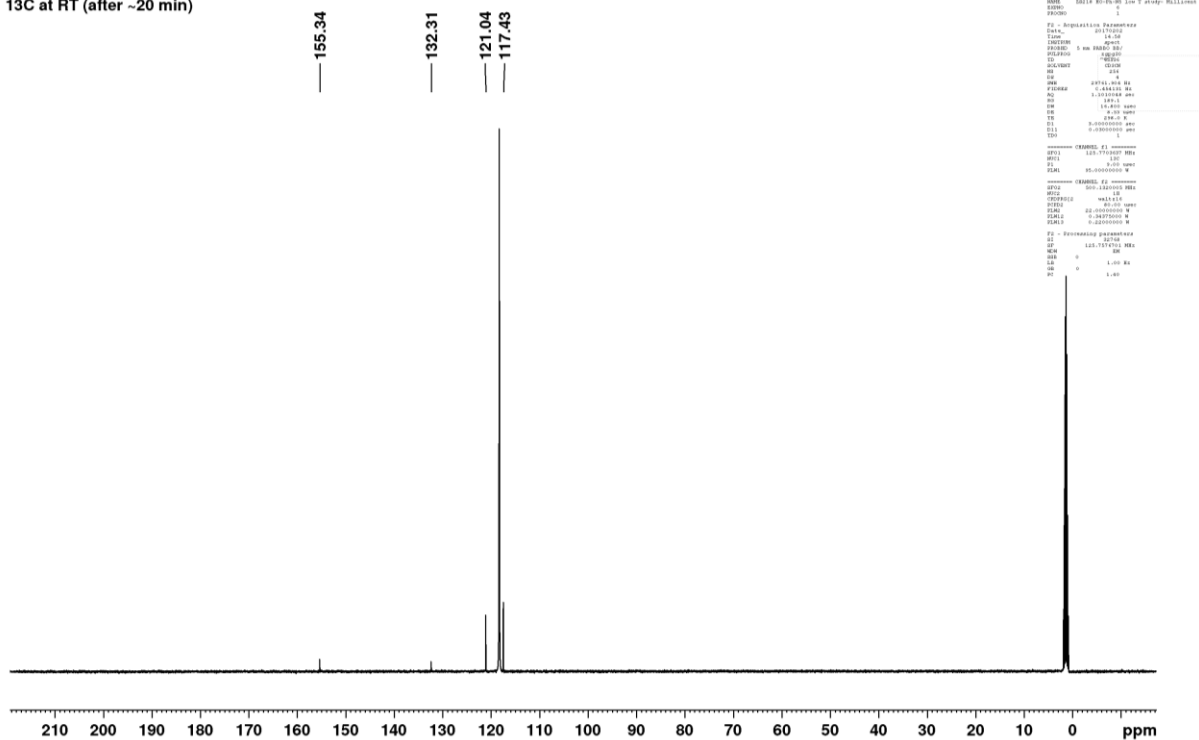
Figure A9.20. ^{13}C NMR spectrum of HOP-N$_3$ at room temperature in CD$_3$CN.
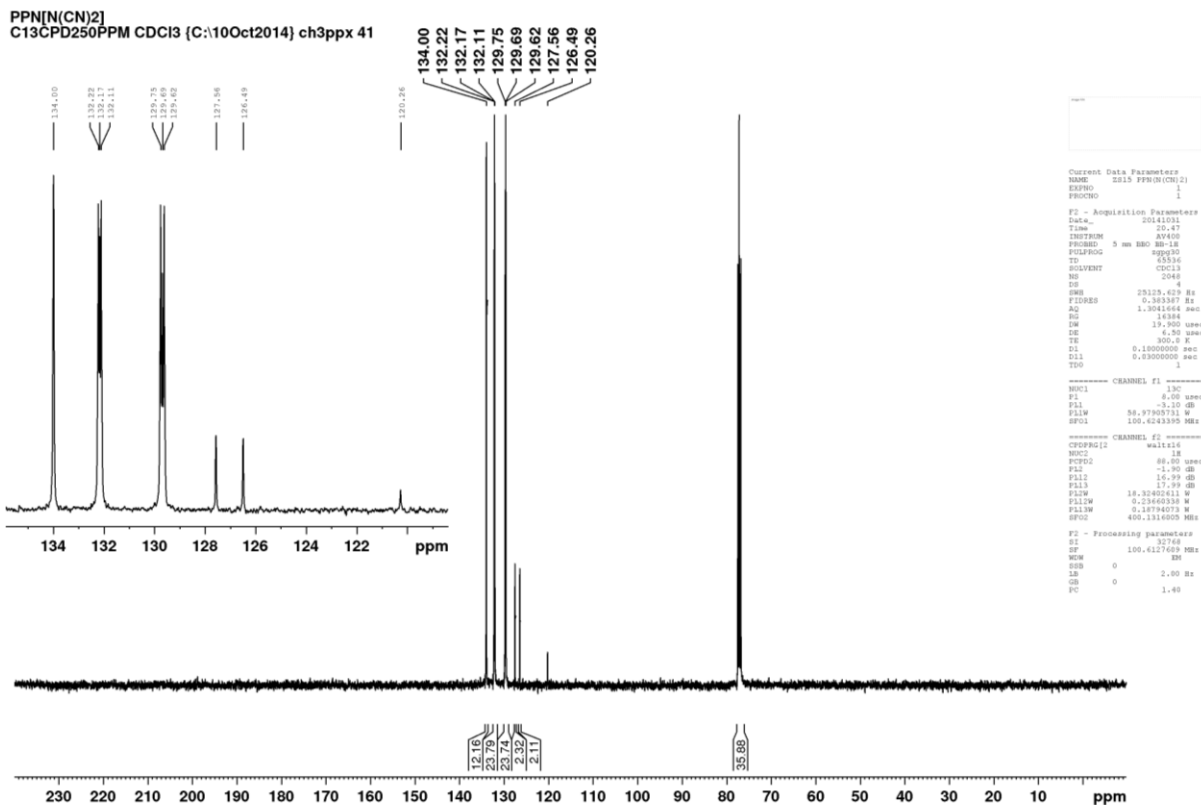
Figure A9.21. ^{13}C NMR spectrum of [PPN][N(CN)$_2$] in CDCl$_3$.
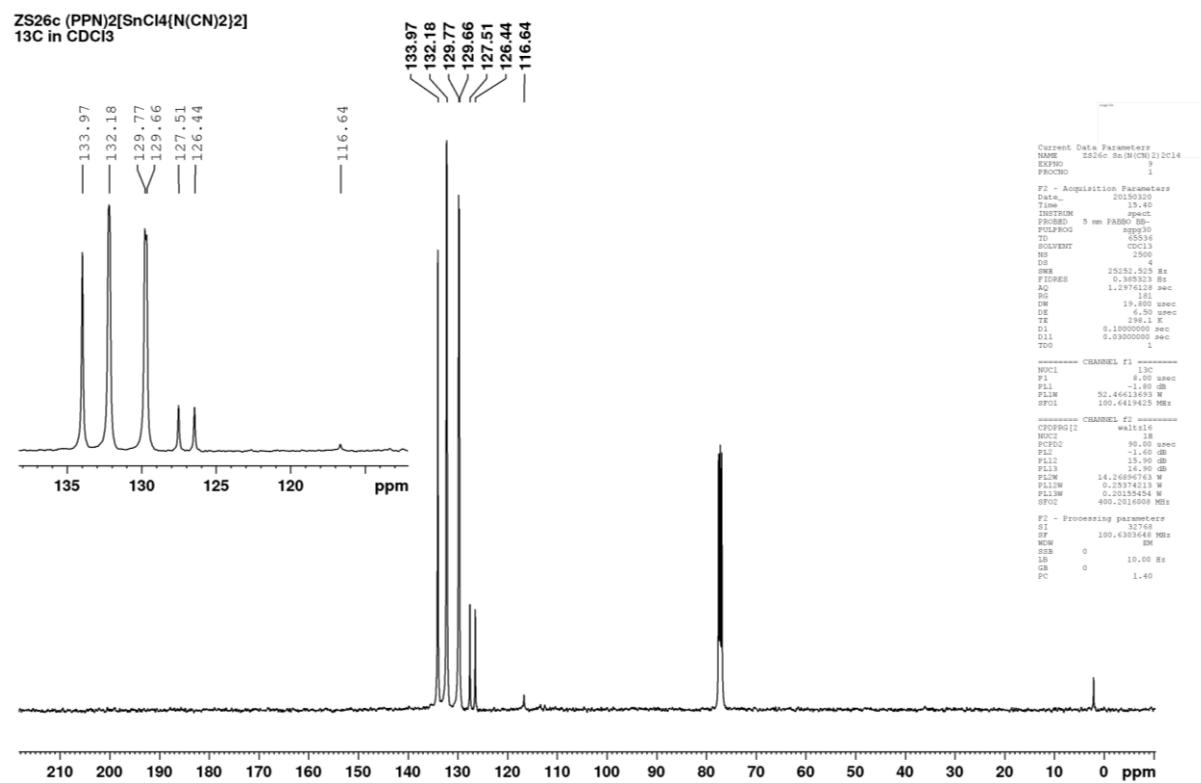
Figure A9.22. ^{13}C NMR spectrum of [PPN]$_2$[SnCl$_4${N(CN)$_2$}$_2$] in CDCl$_3$.

A10. Mass Spectra
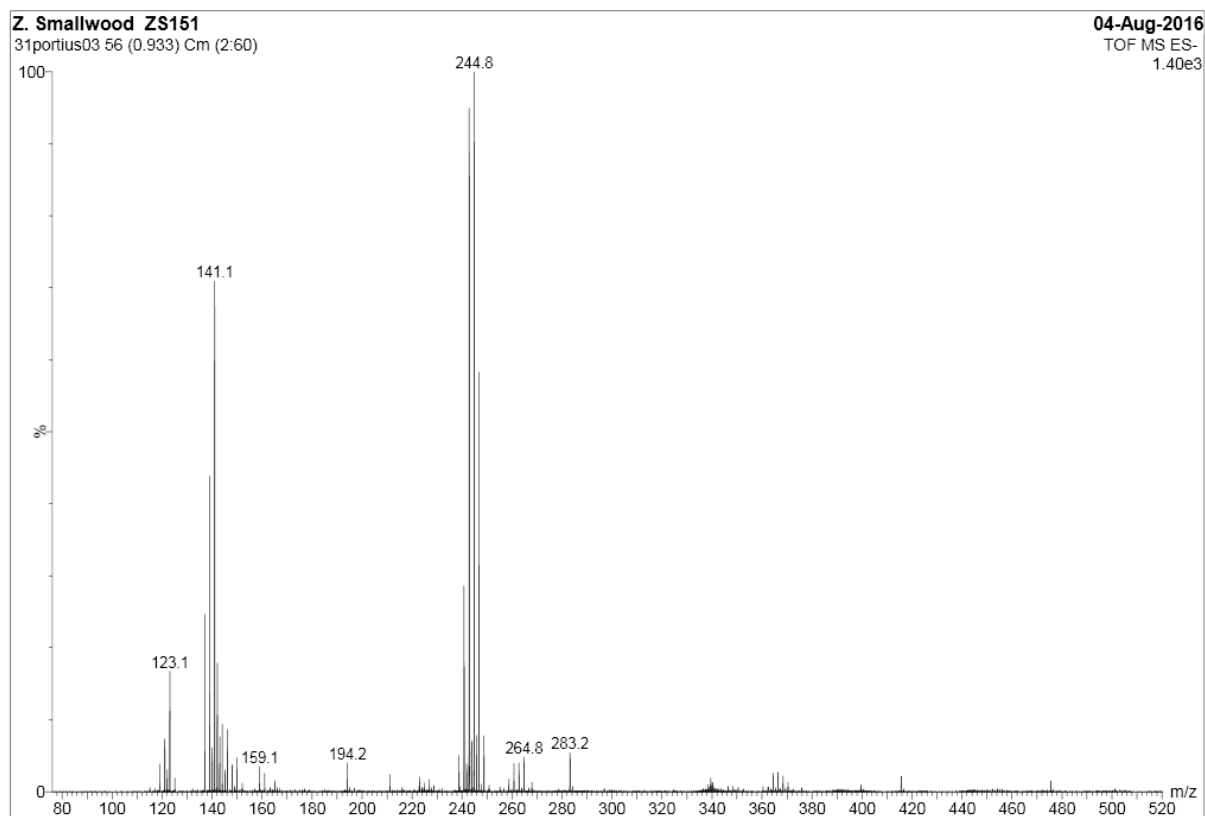
Figure A10.1. ESI-TOF mass spectrum of [PPN]$_2$[Ge(CN)$_6$] in MeCN.
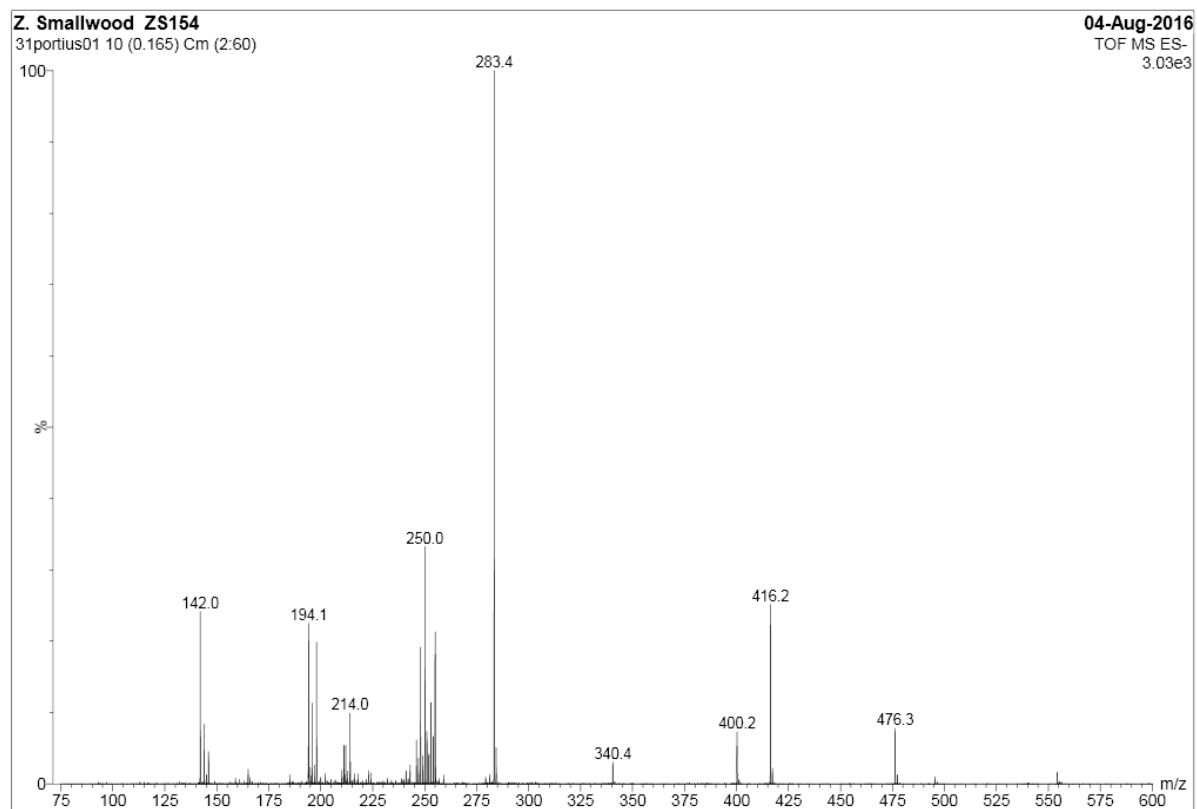
Figure A10.2. ESI-TOF mass spectrum of [PPN]$_2$[Sn(CN)$_6$] in MeCN.
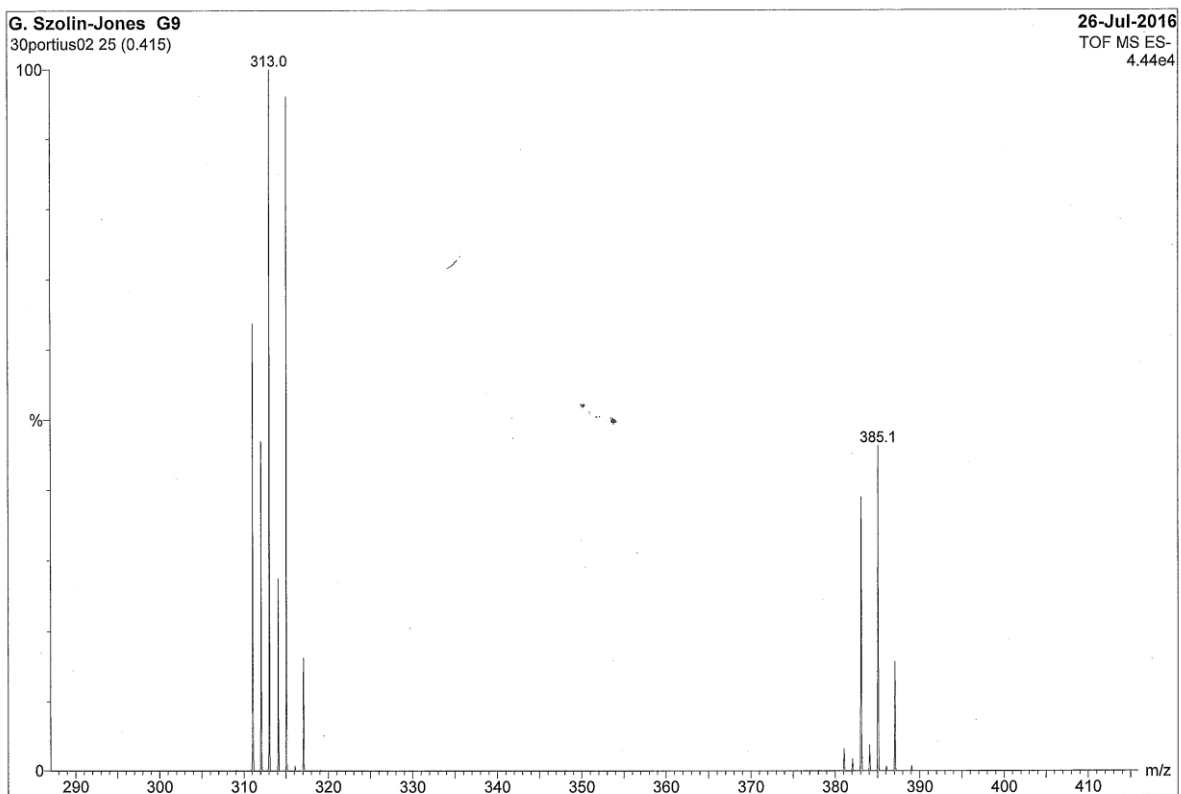
Figure A10.3. ESI-TOF mass spectrum of $(NH_4)_2[PbCl_6]$ in MeCN.
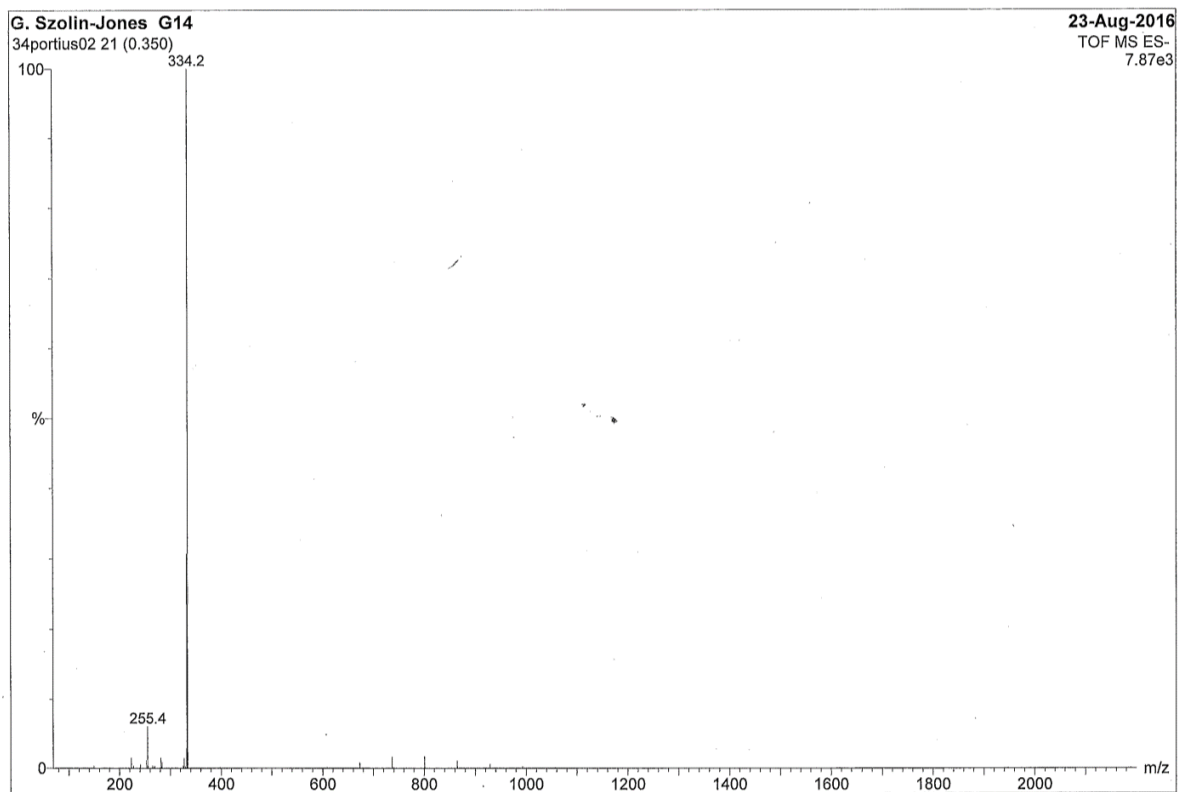
Figure A10.4. ESI-TOF mass spectrum of $[PPN]_2[Pb(N_3)_6]$ in MeCN.

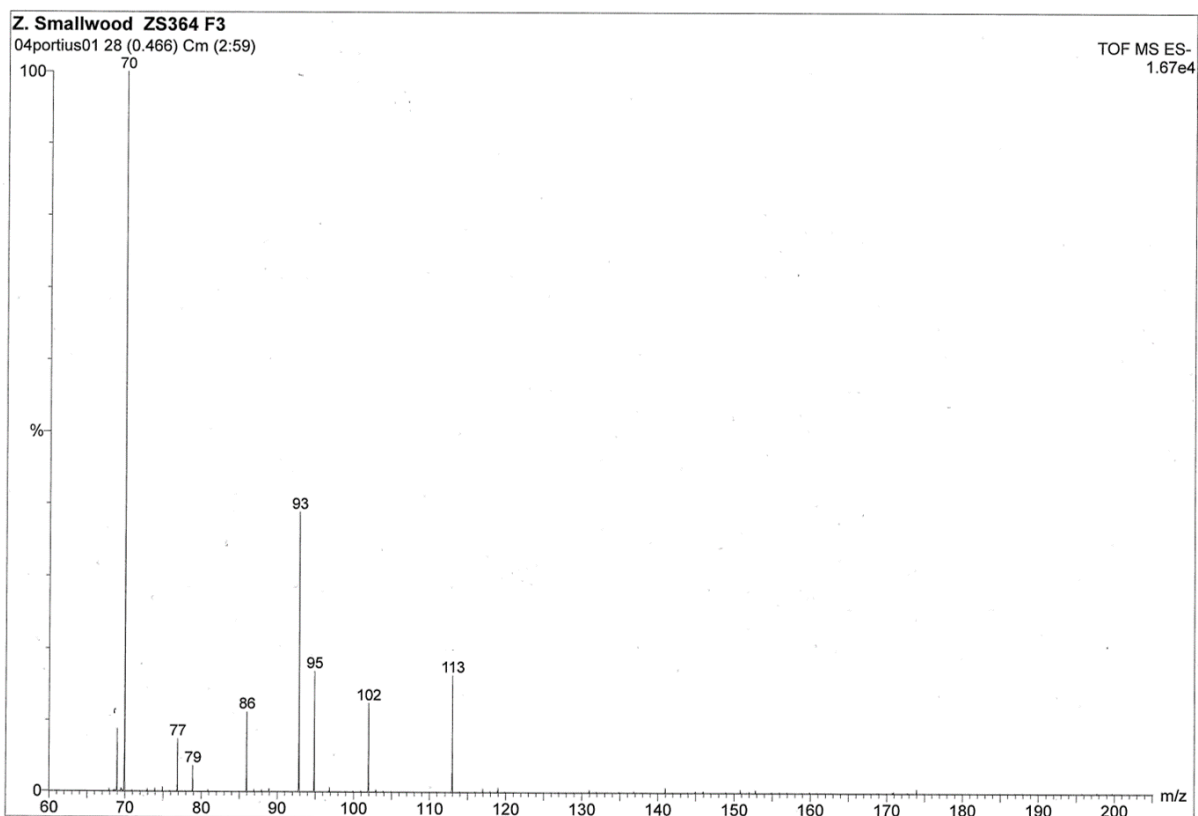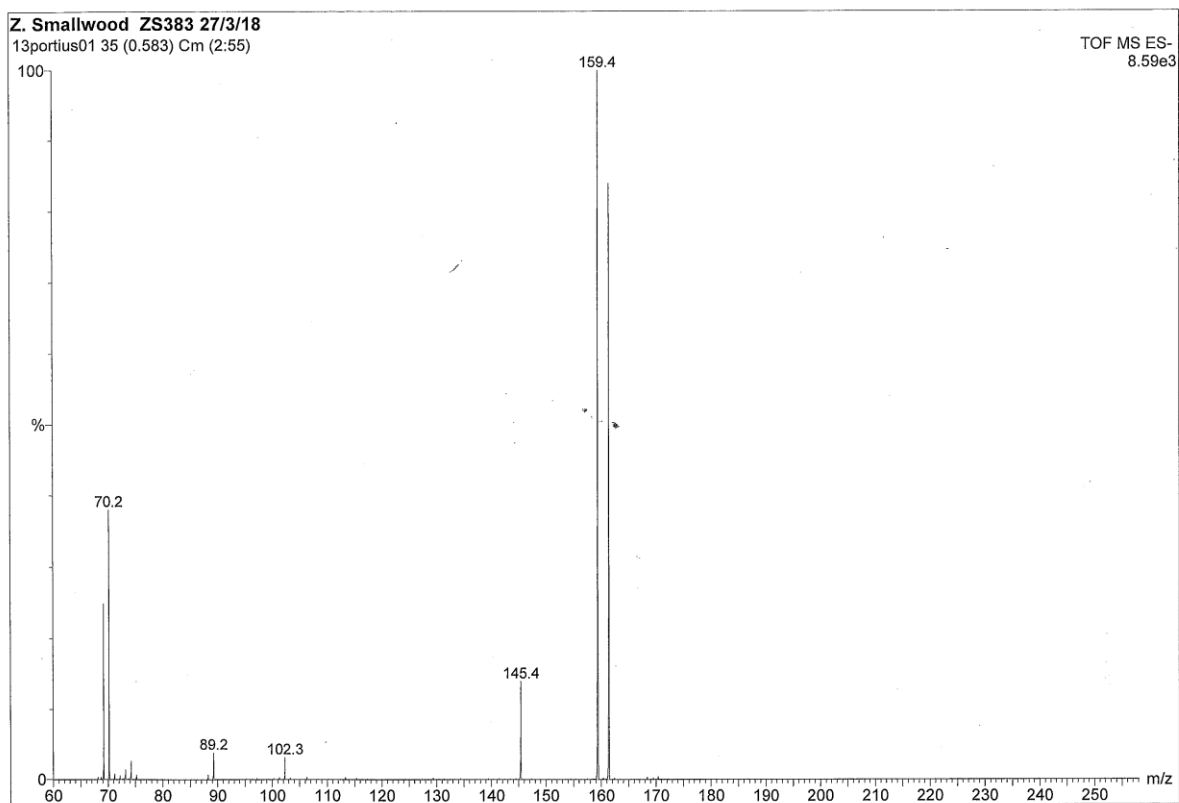Figure A10.5. ESI-TOF mass spectrum of 'NaN$_5$·3H$_2$O' in MeOH:H$_2$O (70%:30%).

Figure A10.6. ESI-TOF mass spectrum of '[PPN]N$_5$' in MeCN.